THE JOURNAL
OF
CHEMICAL PHYSICS

VOLUME 18, NUMBER 4 APRIL, 1950

Second-Order Transitions and Mesh Distribution Functions of Cross-Linked Polystyrenes

KURT UEBERREITER AND GERHARD KANIG
Kaiser-Wilhelm Institute for Physical Chemistry, Berlin-Dahlem, Germany
(Received July 13, 1949)

To the definition of the state of "liquid with thermally fixed structure" is added that of "liquid with chemically fixed structure." Polystyrene is combined with increasing proportions of divinylbenzene. The resulting space network is represented analytically by means of the definition of a mesh width. The second-order transition temperatures of these copolymers are determined from $V-T$ curves. They obey a function where the constant $586[Me \cdot T]$ characterizes the stiffening of the polystyrene by the addition of divinylbenzene. These polystyrene space networks are capable of being thermally activated up to a critical mesh width of 4 C atoms. The mesh widths are of varying sizes, the distribution is called the "polydictiality." The mesh distribution function can be obtained from the $V-T$ curves. The capacity of the space network to be thermally activated ceases fairly suddenly. This can be understood from a function of the capacity to be activated. The experimentally determined mesh distribution functions are expressed by means of a Gauss error curve. The width of this curve, about 1.7, is in surprising agreement for all copolymers. This means that approximately 50 percent of all meshes lie around the average mesh width with a variation of ± 2 meshes. The method can be applied to all cross-linked high polymers.

I. LIQUID WITH THERMALLY FIXED STRUCTURE

FOR every macromolecular substance which can be represented as a homogenous series, there is a transition range from micro- to macromolecular behavior which makes its appearance with a certain chain length (Fig. 1).[1] The molecules of lower energy present within a Maxwell distribution in a micromolecular liquid at a certain temperature form molecule associations. Within a highly molecular chain molecule on the other hand, the same units of low energy, which now appear as chain units, form points of adhesion with neighbors of low energy in adjacent chains. A change of position of the immense molecules is thus prevented. This is not possible until the temperature has so greatly increased that no molecules are present within the energy distribution with such low activation that they are able to form points of adhesion. The fixation of the structure in the case of normal chain molecules is thus of a purely thermal nature, and for this reason we shall call this state for chain molecular substances in the future, liquid with thermally fixed structure.

[1] K. Ueberreiter, Kolloid Zeits. **102**, 272 (1943); K. Ueberreiter, Kautschuk **19**, 12 (1943).

II. LIQUID WITH CHEMICALLY FIXED STRUCTURE

The purely thermal fixation of the structure can be replaced by a chemical one by preparing cross-linked polymers where the thermal adhesion points are replaced by normal bonds permanently fixed. It must therefore be possible to find a critical substance where the chain units become immovable by reducing the distance between the cross links further and further.

III. CHOICE OF A SUBSTANCE AS MODEL

The chemical fixation of macromolecules can be undertaken in two ways:

(1) by the addition or splitting off of atoms or molecules at specially reactive points of macromolecules which are already polymerized (vulcanization of rubber, hardening of Bakelite, $\cdots$),
(2) by the preparation of copolymers whose structure is in the form of a network from the start.

It is of decisive importance when choosing a substance as an ideal model, that no alien atoms are required for the chemical fixation which influence the play of intermolecular forces in any unforeseen way. This is almost always the case with the first method. The second method, fortunately, supplies a highly suitable model

substance in the copolymer styrene-divinylbenzene.*[2,3] Diagrammatically speaking, the free benzene rings in polystyrene are simply joined to a neighboring chain by normal valency bonds, which takes place chemically by the second vinyl group attached to the divinylbenzene being built into a neighboring chain.

IV. THE DEFINITION OF WIDTH OF MESH

The structure existing in the copolymer styrene-divinylbenzene corresponds to that of a space lattice whose points are connected by normal valency bonds. But on studying the model it is seen that a two-dimensional consideration of the system suffices, which simplifies the calculations. Figure 2 which is to be imagined as being continued regularly in all directions, can be built up from the units in chains 2 and 4 indicated by a dotted line. These are divided into chain units (monomer units) in chain 2, and C atoms in chain 4. The C atoms forming cross links with the aid of a benzene ring are marked with an asterisk. The two units at the end of the elementary structure making up the whole network form together a divinylbenzene molecule. The distinction was only made diagrammatically in order to study a single chain. We shall define the distance between two of the cross-linking C atoms marked with an asterisk in one chain, as the width of mesh Me.** If n_{St} denotes the mole fraction of the monomeric styrene chain units present in a basic molecule, and n_{Di} the mole fraction of the divinylbenzene chain units present in the same basic molecule, the relation

$$n_{St}+n_{Di}=1 \tag{1}$$

is obtained for the cross-linked styrene-divinylbenzene copolymer. For the width of mesh Me in chain units one obtains

$$Me_u=\frac{\frac{1}{2}n_{St}}{n_{Di}}=\frac{1}{2}\frac{1-n_{Di}}{n_{Di}}=\frac{1}{2}\left(\frac{1}{n_{Di}}-1\right) \tag{2}$$

(n denotes chain units). For a future comparison with other types of polymers, the expression in chain units has the disadvantage that the meshes have relatively different lengths, if the chain unit consists of more than 2 C atoms. We therefore define the mesh width in C atoms and obtain

$$Me_c=1/(n_{Di}) \tag{3}$$

(C denotes C atoms between two C* atoms). The conversion into terms of monomer units (chain units) is carried out according to the relation

$$Me_c=2Me_u+1. \tag{3a}$$

V. THE DEPENDENCE OF THE SECOND-ORDER TRANSITION TEMPERATURE ON THE WIDTH OF MESH

(a) Determination of the Second-Order Transition Temperature

The second-order transition temperature of a high molecular substance can be determined best from the

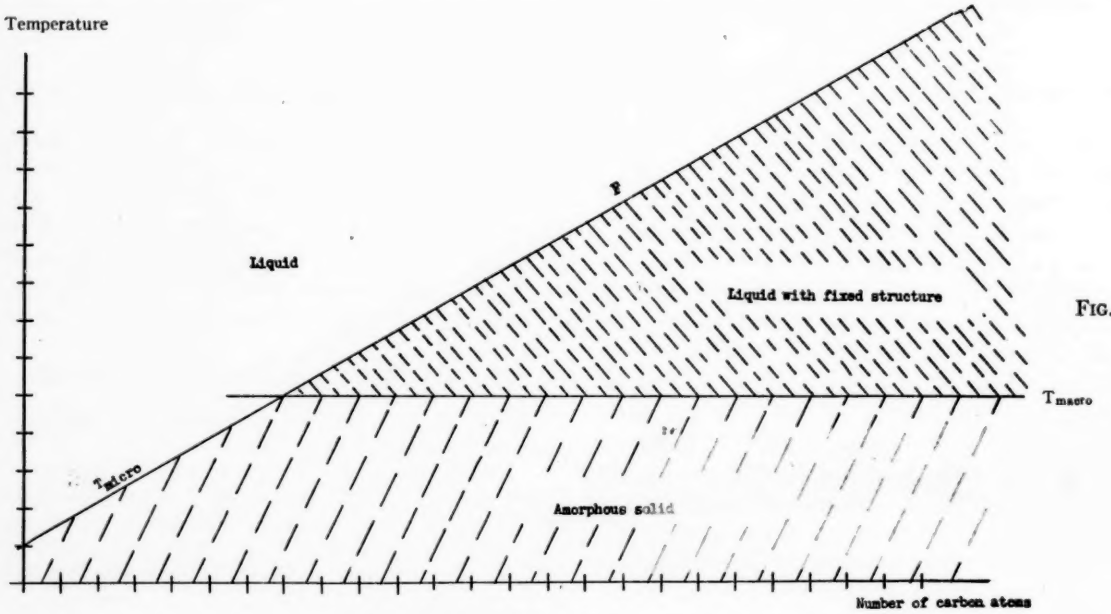

FIG. 1.

Tmicro = second-order transition temperature of micromolecules
Tmacro = second-order transition temperature of macromolecules
F = flow temperature.

* This copolymer was first investigated chemically by Staudinger (see reference 2) from the standpoint of second-order transition temperature by Ueberreiter (see reference 3).

[2] Staudinger and Husemann, Ber. d.d. chem. Ges. **68**, 1618 (1935).

[3] K. Ueberreiter, Zeits. f. physik. Chemie (**B**)**45**, 361 (1940); K. Ueberreiter, Zeits. f. physik. Chemie (**B**)**46**, 157 (1940).

** This definition departs from the usual nomenclature. In considering the network of a net, the length 2 Me would be taken as the mesh length. This is not suitable where the linking of the chains is concerned.

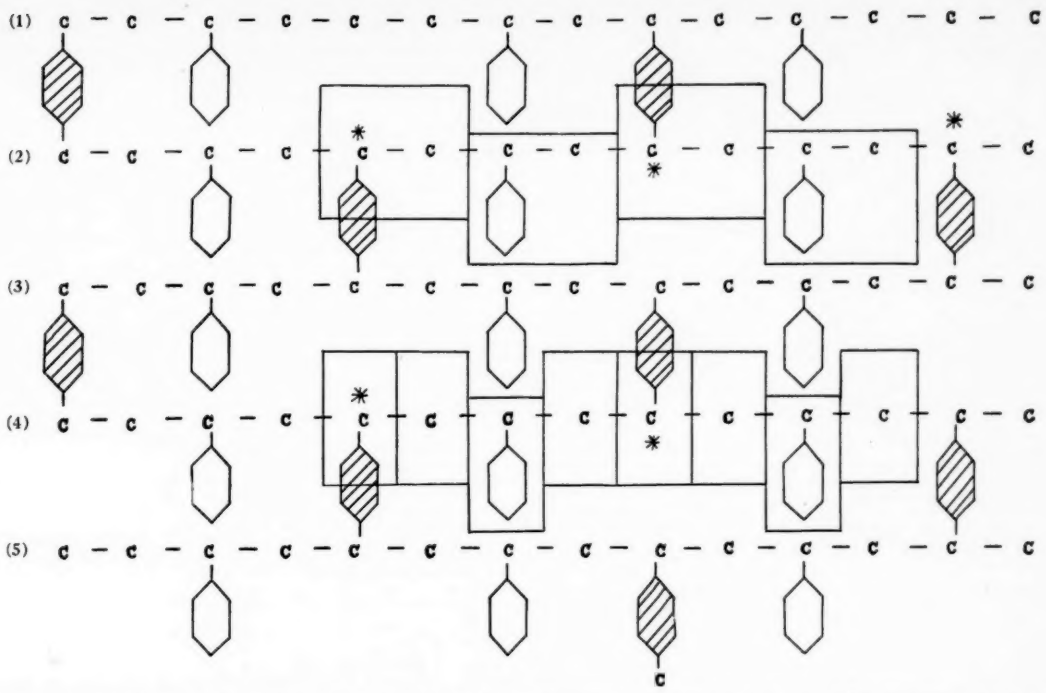

FIG. 2.

volume-temperature curve. If straight lines are drawn through the volume in the range of solid and fixed structure, these are found to cut one another at a point which lies within the second-order transition region and can be used in the determination of this region. The $V-T$ curves of the styrene-divinylbenzene copolymers investigated in this paper are shown in Fig. 3. If the second-order transition range of normal polystyrene is compared with that of the most highly cross-linked polymer which still shows signs of second-order transition, a pronounced widening of this range is observed. This fact makes the determination of the second-order transition temperature by the method just mentioned more difficult. A method already described by Tammann was therefore used which defines the temperature of the maximum of d^2V/dt^2 as the second-order transition temperature. This temperature represents the position of the greatest alteration in the coefficient of volume expansion, that is a temperature at which the great mass of the molecules changes to the state of fixed structure.

(b) Second-Order Transition Temperature and Mesh Width

If one plots the second-order transition temperature of the cross-linked polymers thus obtained against the mesh width, one obtains Fig. 4. If one wishes to determine the connection between the transition temperature T_N and mesh width, i.e. the function $T_N=f(Me)$, it is best to start with the assumption that, with a rise in transition temperature, DT_N will be inversely proportional to the mesh width. One obtains

$$DT_N=\frac{k}{Me} \quad \text{with} \quad DT_N=T_N-T_C \qquad (4)$$

(D=difference), where T_N denotes the second-order transition temperature of the network with mesh width Me, and T_C the second-order transition temperature of the normal chain-polymer.

If the constant k is determined from the measurements in Fig. 4, the value $586[Me\cdot T]$ is obtained. The function for these polymers is thus

$$DT_N=\frac{586}{Me} \quad \text{or} \quad T_N=\frac{586}{Me}+82, \qquad (4a)$$

when $T_C=82°C$ (pure polystyrene). The constant k could be described as the rigidity of the network. It would be interesting for the purposes of comparison, to know its value for as many cross-linked polymers of different structure as possible. It can be seen from Fig. 4 that this function gives a good interpretation of the measurements obtained. It permits the calculation now of the value T_N for any mesh width. According to these measurements, the critical mesh width for divinylbenzene-styrene cross linked structures is 4–5 carbon atoms, corresponding to 2 chain units between two links. The network remains capable of being activated thermally for an astonishing length of time. By being activated thermally is understood that the chain units with benzene rings attached to them which are not cross linked are able to carry out micro-Brownian wriggling movements, and therefore are in the state of liquid with chemically fixed structure.

VI. EXPLANATION OF THE INCREASE IN SECOND-ORDER TRANSITION TEMPERATURE WITH CROSS LINKING

By raising the temperature it is possible to increase the thermal activation of the chain units of polystyrene

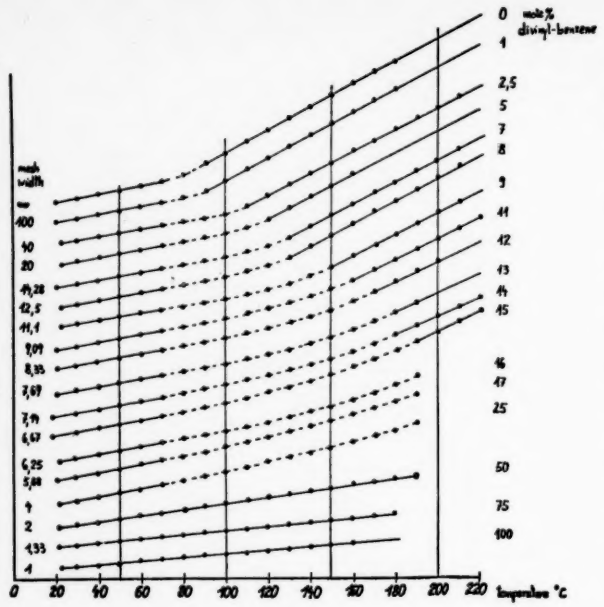

FIG. 3.

to such an extent that these enter the state of liquid with fixed structure characteristic of high polymers.[3] The chain units rotate around the bent valency bonds of the chain in restricted half-rotations, the so-called micro-Brownian[4] or wriggling movements.[5] If all the units in a chain are activated thermally they try to roll the chain up spirally. The chain units with very low thermal energy which function as points of adhesion, constitute a hindrance here. Whilst in the case of thermally fixed structure, it is only the low thermal energy content of a few chain units which makes them into points of adhesion, the linking of these with neighboring chains by means of normal valency bonds has rendered them completely incapable of a change in position. A systematic reduction of the mesh width is therefore bound to lead to a critical width where the chain is so strongly fixed that it resists the coiling tendency of the chain units still capable of wriggling, and thus prevents them doing so.

The results of measurements for polystyrenes show, with the aid of the transition Eq. (4a), that the critical distance for these substances is approximately 4 carbon atoms.

VII. THE POLYDICTIALITY

The picture of a cross-linked polymer given in Fig. 2 does not comply with the real situation in one point. The meshes in this diagram have a constant length and this will not be the case actually. It must be assumed that the meshes of a cross-linked polymer are not of uniform length. We will use the term "polydictiality"† to describe this. One might assume that the conception of the polymolecularity of a polymer is based on a similar foundation. The superficial analogy, however, must not hide the fact that the inner cause for the appearance of the polydictial distribution is different from that of the polymolecular. Chains of varying length are formed in the course of the growing and breaking down processes during polymerization. Thus the polymolecular distribution can be changed by conciously directing the course of the reaction. The polydictial distribution, on the other hand, is a product of the distribution of the molecules of both reaction partners. During the act of polymerization the monomeric molecules are joined together according to their arrangement, their liquid structure is thus fixed chemically and determined for the duration of the existence of the substance. The polydictial distribution thus reflects the arrangement of the molecules in the monomeric reaction liquid. The polymolecular, on the other hand, gives a picture of the mechanism of the reaction.

In the case of a subsequent cross linking of a chain polymer (method 1), the polydictial distribution depends, of course, on the arrangement of the reactive points of the chain. If these are distributed very regularly the meshes will be closely distributed. In the preparation of chain polymers capable of further cross linking, in this case, the polydictiality will again be indirectly dependent on the reaction mechanism, as this directs the construction of the chain. This is the case, for example, in the cross linking of rubber which can be vulcanized.

VIII. ANALYSIS OF THE POLYDICTIAL DISTRIBUTION

(a) The Widening of the Second-Order Transition Region with Cross Linking

The transition equation, (4), shows how the second-order transition temperature rises with decreasing mesh width. But it gives no explanation for the pronounced widening of the transition region. This can now be done with the aid of the polydictial distribution. The chain units of a substance with uniform mesh width would be activated thermally at a certain transition temperature. If there is a number of chain units of varying mesh width present in a substance, the chain units in the longest mesh will be the first to become flexible with a rise of temperature, and following these the remaining meshes. The transition equation indicates the mesh widths whose chain units will be stimulated at the temperature reached.

The principle difference between a polymer with thermally and one with chemically fixed structure comes to light with this result. A chain polymer is also a network, where the knots are made up of chain units of low energy. This network is "torn thermally" at the transition temperature, as the knots can only function as such, as a result of a low energy content which lies under the threshold value necessary for activating the wriggling. The rise in temperature above the transition

[4] W. Kuhn, Zeits. f. physik. Chemie (B)42, 1 (1939).
[5] C. W. Bunn, Proc. Roy. Soc. 180, 82 (1941).
† δικτυόν, network. Thus polydictiality actually means a state of many networks, but we employ this term in preference to a literal translation.

temperature very quickly removes these fixing points. A network with chemically fixed structure, on the other hand, cannot be destroyed by an increase to a temperature at which the substance does not decompose. The transition temperatures corresponding to certain meshes are superimposed, and yield a widened transition region dependent on the polydictial distribution.

(b) The Calculation of an Experimental Mesh Distribution Function

An analysis of the polydictial distribution can be attempted on the basis of these theories. The aim is to obtain a mesh distribution function $h(Me)$, which gives the number of meshes of width Me in the interval dMe.

In order that this function can be differentiated and integrated the mesh width must be regarded as varying continuously. This is perfectly possible, as the difference between two neighboring mesh widths Me and $Me+1$, where the experimental method is concerned, is of no importance for highly polymeric compounds.

The number of gram molecules present in a basic molecule with mesh width Me, besides being dependent on this width Me, is also dependent on the interval in which they lie. Thus

$$dn_{Me}=h(Me)dMe. \tag{5}$$

This function will be denoted in the following as mesh distribution function.

The processes in the transition region will serve as a starting point for our considerations. The calculation must be referred to the chain units and not to the mesh widths, as it is the former and not the meshes which represent the kinetic units. The relation between the number of meshes in an interval and the chain units corresponding to them is found to be,

$$dn_{Me}=-[2/(Me-1)]dn_{St}. \tag{6}$$

The calculation can thus be made on chain units, whereby the alterations in volume with temperature are made use of. The increase in volume with temperature below the transition region is linear, the expansion coefficient constant. The chain units are stimulated thermally in the transition region, and the coefficients of expansion of the activated chain units are greater than those of the non-stimulated. A greater increase in volume therefore appears, which does not increase linearly again with temperature until all chain units are activated thermally.

Therefore, the following relation can be fixed for the number of chain units activated with an increase in temperature of dT,

$$dn_{St}/dT=c(d^2V/dT^2). \tag{7}$$

For the total number of stimulated chain units in the transition region therefore, the following holds good,

$$n_{St}=\int_{t_s}^{t_l} dn_{St}=c\int_{t_s}^{t_l}(d^2V/dT^2)dT$$
$$=c(\alpha_l-\alpha_s)=cD\alpha \tag{8}$$

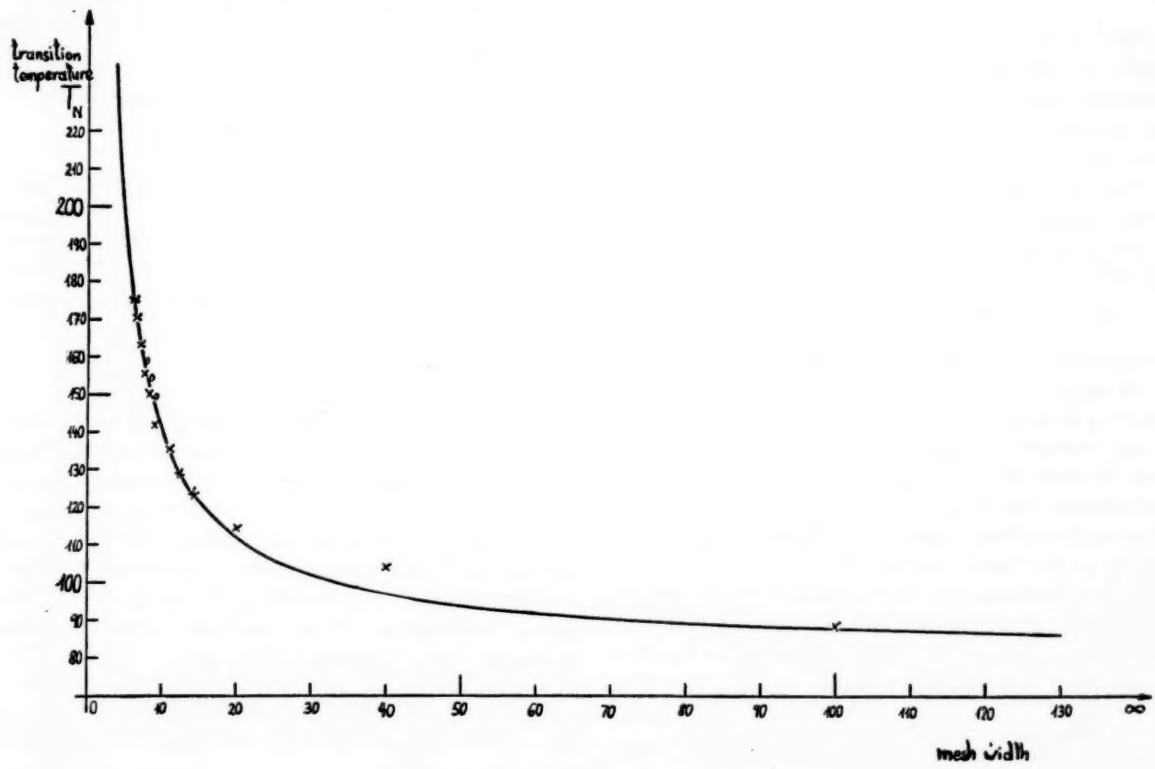

FIG. 4.

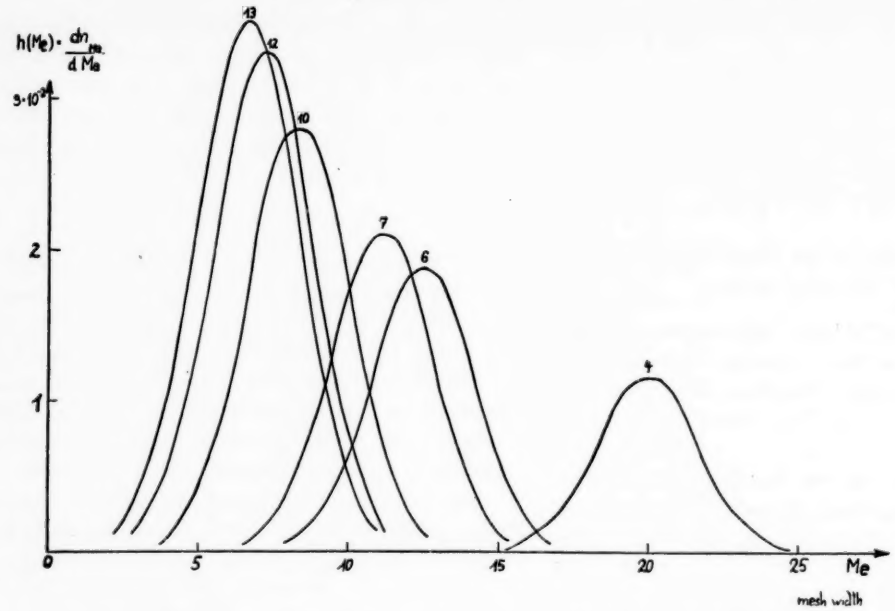

FIG. 5.

(D=difference). The integration here has to extend over the whole transition region, wherefore t_s is to represent a temperature in the range of the solid and t_l a temperature in that of the liquid with fixed structure. In the case of cross-linked substances the relation (1) applies as well for n_{St}, the total number of chain units, capable of being stimulated.

The constant c can now be calculated for every copolymer. The following is obtained,

$$c=n_{St}/D\alpha. \tag{9}$$

The value of $D\alpha$ is derived from the curves in Fig. 3. It shows an insignificant trend, negligible in these calculations, which indicates, like the extreme widening of the transition region for highly cross-linked substances, that the expansion coefficient decreases somewhat with decreasing mesh width. The following equation now applies in place of Eq. (7) for the number of chain units stimulated with an increase in temperature of dT,

$$dn_{St}=cV''(T)dT=(n_{St}/D\alpha)V''(T)dT. \tag{10}$$

An analysis of the mesh distribution will be attempted with the aid of these equations, whereby the following assumption is made.

In the transition region of a polydictial substance, with an increase in temperature of dT, the chain units are stimulated thermally, i.e. they begin to wriggle, in those meshes whose transition temperature is reached according to the transition equation (4).

If Me is substituted for the variable T in the relation (10) with the aid of the Eq. (4), it is possible with this assumption to derive the mesh distribution function from the $V-T$ curves. One obtains

$$dn_{Me}=\frac{2\cdot 586\cdot n_{St}}{D\alpha}\cdot\frac{V''(T)}{Me^2(Me-1)}dMe=h(Me)dMe. \tag{11}$$

If the mesh distribution function is calculated from the values of the $V-T$ curves in Fig. 3 according to Eq. (11), and its values plotted against the mesh widths, curves appear which resemble those of Gauss' law of errors. For this reason and because it is highly probable that the molecules in divinylbenzene-styrene mixtures are present in statistical distribution, Gauss' law will be used below in formulating the mesh distribution function. In contrast to function (11), which was derived from the experimentally determined $V-T$ curves, this function will be described as theoretical mesh distribution function.

(c) The Activation of the Chain Units in Cross-Linked Polymers

The area under the function (11) gives the number of meshes capable of being activated, as is seen on working out this relation. The question now arises, whether this number coincides with the number of meshes actually existing. The latter can be stated immediately for every cross-linked polymer, and is,

$$n_{Me}=2n_{Di} \tag{12}$$

where Eq. (1) applies for n_{Di}. One could now integrate the experimental mesh distribution curves (11) graphically and compare the values with those of Eq. (12). It is simpler, however, as it is only a question of a method which offers an approximate survey, to calculate an activity function which expresses the capacity of the chain units to be activated, using certain simplifying assumptions. We, therefore, define as follows, capacity to be thermally activated

$$A=\frac{\text{number of activated chain units}}{\text{number of chain units capable of being activated}}.$$

The values of the function are thus limited to the range

of $0 \leqq A \leqq 1$. Equation (8) applies for the number of activated chain units, and Eq. (1) still applies for the number of those capable of being activated, whereby n_{St} represents the number of chain units in the basic molecule and $D\alpha_{St}$ refers to pure polystyrene. If one assumes that the coefficient of expansion only varies insignificantly with the mesh width, the following still holds good,

number of chain units
capable of being activated $= n_{St} \cdot D\alpha_{St}$ (13)

so that, for the function of the capacity to be stimulated, the following equation is obtained,

$$A = \frac{c_{Mi} \cdot D\alpha_{Mi}}{n_{St} \cdot c_{St} \cdot D\alpha_{St}} = \frac{D\alpha_{Mi}}{n_{St} \cdot D\alpha_{St}} \quad \text{as} \quad c_{Mi} \cong c_{St}. \quad (14)$$

Mi denotes the cross-linked polymer in question, *St* pure polystyrene. The numbers $100A$ state directly what percentage of chain units in a cross-linked styrene is still capable of being activated thermally. It is found from Table I that with high degrees of cross linking, up to 90 percent of the substance is still capable of being stimulated thermally. This result may be traced back to the fact that the mesh distribution is relatively small, as already indicated by the experimental curves (11).

(d) The Calculation of the Theoretical Mesh Distribution Function

The ground having been prepared, the calculation of the mesh distribution function according to Gauss' law of errors can now follow. It should be formulated so that the integration over all mesh widths gives just that number of meshes present in the substance according to Eq. (12). But the study of the capacity to be activated showed that if cross-linked polystyrene can be activated at all, this can take place in almost all chain units. Therefore the calculation was attempted for all networks by means of the function,

TABLE I.

Mol % Div.	*Me*	$\frac{D\alpha_{Mi}}{D\alpha_{St} \cdot n_{St}} = A$
0		1
1	100	1.040
2.5	40	0.992
5	20	1.065
7	14.28	1.031
8	12.5	1.077
9	11.12	1.037
11	9.1	0.935
12	8.34	0.912
14	7.14	0.865
15	6.66	0.924

$$dn_{Me} = h(Me)dMe = \frac{n_{Me}}{\sigma(2\pi)^{\frac{1}{2}}} \exp\left(-\frac{(Me - Me_{\max})^2}{2\sigma^2}\right) dMe. \quad (15)$$

As a check, the average theoretical mesh widths which were calculated from Eq. (2) were compared with the actual ones calculated, as is usual in error calculation, from the following relation,

$$Me_{\exp} = \frac{[dn_{Me} \cdot Me]}{[dn_{Me}]}, \quad [\,] \text{ denotes } \Sigma. \quad (16)$$

A glance at Table II shows that an extremely low asymmetry of 1-2 mesh widths exists. It is not worth while

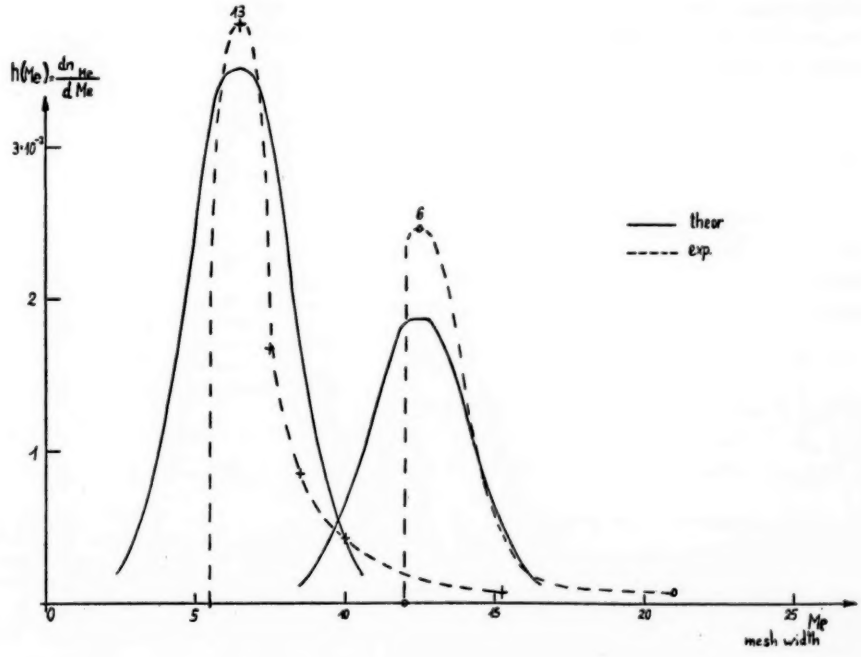

FIG. 6.

TABLE II.

Me_{theor}	Me_{exp}	σ
20	20.91	1.77
12.5	14.35	1.96
11.12	13.85	1.94
8.34	9.82	1.51
7.14	8.33	1.48
6.66	8.15	1.66
6.26	8.25	1.53
		$\bar{\sigma}=1.7$

to take this asymmetry into consideration when constructing the function, as the method only permits a survey actually, and can lay no claim to complete accuracy.

The values on the horizontal axis of the point of inflection are also required for the value σ. Calculated according to the equation known this is,

$$\sigma=([v v\cdot dn_{Me}/d_{Me}]/[dn_{Me}/dMe)] \text{ with } v=Me-Me_{\max}. \quad (17)$$

Its values are also given in Table II. The astonishing result is obtained that the variation of the mesh width is almost independent of the degree of cross linking, and has the value of roughly 1·7. That means that approximately 50 percent of all meshes with a variation of ±2 meshes lie around the average mesh width. A clear idea of the mesh distribution is given in Fig. 5, in which the Gauss' curves for all polymers measured are recorded, namely, the theoretical mesh distribution functions (15) with an average $\sigma=1\cdot7$ for all networks. In view of the fact that the number of meshes increases with an increase in the linking chain units in the basic molecule of polymerizable monomers, the area under the curves increases according to the relation (12). The dotted curve in Fig. 6 is the experimental mesh distribution function on which curve 15 is based. As is to be expected, it falls too steeply in the area of decreasing mesh width, and therefore shows a greater deviation from the theoretical distribution function. This must be explained by the fact that the coefficient of expansion alters somewhat with the mesh width, and probably decreases as this narrows. It is not worth while to use this phenomenon for a further correction of the curves, as a few simplifying assumptions have been made in any case.

(e) The Efficiency of the Method

Although one must emphasize the fact that the theoretical mesh distribution function just described only gives an approximate picture of the situation, the method is still of value in view of the fact that a distribution function cannot be obtained on the basis of chemical fractionating methods, as cross-linked substances are absolutely insoluble in all solvents. Apart from this, it must be added, that in fractionating, an inaccuracy enters through losses during the process and the overlapping of the individual fractions. Finally, it must be observed, how quickly and simply the distribution function above can be obtained from the simple and exact volume measurements. If one starts with the intention of deriving the mesh distribution from the $V-T$ curves of cross-linked substances, one can increase the accuracy by reducing the temperature intervals further. The method can be applied to any cross-linked substance. As will be seen in a continuation of this paper, the knowledge of the mesh distribution can serve to draw conclusions concerning the structure of the chains of the normal substance, by working backwards from the network. But the method, which as yet is the only one permitting an analysis of the network structure, seems to be especially valuable for the investigation of tension and tensile strength problems in polymers which are almost all cross linked when put into use.

The Moments of Inertia of Molecules with Internal Rotation

P. TORKINGTON
*Department of Theoretical Physics, King's College, London, England**
(Received July 5, 1949)

The moments of inertia of some typical molecules with one internal rotational degree of freedom are obtained for all possible configurations; also the directions of the axes of least and greatest inertia. The dependence on the values of the structural parameters is discussed and illustrated.

I. INTRODUCTION

RECENTLY, interest in rotational isomerism and in the potential barrier hindering internal rotation has been revived.[1–7a]† Rotational isomerism may be investigated by electron-diffraction methods,[5,8,9,9a] and by dipole-moment measurements;[4,10] some attempts have been made to draw conclusions from infra-red and Raman spectra, where the different isomers fall into different symmetry point groups and are characterized by different spectra.[6,7,7a,11] Some years ago, it was found possible to deduce the configuration of a molecule with internal rotation from the rotational contour of infra-red absorption bands; chloroprene was shown to have approximately the *trans*-configuration in the gaseous state at ordinary temperatures.[12] The infra-red bands of allyl chloride vapor[13] show signs of rotational contour, but the moments of inertia are too large for this to be properly resolved with the usual prism instruments. It is possible that a proper analysis of the infra-red spectra of selected substances in the gaseous state will prove to be the best method for the investigation of rotational isomerism. The present paper deals with the dependence of the moments of inertia on the configuration. Where the vibrational assignment is certain, a complete analysis of the rotational fine structure of selected vibration-rotation bands, as recorded by a grating instrument, may enable the configuration to be fixed with at least as great a degree of certainty as would be possible from electron-diffraction data. Where the favored configuration is effectively planar, the contour alone may prove sufficient, if the bands are properly chosen. Thus, for the *cis*- and *trans*-forms of allyl chloride, the ethylenic CH_2 bending mode with a frequency of 928 cm^{-1} in the liquid state[13] would give rise to a pure *C*-type band.[13a] Similarly, in the *trans*-form of ethylene dichloride the A_u CH_2 rocking mode would give rise to a pure *C*-type band, and in the *cis*-form the A_1 and B_2 CH_2 rocking modes would give pure *B*- and *C*-type bands respectively. The valence-type symmetry coordinates are readily obtained as functions of the angle for internal rotation, enabling an estimate to be made of the variation of coupling, and thus of frequency, with this angle.

II. THE EVALUATION OF THE MOMENTS OF INERTIA AND THE DIRECTIONS OF PRINCIPAL AXES OF INERTIA[14,14a]

For a system of point masses m_i having Cartesian coordinates x_i, y_i, z_i the moments of inertia about a rotational axis through the center of gravity having direction cosines l, m, n is given by the equation

$$I_{l,m,n}=Al^2+Bm^2+Cn^2-2Dmn-2Eln-2Flm, \quad (1)$$

where A, B, and C are the moments of inertia about the x, y, and z axes respectively, and D, E, and F are the products of inertia involving y_iz_i, x_iz_i, and x_iy_i respec-

---

* *Present address.*—British Rayon Research Association; Research Laboratories, Womston, Lancashire, England.

[1] E. N. Lassettre and L. B. Davis, J. Chem. Phys. **16**, 151, 553 (1948).

[2] W. D. Gwinn and K. S. Pitzer, J. Chem. Phys. **16**, 303 (1948).

[3] J. O. Halford, J. Chem. Phys. **15**, 364, 645 (1947); **16**, 410, 560 (1948); **17**, 111 (1949).

[3a] H. Kuhn, J. Chem. Phys. **15**, 843 (1947).

[4] R. A. Oriani and C. P. Smyth, J. Chem. Phys. **16**, 930 (1948).

[5] Y. Morino and M. Iwasaki, J. Chem. Phys. **17**, 216 (1949).

[6] Szasz, Sheppard, and Rank, J. Chem. Phys. **16**, 704 (1948); **17**, 83 (1949).

[7] N. Sheppard and G. J. Szasz, J. Chem. Phys. **17**, 86, 93 (1949).

[7a] D. W. E. Axford and D. H. Rank, J. Chem. Phys. **17**, 430 (1949).

† Other references will be found in the index to Volume 17 of this journal under "Rotation" and "Rotational Isomerism." While the present paper was in press, a detailed treatment of compound internal rotation appeared [J. E. Kilpatrick and K. S. Pitzer, J. Chem. Phys. **17**, 1064 (1949)]—also, an interesting analysis of the dipole moment-temperature plots for some chlorinated hydrocarbons [R. A. Oriani and C. P. Smyth, *ibid.* **17**, 1174 (1949)]. The determination of the azimuthal angle in H_2S_2 and H_2O_2 from the structure of vibration-rotation infra-red bands has been discussed in two recent papers [M. K. Wilson and R. M. Badger, *ibid.* **17**, 1232 (1949) and P. A. Giguère, *ibid.* **18**, 88 (1950)]. These are both particularly unfavorable cases, as would be anticipated. The examples studied in the present paper still seem worth considering. It should be observed that atomic vibrational displacements have been detected in recent electron diffraction studies [I. L. Karle and J. Karle, *ibid.* **17**, 1052 (1949)].

[8] J. Y. Beach and A. Turkevich, J. Am. Chem. Soc. **61**, 303, 3127 (1939).

[9] V. Schomaker and D. P. Stevenson, J. Chem. Phys. **8**, 637 (1940).

[9a] J. Karle, J. Chem. Phys. **15**, 202 (1947).

[10] J. Y. Beach and K. J. Palmer, J. Chem. Phys. **6**, 639 (1938).

[11] G. Herzberg, *Infrared and Raman Spectra of Polyatomic Molecules* (D. Van Nostrand Company, Inc., New York, 1945), pp. 346–351.

[12] H. W. Thompson and P. Torkington, Proc. Roy. Soc. **A184**, 21 (1945).

[13] H. W. Thompson and P. Torkington, Trans. Faraday Soc. **42**, 432 (1946).

[13a] The classification of band-types is that of R. M. Badger and L. R. Zumwalt, J. Chem. Phys. **6**, 711 (1938).

[14] H. W. Edwards, *Analytic and Vector Mechanics* (McGraw-Hill Book Company, Inc., New York and London, 1933).

[14a] J. O. Hirschfelder, J. Chem. Phys. **8**, 431 (1940).

TABLE I. Constants of inertia of butadiene.

θ	0°	15°	30°	45°	60°	75°	90°	
I_A	43.79	42.82	39.70	34.41	28.10	22.95	20.96	$\times 10^{-40}$
I_B	128.50	133.66	147.74	169.97	186.20	200.28	205.43	g cm²
I_C	172.29	172.54	173.71	176.34	179.99	183.20	184.47	
*S	−0.768	−0.808	−0.896	−0.982	−0.988	−0.976	−0.974	
*ρ	2.19	2.35	2.87	3.98	5.44	7.07	7.90	
c_A	0	0.159	0.319	0.473	0.603	0.691	0.721	
c_C	$-\infty$	−6.302	−3.136	−2.114	−1.657	−1.448	−1.386	

* The parameters S and ρ in Tables I to IV and in Fig. 5 are those introduced by Badger and Zumwalt (see reference 13a) to describe the shape of asymmetric rotors; $S=(2b-a-c)/(a-c)$, $\rho=(a-c)/b$, where a, b, c are the reciprocals of the least, middle, and greatest moments of inertia.

TABLE II. Constants of inertia of ethylene dichloride.

θ	0°	15°	30°	45°	60°	75°	90°	
I_A	107.80	103.89	91.59	72.32	51.39	35.44	29.50	$\times 10^{-40}$
I_B	258.90	280.33	338.86	418.82	498.78	557.32	578.74	g cm²
I_C	356.03	368.36	403.64	454.30	506.63	545.58	559.92	
S	−0.674	−0.753	−0.888	−0.968	−0.996	−0.997	−0.996	
ρ	1.67	1.94	2.86	4.87	8.72	14.42	18.01	
c_A	0	0.277	0.547	0.791	0.982	1.104	1.145	
c_C	$-\infty$	−3.612	−1.828	−1.266	−1.018	−0.906	−0.873	

tively:

$$\left.\begin{aligned} A&=\sum_i m_i(y_i^2+z_i^2) \\ &\quad -\{(\sum_i m_iy_i)^2+(\sum_i m_iz_i)^2\}/(\sum_i m_i), \text{ etc.} \\ D&=\sum_i m_iy_iz_i-(\sum_i m_iy_i)(\sum_i m_iz_i)/(\sum_i m_i), \text{ etc.} \end{aligned}\right\}, \quad (2)$$

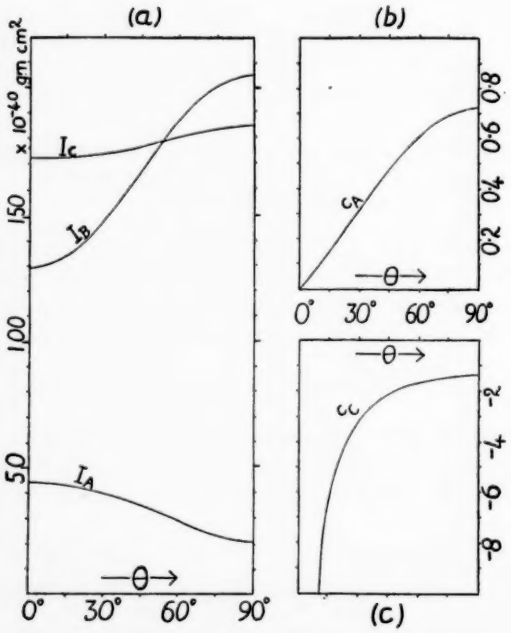

FIG. 1. Butadiene. (a) Principal moments of inertia, (b) direction of axis of least inertia, (c) direction of axis of greatest inertia.

where the center of gravity coincides with the origin of the system of axes, the terms involving $(\sum_i m_i)^{-1}$ vanish. The principal moments of inertia, (i.e., those about axes for which the products of inertia vanish, the principal axes), are the roots of the following cubic equation:

$$\begin{vmatrix} (A-I) & -F & -E \\ -F & (B-I) & -D \\ -E & -D & (C-I) \end{vmatrix}=0, \quad (3)$$

and the ratios of the direction cosines for a given principal axis are given by any row of first minors of the determinant of (3), with the appropriate value of I substituted.

Where the coordinates can be referred to a system of axes in which, for example, the y axis coincides with one of the principal axes of inertia, so that $D=F=0$, and B is a principal moment, then the principal axes and moments in the xz plane are conveniently found as follows: The moment about an axis $(z-z_0)=c(x-x_0)$, passing through the center of gravity (x_0, z_0), is given by

$$I_c=(1+c^2)^{-1}\sum_i m_i[c(x_i-x_0)-(z_i-z_0)]^2+\sum_i m_iy_i^2. \quad (4)$$

The principal axes are found by applying the condition $(\partial I_c/\partial c)=0$, which leads to the following quadratic equation in c:

$$c^2+c[(C-A)/E]-1=0. \quad (5)$$

Substitution of the roots of Eq. (5) in Eq. (4) gives the two moments in the xz plane, which are also the roots of the residual equation

$$I^2-I(A+C)+(AC-E^2)=0. \quad (6)$$

TABLE III. Constants of inertia of chloroprene.

θ	0°	15°	30°	45°	60°	75°	90°	
I_A	90.00	95.68	110.4_2	128.2_6	142.6_4	150.1_7	152.0_8	$\times 10^{-40}$
I_B	319.4_1	315.4_1	302.0_2	277.6_8	247.6_7	224.0_4	215.4_2	g cm²
I_C	409.4_1	402.1_1	385.4_3	370.9_5	365.6_3	366.3_9	367.4_9	
S	−0.841	−0.828	−0.778	−0.645	−0.391	−0.117	-0.003_5	
ρ	2.77	2.51	1.95	1.42	1.06	0.880	0.831	
l_A	−0.739	−0.754	−0.799	−0.866	−0.936	−0.984	−0.998	
m_A	0.674	0.654	0.590	0.478	0.322	0.152	0	
n_A	0	0.060	0.114	0.149	0.145	0.093	0.052	
l_C	0	−0.108	−0.221	−0.285	−0.244	−0.133	0	
m_C	0	−0.214	−0.464	−0.715	−0.886	−0.974	−1	
n_C	1	0.971	0.858	0.638	0.394	0.185	0	

TABLE IV. Constants of inertia of allyl chloride.

θ	0°	30°	60°	90°	120°	150°	180°	
I_A	66.56	65.24	60.32	51.06	39.92	30.87	27.34	$\times 10^{-40}$
I_B	196.2_0	205.2_9	230.2_3	265.3_8	298.1_3	312.1_4	317.7_5	g cm²
I_C	257.4_3	260.6_8	270.8_0	286.0_2	305.5_7	330.7_0	339.7_8	
S	−0.782	−0.820	−0.899	−0.966	−0.993	−0.988	−0.988	
ρ	2.19	2.36	2.97	4.27	6.49	9.17	10.69	
l_A	0.926	0.913	0.875	0.820	0.767	0.732	0.720	
m_A	0.377	0.390	0.438	0.520	0.608	0.671	0.694	
n_A	0	0.112	0.204	0.240	0.206	0.118	0	
l_C	0	−0.198	−0.367	−0.475	−0.292	−0.044	0	
m_C	0	0.187	0.329	0.382	0.043	−0.125	0	
n_C	1	0.962	0.870	0.793	0.956	0.991	1	

For planar molecules, the term involving y_i in Eq. (4) vanishes. Where the x or z axis coincides with a principal axis of inertia, so that A or C is a principal moment, the coefficient of c in Eq. (5) becomes $[(C-B)/D]$ or $[(B-A)/F]$, respectively, where c occurs in the equations for the axes of inertia, $(z-z_0)=c(y-y_0)$ and $(y-y_0)=c(x-x_0)$.

III. APPLICATION TO BUTADIENE, CHLOROPRENE, ETHYLENE DICHLORIDE, AND ALLYL CHLORIDE

For molecules with internally rotating groups, the principal moments of inertia will vary with the configuration. To describe the directions of the principal axes it is necessary to specify some internal coordinate system for each molecule. For the symmetrical molecules butadiene and ethylene dichloride, in which the two halves which mutually rotate are identical, the *cis*-forms fall into the symmetry point group C_{2v}. The plane of symmetry through the C−C bond is in each case taken as σ_{xy} and the vertical plane of symmetry as σ_{yz}. Other configurations are attained by rotating each half of the molecule through an angle θ, in opposite directions, the sense of the rotation being such that $E>0$. The y axis remains a twofold axis of symmetry for all configurations, and the locus of the center of gravity coincides with it. For $\theta=(\pi/2)$, (*trans*-configuration, symmetry C_{2h}), the center of gravity coincides with the center of symmetry at the midpoint of the C−C bond, and σ_{xz} becomes a plane of symmetry. For all configurations, the y axis remains a principal

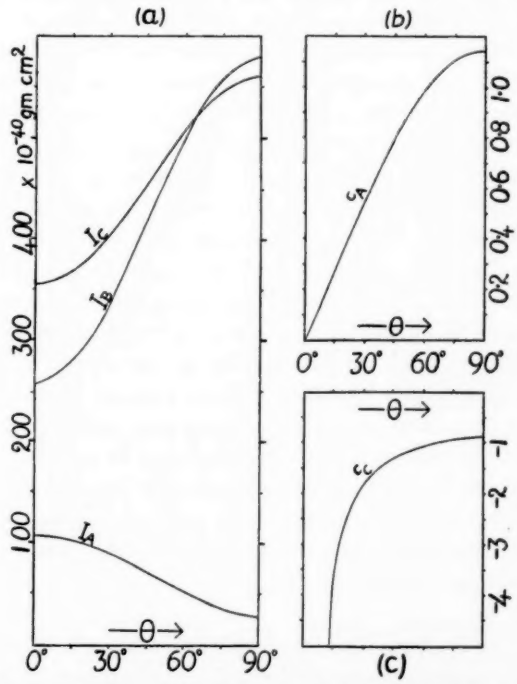

FIG. 2. Etheylene dichloride. (a) Principal moments of inertia, (b) direction of axis of least inertia, (c) direction of axis of greatest nertia.

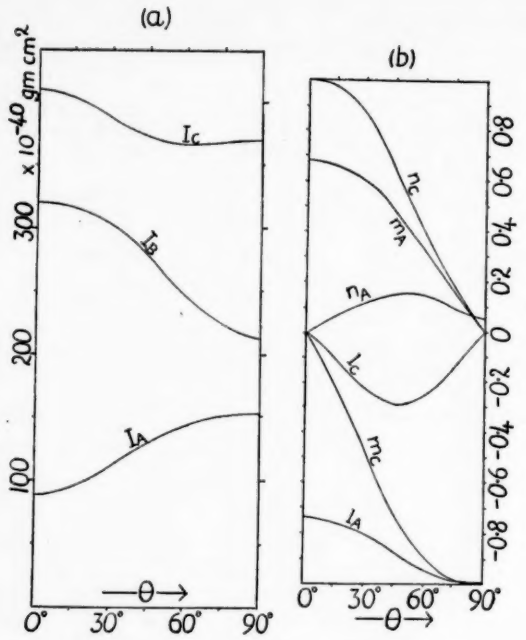

FIG. 3. Chloroprene. (a) Principal moments of inertia, (b) directions of axes of least and of greatest inertia.

axis of inertia, ($D=F=0$), and the directions of the others are conveniently described by the roots of Eq. (5).

Chloroprene is treated in the same manner as butadiene; ($\theta=0$, (*cis*-configuration), $\sigma_{xy}=C_s$; $\theta=(\pi/2)$, (*trans*-configuration), $\sigma_{xz}=C_s$). With the rotation having the same sense as in butadiene, $E<0$; referred to the center of gravity as origin, $D>0>F$. The locus of the center of gravity lies parallel to σ_{yz}. At $\theta=0$, $(\pi/2)$, the axis of greatest inertia is parallel to the z and y axes respectively; at intermediate values all three axes of inertia are inclined to the reference axes. For allyl chloride, the plane of symmetry of the *cis*-configuration is taken as σ_{xy}, the x axis being parallel to the C−C bond. Other configurations are reached by rotating the vinyl group through an angle θ, the $-CH_2Cl$ group remaining fixed. The locus of the center of gravity is again parallel to σ_{yz}. At $\theta=0$ and π, the axis of greatest inertia lies parallel to the z axis; at intermediate configurations there is no element of symmetry. The directions of the coordinate axes and the sense of rotation are such that the products of inertia are all positive except for a small range of D between $\theta=0$ and $(\pi/3)$. For both chloroprene and allyl chloride, the sets of principal axes are conveniently described by the direction cosines of the axes of least and greatest inertia.

The data for the *cis*- and *trans*-isomers and for five intermediate configurations are summarized in Tables I to IV, and the results are plotted in Figs. 1 to 5. The following values were employed for the interatomic distances:

r_{C-H} { 1.071[15] adjacent to double bond.
1.094[11] adjacent to single bond.

r_{C-C} { 1.573[11] in saturated system.
1.54† adjacent to double bond.
1.46† in conjugated system.

$r_{C=C}$ 1.353.[15]

r_{C-Cl} { 1.77[16],‡ adjacent to single bond.
1.69** adjacent to double bond.

The above distances are in angstrom units. All angles were taken as having their ideal hybrid-bonds values, (trigonal: 120°, tetrahedral: 109°28′). The atomic masses used with these models were as follows:

$$m_H=1.008, \quad m_C=12.004, \quad m_{Cl}=34.981.$$

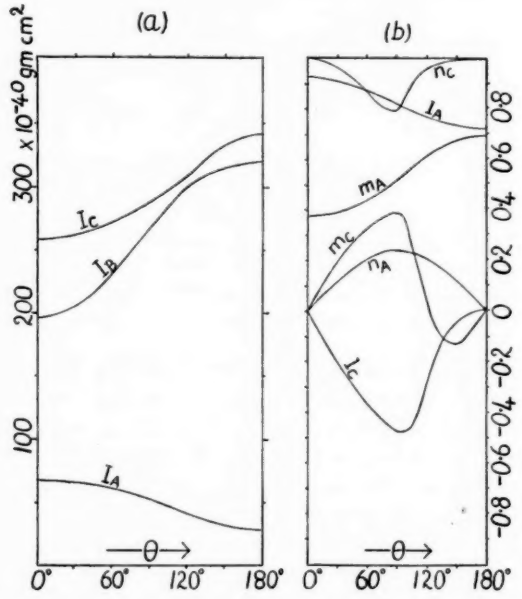

FIG. 4. Allyl chloride. (a) Principal moments of inertia, (b) directions of axes of least and of greatest inertia.

To convert from A.W.-A. units to c.g.s. units the factor employed was 1.6599×10^{-40}.

The coordinates have been chosen so that the subscripts A, B, and C in Tables I to IV refer to the least, middle, and greatest moments at $\theta=0$, and to the moments of inertia as defined in Eq. (2). Thus, at $\theta=0$, $C>B>A$ in all cases; for butadiene and ethylene dichloride $I_A=A$, $I_B=B$, and $I_C=C$, and for chloroprene and allyl chloride $I_C=C$. In the *trans*-configurations, the maximum moment is B, except for allyl

[15] W. S. Gallaway and E. F. Barker, J. Chem. Phys. **10**, 88 (1942).

† Shortening from value for saturated system estimated from C−Cl shortening, and from results for conjugated systems.

[16] L. O. Brockway, Rev. Mod. Phys. **8**, 231 (1936).

‡ Recent microwave measurements give $r_{CCl}=1.779$A in CH_3Cl.

** Taken to be the same as in vinyl chloride. Brockway, Beach, and Pauling, J. Am. Chem. Soc. **57**, 2693 (1935).

TABLE V. Derivatives determining variations in the moments and products of inertia for the ethylene dihalides, CH_2X-CH_2X, (for $D=F=0$, $E>0$).

	$\{[(4/9)K\sqrt{2}]^{-1}(\partial/\partial\alpha)\}$	$\{[(2/9)K]^{-1}r_{CX}(\partial/\partial r_{CX})\}$	$\{(Ka)^{-1}r_{CC}(\partial/\partial r_{CC})\}$	$\{[(1/18)K]^{-1}m_X(\partial/\partial m_X)\}$
A	$-2(1-\rho\cos^2\theta)$	$16(1-\rho\cos^2\theta)$	0	$32\{\sin^2\theta+(1-\rho)^2\cos^2\theta\}$
B	$(3a+2\cos^2\theta)$	$\{3a+2(1+8\sin^2\theta)\}$	$\{(a/\mu)+(\frac{2}{3})(1+2\epsilon)\}$	$\{(3a+2)^2+32\sin^2\theta\}$
C	$\{3a+2(\sin^2\theta+\rho\cos^2\theta)\}$	$\{3a+2+16(1-\rho)\cos^2\theta\}$	$\{(a/\mu)+(\frac{2}{3})(1+2\epsilon)\}$	$\{(3a+2)^2+32(1-\rho)^2\cos^2\theta\}$
E	$[(14-3a)/(4\sqrt{2})]\sin\theta$	$(3a+4)\sqrt{2}\sin\theta$	$(\frac{2}{3})(1-\epsilon)\sqrt{2}\sin\theta$	$4(3a+2)\sqrt{2}\sin\theta$

$K=m_Xr_{CX}^2$ $\quad$ $\epsilon=[(m_Hr_{CH})/(m_Xr_{CX})]$

$\mu=[m_X/(m_X+m_C+2m_H)]$ $\quad$ $\rho=\mu(1-\epsilon)$

$a=(r_{CC}/r_{CX})$ $\quad$ $\alpha=\widehat{CCX}$

chloride, in which it is C. In the two symmetrical molecules, the curves for I_B and I_C intersect, so that towards the *trans*-configurations $I_B>I_C$. The parameters c_A and c_C in Tables I and II define the directions of the axes of least and greatest inertia (see Eqs. (4) and (5)). The l, m, and n in Tables III and IV are the direction cosines of the axes indicated by the subscripts.

The components to the total moment from each of the two mutually rotating groups may be of some interest. These can be evaluated from the formula,

$$I_{l,m,n}=\sum_{i=1}^{n} M_i[(mz_i-ny_i)^2+(mx_i-ly_i)^2+(nx_i-lz_i)^2], \quad (7)$$

giving the moment of inertia I of a system of n particles of masses M_i, coordinates x_i, y_i, and z_i, about an axis of direction (l, m, n). Some results for allyl chloride are given here:

	θ =	0	$(\pi/2)$	π
I_A	Component from $-CH_2Cl$	18.05	29.6	38.31
	Component from $-CH=CH_2$	9.29	21.6	28.25

$\times 10^{-40}$ g cm^2.

The individual moments of the groups about the axis for internal rotation are readily calculated; they are as follows:

For $CH_2=CH-$, 38.47
For $CH_2=CCl-$, 161.4_1
For CH_2Cl-, 165.2_6

$\times 10^{-40}$ g cm.^{2}

IV. VARIATION OF THE MOMENTS OF INERTIA WITH STRUCTURAL PARAMETERS OTHER THAN THE ANGLE FOR INTERNAL ROTATION

From the results given in the last section it is clear that the moments of inertia are in general quite sensitive to the value of the angle θ for internal rotation; particularly the least moment, which is the one principally determining the separation of the Q branches of perpendicular-type bands. Since all examples studied here possess a plane of symmetry in the *cis*- and *trans*-configurations I is least sensitive to θ in the neighborhood of these two extremes; $((\partial I/\partial\theta)=0$ at $\theta=0$ and $(\pi/2)$, (π for allyl chloride).) If we consider determining molecular configurations from the moments of inertia found experimentally, the following question immediately presents itself: What errors in θ can arise from possible errors in the bond-lengths and angles, and from the presence of iotopic species; i.e., what deviation $\Delta\theta$ from a given θ_0 gives the same increment ΔI from $I_0(\theta_0)$ as possible increments in the various structural parameters other than θ. The derivatives of the various moments and products of inertia with respect to any given structural parameter can be obtained from Eq. (2), and the corresponding increments to the principal moments can then be calculated from the variations in the coefficients of the cubic equation (3); where this is factored by a proper choice of coordinates, simple expressions may be obtained (see Appendix I). The various derivatives for ethylene dichloride are given explicitly in Table V.

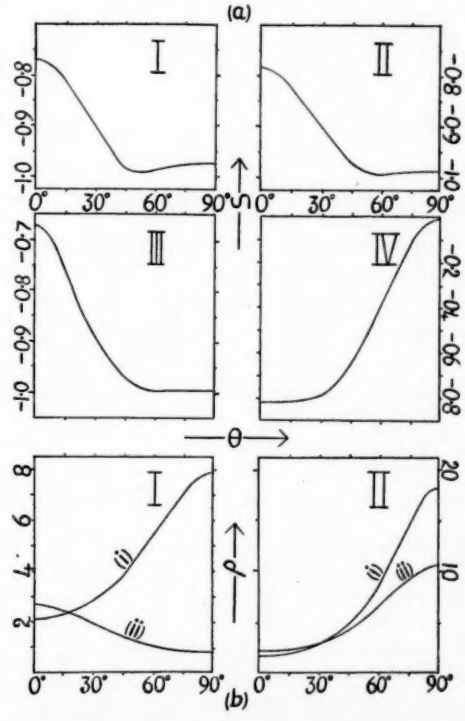

FIG. 5. (a) Plots of $S=(2b-a-c)/(a-c)$. I butadiene, II allyl chloride, III ethylene dichloride, IV chloroprene. (b) Plots of $\rho=(a-c)/b$. I (i) butadiene, (ii) chloroprene. II (i) ethylene dichloride, (ii) allyl chloride.

TABLE VI. Increments to the principal moments of inertia of butadiene, for standard variations in the structural parameters. (In g cm²×10⁻⁴⁰.)

θ		0° Abs.	0° %	30° Abs.	30° %	60° Abs.	60° %	90° Abs.	90° %
For $\Delta\alpha=+1°$	ΔI_A	−0.67	−1.53	−0.66	−1.66	−0.45	−1.60	−0.28	−1.35
($\alpha=\overline{C-C=C}$)	ΔI_B	2.84	2.21	2.50	1.02	1.81	0.59	1.47	0.43
	ΔI_C	2.17	1.26	2.15	1.24	1.93	1.07	1.75	0.95
	ΔI_A	0	0	0.14	0.35	0.59	2.12	0.85	4.08
For $\Delta r_{C-C}=+0.1$A	ΔI_B	10.06	7.83	10.06	6.81	10.06	5.40	10.06	4.90
	ΔI_C	10.06	5.84	9.92	5.71	9.46	5.26	9.20	4.99
	ΔI_A	5.08	11.61	4.18	10.53	1.88	6.71	0.61	2.89
For $\Delta r_{C=C}=+0.1$A	ΔI_B	6.72	5.23	9.22	6.24	14.21	7.63	16.71	8.13
	ΔI_C	11.81	6.85	12.67	7.29	14.87	8.26	16.10	8.73
	ΔI_A	0	0	-0.28_5	−0.72	-0.40_8	−1.45	0	0
For $\Delta\theta=+1°$	ΔI_B	0	0	1.16	0.79	1.16	0.62	0	0
	ΔI_C	0	0	0.12_4	0.07_2	0.24_7	0.14	0	0

TABLE VII. Increments to the principal moments of inertia of ethylene dichloride, for standard variations in the structural parameters. (In g cm²×10⁻⁴⁰.)

θ		0° Abs.	0° %	30° Abs.	30° %	60° Abs.	60° %	90° Abs.	90° %
	ΔI_A	−1.19	−1.11	−1.20	−1.31	−0.72	−1.40	−0.41	−1.39
For $\Delta\alpha=+1°$	ΔI_B	9.30	3.59	8.30	2.45	6.31	1.26	5.31	0.92
($\alpha=\overline{CCCl}$)	ΔI_C	8.11	2.28	7.72	1.91	6.43	1.27	5.72	1.02
	ΔI_A	0	0	0.57	0.62	1.51	2.93	1.84	6.24
For $\Delta r_{CC}=+0.1$A	ΔI_B	19.83	7.66	19.83	5.85	19.83	3.97	19.83	3.43
	ΔI_C	19.83	5.57	19.26	4.77	18.32	3.62	17.98	3.21
	ΔI_A	10.92	10.13	8.66	9.45	3.28	6.38	0.53	1.78
For $\Delta r_{CCl}=+0.1$A	ΔI_B	10.64	4.11	19.78	5.84	38.05	7.63	47.19	8.15
	ΔI_C	21.56	6.06	27.54	6.82	40.23	7.94	46.66	8.33
For $\Delta m_{Cl}=+2{:}00$	ΔI_A	1.65	1.53	1.27	1.39	0.44	0.86	0.02_5	0.08_4
A.W. units	ΔI_B	12.55	4.85	17.17	5.07	26.42	5.30	31.04	5.36
	ΔI_C	14.20	3.99	18.38	4.55	26.80	5.29	31.01	5.54
	ΔI_A	0	0	−1.09	−1.19	−1.30	−2.53	0	0
For $\Delta\theta=+1°$	ΔI_B	0	0	4.83	1.43	4.83	0.97	0	0
	ΔI_C	0	0	2.99	0.74	3.20	0.63	0	0

The absolute and percentage increments to the principal moments are given for butadiene and ethylene dichloride, for four configurations, in Tables VI and VII. The derivatives with respect to θ are readily obtained from the general equations for the various moments and products of inertia. The components for the group CH_2X-CH_2X are given below, referred to the center of gravity as origin.

$$\left.\begin{aligned}
\sum_i m_i x_i^2 &= K[(1/2)(a^2/\mu) \\
&\qquad +(2/9)\{1+2b\epsilon+3a(1+2\epsilon)\}] \\
\sum_i m_i y_i^2 &= (8/9)K[3b\epsilon \\
&\qquad +2\{1-b\epsilon-\rho(1-\epsilon)\}\cos^2\theta] \\
\sum_i m_i z_i^2 &= (8/9)K[3b\epsilon+2(1-b\epsilon)\sin^2\theta] \\
\sum_i m_i x_i z_i &= (2/9)K\sqrt{2}\{3a(1-\epsilon)+2(1-b\epsilon)\}\sin\theta
\end{aligned}\right\}. \quad (8)$$

The subsidiary quantities are as defined for Table V, with the addition $b=(r_{CH}/r_{CX})$. In both butadiene and ethylene dichloride, the least moment is in general least sensitive to uncertainties in the structural parameters at the *trans*-configurations, $(\theta=(\pi/2))$; but errors in r_{C-C} give rise to an error in I_A which increases with θ. The middle and greatest moments become less sensitive to errors in α and r_{C-C} and more sensitive to errors in $r_{C=C}$, r_{CCl} and to the mass m_{Cl}, as θ increases. Disregarding θ itself, the derivatives $(\partial I/\partial p)$ are all positive for the chosen parameters p except $(\partial I_A/\partial\alpha)$, which is negative. Errors are most likely to arise from uncertainties in α and in r_{C-C}. An increase of 2° in the angle $\overline{CCCl}$ over the tetrahedral value changes I_A by −2.8 percent at $\theta=(\pi/2)$; a similar increment, of opposite sign, would arise from an increase of 0.04A in r_{C-C}. The derivatives $(\partial I/\partial\theta)$ are all zero at $\theta=0$, $(\pi/2)$, but inspection of Table II and Fig. 2 shows that the equivalent error in θ will be certainly not greater than 5°. At intermediate configurations, $(\theta\neq 0, (\pi/2))$, the derivatives $(\partial I/\partial\theta)$ have non-zero values and the possible error in θ will be smaller. If the staggered configurations are the more stable, the values of θ of interest are 30° (C_2 isomers), and 90°

(*trans-*); if the eclipsed are favored the significant values are $\theta=0°$ (*cis-*), and 60° (C_2 isomers).

If accurate data could be obtained, the nature of the allowed isomers of the different classes of compound studied here would throw some light on the dependence of the twisting potential on the nature of the rotating groups. We have chosen examples of

(a) Two identical (asymmetrical) tetrahedral rotators ($C_2H_4Cl_2$);
(b) two identical planar rotators (butadiene);
(c) two unlike planar rotators (chloroprene);
(d) one (asymmetrical) tetrahedral and one planar rotator, (allyl chloride).

Where more than one isomer is allowed, a mode of vibration which is fairly sensitive to θ must be chosen for the analysis; thus, the C−Cl stretching modes of ethylene dichloride would be suitable. Where only one isomer is present, a CH bending mode is probably the best, e.g., non-planar CH_2 bending in chloroprene.

APPENDIX I

If Eq. (3) is written in expanded form as follows:

$$I^3 - c_1I^2 + c_2I - c_3 = 0$$

then the increment in a given root I_k produced by increments Δc_i in the coefficients c_i is given by the following formula:[17]

$$\Delta I_k=[(I_k^2\Delta c_1-I_k\Delta c_2+\Delta c_3)/\{(I_k-I_p)(I_k-I_q)\}], \quad (p, q\neq k).$$

[17] P. Torkington, J. Chem. Phys. **17**, 1026 (1949).

The increments in the c_i are readily related to increments in the moments and products of inertia. Where one of the principal moments of inertia factors off, (e.g., $I_B=B$), the following expressions are obtained for the variations:

$$\Delta I_A=[\{\Delta A(C-I_A{}^0)+\Delta C(A-I_A{}^0)-2E\Delta E\}/(I_C{}^0-I_A{}^0)]$$
$$\Delta I_B=\Delta B$$
$$\Delta I_C=[\{\Delta A(I_C{}^0-C)+\Delta C(I_C{}^0-A)+2E\Delta E\}/(I_C{}^0-I_A{}^0)],$$

where $I_{A,B,C}{}^0$ are the null values of the principal moments;

$$(I_C{}^0-A)=(C-I_A{}^0)>0, \quad \text{and} \quad (I_C{}^0-C)=(A-I_A{}^0).$$

APPENDIX II

A convenient method of determining the roots of the cubic equations for the principal moments of inertia is as follows. If I is an approximate root, as found by inspection, then the increment Δ giving the first approximation to the real root $I^0=I+\Delta$ is given by the following expression:

$$\Delta=[(c_1c_2-c_3)/(c_1-I)^2-2I]^{-1}P,$$

where

$$P=[I^3-(c_2I-c_3)/(c_1-I)],$$

c_1, c_2, and c_3 being the coefficients of the expanded form of Eq. (3), as in Appendix I. The quantity P is readily evaluated, and changes sign at $I=I^0$. Application of the method to the equation for the moments of inertia of chloroprene, for $\theta=45°$, gives the following successive approximations for the least moment: $I_A=\left.\begin{matrix}70\\80\end{matrix}\right\}$, 77, 77.27, 77.272_3 A.W.—A units. When the equations for several values of θ have been solved, the first approximation will be quite accurate, and usually only two evaluations of Δ will be necessary, for the degree of accuracy required here.

THE JOURNAL OF CHEMICAL PHYSICS VOLUME 18, NUMBER 4 APRIL, 1950

Near Infra-Red Pleochroism. I. The Perturbed O−H and the C−H Modes in Polyvinyl Alcohol

L. GLATT*, D. S. WEBBER, C. SEAMAN, AND J. W. ELLIS
Department of Physics, University of California, Los Angeles, California

(Received July 21, 1949)

Pleochroism in O−H···O−H bands and >CH_2 bands of polyvinyl alcohol is studied in the 0.6–3.7μ-region, using a quartz recording spectrograph in the 0.6–2.7μ-region and a high dispersion grating instrument with a selenium polarizer in the 2.5–3.7μ-region. Weak pleochroism in the fundamental ν(O−H) bands suggests that either some of the conclusions drawn from x-ray determinations may be in error or that there may be appreciable departure of the positions of the H atoms from the O−O lines. Dichroic bands caused by bound water are also found in this region, complicating interpretation and perhaps explaining discrepancies between this work and that of Elliott, Ambrose, and Temple. Evidence is presented for the presence of "free" carbinol O−H units in the crystalline regions of *well-dried* specimens. Pleochroic bands at 2941 cm^{-1} and 2906 cm^{-1} are tentatively assigned to >CH_2 ν_a and ν_s fundamentals, respectively.

THE pleochroism in the perturbed O−H··· O−H··· absorption bands of polyvinyl alcohol is of interest primarily for the information it yields concerning the O−H alignment in the intermolecular hydrogen bonds. The present knowledge of the crystal structure of this material is not complete. The crystal structure proposed by R. C. L. Mooney[1] has already been criticized by Bunn and Peiser,[2] and by M. L. Huggins of Eastman Kodak (private correspondence). X-ray diffraction investigations cannot locate definitely the positions of the light hydrogen nuclei. It is believed that the relative intensities of the perturbed O−H bands with the *E*-vector respectively perpendicular and parallel to the molecular chain axes, and with both singly and double oriented specimens, can give some indication concerning the orientation of the

* Some of this material was taken from a dissertation presented in partial satisfaction of the requirements for a Ph.D. degree.

[1] R. C. L. Mooney, J. Am. Chem. Soc. **63**, 2828 (1941).

[2] C. W. Bunn and H. S. Peiser, Nature **159**, 161 (1947).

O—H bonds. The pleochroism in the C—H bands gives direct evidence for the types of vibration modes responsible for these bands.

Singly and doubly oriented films of polyvinyl alcohol were examined in the 0.6–3.7μ-region. The 0.6–2.5μ-region was investigated with the same quartz-prism recording spectrograph that was used in an earlier study of polythene[3] and Nylon.[4] The C—H bands in this region will be discussed in the second paper of this series. A very high dispersion grating instrument,[5] together with a selenium polarizer,[6] was used in the 2.5–3.7μ-region.

Stretched films of polyvinyl alcohol have the chain axes of the molecules aligned in the direction of stretch. In addition to the above alignment, rolled specimens have the planes of the carbon backbones, and thus the CH_2 symmetry axes, preferentially oriented in or near the plane of the sheet. There is some evidence that the lines connecting the oxygen atoms of the O—H···O bonds between pairs of adjacent molecules are at ~60° angles to the chain axes and parallel to the carbon backbones, and thus lie also in the plane of the rolled sheet. It is likely, however, that there are departures of considerable magnitude from this orientation, resulting chiefly from a randomness of distribution of the oxygen atoms in each chain relative to the plane of the carbon zigzag. The authors are indebted to Dr. M. L. Huggins for the above information (private correspondence).

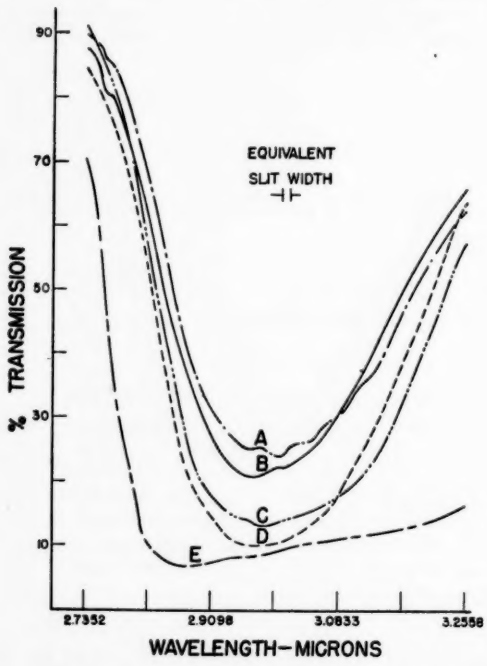

FIG. 1. The fundamental perturbed ν(O—H) bond stretching band in polyvinyl alcohol. A. Oven-dried rolled specimen, ~4μ-thick: *E*-vector ∥ roll direction, B. Same specimen as in A: *E*-vector ⊥ roll direction, C. Oven-dried stretched specimen, ~7μ-thick: *E*-vector ∥ stretch direction, D. Same specimen as in *C*: *E*-vector ⊥ stretch direction, E. Unoriented vacuum desiccator-dried specimen, ~30μ-thick; Unpolarized radiation.

1. THE FUNDAMENTAL ν(O—H) REGION

Figure 1 shows the broad perturbed ν(O—H) band in rolled and in stretched specimens that were oven-dried at 160–170°C. Rolled specimens of the required thinness were prepared by hot-rolling between strips of Nylon. In both types of specimens the absorption is somewhat stronger with the *E*-vector perpendicular to the chain axes. The reversal of the sense of the dichroic ratios on the long wave-length shoulder may possibly indicate an increased displacement perpendicular to the O—H bond directions for the more highly perturbed units.

The ratio of the absorption intensity with the *E*-vector perpendicular to that with it parallel to the chain axes is roughly *the same* in the stretched as in the rolled specimens. For both types of specimens this dichroic ratio is appreciably less than what would be expected for O—H dipoles at mean angles of ~60° to the molecular chain axes; this appears to be true even when allowance is made for the exponential rather than linear, law of absorption, for the incomplete alignment in the specimens, and for the small amount of elliptical polarization introduced by anisotropic refraction in the various crystalline zones traversed by the beam. The above discussed weakness in the pleochroism should not be interpreted, however, as a *conclusive* contradiction of the previously mentioned x-ray determinations of the orientations of the lines connecting the various H bonded oxygen atoms of adjacent molecules. An alternative inference, which appeals to the authors, is that these O···O lines may indeed be oriented as suggested by the x-ray determinations, but that the positions of the H atoms (and thus the directions of the O—H dipoles) may depart significantly from their respective O···O lines. This latter inference is supported by what was found earlier in this laboratory for single crystals of pentaerythritol; a strong perturbed 2ν(O—H) band appeared for this substance even when the polarized *E*-vector was *normal* to the plane containing all of the intermolecular H bonded O···O lines.[7] The above postulation relative to the directions of O—H dipoles must, however, be advanced with caution. In highly perturbed modes of the type under consideration there may readily be an appreciable component of dipole moment displacement normal to the initial O—H bond direction. Also, the orientations involved are not such as to provide a sensitive discrimination, particularly for a band so broad and intense as the perturbed ν(O—H) fundamental. The observed pleochroism appears to indicate, however, that the O—H bonds are inclined at mean angles of approximately 45° to the carbon-backbone planes and

[3] L. Glatt and J. W. Ellis, J. Chem. Phys. **15**, 884 (1947).
[4] L. Glatt and J. W. Ellis, J. Chem. Phys. **16**, 551 (1948).
[5] W. Lyon and E. L. Kinsey, Phys. Rev. **61**, 482 (1942).
[6] A. Elliott, E. J. Ambrose and R. Temple, J. Opt. Soc. Am. **38**, 212 (1948).
[7] J. W. Ellis and J. Bath, J. Chem. Phys. **7**, 862 (1938).

at angles of somewhat greater than 45°, say approximately 50°, to the molecular chain axes.

Elliott, Ambrose, and Temple have previously studied the pleochroism in polyvinyl alcohol. Their results for the perturbed ν(O—H) fundamental of stretched specimens, obtained with the low dispersion of a rocksalt prism instrument,[8] disagree somewhat with ours, with respect to both the position of the minimum and the sense of the dichroic ratio. We believe this discrepancy to have been caused by the presence of a small amount of bound water in their vacuum-desiccated, rather than oven-dried, specimens; the former treatment is not completely efficient. The perturbed O—H···O bond stretching modes of bound water lie at a somewhat higher frequency than do those of the carbinol units (see Fig. 1, *E*) and, judging by what we have found in the overtone bands, have their dichroic ratios in the opposite sense.

2. THE OVERTONE AND COMBINATION O—H BANDS

Figure 2 is a reproduction of spectrograms of oven-dried specimens made on the quartz-prism spectrograph; this instrument plots what is essentially transmitted energy against wave-length. The broad absorption bands originating in the carbinol O—H units are designated by primed numbers. Table I lists the positions and relative intensities of the O—H bands. Some of the intensities are given to two significant figures; these are valid only for the comparison of adjacent bands or of the same band in the two polarization directions. Accurate determinations of absorption intensities are hindered, particularly for broad and overlapping bands such as those characteristic of perturbed O—H units, by the difficulty in obtaining adequately fitting background curves.

Bands 2′ and 3′ of Fig. 2 are attributed to perturbed 2ν(O—H) of the carbinol O—H units. The doubling

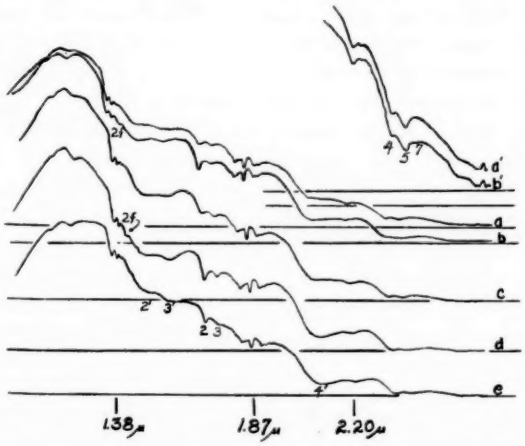

FIG. 2. Spectrograms of oven-dried polyvinyl alcohol (a) Rolled specimen: $E \parallel$ roll direction (a' wide slits). (b) Rolled specimen: $E \perp$ roll direction (b' wide slits). (c) Stretched specimen: Unpolarized radiation. (d) Stretched specimen: $E \perp$ stretch direction. (e) Stretched specimen: $E \parallel$ stretch direction.

[8] Elliott, Ambrose, and Temple, J. Chem. Phys. **16**, 875 (1948).

TABLE I. The perturbed O—H···O bands of polyvinyl alcohol.

Band numbers	Frequency (in 10^{-3}·cm^{-1})	Relative intensities stretched ⊥	stretched ∥	rolled ⊥	rolled ∥
2f	7.067	0.3	0	0.4	0
2″	6.82	—	—	—	—
2′	6.70	4.1	3.4	4.6	3.9
3′	6.33	4.3	3.5	4.4	3.6
4″	5.139	—	—	—	—
4′	4.79	10*	8^+	10*	8^-

* Intensity arbitrarily chosen as 10.
⊥ *E*-Vector perpendicular to stretch (roll) direction.
∥ *E*-Vector parallel to stretch (roll) direction.

in this region, apparently characteristic of alcohols, has been attributed to the fact that each O—H unit donates a proton to form one hydrogen bond and accepts another proton to form a second hydrogen bond—hence two types of perturbation.[7,9] Another possible explanation could be in terms of symmetric and antisymmetric vibrations of the two protons connected to each O atom. The extremely intense absorption in the fundamental perturbed ν(O—H) band made it difficult to tell whether or not there was a similar doubling there. In both of the 2ν(O—H) bands the absorption intensity is greater when the *E*-vector vibrates perpendicular than when it vibrates parallel to the molecular chain axes. The dichroic ratios are thus in the same sense as that found for the fundamental perturbed ν(O—H) mode (Fig. 1). It is probably not significant, owing to the difficulty in estimating the correct background from which to measure the absorption, that the dichroic ratios are slightly larger for the overtone bands than for the fundamental band.

Band 4′ is assigned to the perturbed $\nu+\delta$-band of the carbinol O—H units. The fact that the dichroic ratio in this band is in the same sense as that in the perturbed ν(O—H) and 2ν(O—H) modes may indicate that the bond stretching motion predominates over that of bond bending.

Figure 3 shows a reproduction of spectrograms made for a water saturated specimen. In addition to the

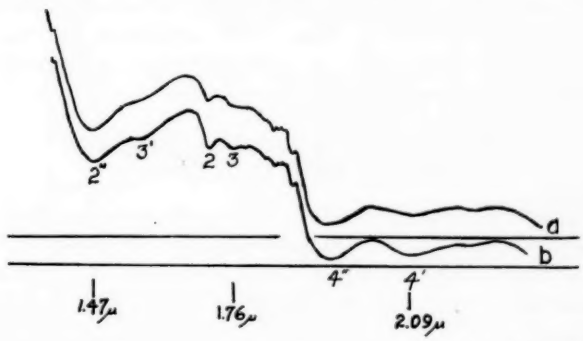

FIG. 3. Spectrograms of a water saturated specimen of stretched polyvinyl alcohol. (a) $E \parallel$ stretch direction. (b) $E \perp$ stretch direction.

[9] Cross, Burnham, and Leighton, J. Am. Opt. Soc. **59**, 1134 (1937).

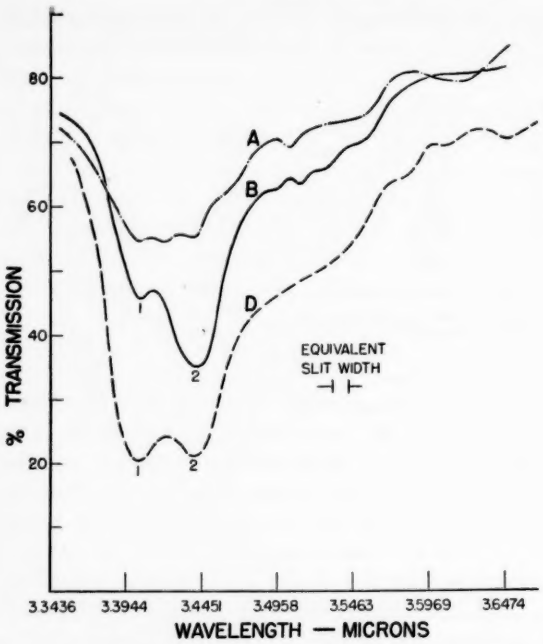

FIG. 4. The fundamental C−H bond stretching bands in polyvinyl alcohol. A. Rolled specimen, ~4μ-thick: E-vector ∥ roll direction. B. Same specimen as in A: E-vector ⊥ roll direction. D. Stretched specimen, ~7μ-thick: E-vector ⊥ stretch direction.

perturbed O−H bands discussed previously, there appear two strong new bands 2″ and 4″ at ~6820 and ~5140 cm^{-1} respectively. Band 2″ is the perturbed 2ν(O−H) band of *bound water;* it somewhat overlaps the corresponding band 2′ of the carbinol O−H units. This is comparable with what was found in the fundamental O−H region (Fig. 1, E). Band 4″ is the perturbed $\nu+\delta$-band of bound water. It is of interest that the slight dichroism observed in both band 2″ and band 4″ is in the opposite sense to that observed in the corresponding carbinol O−H bands. This may possibly indicate that the O−H bonds of the bound water molecules make average angles of less than 45° with the carbon chain axes. Bands 2″ and 4″ were still present, although greatly reduced in intensity, for specimens that were dried for several days in a vacuum desiccator containing P_2O_5. This treatment, as was mentioned previously, is evidently not completely efficient for the removal of bound water.

3. EVIDENCE FOR THE PRESENCE OF UNPERTURBED O−H UNITS

There is some evidence for the presence of a small percentage of "free" carbinol O−H units in the crystalline regions of thoroughly dried specimens. The presence of O−H units of this type, which do *not* participate in hydrogen bonds, would be incompatible with the very regular structure proposed by Mooney.[1] A very weak but sharp and highly dichroic band appears at 7067 cm^{-1} in the spectrograms of oven-dried specimens. This band, labeled 2f in Fig. 2, is at approximately the position to be expected for a 2ν-band of free O−H units. It is apparently absent for specimens which have not been subjected to a certain amount of heat treatment. The marked dichroism of this band shows that it does not arise in the amorphous regions.

A similar *unperturbed* ν(O−H) band was searched for in the fundamental region. While there appears to be considerable structure on the high frequency side of the broad perturbed ν(O−H) band, a definite conclusion as to the presence or absence of a "free" ν(O−H) band was frustrated by the extremely intense absorption in the perturbed band.

4. THE FUNDAMENTAL C−H BANDS

The fundamental C−H bond stretching bands are shown in Fig. 4. Interpretation is somewhat complicated by the presence in the specimens of the >CHOH units. There appears to be no distinct band attributable to the C−H bond of these units. It is possible that some of the shoulder structure is caused by the stretching mode in this latter type of C−H bond. If this is not the case, it may be that the bond stretching in these units couples with the $>CH_2$ ν_a and/or ν_s type vibrations. If these considerations are neglected the observed pleochroism (Fig. 4) would appear to indicate that band 1 at 2941 cm^{-1}, which is greatly weakened in the rolled specimen, is caused by the $>CH_2$ ν_a fundamental and band 2 at 2906 cm^{-1} by the $>CH_2$ ν_s fundamental. Bands occurring in the paraffinic hydrocarbons at ~2925 cm^{-1} and ~2850 cm^{-1} are usually, on the basis of theoretical considerations, assigned to $>CH_2$ ν_a and ν_s modes respectively.

A very recent brief paper by Elliott and his associates[10] discusses some work done on doubly oriented specimens of polyvinyl alcohol, using a lithium fluoride prism to given an adequate dispersion in the 3μ-region. They report *no* dichroism for the perturbed ν(O−H) fundamental and results presumably similar to ours for the C−H region; no figures are shown. Their technique of inclining the plane of their specimen to the direction of the polarized beam introduces the complication of crystal refraction at *oblique incidence* which alters the vibration direction from that of the impinging beam, and thus makes interpretation more difficult.

[10] Elliott, Ambrose, and Temple, Nature **163**, 567 (1949).

The Photovoltaic Behavior of Organic Substances in Solution*

IRVIN LEVIN AND CHARLES E. WHITE
Department of Chemistry, University of Maryland, College Park, Maryland
(Received July 21, 1949)

A number of organic compounds have been studied for a comparison of photovoltaic behavior and fluorescent properties. No definite correlation could be found between visual fluorescence and the photovoltaic response. The photopotentials were measured by using a platinum point as the irradiated electrode connected to a vacuum tube electrometer. The irradiated electrode is assumed to act as a collector in the "space charge" of the photoactive molecules. Both positive and negative photopotentials were obtained. Compounds possessing a carbonyl group adjacent to an aromatic nucleus invariably produced a positive photopotential.

INTRODUCTION

THE production of a potential difference between two inert metallic electrodes immersed in a fluorescent solution, one of the electrodes being in the excited fluorescing region and the other in the dark, has received scant attention since the photovoltaic effect was discovered over 100 years ago by Becquerel.[1] In contrast, the behavior of semiconductors has attracted many workers who have already evolved a sound theoretical explanation and have produced several important applications, such as rectifiers, photo-cells, thermistors, and transistors. A historical summary of the effect of light on "fluorescent electrolytes" is given by Hughes and DuBridge.[2] Zworykin and Wilson[3] mention "sensitive electrolytes" very briefly. An extensive review and discussion of the photovoltaic effect is given by Copeland, Black, and Garrett[4] who classify photovoltaic cells into six types, two of which include those studied here. These two types are (1) metal electrodes immersed in fluorescent solutions and (2) metal electrodes immersed in non-fluorescent organic liquids or solutions. The work on photovoltaic cells of this second type, reviewed by these authors, has been done chiefly on Grignard solutions. The present work continues the study of photovoltaic cells containing both fluorescent and non-fluorescent solutions.

Since a potential is assumed by an inert metallic electrode placed in a fluorescing volume, this irradiated volume can be considered as having a space charge. For this reason, an inert point electrode should act as a suitable collector and should provide a means of determining the potential difference between any point in the fluorescing volume and an electrode placed in the dark unexcited volume. An adequate device such as an electrometer is necessary to measure this potential difference.

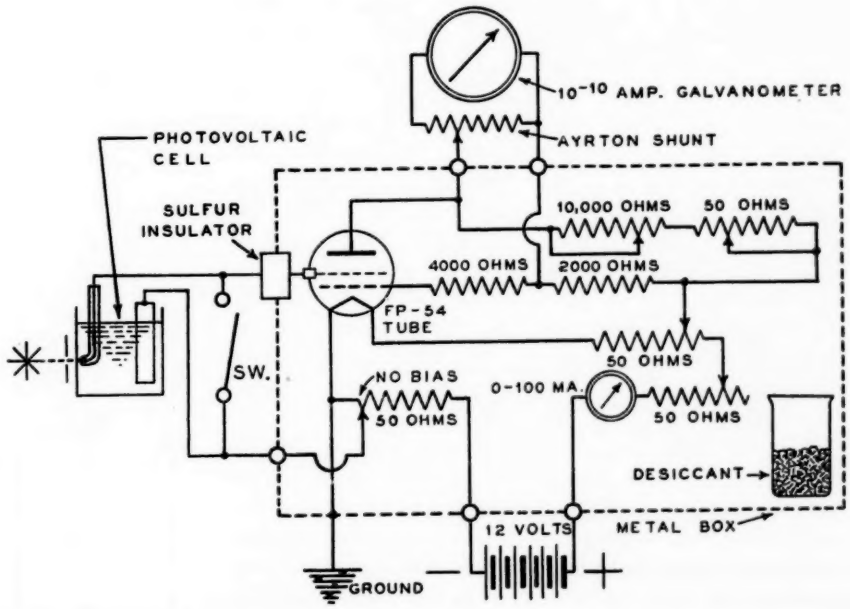

FIG. 1. The electrometer circuit with photovoltaic cell.

* From a thesis submitted in partial fulfilment of the requirements for the Doctor of Philosophy degree by Irvin Levin, University of Maryland, June, 1948. The work was supported in part by a grant from the National Dairy Products Corporation.

[1] E. Becquerel, Comptes Rendus **9**, 145, 561, 711 (1839).

[2] A. L. Hughes and L. A. DuBridge, *Photo Electric Phenomena* (McGraw-Hill Book Company, Inc., New York, 1932).

[3] V. K. Zworykin and E. D. Wilson, *Photocells and Their Application* (John Wiley and Sons, Inc., New York, 1934).

[4] Copeland, Black, and Garrett, Chem. Rev. **31**, 177 (1942).

TABLE I. Effect of light intensity on the photopotential. (0.06 molal benzoin in absolute ethyl alcohol, G.E. 100-watt clear-glass covered mercury lamp, 1.5-mm probe-point at glass cell wall, 1.5-cm diaphragm opening, no grid bias, 25°C.)

Distance D between lamp and cell wall in cm	Galvanometer units Without filter	With filter No. 5543	$1/D^2 \equiv I$ $\times 10^{-4}$	$\log_{10} 1/D^2$
47	500	—	4.53	−3.34
41	—	55	5.95	−3.23
36	750	—	7.72	−3.11
23	1340	360	18.9	−2.72
8.5	2500	1350	138.4	−1.85

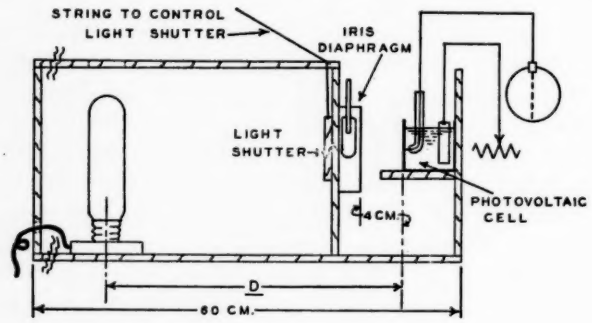

FIG. 2. The irradiation system.

EXPERIMENTAL

A. Apparatus

The Photovoltaic Cell

A platinum wire, of B. and S. No. 24 gauge (0.5 mm diameter), soldered to a copper wire lead was fused into the closed end of a 20-cm length of 6-mm soft glass tubing, leaving a small exposed length of approximately 1.5 mm (this length was found the optimum for producing the maximum photopotential as shown in Fig. 4). This "point" electrode was supported in the photovoltaic cell usually against the center of the irradiated flat side of a cubical glass cell (5×5×5 cm) or an improvised cell having a fused silica wall to yield the maximum photopotential, as shown in Figs. 1 and 2. This point-probe was connected to the grid of the electrometer tube as indicated in Fig. 1. Several advantages of the point-probe are: (1) its simplicity and ruggedness; (2) more light from the lamp can be utilized in excitation as compared with the previous semi-transparent film electrodes of platinum; (3) the diameter of the light beam has little effect on the photopotential; (4) the adaptability of the probe makes interchanging it among various cells a simple procedure; and (5) small volumes of solutions can be studied. Points of copper and nichrome were just as satisfactory as those of platinum in detecting the photopotential. One disadvantage of the point is the possibility of polarization due to current flow and the small area of the point. However, exhaustive studies to be discussed below indicated that polarization effects were not present.

A piece of clean platinum foil 2×6 cm and 0.013 cm thick partly immersed to 5 cm was used as the dark electrode. It was carefully placed at a side of the cubical cell where light could not strike it. The size or shape of this electrode is of course not critical.

The Electrometer

Figure 1 shows the complete electrical circuit of the apparatus. The electrometer circuit is an improved d.c. amplifier developed by DuBridge and Brown.[5] It was mounted in a closed metal light-tight box which also contained a 500-ml beaker half-filled with anhydrous lump calcium chloride as a desiccant. The control-grid lead emerged from the metal box through a large molded sulfur insulator. The electrometer circuit gave consistent results and proved satisfactory for this work. No actual voltage readings of the photopotentials were taken. Readings were obtained in galvanometer scale units (cm) after the galvanometer deflection became constant during irradiation of the point electrode in the solution. The calibration of the vacuum-tube electrometer with zero grid bias voltage indicated a sensitivity of 1.1×10^{-4} volt per cm or unit division. Consequently, the galvanometer scale reading in cm units may be converted to approximate millivolts by multiplying by the factor 0.11, assuming that the resistivity of the photovoltaic cell produces no appreciable self-bias on the grid. The grid bias voltage was set at zero for reasons given below. The Ayrton shunt was used for the larger values of photopotentials in order to bring the galvanometer indicator-line within the linear range of its scale.

The Irradiation System

The light source, either a mercury vapor or incandescent lamp, and the photovoltaic cell system were

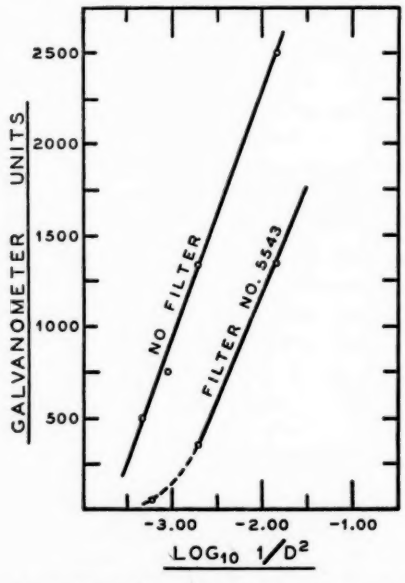

FIG. 3. Linearity of logarithm of light intensity *vs.* photopotential.

[5] L. A. DuBridge and H. Brown, Rev. Sci. Inst. 4, 532 (1933).

mounted in a wooden box as shown in Fig. 2. The mercury vapor lamp was either the "Fluorolight" low pressure fused silica or the G. E. high pressure 100-watt H-4 clear-glass covered type with auxiliary transformer. The incandescent lamp was a 150-watt clear-glass type. No effort was made for regulating the line voltage to these light sources and no lenses were used in the incident light path. An iris diaphragm controlled the cross section of the incident light beam. Filters when used were placed between the iris diaphragm and the photovoltaic cell.

B. The Effect of Varying Conditions on the Photopotential

Grid Bias Voltage

Numerous tests were made to determine whether the small current flowing through the grid circuit with photovoltaic cell could cause polarization at the point electrode. Photopotentials of several compounds were obtained with and without grid bias voltage, using a 1.5-mm probe-point as described, and the results are shown in Table V. Photopotential readings in galvanometer units were larger and more rapidly obtainable without grid bias voltage. The vacuum-tube electrometer also gave optimum results when balanced with the unirradiated photovoltaic cell in the grid circuit. This procedure allows a self-biasing voltage to form on the grid due to the high resistance of the photovoltaic cell. Galvanometer deflections caused only during irradiation were noted as photopotentials. Further measurements indicated that a current of less than 10^{-8} amp. or a current density of approximately 5×10^{-7} amp. per sq. cm. could exist at the point if the photovoltaic cell were to have a resistance of zero; since the alcoholic and other non-ionized solutions have a large resistivity, the grid current would be much less. Willard and Fenwick[6] have shown that polarized electrodes in titrations in aqueous media using a platinum point usually have a current density of approximately 10^{-4} amp. per sq. cm. It has therefore been concluded that polarization or other electrolytic effects do not enter into the production of the photopotential as determined in these studies.

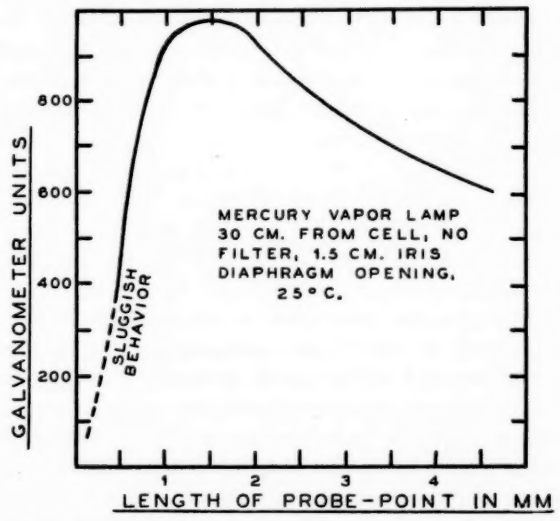

FIG. 4. Effect of size of probe-point on the photopotential using a B. and S. No. 24 gauge platinum wire and 0.06 molal benzoin in absolute ethyl alcohol.

TABLE II. Effect of incident light beam cross section on the photopotential. (0.009 molal benzoin in absolute ethyl alcohol, 1.5-mm probe-point at cell wall, G.E. mercury lamp 25 cm from glass cell wall, no grid bias, 25°C.)

Diameter of iris diaphragm opening in cm	Relative photopotential in galvanometer units
0.5	300
1	320
2	350
3	360

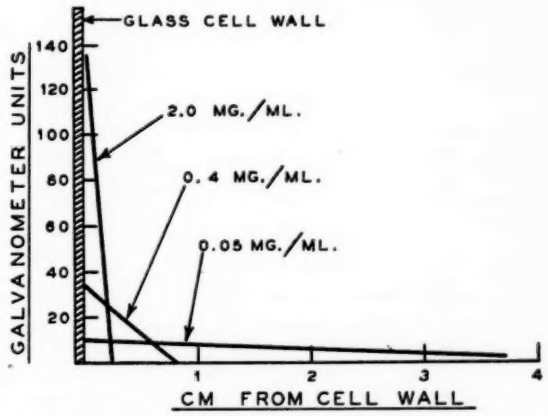

FIG. 5. Approximate effects of position of probe-point and concentration of rhodamine *B* in ethyl alcohol on the photopotential within the solution.

The procedure for balancing the vacuum-tube electrometer for determining photopotentials was as follows: With the control grid connected directly to the negative or grounded end of the filament, the filament current was set close to the rated value of 0.09 amp. at a minimum galvanometer deflection according to the method of DuBridge and Brown,[5] using the plate rheostats and the plate-voltage adjusting potentiometer. Then the darkened photovoltaic cell was placed in the grid circuit and the electrometer rebalanced using only the plate rheostats. After stability and no drifting were obtained, the cell was irradiated and the galvanometer deflection noted.

The Intensity of the Incident Light

The effect of the intensity of the light on the cell was determined by moving the mercury vapor lamp varying distances from the photovoltaic cell. For this study a 0.06 molal solution of benzoin in absolute ethyl alcohol was used. Table I indicates the effect of lamp distance

[6] H. H. Willard and F. Fenwick, J. Am. Chem. Soc. 44, 2516 (1922).

TABLE III. Effect of the solvent on the photopotential and fluorescence intensity. (1 mg sodium eosin per ml of solution, G.E. mercury lamp 25 cm from glass cell wall, 1.5-mm probe-point at cell wall, 1.5-cm iris diaphragm opening, no filter, no grid bias, 25°C.)

Solvent (parts by volume)	Photopotential in galvanometer units	Relative fluorescence intensity	Dielectric constant of solvent
Water	Nil	1	81
1 water: 1 methanol	5	—	—
Methanol	15	2.6	31
3 methanol: 1 benzene	13	—	—
1 methanol: 1 benzene	36	2.3	—
1 methanol: 3 benzene	129	2.0	—
Benzene	Eosin insol.	—	2.3

(D) on the galvanometer scale reading (V) without a filter and with a Corning glass color filter No. 5543. Since the intensity (I) of a source of radiation on a surface is proportional to the reciprocal of the square of the distance (D) of the source from that surface, a plot of $\log 1/D^2$ *vs.* galvanometer readings V yields the linear relationship indicated in Fig. 3. The equation for this relationship is:

$$V = m \cdot \log I + b \qquad (1)$$

where m is the slope of the line and b is a constant, both depending on filters used (wave-lengths of incident light), temperature, and other factors as described. This equation is analogous to the thermodynamic e.m.f. pressure (or concentration) relationship

$$E = k \cdot \log P_a/P_b \qquad (2)$$

and supports the theory that the photopotential is produced from a Maxwell-Boltzmann distribution of stable and unstable molecules.

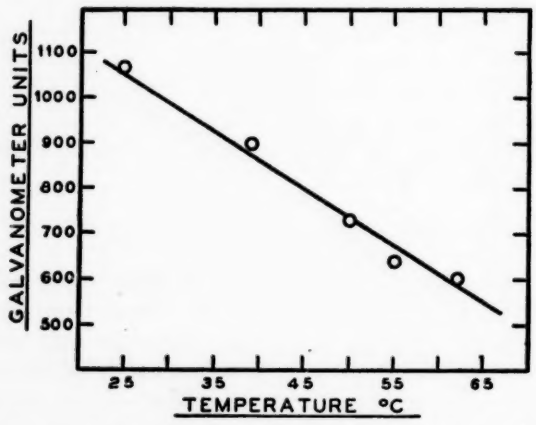

FIG. 6. Effect of temperature on the photopotential using a 0.06 molal solution of benzoin in absolute ethyl alcohol.

The potential of a space charge is dependent among other factors on the number of charged particles within that space. This would lead further to the relationship

$$V = m \cdot \log N_e/N_u \qquad (3)$$

where N_e is the number of excited photoactive molecules forming the space charge and N_u is the number of unexcited molecules or the initial concentration. This last equation is based on the assumption that the number of excited photoactive molecules (N_e) is directly proportional to the light intensity according to photoelectric principles. Equation (3) would then take the form of Eq. (1) since the initial concentration (N_u) is a constant for a given solution.

Figure 3 and Table I indicate also that for very weak intensities of light, as obtained with filter No. 5543 and the mercury vapor lamp at a distance of 41 cm from the cell, marked deviation from Eq. (1) occurs and this relationship does not apply. Copeland, Black, and Garrett[4] point out that in photovoltaic cells, "the photovoltaic potential is directly proportional to light intensity at low intensities and then to the logarithm of the intensity and finally reaches a steady maximum on increasing the light intensity." The effect of low intensities has not been quantitatively studied here; high light intensities caused a rapid decrease in the photopotential most likely due to secondary chemical effects of the light on the photoactive solute in solution. The studies recorded here therefore were confined to medium light intensities.

The Wave-Length of the Incident Light

For the production of the photopotential, light energy must of course be absorbed by the solution. Table V lists compounds which were studied with light of wave-lengths longer than 3000A, glass cells being used which absorbed the shorter wave-lengths. However, the photoinactive compounds of Table V, benzhydrol, hydroquinone, and triphenylmethane, did produce a photopotential when studied with a commercial (Fluorolight) fused silica low pressure mercury vapor lamp rich in the 2536A line and a fused silica cell. The light-absorption property of these compounds is fairly marked for wave-lengths around 2500A.[7] Pure absolute ethyl alcohol absorbs light to a small degree in the ultraviolet beginning at 2500A,[7] and produced a slight photopotential with the 2536A mercury line; with longer wave-lengths, no photopotential was obtained.

The light absorption characteristic of benzoin becomes noticeable at 3500A and increases toward the shorter wave-lengths.[7] A 0.06 molal alcoholic benzoin solution did not yield any photopotential with wave-lengths longer than 4400A as determined with Corning glass color filters. With the General Electric 100-watt high pressure mercury vapor lamp 8.5 cm from the glass cell, 2500 galvanometer units were obtained as shown in

[7] *International Critical Tables* (McGraw-Hill Book Company, Inc., New York, 1929), Vol. V, pp. 326–379.

Table I. With the commercial low pressure lamp rich in the 2536A line approximately 8 cm from the same solution in a fused silica cell, 1900 galvanometer units were obtained. Therefore, wave-lengths from 4360 to 2536A can produce a photopotential with 0.06 molal benzoin in absolute ethyl alcohol. Intensity measurements and further spectrometric studies have not yet been made, and a photopotential *vs.* wave-length characteristic for benzoin and other substances in solution will be given in a later paper. It appears at present that most substances, either pure or in solution, can probably yield a photopotential with the proper light if their liquid resistivities are not too high for the electrode system. Whether the photopotential spectrum will be shifted with respect to the light absorption spectrum as in fluorescence is yet to be determined.

The Cross Section of the Incident Light Beam

The light beam striking the photovoltaic cell was controlled in circular cross section by the iris diaphragm depicted in Fig. 2. The increase in cross section had a small but definite effect of increasing the photopotential as shown in Table II. This small increase in photopotential is probably due to an increase in light scattering as the light beam increases in diameter.

The Size of the Probe-Point

The effect of the size of the probe-point on the photopotential was studied by starting with a 4.5-mm exposed length of the B. and S. No. 24 gauge platinum wire. The exposed wire was cut shorter after determining the photopotential for each length. Figure 4 shows the effect of the size of the point on the photopotential and that a length of about 1.5 mm produces the maximum photopotential. A large "point" in a charged space or volume which possesses a marked charge gradient cannot yield the maximum potential at a given position. A very small point builds up its charge very slowly and cannot be influenced by all the excited molecules around it, as indicated by the 0.5-mm exposed length. The 1.5-mm probe-point has therefore been used throughout these studies.

The Effect of Concentration and the Position of the Probe-Point in the Solution

These effects are perhaps the most striking in illustrating the electrostatic nature of the photoactive solution. The use of a substance which is photoactive and also fluorescent provides a means of observing the position of the light path by the fluorescence and an opportunity to correlate this with the position of the probe-point. If the concentration of a given photoactive fluorescent substance in solution could be made sufficiently high, the solution displayed only a "surface fluorescence"[8] due to the light being absorbed only in a thin layer of solution at the interface between the glass cell wall and solution. At this interface, the fluorescence could only be seen with the eye in a direction parallel with the incident light. When the probe-point was

[8] E. Hirschlaff, *Fluorescence and Phosphorescence* (Chemical Publishing Company, Inc., Brooklyn, 1939).

TABLE IV. Effect of concentration of various substances in absolute ethyl alcohol on the photopotential. (Excitation with wave-lengths longer than 3000A using a G.E. 100-watt clear-glass covered mercury lamp.)

Concentration in mg per ml	Average photopotential in galvanometer units
Benzoin	
16 (sat.)[a]	1300
10	1070
8	950
4	700
2	460
1	330
0.50	220
0.25	85
0.10	60
Benzil	
10[b]	710
5	520
2.5	240
1.25	160
Rhodamine *B*	
14[c]	100
10	100
7	100
3.5	147
1.75[d]	142
0.88	80
0.44	25
0.22	6

[a] The probe-point 1 mm away from the cell wall yielded 900 units with this solution; 3 mm away, 150 units sluggishly. This indicates a volume type of fluorescence which in this case was faint to the eye.
[b] The probe-point 1 mm away from the cell wall yielded 400 units with this solution; 2 mm away, 120 units. This indicates a volume type of fluorescence which in this case was faint to the eye.
[c] The probe-point 1 mm away from the cell wall yielded no photopotential with this solution. This indicates surface fluorescence.
[d] Slight volume fluorescence appeared to the eye. Note Figs. 5 and 7.

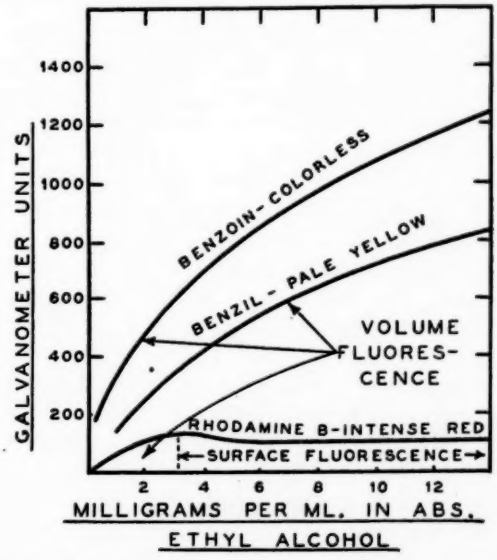

FIG. 7. Comparison of the photopotential *vs.* concentration characteristics of benzoin, benzil, and rhodamine *B* plotted from Table V.

placed so as to touch the glass wall as in Fig. 1, a definite and often very large photopotential was obtained; but when the point was placed about 1 mm away from the glass wall, no photopotential was obtained. Also with the probe-point at the fluorescing plane, the photopotential was found to be independent of the concentration of the substance as long as only surface fluorescence was displayed and the light could not penetrate into the solution. Obviously, therefore, the photopotential is coexistent with light absorption and electronic excitation.

On the gradual dilution of the above concentrated fluorescent solution, the fluorescence and therefore the light absorption spread out from the solution-glass interface plane into the volume of the solution. During the first processes of dilution, the fluorescence gradient appeared marked but continued dilution caused the fluorescence to become not only more uniform throughout the volume of the cell, but also weaker. This type of fluorescence is called "volume fluorescence"[8] and is easily discernible by the eye. The position of the probe-point in the fluorescing volume influenced the photopotential. This is illustrated in Fig. 5 for various concentrations of rhodamine *B* in absolute ethyl alcohol. Rhodamine *B*, which forms an intense red solution, apparently increases its photopotential to a small degree when passing from surface to volume fluorescence, as indicated in Fig. 7. Similar effects have also been obtained with other photoactive and highly colored solutions, to be described in a later paper.

Table IV and Fig. 7 indicate the effect of concentration of benzoin, benzil and rhodamine *B* in absolute ethyl alcohol using mercury lines with wave-lengths longer than 3000A for excitation.

The Effect of Stirring

Stirring the photoactive solution diminished the photopotential. A similar result has been reported by other workers.[2,4] Throughout these studies, therefore, the solution was not stirred during photopotential measurements.

The Effect of Temperature

Using a 100-ml Pyrex beaker instead of the cubical glass cell, the effect of temperature variation on the photopotential was noted with a slowly cooling 0.06 molal benzoin solution in absolute ethyl alcohol. In these experiments the mercury lamp was 25 cm from the cell, a 1.5-mm probe-point was used at the cell wall and the iris diaphragm opening was set at 1.5 cm. Figure 6 shows that the higher the temperature, the smaller the photopotential. This same result is well known in visual fluorescence measurements and fluorescence polarization.

The Nature of the Solvent

The physical properties of the solvent are undoubtedly a very important factor in determining the magnitude of the photopotential. As a very rough indication water-methanol and methanol-benzene mixtures were studied using sodium eosin at a fixed concentration of 1 mg per ml of solution for each test. Table III summarizes the results of the studies showing the effect of the solvent on the photopotential and also on the fluorescence as measured by the Lumetron fluorescence meter. Although the intensity of fluorescence decreased slightly from methanol to the 1 methanol: 3 benzene mixture, the photopotential increased to a much greater extent indicating that the photopotential is not directly related to fluorescence and that each is a separate and distinct effect of light excitation.

Sodium fluorescein at a concentration of 1 mg per ml yielded a slight or practically no photopotential in various solvents. After the addition of a few drops of aqueous sulfuric acid to form the fluorescein acid molecule from the sodium fluorescein in methanol large photopotentials resulted. The fluorescein acid molecule being weakly ionized produced the large photopotenial while the fluorescein ion yielded practically no photopotential. This may be explained as follows:

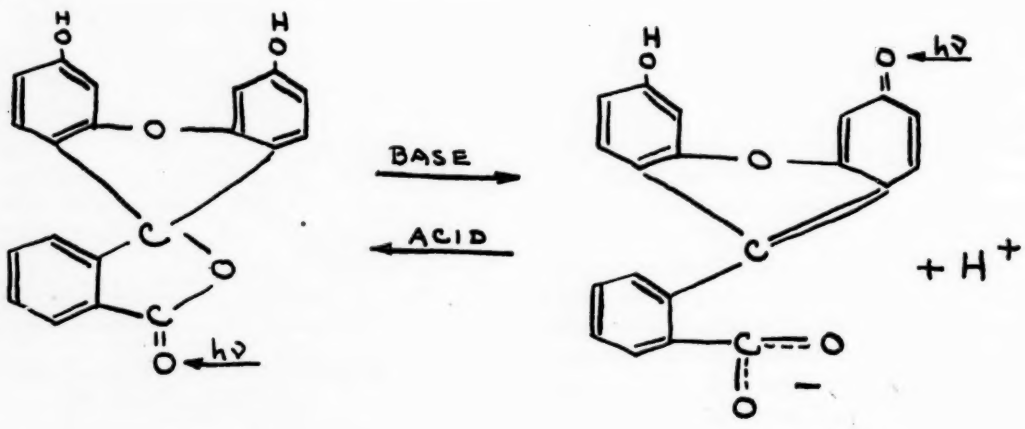

Photoactive Form 1 — Photoinactive Form 2

Since the basic ionic Form 2 produced a poor photopotential, the carbonyl group of the five-membered ring of unionized Form 1 seems to be an active electron-sink for producing the large positive photopotential of the acid Form 1. The carbonyl group of the quinoid structure of Form 2 was probably responsible for producing any photopotential in basic solution. This difference in photopotential behavior between the two forms may probably be due to a difference in light absorption, or to the over-all charge of the ion preventing the detection of the photopotential.

The presence of ions generally lowered the photopotential. For example, the addition of alcoholic solutions of potassium chloride, aluminum chloride, ammonium iodide, zinc chloride, lithium chloride, sodium hydroxide, and potassium acetate to alcoholic solutions of 0.06 molal benzoin decreased the photopotentials. The last two inorganic substances produced a peculiar effect, probably because of their alkaline nature; this effect, designated here as the "transient photo-inductive effect," is discussed further below.

Studies on the photoactivity of miscible liquids, one photoactive and the other -inactive, such as benzaldehyde and ethyl alcohol, respectively, yielded promising results. When the mole fraction was greater than 0.5 with respect to the alcohol, the photopotential was positive as in the usual case; but when the mole fraction was greater in benzaldehyde, the photopotential was negative. This special case of a stable negative photopotential is being investigated further.

As mentioned, it appears from preliminary work so far done that a solvent should have a relatively low electrical resistivity and should tend to associate with the solute in order for it to produce a photopotential.

C. The Photovoltaic Behavior of Organic Substances in Solution

The photovoltaic cell in these studies contained the solution at 25°C and the irradiated probe-point of 1.5 mm at the glass cell wall. The iris diaphragm was set at 1.5 cm. The mercury lamp light source, a G.E. 100-watt H-4 clear-glass covered type, was usually set at 25 cm from the glass cell and was used without filters. With this arrangement, only wave-lengths longer than 3000A were available for excitation. No grid bias voltage was applied unless otherwise stated. No photopotential was obtainable with the absolute ethyl alcohol which was used as the solvent throughout the following studies.

The Behavior of Rhodamine B

This was the first solution to be studied because of its apparently great popularity among workers studying the photovoltaic effect with fluorescent solutions. Since the rhodamine *B* contained much foreign salt as inert and insoluble material, the concentration of the rhodamine in ethanol was determined by evaporating to dryness a known volume of the supernatant liquid and weighing the residue. Table IV and Fig. 7 indicate the variation of the photopotential in galvanometer units with concentration of rhodamine *B*. The maximum "hump" in the curve is probably due to a light absorption-concentration effect.

When the probe-point was placed about 1 mm away from the glass surface, no photopotential was obtainable as indicated in Fig. 5 and Table IV. When the concentration was low, a volume fluorescence was produced and the probe yielded a photopotential throughout the solution of a magnitude depending on the distance from the cell wall. Stirring the fluorescing solution in the photovoltaic cell decreased the photopotential.

Another observation made here and throughout these studies was that the erratic drift of the galvanometer became less as the concentration and photopotential increased. This stabilization may result from the increase in the number of charged molecules around the point.

The Behavior of Benzoin and Benzil

During a photopotential study of the method of detecting boron by means of a fluorescent benzoin complex[9] it was found that benzoin in absolute ethanol yielded very large photopotentials when compared with other substances at similar concentrations. Table IV and Fig. 7 indicate the potentials developed at various concentrations of benzoin.

Benzil dissolved in absolute ethyl alcohol has a pale-yellow color. Table IV and Fig. 7 indicate the photopotential characteristic with the variation in concentration.

The Transient Photoinductive Effect

When sodium fluorescein, benzoin, or benzil in ethyl alcohol were rendered alkaline with sodium hydroxide, a peculiar photoeffect was obtained. On being irradiated, the photopotential first went to a negative and then assumed a positive value. On removing the light quickly, the photopotential increased positively and then reverted to zero. As a typical example, 100 ml of a 0.06 molal benzoin solution in ethyl alcohol yielded a photopotential of 1070 galvanometer units (Fig. 7). The addition of two drops of a 20 percent aqueous sodium hydroxide solution did not seem to affect the volume fluorescence according to the eye. However, immediately on irradiating, a maximum negative photopotential of about 30 units resulted and then the photopotential became positive to about 25 units, which is much lower than the former 1070 units. In another experiment 10 ml of a saturated alcoholic solution of potassium acetate were added to 100 ml of a 0.06 molal alcoholic benzoin solution in the photovoltaic cell; a definite transient effect was again obtained. In order to test the effect of electrolytes on this phenomenon, alcoholic solutions of

[9] White, Weissler, and Busker, Analytical Chem. **19**, 802 (1947).

TABLE V. Effect of various molecular structures on the photopotential. (Excitation with wave-lengths longer than 3000A using a G.E. 100-watt clear-glass covered mercury lamp.)

Substance	Molecular structure	Concentration, molality	Relative photopotential in galv. units		Approximate degree and type of fluorescence (visual with u.v. filter)
			0 grid bias	−3 volt bias	
Benzoin	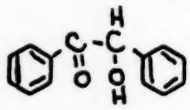	0.060	1070	500	Faint blue volume
Benzil	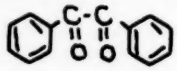	0.061	710	360	Faint blue volume
Benzophenone	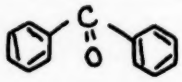	0.070	700	330	Faint blue volume
Benzaldehyde	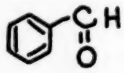	0.12	450	200	Questionable blue volume
Benzhydrol	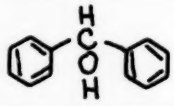	0.070	None	None	Faint blue volume
Benzonitrile	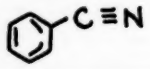	0.1	None	None	None
Anthraquinone	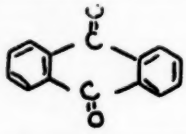	0.003	350	160	Blue volume
Acetophenone	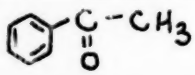	0.10	200	100	Faint blue volume
Acetone	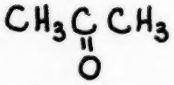	0.10	None		None
Hydroquinone		0.12	None	None	None
Quinone	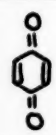	0.12	Tran. then 60	Tran. then 30	Faint blue volume
Triphenyl methane	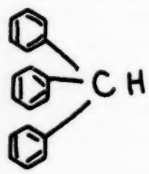	0.052	None	None	Blue volume

TABLE V.—*Continued.*

Substance	Molecular structure	Concentration, molality	Relative photopotential in galv. units: 0 grid bias	Relative photopotential in galv. units: −3 volt bias	Approximate degree and type of fluorescence (visual with u.v. filter)
n-Hexyl phenyl Carbinol	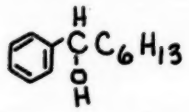	0.066	10		Blue volume
1-amino-4-hydroxy Anthraquinone	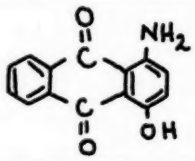	0.053	2		Faint red surface
Sodium eosin	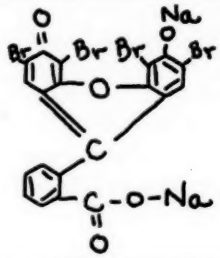	0.002	45		Yellow volume
Fluorescein acid	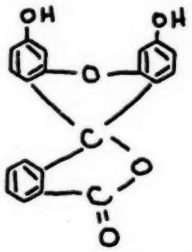	0.020	115		Greenish-blue volume
Sodium fluorescein	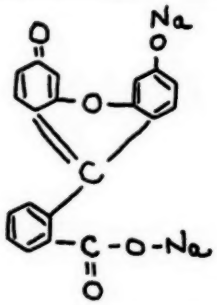	0.017	9		Intense yellow-orange volume
Rhodamine *B*		1 percent	100		Intense red surface

potassium chloride, aluminum chloride, ammonium iodide, zinc chloride, and lithium chloride were added to the benzoin solution. The solutions of these inorganic ions are not photoactive; they do, however, lower the photopotential of benzoin but do not produce the transient effect noted with alkaline solutions. Thus, the transient photo-inductive effect can be attributed to the effect of basic substances, such as the photoinactive hydroxyl and acetate radicals, on photopositive compounds. The transient effect may probably be a competitive one between two separate photoeffects.

The Effect of the Molecular Structure on the Photopotential

It may be noted from the molecular structures of the compounds studied in this research that a ring and carbonyl or other unsaturated group are present in the

compounds which produce definite positive photopotentials with wave-lengths of light longer than 3000A. Preliminary comparative studies were made on organic compounds with and without unsaturated groups. Table V briefly summarizes the experimental work.

DISCUSSION

It is known that when light of a suitable wave-length excites an atom or molecule, distinct effects may occur, some of which may be fluorescence, photochemical activation, the Raman effect, and a photoelectric or electronic excitation effect. These studies seem to indicate that for the production of the photopotential, the probe-point is detecting an activation of a purely electronic type and not a photochemical activation, since the photopotentials are stable and reproducible and return to zero when the light is removed. The charge on the probe-point is probably caused by two separate and distinct processes, one of which is the photoelectronic excitation process of the molecules around the probe-point and the other the effect of the resulting electronically excited molecules on the probe-point. The electrode-solution interface does not seem to be the seat of photoactivity; as mentioned, probe-points made of different metals yielded similar results.

The production of the photopotential may also be considered as a *change* in the oxidation-reduction potential of the solution due to light absorption and electronic excitation. Practically all of the photoactive organic compounds studied here produced positive photopotentials, indicating that they may tend to undergo photo-oxidation. An unsaturated group such as a benzoyl in the photoactive molecule may probably act as an electron sink or oxidizing group to which electrons can concentrate. These electrons, perhaps as photoelectrons, may probably shift either (1) within the photoactive molecule itself to form a more positive molecule or (2) from the solvent to the photoactive molecule to form a more positive volume in the irradiated solution in which the probe-point is immersed. In order for the second effect to occur, association between a photoactive solute and a polar solvent would be necessary to facilitate electronic shifting between them. The degree of association between a solute and different solvents having approximately the same resistivities is probably the main factor in determining the magnitude of the photopotential.

Mean Lifetime of the Fluorescence of Acetone and Biacetyl Vapors*

W. E. KASKAN** AND A. B. F. DUNCAN
Department of Chemistry, University of Rochester, Rochester, New York
(Received August 15, 1949)

The effects of pressure, temperature, and exciting intensity on the lifetime of fluorescence of acetone and biacetyl vapor have been investigated. The pressure dependence of the lifetime in acetone was interpreted in terms of the formation of double molecules, and part of the temperature dependence was interpreted in terms of the formation of double molecules. The lifetime in biacetyl was found to be independent of pressure at a constant temperature, but dependent on temperature. The effect of oxygen on the lifetime in biacetyl was explained by assuming a simple Stern-Volmer mechanism for quenching. The lifetimes of fluorescence in both acetone and biacetyl were found to be dependent on the incident intensity. This effect was explained by assuming that the fluorescing molecules of both compounds were quenched by the products of photochemical decomposition.

IN the theoretical treatment of the rate constants of photochemical reactions the lifetimes of the activated species are of considerable importance. Direct measurements of these quantities are therefore of considerable value. In most cases the lifetime, τ, has been determined indirectly through a study of the quenching of fluorescence under steady state conditions.[1] This type of data leads to a ratio of the constant for quenching to that for spontaneous emission, and in order to determine the lifetime (which is the reciprocal of the rate constant for emission) some assumptions have to be made regarding the numerical value for the quenching rate constant.

To avoid confusion later, the meaning of the terms fluorescence and phosphorescence will be discussed here, since there has been disagreement in past and current literature as to the use of these terms. It has been suggested by Lewis and Kasha[2] that a distinction be made between fluorescence and phosphorescence on the basis of the lifetime of emission, short-lived emissions (around 10^{-6} sec.) being called fluorescence, and longer lived emissions, phosphorescence. On the other hand, the term phosphorescence has been applied extensively to the emission of light by minerals and inorganic phosphors, where the phenomenon appears to be connected with lattice imperfections and not with a definite chemical species; while emissions traceable to transitions between energy levels of a definite chemical species have often been termed fluorescence. It would appear that the latter usage is preferable; hence the term fluorescence will be used exclusively in this paper to describe the afterglow of the organic compounds discussed.

The lifetime of a species in an excited state is connected by the usual theory with the Einstein coefficient of spontaneous emission and hence with the absorption coefficient for the transition to that state.[3] In the case of a molecule in an excited electronic state, the absorption coefficient which is usually used is obtained by summing over the vibration-rotation levels belonging to that state. The lifetime in this case corresponds to an average coefficient for spontaneous emission for the transition from any one of the levels in the upper state to the lower levels. The effects of pressure and temperature have often been neglected in computation of the lifetime.

On the other hand it has been recognized that the lifetime is limited by factors other than the coefficient for spontaneous emission. The Stern-Volmer mechanism for the quenching of fluorescence predicts a linear dependence of the reciprocal of lifetime on pressure. It is also to be expected that τ will depend on temperature in the case where the transition is forbidden by the electronic selection rules but allowed by vibrational perturbation.[4] It is therefore of interest to measure the dependence of lifetime on pressure and temperature.

We have chosen the two compounds acetone and biacetyl for a more detailed study of the effects on lifetime of pressure, temperature, and exciting intensity. Acetone has a region of absorption extending from 2400 to 3200A.[5] This absorption region in aldehydes and ketones has been interpreted as a transition forbidden by the electronic selection rules but allowed by vibrational perturbations.[6] Excitation in this region produces a blue[7] fluorescence consisting of a broad band from 4000 to 5000A.[8] Biacetyl has an absorption region

* This work was supported in part under Contract N6onr-241, Task I, with the Office of Naval Research, United States Navy.
** Eastman Kodak Fellow, 1948–49. Part of a dissertation presented to the Faculty of the Graduate School of the University of Rochester in partial fulfillment of the requirements for the degree of Doctor of Philosophy.
[1] W. A. Noyes, Jr. and P. A. Leighton, *The Photochemistry of Gases* (Reinhold Publishing Corporation, New York, 1941) p. 189 ff.
[2] G. N. Lewis and M. Kasha, J. Am. Chem. Soc. **66**, 2100 (1944); **67**, 994 (1945).
[3] R. S. Mulliken, J. Chem. Phys. **7**, 14 (1939).
[4] R. S. Mulliken and C. A. Rieke, Reports on Progress in Physics **VIII**, 231 (1941).
[5] F. O. Rice, Proc. Roy. Soc. (London) **A91**, 76 (1914).
[6] H. L. McMurry, J. Chem. Phys. **9**, 231 (1941).
[7] The green fluorescence of acetone vapor has been ascribed to the presence of small amounts of photochemically formed biacetyl; the blue has been ascribed to acetone itself (see reference 8). In this paper, the fluorescence of acetone is identified with the blue fluorescence.
[8] G. H. Damon and F. Daniels, J. Am. Chem. Soc. **56**, 2370 (1933).

TABLE I.

	k_1 in sec.$^{-1}$	k_2 in sec.$^{-1}$ mm^{-1}	k_3 in mm^{-1}
25°	4.1×10^3	0.1×10^3	0.018
50°	5.25×10^3	0.11×10^3	0.011

extending from 3500 to 4500A,[9] which has been interpreted as a transition allowed by the electronic selection rules but nevertheless gaining most of its intensity from electronic vibrational interactions.[10] Excitation in this region produces a series of fluorescence bands extending from 4600 to 6000A.

No direct measurements of the lifetime of fluorescence of acetone have been reported, but Hunt and Noyes[11] from a study of the quenching of fluorescence as a function of the pressure of acetone have indicated that there may be two fluorescing levels, with lifetimes of about 10^{-5} sec. and 10^{-7} sec. For biacetyl, Almy and Anderson have measured the lifetime using both a diffusion method and a phosphoroscope employing a rotating disk and found it to be 2.0×10^{-3} sec. from the first method and 1.65×10^{-3} sec. from the second.[12] In the first method, the pressures used were from 0.01 to 0.13 mm and in the second, the pressures were not reported. Rawcliffe[13] found τ for biacetyl to be 1.40×10^{-3} sec. in an unreported pressure range, and independent of pressure.

In this paper are reported the results of direct experimental measurements of the lifetime of excited acetone and biacetyl molecules as a function of pressure, temperature, and exciting intensity.

Experimental Details

The apparatus used in this work has been described previously.[14] The previously reported error of 15 percent in the lifetime has been reduced to 3 percent by more refined measurements of the photographs of the decay curves using a precision comparator.

The acetone used contained a minimum of 99.5 percent acetone; presumably water was the principal impurity. The acetone was dried and outgassed in a vacuum line and stored in a light tight reservoir from which it could be admitted to a conventional T-shaped fluorescence cell. Fresh samples were used for each determination of lifetime. The biacetyl (Eastman Kodak Company) was dried and fractionated three times in a glass bead filled column; each time the middle third was collected for the next operation. The final product was outgassed and stored in a light tight reservoir, and handled in the same manner as acetone.

The procedure used in photographing a decay curve was as follows. With a sample of gas at the desired pressure and temperature in the fluorescence cell, the oscillograph gain, time base frequency, and timing mark frequency were all adjusted so as to give a satisfactory trace. Then this sample of gas was permanently discarded and a fresh sample admitted. The trace of the decay of fluorescence was photographed with the first pulse of light to pass through the sample. Duplicate measurements were made with each sample, and then this sample was permanently discarded. A fixed intensity, reproducible to about 10 percent was obtained by allowing the condenser to charge to the same voltage each time.

In experiments with acetone the light was filtered by a 5-cm layer of solution 0.178 M in $NiCl_2$ and 0.0005 M in K_2CrO_4, supplemented by a 5-mm thickness of Corning filter No. 9863. In the case of biacetyl, 4 mm of Corning No. 5113 and 3 mm of Corning No. 3389 were used.

Pressure and Temperature Dependence of Lifetime

The lifetime of fluorecence of acetone vapor at 25°C and at 50°C and a low exciting intensity was found to be a function of the pressure of acetone vapor, as shown in Fig. 1. The data at both temperatures can be fitted by an equation of the type

$$1/\tau=(k_1+k_2P)/(1+k_3P). \quad (1)$$

The numerical values for the constants at the two temperatures are given in Table I. The decay of fluorescence was exponential within experimental error at all pressures.

Since the relationship between $1/\tau$ and P is not linear the quenching of the fluorescence of acetone vapor does not follow a simple Stern-Volmer mechanism. However, a pressure dependence of the proper form is predicted by the following sequence of steps:

$$\begin{array}{lll} \text{(a)} & A'\rightarrow A+h\nu & k_1 \\ \text{(b)} & A'+A\rightarrow 2A & k_2 \\ \text{(c)} & A'+A\rightleftarrows A_2' & K \end{array} \quad (2)$$

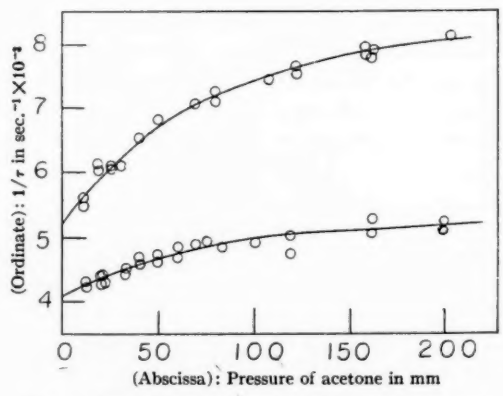

FIG. 1. Pressure dependence of lifetime in acetone. Upper curve, 50°C. Lower curve 25°C.

[9] L. Light, Zeits. f. physik. Chemie **122**, 447 (1926).
[10] H. L. McMurry, J. Chem. Phys. **9**, 241 (1941).
[11] R. E. Hunt and W. A. Noyes, Jr., J. Am. Chem. Soc. **70**, 467 (1948).
[12] G. M. Almy and S. Anderson, J. Chem. Phys. **8**, 805 (1940).
[13] R. D. Rawcliffe, Rev. Sci. Inst. **13**, 413 (1942).
[14] W. E. Kaskan and A. B. F. Duncan, J. Chem. Phys. **16**, 223 (1948).

(d) $A_2' \rightarrow 2A + h\nu \quad k_3$.

In this sequence step (a) is spontaneous emission from the electronic excited state A' to the normal state, with a coefficient k_1; step (b) is deactivation by normal molecules, step (c) is an equilibrium between a molecule in state A', and A, a molecule in the ground electronic state, and A_2', a double molecule held together by van der Waals' forces; step (d) represents fluorescence of the double molecule with a spontaneous emission coefficient k_3. It is assumed that the equilibrium in step (c) is very mobile, so much so that the expression for K

$$K=(A_2')/(A')(A) \tag{3}$$

is effectively satisfied at all times during the decay.

To derive the expression for $1/\tau$ as a function of pressure and of the parameters appearing in (2) the procedure is to set up the differential equation for the disappearance of excited acetone molecules and to solve this equation with the proper boundary conditions. Since excited molecules are present as the two species A' and A_2', which may have different coefficients for spontaneous emission (k_1 and k_3 respectively), we define A_T' as the total concentration of excited molecules:

$$A_T'=A'+A_2' \tag{4}$$

and from Eq. (3)

$$A_T'=(1+KA)A'. \tag{5}$$

The differential equation for the disappearance of A_T' is then

$$-dA_T'/dt=k_1A'+k_2AA'+k_3A_2'; \tag{6}$$

which becomes from Eqs. (3) and (5)

$$-(1+KA)dA'/dt=(k_1+k_2A+k_3KA)A'. \tag{7}$$

Experimentally, the intensity of fluorescence was found to be a maximum at the time of irradiation. Thus we can take as our boundary condition the fact that at $t=0$ (the time of irradiation), $A'=A_0'$. The solution of Eq. (7) making the assumption that A is constant is thus

$$A'=A_0' \exp[(-(k_1+k_2A+k_3KA)/(1+KA))t] \tag{8}$$

and thus

$$1/\tau=(k_1+k_2A+k_3KA)/(1+KA). \tag{9}$$

Equation (9) is of the same form as Eq. (1), which was found to fit the experimental data.

$1/\tau$ will depend on temperature insofar as the constants k_1, k_2, k_3, and K depend on temperature. The temperature dependence of K will be discussed first. The value of K at 25°C from Table I, along with other data to be described, will be used to compute a value for K at 50°C which may be compared with the value of K at 50°C given in Table I.

Assumption of the equilibrium, step (c), in Eq. (2) is similar to an idea used by Fowler and Guggenheim[15] and by Hirschfelder, McClure, and Weeks,[16] in which imperfections in real gases are treated as association problems; that is, an equilibrium is postulated of the type

$$M+M \rightleftarrows M_2 \tag{10}$$

where M is a molecule of a gas in its ground electronic state and M_2 is a double molecule, held together by van der Waals' forces. We adopt the same simplified model which considers the molecules as single particles, neglects all degrees of freedom except the one which describes motion of one particle with respect to the other, and approximates the attractive potential with a box type potential well. In terms of this model, the equilibrium constant K may be written as

$$K=bc \exp(-\Delta E/RT), \tag{11}$$

where

$$b=2\pi N r_a^3/3 \tag{12}$$

$$c=r_a^3-r_0^3/r_a^3. \tag{13}$$

In these formulas, r_a is the effective radius of interaction, r_0 the distance of closest approach at which the potential function rises to infinity, N is Avogadro's number, and ΔE is the depth of the well. The zero of energy is taken as the energy at infinite separation; thus ΔE is a negative quantity.

Numerical values of b, c, and ΔE for several compounds, are listed.[16] Acetone is not listed, but for propane, which is somewhat similar, b is 341 cc/mole, c is 0.681, and ΔE is -694 cal./mole. If we assume that the product bc for propane is equal to that for acetone, Eq. (11) can be used to predict the equilibrium constant at 50° using the value of K obtained at 25°. At 25°, K_{298} (converted to the units appropriate to Eq. (11)) is 332 liter/mole and ΔE becomes -4330 cal./mole.

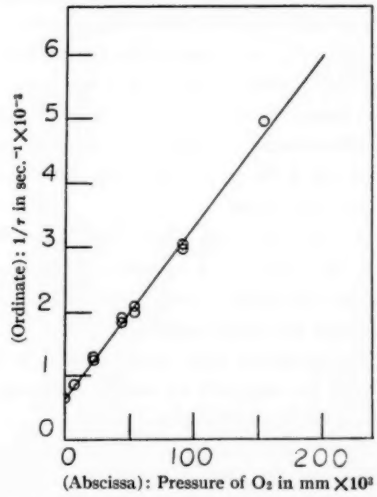

FIG. 2. Dependence of lifetime in biacetyl on pressure of O_2 at 25°. All data obtained with biacetyl at 14 mm, except points at oxygen pressure of 44×10^{-3} mm which were obtained with biacetyl at 33 mm.

[15] R. H. Fowler and E. A. Guggenheim, *Statistical Thermodynamics* (Cambridge University Press, London, 1939), pp. 267–270.

[16] Hirschfelder, McClure, and Weeks, J. Chem. Phys. **10**, 201 (1942).

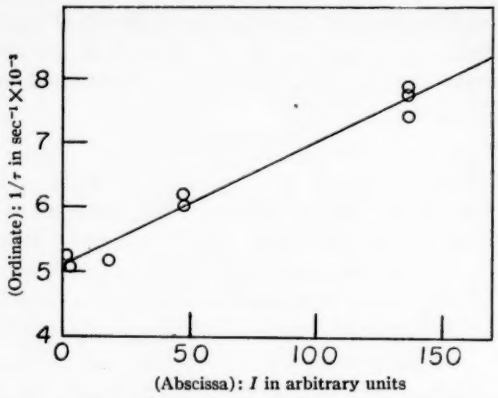

FIG. 3. Dependence of lifetime in acetone on exciting intensity. Acetone at 150 mm and 25°C.

With this value of ΔE, Eq. (11) predicts that K_{323} will be 0.010 mm^{-1}. Alternatively, using the two experimental values for K, ΔE is found to be -3960 cal./mole, which is in good agreement with the theoretical result, considering the fact that the experimental equilibrium constants are determined by fitting the curves to the data.

The mechanism presented above to explain the pressure dependence of lifetime should be quite general. However, it was found that at moderate exciting intensities the lifetime of fluorescence of biacetyl at 25°C and 79°C was independent of the pressure of biacetyl in the pressure range of from 2 to 30 mm, the lifetimes being 1.80×10^{-3} sec. at 25°C and 1.27×10^{-3} sec. at 79°C. Consideration of Eq. (9) shows however that $1/\tau$ might be independent of pressure in the pressure range in which KP is large compared with unity. If, for example, K_{298} for biacetyl were 10 mm^{-1}, KP for the lowest pressure used would be 20. Assuming that the product bc in Eq. (11) is the same for biacetyl as it is for propane, ΔE is found to be only -8120 cal./mole for $K_{298}=10$ mm^{-1}, in reasonable agreement with the value found for acetone. Furthermore, with this value for ΔE, K_{352} becomes 1.2 mm^{-1}, which is probably too large to be observable. Thus it would seem that the results for biacetyl do not provide a conclusive test of the mechanism proposed.

Not much can be said that the temperature dependence of the constants k_2 and k_3. Both k_2 and k_3 are expected to be temperature dependent but the data are not sufficient to distinguish the effects of either one alone. It is to be noted that either step (b) or step (d) in Eq. (2) can be omitted without changing the form of the pressure dependence of $1/\tau$.

Explanation of the temperature dependence of the transition probability, k_1, requires an elaborate theoretical investigation of the effect of the rotation-vibration states concerned. A method of approach to this problem has been given by Mulliken.[4]

The dependence of the lifetime of biacetyl vapor at 25° and 14 mm on the pressure of oxygen was investigated. The results are shown in Fig. 2 from which it can be seen that $1/\tau$ is a linear function of the pressure of oxygen. This suggests that the quenching of excited biacetyl molecules by oxygen follows a simple Stern-Volmer mechanism which may be represented by the two steps

$$\begin{aligned} &(a)\quad B'\rightarrow B+h\nu \qquad k_1 \\ &(b)\quad B'+O_2\rightarrow B+O_2 \quad k_2. \end{aligned} \tag{14}$$

Assuming that the concentration of O_2 is constant, Eq. (14) leads to the following expression for $1/\tau$:

$$1/\tau=k_1+k_2O_2. \tag{15}$$

From the slope of the curve in Fig. 2, k_2 is found to be 8.55×10^{-13} per sec. per molecule of O_2 per cc. If this value for k_2 is used in the simple kinetic theory expression for a bimolecular rate constant

$$k_2=PZ\exp(-E/RT) \tag{16}$$

where P is the probability factor, Z the collision number and E the activation energy, with a collision diameter of 7.5A and with $E=0$, P becomes 0.0095. Thus only one collision between B' and O_2 in 106 such collisions is effective in quenching. This figure may be compared to that given by Almy and Anderson,[12] who estimate, from the measured lifetime of pure biacetyl and from the results of steady state measurements on the quenching of the fluorescence of biacetyl by oxygen, that only one in every one hundred collisions between an excited biacetyl molecule and a oxygen molecule is effective in quenching.

In Fig. 2 the point at an oxygen pressure of 44×10^{-3} mm was obtained with a biacetyl pressure of 33 mm rather than 14 mm as were the rest of the data. The point falls on the same straight line as do the rest of the data as would be expected from Eq. (15) which predicts that $1/\tau$ should be independent of the pressure of biacetyl.

Intensity Dependence of Lifetime

The intensity of exciting radiation was varied usually by means of calibrated blackened copper screens, except that the two highest intensities used with acetone were obtained by the removal of the Ni–K_2CrO_4 filter. The intensity change produced by the removal of this filter was estimated from the change in the amplitude of the fluorescence deflection on the oscillograph screen. It was assumed that the resulting change in spectral distribution of the exciting light was without effect.

Within experimental error, $1/\tau$ was found to be a linear function of exciting intensity in both acetone and biacetyl at a constant T and P as shown in Fig. 3. The errors in this data are probably somewhat larger than those in the data presented in the previous section, because of the method of intensity control.

This dependence on incident intensity was a somewhat unexpected result, especially since the decays

were all purely exponential within experimental error, indicating that the disappearance of excited molecules is a reaction which is first order with respect to the excited molecules. If however, the excited molecules are quenched by products of photochemical decomposition, and intensity dependence can be explained by the following considerations.

The absorption of light is followed by a rapid decomposition process and a process by which the molecule goes to the level from which light is to be emitted. Then we may write

$$\begin{array}{lll} \text{(a)} & A' \rightarrow A + h\nu & k_1 \\ \text{(b)} & A' + D \rightarrow A + D & k_2, \end{array} \tag{17}$$

where A' is either an acetone or biacetyl molecule in the fluorescing state, and D is the quenching decomposition product molecule, which appears immediately on exposure to the light. The steps involving the formation of double molecules have been omitted since this discussion concerns data obtained at constant pressure. It is considered in these steps that the concentration of D does not change appreciably during decay. The differential equation for the disappearance of A' is then

$$-dA'/dt = (k_1 + k_2 D)A'. \tag{18}$$

Thus the decay is exponential and

$$1/\tau = k_1 + k_2 D. \tag{19}$$

Assuming that D is proportional to I_a, the absorbed intensity, Eq. (19), becomes

$$1/\tau = k_1 + k_2 \phi I_a \tag{20}$$

where ϕ is the quantum yield for the formation of D. Since I_a is proportional to the incident intensity, Eq. (20) is of the same form as the observed dependence.

In order to see whether there was a sufficiently high concentration of D present to cause an effect of the order of magnitude observed, a rough estimation of the absolute intensities of fluorescence was made, assuming that the concentration of A' was uniform throughout the illuminated volume. From the amplitude of the fluorescence deflection on the cathode-ray screen, the estimated multiplication factor of the tube,[17] and the geometry of the system, it was estimated that in acetone vapor at 25°C and 150 mm, and at an exciting intensity of one arbitrary unit, about 6×10^9 acetone molecules per cc were excited to fluorescence. From the reported quantum yields for fluorescence[8] and for decomposition[18] at 150 mm and 25°C it is estimated that there are 20 times more molecules decomposing than fluorescing. Assuming that this value can be used at the higher intensities employed in this work, D in Eq. (19) becomes 1.2×10^{11} molecules per cc per pulse of light at an intensity of one in arbitrary units. Using this value, k_2 in Eq. (19) evaluated from the slope of Fig. 3, is 5×10^{-10} per sec. per molecule of D per cc.

The theoretical value for k_2 as computed from the simple kinetic theory expression, Eq. (16) is 5×10^{-10} per sec. per molecule of D per cc, when P is taken as one, E as zero, the collision diameter as 5×10^{-8} cm and the molecular weight of D as 30. The good agreement between the two values of k_2 is probably fortuitous in view of the approximate nature of the calculations, but seems to indicate that the intensity dependence of lifetime can probably be explained through quenching by products of photochemical decomposition.

The data for biacetyl have been treated in a similar way. From the experimental results, k_2 for biacetyl at 25°C is 0.4×10^{-9} per sec. per molecule of D per cc, while k_2 computed from Eq. (16) is 1×10^{-9} per second per molecule of D per cc.

[17] R. W. Engstrom, J. Opt. Soc. Am. **37**, 420 (1947).

[18] W. A. Noyes, Jr. and P. A. Leighton, *The Photochemistry of Gases* (Reinhold Publishing Corporation, New York 1941) pp. 189–190.

Effect of Temperature on the Lifetime of Fluorescence of Solid Acetone*

W. E. KASKAN** AND A. B. F. DUNCAN
University of Rochester, Rochester, New York
(Received August 15, 1949)

The lifetime of fluorescence of solid acetone was found to be a function of temperature, and of an unknown parameter which was interpreted as the state of aggregation of the sample. Both of these effects were interpreted in terms of the exciton theory, in which a quantum of electronic excitation energy is capable of wandering through the crystal before it is emitted as light.

WE have continued the experiments on the lifetime of fluorescence, τ, of solid acetone[1] and wish to report the results of these measurements together with some observations on the fluorescence of solid biacetyl. In view of the reduction of the error in the determination of lifetime from 15 percent to 3 percent as described in the preceding paper[2] we have been able to study relatively small changes in the lifetime produced by the variation of temperature and the state of aggregation.

The lifetime of fluorescence of samples of solid acetone was found to be dependent on the state of aggregation of the crystalline mass and on the temperature, and independent of exciting intensity. All of the decays were purely exponential within experimental error.

The dependence of τ on the state of aggregation manifested itself in the following way. If a sample of acetone were frozen and the lifetime measured several times without disturbing the sample or allowing it to melt, the results always agreed within 3 percent. This was true even though two hours were allowed to elapse between successive determinations. But when a sample was frozen with liquid nitrogen and τ measured after rotation of the samples by intervals of $\pi/2$ about an axis perpendicular to the direction of the exciting beam, it was found that the measured lifetimes might differ by as much as 50 percent.

Furthermore, a sample can be frozen, the lifetime measured several times, melted, refrozen in exactly the same position, and the lifetime remeasured several times. The results after each freezing will agree within three percent; the two sets may vary as much as fifty percent.

Lifetime measurements were made also on a film of solid acetone, condensed from vapor onto a tube internally cooled to 78°K. The tube extended into a bulb, fitted with windows for observation, which could be evacuated and filled with acetone vapor. The lifetime measured with this film was shorter than any values obtained with the material in bulk. It is possible, however that the film may have been at a temperature slightly higher than the surface on which it was condensed.

All of these experiments indicate that the lifetime, *at constant temperature*, depends on a variable which can change the lifetime by a large factor. It appeared probable that this variable was connected with *macroscopic* properties of the solid rather than molecular properties; the latter should be reproducible at constant temperature.

At this point we should examine critically the conception of the lifetime of an excited molecule in a solid in relation to the structure of the solid. In a crystal lattice we may expect that the excitation will not remain localized on a particular molecule but may travel through the crystal. The lifetime will thus be affected by the dimensions of the crystal, displaced lattice points, and impurities in the crystal.

It is of interest to draw an analogy between the motion of excitation energy in a molecular crystal and an electron in a metal. According to a simple treatment[3] of this problem, an electron moving in a perfect infinite metallic lattice would suffer no collisions and its mean free path would be infinite. However a perfect metallic lattice will exist only in a pure metal at the absolute zero of temperature. At other temperatures, the lattice becomes imperfect due to temperature motion, and in any real metallic crystal (i.e., not perfectly pure) the mean free path is given by the expression:

$$l=l_0/(a+T) \qquad (1)$$

where l is the mean free path, T is the temperature, a is a constant dependent on the impurities present, and l_0 is numerically equal to the temperature at which the mean free path is 1 cm in a pure crystal. It can be seen that l_0 must include the effect of crystal size and shape, since for sufficiently small crystals l can never be equal to 1 cm. under any conditions. It is of importance, therefore, to study the effect of temperature on lifetime.

To control the temperature of the solid acetone two holes were bored in a solid aluminum cylinder 2 in. in diameter and 3 in. long; one for the sample tube and the

* This work was supported in part under Contract N6onr-241, Task I, with the Office of Naval Research, United States Navy.
** Eastman Kodak Fellow, 1948–49. Part of a dissertation presented to the Faculty of the Graduate School of the University of Rochester in partial fulfillment of the requirements for the degree of Doctor of Philosophy.
[1] W. E. Kaskan and A. B. F. Duncan, J. Chem. Phys. **16**, 223 (1948).
[2] W. E. Kaskan and A. B. F. Duncan, J. Chem. Phys. **18**, 427 (1950).
[3] J. E. Mayer and M. G. Mayer, *Statistical Mechanics* (John Wiley and Sons, Inc., New York, 1940), pp. 397–400.

other for a thermocouple. These holes were close together and parallel to the axis of the cylinder and an opening was made in the side of the cylinder so that the sample could be irradiated. This block of metal, when situated inside the quartz Dewar flask required about an hour to warm from 78° to 178°K. With the sample tube in place, it was found that during the warming period, the acetone was 1°K colder than the thermocouple, so that a 1°K correction was later applied to the data. The procedure used was to cool the block and sample to 78°K with liquid nitrogen, and then, as the metal and sample warmed slowly the lifetime was measured at about 20°K intervals.

In the temperature range of 78°K to 170°K, $1/\tau$ was found to be a linear function of temperature, as shown in Fig. 1. In this figure, experiments one and two were made with the aluminum block as explained above. Experiment three was made without the aluminum block, in which case the data are less accurate because of the more rapid rate of warming. These data are included, however, because of the quite different lifetime of this sample at 78°K.

The interpretation of the temperature data can be made conveniently in terms of the "exciton" hypothesis,[4] which considers electronic energy as a material particle, with a mass determined by the energy of excitation. According to this picture therefore it is conceivable that excitation energy in a crystal can persist for an average time which is larger than the lifetime of an isolated excited molecule at the same temperature, because of the fact that in a crystal this excitation energy can be handed on from one molecule to another before it can be emitted as radiation from the first molecule. This sort of mechanism could lead to a lifetime which is larger than that which would be observed in a gas at the same temperature.

Making use of this hypothesis, we can describe the process of disappearance of excitation energy in solid acetone by means of the following two steps:

$$\begin{aligned} &\text{(a)}\quad E \rightarrow h\nu \qquad\qquad k_1, \\ &\text{(b)}\quad E+A_u \rightarrow A+h\nu k_2. \end{aligned} \tag{2}$$

E is an exciton, and A_u is an acetone molecule which is located at a distance sufficiently far from its equilibrium position to allow a collision with the exciton. Step (a) takes place because the exciton as it moves along has a finite probability for localizing itself on any acetone molecule in the lattice and subsequently being emitted as radiation. Step (b) formulates the process in which an exciton collides with a displaced acetone molecule, and as a consequence is converted into radiation. From these two steps we have

$$-dE/dt=(k_1+k_2A_u)E \tag{3}$$

and

$$1/\tau=k_1+k_2A_u. \tag{4}$$

The concentration of A_u essentially determines the mean free path of the exciton. Just as in a perfect gas where the mean free path is inversely proportional to pressure, we may write for A_u

$$A_u=k_3/l=k_3(a+T)/l_0, \tag{5}$$

where k_3 is a proportionality factor. Equation (4) thus becomes

$$1/\tau=k_1+k_2k_3(a+T)/l_0. \tag{6}$$

This equation predicts a linear dependence of $1/\tau$ on T, which was experimentally observed (Fig. 1). It is to be noted that omission of step (a) in Eq. (2) does not change the form of Eq. (6).

In Fig. 1 it can be seen that the slopes of the $1/\tau$ *versus* T plots are different, and that there is a tendency for all of the samples to approach the same lifetime at the melting point, which is 178°K. This is to be interpreted qualitatively as an effect arising from variation in l_0 from sample to sample. As was pointed out in the previous discussion, l_0 for any single crystal must be a function of crystal size and shape; the l_0 which appears in the slope of Eq. (6) is really a quantity averaged over the illuminated mass, and is thus a function of what we have called the state of aggregation. Thus l_0 may be expected to be different for different parts of the sample. Now at the melting point, the average molecule in the crystal has almost enough thermal energy to disrupt the forces holding the lattice together. Under these conditions, the concentration of A_u will be high and the mean free path can be expected to be more dependent on A_u, and less dependent on crystal size and shape. Thus at the melting point, all samples are expected to have the same lifetime, as is experimentally observed.

A further possibility must be examined, which is that the decrease in lifetime with rising temperature is due to thermal quenching. This will occur because of increase in amplitudes of crystal vibrations with temperature. Such a mechanism leads to an exponential dependence

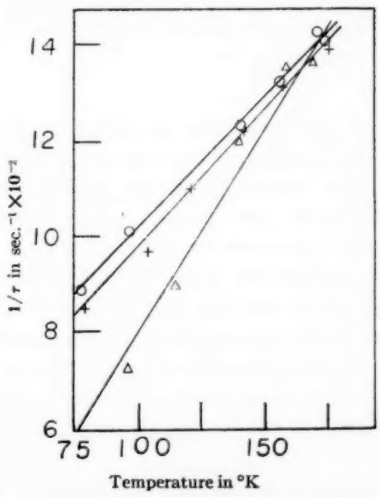

FIG. 1. Temperature dependence of lifetime in solid acetone. Circles and crosses are experiments 1 and 2 respectively. Triangles are experiment 3.

[4] J. Franck and E. Teller, J. Chem. Phys. 6, 861 (1938).

of the lifetime on the temperature. If the amplitudes increase only slightly with T in the range covered, the curves of $1/\tau$ against T will appear to be linear. In the present case, the range of T may be too small to allow decision between a truly linear curve and an exponential curve which is linear only in a first approximation.

The variations in *slope* of the $1/\tau - T$ curves of Fig. 1 are not easily explained, however, by a thermal quenching mechanism. The latter mechanism depends essentially on microscopic properties of the crystal, which are confined to distances of a few molecular diameters for true molecular vibrations. It appears that values of these properties should be the same in every crystal, which requires that the slopes of the $1/\tau - T$ curves should all be the same. This is clearly not the case. On the other hand, if thermal quenching arises from low frequency lattice vibrations of large amplitude, so that waves extend through large aggregates, then there is nothing to distinguish this mechanism from the exciton picture except a change in descriptive notation.

From the preceding discussion it appears that the exciton picture is capable of giving a qualitative explanation of the observed results on the lifetime in solid acetone. The possibility of thermal quenching is not excluded, but is considered inadequate as a basis of explanation of the curves of Fig. 1.

Observation on Solid Biacetyl

The decay of the fluorescence of solid biacetyl at 78°K, when irradiated with wave-lengths in the region 4350A, was found to be non-exponential at high exciting intensities. At lower exciting intensities, the decays became non-exponential as the temperature increased. At those intensities where the decays of fluorescence of biacetyl at 78°K appeared to be exponential, the average of the observed lifetimes was 1.26×10^{-3} sec. Thus the theory developed above for the temperature dependence of the lifetime of fluorescence in solid acetone cannot be applied even qualitatively to biacetyl because of the non-exponential nature of the decays.

A single experiment was done in which solid biacetyl at 78°K was irradiated with wave-lengths in the region 2500A. Absorption of light of this wave-length excites the biacetyl molecules to a electronic energy level different from that reached on absorption of 4350A. The lifetime under these conditions was found to be unchanged however, indicating that in both cases, the fluorescence transition is the same. The large difference in energy between the two upper electronic states must be lost in a time small compared with the time resolving power of our oscillograph, (10^{-5} sec.) since no time lag was observed between excitation and fluorescence.

THE JOURNAL OF CHEMICAL PHYSICS VOLUME 18, NUMBER 4 APRIL, 1950

Near Ultraviolet Absorption Spectra of Melamine and Some Related Compounds

GEORGE W. COSTA,* ROBERT C. HIRT, AND D. J. SALLEY
Stamford Research Laboratories, American Cyanamid Company, Stamford, Connecticut
(Received October 3, 1949)

An absorption band of low intensity has been found in the 2800 to 3400A region for solutions of melamine, trimethylol melamine, trimethyl ether of trimethylol melamine, hexamethylol melamine, and cyanuric chloride. The band has also been observed in gaseous melamine at elevated temperatures. The band is believed to be due to a singlet-triplet transition, rather than analogous to the 2600A absorption system of benzene.

MELAMINE is usually considered to have a symmetrical "amino" structure containing three conjugated double bonds[1] analogous to those in benzene. General empirical observation suggests that such a system should show an absorption band in the region of 2500 to 3400A, and indeed Maccoll[2] has predicted that symmetrical triazine ($C_3N_3H_3$) should exhibit a band near 3700A. In addition, considerations of the symmetry of the molecule suggest that a forbidden electronic transition would be involved and hence that the absorption would be relatively weak. Two earlier articles[3,4] on the ultraviolet absorption spectra of melamine and related compounds were not concerned with these aspects but with the absorption in the 2350A region. Consequently, a search of the longer wave-length region has been made for solutions of melamine and some related compounds and for melamine vapor.

EXPERIMENTAL

Melamine, trimethylol melamine, hexamethylol melamine, the trimethyl ether of trimethylol melamine, and cyanuric chloride, all prepared by various members of these Laboratories, were recrystallized, resublimed,

* Present address: Department of Chemistry, Northeastern University, Boston, Massachusetts.

[1] E. H. Hughes, J. Am. Chem. Soc. **63**, 1737 (1941).

[2] A. Maccoll, J. Chem. Soc., 670–672 (1946).

[3] Dixon, Woodberry, and Costa, J. Am. Chem. Soc. **69**, 599 (1947).

[4] I. M. Klotz and T. Askounis, J. Am. Chem. Soc. **69**, 801 (1947).

or otherwise treated in an effort to obtain the highest possible purity. For melamine and cyanuric chloride these efforts undoubtedly succeeded in producing a very pure material, but they may not have succeeded entirely for the other compounds which are somewhat unstable and which are initially obtained in admixture with other closely related compounds. Aqueous solutions were made of all but cyanuric chloride; this latter was examined in cyclohexane. Ethylene glycol was also used as a solvent for melamine. Since the absorption was weak in the region examined, relatively concentrated solutions were employed. Cell lengths (5 to 100 mm) and solution concentrations (0.2 percent to 3.5 percent) were so chosen that in all cases the observed absorbances (optical densities) were within the range of 0.1 to 0.8, where a precision of ±1 percent could be obtained.

In the case of melamine, the solubility[5] in water at room temperature was not sufficient to allow adequate absorption with the cell length available. Consequently, it was examined in a nearly saturated solution at about 75°C in an electrically heated cell, or as a solution supersaturated at room temperature. In the latter, the solution could be held as long as an hour before crystallization set in.

A Beckman spectrophotometer, Model DUV, accommodating 5 to 100 mm length cells and using a water-cooled hydrogen lamp of high intensity,[6] was employed for most of the measurements on solutions, but some examinations were also made with a Cary automatic recording spectrophotometer.[7]

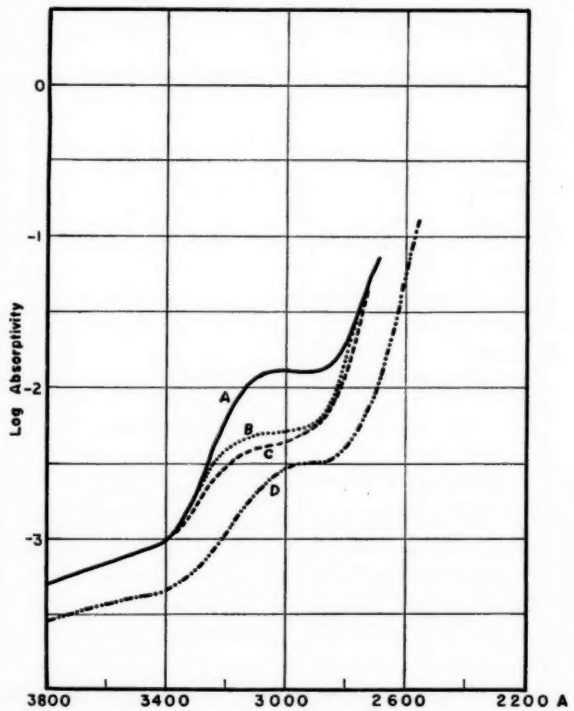

FIG. 1. Near ultraviolet absorption spectra of: *A*————Trimethyl ether of trimethylol melamine; *B*. . . . . Hexamethylol melamine; *C*– – – – –Trimethylol melamine; *D*—··—··—Melamine.

[5] Chapman, Averell, and Harris, Ind. and Eng. Chem. **35**, 137 (1943).

TABLE I. Near ultraviolet bands.

Compound	*p*H	Band wave-length, A	Absorptivity Specific	Absorptivity Molar
Melamine, recrystallized	1.4	2950	0.0103	1.3
Melamine, recrystallized	8.4	2950	0.0021	0.26
Melamine, recrystallized	11.7	2950	0.0079	1.0
Melamine, resublimed, 3×	1.5	2950	0.0092	1.2
Melamine, resublimed, 3×	8.0	2950	0.0031	0.39
Trimethylol melamine	0.8	3000	0.0160	3.5
Trimethylol melamine	7.9	3000	0.0046	1.0
Trimethylol melamine	11.4	3000	0.0050	1.1
Trimethyl ether of trimethylol melamine	1.3	2980	0.056	14.2
Trimethyl ether of trimethylol melamine	8.6	2980	0.013	3.3
Trimethyl ether of trimethylol melamine	11.7	2980	0.014	3.6
Hexamethylol melamine	8.0	3100	0.0047	1.3
Cyanuric chloride	(*c*-hexane)	3400	0.0009	0.17

For photographing the vapor spectrum of melamine, a Hilger medium quartz spectrograph with a water-cooled Nestor hydrogen lamp and Eastman Kodak Type III-O plates were used. A 50 mm vapor cell was equipped with quartz windows and was enclosed in a small electrically heated furnace having quartz windows. The temperature inside the furnace was measured with a thermocouple. The vapor was maintained at about 198°C and 243°C to obtain a concentration sufficiently high to give satisfactory spectrograms in less than a hour of exposure. The plates were traced on a Leeds and Northrup recording microphotometer. The absorbance (optical density) values obtained from the tracings were corrected by use of H and D curves for the emulsion at various wave-lengths; they were also corrected for the variation in intensity of the hydrogen lamp with wave-length, which was obtained from a microphotometer tracing of the hydrogen lamp spectrum, photographed on the same plate.

RESULTS

The ultraviolet absorption spectra were expressed as the logarithm of the absorptivity *versus* wave-length, using Beer's law in the form:

$$\log_{10} I_0/I = A = a \cdot b \cdot c,$$

where I_0 is the intensity of the incident light, I is the intensity of the transmitted light, A is the absorbance (optical density), a is the absorptivity (specific extinction), b is the cell thickness in mm, c is the concentration in g/100 ml.

[6] The lamp was of the type described by A. J. Allen and R. G. Franklin, J. Opt. Soc. Am. **29**, 453 (1939) and was obtained from A. G. Nestor of the Bartol Foundation.

[7] We are indebted to Drs. R. H. Kienle and G. L. Buc of the Calco Chemical Division of this Company for the use of this instrument.

A weak, unresolved band or shoulder was displayed by all the compounds in the region of 2800 to 3400A. Figure 1 shows the spectra for aqueous solutions of melamine (supersaturated solution), trimethylol melamine, hexamethylol melamine, and the trimethyl ether of trimethylol melamine. Curves similar to these were obtained for melamine in water at 75°C and in ethylene glycol at room temperature. No fine structure was found in these bands even with the Cary instrument. The intensity of the band was very low, with absorptivity values in the range 0.001 to 0.1, as shown in Table I. The effect of *p*H changes was to enhance the band at either low or high *p*H values as is evident in Table I. For the compounds tested, Beer's law was obeyed within the limit of experimental error in the concentration range of 0.2 to 3.5 percent; changes in both cell thickness and concentration were made in verification of this behavior.

Cyanuric chloride in cyclohexane solution displayed a low intensity band near 3400A, as shown in Fig. 3. This band, like the band near 2500A, appeared to be partially resolved into two bands.

The spectrum of melamine vapor also showed a shoulder band appearing at 3100 to 3200A, similar to that in the solution spectra at 2900 to 3000A. This is shown in Fig. 4. Measurable absorption could be found from the microphotometer tracings as far as 3400A and there was strong absorption below 2450A. Since the absorption in the near ultraviolet range was of primary interest, the strong absorption below 2450A was not investigated at this time. No fine structure was observed.

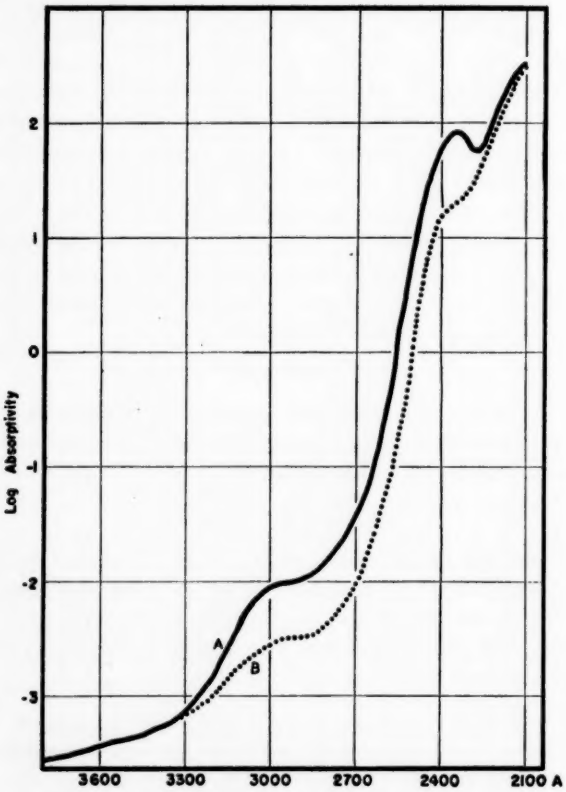

FIG. 2. Ultraviolet absorption spectra of melamine: *A*———— at *p*H 1.4; B..... at *p*H 8.4.

DISCUSSION

Although the bands observed in the 2800 to 3400A region are of very low intensity, their reality appears unquestionable. The intensity of the band for samples of melamine obtained from various sources and subjected to repeated purification did not change, showing that it did not arise from an impurity. The facts that Beer's law is obeyed at high concentrations and that the band is observed in organic solvents means that it

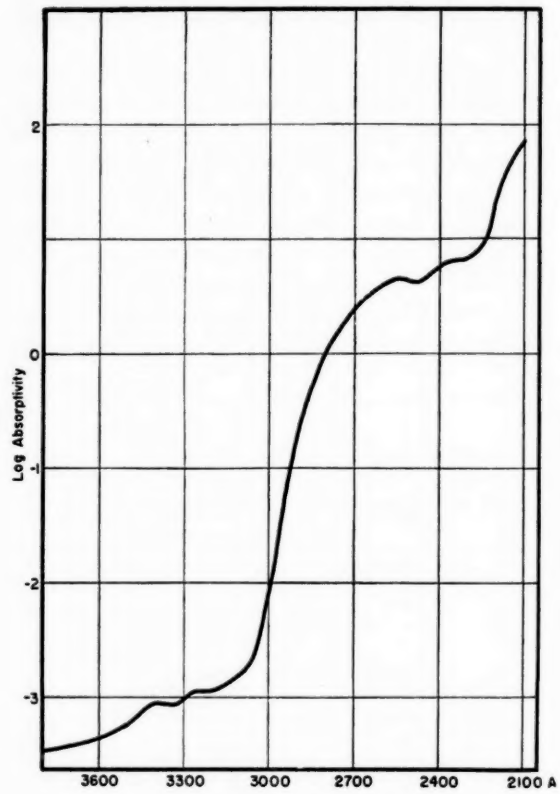

FIG. 3. Cyanuric chloride in cyclohexane.

cannot be attributed to the presence of ions or solvated molecules. The enhancement by *p*H changes indicates, however, that the ions so formed have a somewhat higher absorptivity than that of the neutral molecule. Finally the appearance of the band in the vapor phase indicates that it is characteristic of the melamine molecule.

It would appear that the band is due to an electronic transition arising from the triazine nucleus of the molecule, and two alternative suggestions may be offered at this time concerning the nature of this transition. The proposal which stimulated the investigation of the 2500 to 3400A region was that a band corresponding to the 2600A absorption of benzene

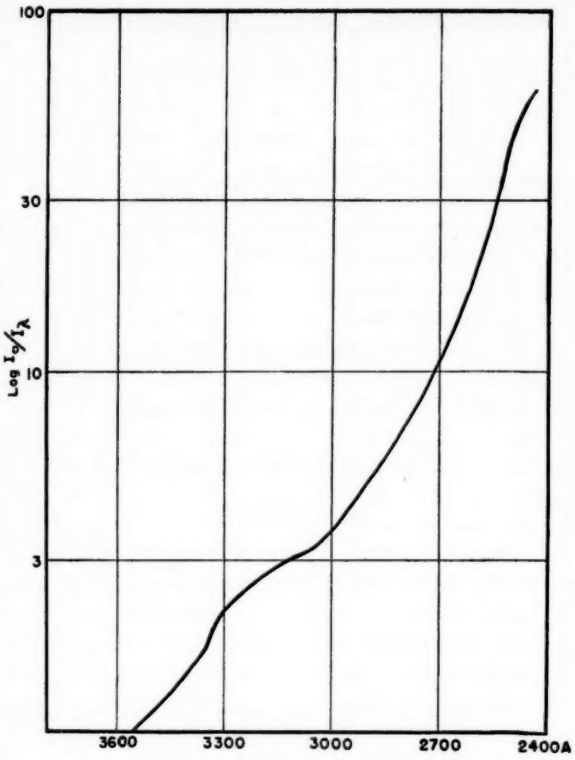

FIG. 4. Melamine vapor at 243°C.

and its derivatives should exist for melamine. That the band should be weak in intensity was expected from the fact that the trigonal symmetry of the "amino" or "normal" structure of the melamine molecule places it in the D_{3h} symmetry point group (neglecting the hydrogen atoms). Symmetry considerations for molecules belonging to this point group show that the transition analogous to the 2600A ($^1A_{1g} \rightarrow {}^1B_{2u}$) benzene transition is forbidden electronically. This has been demonstrated in the cases of 1,3,5-trichlorobenzene and 1,3,5-trimethylbenzene.[8] However, the intensity of the observed band in melamine is roughly 10^{-3} that for benzene. This large intensity difference argues against this explanation, for it is unlikely that such a transition should be any *more* forbidden in melamine than in benzene.

The alternative suggestion is that a singlet-triplet transition is involved. Benzene has very weak absorption bands near 3400A[9,10] arising from a symmetry-forbidden, singlet-triplet transition ($^1A_{1g} \rightarrow {}^3B_{1u}$); this has been discussed in detail by Kasha[11] and by Shull.[12] The intensity of this benzene absorption, however, is about 10^{-2} that of the melamine band. Another singlet-triplet transition ($^1A_{1g} \rightarrow {}^3E_u^-$) in benzene (though not observed probably due to the overlapping of the 2600A absorption) was expected by Roothaan and Mulliken[13] to have an intensity 10^3 stronger than the $^3B_{1u}$ and thus about 10^2 weaker than the $^1B_{2u}$ transition. This expected intensity for the benzene band is thus about the observed intensity of the melamine band. If then, the 2950A melamine absorption arises from a singlet-triplet transition, the strong absorption of the triazines in the 2200–2500A region[3,4] (Fig. 2) may be considered as corresponding to the 2600A region bands of benzene and substituted benzenes.[14]

Cyanuric chloride can exist only in the "normal" form[4] and hence is also a planar, trigonally symmetrical molecule belonging in the symmetry point group D_{3h}. The low intensity band near 3400A is thought to correspond to that of melamine at 2950A, and that near 2500A to that of melamine near 2350A. The differences near 2500A between the cyanuric chloride spectrum shown on Fig. 3 and that reported by Klotz[4] are believed to be due to the different solvents used. The presence of this weak band in cyanuric chloride spectra argues against explanations involving ions or contributions from the amino nitrogen atoms.

A choice between the two alternative explanations at this time would be in favor of the singlet-triplet hypothesis. Both of these explanations attribute the absorption to electronic transitions arising from symmetrical, benzene-like structures in these triazines. The increase in molar absorptivity in the weak band from melamine to trimethylol melamine to the trimethyl ether of trimethylol melamine is consistent with the reduction in symmetry due to the additional atoms, although admittedly but little can be said with regard to the configuration of the latter two compounds. The similarity of the melamine and cyanuric chloride spectra, together with the correlation between melamine and benzene spectra, support the opinion that melamine itself in aqueous solution has the symmetrical amino structure.[4] Further investigations on the ultraviolet absorption spectra of melamine and related compounds, especially unsymmetrically substituted triazines, are being pursued here in the hope that new evidence on the structure of these compounds and the origin of their spectra may result.

ACKNOWLEDGMENT

We are grateful to Dr. R. F. Stamm and Dr. F. Halverson for many helpful suggestions and discussions, and to Mrs. D. M. Sousa for aid with the experimental work.

[8] H. Sponer, Chem. Rev. **41**, 281 (1947).
[9] A. L. Sklar, J. Chem. Phys. **5**, 669 (1937).
[10] G. N. Lewis and M. Kasha, J. Am. Chem. Soc. **66**, 2100 (1944), and **67**, 994 (1945).
[11] M. Kasha, Chem. Rev. **41**, 401 (1947).
[12] H. Shull, J. Chem. Phys. **17**, 295 (1949).
[13] C. C. J. Roothaan and R. S. Mulliken, J. Chem. Phys. **16**, 118 (1948).
[14] R. C. Hirt and J. P. Howe, J. Chem. Phys. **16**, 480 (1948).

A Single Exposure Photographic Method for Depolarization Factor Measurements*

PAUL BENDER AND PHILIP A. LYONS**
University of Wisconsin, Madison, Wisconsin
(Received August 24, 1949)

A single exposure photographic method for the measurement of depolarization factors in Raman spectroscopy is described. The accuracy of the results was tested by measurements with carbon tetrachloride and chloroform. The depolarization factors found for highly polarized lines were in good agreement with those given by the photoelectric method rather than with those of other photographic investigations.

INTRODUCTION

THE experimental methods for depolarization factor measurements receiving particular attention in recent years have been the two exposure photographic method[1,2] and the photoelectric technique.[3] The latter is especially adapted to measurements on highly polarized lines but its application is difficult with equipment having low light gathering power, and very weak Raman lines would require some integrating method for recording in any event. The disadvantages of the two exposure method, which include errors due to fluctuations in the incident light, progressive sample discoloration and decomposition, and fluctuations in the response of the photographic emulsion caused by changes in temperature and humidity and by decay of the photographic latent image, would seem to outweigh the superiority in speed over a single exposure method, particularly in the usual case where the investigation of a large number of samples in a short time was not contemplated. The present paper is a report on a modified version of the single exposure method of Reitz[4] which has yielded satisfactory results.

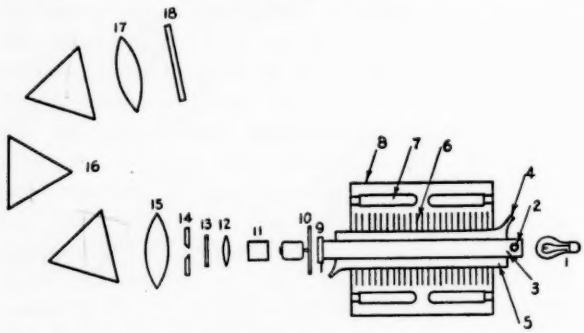

FIG. 1. Schematic diagram of equipment for depolarization factor measurements.

1. Lamp
2. Sample inlet
3. Raman tube
4. Filter solution inlet
5. Filter jacket
6. Baffles
7. Lamps
8. Housing
9. Iris diaphragm
10. Sector wheel
11. Wollaston prism
12. Condensing lens
13. Quarter wave plate
14. Slit
15. Collimator lens
16. Prisms
17. Camera lens
18. Plate holder

EXPERIMENTAL DETAILS

Equipment

A schematic diagram of the assembled equipment is given in Fig. 1. To avoid the convergence of the incident light produced by a cylindrical Raman tube, the jacket and tube were made of square cross section in the illuminated region. The internal diameter of the tube proper was approximately 12 mm. Instead of the conventional horn, the back end of the tube was closed by a plane glass window which facilitated alignment of the tube.

Four Type AH-11 mercury vapor lamps were employed for illumination as shown; the bright core of the lamp was approximately three inches from the tube jacket. To define correctly the illuminated area of the tube, a shield of blackened metal was provided which covered the tube completely except for two longitudinal strips three-eighths of an inch wide. This shield also served as a mount for two-inch long blackened metal baffles which could be clipped on at one-quarter inch intervals. Air was circulated by a blower through the transite box which housed the excitation unit.

The filter solution, which consisted of 4 percent paranitrotoluene and 0.03–0.06 percent crystal violet in ethyl alcohol, was circulated from a reservoir where it was maintained at room temperature to eliminate refractive index gradients in the scattering liquid.

Resolution of the scattered light was accomplished by a large aperture (1 sq. in) 2° quartz Wollaston prism which permitted complete separation of two 3 mm images at the spectrograph slit. A quarter-wave plate was used to convert the resolved, plane-polarized components into circularly polarized beams.

A Steinheil Type GH spectrograph with short (f/3.5) focal length optics, and a microphotometer of essentially conventional design were used in all work reported here. The photomultiplier unit employed was identical with one previously described[5] except for the addition of an electrometer tube input stage to the amplifier section.

* This paper is based on part of a dissertation presented by Philip A. Lyons to the faculty of the graduate school of the University of Wisconsin in partial fulfillment of the requirements for the degree of Doctor of Philosophy in June, 1948.

** Present address: Department of Chemistry, Yale University, New Haven, Connecticut.

[1] F. F. Cleveland, J. Chem. Phys. **13**, 101 (1945).

[2] B. L. Crawford and W. Horowitz, J. Chem. Phys. **15**, 268 (1947).

[3] A. E. Douglas and D. H. Rank, J. Opt. Soc. Am. **38**, 281 (1948).

[4] A. Reitz, Zeits. Physik. Chemie **B33**, 368 (1936).

[5] J. Y. Chien and P. Bender, J. Chem. Phys. **15**, 376 (1947).

Experimental Procedure

After alignment of the Raman tube, the orientation of the quarter-wave plate was changed until the intensities of the resolved components of an unpolarized beam* were equal as measured at the focal plane of the camera lens by the photo-multiplier unit. The apparatus correction usually required to compensate for the differing losses in reflection suffered by the two resolved linearly polarized beams in passage through the spectrograph was thus made negligible. To check the maintenance of this correct setting and to provide for any required correction a photographic record of the resolved components of an unpolarized source was made on each plate on which a Raman spectrum was recorded.

After the Raman exposure was taken plate calibration was carried out with a continuous unpolarized source. A wide range of relative intensities was obtained by use of a sector wheel in conjunction with varying slit widths. The slit had previously been calibrated with the help of the photo-multiplier unit, and the response found to be linear in the range of slit widths employed. Plate calibration curves were prepared by plotting the microphotometer galvanometer deflection *versus* log (relative intensity $+1$).** Microphotometer tracings of the Raman spectra were obtained, the difference between peak line and background intensities determined for both the $\perp$ and $\parallel$ components, and the depolarization factor calculated for each line in the usual way, the background reading being taken as the interpolated value of the actual background curve at the position of the peak of the Raman line.

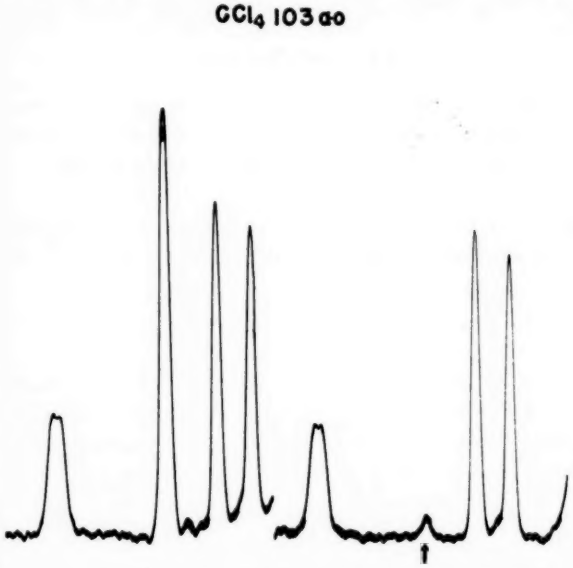

FIG. 2. Densitometer tracings of the $\perp$ and $\parallel$ spectra for carbon tetrachloride.

TABLE I. Depolarization factors for the Raman lines of carbon tetrachloride.

$\Delta\nu'$, cm^{-1}	218	314	459	762–790
I	0.90	0.88	0.02	0.90
	0.86	0.85	0.01	0.86
	0.88	0.91	0.02	0.88
	0.83	0.84	0.03	0.84
	0.88	0.84	0.02	0.91
	0.87	0.86	0.02	0.90
II	0.85	0.87		0.88
	0.84	0.84		0.87
	0.86	0.83		0.88
	0.83	0.84		0.90
	0.80	0.80		0.82
	0.86	0.86		0.87
	0.84	0.87		0.89
	0.85	0.87		0.90
III			0.02	
			0.02	
			0.02	
Mean	0.85_4	0.85_4	0.02	0.87_8
Av. dev. from mean	0.019	0.020		0.019

Series I: Medium exposure (about 90 minutes).
II: Shorter exposure for strong lines.
III: Longer exposure for polarized line.
Baffle spacing $\frac{1}{4}''$ in all above runs.

Low inertia plates (Types 103a-o and 103a-j) were used. Of a number of developers tested,*** D-91 (a para-aminophenol developer) was chosen as giving lowest fog and grain with fair contrast and without undue loss of emulsion speed. At 18°C a $3\frac{1}{2}$ minute development was used followed by 2-minute washing before fixing.

Experimental Results

Carbon tetrachloride has regularly been employed as a test liquid because it provides a close approach to an absolute standard with which the actual experimental results can be compared. The results of a series of determinations on this compound are given in Table I, while typical microphotometer tracings of the spectra are given in Fig. 2. The accuracy obtained in these cases represents the limiting value available with the technique employed since the measurements were made on lines which were well separated (except for the 762–790 cm^{-1} doublet) and which have a high line to background intensity ratio. Further comparative data on chloroform are listed in Table II.

The effect of the baffle spacing on the results obtained was followed by observations on carbon tetrachloride. The results given in Table III for the 459 cm^{-1} line show clearly that baffles are necessary for accurate measurements on polarized lines.

* Whenever reference is made to an unpolarized light source it will mean a small ground glass screen placed at the front stop of the Raman tube and illuminated from the rear by an incandescent lamp operated from a regulated voltage supply.

** Any arbitrary function of the intensity which would reduce to zero for zero deflection and which when plotted against deflection would be substantially linear over a wide range of densities would be equally convenient.

*** D-11, D-8, D-19, D-76, D-91, DK-60A, Microdol, Edwal 12, and a *p*-phenylene diamine developer were tested.

TABLE II. Depolarization factors for the Raman lines of chloroform.

$\Delta\nu'$, cm^{-1}	This research	Douglas and Rank[a]	Crawford and Horowitz[b]
262	0.84		0.86
366	0.14	0.13	0.18
668	0.02	0.026	0.08
760	0.84		0.92
1214	0.9		0.9
3020	0.3		0.4

[a] See reference 3.
[b] See reference 2.

TABLE III. Effect of baffle spacing on the depolarization factor for the $\Delta\nu'=459$ cm^{-1} line of carbon tetrachloride.

Baffle spacing	ρ
$\frac{1}{4}''$	0.02
$\frac{1}{2}''$	0.03
$1''$	0.05
no baffles	0.10

The low value of $\rho=0.02$ found for the $\Delta\nu'=459$ cm^{-1} line is substantiated by the value of 0.013 recently reported by Douglas and Rank, who have commented on the contrast between this figure and the previously reported values of 0.045 and higher.

DISCUSSION

The most difficult problem in the evaluation of the depolarization factor lies in the correction for the background present. For satisfactory results the background must be low, and of comparable intensity for both components, which requires the use of a source with a low background to line intensity ratio such as the AH-11 (see Fig. 2).

The spectra themselves provide a means for checking the self-consistency of the method of taking background readings. If two lines are depolarized to the limit, ($\rho=6/7$), the ratio of the line intensities for the pair should be the same in both the $\perp$ and $\parallel$ spectra. For the 217 cm^{-1} and 313 cm^{-1} lines of the carbon tetrachloride spectrum such an agreement was actually found, within an average deviation of 1.5 percent, in each of a series of twelve determinations when the aforementioned standard method for background correction was employed. If the background reading was assumed to be the reading at the low wave-number side of the Raman line,[2] this ratio was slightly higher for the $\perp$ spectrum than for the $\parallel$ spectrum in consequence of the difference in the shape of the background curve in the two spectra.

At least for fairly intense, depolarized lines the limiting accuracy can safely be assumed to be that permitted by the photographic process. The precision of 1.5 percent noted above is somewhat superior to the accuracy achieved in the measurements recorded in Table I. This may be due to reciprocity law failure, to the use of a continuous source for calibration, or to the lack of validity of making background corrections assuming additive intensities. However, since the reciprocity law error results essentially only in a change of the gamma of the calibration curve and since, for the depolarized lines considered, the background and peak line readings correspond to nearly the same positions on the calibration curve for both the $\perp$ and $\parallel$ spectra, reciprocity law failure may be expected to be of secondary importance. Attempts to use neon and argon lamps as line calibration sources were unsuccessful because of fluctuations in the light intensity which occurred in spite of excellent regulation of the lamp power supply.

ACKNOWLEDGMENTS

This research was supported in part by the Research Committee of the Graduate School from funds supplied by the Wisconsin Alumni Research Foundation.

The special Raman tube was constructed by the Research and Development Division of the Corning Glass Works through the courtesy of Dr. E. M. Guyer.

Measurement of Normal Burning Velocities of Propane-Air Flames from Shadow Photographs*

J. W. ANDERSEN** AND R. S. FEIN***
Naval Research Laboratory, Department of Chemistry, University of Wisconsin, Madison, Wisconsin
(Received August 26, 1949)

The limitation placed upon the stroboscopically illuminated particle method of measuring the normal burning velocity by the heat capacity of the particles is discussed. A supplementary method of measuring the normal burning velocity using a modified Gouy procedure is presented. The line between the dark and light spaces on shadow photographs, taken at different distances from the flame to the film, is used in this method to define the flame area. This area is then extrapolated to the diametral plane of the flame. This procedure gives results that are consistent with the particle method of determining the normal burning velocity and its use is justified empirically. Burning velocities of propane-air flames are given.

Nomenclature

α = Angle between flame front and vertical
u_f = Gas filament velocity in vertical direction
u = Burning velocity
A = Area of flame surface
V = Volumetric flow rate

INTRODUCTION

In order to obtain a knowledge of the mechanism of flame propagation it is necessary to measure accurately parameters that are characteristic of the burning mixture. One parameter that is commonly measured is the "burning" or "transformation" velocity. This is defined as the rate of propagation of a flame through gas in a direction normal to the flame surface. However, this is not a quantity that is readily defined unless the velocity is measured relative to the cold unburned gas. When this velocity is measured relative to the cold gas, it is known as the "normal burning velocity."

Measurement of the burning velocity has been accomplished by three general methods. First, the propagation of a flame in a tube or a spherical bomb has been used to measure this quantity.[1] Second, the propagation of a flame in a soap bubble has been used.[2,3] These two methods are inaccurate because they perturb the burning mixture with changing pressures, water vapor, cold walls quenching the flame, or an irregularly shaped flame front. For these reasons the third method, which consists of measurements made on stationary Bunsen flames, has been most commonly used. The use of a laminar Bunsen flame has the advantage of steady-state determinations which are easier to make than measurements of transients.

Generally, Bunsen burner methods of obtaining burning velocities are either a modification of the Michelson method[1]

$$u = u_f \sin\alpha, \tag{1}$$

or of the Gouy method[1]

$$u = V/A. \tag{2}$$

The Michelson method will yield the normal burning velocity if the angle and gas filament velocity can be determined. The angle can be measured fairly accurately, but measurement of the filament velocity offers some difficulties.

Smith and Pickering,[4] in using the Michelson method, assumed that with laminar flow the parabolic velocity distribution across the tube continued for some distance above the mouth of the burner tube. They then used this assumption to determine the filament velocity. This process introduces systematic errors because the velocity distribution is not parabolic due to the back pressure of the flame; and the visible flame cone from which the angle is determined lies in the hot gas region and therefore the streamlines have diverged.[5] Since the streamlines diverge, burning velocities measured near the center portion of the cone are low.

Lewis and von Elbe[6] introduced small particles into the flowing gas and stroboscopically illuminated them to obtain the filament velocity. The addition of a constant-velocity profile nozzle to give straight-sided flame cones and an improved method of feeding particles into the gas stream[5] has made this an accurate and simple method of obtaining normal burning velocities for a limited range of fuel-air mixtures.

Further work at this laboratory has indicated that the development of a method of measuring normal burning velocity other than the stroboscopically illuminated particle method is necessary. For the propane-air system, it has been observed that the addition of particles to mixtures leaner than 3.8 percent propane causes a significant decrease in the burning velocity. This is evidenced by an increase in the height of the

* This work was carried out under Contract NOrd 9938 with the Navy Bureau of Ordnance.
** Present address: Monsanto Chemical Company, Dayton, Ohio.
*** Present address: The Texas Company, Beacon, New York.
[1] Jost-Croft, *Explosion and Combustion Processes in Gases*, (McGraw-Hill Book Company, Inc., New York, 1946), Chap. III.
[2] Fiock and Marvin, Chem. Rev. **21**, 367 (1937).
[3] Stevens, NACA, T.M. 305 (1929); NACA, T.M. 372 (1930).
[4] Smith and Pickering, J. Research Nat. Bur. Stand. **17**, 7 (1936).
[5] J. W. Andersen and R. S. Fein, J. Chem. Phys. **17**, 1268 (1949).
[6] B. Lewis and G. von Elbe, J. Chem. Phys. **11**, 75 (1943).

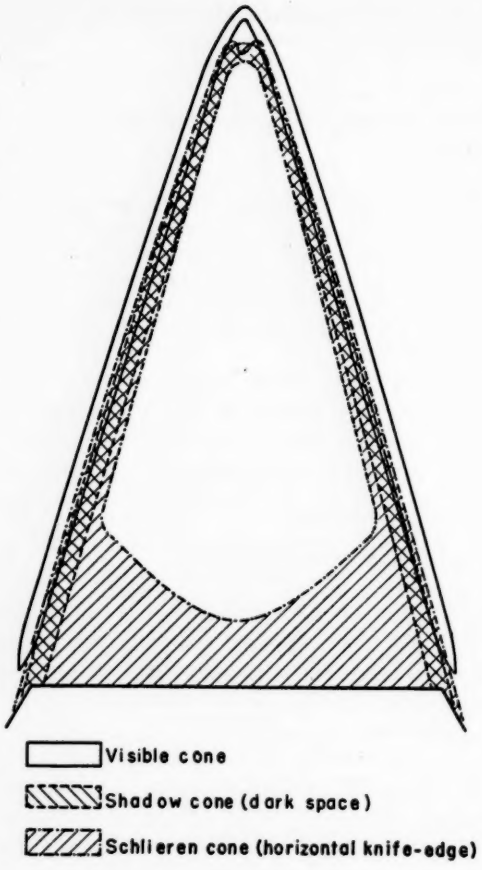

FIG. 1. Propane-air flame cones.

flame cone upon the addition of the particles. The decrease in the burning velocity is probably the result of the large heat capacity of the magnesium oxide particles. As leaner mixtures are approached, the residence time of the particles in the flame zone increases and, as a result, the particles take up enough heat to appreciably disturb the flame. The increased residence time is caused by the decreased burning velocity and the increased thickness of the flame zone. To circumvent this difficulty, it is necessary to develop a method of measuring the normal burning velocity that will not disturb the flame.

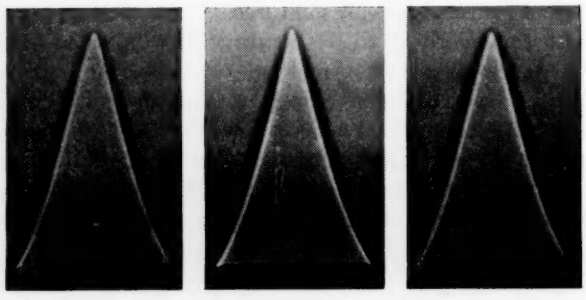

FIG. 2. Shadow photographs of 2.87 percent propane-air flame; flow rate 108 cc/sec., $\frac{5}{8}$" I.D. burner tube. Distance from diametral plane of flame to film (a) 23.8 cm, (b) 33.0 cm, (c) 43.3 cm.

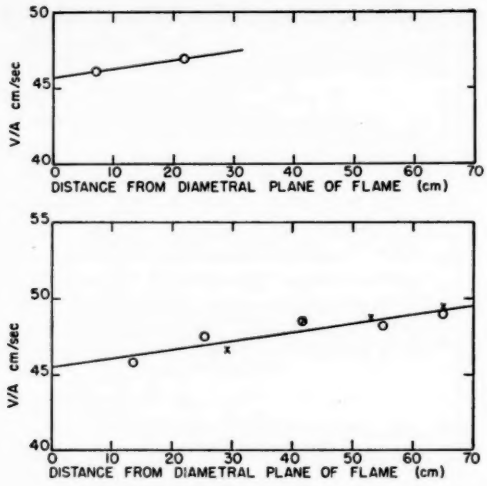

FIG. 3. Determination of normal burning velocity of a 4.12 percent propane-air flame from the flame area defined by line between dark and light spaces on shadow photograph. Top: $\frac{1}{2}$-inch constant velocity profile nozzle. Bottom: $\frac{1}{2}$-inch straight tube. ○, flow rate=119 cc/sec.; ×, flow rate=237 cc/sec.

The Gouy method of measuring the burning velocity will give the normal burning velocity provided the following conditions are true: (1) the flame area that is measured is at the base of the temperature gradient through the flame zone; and (2) if the quenching of the flame at the base of the cone and the increased burning velocity at the tip of the cone caused by preheating of the unburnt gases and/or diffusion of active centers into the unburnt gases are negligible or compensate for each other. It is apparent that to obtain results consistent with the definition of normal burning velocity, an experimental procedure for the detection of the base of the temperature gradient is necessary.

Flame areas for the Gouy method of measuring burning velocities have been determined by direct, schlieren, and shadow photographs.

The flame cones obtained by these three types of photographs for a 4.12 percent propane-air flame on a constant-velocity profile nozzle are illustrated in Fig. 1. It should be observed that the three cones do not coincide. Since it can readily be shown that the outer edge of the dark shadow cone must correspond to the top of the temperature gradient,[7] it is apparent from Fig. 1 that the visible cone lies in the hot gas region. This is in agreement with the results of the determination of the temperature gradient through the flame front from stroboscopically illuminated particle tracks[5] and rules out the use of the visible cone for the determination of normal burning velocity. The use of the Schlieren cone is not practical because the Schlieren method is too sensitive to give a well-defined flame cone. Thus, the shadow cone remains as a possible source of flame area data that is consistent with the definition of the normal burning velocity.

[7] Sherratt and Linnett, Trans. Faraday Soc. 44, 596 (1948).

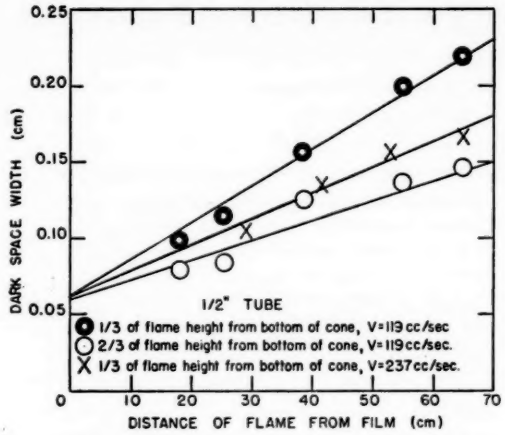

FIG. 4. Extrapolation of dark space width to the flame.

EXPERIMENTAL METHOD AND JUSTIFICATION

Sherratt and Linnett[7] have used the line between the dark and the light space (inside line of dark space in Fig. 1) to measure the burning velocity. This gives a burning velocity that is too large because the width of the dark space increases with increasing radius of curvature and with distance from the diametral plane of the flame to the photographic plate.[8] This is illustrated in Fig. 2.

Since the width of the dark space decreases as the film is brought close to the flame, the velocity, V/A, determined from numerical integration of the area defined by the line between the dark and light spaces and from the flow rate, also decreases. It is found that if V/A, determined in this manner, is extrapolated back to zero distance between the flame and the film, the velocity obtained agrees with the normal burning velocity obtained with stroboscopically illuminated particles.[5] This is shown in Fig. 3, which illustrates the extrapolation for 4.12 percent propane-air flames under widely varying flow conditions. It is apparent that 45.5 cm/sec. is obtained from the extrapolation of V/A. This value agrees well with 45.0 cm/sec. from the particle method.[5]

[8] Keenan and Polachek, Nav. Ord. Report No. 86–46.

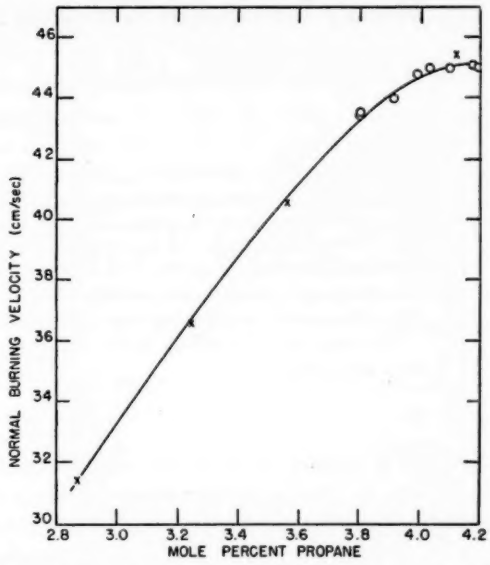

FIG. 5. Normal burning velocities of propane-air mixtures. ○—measured by stroboscopically illuminated particle tracks. ×—measured by shadow photographs.

On the presumption that this method of determining the flame area is correct, the width of the dark space at zero distance should correspond to the length of the temperature gradient through the flame (since the outer edge of the dark space indicates the top of the temperature gradient). Figure 4 shows the extrapolation of dark space widths determined with a pair of dividers, for the 4.12 percent propane-air flame. The extrapolated width of 0.6 mm is in good agreement with the length of the steep portion of the temperature gradient.[5,9]

From the preceding evidence, it is concluded that this is an accurate technique for the determination of the normal burning velocity. The method has been used to supplement the data obtained by the particle method for lean propane-air flames and the results are presented in Fig. 5.

[9] St. John and Olsen, UW/APL, CM Report No. 549 (1949).

THE JOURNAL OF CHEMICAL PHYSICS VOLUME 18, NUMBER 4 APRIL, 1950

Energy Levels and Thermodynamic Properties of the Internal Rotator

J. O. HALFORD
Chemistry Department, University of Michigan, Ann Arbor, Michigan

(Received August 31, 1949)

To facilitate the calculation of the thermodynamic properties of internal rotators lying outside the limits of available tabulations, methods of determining the energy levels are studied for the purpose of finding the most expeditious route to accurate results. It proves to be unnecessary in any case to calculate many levels from the wave mechanics. A partition function is set up in terms of the correct ground state and a series of approximate levels derived from the old quantum theory, and this is corrected to constancy by the successive substitution of correct levels, starting with the first excited state. A set of levels obtained in this way which gives the correct partition function always leads to correct values of all the thermodynamic properties.

To obtain accurate energy levels, the continued fractions of Koehler and Dennison are recommended as most convenient.

EXTENSIVE tables of the four thermodynamic properties of the hindered internal rotator have been published by Pitzer and Gwinn.[1] These tables are based upon energy levels obtained from rigorously derived relations for a system of two coaxial rotators, one symmetrical, the other "accidentally" symmetrical, and are recommended as accurate enought for the more general case of a rigid framework with non-interacting symmetrical tops attached at any angles. The energy levels come out as regions within which individual levels may appear, such that for any fixed combination of quantum states of the remaining degrees of freedom, a particular level is determined within each region, and, by numerical summation, a partition function and the derivable thermodynamic properties are determined.

For a given temperature, potential barrier, moment of inertia and symmetry number, there are two limiting values of each property of the internal rotator between which the representative average value must lie. Pitzer and Gwinn[1] found it unnecessary to develop a valid solution for the average, but limited their calculations to those regions of the variables in which the differences between the limiting values are negligible, and found that they had apparently covered all cases for which the tables were likely to be used.

The recent accurate determination of a low potential barrier and a low internal moment of inertia from spectroscopic data for methyl alcohol by Burkhard and Dennison[2] places this compound well outside the limits of the Pitzer and Gwinn[1] tabulations and probably means that there will be other cases as well which are not covered by the tables.

As yet there appears to be no basis upon which any considerable general extension of the tables could be founded, and, even if there were, the extension could hardly be justified when few compounds are expected to require it. In order to deal with the methyl alcohol case, for which the thermodynamic properties are now being calculated, available methods of setting up the required energy levels, or regions of energy levels, have been examined, and a scheme had been devised which makes liberal use of rapidly calculated old quantum theory levels at higher energies. In this paper this scheme is developed and illustrated with cases lying within the limits of the tables of Pitzer and Gwinn.[1]

The energy levels used by Pitzer and Gwinn[1] were obtained from Hill's determinant and an equation representing a theorem discovered by Hill.[3] The description of the actual calculation is extremely brief and is likely to give the reader the impression that the required levels can be obtained only with extensive laborious calculations. An equivalent solution, developed by Koehler and Dennison[4] for the simple cosine potential function and the symmetry number 3, is readily generalized for all symmetry numbers, contains the coupling constant within the determinant, thereby eliminating the need for Hill's theorem, and can be expressed in terms of infinite continued fractions which are easier to solve than the determinant. As compared with Hill's determinant, which includes solutions for more complicated potential functions, the simple continued fractions are limited to the form $V=V_0(1-\cos nx)/2$, but they contain all the information necessary to calculate the available tabulated properties.

An outline of the derivation of the continued fractions, following Koehler and Dennison[3] except for the introduction of the general symmetry number n, is given below. The wave equation for the internal motion is:

$$d^2M/dx^2+(R+2\alpha\cos nx)M=0. \tag{1}$$

The solution has the form

$$M=e^{i\sigma x}\sum_{-\infty}^{+\infty}a_r e^{irx} \tag{2}$$

in which the a_r are Fourier coefficients, and $\sigma=-KC_1/C$ where K is the quantum number of the rotation of the whole molecule around the axis of the internal rotation,

[1] K. S. Pitzer and W. D. Gwinn, J. Chem. Phys. **10**, 428 (1942).
[2] D. G. Burkhard and D. M. Dennison, private communication.
[3] Hill, Whittaker, and Watson, *Modern Analysis* (Cambridge University Press, London, 1935), p. 413.
[4] J. S. Koehler and D. M. Dennison, Phys. Rev. **57**, 1006 (1940).

C_1 is the moment of inertia of one of the coaxial rotators, and C is the sum of the moments of the two rotating parts. The symmetry number of the symmetrical top appears as n in Eq. (1). By substituting from Eq. (2) and its differentiated forms into Eq. (1) and recognizing that the coefficient of each $e^{i\tau x}$ must be zero, the valid solutions are obtained as those which conform to the recursion formula

$$\frac{\alpha}{R-(\sigma+\tau)^2}a_{\tau-n}+a_\tau+\frac{\alpha}{R-(\sigma+\tau)^2}a_{\tau+n}=0. \quad (3)$$

Equation (3), in effect, divides the a_τ into n sets, for each of which a determinant of the coefficients can be set equal to zero, or a more convenient equation in continued fractions can be written. Present purposes require only the solution derived from those Eqs. (3) which contain a_0, a_{-n}, a_n, etc. The continued fraction is obtained by setting an arbitrary a_τ, where τ is large, equal to zero, and expressing each lower a_τ in terms of $a_{\tau-n}$ until a_{-n} and a_n are obtained in terms of a_0. The Eq. (3) centered on a_0 then becomes

$$-\cfrac{\alpha^2}{\{0\}\{-n\}}\qquad +1-\cfrac{\alpha^2}{\{0\}\{n\}}\qquad =0 \quad (4)$$

$$1-\cfrac{\alpha^2}{\{-n\}\{-2n\}}\qquad 1-\cfrac{\alpha^2}{\{n\}\{2n\}}$$

$$1-\cfrac{\alpha^2}{\{-2n\}\{-3n\}}\qquad 1-\cfrac{\alpha^2}{\{2n\}\{3n\}}$$

$$1-\text{etc.}\qquad 1-\text{etc.}$$

in which $R-(\sigma+n)^2$ is represented by $\{n\}$. From the definition of α,

$$\alpha=2\pi^2cC_1C_2H/hC, \quad (5)$$

where H is the barrier height in wave numbers and C_1C_2/C is the reduced internal moment of inertia, combined with the classical partition function of the limiting free rotator,

$$Q_f=(8\pi^3C_1C_2kT/n^2Ch^2)^{\frac{1}{2}}; \quad (6)$$

it follows that

$$\alpha=n^2Q_f^2Hch/4\pi kT=(n^2/4\pi)Q_f^2V/\mathrm{R}T. \quad (7)$$

In Eq. (7), and subsequently where the fraction $V/\mathrm{R}T$ appears, R is the gas constant and V is the potential barrier in the same energy units. Here α is expressed in terms of the variables tabulated by Pitzer and Gwinn.[1]

For the energy corresponding to a given value of the characteristic number R,

$$W(cm^{-1})=hC(R+2\alpha)/8\pi^2cC_1C_2=H(R+2\alpha)/4\alpha \quad (8)$$

which takes the more convenient form for calculating thermodynamic properties

$$W/H(=E/V)=R/4\alpha+\tfrac{1}{2}, \quad (9)$$

where the energy appears as a ratio to the barrier height which is independent of the units of energy.

At a fixed value of σ/n and a given Q_f and $V/\mathrm{R}T$, the α introduced into Eq. (4) is proportional to n^2, and consequently the derived R will also be proportional to n^2. Therefore E/V (Eq. (9)) is independent of the symmetry number, and the energy level system at constant σ/n will always be the same for a given value of $Q_f(V/\mathrm{R}T)^{\frac{1}{2}}$.

The energy levels from Eq. (4) are periodic in σ, repeating themselves each time this quantity is changed by n units. For a given continuous region of energy levels, all possible numerical values will occur between $\sigma=0$ and $\sigma=\pm n/2$. To obtain the tabulated results of Pitzer and Gwinn,[1] two sets of levels, one for $\sigma=0$, the other for $\sigma=\pm n/2$, are used at each point.

The selection of $-KC_1/C$ for σ gives the result an apparent asymmetry which is interesting because either moment of inertia could be defined as C_1. The actual boundary conditions are, more generally, $KC_1/C+\sigma=S_1$ and $KC_2/C-\sigma=S_2$ where S_1 and S_2 must be integers. If, as in the above definition, either S_1 or S_2 is given an arbitrary value, a complete set of energy levels will be obtained, such that, for a given value of K, a level of a particular symmetry class always appears at the same energy. The solution, however, may come from any one of the n equations of the type of Eq. (4), according to what integer has been selected for S_1 or S_2.

To obtain the ratios E/V (Eq. (9)) which define the energy levels, σ is chosen, α is calculated and the R values which satisfy Eq. (4) are found by successive approximation. If the energy regions are numbered off, starting with zero, the condition $\sigma=0$ corresponds to the lower limits of the even numbered regions and the upper limits of the odd-numbered regions. For this condition, Eq. (4) takes the form

$$\cfrac{\cfrac{\alpha^2}{\{0\}\{n\}}}{1-\cfrac{\alpha^2}{\{n\}\{2n\}}}{\Big/}1-\text{etc.}=0.5. \quad (10)$$

When, however, Eq. (10) is used, it develops that only the lower limits of the even numbered regions are directly obtainable, while a singularity is encountered in each region where one of the other solutions is expected to lie. These singularities prove to be valid solutions. Apparently, the derivation of Eq. (4), which involves a succession of divisions, has included an inadvertent division by zero for the case $\sigma=0$. If an appropriate portion of the corresponding determinant of the coefficients is expanded, the determinant is

TABLE I. Energy levels, internal rotator, $n=3$, $\alpha^2=10$.

	$\sigma=0$			$\sigma=\pm 3/2$	
l	R	$\Delta E/V$	l	R	$\Delta E/V$
0	−1.88346	0	0	−1.37838	0.039931
1	+8.63274	0.831381	1	+4.75855	0.525097
2	10.50870	0.979687	2	20.43826	1.764687
3	36.14499	3.006413	3	20.62572	1.779507
4	36.15251	3.007008	4	56.34264	4.603177
5	81.06352	6.557534	5	56.34280	4.603190
6	81.06353	6.557535	6, 7	110.29631	8.868589
7, 8	144.03528	11.535888			

reduced to zero by the condition,

$$1-\cfrac{\alpha^2}{\{n\}\{2n\}\;\;=0,} \qquad (11)$$
$$1-\cfrac{\alpha^2}{\{2n\}\{3n\}}$$
$$1-\text{etc.}$$

which gives the R values for the upper limits of the odd-numbered regions. Further, for $\sigma=0$, the determinant can be factored into two parts corresponding, respectively, to Eq. (10) and Eq. (11).

At the opposite limits, for $\sigma=-n/2$, $\{0\}$ becomes equal to $\{n\}$, $\{-n\}$ to $\{2n\}$, etc., leading to the equation

$$1-\cfrac{\alpha^2}{\{n\}\{2n\}\;\;=\pm\dfrac{\alpha}{\{0\},}} \qquad (12)$$
$$1-\cfrac{\alpha^2}{\{2n\}\{3n\}}$$
$$1-\text{etc.}$$

in which the negative roots go with the even-numbered regions, the positive roots with the odd-numbered ones.

To reproduce the tables of Pitzer and Gwinn,[1] sets of energy levels according to Eqs. (7), (9), (10), (11) and (12) can be obtained for values of α/n^2 chosen at appropriate intervals, and from each set a series of points running through each table according to Eq. (7) can be obtained, again at chosen intervals. For present purposes, interest is centered upon low values of α/n^2 for which fewer than three complete regions of levels lie within the potential valley. For higher values of α/n^2, which cover the major part of the tabulations, it has already been shown that the old quantum theory, with an arbitrary assignment of quantum numbers, will yield accurate results.[5] These can be obtained most expeditiously with the aid of a subsequently published table.[6]

It is now of interest to inquire, for the region of low α/n^2, that is, the region of widely spaced levels relative to the barrier height, how and to what extent the old quantum theory can be used to expedite the calculation without undue loss of accuracy. For this purpose, the limiting free rotator is examined. According to Hill's theorem, the free rotator solutions follow the equation

$$W=\frac{Rh^2C}{8\pi^2C_1C_2}. \qquad (13)$$

If R is the square of an integral multiple of n, the solutions correspond to $\sigma=0$, while for R equal to $[n(2S+1)/2]^2$, where S is an integer, the results are valid for $\sigma=\pm n/2$. Each level except the lowest is both the upper limit of one region and the lower limit of the next, and the forbidden energies between the eligible regions have disappeared.

Equation (13), for $\sigma=0$, is also the old quantum theory solution for the one-dimensional rotator, and, if the privilege of assigning the intervening half quantum numbers is assumed, the free rotator solution can be said to have been derived from the old quantum theory. Further, since the level system of the hindered rotator rapidly takes on the character of free rotation as the energy increases, there must be some point beyond which the old quantum theory energy levels can be substituted for the more accurate ones without undue loss of accuracy, even when the barrier is appreciable.

The results of a series of old quantum theory graphical integrations are contained in a previously published table[6] which gives E/V as a function of an index ρ which is defined as:

$$\rho=r/[Q_f(V/RT)^{\frac{1}{2}}]. \qquad (14)$$

If the hindered rotator is treated like the free rotator, the corresponding assignment of integers and half-integers to r will again divide the energy space into contiguous regions which should be the same as the correct regions at high energies. At lower energies, the old quantum theory solutions will lie in the forbidden spaces, and each one will represent some kind of an average of the upper limit of one region and the lower limit of the next.

It is proposed to minimize the rather laborious use of Eqs. (10), (11) and (12) in the calculation of thermodynamic properties in the following manner. The old quantum theory limits of the regions are first laid out. Then, starting at the lowest energies, the correct levels are successively substituted until further substitution no longer appreciably changes the partition function or its derivatives. In general, an accurate result will require at least one solution of Eq. (10) and the first pair of solutions of Eq. (12), while the further substitution of accurate levels will depend upon the particular system being evaluated and the desired accuracy of the result.

The proposed method is illustrated below by calculations for the case $\alpha^2=10$, $n=3$, that is, for $1/[Q_f(V/RT)^{\frac{1}{2}}]=0.4759$. For any other symmetry number n', the same energies would be obtained with

[5] J. O Halford, J. Chem. Phys. **15**, 645 (1947).
[6] J. O. Halford, J. Chem. Phys. **16**, 410 (1948), Table II.

TABLE II. Energy levels, internal rotator, $1/[Q_f(V/RT)^{\frac{1}{2}}]=0.4759$ from old quantum theory graphical integrals.

$\sigma=0$		$\sigma=\pm 3/2$	
l	E/V	l	E/V
0	0	0, 1	0.7413
1, 2	1.2575	2, 3	2.1209
3, 4	3.3572	4, 5	4.9545
5, 6	6.9081	6, 7	9.2198
7, 8	11.8857	8, 9	14.9144
9, 10	18.2895	10, 11	22.0490
11, 12	26.1156	12, 13	30.5470
13, 14	35.3649	14, 15	40.5244
15, 16	46.0374	16, 17	51.9085
17, 18	58.1329	18, 19	64.7158
19, 20	71.6514	20, 21	78.9460
21, 22	86.5932	22, 23	94.5993
23, 24	102.9578	24, 25	111.6757
25, 26	120.7456	26, 27	130.1750

$\alpha'=(n')^2\alpha/9$. For all values of V/RT below 1.2, the properties will fall within the limits of the tables of Pitzer and Gwinn.[1] Table I shows the R values from Eqs. (10), (11) and (12). On the left are the solutions for $\sigma=0$, on the right those for $\sigma=\pm\frac{3}{2}$.

Table II contains the approximations to the same limiting levels given by the old quantum theory.

Calculations are now carried out for $V/RT=1.0$, $1/Q_f=0.4759$. First, Q is added for the case $\sigma=0$ with all levels except the lowest taken from the old quantum theory, then the sum is corrected by substituting the values for $l=1$ and $l=2$ for the corresponding old quantum theory approximation, the substitution is then made for $l=3$ and 4, etc., as shown in Table III. For $\sigma=\frac{3}{2}$, the first summation involves entirely old quantum theory levels, referred, however, to the accurate lowest level for $\sigma=0$ as the zero of energies. Substitutions are then made as indicated in the table. Except for the first row, all of the partition functions lead to the same result, $-F/T=1.289$, $(F-F_f)/T=0.187$. By linear interpolation, from Table II of Pitzer and Gwinn,[1] the latter value is 0.185. For this case the free energy has been accurately reproduced with five correct energy levels, although in an independent calculation it would be necessary to increase this number to nine in order to be sure of the accuracy of the result.

In Table IV, the sum $Q'=\sum(\Delta E/RT)e^{-\Delta E/RT}$ is examined in the same way, for the purpose of calculating $H/T=RQ'/Q$ and $S=(H-F)/T$. The values in the second and subsequent rows, used either with the corresponding Q's or the limiting Q's from Table III, all lead to 1.087 for H/T, against 1.085 from Pitzer and Gwinn.[1] The entropy, $S_f-S=0.093$, equals the Pitzer and Gwinn value. Again five accurate energy levels suffice.

The heat capacity is now calculated, for which purpose $Q''=\sum(\Delta E/RT)^2e^{-\Delta E/RT}$, as shown in Table V. Again, all of the summations except the first row lead to the same heat capacity, 1.151 at $\sigma=0$, and 1.150 at $\sigma=\frac{3}{2}$ as against 1.149 from the tables of Pitzer and Gwinn.[1]

TABLE III. Partition function, internal rotator, $\alpha^2=10$, $n=3$, $1/[Q_f(V/RT)^{\frac{1}{2}}]=0.4759$, $V=RT$, referred to correct zero energy level.

$\sigma=0$ Levels from quantum theory			$\sigma=\pm 3/2$ Levels from quantum theory		
New	Old	Q	New	Old	Q
0	1 etc.	1.90980		0 etc.	1.71490
0, 1, 2	3 etc.	1.91272	0, 1	2 etc.	1.91337
0–4	5 etc.	1.91265	0–3	4 etc.	1.91259
all		1.91265	all		1.91264

TABLE IV. Internal rotator, $\alpha^2=10$, $n=3$, $1/[Q_f(V/RT)^{\frac{1}{2}}]$ 0.4759, Sum $Q'=\Sigma(\Delta E/RT)e^{-\Delta E/RT}$.

$\sigma=0$ Levels from quantum theory			$\sigma=\pm 3/2$ Levels from quantum theory		
New	Old	Q'	New	Old	Q'
0	1 etc.	1.04876		0 etc.	1.22606
0–2	3 etc.	1.04624	0, 1	2 etc.	1.04676
0–4	5 etc.	1.04610	0–3	4 etc.	1.04615
all		1.04610	all		1.04615

For the particular case here illustrated, accurate values of all the thermodynamic properties have been obtained with only five levels derived from the wave mechanics, while the rest are introduced as approximate averages from the old quantum theory. In order to be sure of the result, however, without bringing outside experience into the problem, it would be necessary to increase the number of accurate levels to seven or nine. It appears from these calculations that, whenever the upper limit of one region is close enough to the lower limit of the next, the substitution of an old quantum theory average can be made. Since the required proximity of the two limits is determined by the ratio E/V (i.e., W/H), the illustration indicates that the substitution can be made whenever this ratio lies above 1.5.

This statement can be tested, with the above set of energy levels, at other values of V/RT. If the approximation is accurate at $V/RT=0.20$ ($1/Q_f=0.2128$), it is reasonable to say that it will be satisfactory at all values of V/RT between 0.20 and 1.00. The results, with only five accurate levels, three at $\sigma=0$ and two at $\sigma=3/2$, are summarized in Table VI. The last row gives the results obtained by interpolation from the tables of Pitzer and Gwinn.[1] The two correct levels for l equal to 1 and 2 at $\sigma=0$ are not essential to the production of an accurate result at this point. Consequently, the result at $\sigma=0$ can be reproduced exactly as tabulated with only one level correctly evaluated.

To the writer's knowledge, the tabulations of Pitzer and Gwinn have never been independently checked. It may therefore be of some interest that the thermodynamic properties obtained with the energy levels of Table I at several points within the limits of the Pitzer and Gwinn tabulations have always been very close to the tabulated values. A similar set of checks with

TABLE V. Internal rotator, $\alpha^2=10$, $n=3$; $1/[Q_f(V/RT)^{\frac{1}{2}}]=0.4759$
Sum $Q''=\Sigma(\Delta E/RT)^2 e^{-\Delta E/RT}$.

$\sigma=0$ Levels from quantum theory			$\sigma=\pm 3/2$ Levels from quantum theory		
New	Old	Q''	New	Old	Q''
0	1 etc.	1.68327		0 etc.	1.72034
0–2	3 etc.	1.68078	0, 1	2 etc.	1.67884
0–4	5 etc.	1.68051	0–3	4 etc.	1.67912
all		1.68059	all		1.67914

TABLE VI. Internal rotator at $1/Q_f=0.2128$, $V/RT=0.2$.

	$(F-F_f)/T$	H/T	S_f-S	C
$\sigma=0$	0.055	1.043	0.005	1.002
$\sigma=n/2$	0.055	1.043	0.005	1.003
P & G	0.057	1.045	0.004	1.001

energy levels for the case $\alpha^2=100$, $1/[Q_f(V/RT)^{\frac{1}{2}}]=0.26762$, has likewise produced complete agreement. These levels are shown in Table VII.

Tables I and VII contain solutions for fairly high values of R, and a few comments upon their derivation from Eqs. (10), (11) and (12) may be in order, although the results of Tables III–VI, inclusive, show that it will not, in general, be necessary to make such evaluations. Since, in general, R must lie between two of the quantities $(\sigma+\tau)^2$ and $(\sigma+\tau+n)^2$, all of the fractions $\alpha^2/[\{\tau\}\{\tau+n\}]$ will be positive except the one for which R lies between the two squares appearing in the denominator. In the numerically evaluated continued fraction, there will therefore be one plus sign, which will appear further down the fraction for the successively higher values of R. Beyond this point, the fractions always converge rapidly. Since the continued fractions are equivalent to a determinant of the coefficients of the Eqs. (3), and a solution could be obtained from a limited part of the determinant centered around the point corresponding to the above plus sign, it should be possible to dispense with much of the superstructure of the continued fraction. When the point is reached at which two values of R are indistinguishable (e.g., $l=7$, 8 for $\sigma=0$ in Table VII), it is found in this connection that the solution may be obtained by setting a part of the continued fraction equal to zero. For R between $\{\tau\}$ and $\{\tau+n\}$, the following equation gives an accurate enough solution for the higher energy levels.

TABLE VII. Energy levels, internal rotator, $n=3$, $\alpha^2=100$.

	$\sigma=0$			$\sigma=3/2$	
l	R	$\Delta E/V$	l	R	$\Delta E/V$
0	−11.1345	0	0	−11.0997	0.00087
1	5.5634	0.41745	1	4.8165	0.39878
2	16.0374	0.67930	2	20.8324	0.79917
3	37.2109	1.20864	3	24.8658	0.90001
4	37.8690	1.22509	4	57.1643	1.70747
5	81.6375	2.31930	5	57.2140	1.70871
6	81.6399	2.31936	6	110.7146	3.04623
7, 8	144.3330	3.88669	7	110.7147	3.04623

$$1-\cfrac{\alpha^2}{\{\tau-2n\}\{\tau-n\}}\Bigg/1-\cfrac{\alpha^2}{\{\tau-n\}\{\tau\}}\Bigg/1-\cfrac{\alpha^2}{\{\tau\}\{\tau+n\}}\Big/1-\text{etc.}=0. \tag{14}$$

From the above examples and the results of an earlier paper,[5] the following conclusions can be drawn. If three or more old quantum theory vibrational states lie below the top of the barrier (i.e., if $1/[Q_f(V/RT)^{\frac{1}{2}}]<0.287$), the thermodynamic properties can be obtained accurately with the old quantum theory alone. For $1/[Q_f(V/RT)^{\frac{1}{2}}]>0.287$, only a few of the now widely spaced lower levels, up to about $E=1.5\,V$, need to be derived accurately from the wave mechanics. It should be clearly understood that, in the above two regions, the assignment of quantum numbers in the old quantum theory is made in different ways.

For the calculations now in progress for methyl alcohol, which lie outside the limits of present tabulations, it may prove to be necessay, in using old quantum theory levels, to introduce their dependence upon K in a proper way. If K, and therefore σ, is taken for some point between the limits $\sigma=0$ and $\sigma=\pm n/2$, it is valid to assign the old quantum theory numbers in the free rotator limit on a linear scale. This linear assignment, by analogy to the methods developed here, will then be carried over to the hindered rotator.

On the Thermodynamic Relation between Surface Tension and Curvature

FREDERICK O. KOENIG
Stanford University, California

(Received September 12, 1949)

From the Gibbs theory of surface tension general equations are deduced for the change of surface tension with curvature in the system having an arbitrary number of components but no insoluble surface film. For the special case that the surface layer is spherical, the equations are shown to be reducible, by an appropriate choice of auxiliary Gibbs surfaces, to a simple form identical with that recently found by Tolman for the system of one component. Some of the consequences of physical interest following from the equation for the spherical surface layer are pointed out.

I. INTRODUCTION

In a recent article R. C. Tolman has deduced, from the Gibbs theory of surface tension, two exact thermodynamic equations relating surface tension to radius of curvature.[1] Tolman's analysis is confined to the case of a pure liquid in equilibrium with its vapor, that is, to a system of one component. This system has two degrees of freedom, as which Tolman naturally takes, in addition to the radius, the temperature. Although in his discussion Tolman refers only to spherical droplets, actually only the second of his two chief equations (Eq. T(4.1) is restricted to this case; the first (Eq. T(2.6)) applies to a surface of any shape compatible with equilibrium (provided the "radius" is taken to be the harmonic mean of the principal radii of curvature). Our object in the present article is to extend the investigation to the system containing an arbitrary number of components, but no insoluble surface film (Part II, §A). We shall do this in the most general way which seems at all useful, by taking a set of independent variables whose members, except for curvature and temperature, remain unspecified (Part II, §§B, C, D). We shall then find in the first place (Part III), that we can deduce two equations (Eqs. (31) and (44)) which jointly constitute a generalization of Eq. T(2.6), and whose form is such that it permits ready deduction of special equations for the experimental situations ordinarily encountered in surface tension measurement (with independent variables completely specified, see Part III, §C); and we shall find in the second place (Part IV), that our two equations, (31) and (44), are reducible, for the special case of the spherical surface layer, to a single equation (Eq. (80) or (81)) which not only constitutes a generalization of Eq. T(4.1), but also is identical in form with the latter. This finding for the spherical surface layer is valuable because it leads (Part V), for the multicomponent case here considered, to conclusions of physical interest much like those reached by Tolman for the case of one component.

In his article Tolman has given a review of previous inquiries into the relation between surface tension and curvature. We may supplement this review by calling attention to the contributions of Defay[2] and of Guggenheim.[3] Defay has carried out a systematic theoretical study of the thermodynamics of surface layers, based upon the theory of Gibbs as extended by DeDonder to include irreversible chemical reactions. In this study Defay deduces, in addition to an equation already given by Gibbs[4] for change of surface tension with curvature, also a new equation with which our Eq. (47) is identical. Guggenheim has given an instructive analysis of the thermodynamics of surface layers in multicomponent systems, based upon the theory of Bakker and of Verschaffelt—which differs markedly from the Gibbs theory, in that it employs not a single geometrical dividing surface, but rather two such surfaces, one on each side of the inhomogeneous region. At the end of his article Guggenheim discusses the effect of curvature upon surface tension, and, without deducing equations for this effect, gives an argument to show that it is negligibly small under the conditions ordinarily obtaining in the experimental measurement of surface tension.

II. ASSUMPTIONS

A. Specification of the System to Be Studied

Our system is specified by the following five conditions: (i) It consists of two effectively homogeneous fluid masses (i.e. phases) in contact, and of the inhomogeneous layer (to be called the "surface layer") formed by this contact; (ii) it has an arbitrary number, κ, of independent components, each of which is present in

[1] R. C. Tolman, J. Chem. Phys. **17**, 333 (1949). The two equations in question are (2.6) and (4.1) of Tolman's article, and we shall henceforth refer to them as Eqs. T(2.6) and T(4.1). We need not quote these equations at this point because we shall meet them later in the present article: Our Eq. (48) is equivalent to Eq. T(2.6) and our Eq. (81) is identical in form with Eq. T(4.1). We shall similarly designate with a "T" the other equations of Tolman's article to which we shall have occasion to refer.

[2] R. Defay, "Étude Thermodynamique de la Tension Superficielle" (Extrait des Bulletins de l'Académie Royale de Belgique (Classe des Sciences). (Années 1929, 1930 et 1931) (Marcel Hayez, Brussels, 1931). See Eqs. (206) to (217) of this monograph.

[3] E. A. Guggenheim, Trans. Faraday Soc. **36**, 397 (1939).

[4] J. W. Gibbs, *Collected Works* (Longmans, Green and Company, New York, 1928), Vol. I. The equation in question is the next to the last on p. 232. Owing to the nature of its independent variables, this equation is not directly applicable to experimental situations of the usual type, except when the number of components is unity, in which case the equation becomes identical with Eq. T(2.6).

at least one of the two phases (i.e. no component is present only in the surface layer); (iii) external fields of force are absent; (iv) it is in mechanical, thermal and chemical equilibrium, and this equilibrium is stable; (v) the surface layer is curved in any way compatible with equilibrium, and the radii of curvature are great compared to 1A. It will be convenient to refer to the two phases of the system by α and β, respectively, and to its surface layer by ω.

B. Curvature as a Variable of State

We denote the principal curvatures at any point of the surface of tension[5] by q_1 and q_2, and their arithmetic mean by q, i.e.[6]

$$q=\tfrac{1}{2}(q_1+q_2).$$

For any given state of the system the quantities q_1 and q_2 in general vary from point to point of the surface of tension, but always in such a way that q remains constant. This follows from the conditions for the mechanical equilibrium of the system (strictly valid only in the absence of a gravitational field):

$$P^\alpha=\text{const.},\quad P^\beta=\text{const.},\quad P^\alpha-P^\beta=2\sigma q, \tag{1}$$

in which P^α and P^β are the pressures of the phases α and β respectively, and σ is the surface tension. The quantity q is thus seen to be a variable of state, and we shall call it for simplicity "the curvature." It is furthermore to be noted that, since in a stable system σ is always positive, Eq. (1) implies the convention that q is positive or negative, according as the index α or the index β has been assigned to the phase having the greater pressure. The variable q thus has the range $-\infty<q<\infty$. Finally we may note that, since q is defined at every point of a specified geometrical region (in this case a two-dimensional region, the surface of tension) within the system, it may be regarded as an intensive variable.

In this article we shall take q as our principal variable of differentiation (i.e. we shall seek expressions for the derivatives $\partial\sigma/\partial q$. Instead of q one could of course choose its reciprocal, $r=1/q$ (which may be seen to be equal to the harmonic mean of the principal radii of curvature), as the variable of differentiation; and this is what Tolman does (i.e. he calculates $\partial\sigma/\partial r$). The variable q is however more convenient, because q is continuous over all the states of the system, whereas r has a discontinuity ($r=\pm\infty$) when the surface layer is plane.

C. The Independent Variables

If, in the system specified above, the surface layer were constrained to remain plane ($q=0$), the system would obey the phase rule, and would therefore have κ degrees of freedom. Removal of this constraint evidently increases the number of degrees of freedom by one. The system specified therefore has $\kappa+1$ degrees of freedom, or in other words, $\kappa+1$ independent intensive variables are necessary and sufficient to fix each of the other intensive variables. Since the curvature q is an intensive variable, sets of $\kappa+1$ independent intensive variables can be chosen which contain q. In the present investigation we shall use sets of independent variables which contain, in addition to the curvature q, also the temperature T, and whose other members are unspecified. We shall denote this set of generalized independent variables by q, T, $x_3\cdots x_{\kappa+1}$. We may then formulate our object as follows: to deduce expressions for the derivatives, $\partial\sigma/\partial q$, of the functions:

$$\sigma=\sigma(q, T, x_3\cdots x_{\kappa+1}). \tag{2}$$

In pursuing this object we shall exclude the case in which the set $x_3\cdots x_{\kappa+1}$ contains simultaneously P^α (or a function of P^α), and P^β (or a function of P^β), because Eq. (1) requires that in this case the function on the right side of Eq. (2) reduces to $(P^\alpha-P^\beta)/2q$.

D. Case A and Case B

In calculating the derivatives $\partial\sigma/\partial q$ corresponding to Eq. (2), we shall need to give separate consideration to the two following cases, which we shall call Case A and Case B, respectively. Case A: the set $x_3\cdots x_{\kappa+1}$ does not contain P^α (or a function of P^α); Case B: the set $x_3\cdots x_{\kappa+1}$ contains P^α (or a function of P^α). In Case B we shall write Eq. (2) in the form:

$$\sigma=\sigma(q, T, P^\alpha, x_4\cdots x_{\kappa+1}).$$

We shall refer to the sets q, T, $x_3\cdots x_{\kappa+1}$, (without P^α), and q, T, P^α, $x_4\cdots x_{\kappa+1}$, as Set A and Set B respectively. It is important to note that Set A, although it does not contain P^α, may or may not contain P^β, but that Set B (owing to the restriction made above in Part II, §C) does not contain P^β.

E. Classification of the Components

To attain our object we shall need to divide the κ components of the system into three classes, to be called Classes 1, 2, and 3 respectively, and defined as follows. Class 1: those components appreciably present in both phase α and phase β; Class 2: those appreciably present in α but not in β; Class 3: those appreciably present in β but not in α. We shall denote the number of components in Class 1 by κ', in Class 2 by κ'', and in Class 3 by κ''', and furthermore, the total number of components appreciably present in α by κ^α, and the total number appreciably present in β by κ^β. We note the relations:

$$\kappa=\kappa'+\kappa''+\kappa''', \tag{3}$$

$$\kappa^\alpha=\kappa'+\kappa'', \tag{4}$$

$$\kappa^\beta=\kappa'+\kappa'''. \tag{5}$$

[5] For the definition of the surface of tension see J. W. Gibbs, reference 4, pp. 227–229; also R. C. Tolman, J. Chem. Phys. **16**, 758 (1948); for criticism of Gibb's exposition see E. A. Guggenheim, reference 3.

[6] We use q_1, q_2 and q rather than the more customary c_1, c_2 and c because we shall later need c_i to denote concentration of the ith component.

F. Notation

We shall denote the surface concentrations of the components of Class 1 by $\Gamma_1' \cdots \Gamma_{\kappa'}'$, of the components of Class 2 by $\Gamma_1'' \cdots \Gamma_{\kappa''}''$, of the components of Class 3 by $\Gamma_1''' \cdots \Gamma_{\kappa'''}'''$, and of all the components without reference to the three classes, by $\Gamma_1 \cdots \Gamma_\kappa$. We shall denote the chemical potentials of the components of Class 2 by $\mu_1''^\alpha \cdots \mu_{\kappa''}''^\alpha$, and of Class 3 by $\mu_1'''^\beta \cdots \mu_{\kappa'''}'''^\beta$, and we shall write the conditions for the heterogeneous chemical equilibrium between the phases α and β, in which the components of Class 1 alone are involved, in the form:

$$\mu_i'^\alpha = \mu_i'^\beta \quad (i = 1 \cdots \kappa'). \tag{6}$$

And we shall denote the chemical potentials of all the components, without reference to the three classes, by $\mu_1 \cdots \mu_\kappa$. We shall denote the mole fractions, in phase α, of the components there present (Classes 1 and 2), by $N_1'^\alpha \cdots N_{\kappa'}'^\alpha$, $N_1''^\alpha \cdots N_{\kappa''}''^\alpha$, or alternatively, when there is no need to distinguish between the classes, by $N_1^\alpha \cdots N_\kappa^\alpha$; and likewise we shall denote the mole fractions, in phase β, of the components there present (Classes 1 and 3) by $N_1'^\beta \cdots N_{\kappa'}'^\beta$, $N_1'''^\beta \cdots N_{\kappa'''}'''^\beta$, or alternatively by $N_1^\beta \cdots N_\kappa^\beta$. We shall denote the partial molal volumes in phase α, of the components there present, by $V_1'^\alpha \cdots V_{\kappa'}'^\alpha$, $V_1''^\alpha \cdots V_{\kappa''}''^\alpha$, and likewise the partial molal volumes in phase β, of the components there present, by $V_1'^\beta \cdots V_{\kappa'}'^\beta$, $V_1'''^\beta \cdots V_{\kappa'''}'''^\beta$. Finally (in Part IV) we shall denote the total number of moles of the components in the system by $n_1' \cdots n_{\kappa'}'$, $n_1'' \cdots n_{\kappa''}''$, $n_1''' \cdots n_{\kappa'''}'''$, or alternatively by $n_1 \cdots n_\kappa$; the volume concentrations in phase α by $c_1'^\alpha \cdots c_{\kappa'}'^\alpha$, $c_1''^\alpha \cdots c_{\kappa''}''^\alpha$, or alternatively by $c_1^\alpha \cdots c_\kappa^\alpha$ with the understanding that $c_i^\alpha = 0$ for each component of Class 3 (note the difference between this scheme and that just introduced for the mole fractions); and the volume concentrations in phase β by $c_1'^\beta \cdots c_{\kappa'}'^\beta$, $c_1'''^\beta \cdots c_{\kappa'''}'''^\beta$, or alternatively by $c_1^\beta \cdots c_\kappa^\beta$ with $c_i^\beta = 0$ for each component of Class 2.

G. Gibb's Adsorption Theorem

The system specified above (Part II, §A) is subject to the familiar equation:

$$d\sigma = -s^\omega dT - \sum_{i=1}^{\kappa} \Gamma_i d\mu_i, \tag{7}$$

in which s^ω denotes the entropy of the surface layer per unit area, and the meanings of the other symbols have already been given. This equation, which is frequently referred to as Gibbs's adsorption theorem, is the principal starting point of our deduction. When, as is here the case, Eq. (7) is to be applied to a *curved* surface layer, it is important to note that the Gibbs surface defining the quantities s^ω and Γ_i *which go into the equation*, is not arbitrary, but is just the surface of tension (already mentioned in Part II, §B). This fact, although apparent from Gibbs's original exposition, has been all too frequently overlooked in subsequent expositions, and we must be grateful to Tolman for having emphasized it in his recent papers (references 1, 5, 10). For our present purpose we shall need to write Eq. (7) so as to distinguish the terms for Classes 1, 2 and 3 as explained above in Part II, §F:

$$d\sigma = -s^\omega dT - \sum_{i=1}^{\kappa'} \Gamma_i' d\mu_i'^\alpha - \sum_{i=1}^{\kappa''} \Gamma_i'' d\mu_i''^\alpha - \sum_{i=1}^{\kappa'''} \Gamma_i''' d\mu_i'''^\beta. \tag{8}$$

H. The Gibbs-Duhem Equations

In addition to Gibbs's adsorption theorem we shall need also the two Gibbs-Duhem equations for the phases α and β respectively. In terms of the notation explained above in Part II, §F, these equations are:

$$\bar{S}^\alpha dT - \bar{V}^\alpha dP^\alpha + \sum_{i=1}^{\kappa'} N_i'^\alpha d\mu_i'^\alpha + \sum_{i=1}^{\kappa''} N_i''^\alpha d\mu_i''^\alpha = 0, \tag{9}$$

$$\bar{S}^\beta dT - \bar{V}^\beta dP^\beta + \sum_{i=1}^{\kappa'} N_i'^\beta d\mu_i'^\beta + \sum_{i=1}^{\kappa'''} N_i'''^\beta d\mu_i'''^\beta = 0, \tag{10}$$

in which $\bar{S}^\alpha$ and $\bar{V}^\alpha$ denote respectively the mean molal entropy and mean molal volume of phase α, and $\bar{S}^\beta$ and $\bar{V}^\beta$ denote the same quantities for phase β.

III. RELATIONS FOR THE SURFACE LAYER OF ARBITRARY SHAPE

A. Treatment of Case A

In addition to

$$\text{Set A:} \quad q,\ T,\ x_3 \cdots x_{\kappa+1}$$

(which, we recall, does not contain P^α), we shall need the following three auxiliary sets of independent variables, to be called Sets I, II and III:

$$\begin{aligned} &\text{Set I:} && P^\alpha,\ T,\ x_3 \cdots x_{\kappa+1}, \\ &\text{Set II:} && P^\alpha,\ T,\ N_2^\alpha \cdots N_\kappa^\alpha, \\ &\text{Set III:} && P^\beta,\ T,\ N_2^\beta \cdots N_\kappa^\beta. \end{aligned}$$

Set I, like Set A, applies to the system specified above in Part II, §A, but Sets II and III do not: Set II applies to the system consisting of phase α *alone* (hence $\kappa^\alpha + 1$ independent intensive variables, in accord with the phase rule), and Set III to the system consisting of phase β alone ($\kappa^\beta + 1$ independent intensive variables). Partial derivatives corresponding to Set A will be written without subscript, and partial derivatives corresponding to the Sets I, II, and III will be distinguished by the subscripts I, II, and III respectively.

From Eq. (8) we deduce for the desired derivative $\partial\sigma/\partial q$:

$$\frac{\partial \sigma}{\partial q} = -\sum_{i=1}^{\kappa'} \frac{\partial \mu_i'^\alpha}{\partial q} \Gamma_i' - \sum_{i=1}^{\kappa''} \frac{\partial \mu_i''^\alpha}{\partial q} \Gamma_i'' - \sum_{i=1}^{\kappa'''} \frac{\partial \mu_i'''^\beta}{\partial q} \Gamma_i'''. \tag{11}$$

We accordingly seek convenient expressions for the derivatives of the potentials $\mu_i'^\alpha$, $\mu_i''^\alpha$, $\mu_i'''^\beta$ occurring

in this equation. For this purpose we note that the quantities $\mu_i'^{\alpha}$ and $\mu_i''^{\alpha}$ are functions of the variables of Set II, and the quantities $\mu_i'''^{\beta}$ are functions of the variables of Set III, and that it therefore follows, in accord with familiar principles, that

$$d\mu_i'^{\alpha}=-S_i'^{\alpha}dT+V_i'^{\alpha}dP^{\alpha}+\sum_{j=2}^{\kappa^{\alpha}}\left(\frac{\partial\mu_i'^{\alpha}}{\partial N_j^{\alpha}}\right)_{\mathrm{II}}dN_j^{\alpha}, \tag{12}$$

$$d\mu_i''^{\alpha}=-S_i''^{\alpha}dT+V_i''^{\alpha}dP^{\alpha}+\sum_{j=2}^{\kappa^{\alpha}}\left(\frac{\partial\mu_i''^{\alpha}}{\partial N_j^{\alpha}}\right)_{\mathrm{II}}dN_j^{\alpha}, \tag{13}$$

$$d\mu_i'''^{\beta}=-S_i'''^{\beta}dT+V_i'''^{\beta}dP^{\beta}+\sum_{j=2}^{\kappa^{\beta}}\left(\frac{\partial\mu_i'''^{\beta}}{\partial N_j^{\beta}}\right)_{\mathrm{III}}dN_j^{\beta}, \tag{14}$$

in which $S_i'^{\alpha}$, $S_i''^{\alpha}$ and $S_i'''^{\beta}$ denote partial molal entropies, and the meanings of the other symbols have been given in Part II, §F. Applying the fact that the quantities $\mu_i'^{\alpha}$, $\mu_i''^{\alpha}$, $\mu_i'''^{\beta}$ and P^{α} are functions of the variables of Set A, and that the quantities P^{β}, N_j^{α} $(j=2\cdots\kappa^{\alpha})$ and N_j^{β} $(j=2\cdots\kappa^{\beta})$ are functions of the variables of Set I, we deduce from Eqs. (12), (13), and (14):

$$\frac{\partial\mu_i'^{\alpha}}{\partial q}=V_i'^{\alpha}\frac{\partial P^{\alpha}}{\partial q}+\sum_{j=2}^{\kappa^{\alpha}}\left(\frac{\partial\mu_i'^{\alpha}}{\partial N_j^{\alpha}}\right)_{\mathrm{II}}\left(\frac{\partial N_j^{\alpha}}{\partial P^{\alpha}}\right)_{\mathrm{I}}\frac{\partial P^{\alpha}}{\partial q}, \tag{15}$$

$$\frac{\partial\mu_i''^{\alpha}}{\partial q}=V_i''^{\alpha}\frac{\partial P^{\alpha}}{\partial q}+\sum_{j=2}^{\kappa^{\alpha}}\left(\frac{\partial\mu_i''^{\alpha}}{\partial N_j^{\alpha}}\right)_{\mathrm{II}}\left(\frac{\partial N_j^{\alpha}}{\partial P^{\alpha}}\right)_{\mathrm{I}}\frac{\partial P^{\alpha}}{\partial q}, \tag{16}$$

$$\frac{\partial\mu_i'''^{\beta}}{\partial q}=V_i'''^{\beta}\left(\frac{\partial P^{\beta}}{\partial P^{\alpha}}\right)_{\mathrm{I}}\frac{\partial P^{\alpha}}{\partial q}+\sum_{j=2}^{\kappa^{\beta}}\left(\frac{\partial\mu_i'''^{\beta}}{\partial N_j^{\beta}}\right)_{\mathrm{III}}\left(\frac{\partial N_j^{\beta}}{\partial P^{\alpha}}\right)_{\mathrm{I}}\frac{\partial P^{\alpha}}{\partial q}. \tag{17}$$

Introducing the abbreviations:

$$\sum_{j=2}^{\kappa^{\alpha}}\left(\frac{\partial\mu_i'^{\alpha}}{\partial N_j^{\alpha}}\right)_{\mathrm{II}}\left(\frac{\partial N_j^{\alpha}}{\partial P^{\alpha}}\right)_{\mathrm{I}}=u_i', \tag{18}$$

$$\sum_{j=2}^{\kappa^{\alpha}}\left(\frac{\partial\mu_i''^{\alpha}}{\partial N_j^{\alpha}}\right)_{\mathrm{II}}\left(\frac{\partial N_j^{\alpha}}{\partial P^{\alpha}}\right)_{\mathrm{I}}=u_i'', \tag{19}$$

$$\sum_{j=2}^{\kappa^{\beta}}\left(\frac{\partial\mu_i'''^{\beta}}{\partial N_j^{\beta}}\right)_{\mathrm{III}}\left(\frac{\partial N_j^{\beta}}{\partial P^{\alpha}}\right)_{\mathrm{I}}=u_i''', \tag{20}$$

we obtain from Eqs. (15), (16), and (17):

$$\frac{\partial\mu_i'^{\alpha}}{\partial q}=\frac{\partial P^{\alpha}}{\partial q}[V_i'^{\alpha}+u_i'], \tag{21}$$

$$\frac{\partial\mu_i''^{\alpha}}{\partial q}=\frac{\partial P^{\alpha}}{\partial q}[V_i''^{\alpha}+u_i''], \tag{22}$$

$$\frac{\partial\mu_i'''^{\beta}}{\partial q}=\frac{\partial P^{\alpha}}{\partial q}\left[\left(\frac{\partial P^{\beta}}{\partial P^{\alpha}}\right)_{\mathrm{I}}V_i'''^{\beta}+u_i'''\right]. \tag{23}$$

We now differentiate Eq. (1) and obtain:

$$\frac{\partial P^{\alpha}}{\partial q}-\frac{\partial P^{\beta}}{\partial q}=2\left[\sigma+q\frac{\partial\sigma}{\partial q}\right],$$

$$\therefore\quad \frac{\partial P^{\alpha}}{\partial q}-\left(\frac{\partial P^{\beta}}{\partial P^{\alpha}}\right)_{\mathrm{I}}\frac{\partial P^{\alpha}}{\partial q}=2\left[\sigma+q\frac{\partial\sigma}{\partial q}\right],$$

$$\therefore\quad \frac{\partial P^{\alpha}}{\partial q}=\frac{2\left[\sigma+q\dfrac{\partial\sigma}{\partial q}\right]}{1-\left(\dfrac{\partial P^{\beta}}{\partial P^{\alpha}}\right)_{\mathrm{I}}}. \tag{24}$$

We introduce the further abbreviation:

$$U=\frac{1}{1-\left(\dfrac{\partial P^{\beta}}{\partial P^{\alpha}}\right)_{\mathrm{I}}}, \tag{25}$$

the substitution of which into Eq. (24) gives:

$$\partial P^{\alpha}/\partial q=2U[\sigma+q(\partial\sigma/\partial q)]. \tag{26}$$

From Eq. (25) we obtain:

$$\left(\frac{\partial P^{\beta}}{\partial P^{\alpha}}\right)_{\mathrm{I}}=\frac{U-1}{U}. \tag{27}$$

Substitution of Eqs. (26) and (27) into Eqs. (21), (22), and (23) gives the desired expressions for the derivatives of $\mu_i'^{\alpha}$, $\mu_i''^{\alpha}$ and $\mu_i'''^{\beta}$:

$$\partial\mu_i'^{\alpha}/\partial q=2U[\sigma+q(\partial\sigma/\partial q)][V_i'^{\alpha}+u_i'], \tag{28}$$

$$\partial\mu_i''^{\alpha}/\partial q=2U[\sigma+q(\partial\sigma/\partial q)][V_i''^{\alpha}+u_i''], \tag{29}$$

$$\partial\mu_i'''^{\beta}/\partial q=2U[\sigma+q(\partial\sigma/\partial q)]\times[(U-1/U)V_i'''^{\beta}+u_i''']. \tag{30}$$

Substitution of these three equations into Eq. (11) gives an equation which can be solved for $\partial\sigma/\partial q$ or, a little more compactly, for $\partial\log\sigma/\partial q$; the result is:

$$\frac{\partial\log\sigma}{\partial q}=-\frac{2U\left[\sum_{i=1}^{\kappa'}(V_i'^{\alpha}+u_i')\Gamma_i'+\sum_{i=1}^{\kappa''}(V_i''^{\alpha}+u_i'')\Gamma_i''+\sum_{i=1}^{\kappa'''}((U-1/U)V_i'''^{\beta}+u_i''')\Gamma_i'''\right]}{1+2qU\left[\sum_{i=1}^{\kappa'}(V_i'^{\alpha}+u_i')\Gamma_i'+\sum_{i=1}^{\kappa''}(V_i''^{\alpha}+u_i'')\Gamma_i''+\sum_{i=1}^{\kappa'''}((U-1/U)V_i'''^{\beta}+u_i''')\Gamma_i'''\right]}. \tag{31}$$

This is the general and exact solution for Case A.

The quantity U occurring in Eq. (31) is defined by Eq. (25). It will be useful to supplement this definition by giving a further expression for U which follows from the Gibbs-Duhem equation for phase β. We substitute Eq. (6) into Eq. (10), and from the result deduce:

$$-\bar{V}^\beta\left(\frac{\partial P^\beta}{\partial P^\alpha}\right)_{\mathrm{I}}+\sum_{i=1}^{\kappa'}N_i{}'^\beta\left(\frac{\partial \mu_i{}'^\alpha}{\partial P^\alpha}\right)_{\mathrm{I}}+\sum_{i=1}^{\kappa'''}N_i{}'''^\beta\left(\frac{\partial \mu_i{}'''^\beta}{\partial P^\alpha}\right)_{\mathrm{I}}=0. \tag{32}$$

From Eqs. (12), (14), (18), (20) we readily see that

$$\left(\frac{\partial \mu_i{}'^\alpha}{\partial P^\alpha}\right)_{\mathrm{I}}=V_i{}'^\alpha+u_i', \tag{33}$$

$$\left(\frac{\partial \mu_i{}'''^\beta}{\partial P^\alpha}\right)_{\mathrm{I}}=\left(\frac{\partial P^\beta}{\partial P^\alpha}\right)V_i{}'''^\beta+u_i'''. \tag{34}$$

Substitution of Eqs. (33) and (34), and of the further equation drawn from familiar principles:

$$\bar{V}^\beta=\sum_{i=1}^{\kappa'}N_i{}'^\beta V_i{}'^\beta+\sum_{i=1}^{\kappa'''}N_i{}'''^\beta V_i{}'''^\beta \tag{35}$$

into Eq. (32) gives:

$$-\left(\frac{\partial P^\beta}{\partial P^\alpha}\right)_{\mathrm{I}}\sum_{i=1}^{\kappa'}N_i{}'^\beta V_i{}'^\beta+\sum_{i=1}^{\kappa'}N_i{}'^\beta(V_i{}'^\alpha+u_i')+\sum_{i=1}^{\kappa'''}N_i{}'''^\beta u_i{}'''=0.$$

Into this equation we substitute Eq. (27) and obtain, on solving for U:

$$U=\frac{\sum_{i=1}^{\kappa'}N_i{}'^\beta V_i{}'^\beta}{\sum_{i=1}^{\kappa'}N_i{}'^\beta(V_i{}'^\beta-V_i{}'^\alpha-u_i')-\sum_{i=1}^{\kappa'''}N_i{}'''^\beta u_i{}'''}. \tag{36}$$

This is the desired supplementary expression for U. We may note, furthermore, that whenever $(\partial P^\beta/\partial P^\alpha)_{\mathrm{I}}$ is zero, Eq. (25) requires that

$$U=1. \tag{37}$$

There are two important cases in which this occurs: (i) P^β is contained in Set A (and therefore in Set I); (ii) $\kappa^\beta=0$ (i.e. α is a liquid of negligible vapor pressure and β is the vacuum, so that $P^\beta=0$).

B. Treatment of Case B

In addition to

Set B: $q, T, P^\alpha, x_4\cdots x_{\kappa+1}$

(which, we recall, does not contain P^β), we introduce three auxiliary sets of independent variables, of which the first will be called Set IV, and the second and third are respectively identical with Sets II and III under Case A; that is:

Set IV: $P^\beta, T, P^\alpha, x_4\cdots x_{\kappa+1}$,
Set II: $P^\alpha, T, N_2{}^\alpha\cdots N_\kappa{}^\alpha$,
Set III: $P^\beta, T, N_2{}^\beta\cdots N_\kappa{}^\beta$.

Set IV, like Set B, applies to the system specified in Part II, §A. Partial derivatives corresponding to the Set B will be written without subscript, and partial derivatives corresponding to the auxiliary sets will be distinguished by the subscripts IV, II, or III.

The deduction is parallel to that for Case A. We first deduce an equation identical in form with Eq. (11). Equations (12)–(14) hold as before. In place of Eqs. (15)–(17) we obtain the three equations:

$$\frac{\partial \mu_i{}'^\alpha}{\partial q}=\sum_{j=2}^{\kappa^\alpha}\left(\frac{\partial \mu_i{}'^\alpha}{\partial N_j{}^\alpha}\right)_{\mathrm{II}}\left(\frac{\partial N_j{}^\alpha}{\partial P^\beta}\right)_{\mathrm{IV}}\frac{\partial P^\beta}{\partial q},$$

$$\frac{\partial \mu_i{}''^\alpha}{\partial q}=\sum_{j=2}^{\kappa^\alpha}\left(\frac{\partial \mu_i{}''^\alpha}{\partial N_j{}^\alpha}\right)_{\mathrm{II}}\left(\frac{\partial N_j{}^\alpha}{\partial P^\beta}\right)_{\mathrm{IV}}\frac{\partial P^\beta}{\partial q},$$

$$\frac{\partial \mu_i{}'''^\beta}{\partial q}=V_i{}'''^\beta\frac{\partial P^\beta}{\partial q}+\sum_{j=2}^{\kappa^\beta}\left(\frac{\partial \mu_i{}'''^\beta}{\partial N_j{}^\beta}\right)_{\mathrm{III}}\left(\frac{\partial N_j{}^\beta}{\partial P^\beta}\right)_{\mathrm{IV}}\frac{\partial P^\beta}{\partial q},$$

which, on introduction of the abbreviations:

$$\sum_{j=2}^{\kappa^\alpha}\left(\frac{\partial \mu_i{}'^\alpha}{\partial N_j{}^\alpha}\right)_{\mathrm{II}}\left(\frac{\partial N_j{}^\alpha}{\partial P^\beta}\right)_{\mathrm{IV}}=w_i', \tag{38}$$

$$\sum_{j=2}^{\kappa^\alpha}\left(\frac{\partial \mu_i{}''^\alpha}{\partial N_j{}^\alpha}\right)_{\mathrm{II}}\left(\frac{\partial N_j{}^\alpha}{\partial P^\beta}\right)_{\mathrm{IV}}=w_i'', \tag{39}$$

$$\sum_{j=2}^{\kappa^\beta}\left(\frac{\partial \mu_i{}'''^\beta}{\partial N_j{}^\beta}\right)_{\mathrm{III}}\left(\frac{\partial N_j{}^\beta}{\partial P^\beta}\right)_{\mathrm{IV}}=w_i''', \tag{40}$$

become:

$$\frac{\partial \mu_i{}'^\alpha}{\partial q}=\frac{\partial P^\beta}{\partial q}\cdot w_i', \tag{41}$$

$$\frac{\partial \mu_i{}''^\alpha}{\partial q}=\frac{\partial P^\beta}{\partial q}\cdot w_i'', \tag{42}$$

$$\frac{\partial \mu_i{}'''^\beta}{\partial q}=\frac{\partial P^\beta}{\partial q}[V_i{}'''^\beta+w_i''']. \tag{43}$$

Differentiation of Eq. (1) gives immediately:

$$\frac{\partial P^\beta}{\partial q}=-2[\sigma+q(\partial\sigma/\partial q)],$$

the substitution of which into Eqs. (41), (42) and (43) gives:

$$\frac{\partial \mu_i{}'^\alpha}{\partial q}=-2[\sigma+q(\partial\sigma/\partial q)]w_i',$$

$$\frac{\partial \mu_i{}''^\alpha}{\partial q}=-2[\sigma+q(\partial\sigma/\partial q)]w_i'',$$

$$\frac{\partial \mu_i{}'''^\beta}{\partial q}=-2[\sigma+q(\partial\sigma/\partial q)][V_i{}'''^\beta+w_i'''].$$

Substitution of these equations into Eq. (11) yields:

$$\frac{\partial \log\sigma}{\partial q}=\frac{2\left[\sum_{i=1}^{\kappa'}w_i'\Gamma_i'+\sum_{i=1}^{\kappa''}w_i''\Gamma_i''+\sum_{i=1}^{\kappa'''}(V_i'''^{\beta}+w_i''')\Gamma_i'''\right]}{1-2q\left[\sum_{i=1}^{\kappa'}w_i'\Gamma_i'+\sum_{i=1}^{\kappa''}w_i''\Gamma_i''+\sum_{i=1}^{\kappa'''}(V_i'''^{\beta}+w_i''')\Gamma_i'''\right]}. \tag{44}$$

This is the general and exact solution for Case B.

C. Some Special Cases

We shall now show that the generality of the solutions obtained in the form of Eqs. (31) and (44) does not stand in the way of the deduction from these solutions of special equations applying to the experimental situations commonly encountered in the measurement of surface tension. For this purpose we shall consider a series of special cases, each defined by the dual operations of (i) restricting to some extent the chemical nature of the system specified in Part II, §A, and (ii) specifying completely the independent variables.

Case 1: Nature of the system: $\kappa'>0$, $\kappa''>0$, $\kappa'''>0$; independent variables: q, T, P^{β}, $N_2^{\alpha}\cdots N_{\kappa}{}^{\alpha}$, $N_2'''^{\beta}\cdots N_{\kappa'''}'''^{\beta}$. This comes under Case A. The membership of Sets I and II is given, and for Set III we make the particular selection P^{β}, T, $N_1'^{\beta}\cdots N_{\kappa'}{}^{\beta}$, $N_2'''^{\beta}\cdots N_{\kappa'''}'''^{\beta}$. From Eqs. (18), (19), and (20) we then readily see that

$$u_i'=u_i''=0,$$

$$u_i'''=\sum_{j=1}^{\kappa'}\left(\frac{\partial \mu_i'''^{\beta}}{\partial N_j'^{\beta}}\right)_{\mathrm{III}}\left(\frac{\partial N_j'^{\beta}}{\partial P^{\alpha}}\right)_{\mathrm{I}}.$$

Since Set A here contains P^{β}, we have $U=1$ (see Eq. (37)). The general Eq. (31) accordingly reduces to:

$$\frac{\partial \log\sigma}{\partial q}=-\frac{2\left[\sum_{i=1}^{\kappa'}V_i'^{\alpha}\Gamma_i'+\sum_{i=1}^{\kappa''}V_i''^{\alpha}\Gamma_i''+\sum_{i=1}^{\kappa'''}u_i'''\Gamma_i'''\right]}{1+2q\left[\sum_{i=1}^{\kappa'}V_i'^{\alpha}\Gamma_i'+\sum_{i=1}^{\kappa''}V_i''^{\alpha}\Gamma_i''+\sum_{i=1}^{\kappa'''}u_i'''\Gamma_i'''\right]}.$$

Case 2: Nature of the system: $\kappa'>0$, $\kappa''>0$, $\kappa'''>0$; independent variables: q, T, P^{α}, $N_2^{\alpha}\cdots N_{\kappa}{}^{\alpha}$, $N_2'''^{\beta}\cdots N_{\kappa'''}'''^{\beta}$. This comes under Case B. The membership of Sets IV and II is given, and for Set III we select again P^{β}, T, $N_1'^{\beta}\cdots N_{\kappa'}{}^{\beta}$, $N_2'''^{\beta}\cdots N_{\kappa'''}'''^{\beta}$. From Eqs. (38), (39), and (40) we then see that

$$w_i'=w_i''=0,$$

$$w_i'''=\sum_{j=1}^{\kappa'}\left(\frac{\partial \mu_i'''^{\beta}}{\partial N_j'^{\beta}}\right)_{\mathrm{III}}\left(\frac{\partial N_j'^{\beta}}{\partial P^{\beta}}\right)_{\mathrm{IV}}.$$

The general Eq. (44) accordingly reduces to:

$$\frac{\partial \log\sigma}{\partial q}=\frac{2\sum_{i=1}^{\kappa'''}(V_i'''^{\beta}+w_i''')\Gamma_i'''}{1-2q\sum_{i=1}^{\kappa'''}(V_i'''^{\beta}+w_i''')\Gamma_i'''}.$$

Case 3: Nature of the system: $\kappa'=0$, $\kappa''>0$, $\kappa'''>0$; (i.e. α and β are mutually insoluble); independent variables: q, T, P^{β}, $N_2''^{\alpha}\cdots N_{\kappa}{}''^{\alpha}$, $N_2'''^{\beta}\cdots N_{\kappa'''}'''^{\beta}$, or q, T, P^{α}, $N_2''^{\alpha}\cdots N_{\kappa}{}''^{\alpha}$, $N_2'''^{\beta}\cdots N_{\kappa'''}'''^{\beta}$. With the first choice of independent variables, the treatment is derivable from that for Case 1 by deleting the terms in single prime (since $\kappa'=0$), and noting that then Eq. (20) requires $u_i'''=0$; the result is accordingly:

$$\frac{\partial \log\sigma}{\partial q}=-\frac{2\sum_{i=1}^{\kappa''}V_i''^{\alpha}\Gamma_i''}{1+2q\sum_{i=1}^{\kappa''}V_i''^{\alpha}\Gamma_i''}.$$

With the second choice of independent variables, the treatment is derivable from that for Case 2 by noting that Eq. (40) now requires $w_i'''=0$; the result is accordingly:

$$\frac{\partial \log\sigma}{\partial q}=\frac{2\sum_{i=1}^{\kappa'''}V_i'''^{\beta}\Gamma_i'''}{1-2q\sum_{i=1}^{\kappa'''}V_i'''^{\beta}\Gamma_i'''}.$$

Case 4: Nature of the system: $\kappa'\geq 0$, $\kappa''\geq 0$, $\kappa'''=0$, with $\kappa'=\kappa''=0$ excluded (i.e. all the components are present in at least one phase, which is taken to be α); independent variables: q, T, $N_2^{\alpha}\cdots N_{\kappa}{}^{\alpha}$. This comes under Case A. Since $\kappa'''=0$, the terms with triple prime drop out. Equations (18) and (19) are seen to give $u_i'=u_i''=0$. The general equation (31) accordingly reduces to:

$$\frac{\partial \log\sigma}{\partial q}=-\frac{2U\left[\sum_{i=1}^{\kappa'}V_i'^{\alpha}\Gamma_i'+\sum_{i=1}^{\kappa''}V_i''^{\alpha}\Gamma_i''\right]}{1+2qU\left[\sum_{i=1}^{\kappa'}V_i'^{\alpha}\Gamma_i'+\sum_{i=1}^{\kappa''}V_i''^{\alpha}\Gamma_i''\right]}.$$

Since in this case $\kappa'+\kappa''=\kappa^\alpha=\kappa$, we may denote the partial molal volumes in phase α by $V_1{}^\alpha \cdots V_\kappa{}^\alpha$, and then write the above equation more compactly as:

$$\frac{\partial \log\sigma}{\partial q}=-\frac{2U\sum_{i=1}^{\kappa}V_i{}^\alpha\Gamma_i}{1+2qU\sum_{i=1}^{\kappa}V_i{}^\alpha\Gamma_i}. \tag{45}$$

With regard to U, we now see from Eqs. (36) and (37) that when

$$\kappa^\beta>0, \quad U=\frac{\sum_{i=1}^{\kappa'}N_i{}'^\beta V_i{}'^\beta}{\sum_{i=1}^{\kappa'}N_i{}'^\beta(V_i{}'^\beta-V_i{}'^\alpha)}, \tag{46}$$

$$\kappa^\beta=0, \quad U=1.$$

Moreover, since in this case $\kappa'=\kappa^\beta$, the quantity on the right side of Eq. (46) has a simple physical interpretation, in that the numerator equals the mean molal volume, $\bar{V}^\beta$, of the phase β (see Eq. (35)), and the denominator equals minus the gain in volume when one mole of the material of β is dissolved, at equilibrium, in a very large quantity of α.

Case 5: Under Case 4, phase β is a gaseous mixture, not necessarily perfect, but of density negligible compared to phase α. In this case $V_i{}^\beta \gg V_i{}^\alpha$, and therefore, by Eq. (46), $U\sim 1$. Equation (45) accordingly yields the accurate approximation:

$$\frac{\partial \log\sigma}{\partial q}\sim-\frac{2\sum_{i=1}^{\kappa}V_i{}^\alpha\Gamma_i}{1+2q\sum_{i=1}^{\kappa}V_i{}^\alpha\Gamma_i}.$$

Case 6: Under Case 4, phase α is a perfect gaseous mixture of density negligible compared to that of phase β. In this case:

$$V_i{}^\alpha=RT/P^\alpha \quad (i=1\cdots\kappa),$$
$$V_i{}'^\alpha \gg V_i{}'^\beta \quad (i=1\cdots\kappa').$$

Noting that in Eq. (46) the numerator equals $\bar{V}^\beta$, we then see that

$$U\sim-(\bar{V}^\beta P^\alpha)/(RT).$$

Equation (45) accordingly yields the accurate approximation:

$$\frac{\partial \log\sigma}{\partial q}\sim-\frac{2\bar{V}^\beta\sum_{i=1}^{\kappa}\Gamma_i}{1-2q\bar{V}^\beta\sum_{i=1}^{\kappa}\Gamma_i}. \tag{47}$$

This equation is identical (except for slight differences of notation) with one deduced by Defay.[7]

Case 7: Nature of the system: $\kappa=\kappa^\alpha=1$; independent variables: q, T. This comes under Case 4. If the single component is present in both phases, we have $V_1{}'^\alpha=\bar{V}^\alpha$ and $V_1{}'^\beta=\bar{V}^\beta$. Equation (46) then becomes:

$$U=\bar{V}^\beta/(\bar{V}^\beta-\bar{V}^\alpha),$$

and Eq. (45) therefore yields:

$$\frac{\partial \log\sigma}{\partial q}=-\frac{2\bar{V}^\beta\bar{V}^\alpha\Gamma_1'}{\bar{V}^\beta-\bar{V}^\alpha+2q\bar{V}^\beta\bar{V}^\alpha\Gamma_1'}. \tag{48}$$

This equation is equivalent to the first of Tolman's two chief equations (i.e. Eq. T(2.6)). If on the other hand the component is involatile and β is the vacuum, then $V_1{}''^\alpha=\bar{V}^\alpha$, and $U=1$, so that Eq. (45) yields:

$$\frac{\partial \log\sigma}{\partial q}=-\frac{2\bar{V}^\alpha\Gamma_1''}{1+2q\bar{V}^\alpha\Gamma_1''}. \tag{49}$$

D. Remarks

We may point out the following four features of Eqs. (31) and (44). (i) These two equations jointly constitute a general solution, in terms of the Gibbs theory, of the problem of the change of surface tension with curvature for the multicomponent system without insoluble surface film, and moreover in a form from which special equations for experimental situations of the usual type are readily deducible. (ii) The two equations jointly constitute a generalization of the *first* of Tolman's two chief equations, i.e. Eq. T(2.6). (iii) The equations, like Eq. T(2.6), apply to a surface layer of any shape compatible with equilibrium. (iv) In each of the Eqs. (31) and (44), the numerator of the expression on the right is a linear combination of the surface concentrations Γ_i referred to the surface of tension, and moreover has the physical dimensions of length; these facts suggest that the numerator represents in generalized form, a kind of *characteristic length* associated with the surface layer.

In Part IV we shall obtain, as a by-product of the deduction there to be carried out for the special case of the spherical surface layer, a physically more concrete interpretation of the numerator in Eq. (31) or (44) as a characteristic length.

IV. THE RELATION FOR THE SPHERICAL SURFACE LAYER

A. Change of Surface Concentration with Position of Gibbs Surface

For the purpose here in hand we shall need to know, for the spherical surface layer, how the value of a surface concentration changes with the position of the

[7] See reference 2. The equation in question is the not numbered equation preceding Eq. (211) of Defay's monograph.

Gibbs surface defining that value. To obtain this information we consider the case in which the system consists of a sphere of one phase imbedded in the other phase. In order to make our result general, we introduce the convention that the radius of any Gibbs surface shall be positive or negative, according as the spherical phase has the index α or β. This convention is in accord with that for the sign of the curvature, q, of the surface of tension, introduced in Part II, §B. We now consider two arbitrary Gibbs surfaces of radii r_1 and r_2 respectively, and suppose for the moment that α is the spherical phase, so that r_1 and r_2 are positive. Then the Gibbs definition of surface concentration gives us the two equations:

$$n_i=\frac{4\pi}{3}r_1^3c_i^\alpha+\left(V-\frac{4\pi}{3}r_1^3\right)c_i^\beta+4\pi r_1^2\Gamma_{i1},$$

$$n_i=\frac{4\pi}{3}r_2^3c_i^\alpha+\left(V-\frac{4\pi}{3}r_2^3\right)c_i^\beta+4\pi r_2^2\Gamma_{i2},$$

in which V denotes the total volume of the system and Γ_{i1} and Γ_{i2} denote the surface concentrations of the ith component referred respectively to the two Gibbs surfaces in question. Subtraction and rearrangement gives:

$$r_2^2\Gamma_{i2}-r_1^2\Gamma_{i1}=-\tfrac{1}{3}(r_2^3-r_1^3)(c_i^\alpha-c_i^\beta). \tag{50}$$

Now we suppose, instead, that β is the spherical phase, so that r_1 and r_2 are negative, and we repeat the argument just given. The result is again Eq. (50), which is thus seen to be the general relation between surface concentration and position of the Gibbs surface, for the spherical surface layer. We may note for clarity that Eq. (50) applies to each of the κ components of the system, with $c_i^\alpha=0$ for each component of Class 3, and $c_i^\beta=0$ for each of Class 2 (see Part II, §F). For the purpose in hand it will be convenient to eliminate r_2 from Eq. (50) by the substitution:

$$r_2=r_1+\delta,$$

and then to write the result in the form:

$$\left(1+\frac{\delta}{r_1}\right)^2\Gamma_{i2}-\Gamma_{i1}=-\delta\left(1+\frac{\delta}{r_1}+\frac{1}{3}\frac{\delta^2}{r_1^2}\right)(c_i^\alpha-c_i^\beta). \tag{51}$$

The quantity δ is evidently the distance *from* the Gibbs surface of radius r_1, *to* that of radius r_2, *measured in the direction from α to β*. We may verify Eq. (51) by noting that $r_1=\infty$ gives:

$$\Gamma_{i2}-\Gamma_{i1}=-\delta(c_i^\alpha-c_i^\beta),$$

which is the well-known formula for the plane surface layer.[8]

[8] See J. W. Gibbs, reference 4, p. 234; also E. A. Guggenheim and N. K. Adam, Proc. Roy. Soc. **A139**, 218 (1933).

B. Treatment of Case A

We recall that in Eq. (31) the surface concentrations Γ_i', Γ_i'', Γ_i''' are defined with reference to the surface of tension. We now introduce a new Gibbs surface, to be called the *auxiliary surface*, which is so located that the surface concentrations referred to it, which we shall denote by $\Gamma_i^{*\prime}$, $\Gamma_i^{*\prime\prime}$, $\Gamma_i^{*\prime\prime\prime}$, obey the equation which is generated by replacing Γ_i in the numerator of Eq. (31) by Γ_i^* and setting the result equal to zero; this gives, after dividing through by $2U$:

$$\sum_{i=1}^{\kappa'}(V_i'^\alpha+u_i')\Gamma_i^{*\prime}+\sum_{i=1}^{\kappa''}(V_i''^\alpha+u_i'')\Gamma_i^{*\prime\prime}$$

$$+\sum_{i=1}^{\kappa'''}(((U-1)/U)V_i'''^\beta+u_i''')\Gamma_i^{*\prime\prime\prime}=0. \tag{52}$$

That this equation actually does define a set of surface concentrations Γ_i^*, and therefore locates a Gibbs surface, for any given state of the system, may be shown as follows. We denote the radius of any Gibbs surface by r, take α to be the spherical phase, and apply the Gibbs definition of surface concentration, writing the equations for components of Classes 1, 2, and 3 separately:

$$\left.\begin{aligned} n_i'&=\frac{4\pi}{3}r^3c_i^\alpha+\left(V-\frac{4\pi}{3}r^3\right)c_i'^\beta+4\pi r^2\Gamma_i^{*\prime} \qquad (i=1\cdots\kappa'),\\ n_i''&=\frac{4\pi}{3}r^3c_i''^\alpha+4\pi r^2\Gamma_i^{*\prime\prime} \quad (i=1\cdots\kappa''),\\ n_i'''&=\left(V-\frac{4\pi}{3}r^3\right)c_i'''^\beta+4\pi r^2\Gamma_i^{*\prime\prime\prime} \quad (i=1\cdots\kappa'''). \end{aligned}\right\} \tag{53}$$

These equations, together with Eq. (52), make a set of $\kappa'+\kappa''+\kappa'''+1(=\kappa+1)$ equations which can be solved for the $\kappa'+\kappa''+\kappa'''+1$ unknowns $\Gamma_i^{*\prime}$, $\Gamma_i^{*\prime\prime}$, $\Gamma_i^{*\prime\prime\prime}$, r in terms of variables of state whose values are independent of the position of a Gibbs surface.

Having thus defined the auxiliary surface and the associated surface concentrations Γ_i^*, we now apply Eq. (51) as follows. We take:

$$\Gamma_{i1}=\Gamma_i \quad (i=\cdots 1\kappa), \tag{54}$$

$$\Gamma_{i2}=\Gamma_i^* \quad (i=1\cdots\kappa), \tag{55}$$

and we note that since the quantities Γ_i are referred to the surface of tension, Eq. (54) implies:

$$r_1=1/q. \tag{56}$$

Substituting Eqs. (54), (55), and (56) into Eq. (51), and solving for Γ_i, we obtain:

$$\Gamma_i=(1+\delta q)^2\Gamma_i^*+\delta(1+\delta q+\tfrac{1}{3}\delta^2q^2)(c_i^\alpha-c_i^\beta), \tag{57}$$

in which δ now stands for the distance *from* the surface of tension *to* the auxiliary surface, *measured in the direction from α to β*. For abbreviation we set

$$(1+\delta q)^2=a, \tag{58}$$

$$\delta(1+\delta q+\tfrac{1}{3}\delta^2q^2)=b, \tag{59}$$

so that Eq. (57) may be written as:

$$\Gamma_i=a\Gamma_i^*+b(c_i^\alpha-c_i^\beta). \tag{60}$$

We write this equation separately for each of the Classes 1, 2, and 3:

$$\Gamma_i'=a\Gamma_i^{*\prime}+b(c_i'^\alpha-c_i'^\beta) \quad (i=1\cdots\kappa'), \tag{61}$$

$$\Gamma_i''=a\Gamma_i^{*\prime\prime}+bc_i''^\alpha \quad (i=1\cdots\kappa''), \tag{62}$$

$$\Gamma_i'''=a\Gamma_i^{*\prime\prime\prime}-bc_i'''^\beta \quad (i=1\cdots\kappa'''). \tag{63}$$

We then substitute Eqs. (61), (62) and (63) into Eq. (31), and note that the terms in $\Gamma_i^{*\prime}$, $\Gamma_i^{*\prime\prime}$, $\Gamma_i^{*\prime\prime\prime}$ disappear by virtue of Eq. (52). We write the result in the form:

$$\frac{\partial\log\sigma}{\partial q}=-\frac{2bQ_A}{1+2qbQ_A}, \tag{64}$$

in which Q_A is given by:

$$Q_A=U\Big[\sum_{i=1}^{\kappa'}(V_i'^\alpha+u_i')(c_i'^\alpha-c_i'^\beta)+\sum_{i=1}^{\kappa''}(V_i''^\alpha+u_i'')c_i''^\alpha - \sum_{i=1}^{\kappa'''}(((U-1)/U)V_i'''^\beta+u_i''')c_i'''^\beta\Big]. \tag{65}$$

This quantity Q_A however, is identically equal to unity. To prove this we substitute into Eq. (65) the following:

$$\left.\begin{aligned} c_i'^\alpha&=N_i'^\alpha/\bar V^\alpha, \quad c_i''^\alpha=N_i''^\alpha/\bar V^\alpha,\\ c_i'^\beta&=N_i'^\beta/\bar V^\beta, \quad c_i'''^\beta=N_i'''^\beta/\bar V^\beta,\end{aligned}\right\} \tag{66}$$

and find, on taking account of the further equation, drawn from familiar principles:

$$\sum_{i=1}^{\kappa'}N_i'^\alpha V_i'^\alpha+\sum_{i=1}^{\kappa''}N_i''^\alpha V_i''^\alpha=\bar V^\alpha, \tag{67}$$

that we can write the result in the form:

$$Q_A=U\Big[1+(1/\bar V^\alpha)\Big(\sum_{i=1}^{\kappa'}N_i'^\alpha u_i'+\sum_{i=1}^{\kappa''}N_i''^\alpha u_i''\Big) -1/\bar V^\beta\Big(\sum_{i=1}^{\kappa'}N_i'^\beta V_i'^\alpha+\sum_{i=1}^{\kappa'}N_i'^\beta u_i'+\sum_{i=1}^{\kappa'''}N_i'''^\beta u_i'''\Big) -1/\bar V^\beta((U-1)/U)\sum_{i=1}^{\kappa'''}N_i'''^\beta V_i'''^\beta\Big]. \tag{68}$$

We now obtain values for the two terms in bold parentheses in this equation, as follows. We turn back to Eq. (9) and from it deduce:

$$-\bar V^\alpha+\sum_{i=1}^{\kappa'}N_i'^\alpha\left(\frac{\partial\mu_i'^\alpha}{\partial P^\alpha}\right)_I+\sum_{i=1}^{\kappa''}N_i''^\alpha\left(\frac{\partial\mu_i''^\alpha}{\partial P^\alpha}\right)_I=0.$$

Into this equation we substitute Eq. (33) and the parallel equation:

$$(\partial\mu_i''^\alpha/\partial P^\alpha)_I=V_i''^\alpha+u_i'',$$

and then find the result, by virtue of Eq. (67), reduces to:

$$\sum_{i=1}^{\kappa'}N_i'^\alpha u_i'+\sum_{i=1}^{\kappa''}N_i''^\alpha u_i''=0. \tag{69}$$

Next, we turn back to Eq. (36), and find, by rearrangement of terms:

$$\sum_{i=1}^{\kappa'}N_i'^\beta V_i'^\alpha+\sum_{i=1}^{\kappa'}N_i'^\beta u_i'+\sum_{i=1}^{\kappa'''}N_i'''^\beta u_i''' =(U-1)/U\sum_{i=1}^{\kappa'}N_i'^\beta V_i'^\beta. \tag{70}$$

On replacing the two terms in bold parentheses in Eq. (68) by their values as given by Eqs. (69) and (70), we find:

$$Q_A=U\Big[1-(1/\bar V^\beta)((U-1)/U) \times\Big(\sum_{i=1}^{\kappa'}N_i'^\beta V_i'^\beta+\sum_{i=1}^{\kappa'''}N_i'''^\beta V_i'''^\beta\Big)\Big],$$

and this, owing to Eq. (35), is seen to reduce to:

$$Q_A=1.$$

Equation (64) accordingly reduces to:

$$\partial\log\sigma/\partial q=-2b/(1+2qb),$$

which, on replacing b by its value given by Eq. (59), becomes:

$$\frac{\partial\log\sigma}{\partial q}=-\frac{2\delta(1+\delta q+\frac{1}{3}\delta^2q^2)}{1+2\delta q(1+\delta q+\frac{1}{3}\delta^2q^2)}. \tag{71}$$

This is the final result for the spherical surface layer under Case A.

C. Treatment of Case B

The deduction is parallel to that for Case A. We locate the auxiliary surface by replacing Γ_i in the numerator of Eq. (44) by Γ_i^* and setting the result equal to zero, thus obtaining:

$$\sum_{i=1}^{\kappa'}w_i'\Gamma_i^{*\prime}+\sum_{i=1}^{\kappa''}w_i''\Gamma_i^{*\prime\prime}+\sum_{i=1}^{\kappa'''}(V_i'''^\beta+w_i''')\Gamma_i^{*\prime\prime\prime}=0. \tag{72}$$

That this equation actually does define a set of surface concentrations Γ_i^*, and therefore locates a Gibbs surface, follows (as in the case of Eq. (52)) from the fact that it can be solved simultaneously with the Eqs. (53). We now apply Eq. (51) exactly as under Case A, and find, on substituting Eqs. (61), (62) and (63) into Eq. (44), that the terms in $\Gamma_i^{*\prime}$, $\Gamma_i^{*\prime\prime}$, $\Gamma_i^{*\prime\prime\prime}$ disappear by virtue of Eq. (72), and that we are left with a result of the form:

$$\frac{\partial \log\sigma}{\partial q}=\frac{2bQ_B}{1-2qbQ_B}, \tag{73}$$

in which Q_B is given by:

$$Q_B=\sum_{i=1}^{\kappa'} w_i'(c_i'^{\alpha}-c_i'^{\beta})+\sum_{i=1}^{\kappa''} w_i'' c_i''^{\alpha}-\sum_{i=1}^{\kappa'''}(V_i'''^{\beta}+w_i''')c_i'''^{\beta}.$$

This quantity Q_B is identically equal to minus one. To prove this we substitute Eqs. (66) into Eq. (74) and obtain:

$$Q_B=1/\bar{V}^{\alpha}\left[\sum_{i=1}^{\kappa'} N_i'^{\alpha}w_i'+\sum_{i=1}^{\kappa''} N_i''^{\alpha}w_i''\right]$$

$$-1/\bar{V}^{\beta}\left[\sum_{i=1}^{\kappa'} N_i'^{\beta}w_i'+\sum_{i=1}^{\kappa'''} N_i'''^{\beta}(V_i'''^{\beta}+w_i''')\right]. \tag{75}$$

From Eq. (9) we deduce:

$$\sum_{i=1}^{\kappa'} N_i'^{\alpha}\left(\frac{\partial\mu_i'^{\alpha}}{\partial P^{\beta}}\right)_{\mathrm{IV}}+\sum_{i=1}^{\kappa''} N_i''^{\alpha}\left(\frac{\partial\mu_i''^{\alpha}}{\partial P^{\beta}}\right)_{\mathrm{IV}}=0, \tag{76}$$

and from Eq. (10), after taking account of Eq. (6):

$$-\bar{V}^{\beta}+\sum_{i=1}^{\kappa'} N_i'^{\beta}\left(\frac{\partial\mu_i'^{\alpha}}{\partial P^{\beta}}\right)_{\mathrm{IV}}\quad\sum_{i=1}^{\kappa'''} N'''^{\beta}\left(\frac{\partial\mu_i'''^{\beta}}{\partial P^{\beta}}\right)_{\mathrm{IV}}=0. \tag{77}$$

From Eqs. (12), (13), (14) and (38), (39), (40) we readily see that:

$$\left(\frac{\partial\mu_i'^{\alpha}}{\partial P^{\beta}}\right)_{\mathrm{IV}}=w_i',$$

$$\left(\frac{\partial\mu_i''^{\alpha}}{\partial P^{\beta}}\right)_{\mathrm{IV}}=w_i'',$$

$$\left(\frac{\partial\mu_i'''^{\beta}}{\partial P^{\beta}}\right)_{\mathrm{IV}}=V_i'''^{\beta}+w_i'''.$$

Substitution of these equations into Eqs. (76) and (77) yields:

$$\sum_{i=1}^{\kappa'} N_i'^{\alpha}w_i'+\sum_{i=1}^{\kappa''} N_i''^{\alpha}w_i''=0, \tag{78}$$

$$\sum_{i=1}^{\kappa'} N_i'^{\beta}w_i'+\sum_{i=1}^{\kappa'''} N_i'''^{\beta}(V_i'''^{\beta}+w_i''')=0. \tag{79}$$

On replacing the terms in brackets in Eq. (75) by their values as given by Eqs. (78) and (79) we find:

$$Q_B=-1.$$

Substitution into Eq. (73) of this value for Q_B, and of the value of b given by Eq. (59), yields:

$$\frac{\partial \log\sigma}{\partial q}=-\frac{2\delta(1+\delta q+\frac{1}{3}\delta^2q^2)}{1+2\delta q(1+\delta q+\frac{1}{3}\delta^2q^2)}, \tag{80}$$

which is identical with Eq. (71), and is the final result for the spherical surface layer under Case B.

D. The Characteristic Length

The two Eqs. (31) and (44) applying respectively to Cases A and B are thus seen to reduce, when the surface layer is spherical, to the single Eq. (80). This reduction moreover comes about through the fact that in Eq. (31) the numerator becomes equal to $2\delta(1+\delta q+\frac{1}{3}\delta^2q^2)$, and in Eq. (44) to $-2\delta(1+\delta q+\frac{1}{3}\delta^2q^2)$, where δ is the distance (measured in the direction from α to β) from the surface of tension to an auxiliary Gibbs surface which is fixed in both cases by the same procedure. We may note further that when the surface layer is plane, the numerators in question reduce to $\pm 2\delta$, and Eq. (80) becomes simply:

$$\frac{\partial \log\sigma}{\partial q}=-2\delta.$$

The quantity $2\delta(1+\delta q+\frac{1}{3}\delta^2q^2)$ may therefore be regarded as a characteristic length for the spherical surface layer, obtained by multiplying the length 2δ characteristic of the plane surface layer by a correction factor to take account of the deviation from the plane. This interpretation must however not be taken to imply that δ itself is independent of the curvature, although we may expect it to be very nearly so in many cases. It is also important to remember that even when the state of the system is fixed, the value of δ still depends upon the choice of the variables $x_3\cdots x_{\kappa+1}$, which are of course unspecified as far as Eq. (80) is concerned. The simplicity of these results, which may seem remarkable in view of the complexity of the multicomponent situation with generalized independent variables, comes from the fact that this complexity is as it were cancelled by an equivalent complexity in the Eq. (52) or (72) fixing the auxiliary surface.

E. Remarks

We may point out four further features of our results for the spherical surface layer. (i) Equation (80) is a generalization of the *second* of Tolman's two chief equations (i.e. Eq. T(4.1), and is converted by the

substitution $q=1/r$ into:

$$\frac{\partial \log\sigma}{\partial r}=\frac{\frac{2\delta}{r^2}\left(1+\frac{\delta}{r}+\frac{1}{3}\frac{\delta^2}{r^2}\right)}{1+\frac{2\delta}{r}\left(1+\frac{\delta}{r}+\frac{1}{3}\frac{\delta^2}{r^2}\right)}, \tag{81}$$

which is identical in form with Eq. T(4.1). (ii) The two Eqs. (52) and (72), fixing the auxiliary surface, are generalizations of Tolman's equation $\Gamma=0$, and our Eq. (57) is a generalization of Eq. T(3.4).[9] (iii) For some of the special cases considered in Part III, §C, the equations locating the auxiliary surface are simple and already known; thus for Case 4 we have, from Eq. (45):

$$\sum_{i=1}^{\kappa} V_i^{\alpha}\Gamma_i^{*}=0, \tag{82}$$

and for Case 6, from Eq. (47):

$$\sum_{i=1}^{\kappa}\Gamma_i^{*}\sim 0. \tag{83}$$

Surface concentrations defined according to Eqs. (82) and (83) have been calculated by Guggenheim and Adam[8] for aqueous solutions of alcohol and water, of all concentrations, in contact with their vapor. (iv) If we treat δ as a constant independent of q, Eq. (80) gives:

$$\frac{\partial \log\sigma}{\partial \delta q}=-\frac{2(1+\delta q+\frac{1}{3}\delta^2 q^2)}{1+2\delta q(1+\delta q+\frac{1}{3}\delta^2 q^2)}, \tag{84}$$

which on integration would give:

$$\sigma/\sigma_0=f(\delta q), \tag{85}$$

where σ and σ_0 refer respectively to a spherical surface layer, and to a plane one for which all the independent variables (given by Set A or B) except q have the same value as for the spherical one. For $\delta q \ll 1$, Eq. (84) yields the approximation $f(\delta q)\sim 1-2\delta q$, and therefore:

$$(\sigma_0-\sigma)/\sigma_0\sim 2\delta q.$$

V. APPLICATION OF THE RELATION FOR THE SPHERICAL SURFACE LAYER

Tolman has carried out exactly the integration indicated in Eq. (85), and calculated values of σ/σ_0 for values of $\delta q(=\delta/r)$ ranging from 0 to 0.3 (see reference 1, p. 337, Table I). These results are of course applicable to the general case here considered.

In order to go further, and calculate σ as a function of q, it is necessary to know δ. But this information, as it happens, is not obtainable, from experimental data of any type at present available, by means of thermodynamic equations alone. The reason for this may be indicated by considering the case of the plane surface layer, as follows. In this case Eq. (57) gives:

$$\Gamma_i=\Gamma_i^{*}+\delta(c_i^{\alpha}-c_i^{\beta}). \tag{86}$$

Now it can be shown that (when the variables $x_3\cdots x_{\kappa+1}$ are observable) the quantities Γ_i^{*} for the plane surface layer are exactly computable from ordinary experimental data (surface tensions, partial molal volumes, activity coefficients) by means of thermodynamic equations (Gibbs' adsorption theorem, etc.). It then follows from Eq. (86) that the computability of δ is equivalent to that of the surface concentrations Γ_i referred to the surface of tension. These quantities are however not computable as are the quantities Γ_i^{*}; it can be shown that in order to compute Γ_i it is necessary to know $\partial\sigma/\partial q$ (i.e., just the quantity with whose independent calculation we are here concerned), and the direct measurement of this quantity is not experimentally feasible owing to its extreme smallness. Consequently, δ eludes determination by thermodynamic methods. For the one-component system Tolman met this situation by devising a "quasi-thermodynamic" method which led to a rough estimate of Γ_1 (referred to the surface of tension) for a number of common liquids,[10] and in this way found δ to be positive (α being the liquid phase) of the order of 10^{-8} cm. This then led to an undetectably small effect of curvature upon surface tension[1] for the one-component case, in agreement with empirical experience. Still more recently Kirkwood and Buff[11] have given a statistical mechanical analysis of surface tension which yields values of δ in simple cases; for liquid argon at 90°K they find $\delta=3.63\times10^{-8}$ cm (α being the liquid), in good agreement with Tolman's result for other liquids.

For the multicomponent case here considered we have as yet no specific information concerning δ. In the absence of such information we can still use our result in the following two ways. (i) In any particular case (involving a specific choice of independent variables, see Part III, §C) in which direct measurement shows surface tension to be independent of curvature within experimental error (and this is of course usually the case, if not indeed always), we may conclude that δ is extremely small, and therefore, since the surface of tension certainly lies within the surface layer, that the auxiliary surface lies within or extremely close to the surface layer. (ii) In any particular case in which we may assume that the auxiliary surface lies within or extremely close to the surface layer, we may conclude, since the surface of tension does lie within the surface layer, and this layer is extremely thin, that the effect of curvature upon surface tension will be extremely small, over the range of curvature ordinarily used in surface tension measurements (say $0\leq|q|\leq 10^4$ cm^{-1}).

[9] It is also worth noting that the two equations (52) and (72), which locate the auxiliary surface for Cases A and B respectively, can be compactly subsumed under the single equation $\sum_{i=1}^{k}\frac{\partial\mu_i}{\partial q}\Gamma_i^{*}=0$. This follows immediately on comparing with Eq. (11), on the one hand Eqs. (52) and (31), and on the other hand Eqs. (72) and (44).

[10] R. C. Tolman, J. Chem. Phys. **17**, 118 (1949).

[11] J. G. Kirkwood and R. P. Buff, J. Chem. Phys. **17**, 338 (1949).

Appearance Potentials of Some Metastable Transition Ions Found in Hydrocarbon Mass Spectra

R. E. Fox and Alois Langer
Westinghouse Research Laboratories, Pittsburgh, Pennsylvania
(Received October 3, 1949)

The appearance potentials of some metastable transition peaks in normal butane, isobutane, the butenes, and 1,3-butadiene have been studied along with the parent ions in each metastable transition. A comparison shows that in most cases studied, an additional energy of about 2 ev is required for the formation of the metastable state. However, in the case of normal butane, two transitions were studied in which no additional energy was required within an experimental error of 0.3 ev. Evidence is presented which indicates that in some cases the appearance potentials of ions in hydrocarbon spectra are affected by these metastable ion contributions. This effect may account for some of the unexplained discrepancies found in published data on hydrocarbon gases. Check values of some ions in methane, ethane, and propane were taken to determine the performance of the instrument. A comparison of these results is made with previously published data.

I. INTRODUCTION

THE study of various hydrocarbon gases with a mass spectrometer revealed several diffuse peaks in their spectra. These peaks have been attributed to metastable ions* which spontaneously dissociate during transit through the mass spectrometer tube[1–3] with very little, if any, energy release at the instant of dissociation. Calculations have shown that the half-life of these ions is of the order of 2×10^{-6} second.[4]

The object of this study was to determine if any excess energy is associated with this metastable condition. A comparison of the appearance potential of a metastable transition ion with that for the parent ion in a dissociation process would then give a measure of the excess energy required for the formation of the metastable state. Fortunately, some of these metastable transition ions give rise to peaks at masses where there is little (or no) interference by other ions.

II. APPARATUS AND EXPERIMENTAL PROCEDURE

The mass spectrometer used in these experiments has a sectored magnetic field, the ions being deflected through a 90° angle on a 5-inch radius of curvature. The ion currents were measured with a pen and ink recorder having sensitivity sufficient to record currents of 2×10^{-15} ampere. This recorder and certain features of the mass spectrometer have been previously described.[5,6]

Two methods of taking the data with the recorder were employed. In the first method the electron energy was successively decreased by small decrements, the peak heights being recorded for each value. A plot of these peak heights as a function of the electron energy gave a relative ionization efficiency curve.

The second method employed the use of a motor driven potentiometer to vary the electron accelerating voltage continuously. The mass scanning mechanism was disconnected so that the recorder pen was recording only the top of the peak in question. The recorder then gave a continuous trace of the ion current as a function of the electron energy. The voltage drop across the motor driven potentiometer could be adjusted so that any desired rate of changing the electron energy could be selected. This then meant that the voltage scale on the charts could be selected to give the desired accuracy in the voltage readings. A series of tests indicated that these voltage readings could be determined to better than ±0.1 volt.

A series of fixed shunts combined with a variable sensitivity control on the recorder allowed the over-all sensitivity of the recorder to be adjusted so that ion currents covering a range in values of 10,000 to 1 could be recorded linearly. It was thus possible to adjust the recorder sensitivity so as to give approximately the same slope to the ionization efficiency curves at their straight portions near the point of vanishing ion current.

The appearance potentials of all ions discussed in this paper was taken at that electron energy (ev) which gave the first detectable ion current. This method has been used extensively by many investigators in the studies of ionization by electron impact. A paper by Mariner and Bleakney[7] gives a discussion of the significance of this method of vanishing current along with a discussion of the linear extrapolation method used recently by Vought.[8]

The filament was a 5-mil diameter tungsten wire heated with current from storage batteries. In all cases the ion accelerating voltage was maintained at 600 volts.

* Those delayed transitions which give rise to peaks at non-integral or irrational masses have been termed "metastable transitions." For want of a more suitable short descriptive phrase, such peaks arising from these transitions are designated as metastable transition peaks.

[1] J. A. Hipple and E. U. Condon, Phys. Rev. **68**, 54 (1945).
[2] Hipple, Fox, and Condon, Phys. Rev. **69**, 347 (1946).
[3] Bloom, Mohler, Legel, and Wise, J. Research Nat. Bur. of Stand. **40**, 437 (1948).
[4] J. A. Hipple, Phys. Rev. **71**, 594 (1947).
[5] Hipple, Grove, and Hickam, Rev. Sci. Inst. **16**, 69 (1945).
[6] D. J. Grove and J. A. Hipple, Rev. Sci. Inst. **18**, 837 (1947).
[7] Thomas Mariner and Walker Bleakney, Phys. Rev. **72**, 807 (1947).
[8] R. H. Vought, Phys. Rev. **71**, 93 (1947).

III. PRECAUTIONARY TESTS

In order to insure that there were no secondary effects entering into the results due to instrumental design, several precautionary tests were made. The appearance potential of mass 58 in normal butane was measured several times over a 5 to 1 range in ionizing electron current. No change in the appearance potential greater than ±0.1 volt was detected. In addition, the pressure of the normal butane in the mass spectrometer tube was varied by a factor of 3 with no measurable difference in the appearance potential.

Appearance potential measurements on methane, ethane, and propane were made to determine the operation of the apparatus over a fairly wide mass range. The data on these gases are given in Table I.

The results indicated that though the values appeared to be constantly higher than previously published values by a little over 0.1 volt, they fall largely within the limits of experimental error.

In this work all values of the electron energies were corrected by measuring the appearance potential of argon ($m/e=40$) and correcting this value against the spectroscopic value of 15.76 ev.[9] Whenever possible the argon was admitted to the mass spectrometer tube simultaneously with the gas being studied. However, in some cases when the hydrocarbon gave an appreciable mass 40 peak this was not feasible. Several check runs gave no detectable difference in the values of the appearance potentials with and without argon being admitted simultaneously.

IV. RESULTS ON SOME METASTABLE TRANSITION IONS

1. Normal Butane

In normal butane there are three transitions which give rise to metastable transition peaks of sufficient size that ionization efficiency curves could be taken with the instrument described above. These transitions are:

$$C_4H_{10}^+(58)\rightarrow C_3H_7^+(43)+15 \qquad M^*=31.9$$
$$C_4H_{10}^+(58)\rightarrow C_3H_6^+(42)+16 \qquad M^*=30.4$$
$$C_3H_7^+(43)\rightarrow C_3H_5^+(41)+2 \qquad M^*=39.2$$

M^* denotes the apparent mass of the metastable transition ion appearing in the spectrum. The neutral fragment is merely designated by the mass number since we have no information as to its structure (i.e. one or more fragments). Figures 1 and 2 show the ionization efficiency curves near the appearance potentials for some of the ions in normal butane. Figure 2 gives a comparison of the ionization efficiency curves for the metastable transition peaks 30.4 and 31.9 with that of the parent mass (58) in the dissociation process. The curves indicate that these three peaks have the same appearance potential although the shape of curves for the metastable transition ions differs slightly from

TABLE I. Appearance potentials of parent ions in methane, ethane, and propane.

Compound	Appearance pot. (A^+) This research (ev)	Appearance pot. (A^+) Previously published (ev)
Methane ($m/e=16$)	13.4±0.2	13.1$_8$,[a] 13.0$_4$,[b] 13.0$_4$,[c] 13.0[d]
Ethane ($m/e=30$)	11.9±0.2	11.59,[c] 11.76,[b] 11.77,[e] 11.5,[d]
Propane ($m/e=44$)	11.4±0.2	11.3,[f] 11.21,[b] 11.30,[e] 11.2[d]

[a] L. G. Smith, Phys. Rev. **51**, 263 (1937).
[b] R. E. Honig, J. Chem. Phys. **16**, 105 (1948).
[c] J. J. Mitchell and F. F. Coleman, J. Chem. Phys. **17**, 44 (1949).
[d] M. B. Koffel and R. A. Lad, J. Chem. Phys. **16**, 420 (1948).
[e] D. P. Stevenson and J. A. Hipple, J. Am. Chem. Soc. **64**, 1588 (1942).
[f] J. Delfosse and W. Bleakney, Phys. Rev. **56**, 256 (1939).

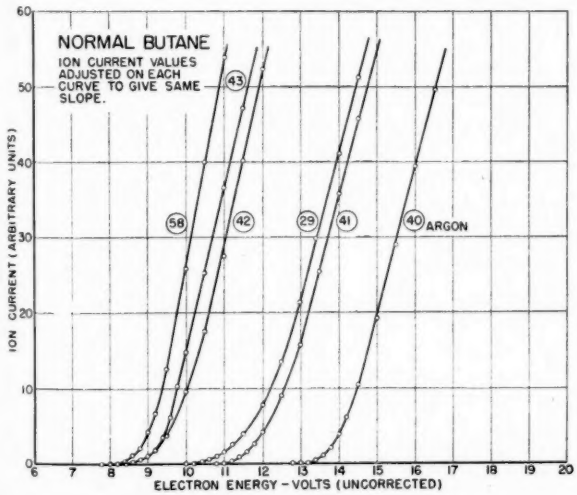

FIG. 1. Ionization efficiency curves for some ions in the normal butane spectrum. The voltage scale has not been corrected against the spectroscopic value of 15.76 ev for argon (40).

[9] R. F. Bacher and S. Goutsmit, *Atomic Energy States* (McGraw-Hill Book Company, Inc., New York, 1932). Recomputed using the new conversion factor 1 ev=8066 cm^{-1}.

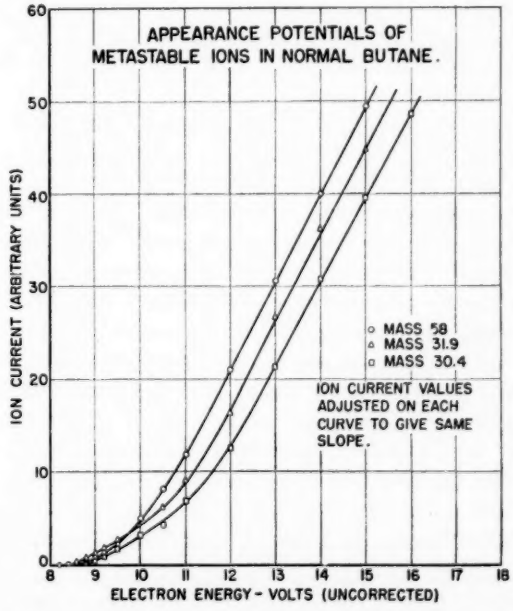
APPEARANCE POTENTIALS OF METASTABLE IONS IN NORMAL BUTANE.
o MASS 58
Δ MASS 31.9
o MASS 30.4
ION CURRENT VALUES ADJUSTED ON EACH CURVE TO GIVE SAME SLOPE.
ION CURRENT (ARBITRARY UNITS)
ELECTRON ENERGY - VOLTS (UNCORRECTED)

FIG. 2. A comparison of the ionization efficiency curves for two metastable transition peaks with that of the parent ion in the transitions. The relative abundance of the metastable transition peaks to the mass 58 ion is about 0.1.

TABLE II. Appearance potentials of metastable ions in hydrocarbon gases.

Ion	A (ion) ev	Energy difference (ev)
	Normal Butane	
$C_4H_{10}^+(58)$	11.0±0.1	$A(58)^+-A(31.9)^*=0$
$C_3H_7^+$ (43)	11.6±0.1 (low sens.)	$A(58)^+-A(30.4)^*=0$
$C_3H_7^+$ (43)	11.0±0.1 (high sens.)	$A(43)^+-A(31.9)^*=0$
$C_3H_6^+$ (42)	11.3±0.2 (low sens.)	$A(42)^+-A(30.4)^*=0$
$C_3H_6^+$ (42)	11.0±0.2 (high sens.)	$A(41)^+-A(39.2)^*=0.1$
$C_3H_5^+$ (41)	13.6±0.2	$A(39.2)^*-A(43)^+=2.1$
$C_3H_3^+$ (39)	15.9±0.5	
$M^*=39.2$	13.7±0.5	
$M^*=31.9$	11.0±0.2	
$M^*=30.4$	11.0±0.2	
	Isobutane	
$C_4H_{10}^+(58)$	10.7±0.2	
$C_3H_7^+$ (43)	11.7±0.2 (low sens.)	$A(41)^+-A(39.2)^*=0$
$C_3H_7^+$ (43)	10.9±0.2 (high sens.)	$A(39.2)^*-A(43)^+=1.9$
$C_3H_5^+$ (41)	13.6±0.2	
$M^*=39.2$	13.6±0.3	

TABLE III. Appearance potentials of metastable ions in hydrocarbon gases.

Ion	A (ion) ev	Energy difference (ev)
	Butene-1	
$C_4H_8^+(56)$	9.77±0.1	$A(41)^+-A(30)^*=0.1$
$C_3H_5^+(41)$	11.72±0.2	$A(30)^*-A(56)^+=1.9$
$M^*=30$	11.63±0.2	
	Cis-butene-2	
$C_4H_8^+(56)$	9.24±0.1	$A(41)^+-A(30)^*=0.1$
$C_3H_5^+(41)$	11.59±0.2	$A(30)^*-A(56)^+=2.3$
$M^*=30$	11.47±0.2	
	Isobutylene	
$C_4H_8^+(56)$	8.78±0.1	$A(41)^+-A(30)^*=0.6$
$C_3H_5^+(41)$	11.36±0.2	$A(30)^*-A(56)^+=2.0$
$M^*=30$	10.76±0.2	
	1,3-Butadiene	
$C_4H_6^+(54)$	9.2±0.1	$A(39)^+-A(28.2)^*=0.4$
$C_3H_3^+(39)$	11.9±0.2	$A(28.2)^*-A(54)^+=2.3$
$M^*=28.2$	11.5±0.5	

that of mass 58. The ion current values of the metastable transition peaks were multiplied by a constant factor in order to match the slopes of the straight line portions of the curves. Within the accuracy of the measurements, these three appearance potentials are identical (±0.2 ev).

The mass 42 and 43 peaks are interesting in that they are composed of ions arising from two different processes: those which are formed by electron impact immediately, and those which arise from the delayed transitions mentioned above.** Since this metastable state has a half-life of 10^{-6} second, a large fraction of these ions will dissociate in the ionizing region before they can be drawn out and accelerated through the analyzer. Consequently, these ions will appear as normal mass 42 and mass 43 ions. However, these ions should have the same appearance potential as the metastable transition peaks with which they are associated in the transitions.

The first studies made on these peaks indicated that in normal butane the appearance potential of mass 43 was about 0.6 volt greater than that of mass 58 which was in some agreement with previously published data by Stevenson and Hipple (see reference e of Table I), but which did not agree with data given by Mitchell and Coleman (see reference c of Table I), who found the difference to be about 0.15 ev. However, since the 43 peak in normal butane is about seven times more abundant than the 58 peak, and since the evidence pointed to the fact that only a small percentage of the 58 ions experienced a delayed dissociation, it was felt that the effect in question was lost due to the insensitive range which was used in taking the mass 43 ionization curve. In view of this, the ionization efficiency curve for mass 43 was retaken at low electron energies using a considerably more sensitive recorder range. The results are shown in Fig. 3. In this figure the high and low sensitivity differ by a factor of approximately 10. Note that in Fig. 3B the appearance potential is 9.0 volts (uncorrected). The high sensitivity curve Fig. 3A shows the uncorrected value of the appearance potential to be 8.4 volts which agrees with the value for mass 58. The sharp break B in Figure 3A occurs at about 9.0 volts (uncorrected) which is interpreted as being the appearance potential of the mass 43 ions formed by immediate fragmentation due to electron impact. This checks with the value of the appearance potential (9.0 volts) obtained in Fig. 3B. In addition, there is an unexplained sharp break (A) occuring in the two curves at about 9.6 volts.

The second transition listed involved the mass 58 ion dropping 16 mass units becoming a mass 42 ion.

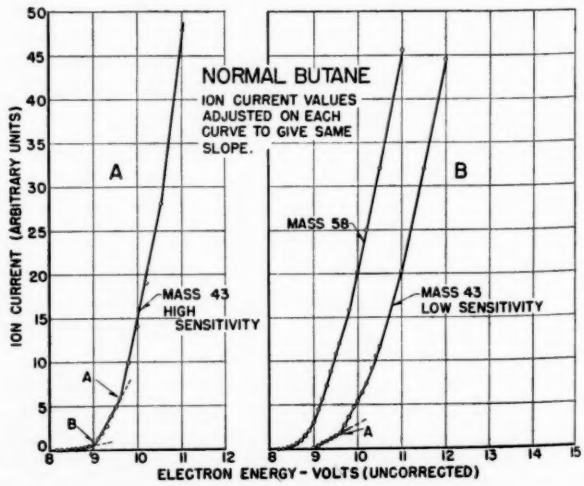

FIG. 3. Ionization efficiency curves for mass 43 in normal butane showing the effect of the metastable ions on the appearance potential.

** Since the mechanism for ion fragmentation is not clearly understood, those mechanisms which occur in times short compared to 1 microsecond are designated as due to direct electron impact as differentiated from those which occur with a delayed dissociation. It is of course understood that all the mechanisms discussed arise primarily from electron impact phenomena.

As discussed above, the 42 ion should then have the same appearance potential as the metastable transition peak 30.4. It was found that the mass 42 ionization curve broke over to give a value for the appearance potential identical to the mass 58 ion. The corrected values for the appearance potentials observed in normal butane are given in Table II.

The third metastable transition gives rise to a peak appearing at mass 39.2. In the spectrum this peak appears as a prominent "hump" on the side of the normal 39 peak which is formed by indirect fragmentation due to electron impact. In this transition the parent ion is mass 43, presumably those formed by electron-impact fragmentation rather than those formed by a delayed dissociation. From Table II it is seen that the appearance potential of the metastable transition ion is 13.7 volts while that of the 43 ion is 11.6 volts (corrected value). This gives an energy difference of 2.1 volts. The inaccuracy of the value for the 39.2 peak is due primarily to a long tailing of the ionization efficiency curve. There should be little interference from the mass 39 peak since its appearance potential is 15.9 volts which is some 2 volts greater than the value for the metastable transition peak 39.2. This transition then requires about 2 volts additional energy.

Applying the same reasoning here as was used above for the other transitions, the appearance potential of the mass 41 peak should agree with that of the metastable transition peak 39.2. The values given in Table II are 13.6 volts for mass 41 and 13.7 volts for mass 39.2, in good agreement within the experimental error.

2. Isobutane

In isobutane the two metastable transition peaks at masses 31.9 and 30.4 were too small to permit ionization efficiency curves to be taken which would have any significance. For this reason no attempt was made to determine these appearance potentials.

On the other hand the mass 39.2 peak is larger in this case than for normal butane, which undoubtedly is due to the fact that the 43 peak in isobutane is also larger.

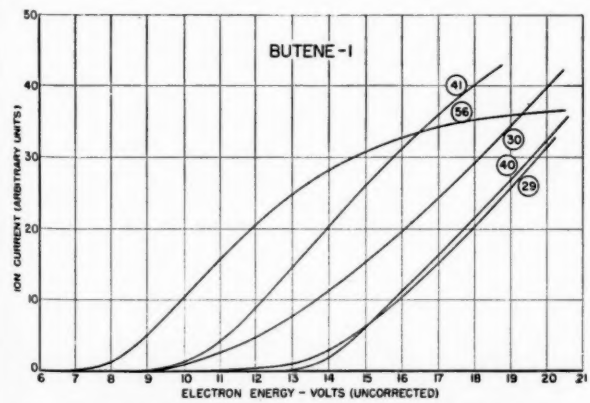

FIG. 4. Ionization efficiency curves for some ions in butene-1. These curves are continuous recorder tracings. The encircled numbers are the mass numbers of the ions. Mass 40 is that from argon.

The transition giving rise to the 39.2 peak is the same as the one discussed for normal butane. The appearance potentials obtained for isobutane are also listed in Table II. From this table, it is seen that the appearance potential of mass 43 is 11.7 volts whereas that for the metastable transition peak 39.2 is 13.6 volts. This gives a difference in energy of 1.9 ev which is about the same as the value of 2.0 volts obtained in normal butane. One should note here also that the 41 peak and 39.2 peak again have the same appearance potential.

3. The Butenes

In butene-1 *cis*-butene-2, and isobutylene only one metastable transition peak was studied. This peak occurs through the same transition in all three compounds and is present in all three spectra at mass 30 with approximately the same abundance. The transition giving rise to this peak is:

$$C_4H_8^+(56) \rightarrow C_3H_5^+(41)+15; \quad M^*=30.$$

The results on the appearance potentials studied for these compounds are listed in Table III. From the values listed in this table, it is observed that for all three compounds the energy difference between the appearance potentials of the parent ion and the metastable transition peak is about 2 ev, the agreement being within the limits of experimental error. It is interesting to note that this energy difference is the same as that observed for the mass 43 transition in normal and isobutane.

Here again, as in the case of the butanes, those ions after dissociation (in this case mass 41) have the same appearance potential as the metastable transition peak. For isobutylene, however, the difference between these two values is 0.6 ev which is outside the limits of error by 0.2 ev. The values for the appearance potentials of mass 56 and 41 for these three compounds agree quite well with previously published results. A comparison of these data is given in Table IV.

Figure 4 shows the ionization efficiency curves taken for several masses in butene-1. These curves are continuous recorder tracings of the peaks with the electron energies decreasing as outlined in the second method discussed above.

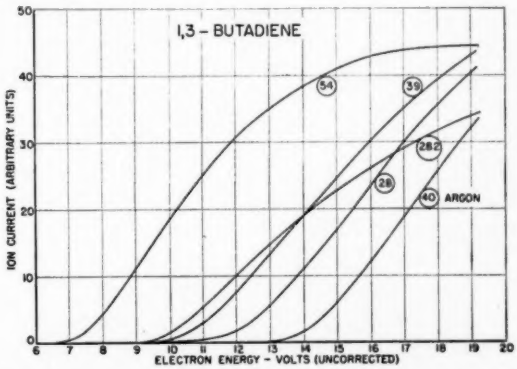

FIG. 5. Ionization efficiency curves for some ions in 1,3-butadiene. These curves are continuous recorder tracings, the encircled numbers designating the mass of the ion.

TABLE IV.

Compound	Appearance potential A (ion) ev This research	A (ion) ev Previously published
Butene-1		
$C_4H_8^+(m/e=56)$	9.77±0.1	9.65[a], 9.76[b], 10.0[c]
$C_3H_5^+(m/e=41)$	11.72±0.2	11.65[a], 11.80[c]
Cis-butene-2		
$C_4H_8^+(m/e=56)$	9.24±0.1	9.41[d], 9.29[b]
$C_3H_5^+(m/e=41)$	11.59±0.2	11.66[d]
Isobutylene		
$C_4H_8^+(m/e=56)$	8.78±0.1	8.86[e], 9.64[c]
$C_3H_5^+(m/e=41)$	11.36±0.2	11.51[e], 11.80[e]

[a] See reference 11.
[b] R. E. Honig, J. Chem. Phys. 16, 105 (1948).
[c] J. J. Mitchell and F. F. Coleman, J. Chem. Phys. 17, 44 (1949).
[d] See reference 12.
[e] See reference 10.

4. 1,3-Butadiene

There is a large metastable transition peak in the 1,3-butadiene spectrum at mass 28.2 which is given by the transition

$$C_4H_8^+(54)\rightarrow C_3H_3^+(39)+15, \quad M^*=28.2.$$

The values of the appearance potentials of these peaks ore also given in Table III. The value of A (54) is 9.2 ev while that for A (28.2) is 11.5 ev giving an energy difference of 2.3 ev. This value agrees within the limits of error with the energy differences obtained in the other compounds. Hence again, as in the other cases cited, the ion after transition (mass 39) has the same appearance potential as the metastable peak within the limits of error. The ionization efficiency curves for some peaks in 1,3-butadiene are shown in Fig. 5. These curves were also taken by the second method outlined above.

The shape of the ionization efficiency curve for mass 54 differs considerably from a curve obtained by Sugden and Walsh.† However, in view of the difference in methods used in the two cases no real comparison can be made. Sugden and Walsh observed a double maximum in the ionization curve which gave rise to ionization potentials at 8.71 ev and 9.02 ev. They attributed these two values as belonging to the "*cis-*" and "*trans-*" isomers, respectively. Since, in the present work, the temperature was at least 100°C one might possibly explain the lack of a double ionization maximum on the grounds that the butadiene was composed largely of the "*trans-*" isomer. The value of 9.02 ev quoted by Sugden and Walsh for the "*trans-*" isomer ionization potential is then in substantial agreement with the value of 9.2 ev obtained in this work.

V. DISCUSSION

An interpretation of the various dissociations discussed above was made using thermochemical data along with appearance potential data previously taken.[10–15]‡ These data were used in conjunction with the energies involved in the processes in an attempt to determine the nature of the neutral fragments. If it is assumed, as is quite reasonable, that the ionization potentials of hydrocarbon-free radicals are in the range, 6–8 ev, then the appearance potentials observed in this paper are only consistent with the processes involving the "loss" of one C−C or one C−H bond, since the dissociation energies of these bonds are known to lie in the ranges, 3.4–3.6 and 4.0–4.4 ev, respectively. As an example, in the case of the transitions involving the loss of 15 mass units, the energy requirements are only consistent if one assumes that this mass is lost as a CH_3 radical. Similarly, in the case of the butanes where the transition involves the loss of 16 mass units, the energy requirements are consistent only if we assume this mass to be lost as a CH_4 molecule.

VI. SUMMARY

The appearance potentials of several metastable transition ions in six hydrocarbon gases were studied. In most cases the appearance potential of the metastable transition peak was about 2 ev in excess of that for the parent ion in the transition in question.

In two cases involving normal butane, no additional energy was observed. However, in all cases it was possible to show that the energy requirements for the transitions were satisfied by the energy required for the appearance potential of the metastable transition peaks in question. In fact, in most cases the agreement was very good.

It is felt that quite possibly a large amount of the discrepancies in appearance potential data found in the literature may arise from metastable transition ions formed in hydrocarbon gases as evidenced by the data on the mass 43 and 42 peaks from the butanes. If the ion mass in question arises from two different processes, then different values for the appearance potential can be obtained depending on the sensitivity of the instrument.

The writers wish to express their appreciation to Dr. J. A. Hipple of the National Bureau of Standards, Washington, D. C., for his many discussions and suggestions.

Appreciation is also expressed to Mr. D. J. Grove of this laboratory for his many helpful suggestions; in particular his suggestion that we search for the break in the ionization efficiency curve of mass 43 in normal butane due to the metastable transition ions which dissociate in the ionization chamber.

† T. M. Sugden and A. D. Walsh, Trans. Faraday Soc. 41, 76 (1945).

[10] D. P. Stevenson and J. A. Hipple, J. Am. Chem. Soc. 64, 2769 (1942).
[11] D. P. Stevenson, J. Am. Chem. Soc. 65, 209 (1943).
[12] V. H. Dibeler, J. Research Nat. Bur. Stand. 38, 329 (1947).
[13] D. P. Stevenson, J. Chem. Phys. 10, 291 (1942).
[14] Selected Thermochemical Data, U. S. Department of Commerce, National Bureau of Standards, December 31, 1947.
[15] F. O. Rice and K. K. Rice, *The Aliphatic Free Radicals* (The Johns Hopkins Press, Baltimore, 1935).
‡ See also reference f of Table I.

The Ratio of the Specific Heats of Gases, C_p/C_v, by a Method of Self-Sustained Oscillations*

W. F. KOEHLER**
Department of Physics, The Johns Hopkins University, Baltimore, Maryland
(Received October 3, 1949)

The ratio c_p/c_v at room temperature has been determined for He, A, H_2, N_2, O_2, CO_2, N_2O, SO_2, CH_4, and C_2H_4 by a method of self-sustained oscillations. The results are reproducible to within 0.1 percent and agree with the best values reported by other observers to within 0.1 percent. The method requires the measurement of a temperature, a pressure and a period of oscillation. The theory of the self-sustained oscillations has been developed to include the effects of the mass of the oscillating gas, damping, heat conduction, and the departure of the behavior of actual gases from the ideal gas law.

INTRODUCTION

THE method of self-sustained oscillations is an extension of the method reported by Rüchardt.[1] His apparatus consists of a large flask in which is inserted a vertical, precision-bored tube containing a matching ball bearing. His procedure consists of filling the flask and tube with gas until the ball bearing is raised to a position near the top of the tube. The ball bearing is then given an impulse to start an oscillatory motion. If one assumes that the pressure is uniform throughout the container, that the change in pressure is small in comparison with the equilibrium value, that the damping is negligible, that the oscillations occur adiabatically and that the thermal conductivity is negligible, then the ball bearing should execute simple harmonic motion of angular frequency

$$\omega=[\gamma A^2P_0/(mV_0)]^{\frac{1}{2}}.$$

γ is the ratio of the specific heats c_p/c_v, A and m are the cross-sectional area and mass of the ball bearing. P_0 and V_0 are the average values of the pressure and volume. Thus, γ can be determined from relatively simple measurements. However, the results obtained by this method disagree with the accepted values of γ by as much as 10 percent.

The apparatus used in the method of self-sustained oscillations is shown in Fig. 1. It is a Rüchardt apparatus with a small hole drilled in the wall of the tube and an inlet to compensate for the escaping gas. Briefly, the method of measuring γ using this new apparatus is as follows. The container is filled with a gas and by adjustment of the needle valve the ball is caused to rise slowly in the tube until it passes the hole, at which time a small amount of gas escapes to start the oscillation. The ball is then caused to oscillate symmetrically with respect to the hole, by finer adjustment of the needle valve. The value of γ can be calculated to within 0.1 percent of the accepted value from measurements of period of oscillation, pressure, temperature and constants of the apparatus.

THEORY OF SELF-SUSTAINED OSCILLATIONS

The ball is caused to oscillate by allowing a small amount of gas to escape through the small hole in the wall of the tube during the positive half of the displacement cycle. If y represents the displacement of the ball from its equilibrium position, then its equation of motion is of the form

$$m_e\ddot{y}+R\dot{y}=(P-P_0)A,$$

where m_e is the effective mass of the oscillator, R is a constant of proportion between the mechanical friction and the velocity, P is the instantaneous value of the pressure, P_0 is the equilibrium value of the pressure, and A is the cross-sectional area of the ball.

In the following section, it is shown that when $y=y_0\sin\omega t$

$$(P-P_0)=-\left[M-\frac{cfN}{\omega}\right]\sin\omega t -\left[N+\frac{4cfM}{3\omega}-\frac{4f}{\pi\omega}(P_0-B)\right]\cos\omega t,$$

where M and N are quantities which depend upon the physical properties of the gas, c is a geometrical factor, B is the corrected barometer reading, and f is a constant governing the rate of escape of the gas through the small hole. Furthermore, it is shown that $y=y_0\sin\omega t$ represents the displacement of the ball to a high degree of approximation.

Substitution of the expression for $(P-P_0)$ in the equation of motion yields

$$\ddot{y}+\left[\frac{R}{m_e}+\frac{NA}{m_e\omega y_0}\right]\dot{y}+\frac{MA}{m_ey_0}y=\frac{A}{m_e}\frac{cfN}{\omega}\sin\omega t +\frac{A}{m_e}\left[\frac{4f}{\pi\omega}(P_0-B)-\frac{4cfM}{3\omega}\right]\cos\omega t.$$

The right side of the equation can be interpreted as a

* From the dissertation submitted in partial fulfillment of the requirements for the degree of Doctor of Philosophy at The Johns Hopkins University.
** Present address: Department of Physics, U. S. Naval Postgraduate School, Annapolis, Maryland.
[1] E. Rüchardt, Physik. Zeits. **30**, 58 (1929).

UNIVERSITY OF MICHIGAN LIBRARIES

periodic driving force resulting from the escape of gas through the small hole during the positive half of the displacement cycle. The coefficient of the y term is the square of the natural frequency of oscillation, that is

$$\omega_0^2 = MA/m_e y_0.$$

The dependence of M upon the physical properties of the gas is given by

$$M = \frac{-\gamma A y_0 (v_0/V_0)(\partial P_0/\partial v_0)_T}{1+h+h^2},$$

where h is a quantity much smaller than unity which takes account of thermal conduction and the consequent deviation of the actual process from the ideal adiabatic process. It is convenient to denote $1+h+h^2$ by H, so that H is a correction factor for thermal conduction with a value near unity. If also the factor $-(v_0/P_0)(\partial P_0/\partial v_0)_T$ be replaced by $1/G$, then G is a factor which would be unity if the gas were ideal and is actually a number approximately equal to unity. By the use of these factors, the expression for M may be written

$$M = \gamma \frac{AP_0}{V_0 HG}.$$

Combining this equation with the expression for ω_0^2 yields

$$\gamma = m_e V_0 \omega_0^2 GH/(A^2 P_0).$$

If the mass of the oscillating gas is appreciable in comparison with the mass of the ball, then the pressure will not be uniform throughout the volume. If the container were a uniform cylinder with a diameter equal to that of the ball, then the oscillation would be analogous to that of a weight at the end of a spring of appreciable mass. The effective mass would then be obtained by adding one-third of the mass of the gas to the mass of the ball. Accordingly, it is assumed that for containers of other shapes the effective mass is obtained by adding to the mass of the gas a fraction of the mass of the oscillating gas. Since the mass of the gas is proportional to the density, one can write the following expression for the effective mass.

$$m_e = m + c\rho = m(1+c'\rho) = mE, \tag{1}$$

where m is the mass of the ball. Substituting this for m_e in the preceding expression for γ yields

$$\gamma = mV_0\omega_0^2 EGH/(A^2 P_0).$$

Another correction factor is necessary to account for the difference between the measured frequency and the natural frequency ω_0. This difference is due to the mechanical friction and a component of the pressure, N, which is 180° out of phase with the velocity of the ball and, therefore, acts like a dissipative force. The dependence of N upon the physical properties of the gas is given by

$$N = Mh/(1+h),$$

where h is a quantity small compared to 1 and proportional to the square root of the thermal conductivity. Thus, the N-component of the pressure vanishes for gases with negligible thermal conductivity. To evaluate this damping correction factor, $y = y_0 \sin\omega t$ is substituted in the equation of motion. Then, equating the coefficients of the sine terms yields

$$\omega_0^2 \doteqdot \omega^2\left[1+\frac{cf}{\omega}\frac{h}{1+h}\right] = \omega^2 D. \tag{2}$$

Substitution of this expression for ω_0^2 in the equation for γ yields

$$\gamma = mV_0\omega^2 DEGH/(A^2 P_0). \tag{3}$$

This result reduces to that of the elementary theory under the following conditions: (1) When the thermal conductivity of the gas is negligible, D and H are approximately one; (2) when the mass of the gas is negligible in comparison with the mass of the ball, E is approximately one; and (3) when the gas obeys $PV = RT$, G is one. These conditions are three of the five assumptions of the elementary theory. The fourth assumption of the elementary theory, namely,

$$P - P_0 = (V - V_0)(dP/dV)_0$$

is also used in this more rigorous theory. It is used in the computation of the quantities M and N. This assumption can be satisfied experimentally by using a very small hole in the wall of the tube. The size of the hole is the dominant factor in determining the amplitude of oscillation and the amplitude is proportional to $(V - V_0)$. The fifth assumption of the elementary theory, namely, that the mechanical friction is negligible, is less stringent in this more rigorous theory. It is assumed that the mechanical friction force is less than $0.01\,MA$ where MA is the force due to the largest component of the pressure $(P - P_0)$. This assumption is

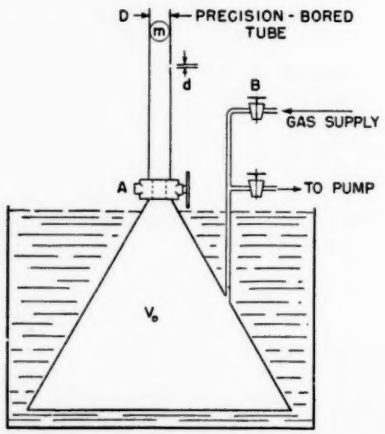

FIG. 1. Self-sustained oscillation apparatus. $D = 1.587$ cm, $d = 0.058$ cm, $m = 16.25$ g, $V_0 = 1.07$ l; A is a ½-inch gas cock, and B is a No. 315 Hoke needle valve.

used in the derivation of the expression for $(P-P_0)$ and can be satisfied experimentally by using a very clean, smooth tube and ball.

SOLUTION FOR $(P-P_0)$

Clark and Katz[2] analyzed the system shown in Fig. 2. They assumed a displacement of the piston small enough so that

$$(\underline{P}-P_0)=(\partial P/\partial v)_T\Delta\underline{v}+(\partial P/\partial T)_v\Delta\underline{T}$$

would be a sufficient approximation for the variation in pressure. The quantities underscored are complex functions to allow for phase differences. v represents the volume of unit mass of gas. T represents the temperature. They solved this equation considering the heat conducted to the walls of spherical and cylindrical containers and obtained the following expression for the change in pressure when the piston oscillates according to $y=y_0\sin\omega t$:

$$\text{(Real)}\quad (P-P_0)=-M\sin\omega t-N\cos\omega t, \qquad (4)$$

where P is the instantaneous value of the pressure in the left container, $N=hM/(1+h)$, $h=(S/V)\times(\gamma-1)(1-\epsilon)/\alpha 2^{\frac{1}{2}}$, (S/V) is surface area/volume, $\alpha^2=(\omega c_p\rho)/k$, ρ is the mean density of the gas, k is the thermal conductivity, c_p is the specific heat at constant pressure, ϵ is the ratio of the discontinuity in the temperature at the gas-metal surface to the discontinuity that would exist if no heat exchange took place between the gas and the walls of the container.

$$M=F/(1+h+h^2-h^3+--)=F/H, \qquad (5)$$

and

$$F=-Ay_0\gamma v_0(\partial P_0/\partial v_0)_T/V_0=Ay_0\gamma P_0/(V_0G). \qquad (6)$$

In the apparatus shown in Fig. 1 the rate of change of pressure, dP/dt, is composed of several contributions. The contributing processes, in order of decreasing magnitude, are the displacement of the ball, the supply of gas, the escape of gas through the annular area between the ball and the wall of the tube, and the escape of gas through the small hole in the wall of the tube. At this place in the analysis it will be assumed that the displacement of the ball can be represented by $y=y_0\sin\omega t$. Later in the analysis the validity of this assumption is considered. If $y=y_0\sin\omega t$ is the displacement of the ball then the contribution to dP/dt due to the displacement can be obtained by differentiating the Clark and Katz expression for $(P-P_0)$, that is,

$$-\omega M\cos\omega t+N\sin\omega t.$$

The contribution to dP/dt due to the supply of gas is a positive constant, J. The contribution to dP/dt due to the gas escaping through the annular area around the ball is negative and proportional to the difference in pressure between the inside and outside of the container,

$$-e(P-B).$$

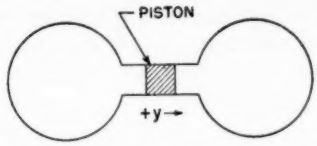

FIG. 2. System analyzed by Clark and Katz.

The contribution to dP/dt due to the gas escaping through the small hole in the wall of the tube is negative and proportional to the difference in pressure between the inside and outside of the container. This contribution is made only during the positive half of the displacement cycle. Therefore, this contribution can be represented by

$$\begin{aligned} -f(P-B) &\quad \text{for} \quad 0\leq t\leq\tau/2 \\ 0 &\quad \text{for} \quad \tau/2\leq t\leq\tau. \end{aligned}$$

If e/f be denoted by r, then

$$e=rf \quad \text{or} \quad e+f=(1+r)f=uf.$$

The ratio r is of the order of the ratio of the annular area between the ball and the tube to the area of the hole. For this apparatus the value of r is between 0 and 2. Summing the contributions to (dP/dt) yields

$$(dP/dt)_1=-M\cos\omega t+N\sin\omega t-uf(P-B)+J \quad \text{for} \quad 0\leq t\leq\tau/2$$

$$(dP/dt)_2=-M\cos\omega t+N\sin\omega t-rf(P-B)+J \quad \text{for} \quad \tau/2\leq t\leq\tau.$$

Note that the subscripts 1 and 2 indicate the positive half and negative half of the cycle respectively.

Since the contribution to dP/dt due to the displacement of the ball is by far the largest contribution, the expression

$$P=P_0-M\sin\omega t-N\cos\omega t$$

is used as *zero-order approximation* for the value of P in the expressions for $(dP/dt)_1$ and $(dP/dt)_2$. An integration yields

$$P_1=\left[\frac{ufN}{\omega}-M\right]\sin\omega t-\left[\frac{ufM}{\omega}+N\right]\cos\omega t+K_1t+c_1,$$

$$P_2=\left[\frac{rfN}{\omega}-M\right]\sin\omega t-\left[\frac{rfM}{\omega}+N\right]\cos\omega t+K_2t+c_2,$$

where $K_1=J-uf(P_0-B)$, $K_2=J-rf(P_0-B)$ and the c's are the constants of integration. Consequently, $K_2-K_1=f(P_0-B)$. Thus, the slow passage of gas through the apparatus, which is necessary to maintain the oscillations, contributes the terms K_1t and K_2t in the preceding equations and these linear terms may be considered as a saw-tooth component in the pressure. Making use of the continuity of the pressure at the middle and at the beginning and end of the cycle

[2] A. L. Clark and L. Katz, Can. J. Research **21A**, 1 (1943).

provides still other relations which are used to reduce the number of constants to a minimum.

To obtain $P=P(t)$ which is continuous in the interval $0\leq t\leq\tau$ and which may be used to investigate the effects of higher harmonics in P, the pressure

$$P=P_1 \quad \text{for} \quad 0\leq t\leq\tau/2$$

and

$$P=P_2 \quad \text{for} \quad \tau/2\leq t\leq\tau$$

is expanded in a Fourier series,

$$P(t)=P_0+\sum_1^\infty a_n \sin n\omega t+\sum_1^\infty b_n \cos n\omega t.$$

Computation of a_n and b_n by the usual procedure yields a first approximation for the pressure which is continuous. A second approximation for a continuous pressure function can be obtained by substituting the result of the first approximation in the equations for $(dP/dt)_1$ and $(dP/dt)_2$ and then repeating the procedure used to obtain the first approximation. The result of the second approximation, neglecting the harmonics beyond the second, is

$$\begin{aligned}P(t)=P_0&-\left[M-(1+2r)\frac{f}{\omega}N-\left(\frac{1+2r}{2}\right)^2\frac{f^2}{\omega^2}M\right.\\&\left.+\left(\frac{1+2r}{\pi}\right)\frac{f^2}{\omega^2}(P_0-B)+\frac{4(1+2r)}{18\pi^2\omega}\frac{f}{\omega}N\right]\sin\omega t\\&-\left[N+(1+2r)\frac{f}{\omega}M-\left(\frac{1+2r}{2}\right)^2\frac{f^2}{\omega^2}N\right.\\&\left.-\frac{4f}{\pi\omega}(P_0-B)\right]\cos\omega t\\&-\left[\frac{fM}{3\pi\omega}-\frac{2(1+2r)}{3\pi}\frac{f^2}{\omega^2}N\right]\sin 2\omega t\\&-\left[\frac{2fN}{3\pi\omega}+\frac{1+2r}{3\pi}\frac{f^2}{\omega^2}M-\frac{4}{3\pi^2}\frac{f^2}{\omega^2}(P_0-B)\right]\cos 2\omega t.\end{aligned}$$

It is desirable to simplify the coefficient of the sine term because it is used to derive the damping factor D of Eq. (2). Simplification can be obtained by equating $(m/A)\ddot{y}+(R/A)\dot{y}$ to the first harmonic of $P(t)$. When the first harmonic of the displacement $y'=y_0'\sin\omega t$ is substituted, then the equation is an identity in $\sin\omega t$ and $\cos\omega t$. From the coefficients of the cosine terms one obtains

$$y_0'\frac{R}{A}=-N-(1+2r)\frac{f}{\omega}M+\left(\frac{1+2r}{2}\right)^2\frac{f^2}{\omega^2}N+\frac{4f}{\pi\omega}(P_0-B).$$

Solving this identity for $(1+2r)f^2(P_0-B)/\pi\omega^2$ and then substituting in the coefficient of the sine component of $P(t)$ yields

$$\begin{aligned}-\left[M-\frac{3}{2}\frac{(1+2r)}{2}\frac{f}{\omega}N-\left(\frac{1+2r}{2}\right)^3\frac{f^3}{\omega^3}\frac{N}{2}\right.\\\left.+\frac{1}{2}\frac{(1+2r)}{2}\frac{f}{\omega}M\frac{R\omega y_0'}{MA}+\frac{4(1+2r)}{18\pi^2\omega}\frac{f}{\omega}N\right]\sin\omega t.\end{aligned}$$

The ratio of the fifth term to the second term is 0.002 and this term is therefore negligible. The ratio of the fourth term to the second term is

$$\frac{M}{3N}\frac{R\omega y_0'}{MA}.$$

The fraction $R\omega y_0'/MA$ is the ratio of the mechanical friction force to the force due to the largest component of the pressure, M. For helium, which is the extreme case, the fourth term is only 0.01 of the second term if the mechanical friction force is 0.002 of the force due to the largest component of the pressure. It seems reasonable to assume that the mechanical friction force is not larger than 0.002 of MA when the tube is mounted vertically and both the tube and ball are clean. When so mounted, it is found experimentally that the ball spins very rapidly within the tube. Therefore, the fourth term is negligible in comparison with the second. Incidentally, the determination of γ for helium from experimental data would be changed by 0.1 percent if the ratio $R\omega y_0'/MA$ were as large as 0.01. When this simplification is introduced in the coefficient of $\cos 2\omega t$, the second approximation reduces to

$$\begin{aligned}P(t)=P_0&-\left[M-\frac{3}{2}\left(\frac{1+2r}{2}\right)\frac{f}{\omega}N-\frac{1}{2}\left(\frac{1+2r}{2}\right)^3\frac{f^3}{\omega^3}N\right]\sin\omega t\\&-\left[N+2\left(\frac{1+2r}{2}\right)\frac{f}{\omega}M-\left(\frac{1+2r}{2}\right)^2\frac{f^2}{\omega^2}N\right.\\&\left.-\frac{4f}{\pi\omega}(P_0-B)\right]\cos\omega t\\&-\left[\frac{fM}{3\pi}-\frac{4}{3\pi}\left(\frac{1+2r}{2}\right)\frac{f^2}{\omega^2}N\right]\sin 2\omega t\\&-\frac{fN}{3\pi\omega}\cos 2\omega t.\end{aligned}$$

To investigate the relative magnitudes of the remaining components of the pressure, it is necessary to obtain an approximate value of f/ω. Consider the apparatus with the ball removed, the open end capped and the small hole closed. Then consider the apparatus filled with a gas so that the pressure is equal to P_0 and the temperature is T_0. When the small hole is opened, the pressure will decrease initially according to

$$(dP/dt)=-f(P_0-B)=-fmg/A, \qquad (7)$$

TABLE I. Data used to determine the constants of apparatus No. 3.

Date	6/26/48	7/3/48	6/30/48	6/26/48
Gas	CO_2	N_2	H_2	He
γ, ratio of c_p to c_v	1.3000	1.4028	1.4047	1.6667
G, correction to ideal gas	1.0052	1.0002	.99975	1.0006
$k\times10^5$, cal./sec. cm °C	3.950	5.986	42.40	35.85
$R_m\times10^{-6}$, erg/g °C	1.890	2.968	41.25	20.78
Temperature at barometer, °C	29.2	28.6	30.7	28.0
Barometer reading, cm Hg	75.910	75.990	75.680	75.950
Barometer reading, cm Hg	75.900	75.990	75.685	75.960
Barometer reading, cm Hg	75.900	76.000	75.680	75.960
Barometer reading, cm Hg	75.900	76.000	75.675	75.970
Average value, cm Hg	75.902	75.995	75.680	75.960
Barometer correction, cm Hg	−.401	−.395	−.419	−.388
B, atmospheric pressure, cm Hg	75.501	75.600	75.261	75.572
ΔP, weight of ball/area, cm Hg	.622	.622	.622	.622
P_0, mean gas pressure, cm Hg	76.123	76.222	75.883	76.194
T_0, mean gas temperature, °K	298.2	299.3	301.4	298.1
y_0, displacement amplitude, cm	1.3	1.8	2.2	1.8
Time of 500 oscillations, sec.	185.64	178.78	182.74	171.21
Time of 500 oscillations, sec.	185.63	178.67	182.76	171.18
Time of 500 oscillations, sec.	185.64	178.87	182.60	171.08
Time of 500 oscillations, sec.	185.63	178.76	182.71	170.98
Average value, sec.	185.63	178.77	182.70	171.11
τ, period of oscillation, sec.	.37127	.35754	.36540	.34222
c'', an estimate	9.75	9.75	9.75	9.75

where mg is the weight of the ball and A is its cross-sectional area. Since f is used to compute small correction terms, it is sufficient to write

$$\frac{dP}{dt}=-\frac{\gamma P_0}{V_0}\frac{dV}{dt}=-\frac{\gamma P_0}{V_0}Wa \tag{8}$$

where W is the initial velocity of escape and a is the area of the hole. W can be computed by making use of the fundamental equation of fluid dynamics, that is,

$$(\partial \underline{w})/(\partial t)+\underline{w}\ \text{grad}\cdot\underline{w}=\underline{F}-(1/\rho)\ \text{grad}P,$$

where $\underline{w}$ is the velocity and $\underline{F}$ is the body force on unit mass of the fluid, which in this case is the vector sum of a horizontal friction force and the vertical gravitational force. The energy dissipated due to friction in the escape channel through the wall of the tube decreases with the length of the channel. In this case the length of the channel, along which a pressure gradient exists, is very small since the hole through the wall of the tube was bored with a wide-angle drill. Therefore, it is assumed that the friction force encountered by unit mass of the gas as it escapes through the wall of the tube may be ignored. Assuming a steady linear flow in the horizontal x direction during a short interval of time after the hole is opened, the preceding equation reduces to

$$w(dw/dx)=-(1/\rho)(dP/dx).$$

Assuming that the gas escapes adiabatically, use can be made of $P/\rho^\gamma=K$ to integrate the preceding equation. The limits of integration are determined by the condition that inside the container $P=P_0$ and $w=0$, while outside the container $P=B$ and $w=W$, the initial velocity of escape. Accordingly,

$$\frac{W^2}{2}=\frac{\gamma R_m T_0}{\gamma-1}\left[1-\frac{B}{P}\right]^{(\gamma-1)/\gamma}\doteq R_m T_0 \ln P_0/B. \tag{9}$$

Combining Eqs. (7), (8) and (9) and then dividing by ω yields

$$\frac{f}{\omega}=c(\gamma P_0\tau)(10^{-6}R_m T_0 \ln P_0/B)^{\frac{1}{2}}, \tag{10}$$

where $c=9600aA/(\pi m V_0)$ when P_0 is measured in cm of Hg and R_m is measured in ergs/g degree. Substituting measured values of a, A, m and V_0 the numerical value of c is 9.3×10^{-4}. The value of f/ω for helium, which is the largest possible due to its values of γ and R_m, is approximately 0.25. This estimate of f/ω for helium is high because the effective area of the hole is less than the measured area. A minimum value of f/ω for helium is 0.06 which is obtained by considering the effective diameter of the hole equal to one-half of the measured diameter. The corresponding maximum and minimum values of $(1+2r)f/2\omega$ for helium are 0.6 and 0.06. Incidentally, the value of $(1+2r)f/2\omega$ obtained from an experimental determination of the constants of the apparatus, which is described later, is 0.102. Consequently, the terms in the expression for $P(t)$ containing powers of $(1+2r)f/2\omega$ higher than the first are negligible in comparison with terms containing $(1+2r)f/2\omega$. Thus, the second approximation for $P(t)$ reduces to

$$P(t)=P_0-\left[M-\frac{3}{2}\left(\frac{1+2r}{2}\right)\frac{f}{\omega}N\right]\sin\omega t$$

$$-\left[N+2\left(\frac{1+2r}{2}\right)\frac{f}{\omega}M-\frac{4f}{\pi\omega}(P_0-B)\right]\cos\omega t$$

$$-\frac{fM}{3\pi\omega}\sin2\omega t-\frac{fN}{3\pi\omega}\cos2\omega t.$$

To determine the effects of the second harmonic in the expression for $P(t)$ it is necessary to estimate the

TABLE II. Comparison of apparatus constants.

	c_0	C	c'	c''
Appears in equation	(11)	(12)	(13)	(14)
Estimate from rough measurements	13.2	1.5×10^{-4} to 47.0×10^{-4}	—	9.75
From Fig. 3	13.307	5.03×10^{-4}	.0590	10.25

amplitudes of the harmonics of the displacement. The amplitude of the harmonics of the displacement can be obtained by equating $(m/A)\ddot{y}+(R/A)\dot{y}$ to each harmonic of $P(t)$ and solving the resulting differential equations. The harmonic solutions are of the form $y'=y_0'\sin\omega t$, $y''=y_0''\sin2\omega t$, etc. The maximum value of the ratio y_0''/y_0', for all the gases investigated, is 0.01 and the ratio of the higher harmonics to the first is much less than 0.01. This indicates that the maximum value of the average kinetic energy of the second harmonic vibration is at most 0.0004 of the average kinetic energy of the first harmonic vibration. Thus, one may conclude that the second harmonic of $P(t)$ is negligible in comparison with the first harmonic and that $y=y_0\sin\omega t$ represents the displacement of the ball to a very high degree of approximation. Finally,

$$P(t)-P_0=-\left[M-\frac{f}{\omega}c-N\right]\sin\omega t$$

$$-\left[N+\frac{4cf}{3\omega}M-\frac{4f}{\pi\omega}(P_0-B)\right]\cos\omega t$$

where $c=3(1+2r)/4$.

EXPERIMENTAL DETERMINATION OF THE APPARATUS CONSTANTS

For the convenience of the reader, Eq. (3) is rewritten as follows:

$$\gamma=\frac{mV_0\omega^2DEGH}{(A^2P_0)}=\gamma'DEGH. \qquad (3')$$

When the pressure P_0 is measured in cm of Hg and the period is measured in seconds, then

$$\gamma'=c_0/P\tau^2 \quad \text{where} \quad c_0=4\pi^2V_0/(A^2g\rho_{Hg}). \qquad (11)$$

Combining Eqs. (2) and (10) yields, for the damping correction factor,

$$D=1+C\left(\frac{h}{1+h}\right)(\gamma P_0\tau)$$

$$\times(10^{-6}R_mT_0\ln P_0/B)^{\frac{1}{2}}=1+Cd \qquad (12)$$

where $C=3(1+2r)(aA\rho_{Hg})/(5.66\pi mV_0 10^{-3})$.

Equation (1) defines E which corrects for the mass of the oscillating gas. One would not expect this factor to be much different from 1 and, therefore, ρ in this equation can be replaced by P_0/R_mT_0 with sufficient accuracy. Thus,

$$E=1+c'\rho=1+c'P_0/R_mT_0, \qquad (13)$$

where c' is a constant depending upon the geometry of the apparatus. The factor G which corrects for the deviation of the actual gas from the ideal gas law is defined by Eq. (6).

$$G=-(P_0/V_0)(\partial v_0/\partial P_0)_{T_0}.$$

It is computed from empirical equations of state such as

$$(Pv)_T=A+BP+CP^2+DP^3\cdots.$$

Thus, the G factor is independent of the constants of the apparatus. The factor H which corrects for the deviation of the process from the ideal adiabatic process is defined by Eq. (5) which is

$$H=1+h+h^2-h^3\cdots,$$

where

$$h=(1-\epsilon)(S/V)(\gamma-1)(k/2\rho c_p\omega)^{\frac{1}{2}}.$$

It is desirable to eliminate ρ and c_p since each would require an independent measurement which is difficult to make. In making this small correction, the gas may be regarded as ideal and ρc_p may be replaced by $(\gamma P)/(\gamma-1)T$, yielding

$$h=c''\left[\frac{(\gamma-1)^3}{\gamma}\frac{kT_0\tau}{P_0}\right]^{\frac{1}{2}}, \qquad (14)$$

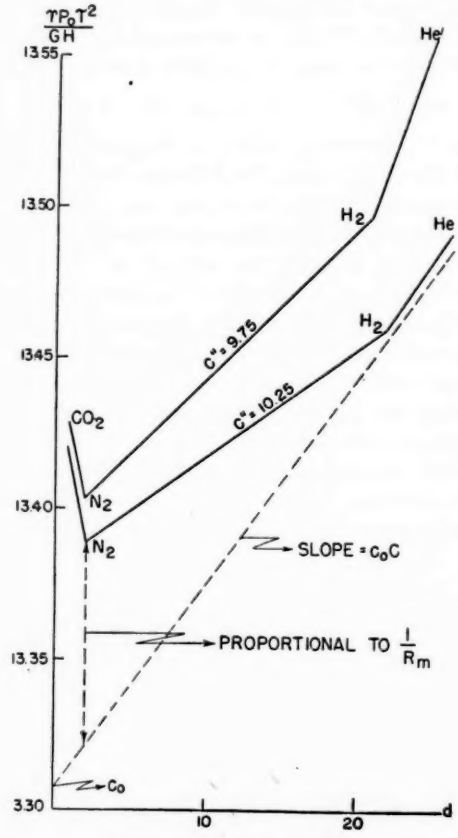

FIG. 3. Graph of Eq. (15).

where c'' is a constant made up of dimensions of the apparatus and conversion factors to take care of the units. The numerical value of this constant is determined by

$$c''=(1-\epsilon)(S/V_0)(J/4\pi g\rho_{Hg}).$$

Thus, there are in Eq. (3′) four constants which depend upon the dimensions of the apparatus; namely, c_0, C, c' and c''. Before one can compute γ by substituting data in this equation, one must determine these four constants. All could be determined from direct measurements but the accuracy would be insufficient unless elaborate methods were used. To simplify the determination of the four constants and to check the foregoing theory, it was decided to choose four gases for which γ, G, k and R_m are known with the greatest possible accuracy and to determine the constants experimentally. A special apparatus, No. 3, was constructed such that none of the four constants would be negligible. To make c'' large, the ratio, surface area/volume, had to be made large. To have a large c'' and a compact apparatus which would minimize temperature gradients, a conical container was chosen. This choice, however, required the additional assumption that the solution for $(P-P_0)$ in a conical container, when the oscillations are non-adiabatic, would be of the same form as Eq. (4) which Clark and Katz[2] derived for spherical and cylindrical containers. The four gases chosen were CO_2, N_2, H_2 and He. The wide range of values of γ, G, k and R_m included by this choice is shown in Table I. The values of γ and G are those reported by Clark and Katz;[2] the values of k are those reported by Johnston and Grilly;[3] and the values of R_m are those tabulated by Kennard.[4]

As a preliminary step in determining the constants, the correction for the mass of the gas is ignored and E is thus taken as 1. Equation (3′) may then be written in the more convenient form

$$\gamma P_0\tau^2/(GH)=c_0+c_0Cd. \qquad (15)$$

Using data of Table I, all quantities of Eq. (15) can be computed except C and c_0. The graph of Eq. (15) is a straight line with a slope equal to c_0C and an intercept equal to c_0. If the four points corresponding to the four gases are plotted, they will probably not lie on a straight line for one or both of two reasons. First, Eq. (15) neglects the mass correction factor; and second, the measured value of c'' used in computing H and d is only an estimate. If the mass of the oscillating gas is appreciable, the points for CO_2 and N_2 are located above the straight line determined by the points for H_2 and He because the mass correction factor for the latter is negligible in comparison with that of the former. The graph obtained with the estimated value of c'' will show the sense of the estimate used and will indicate a better value. Using a better value of c'', H and d are recomputed and the points again plotted. The process is continued until the points for CO_2 and N_2 lie above the straight line determined by the points for H_2 and He, with the deviations inversely proportional to R_m. From these deviations the value of c' is determined. Usually three trials are sufficient to determine the best value of c''. The graph of Eq. (15) is plotted in Fig. 3 for $c''=9.75$, which is an estimate, and for $c''=10.25$, which is the best value for apparatus No. 3. Table II shows the values of the four constants obtained from Fig. 3 compared with the values determined from rough measurements.

Substitution in Eq. (3′) of the numerical values of the four constants, as determined from Fig. 3, yields the equations used in computing the results found in the following section.

$$\gamma=\gamma' DEGH$$
$$\gamma'=13.307/P_0\tau^2$$
$$D=1+0.000503(h/1+h)(\gamma P_0\tau)(10^{-6}R_mT_0\ln P_0/B)^{\frac{1}{2}}$$
$$E=1+0.0590P_0/10^{-6}R_mT_0$$
$$G=-(P_0/v_0)(\partial v/\partial P)_{T_0}$$
$$H=1+h+h^2-h^3\cdots$$
$$h=10.25[(\gamma-1)^2kT_0\tau/\gamma P_0]^{\frac{1}{2}}.$$

To compute the correction terms D and H, approximate values of γ and k are required. In most cases handbook values of these two quantities are sufficient.

RESULTS

To demonstrate the accuracy with which the results can be reproduced and to show the order of magnitude of the four correction factors, the data and results for methane are recorded in detail in Table III. This gas was obtained from the Matheson Company which claims a purity of 99.0 percent with 0.5 percent ethane, 0.3 percent nitrogen and 0.2 percent carbon dioxide as the contaminants. The value of G was calculated by making use of the equation

$$(Pv)_{25}=1.0894-1.804\times10^{-3}P$$

which was determined by interpolation of the data

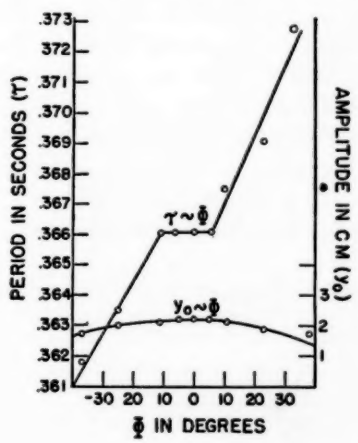

FIG. 4.

[3] H. L. Johnston and E. R. Grilly, J. Chem. Phys. **14**, 233 (1946).
[4] E. H. Kennard, *Kinetic Theory of Gases* (McGraw-Hill Book Company, Inc., New York, 1938) p. 26.

TABLE III. Data and results for methane.

Date	6/27/48	8/3/48	8/4/48	8/10/48
P_0	75.785	75.747	75.481	76.491
T_0	298.4	298.7	298.1	295.8
y_0	1.80	1.80	1.80	1.90
τ	0.37076	0.37064	0.37146	0.36901
$k\times10^5$	8.134	8.144	8.124	8.050
γ'	1.27743	1.27878	1.27768	1.27755
E	1.00290	1.00289	1.00288	1.00294
G	1.00202	1.00202	1.00202	1.00202
D	1.00110	1.00110	1.00110	1.00108
H	1.01712	1.01714	1.01715	1.01680
γ	1.3071	1.3085	1.3074	1.3069

Average value: 1.3075±0.0005
Eucken: 1.31

found in the "International Critical Tables." The value of k was obtained by interpolation of the values reported by Johnston and Grilley.[3] The measured quantities in Table III have the same units as in Table I. The value by Eucken[5] is taken from his table of most probable values.

The values of γ for all the gases investigated by the method of self-sustained oscillations at 25°C and 1 atmosphere are shown in Table IV. Each value is the average of four independent sets of measurements except in the case of argon.

TABLE IV. γ by self-sustained oscillations at 25°C and 1 atmosphere.

Gas	Purity (%)	γ(Koehler)	γ(others)	Reference
A	99.6	1.6647	1.6702	2
He	99.8	1.6671±.0004	1.6667	2
H_2	99.95	1.404±.001	1.4047	2
N_2	99.6	1.4029±.0001	1.4028	2
O_2	99.5	1.3986±.0008	1.396	5
CO_2	99.5	1.2995±.0004	1.3000	2
N_2O	99.0	1.2858±.0004	1.2847	2
SO_2	99.9	1.285±.005	1.2837	2
CH_4	99.0	1.3075±.0005	1.31	5
C_2H_4	99.5	1.2469±.0003	1.25	5

ERRORS

The constant errors, such as occur in the measuring devices and in the determination of the constants of the apparatus, are reduced to a minimum by the experimental method which was used to determine the constants in Eq. (3′).

The magnitude of the possible error in γ due to errors in the auxiliary data, such as thermal conductivity and Pv data, depends upon the gas being investigated. In the case of helium, which has the largest thermal conductivity of all the gases investigated, an error of 1 percent in the value of k causes an error of 0.05 percent in γ. In the case of sulfur dioxide, which has the largest G correction factor of all the gases investigated, a maximum difference of 0.2 percent occurs in the value of γ if G is calculated using Pv data by different observers as was shown by Clark and Katz.[2]

Accidental errors occur when measuring the period of oscillation, pressure and temperature. If the oscillation is stable the period can be measured with an error less than 0.05 percent which causes an error in γ of less than 0.1 percent. Incidentally, the stability of oscillation is very sensitive, being disturbed by slight drafts of air, normal closing of doors and unsettled atmospheric conditions. The pressure can be measured with an error less than 0.05 percent which causes an error in γ of less than 0.05 percent. The temperature can be measured with an error less than 0.1 percent which causes an error in γ of less than 0.005 percent.

Another possible source of error is in the adjustment of the oscillation so that it takes place symmetrically with respect to the hole in the tube. The unique characteristics of this oscillator, as shown in Fig. 4, make the effect of this error in the value of γ less than 0.1 percent. Figure 4 shows the variation of the amplitude with the phase angle of the hole in the tube relative to the center of oscillation. This phase angle is called Φ. Figure 4 also shows the variation of period of oscillation with Φ. The data plotted in Fig. 4 is for hydrogen which has the largest variation of all the gases investigated. For gases which have a small thermal conductivity, the plateau of period is much longer than that for hydrogen. This plateau of period is responsible for the small average deviation of a set of measurements of the period of oscillation (see Table I).

The precision with which the values of γ can be reproduced is apparent from the results. It is believed that the major portion of the average deviation for any particular gas can be accounted for by the simple but not too adequate method of introducing the gas into the apparatus, which causes a slight contamination. Furthermore, it is believed that the method is applicable to most gases because of the range of values included by the selection of the ten investigated gases. The range of values follows.

Ratio C_p/C_v	1.25 to 1.67
Thermal conductivity$\times10^5$	2.10 to 42.0
Gas constant$\times10^{-6}$	1.30 to 41.3
Deviation from ideal gas, G	1.00 to 1.02

ACKNOWLEDGMENTS

The author is grateful to Professor R. T. Cox and Professor J. Strong for the suggestions they made during the course of this work.

[5] A. Eucken, Handbuch der Experimentalphysik 8 (Part 1) 433 (1929).

Elastic Scattering and Neutralization of Low Velocity Hydrogen Ions in Normal Butane and Isobutane

J. H. SIMONS AND W. H. CRAMER
School of Chemistry and Physics, The Pennsylvania State College, State College, Pennsylvania
(Received October 3, 1949)

The low velocity scattering of H^+, H_2^+, and H_3^+ in both normal and isobutane has been measured at ion velocities of less than 150 volts. Ion neutralization was detected and measured for all three ions in both hydrocarbons. The potential functions between the ion and molecule as evaluated from the elastic scattering have been obtained for all three ions in both hydrocarbons. For H^+ these functions in both hydrocarbons have the same form with the same values of the exponent over the same range of distance. The force constant, however, is considerably greater for the branch chain compound. For certain ranges of distances the potential functions of the three different ions in both of the hydrocarbons show values of the exponent less than 4. For substances possessing no permanent dipole similar results have previously been obtained only in those cases where there is a potentiality of chemical combination.

INTRODUCTION

ALTHOUGH isobutane is thermodynamically slightly more stable than normal butane, its rate of reaction in acid catalyzed condensation is very much greater. An explanation for this phenomenon is not easy to obtain. The obvious fact that the branch chain compound contains a tertiary hydrogen atom is difficult to use to explain this phenomenon because the products of the acid catalyzed condensation between isobutane and aliphatic olefins are difficult to rationalize on the basis of an explanation involving the removal of the tertiary hydrogen atom. It would appear, therefore, that some factor significant in the kinetics of the reaction would need to be taken into consideration. As the scattering in the vapor phase of protons by the gas molecules is an unambiguous experimental method of exploring the basic properties of the molecule, it would appear profitable to obtain such data. This basic property is considered of significance in some of the postulated mechanisms in this type of reaction.[1]

Previous experiments in this laboratory have established the technique for studying the scattering of ions in hydrocarbon gases at low pressure.[2]

In order to make measurements of satisfactory precision with molecules of higher molecular weight, it was necessary to improve the precision of pressure measurement. This has been accomplished in this laboratory and has recently been reported.[3]

The hydrocarbons used were samples of very high purity obtained by the courtesy of Dr. Merrell R.

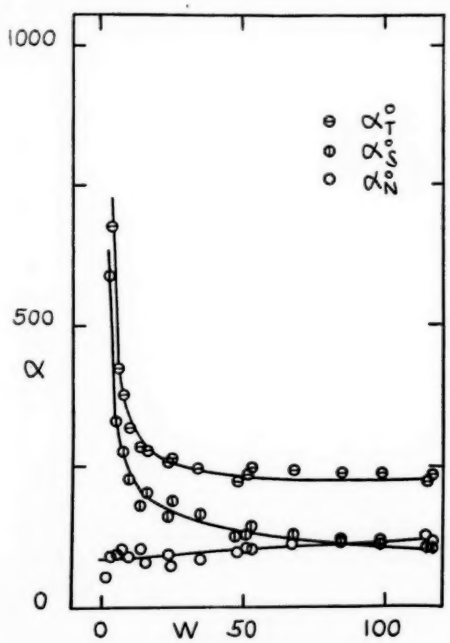

FIG. 1. Scattering of H^+ in normal butane.

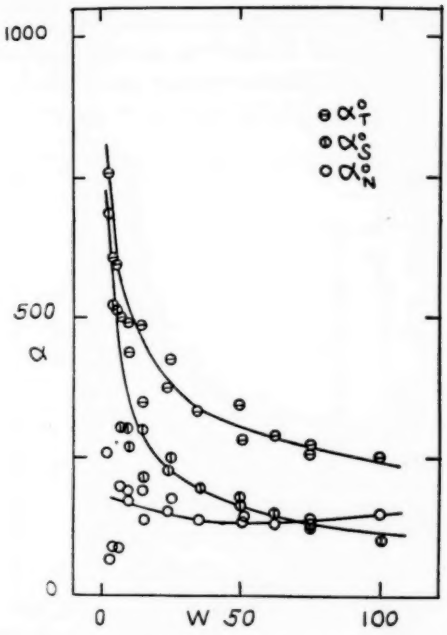

FIG. 2. Scattering of H_2^+ in normal butane.

[1] J. W. Sprauer and J. H. Simons, J. Am. Chem. Soc. **64**, 648 (1942). W. H. Pearlson and J. H. Simons, J. Am. Chem. Soc. **67**, 352 (1945).
[2] J. H. Simons and G. C. Fryburg, J. Chem. Phys. **13**, 216 (1945). J. H. Simons and L. G. Unger, J. Chem. Phys. **13**, 221 (1945).
[3] G. H. Fryburg and J. H. Simons, Rev. Sci. Inst. **20**, 541 (1949).

TABLE I. Scattering of hydrogen ions in normal butane.

H^+			H_2^+			H_3^+		
W volts	$\alpha_T°$*	$\alpha_S°$†	W volts	$\alpha_T°$	$\alpha_S°$	W volts	$\alpha_T°$	$\alpha_S°$
117	236	107	100	250	102	100	116	91
115	226	108	75	256	124	100	135	108
99	239	117	75	272	138	75	177	149
85	239	121	62	288	150	75	201	169
68	245	129	51	279	143	63	184	152
53	248	145	50	344	177	63	218	188
52	234	130	35	332	195	50	247	206
48	224	126	24.5	424	251	50	269	223
34	247	163	23.7	373	224	35	313	273
24.9	265	190	15.0	348	212	35	320	276
24.2	259	163	14.5	488	299	24.9	398	351
16.3	284	204	10.0	438	268	24.8	365	314
14.7	287	183	9.8	491	301	14.5	410	346
10.2	317	227	7.2	502	302	9.8	492	422
8.2	379	276	5.4	599	516	7.0	593	530
5.7	425	330	4.5	606	522	4.5	902	822
3.3	678	589	3.1	757	691	2.5	1251	1168
1.9	1231	1178	1.4	1334	1079	2.0	2061	1972

* $\alpha_T°$ is the total cross section of the molecule extrapolated to zero pressure.
† $\alpha_S°$ is the effective cross section of the molecule for scattering extrapolated to zero pressure.

TABLE II. Scattering of hydrogen ions in isobutane.

H^+			H_2^+			H_3^+		
W volts	$\alpha_T°$*	$\alpha_S°$†	W volts	$\alpha_T°$	$\alpha_S°$	W volts	$\alpha_T°$	$\alpha_S°$
100	279	208	100	228	103	100	96	62.5
100	269	197	100	254	109	100	97	65.0
75	318	234	75	242	116	75	119	85.0
62	300	227	62	250	126	62	122	82.1
62	295	223	50	263	138	62	121	79.4
50	338	228	50	283	144	50	181	132
35	357	254	35	294	175	35	218	161
25	371	268	25	391	220	25	229	171
25	348	269	15	455	294	25	234	184
15	364	280	15	499	359	15	398	348
10	456	334	10	560	430	15	433	380
10	441	338	7.0	635	386	10	737	698
7.0	512	478	5.4	989	826	7.0	799	744
5.2	544	451	3.8	1235	1060	5.2	1008	940
3.7	914	830				3.1	1379	1300
3.2	1434	1356						

* $\alpha_T°$ is the total cross section of the molecule extrapolated to zero pressure.
† $\alpha_S°$ is the effective cross section of the molecule for scattering extrapolated to zero pressure.

Fenske, Director of the Petroleum Refining Laboratory, The Pennsylvania State College.

RESULTS

In Table I are given the results of the scattering of hydrogen ions in normal butane. These results are also shown in Figs. 1, 2, and 3. In the figures the symbols $\alpha_S°$ and $\alpha_T°$ have the same significance as they have in the tables. $\alpha_N°$ is the zero pressure effective cross section of the molecule for electron exchange (ion neutralization). Potential function graphs are shown in Figs. 4, 5, and 6. In Table II the results of the scattering of hydrogen ions in isobutane are shown and also in Figs. 7, 8, and 9, with the potential function graphs in Figs. 10, 11, and 12. The potential laws as evaluated from the graphs are shown in Table III. In evaluating the potential functions an approximate treatment suggested by Kells[4] was used. This gives a value of the force constant within one percent of that obtained by the more elaborate exact treatment. This involves n and Q obtained from the plot of log$W$ *versus* logα_s in the same way as previously used to obtain the approximate value of the force constant. These values are then

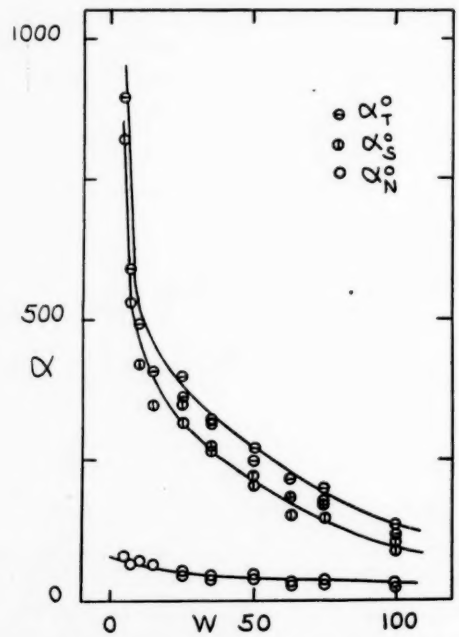

FIG. 3. Scattering of H_3^+ in normal butane.

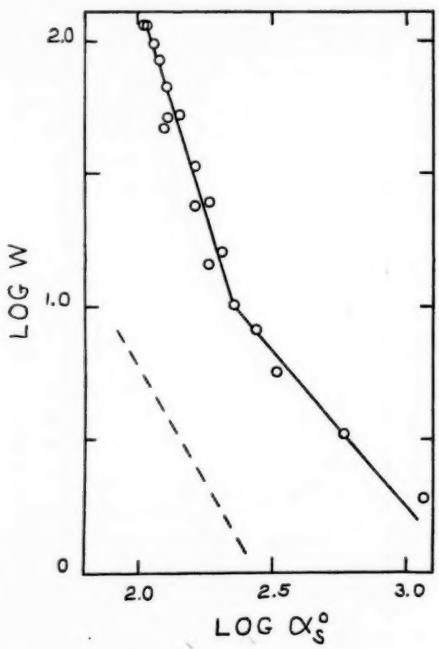

FIG. 4. H^+ in normal butane.

[4] M. C. Kells, J. Chem. Phys. **16**, 1174 (1948).

substituted in the following equation:

$$K_a' = \left[\frac{Q}{n\pi N[(1/\{2+n\})+(m_1/2\mu C)(a/l)]}\right]^{n/2}\left[\frac{a}{lC}\right].$$

The values of the symbols in this equation are identical with those previously used in publications in this field of study but more specifically are as follows: K_a' = force constant in potential law, $V=-K/r^n$, where V is potential energy and r is distance. n = the exponent in the potential law. $Q=\alpha_S W^{2/n}$, where W = initial potential energy of ion in volts, α_S = effective cross section for scattering of the molecule in cm^2/cm^3 $=(1/R_S-1)/(1/R_T-1)\alpha_T$, where R_T = ratio of unscattered current to total current, R_S = ratio of unscattered current to total current less the current lost by electron exchange, α_T = total cross section in $cm^2/cm^3=(F/P)\log 1/R_T$, where P = gas pressure in mm Hg, $F=[2.303(273.1+t)]/[l(273.1)]$, where t = temp. in °C, l = length of scattering cylinder = 4.176 cm. $C=(\pi^{\frac{1}{2}}\Gamma(\frac{1}{2}n+\frac{1}{2}))/(\Gamma(\frac{1}{2}n))$, m_1 = mass of ion, μ = reduced mass of ion and gas molecule, N = number of molecules per cc at 0°C and 1 mm Hg = 3.536×10^{16}, a = radius of ion receiver, $l/a=13.89$. Since the fraction scattered elastically varied with pressure, measurements were made at two pressures. This variation with pressure was probably due to multiple scattering as discussed in previous papers.[2] Determinations of the present experiments did not fit the previous analytical treatment, hence for each voltage the fraction was extrapolated to zero pressure and this value used in the equation. For most series of determinations the total scattering was independent of the gas pressure. In some experiments, however, a trend was noticed at higher pressures. This is probably an apparatus effect caused by pumping rates and the viscosity of the gas going through smaller tubes and orifices. Where this was experienced results were extrapolated to zero pressure.

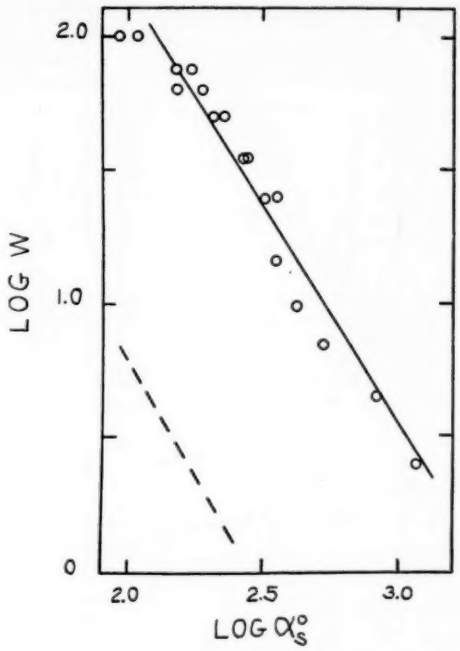

FIG. 6. H_2^+ in normal butane.

The life period of the $C_4H_{10}^+$ ion has been estimated by Hipple.[5] As this ion would be the one initially formed by neutralization of any of the hydrogen ions by the hydrocarbon molecule, a short life period should result in experimentally determinable changes in neutraliza-

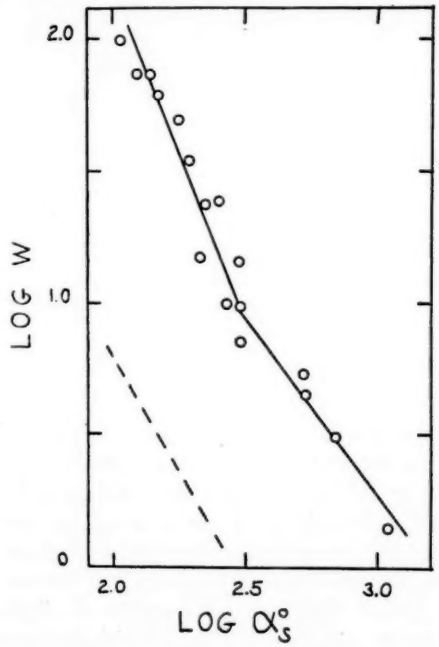

FIG. 5. H_2^+ in normal butane.

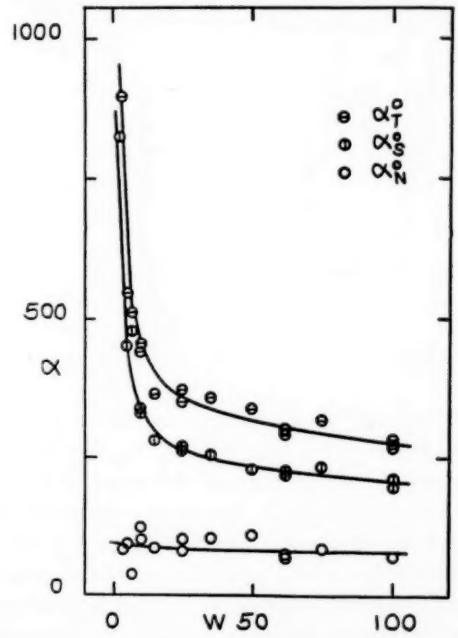

FIG. 7. Scattering of H^+ in isobutane.

[5] J. A. Hipple, J. Phys. and Colloid Chem. **52**, 456 (1948).

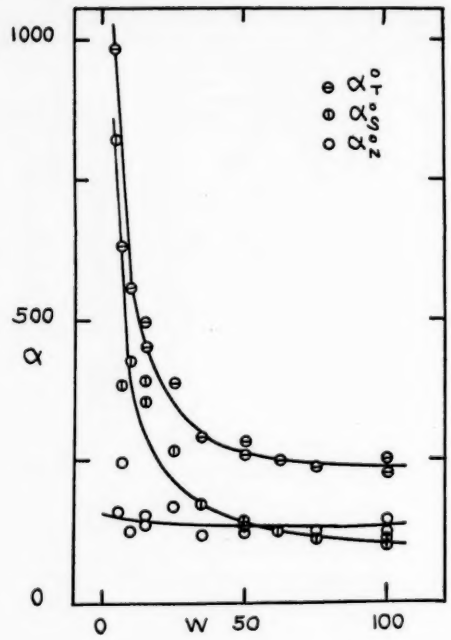

FIG. 8. Scattering of H_2^+ in isobutane.

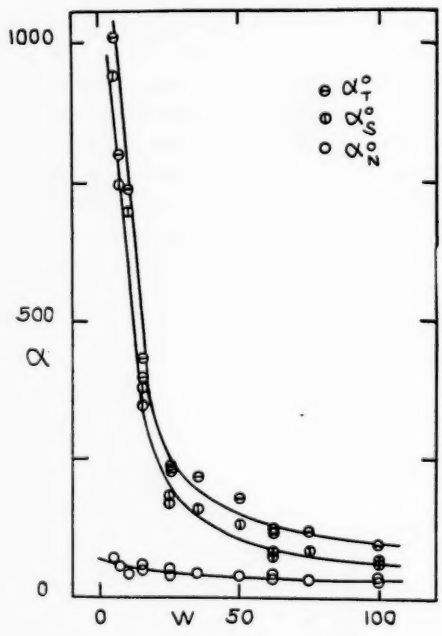

FIG. 9. Scattering of H_3^+ in isobutane.

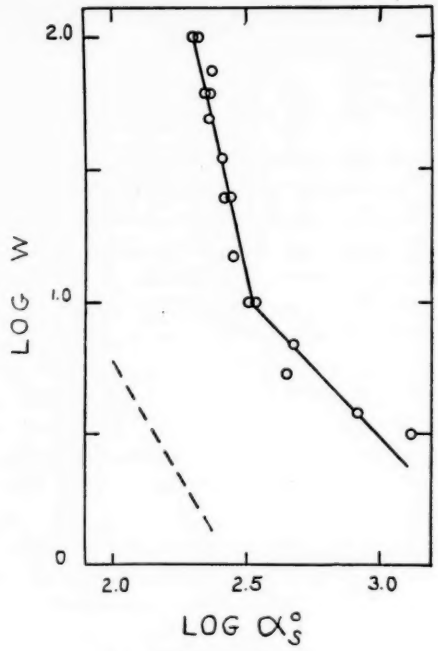

FIG. 10. H^+ in isobutane.

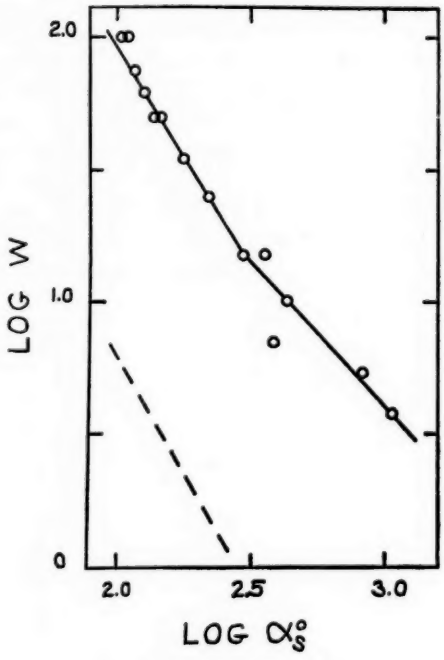

FIG. 11. H_2^+ in isobutane.

tion provided the decomposition of the ion is sufficiently energetic. The ions formed by neutralization would have the random thermal velocities of gas molecules at that temperature. Energetic spontaneous decomposition would result in new ions of higher velocity. A plot, therefore, of the intensity of the thermal velocity ions collected on the lid of the scattering can *versus* the retarding potential should be different depending upon whether the ion formed by neutralization is stable or whether it decomposes energetically with the formation of a new ion traveling at a higher velocity. Values of the intensity of the neutralized ion as a function of the retarding potential were obtained for both hydrocarbons. The plots of these functions were not significantly different from similar plots obtained using substances, the ion formed from which is known to be relatively stable. Thus, no information of significance in regard to the stability of the ion initially formed by neutralization was obtained in these experiments.

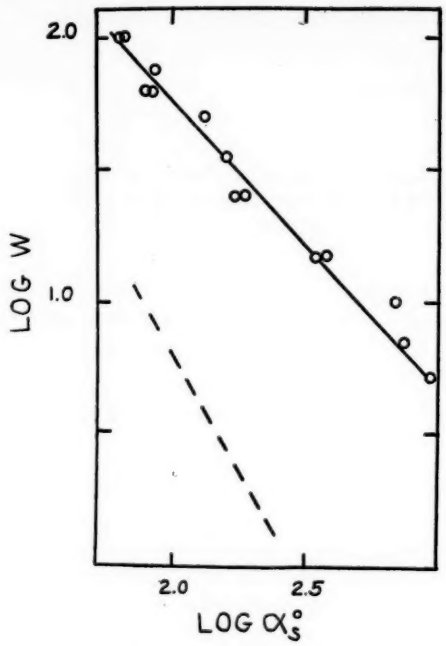

FIG. 12. H_3^+ in isobutane.

DISCUSSION

In Table III it can be seen that the coefficient in the potential function for the scattering of protons in isobutane is considerably larger than that in normal butane. As these potential laws are presumably attributable to attractive forces between the ion and the gas molecule, this indicates a considerably greater proton affinity, i.e., basicity, for isobutane over normal butane. Integrating over the same distance from the center of the hydrocarbon molecule, the value for the force of attraction of isobutane for the hydrogen ion is approximately 50 percent higher than that for normal butane. If this is a significant factor in the formation of a transition state in the acid catalyzed condensation reaction, it would appear that it would result in a difference of activation energy of approximately 50 percent with the greater number being assigned to the normal hydrocarbon. Activation energies of reactions of this kind are frequently in the order of magnitude of 15 kcal. A 50 percent increase in activation energy for a reaction involving binary collisions occurring at room temperature or slightly below and having an activation energy of this order of magnitude would result in a decrease in reaction rate of the order of magnitude of 10^6. As a matter of experience, although isobutane alkylates with olefins in an acid catalyzed reaction at a rapid rate at zero degrees, normal butane does not alkylate at a reasonable rate at least below several hundred degrees.

TABLE III. Summary of potential functions.

Ion	Range		Potential Function
		Normal Butane	
H^+	1.9–10 volts	10.5–4.6A	$V=-20.1/r^{2.25}$
	10–100 volts	4.6–3.1A	$V=-1.55\times10^4/r^{7.25}$
H_2^+	1.4–9.8 volts	10.0–5.3A	$V=-77.1/r^{2.88}$
	9.8–100 volts	5.3–3.1A	$V=-1160/r^{4.66}$
	1.4–100 volts	10.0–3.1A	$V=-623/r^4$
H_3^+	2.0–100 volts	13.5–2.9A	$V=-436/r^{3.40}$
		Isobutane	
H^+	3.2–10 volts	11.2–5.6A	$V=-27.3/r^{2.15}$
	10–100 volts	5.6–4.3A	$V=-8.80\times10^5/r^{8.70}$
H_2^+	3.8–15 volts	9.9–5.5A	$V=-44.0/r^{2.27}$
	15–100 volts	5.5–3.1A	$V=-377/r^{3.70}$
	3.8–100 volts	9.9–3.1A	$V=-174/r^3$
H_3^+	3.1–100 volts	11.0–2.4A	$V=-48.3/r^{2.23}$

It can be noted in Table III that values of the exponent in the potential function less than 4 are recorded for the three hydrogen ions in both hydrocarbons. The significance of this is not apparent. If we use the questionable logic of reasoning by analogy, it might be suggested that there is a possibility of a transitory existence of species $C_4H_{11}^+$, $C_4H_{12}^+$, and $C_4H_{13}^+$. In previous experimental work in this field, low values of the exponent have been found in those cases where ionic species were known that could result from the combination of the molecules and the ion.

The Vibrational Spectrum of Tetrachloroethylene

H. J. BERNSTEIN
National Research Council, Ottawa, Canada

(Received October 3, 1949)

The infra-red spectrum of C_2Cl_4 through long paths has been obtained in the region 2.5–25μ. As many combination tones as possible were observed. An assignment of the fundamentals has been made which interprets satisfactorily 16 lines in the Raman spectrum and 24 bands in the infra-red spectrum.

NOTWITHSTANDING the high symmetry of tetrachloroethylene (D_{2h}), there has been considerable disagreement in the literature as to the proper assignment (see Table I). Primarily this is due to the fact that the low lying infra-red active fundamentals have not as yet been observed.

It was considered worth while to reinvestigate this molecule using longer absorbing paths than have been used hitherto in order to bring out as many of the combination tones as possible. In particular, the region >1700 cm^{-1} should be fruitful in tracing down some of the low lying fundamentals since, as can be seen from Table I, combinations of only ν_1 or ν_5 with the low frequency fundamentals are most likely to appear in this region.

EXPERIMENTAL

The tetrachloroethylene used was the Eastman Kodak product redistilled in a Stedman column of about 30 theoretical plates. The infra-red spectrum of liquid C_2Cl_4 was obtained with a Perkin-Elmer spectrometer (Model 12C) on a Brown recorder (see Fig. 1 and Table II). It is worth emphasizing here that no fundamentals of appreciable intensity were found between 400–780 cm^{-1}.

DISCUSSION

The Raman spectrum has been obtained previously[1] and shows three strong polarized lines at 1571, 447, and 237 cm^{-1} which are Type A_g. The spectrum also contains two depolarized lines of medium intensity at 347 cm^{-1} and 512 cm^{-1}. These could be both of Type B_{1g} or one B_{1g} and the other B_{2g}. Of the bands in the infra-red spectrum the two very strong ones at 782 and 913 cm^{-1} are taken as fundamentals. The band at 913 cm^{-1} is taken as $\nu_{11}(B_{3u})$ since a valence force calculation[2] which permits evaluation of the force constants of the A_g modes gives a solution for the B_{3u} modes with these constants and $\nu_{11}=913$ cm^{-1}, whereas with $\nu_{11}=782$ cm^{-1} the roots are imaginary. The band at 782 cm^{-1} is

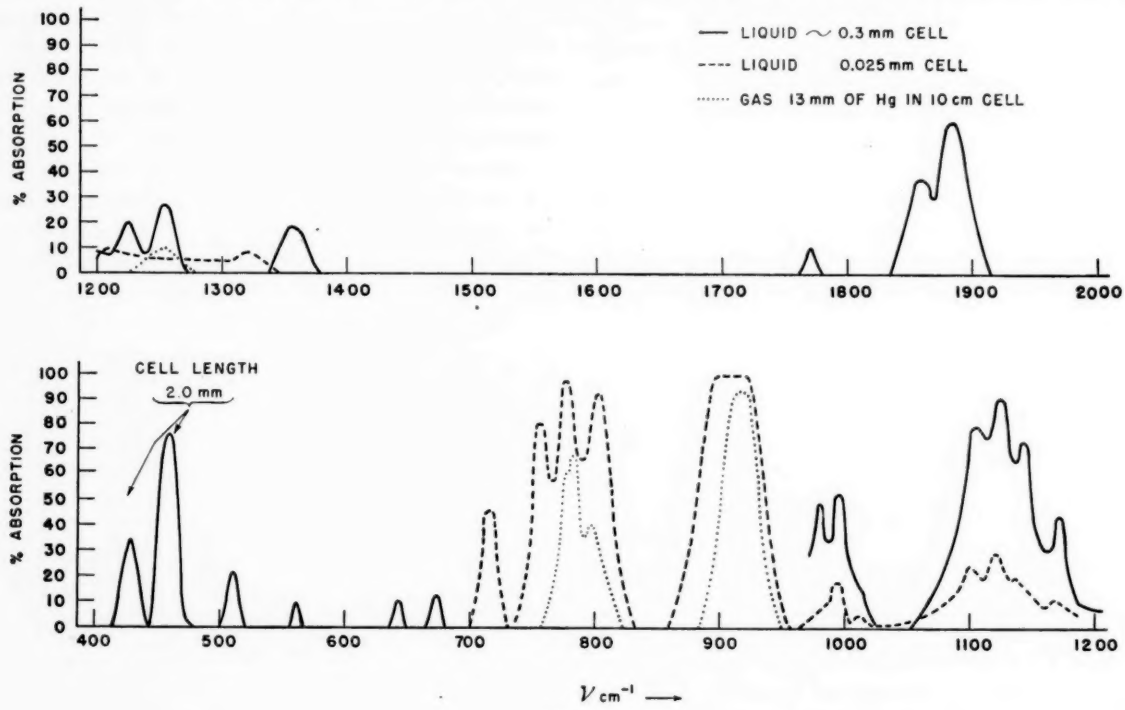

FIG. 1.

[1] See Table II, reference a.
[2] See Table I, reference e.

TABLE I. Assignment of the vibrational modes of C_2Cl_4.

Symmetry type and activity[a]	Herzberg[b]	Wu[c]	Duchesne[d]	Verleysen[e]	This work	
A_g	1571	1569	1569	1569	1571	ν_1
Raman active	447	445	445	445	447	ν_2
	237	236	383	236	237	ν_3
A_u (inactive in both Raman and infra-red)						ν_4
B_{1g}	1000	512	512	[1429]	1000	ν_5
Raman active	347	341	341	[279]	347	ν_6
B_{1u}	(332)				288	ν_7
infra-red active						
B_{2g}	512	383	236		512	ν_8
Raman active						
B_{2u}	913		792	782	782	ν_9
infra-red active	(332)		332	[173]	194	ν_{10}
B_{3u}	782	913	913	913	913	ν_{11}
infra-red active	(387)	345(calc.)	387	[361]	318	ν_{12}

[a] The notation and numbering of frequencies is the same as that employed by G. Herzberg (see reference b).
[b] G. Herzberg, *Infrared and Raman Spectra of Polyatomic Molecules* (D. Van Nostrand Company, Inc., New York, 1945).
[c] T. Y. Wu, *Vibrational Spectra and Structure of Polyatomic Molecules* (J. W. Edward, Ann Arbor, Michigan, 1946).
[d] J. Duchesne, Physica **8**, 144 (1941).
[e] A. Verleysen, Ann. Soc. Sci. Brux., 287 (July, 1939). The figures in square brackets are the results of a valence force calculation using four interaction constants in the potential function.

taken as $\nu_9(B_{2u})$ since $\nu_7(B_{1u})$, $\nu_{10}(B_{2u})$, and $\nu_{12}(B_{3u})$ are expected to have much lower frequencies than this.

Without the use of combination and overtones the following reasonable assignment can be made:

$$\left.\begin{array}{ll} \nu_1 = 1571 & \\ & \nu_6 = 347 \\ \nu_2 = 447 & \\ & \nu_8 = 512 \\ \nu_3 = 237 & \end{array}\right\} \text{Raman active}$$

$$\left.\begin{array}{l} \nu_9 = 782 \\ \\ \nu_{11} = 913 \end{array}\right\} \text{infra-red active.}$$

The line at 347 cm^{-1} is chosen for $\nu_6(B_{1g})$ rather than 512 cm^{-1} since the calculations of Verleysen[2] indicate a low frequency.

Of the observed weak Raman lines several can be interpreted on the basis of the above assignment, *viz.*:

$$\begin{aligned} 218 &= \nu_2 - \nu_3 = 210(A_g) \\ 464 &= 2\nu_3 = 474(A_g) \\ 574 &= \nu_3 + \nu_6 = 584(B_{1g}) \\ 726 &= \nu_3 + \nu_8 = 749(B_{2g}) \\ 784 &= \nu_2 + \nu_6 = 794(B_{1g}) \\ 1025 &= 2\nu_8 = 1024(A_g) \\ 1819 &= 2\nu_{11} = 1826(A_g) \\ 1998 &= \nu_1 + \nu_2 = 2018(A_g). \end{aligned}$$

The remaining weak Raman lines not accounted for are 631 cm^{-1}, 1000 cm^{-1},[3] and 1441 cm^{-1}.[4]

[3] This line is very weak. See Table II.
[4] This line is designated with a question mark (see Table II) indicating doubt as to its reality.

TABLE II. Vibrational spectrum of liquid C_2Cl_4 in cm^{-1}.

Infra-red	Raman[a]
429(w)	218(v.w.)
460(w)	237(s)pol.
511(w)	347(m)depol.
562(w)	447(v.s.)pol.
642(w)	464(w)
673(w)	512(m)depol.
715(w)	574(w)
758(m)	631(v.w.)
782(v.s.)	726(v.w.)
802(s)	784(v.w.)
913(v.s.)	1000(v.w.)
983(w)	1025(w)pol.
995(w)	1441(w?)
1102(w)	1571(s)pol.
1125(w)	1819(w)
1143(w)	1998(w)
1172(w)	
1225(w)	
1254(w)	
1360(w)	
1771(w)	
1858(w)	
1884(w)	
2470(w)	

[a] K. W. F. Kohlrausch, *Ramanspektren* (Edwards Brothers, Ann Arbor, Michigan, 1945).

Of the observed weak infra-red bands the following interpretation can be given on the basis of this assignment, *viz.*:

$$\begin{aligned} 460 &= \nu_{11} - \nu_2 = 466(B_{3u}) \\ 673 &= \nu_{11} - \nu_3 = 676(B_{3u}) \\ 983 &= 758 + \nu_3 = 995^* \\ 995 &= \nu_3 + \nu_9 = 1019(B_{2u}) \\ 1102 &= 758 + \nu_6 = 1105^* \\ 1125 &= \nu_9 + \nu_6 = 1129(B_{3u}) \\ 1143 &= \nu_3 + \nu_{11} = 1150(B_{3u}) \\ 1172 &= 758 + \nu_2 = 1205^* \\ 1225 &= \nu_2 + \nu_9 = 1229(B_{2u}) \\ 1254 &= \nu_6 + \nu_{11} = 1260(B_{2u}) \\ 1360 &= \nu_2 + \nu_{11} = 1360(B_{3u}) \\ 2470 &= \nu_1 + \nu_{11} = 2484(B_{3u}). \end{aligned}$$

The bands not accounted for in the infra-red spectrum are then 429w, 511w, 562w, 642w, 715w, 758m, 802m, 1771w, 1858w, and 1884w.

Of the remaining five fundamentals one would expect ν_{10}, ν_{12}, ν_7, and ν_4 to be low[2] and less than 500 cm^{-1}, whereas ν_5 may be high and in the vicinity of 1000 cm^{-1}. Since $\nu_5+\nu_{11}$ and $\nu_5+\nu_9$ are infra-red active, these combination tones would be above 1700 cm^{-1}. As a result, the infra-red bands over 1700 cm^{-1} can be accounted for in two ways, either by combination with 1571 cm^{-1} or by combination with ν_5.

For the first alternative, two of the infra-red active fundamentals are given by $1858-1571=287$ cm^{-1} and $1884-1571=313$ cm^{-1}, and for the second, the following choices for ν_5 are permitted:

$$\begin{aligned} 1858-782 &= 1076 \text{ cm}^{-1} \\ 1858-913 &= 945 \text{ cm}^{-1} \\ 1884-782 &= 1102 \text{ cm}^{-1} \\ 1884-913 &= 971 \text{ cm}^{-1}. \end{aligned}$$

* Since the bands at 758 cm^{-1} and 802 cm^{-1} are of medium intensity, triple tones are not unreasonable.

TABLE III.

Assignment	Infra-red (liquid)	Raman[a] (liquid)	Assignment	Infra-red (liquid)	Raman[a] (liquid)
$\nu_2-\nu_3(A_g)$		218(v.w.)	$\nu_7+\nu_8(B_{3u})$	802(s)	
ν_3		237(s)pol.	ν_{11}	913(v.s.)	
ν_7	288(s)[b]		$(\nu_2+\nu_{12})+\nu_3(B_{3u})$	983(w)	
ν_{12}	318(s)[b]		$\nu_3+\nu_9(B_{2u})$	995(w)	
ν_6		347(m)depol.	ν_5		1000(v.w.)
?	404(?)[b]		$2\nu_8(A_g)$		1025(w)pol.
$\nu_3+\nu_{10}(B_{2u})$	429(w)[c]		$(\nu_2+\nu_{12})+\nu_6(B_{2u})$	1102(w)	
ν_2		447(v.s.)pol.	$\nu_6+\nu_9(B_{3u})$	1125(w)	
$\nu_{11}-\nu_2(B_{3u})$	460(w)		$\nu_3+\nu_{11}(B_{3u})$	1143(w)	
$2\nu_3(A_g)$		464(w)	$(\nu_2+\nu_{12})+\nu_2(B_{3u})$	1172(w)	
$\nu_3+\nu_7(B_{1u})$	511(v.w.)		$\nu_2+\nu_9(B_{2u})$	1225(w)	
ν_8		512(m)depol.	$\nu_6+\nu_{11}(B_{2u})$	1254(w)	
$\nu_3+\nu_{12}(B_{3u})$	562(w)		$\nu_2+\nu_{11}(B_{3u})$	1360(w)	
$\nu_3+\nu_6(B_{1g})$		574(w)	$\nu_2+\nu_5(B_{1g})$?		1441(w?)
$2\nu_{12}(A_g)$		631(v.w.)	ν_1		1571(s)pol.
$\nu_2+\nu_{10}(B_{2u})$	642(w)		$\nu_1+\nu_{10}(B_{2u})$	1771(w)	
$\nu_{11}-\nu_3(B_{3u})$	673(w)		$2\nu_{11}(A_g)$		1819(w)
$\nu_2+\nu_7(B_{1u})$	715(w)		$\nu_1+\nu_7(B_{1u})$	1858(w)	
$\nu_3+\nu_8(B_{2g})$		726(v.w.)	$\nu_1+\nu_{12}(B_{3u})$	1884(m)	
$\nu_2+\nu_{12}(B_{3u})$	758(m)		$\nu_1+\nu_2(A_g)$		1998(w)
ν_9	782(v.s.)		$\nu_1+\nu_{11}(B_{3u})$	2470(w)	
$\nu_2+\nu_6(B_{1g})$		784(v.w.)			

[a] See Table II, reference a.
[b] Observed by E. K. Plyler, see reference 5.
[c] Observed by E. K. Plyler (reference 5) at 431 cm^{-1}.

Since ν_5 is Raman active and none of the above choices for it are present as a line in the Raman spectrum, it seems probable that the bands above 1700 cm^{-1} are to be accounted for only by combination with 1571 cm^{-1}. It would seem therefore that 1858 cm^{-1} is to be explained by combination with a fundamental around 287 cm^{-1} and 1884 cm^{-1} by combination with the fundamental at 313 cm^{-1}.[5]

Since ν_{11} has combined with ν_1, ν_2, and ν_3 to give bands in the infra-red spectrum, one might expect to observe combination tones of ν_{12} with ν_1, ν_2, and ν_3. Choosing the observed value[5] of 318 cm^{-1} for ν_{12} rather than the value 313 cm^{-1} obtained by difference, the observed bands at 1884, 758, and 562 cm^{-1} may be interpreted as $\nu_{12}+\nu_1$, $\nu_{12}+\nu_2$, and $\nu_{12}+\nu_3$, respectively. Choice of 288 cm^{-1} as ν_{12} on the other hand gives combination tones of which only one is observed.

This seems to justify choosing the band at 318 cm^{-1} as the fundamental ν_{12}. This choice is supported further by a valence force calculation.[6]

The band at 288 cm^{-1} is taken as ν_7 rather than ν_{10} since valence force calculations[6] indicate that ν_{10} is lower than 200 cm^{-1}.

The line at 631 cm^{-1} in the Raman spectrum may now be interpreted as $2\nu_{12}=636(A_g)$. Of the bands in the infra-red spectrum hitherto not accounted for, the following interpretations are possible:

$$511=\nu_3+\nu_7=525(B_{1u})$$
$$802=\nu_8+\nu_7=800(B_{3u})$$
$$715=\nu_2+\nu_7=735(B_{1u}).$$

In the Raman spectrum then, only 1000w and 1441? are not explained and in the infra-red spectrum the bands at 1771, 642, and 429 cm^{-1} are still unexplained.

To interpret some of these bands the unobserved infra-red active fundamental ν_{10} is at our disposal. If ν_{10} is taken as 194 cm^{-1}, then

$$\nu_1+\nu_{10}=1765(B_{2u})$$
$$\nu_2+\nu_{10}=\ 641(B_{2u})$$
$$\nu_3+\nu_{10}=\ 431(B_{2u});$$

all of which are observed, *viz.*, 1771, 642, and 429 cm^{-1}. This choice for ν_{10} is not unreasonable since the valence force calculations[6] indicate a low frequency for this fundamental.

The only choice left for the line at 1000 cm^{-1} appearing in the Raman spectrum is to assign it as ν_5.

The line at 1441 cm^{-1} may then be $\nu_5+\nu_2=1447(B_{1g})$.

Table III gives the complete assignment of the observed Raman and infra-red spectra. This assignment though plausible must still be regarded as tentative inasmuch as ν_{10} and ν_5 are uncertain and ν_4 is not estimated.

On the basis of this assignment an estimate of ν_4 could be made if the specific heat of the gas were known at one temperature.[7] This might prove of interest since the torsional constant could be estimated thus enabling an

[5] E. K. Plyler of the National Bureau of Standards, Washington, D. C., has obtained a spectrum of our sample of C_2Cl_4 in the region 25μ–40μ with a thallium bromide prism. His results, which he has kindly allowed to be quoted, are obtained in a 1.6-mm cell and are 288s, 318s, 404?, and 431w cm^{-1}.
The agreement between the expected and observed fundamentals is quite good.

[6] See Table I, column 5.

[7] See Table I, reference b, p. 512.

approximation of the torsional frequency in ethylene to be made.

Note added in proof: The recent paper on the vibrational spectrum of tetrachloroethylene by P. Torkington [Trans. Farad. Soc. 45, 445–7 (1949)] has just come to the attention of the author. On the basis of the early experimental data listed in column 2 of Table I, Torkington suggests the following assignment:

$A_g = 1571, 447, 237$; $A_u = 135$ (estimated from the torsional frequency in ethylene); $B_{1g} = 512, 347$; $B_{1u} = 185$; $B_{2g} = 215$; $B_{2u} = 913, 332$; $B_{3u} = 782, 387$.

ACKNOWLEDGMENT

Thanks are due Dr. E. K. Plyler for permission to use his results on the far infra-red spectrum of C_2Cl_4 and Miss E. Miller for reduction of the spectra.

THE JOURNAL OF CHEMICAL PHYSICS VOLUME 18, NUMBER 4 APRIL, 1950

Dissociation and Exchange Equilibria of the Tritium Halides*

JACOB BIGELEISEN
Brookhaven National Laboratory, Upton, New York
(Received October 3, 1949)

The ratios of the partition functions of the tritium halides to their respective protium halides have been calculated. These are combined with one another to give the exchange equilibria between the six pairs of tritium and protium halides. The exchange equilibria with water are calculated. From the exchange equilibria between the tritium halides and protium and the free energy of dissociation of the protium halides, the dissociation equilibria of the tritium halides have been calculated.

The experimental data on the dissociation of HI are reviewed and it is shown that the data of Taylor and Crist on DI and HI are self-consistent as well as in good agreement with theory. The heat of formation of HI at absolute zero, ΔH_0^0, is found to be -1007 ± 10 calories per mole.

INTRODUCTION

THE availability of the hydrogen isotope of mass three, tritium, for experimental purposes makes it desirable and important to have available the thermodynamic properties of different chemical compounds of this nuclide. Libby[1] has calculated the exchange equilibria between the isotopic water and the isotopic hydrogen molecules. Urey[2] has calculated these same equilibria as well as the partition function ratios of the various pairs of isotopic water molecules and the isotopic hydrogen molecules. Jones[3] has calculated the thermodynamic functions for tritium and tritium hydride. From these and the free energy function of protium he has calculated the equilibrium between tritium, protium, and tritium hydride. In addition, he has calculated the dissociation of the isotopic hydrogen molecules into atoms.

This paper reports the calculations of the partition function ratios of the tritium to protium halides. The partition function ratios of the four isotopic hydrogen halides are then combined to give the six exchange equilibria between the various tritium and protium halides.

$$TX + HX^1 = TX^1 + HX. \quad (1)$$

The ratios are also combined with the partition function ratios of the tritium water molecules and the protium water molecules to give the exchange equilibria between the tritium halides and water. From the calculated exchange equilibria between the tritium halides and protium and the known free energies of formation of the protium halides,[4] the dissociation equilibria of the tritium halides have been calculated. By means of suitably chosen exchange equilibria, which can be calculated directly from partition function ratios, it is possible to calculate all the thermodynamic equilibrium constants for gaseous tritium compounds from the experimental and theoretical values for the corresponding protium compounds. This is the most rapid procedure for such calculations and the precision and accuracy attained are generally limited by the accuracy of the protium determinations.

PARTITION FUNCTION RATIOS

The formulas and method for the calculation of the partition function ratios have been published previously.[5] Both chlorine and bromine each have two stable isotopes. The partition function ratios TCl/HCl and TBr/HBr are calculated for the normal isotopic abundance of the halogens. The procedure used was to calculate the spectroscopic properties of the tritium chloride and bromide as though they were each monoisotopic. The mass of the halogen taken was the weighted masses of the isotopes. This simplification over the procedure of calculating the ratios for each of the halogen isotopes and weighting the ratios introduces an error of less than one tenth of one percent for the

* Research done at the Brookhaven National Laboratory under the auspices of the AEC.

[1] W. F. Libby, J. Chem. Phys. **11**, 101 (1943).
[2] H. C. Urey, J. Chem. Soc. 562 (1947).
[3] W. M. Jones, J. Chem. Phys. **16**, 1077 (1948).
[4] "*Selected values of chemical thermodynamic properties*," National Bureau of Standards, June 30, 1948.
[5] J. Bigeleisen and M. G. Mayer, J. Chem. Phys. **15**, 261 (1947).

TABLE I.

Nuclide	Mass*
H	1.00813
T	3.01703
F^{19}	19.00450
Cl^{35}	34.97867
Cl^{37}	36.97750
Br^{79}	78.94438
Br^{81}	80.94228
I^{127}	126.95

* The masses for H and T were taken from K. T. Bainbridge, National Research Council Committee on Nuclear Science Report No. 1; those for F and Cl from H. Bethe, *Elementary Nuclear Theory* (John Wiley and Sons, New York, 1947); Br from K. Ogata, Phys. Rev. **75**, 200 (1949); I from chemical atomic weight, J. Am. Chem. Soc. **70**, 3531 (1948).

TABLE II.*

	ω_e	$x_e\omega_e$	σT
HF	4141.31	90.866	29.527
TF	2511.18	33.410	10.948
HCl	2988.95	51.65	15.0160
TCl	1774.71	18.21	5.3255
HBr	2649.67	45.21	12.023
TBr	1550.54	15.48	4.140
HI	2309.53	39.73	9.292
TI	1345.47	13.48	3.146

* The values for the protium halides were taken from G. Herzberg *Molecular Spectra and Molecular Structure* (Prentice-Hall, Inc., New York 1939). The ones for the tritium halides were calculated.

TABLE III.

T°K	TF/HF	f TCl/HCl	TBr/HBr	TI/HI
273.16	40.182	13.736	10.072	7.0768
298.16	28.268	10.556	7.9362	5.7449
300	27.607	10.372	7.8105	5.6660
400	10.630	5.0812	4.0995	3.2295
500	5.9988	3.3225	2.8003	2.3240
600	4.1019	2.5223	2.1868	1.8829
700	3.1325	2.0727	1.8448	1.6326
800	2.5654	1.7998	1.6333	1.4762
900	2.2021	1.6227	1.4930	1.3715
1000	1.9545	1.4980	1.3948	1.2978
1100	1.7770	1.4075	1.3233	1.2443
1200	1.6453	1.3396	1.2694	1.2037
1300	1.5446	1.2889	1.2281	1.1725
1400	1.4659	1.2465	1.1954	1.1479
1500	1.4033	1.2134	1.1695	1.1281
2000	1.2212	1.1175	1.0928	1.0704

tritium to protium chloride ratio at 300°K. The error is smaller at higher temperatures and is smaller at all temperatures for the bromides. The masses of the atoms used in the calculations are given in Table I. The spectroscopic values used are given in Table II. The values of σT were calculated for the ground vibrational state. The conversion factor used, hc/k, was taken as 1.43847 so that the equilibria calculated may be combined directly with those being published by the National Bureau of Standards.[4]

The partition function ratios, f values (Eq. (11), reference 5), corrected for non-classical rotation, Eq. (15), reference 5, for the tritium to protium halides are given in Table III. Interpolations of the values in

TABLE IV.

T°K	TF HF / HF TF	TF HBr / HF TBr	TF HCl / HF TCl	TCl HI / HCl TI	TCl HBr / HCl TBr	TBr HI / HBr TI
273.16	5.6780	3.9895	2.9253	1.9410	1.3638	1.4232
298.16	4.9205	3.5619	2.6778	1.8375	1.3301	1.3814
300	4.8724	3.5346	2.6617	1.8305	1.3279	1.3785
400	3.2915	2.5930	2.0920	1.5734	1.2395	1.2694
500	2.5812	2.1422	1.8055	1.4296	1.1865	1.2049
600	2.1785	1.8758	1.6263	1.3396	1.1534	1.1614
700	1.9187	1.6980	1.5113	1.2696	1.1235	1.1300
800	1.7378	1.5707	1.4254	1.2192	1.1019	1.1064
900	1.6056	1.4749	1.3571	1.1832	1.0869	1.0886
1000	1.5060	1.4013	1.3047	1.1543	1.0740	1.0747
1100	1.4281	1.3429	1.2625	1.1312	1.0636	1.0635
1200	1.3669	1.2961	1.2282	1.1129	1.0553	1.0546
1300	1.3174	1.2577	1.1984	1.0993	1.0495	1.0474
1400	1.2770	1.2263	1.1760	1.0859	1.0427	1.0414
1500	1.2440	1.1999	1.1565	1.0756	1.0375	1.0367
2000	1.1408	1.1175	1.0928	1.0440	1.0226	1.0209

TABLE V.

T°K	HT HF / H_2 TF	HT HCl / H_2 TCl	HT HBr / H_2 TBr	HT HI / H_2 TI	fHT/H_2
273.16	0.31135	0.91080	1.2421	1.7678	12.511
298.16	0.37311	0.99912	1.3290	1.8359	10.547
300	0.37767	1.0053	1.3349	1.8402	10.426
400	0.61718	1.2912	1.6003	2.0315	6.5606
500	0.82820	1.4953	1.7742	2.1378	4.9682
600	1.0064	1.6367	1.8878	2.1925	4.1282
700	1.1547	1.7452	1.9608	2.2156	3.6172
800	1.2776	1.8211	2.0067	2.2203	3.2776
900	1.3792	1.8717	2.0343	2.2145	3.0372
1000	1.4633	1.9092	2.0505	2.2037	2.8600
1100	1.5331	1.9356	2.0588	2.1895	2.7244
1200	1.5914	1.9546	2.0627	2.1753	2.6184
1300	1.6404	1.9659	2.0632	2.1610	2.5338
1400	1.6817	1.9777	2.0622	2.1476	2.4652
1500	1.7162	1.9848	2.0593	2.1349	2.4084
2000	1.9031	1.9995	2.0447	2.0874	2.2344

Table III can best be made by a plot of log$f$ *vs.* $1/T$, which is linear up to 1000°K and then f approaches unity asymptotically at infinite temperature.

EQUILIBRIUM CONSTANTS

The equilibrium constants for exchange reactions between the tritium and protium halides are given in Table IV.

The equilibrium constants for the exchange of the tritium halides with protium, according to Eqs. (2) and (3)

$$H_2+TX=HT+HX \quad (2)$$

$$H_2+2TX=T_2+2HX, \quad (3)$$

are given in Tables V and VI, respectively. Table V also contains the f values for HT/H_2 necessary for the equilibria, while Table VI contains the f values for T_2/H_2. These f values were calculated with constants given in Table VII. The equilibrium constants for the reaction,

$$H_2+T_2=2HT, \quad (4)$$

calculated from the f values in Tables V and VI are in

good agreement with those calculated by Jones[3] using the free energy functions and ΔH_0^0 from spectroscopic data. The slight discrepancy, less than 0.5 percent at 300°K, results from the fact that Jones uses slightly different spectroscopic values for ω_e and $x_e\omega_e$.

Table VIII lists the partition function ratios HTO/H_2O and T_2O/H_2O from 273.16°K to 2000°K. The vibrational frequencies and anharmonicities used were taken from Libby's calculations.[1] These are combined with those of the halides to give the equilibrium constants for the following reactions

$$H_2O+TX=HTO+HX, \quad (5)$$

$$H_2O+2TX=T_2O+2HX. \quad (6)$$

The equilibrium constants are listed in Table VIII.

DISSOCIATION OF THE TRITIUM HALIDES

The exchange equilibria of the tritium halides with protium, Eqs. (2) and (3), can be combined with the dissociation equilibria of the protium halides

$$2HX=H_2+X_2 \quad (7)$$

to give the dissociation equilibria of the tritium halides in dilute and concentrated tritium mixtures.

$$HX+TX=HT+X_2, \quad (8)$$

$$2TX=T_2+X_2. \quad (9)$$

$K_8=K_2K_7$; $K_9=K_3K_7$. From the dissociation equilibria of the tritium halides (Eq. (9)) their respective free energies of formation are calculated. The equilibrium constants and free energies of formation are listed in Table IX. The values of K_7 used for the respective protium halides were obtained from the following sources: HF from the free energy equation of Murphy and Vance;[6] HCl and HBr from the National Bureau of

TABLE VI.

T°K	$\frac{T_2}{H_2}\cdot\left(\frac{HF}{TF}\right)^2$	$\frac{T_2}{H_2}\cdot\left(\frac{HCl}{TCl}\right)^2$	$\frac{T_2}{H_2}\cdot\left(\frac{HBr}{TBr}\right)^2$	$\frac{T_2}{H_2}\cdot\left(\frac{HI}{TI}\right)^2$	fT_2/H_2
273.16	0.039897	0.34141	0.63496	1.2863	64.417
298.16	0.054294	0.38935	0.68884	1.3145	43.385
300	0.055452	0.39285	0.69279	1.3164	42.263
400	0.12797	0.56009	0.86047	1.3865	14.461
500	0.21122	0.68857	0.96932	1.4074	7.6011
600	0.29460	0.77916	1.0366	1.3982	4.9570
700	0.37282	0.85154	1.0749	1.3725	3.6583
800	0.44377	0.90161	1.0948	1.3402	2.9206
900	0.50693	0.93354	1.1028	1.3069	2.4582
1000	0.56205	0.95682	1.1036	1.2748	2.1471
1100	0.61032	0.97279	1.1006	1.2447	1.9272
1200	0.65223	0.98390	1.0957	1.2186	1.7656
1300	0.68870	0.98904	1.0894	1.1952	1.6431
1400	0.72037	0.99627	1.0833	1.1748	1.5480
1500	0.74773	1.0001	1.0766	1.1571	1.4725
2000	0.91077	1.0054	1.0513	1.0957	1.2555

TABLE VII.†

	ω_e	$x_e\omega_e$	σT
H_2	4405.30	125.325	85.365
HT	3598.01	83.601	57.208
T_2	2546.49	41.877	28.836

† See reference * in Table II.

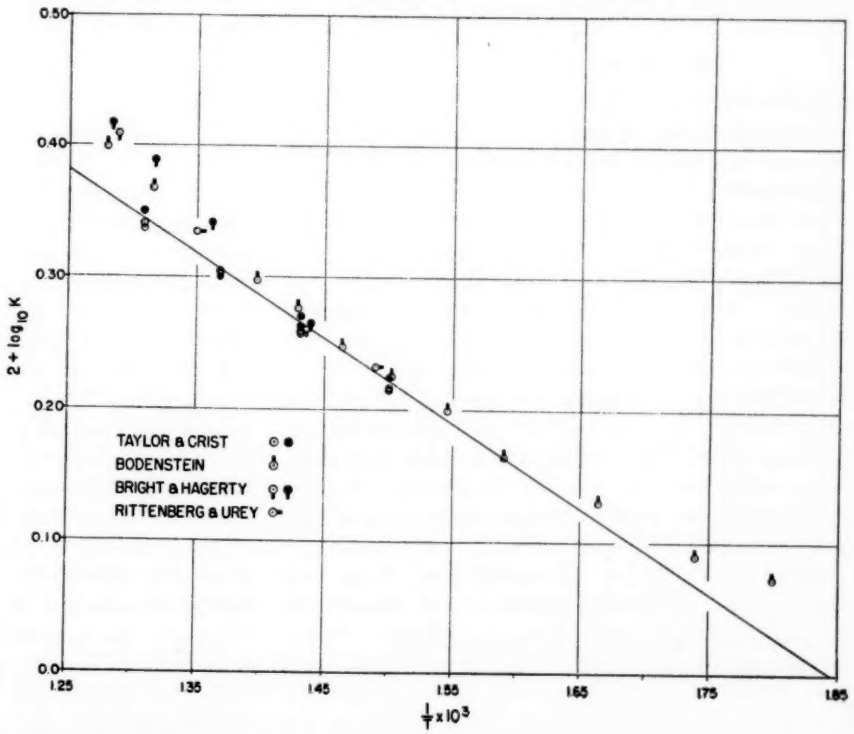

FIG. 1. Equilibrium in the dissociation of HI. $2HI(g)=H_2(g)+O_2(g)$. Open circles HI data; solid circles calculated from DI data.

[6] G. M. Murphy and J. E. Vance, J. Chem. Phys. 7, 806 (1939).

TABLE VIII.

T°K	$\frac{f}{HTO}$ / H_2O	HTO HF / H_2O TF	HTO HCl / H_2O TCl	HTO HBr / H_2O TBr	HTO HI / H_2O TI	$\frac{f}{T_2O}$ / H_2O	$\frac{T_2O}{H_2O}\left(\frac{HF}{TF}\right)^2$	$\frac{T_2O}{H_2O}\left(\frac{HCl}{TCl}\right)^2$	$\frac{T_2O}{H_2O}\left(\frac{HBr}{TBr}\right)^2$	$\frac{T_2O}{H_2O}\left(\frac{HI}{TI}\right)^2$
273.16	95.404	2.3743	6.9455	9.4722	13.481	2723.3	1.6867	14.433	26.844	54.377
298.16	65.206	2.3067	6.1772	8.2163	11.350	1243.3	1.5559	11.158	19.740	37.671
300	63.562	2.3024	6.1282	8.1380	11.218	1179.6	1.5477	10.965	19.336	36.743
400	22.678	2.1334	4.4631	5.5319	7.0221	141.79	1.2548	5.4917	8.4369	13.594
500	12.292	2.0491	3.6996	4.3895	5.2892	40.404	1.1228	3.6601	5.1525	7.4808
600	8.2018	1.9995	3.2517	3.7506	4.3559	17.711	1.0526	2.7839	3.7036	4.9956
700	6.1810	1.9732	2.9821	3.3505	3.7860	9.9546	1.0145	2.3171	2.9250	3.7347
800	5.0248	1.9587	2.7919	3.0765	3.4039	6.5335	0.99274	2.0169	2.4491	2.9981
900	4.2970	1.9513	2.6481	2.8781	3.1331	4.7545	0.98047	1.8057	2.1331	2.5276
1000	3.8068	1.9477	2.5413	2.7293	2.9333	3.7183	0.97335	1.6570	1.9112	2.2076
1100	3.4600	1.9471	2.4583	2.6147	2.7807	3.0627	0.96991	1.5460	1.7490	1.9781
1200	3.2042	1.9475	2.3919	2.5242	2.6620	2.6213	0.96834	1.4607	1.6267	1.8092
1300	3.0108	1.9492	2.3359	2.4516	2.5678	2.3098	0.96814	1.3904	1.5315	1.6801
1400	2.8602	1.9512	2.2946	2.3927	2.4917	2.0814	0.96859	1.3396	1.4565	1.5796
1500	2.7408	1.9531	2.2588	2.3436	2.4296	1.9083	0.96902	1.2961	1.3953	1.4995
2000	2.3982	1.9638	2.1460	2.1945	2.2405	1.4553	0.97586	1.1654	1.2186	1.2701

TABLE IX.

T°K	TF $\log_{10}K_8$	TF $\log_{10}K_9$	TF $\Delta F_f°$ in kcal.	TCl $\log_{10}K_8$	TCl $\log_{10}K_9$	TCl $\Delta F_f°$ in kcal.	TBr $\log_{10}K_8$	TBr $\log_{10}K_9$	TBr $\Delta F_f°$ in kcal.	TI $\log_{10}K_8$	TI $\log_{10}K_9$	TI $\Delta F_f°$ in kcal.
298.16	−95.593	−96.430	−65.78	−33.3796	−33.7888	−23.049	−19.052	−19.337	−13.19	−2.558	−2.703	−1.84
300	−95.007	−95.841	−65.78	−33.1789	−33.5869	−23.052	−18.943	−19.228	−13.20	−2.545	−2.691	−1.85
400	−71.322	−72.005	−65.89	−25.0202	−25.3829	−23.229	−14.350	−14.619	−13.38	−2.066	−2.232	−2.04
500	−57.109	−57.692	−66.00	−20.1153	−20.4520	−23.395	−11.583	−11.846	−13.55	−1.760	−1.942	−2.22
600	−47.609	−48.142	−66.09	−16.8348	−17.1571	−23.552	−9.7278	−9.9882	−13.71	−1.547	−1.742	−2.39
700	−40.823	−41.324	−66.18	−14.4843	−14.7960	−23.696	−8.3974	−8.6584	−13.87	−1.391	−1.599	−2.56
800	−35.728	−36.188	−66.23	−12.7175	−13.0228	−23.835	−7.3969	−7.6601	−14.02	−1.273	−1.492	−2.73
900	−31.762	−32.197	−66.30	−11.3410	−11.6431	−23.974	−6.6160	−6.8819	−14.17	−1.180	−1.409	−2.90
1000	−28.587	−29.003	−66.35	−10.2373	−10.5374	−24.108	−5.9901	−6.2592	−14.32	−1.104	−1.341	−3.07
1100	−25.987	−26.387	−66.41	−9.3346	−9.6334	−24.244	−5.4784	−5.7504	−14.47	−1.043	−1.288	−3.24
1200	−23.818	−24.205	−66.45	−8.5811	−8.8792	−24.377	−5.0504	−5.3251	−14.62	−0.991	−1.243	−3.41
1300	−21.981	−22.358	−66.50	−7.9430	−8.2414	−24.512	−4.6889	−4.9662	−14.77	−0.948	−1.206	−3.59
1400	−20.406	−20.774	−66.54	−7.3958	−7.6936	−24.642	−4.3797	−4.6592	−14.92	−0.912	−1.174	−3.76
1500	−19.040	−19.400	−66.58	−6.9205	−7.2182	−24.771	−4.1105	−4.3921	−15.07	−0.881	−1.147	−3.94

Standards tables;[4] the data used for HI are discussed below.

DISSOCIATION OF HI

The dissociation of protium iodide is one of the most carefully studied gaseous equilibria. Yet, in spite of the considerable amount of careful experimental work and the application of statistical thermodynamics to the problem, there is still a considerable degree of discrepancy between the results of the various workers. Murphy[7] has reviewed and examined critically the experimental data up to 1936 in his paper on the free energy of formation from sprectroscopic data. He concludes that Bodenstein's[8] data below 600°K and above 700°K are probably in error. Taylor and Crist[9] have redetermined the dissociation of HI and determined the dissociation of DI. Their results are in good agreement with the calculations of Murphy on HI and those of Blagg and Murphy[10] on DI. Their analysis of their data leads to a change of Murphy's ΔE_0^0 from 971.83±13.65 cal. mole^{-1} to 990.40±4 cal. mole^{-1} and Blagg and Murphy's ΔE_0^0 from 1014.52±14 cal. mole^{-1} to 1033.09±4 cal. mole^{-1}. Recently Bright and Hagerty[11] have published their data on the dissociation of protium and deuterium iodides. Their data on protium and deuterium iodides are self consistent. They lead to values for the exchange equilibrium

$$H_2+2DI=D_2+2HI, \qquad (10)$$

which are in good agreement with the theoretical calculation of Bigeleisen and Mayer.[5] However, while their data on protium iodide are in good agreement with those of Bodenstein, they are in poor agreement with those of Taylor and Crist and the calculations of Murphy. If we write the equilibrium in the form of Eq. (7) the data of Bright and Hagerty are higher than those of Taylor and Crist.

The free energies of formation of HI(g) given in the National Bureau of Standards tables[4] are larger than all the previous data. Thus the logK values for Eq. (7) are even lower than those of Murphy. There are no experimental data which are consistently below Murphy's calculations for K_7. This discrepancy was called to the attention of Dr. D. D. Wagman. In reply, Dr. Wagman has informed me that his compilation had unfortunately overlooked the measurements of Taylor and Crist in arriving at a value of $\Delta H_f^0{}_{298.16}$. After

[7] G. M. Murphy, J. Chem. Phys. **4**, 344 (1936).
[8] M. Bodenstein, Zeits. f. physik. Chem. **29**, 295 (1899).
[9] A. H. Taylor and R. H. Crist, J. Am. Chem. Soc. **65**, 1377 (1941).
[10] J. C. L. Blagg and G. M. Murphy, J. Chem. Phys. **4**, 631 (1936).
[11] N. F. H. Bright and R. P. Hagerty, Trans. Faraday Soc. **43**, 697 (1947).

consideration of the data of Taylor and Crist, Wagman arrives at the following constants for the reaction

$$\tfrac{1}{2}H_2(g)+\tfrac{1}{2}I_2(c)=HI(g), \qquad (11)$$

$$\Delta H_f{}^0{}_{298.16}=6.28 \text{ kcal.},$$
$$\Delta F_f{}^0{}_{298.16}=0.39 \text{ kcal.},$$
$$\log_{10}K_f=-0.286.$$

These constants together with the heat of vaporization of iodine, the vapor pressure of iodine and the free energy functions for $H_2(g)$, $I_2(g)$, and $HI(g)$ (all from the National Bureau of Standards tables) yield -1007 ± 10 cal. mole^{-1} for the heat of formation of $HI(g)$ at absolute zero. The values of K_7 used for HI were calculated from this $\Delta H_0{}^0$ and the $(F^0-H_0{}^0)$ tables of the National Bureau of Standards.[4] A plot of $\log K_7$ *vs.* 1/T is shown in Fig. 1 together with the experimental data of Taylor and Crist,[9] Bodenstein,[8] Bright and Hagerty,[11] and Rittenberg and Urey.[12] Finally, the equilibrium data of Taylor and Crist and of Bright and Hagerty on DI are combined with the theoretical values[5] of K_{10} to give K_7. It is seen that both the data of Taylor and Crist and Bright and Hagerty on DI are consistent with their respective HI data. Furthermore, the data of Taylor and Crist on HI are in good agreement with those calculated from spectroscopic data and the value of $\Delta H_{f0}{}^0 - 1007$ cal. mole^{-1}.

[12] D. Rittenberg and H. C. Urey, J. Chem. Phys. **1**, 137 (1933); J. Am. Chem. Soc. **56**, 1885 (1934).

THE JOURNAL OF CHEMICAL PHYSICS VOLUME 18, NUMBER 4 APRIL, 1950

Infra-Red and Raman Spectra of Fluorinated Ethylenes II. 1,1-Difluoro-2,2-Dichloroethylene*

J. Rud Nielsen and Howard H. Claassen
Department of Physics, University of Oklahoma, Norman, Oklahoma

and

D. C. Smith
Naval Research Laboratory, Washington, D. C.

The infra-red absorption spectrum of gaseous 1,1-difluoro-2,2-dichloroethylene between 2 and 22.6μ has been investigated with a prism spectrometer of high resolution. The Raman spectrum of $CF_2{:}CCl_2$ in the liquid state has been photographed with a three-prism glass spectrograph of linear dispersion 15A/mm at 4358A. Quantitative polarization measurements have been made. The 12 fundamental vibration frequencies have been assigned, and the observed vibration spectra have been interpreted in detail.

INTRODUCTION

THE Raman spectrum of liquid 1,1-difluoro-2,2-dichloroethylene has been studied by Hatcher and Yost.[1] The infra-red spectrum of the compound in the gaseous state has been investigated by Torkington and Thompson[2] who made an assignment of ten of the twelve fundamental vibration frequencies. In the present paper more accurate experimental data, a complete assignment of fundamentals and a detailed interpretation of the infra-red and Raman spectra of $CF_2{:}CCl_2$ will be given.

EXPERIMENTAL

The sample of $CF_2{:}CCl_2$ was prepared and purified in the Jackson Laboratory of E. I. du Pont de Nemours and Company. No information was available about its purity. However, the infra-red spectrum showed that it contained certain amounts of carbon dioxide and carbon monoxide as impurities.

The infra-red absorption spectrum of gaseous $CF_2{:}CCl_2$ was measured from 2 to 22.6μ in the manner described in the first paper of this series.[3] The Raman spectrum of liquid $CF_2{:}CCl_2$ was photographed by means of a Lane-Wells spectrograph.[3] Quantitative measurements of the depolarization ratios of the Raman bands were made with an apparatus similar to that described by Crawford and Horwitz,[4] except for the use of mercury lamps with internally water-cooled electrodes. The Type *H* polaroid sheets were given a permanent cylindrical shape by bending them tightly around a glass tube of appropriate diameter, wrapping a string around them along the whole length and heating them in an oven for one to two hours at 75°C.

In order to make the two exposures accurately equivalent, an intensity integrator was used. It consists of a glow tube relaxation circuit in which the resistance in series with the condenser is furnished by a 929 photocell and depends on the intensity of the light falling on the cell. The condenser charges at a rate determined by

* This work has been supported by the ONR under Contract N7-onr-398, Task Order I.

[1] J. B. Hatcher and D. M. Yost, J. Chem. Phys. **5**, 992 (1937).
[2] P. Torkington and H. W. Thompson, Trans. Faraday Soc. **41**, 236 (1945).
[3] Smith, Nielsen, and Claassen, J. Chem. Phys. **18**, 326 (1950).
[4] B. L. Crawford, Jr. and W. Horwitz, J. Chem. Phys. **15**, 882 (1947).

TABLE I. Infra-red spectrum of CF_2:CCl_2 (gas).*

Wave number	Description		Interpretation
459 cm^{-1}	vw		B_1 Fundamental
556			
564	s	Type *C*	B_2 Fundamental
573			
~617			
622	m	Type *A*	A_1 Fundamental
~629			
635			
640	s	Type *A*	A_1 Fundamental
~647			
758	vvw		
805	vw		993−(188)=805(A_1); (188)+622=810(B_1)
838	vvw		1032−(188)=844(B_1)
881	m	sh	(258)+622=880(B_2)
884	m		(434)+459=893(B_1)
887	m		
989	vs	Type *B*	B_1 Fundamental
996			
1027			
1032	vs	Type *A*	A_1 Fundamental
1037			
~1051			
1056	vw	Type *A*?	(434)+622=1056(A_1)
1060			
1125			
1131	s	Type *A*	2×564=1128(A_1)
1136			
1171	s	Type *C*?	564+622=1186(B_2); (188)+993=1181(A_1)
1214	m	Type *B*	(188)+1032=1220(B_1)
1221			
1250	vvw		2×622=1244(A_1)
1281	w		2×640=1280(A_1); (258)+1032=1290(B_2)
1323	vs	Type *B*	B_1 Fundamental
1330			
1427	m		(434)+993=1427(B_1)

TABLE I.—*Continued.*

Wave number	Description		Interpretation
1477 cm^{-1}	m		459+1032=1491(B_1)
1485	m		
1543	w		1749−(188)=1561(B_1)?
1575	vvw		2×564+459=1587(B_1)?
1585	vvw		264+1032=1596(B_2)?
1627			
1636	vw	Type *B*?	640+993=1633(B_1)
1745			
1749	vs	Type *A*	A_1 Fundamental
1752			
1798	vvw		459+1327=1786(A_1)
1878	vvw		(188)+640+1032=1860(B_1)?
1894	vvw		2×459+993=1911(B_1)?
1936	vw		(188)+1749=1937(B_1); 622+1327=1949(B_1)
1978	m		2×993=1986(A_1); 640+1327=1967(B_1)
1998	vvw		(258)+1749=2007(B_2)
2058	m		2×1032=2064(A_1)
2175**	m		(434)+1749=2183(A_1)
2296	vvw		564+1749=2313(B_2)
2375	vvw		622+1749=2371(A_1)
2441	vvw		(258)+(434)+1749=2441(B_2)
2500	vvw		(188)+993+1327=2508(B_1)
2563	vvw		258+564+1749=2571(A_1)
2636	s		2×1327=2654(A_1)
2732	w		993+1749=2742(B_1)
2770	s		1032+1749=2781(A_1)
2841	m		(188)+2×1327=2842(B_1); 459+640+1749=2848(B_1)
3062	m		1327+1749=3076(B_1)
3470	w		2×1749=3498(A_1)
3620	w		2×1327+993=3629(B_1)

* Frequencies observed as fundamentals only in the Raman spectrum of liquid CF_2:CCl_2 are enclosed in parentheses, since they may differ somewhat from the corresponding frequencies for the gas.

** Coincides with the maximum in the *R* branch of the CO band.

the applied voltage and the intensity of the light. When the condenser voltage becomes equal to the breakdown voltage of the glow tube the condenser discharges through a sensitive relay that activates a mechanical counter. When the voltage has fallen to the extinction voltage of the glow tube the discharge stops, and the condenser begins to charge again. The photo-cell is mounted, with appropriate shielding, above the reflector in the polarization apparatus, and suitable holes in the reflector transmit light equally from the two mercury lamps to the photo-cell.[5] The two exposures, with the two different polaroid cylinders, are made equal by extending them to the same number of counts. For film calibration two step-sectored spectra of a continuous source were made on another spectrograph. The four films were cut from the same sheet and were developed together in a plastic holder. Their blackening was measured by means of a Leeds and Northrup Knorr-Albers microphotometer.

[5] This intensity integrator was designed by Dr. Russell L. Hudson and will be described by him elsewhere.

RESULTS

The infra-red absorption spectrum of gaseous 1,1-difluoro-2,2-dichloroethylene from 2.5 to 22.6μ is shown in Fig. 1. The infra-red absorption maxima at 668, 720, 2346, and 2355 cm^{-1} are caused by an admixture of carbon dioxide. The rotational structure appearing around 2150 cm^{-1} is caused by a small admixture of carbon monoxide. The wave numbers for the observed absorption maxima (or "shoulders") are given in the first column of Table I. In the second column the relative intensities are indicated as well as the type of the band contours in Badger and Zumwalt's notation.[6]

The observed Raman shifts of liquid $CF_2:CCl_2$ are listed in the first column of Table II. In the second column are given rough estimates of the relative intensities of the bands and, for some bands, information about exceptionally sharp or diffuse appearance. The measured depolarization ratios are listed in the third column.

The infra-red spectrum, as observed in the present work, includes many bands not found by Torkington and Thompson, and the wave number measurements are considerably more accurate. The Raman shift of 883 cm^{-1} reported by Hatcher and Yost was not observed

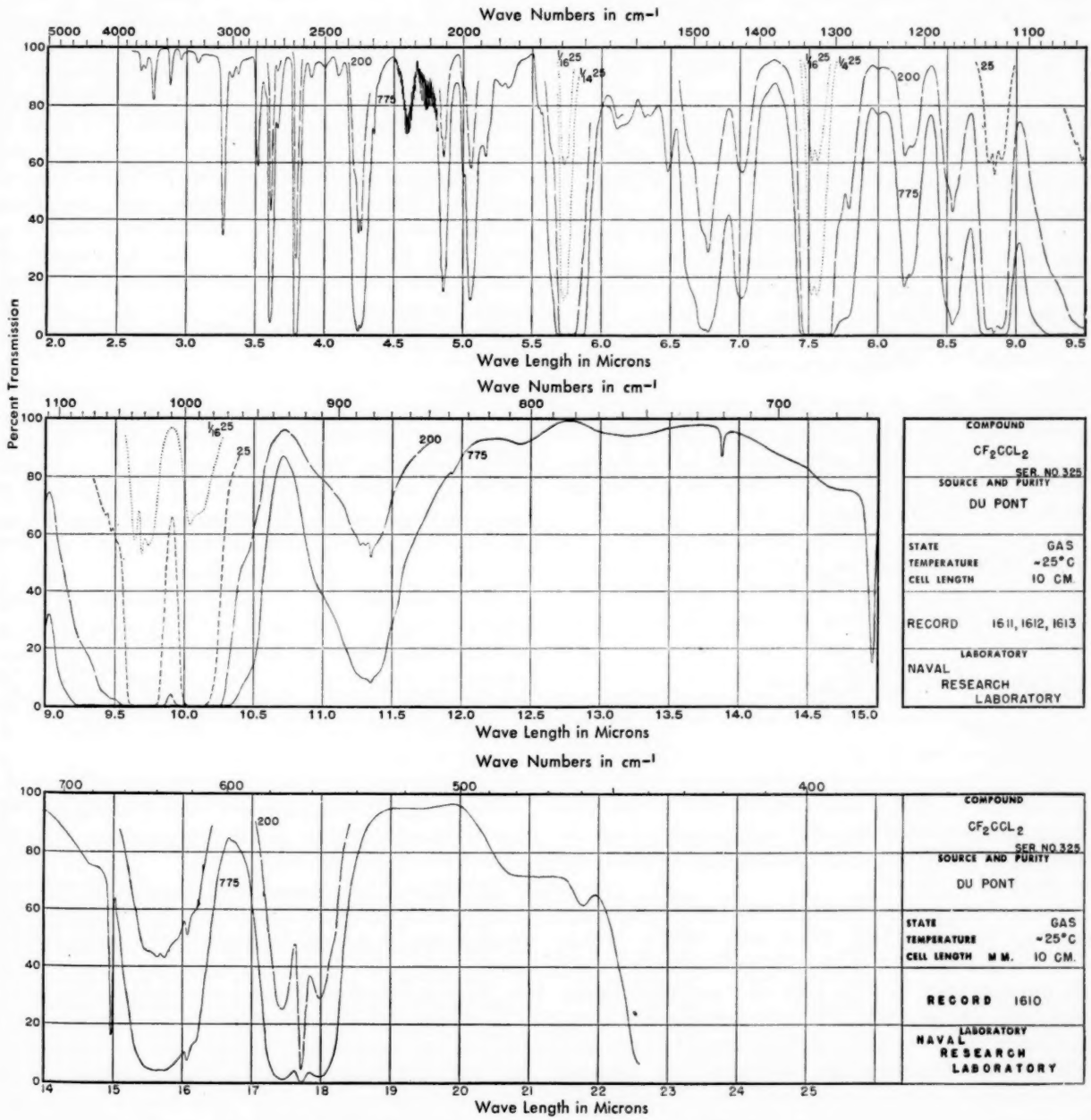

FIG. 1. Infra-red absorption spectrum of 1,1-difluoro-2,2-dichloroethylene.

[6] R. M. Badger and L. R. Zumwalt, J. Chem. Phys. 6, 711 (1938).

TABLE II. Raman spectrum of $CF_2:CCl_2$ (liquid).

Wave number	Description		Depolarization	Interpretation
167* cm^{-1}	vvw			A_2 Fundamental
187.8	w		0.88	B_1 Fundamental
258	vs		0.86	B_2 Fundamental
433.8	vs	sh	0.07	A_1 Fundamental
454	w	d	0.8	B_1 Fundamental
560.8	vs		0.83	B_2 Fundamental
623.0	s	sh	0.12	A_1 Fundamental
646	w	d	0.20	A_1 Fundamental
986	vw		~1	B_1 Fundamental
1027.6	m	sh	0.35	A_1 Fundamental
1121.8	w	sh	0.11	$2\times560.8=1121.6(A_1)$
1313	vvw			B_1 Fundamental
1738.8	s	sh	0.27	A_1 Fundamental
1966	vvw			$2\times986=1972(A_1)$

* This faint band may be spurious, or it may be interpreted as $258-188=170(A_2)$.

here. On the other hand, Table II contains four Raman bands at 1313, 986, 187.8 and 167 cm^{-1}, not found by Hatcher and Yost, and these authors made no polarization measurements. Except for the very faint band at 1966 cm^{-1}, which was observed by Hatcher and Yost at 1976 cm^{-1}, the agreement between the Raman shifts obtained in the present work and those reported by Hatcher and Yost is very good.

INTERPRETATION

If the $CF_2:CCl_2$ molecule has a planar structure of symmetry C_{2v}, the normal vibrations divide themselves into species in the same manner as for $CF_2:CH_2$, i.e., $5A_1+1A_2+4B_1+2B_2$, and the rules for finding the species of combination bands are the same.

Assuming the following dimensions for the $CF_2:CCl_2$ molecule: C=C distance=1.27A, C−F distance=1.32A, C−Cl distance=1.7A, and F−C−F angle=Cl−C−Cl angle=110°, the following moments of inertia are obtained:

$$I_A=298\times10^{-40},\quad I_B=392\times10^{-40},\quad I_C=690\times10^{-40}\ \text{g cm}^2.$$

From these values Badger and Zumwalt's parameters are found to be $\rho=0.74$ and $S=0.16$. Using their curves for $\rho=\frac{3}{4}$ and $S=0$, the values 5.8, 2.7 and 9.7 cm^{-1} for the separation $\nu-\nu_0$ of the rotational branches from the band center for Types A, B and C bands, respectively, are obtained.

Seven of the observed Raman bands are definitely polarized, namely 433.8, 623.0, 646, 1027.6, 1121.8, 1738.8, and 1966 cm^{-1}. The weak band at 1121.8 cm^{-1} and the very faint band at 1966 cm^{-1} are undoubtedly overtones, $2\times560.8=1121.6$ and $2\times986=1972$, respectively. The very strong Raman band at 433.8 cm^{-1}, which lies outside the range covered by the infra-red measurements, must be a fundamental of species A_1. The frequencies 1027.6 and 1738.8 cm^{-1} occur, with small shifts because of the change in the state of aggregation, as intense Type A bands in the infra-red spectrum. They must also be interpreted as A_1 fundamentals. The contours of the two partly overlapping infra-red bands at 622 and 640 cm^{-1} are not quite typical of Type A bands. This may be caused in part by the superposition of two A_1 combination bands, $188+434=622$ and $188+459=647$ cm^{-1}. However, the intensities of the bands in question are so high that the bands must be interpreted as fundamentals, and since the corresponding Raman bands are polarized, they must belong to species A_1. Thus, we have accounted for all of the five totally symmetrical fundamentals.

The strong infra-red band at 564 cm^{-1} is definitely of Type C, and its counterpart in the Raman spectrum, 560.8 cm^{-1}, is very strong and depolarized. There can be no doubt that these bands represent one of the two B_2 fundamentals. Another Raman band at 258 cm^{-1} is strikingly similar to 560.8 in appearance and intensity and is also depolarized. It is undoubtedly the other B_2 fundamental.

The very intense Type B infra-red band at 1327 cm^{-1} must be a fundamental of species B_1. The corresponding Raman band for liquid $CF_2:CCl_2$, at 1313 cm^{-1}, is so weak that its polarization could not be ascertained. Another very strong infra-red band, at 993 cm^{-1}, appears rather definitely to be of Type B. Its counterpart in the Raman spectrum of the liquid is depolarized. It must also be a B_1 fundamental. Although the depolarization ratio for the weak and diffuse Raman band at 454 cm^{-1} is not measured with great accuracy, the band is fairly certainly depolarized. The corresponding band in the infra-red, at 459 cm^{-1}, does not have any clearly defined contour. Nevertheless, it appears rather certain that these bands represent a B_1 fundamental. The depolarized Raman band at 187.8 cm^{-1} must be the last B_1 fundamental.

There remains only the A_2 fundamental. A rough estimate, based on the values of the twisting frequency in C_2H_4 and $CF_2:CH_2$, indicates that this frequency should lie somewhere in the region between 100 and 150 cm^{-1}. Unfortunately, certain spurious light effects in the Raman spectrograph make this region difficult to observe and throw some doubt upon the reality of the observed Raman band at 167 cm^{-1}. Until this doubt can be removed, and the region close to the exciting mercury line investigated, it is tentatively assumed that 167 cm^{-1} is the A_2 fundamental.

The infra-red and Raman bands interpreted as fundamentals for $CF_2:CCl_2$ are listed in Table III. The terms given in the second column serve to indicate in a very rough manner the general nature of the vibrations but do not pretend to describe them with any accuracy.

As mentioned above, Torkington and Thompson,[2] on the basis of Hatcher and Yost's Raman data and their own infra-red observations, made an assignment of ten of the fundamentals for $CF_2:CCl_2$. Two of their assignments, 648 cm^{-1} to B_2 and 255 cm^{-1} to A_1, must be interchanged, since the former is strongly polarized and the latter depolarized. They interpreted the Raman

TABLE III. Fundamental vibration frequencies for $CF_2:CCl_2$.

Symmetry species	Approximate character*	Infra-red (gas) Wave number	Description		Raman (liquid) Wave number	Description		Depolarization
A_1	C=C Stretching	1749 cm^{-1}	vs	Type A	1738.8 cm^{-1}	s	sh	0.27
A_1	CF Stretching	1032	vs	Type A	1027.6	m	sh	0.35
A_1	CCl Stretching	640	s		646	w	d	0.20
A_1	CF_2 Deformation	622	m	Type A	623.0	s	sh	0.12
A_1	CCl_2 Deformation				433.8	vs	sh	0.07
B_2	CF_2 Wagging	564	s	Type C	560.8	vs		0.83
B_2	CCl_2 Wagging				258	vs		0.86
A_2	Twisting				167	vvw		
B_1	CF Stretching	1327	vs	Type B	1313	vvw		
B_1	CCl Stretching	993	vs	Type B	986	vw		~1
B_1	CF_2 Rocking	459	vw		454	w	d	0.8
B_1	CCl_2 Rocking				187.8	w		0.88

* Only very rough meaning can be attached to the terms used in this column.

band at 883 cm^{-1}, which was not observed in the present work, as a B_1 fundamental. If this Raman band should be real, it must be very faint; hence it would be more natural to interpret it as a combination band, 434+454 =888 cm^{-1}. Torkington and Thompson left unassigned one of the B_1 fundamentals, as well as the A_2 twisting frequency.

On the basis of the fundamental vibration frequencies listed in Table III, it has been possible to interpret all of the observed infra-red and Raman bands. The interpretation of the infra-red bands is given in the third column of Table I and that of the Raman bands in the third column of Table II. In the former table, frequencies observed only as fundamentals in the Raman spectrum of liquid $CF_2:CCl_2$ are enclosed in parentheses, since these frequencies may be expected to differ somewhat from the corresponding frequencies for the gas.

DISCUSSION

The interpretation of the two Raman bands not regarded as fundamentals is entirely satisfactory. The majority of the infra-red bands are also interpreted satisfactorily. However, for many of the bands, especially at high wave numbers, alternative interpretations are possible. Except in cases where two assignments are about equally plausible, the alternatives are not listed in the table. About half of the possible binary combination bands have been observed. A third of the missing combination bands may be masked by stronger bands, the others are apparently too weak for observation. Four bands have been interpreted as difference bands, and a number as ternary combination bands.

For some bands, the interpretation given is not quite satisfactory. Thus, the infra-red band at 1936 cm^{-1} is interpreted as a B_1 combination, although its contour more nearly resembles that of a B_2 or A_1 band. If the selection rules were disregarded, the faint infra-red band at 758 cm^{-1} could be interpreted as $1327-564=763(A_2)$, and the band at 1894 cm^{-1} could be interpreted as the corresponding sum band. Also, two or three other bands could be given alternative interpretations. This evidence, however, is hardly sufficient to warrant a serious consideration of the possibility that the $CF_2:CCl_2$ molecule is non-planar. In any case, the fact that both of the B_2 fundamentals give depolarized Raman bands indicates that a deviation from planar structure, if it exists, must be small.

ACKNOWLEDGMENT

The writers wish to express their indebtedness to E. I. du Pont de Nemours and Company for the gift of the sample.

Migration of Sodium Ions through Quartz Plates in an Electric Field. I

RICHARD C. VOGEL* AND GEORGE GIBSON†
Department of Chemistry, Illinois Inltitute of Technology, Chicago, Illinois
(Received October 7, 1949)

The kinetics of the migration of sodium ions through crystalline quartz plates has been studied. This migration, which was induced by an electric field, is assumed to take place through tunnels inherent in the crystal structure and parallel to the principal axis of the quartz. It was shown that the only important mechanism of current flow is the migration of sodium ions through the quartz plate. The activation energy is from 22 to 25 kcal. and depends upon the potential gradient. The rate of migration of the sodium ions is essentially independent of the concentration of the sodium ions.

I. INTRODUCTION

IT was demonstrated by Warburg and Tegetmeier[1] that lithium and sodium ions in an electric field would migrate through crystalline quartz plates cut perpendicular to the Z or principal crystallographic axis. The anode was an amalgam against one side of the quartz plate while the cathode was mercury against the opposite side of the quartz plate. Potassium ions under similar conditions would not migrate. With quartz plates cut parallel to the principal axis, or with fused quartz,[2] no migration of ions was observed.

On the basis of x-ray diffraction data, Gibbs[3] has postulated structures for alpha- (stable below 573°C) and beta-quartz. For alpha-quartz, he indicates the existence of tunnels parallel to the principal axis of the crystal, while similar tunnels are absent in directions perpendicular to the principal axis. It has been proposed[4] that this tunnel-like structure is responsible for the ease of ion migration in quartz plates cut perpendicular to the principal axis; and furthermore, that lithium and sodium ions are small enough to pass through the tunnels while potassium ions are too large.

Harris and Waring[4] made a kinetic study of the migration of lithium ions through quartz plates of varying thicknesses. A Warburg-type cell was used generally with fused lithium nitrate in the anode compartment, but one run was reported using lithium amalgam. Waring and Gibson[5] carried out preliminary kinetic studies on the migration of sodium ions in the Harris-Waring apparatus. Sodium amalgams and mercury were used in the anode and cathode compartments respectively. The data obtained indicated the desirability of a more extensive investigation.

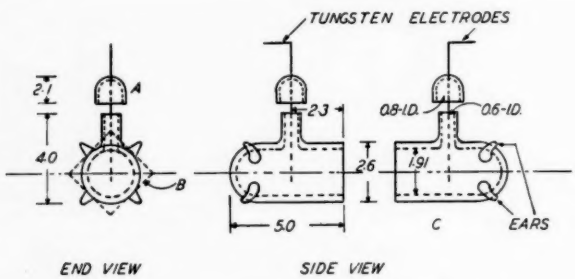

FIG. 1. Diagram of the cell (dimensions in cm).

II. APPARATUS AND EXPERIMENTAL PROCEDURE

The major disadvantages of the Warburg-type of cell used by previous investigators were the contamination of the cell contents by the gaskets between the quartz plate and the cell and the probability of breaking the plate during assembly. Our cell was all glass and constructed of thick walled Pyrex tubing (Fig. 1). The two cell compartments, C, with a quartz plate, B, fixed between them, were held tightly together by four springs hooked over ears fused to the cell body. The springs were made of Chromel-C wire, since it was found to resist attack by mercury vapor at elevated temperatures. The ends of the cell compartments in contact with the quartz plate were polished to prevent mercury and amalgam from leaking out of the cell. The area of the quartz plate exposed to the cell contents was 2.87 cm².

The temperature range selected for the experiments was 210 to 240°C. The range was somewhat predetermined since above 240°C it would have been necessary to avoid vaporization of mercury from the cell while below 210°C the currents would have been quite low for the thicker crystals. A tube furnace was constructed by winding Nichrome wire on an insulated iron pipe. The temperature of the furnace was controlled through a photoelectric-thyratron circuit[6] and could be kept constant to ±0.1°C while readings were taken. We found that this thyratron circuit would not function as Waring and Robison described it unless a variable 10- to 150-$\mu\mu$f condenser was placed in parallel with the photo-cell. A Pyrex tube was centered in the furnace and the ends of the Pyrex tube were closed with rubber stoppers. The electrical leads to the cell, a Pyrex thermocouple well and nitrogen gas inlet and outlet, were brought through these stoppers.

* Present address: Chemical Engineering Division, Argonne National Laboratory, Chicago 80, Illinois.
† Present address: On leave of absence to the Chemistry Division, Argonne National Laboratory, Chicago 80, Illinois.
[1] E. Warburg and F. Tegetmeier, Ann. d. Physik **35**, 455 (1888).
[2] C. E. Waring, *Abstracts of Doctor's Dissertations* (The Ohio State University Press, 1937), No. 21.
[3] R. E. Gibbs, Proc. Roy. Soc. London **A110**, 443 (1926).
[4] P. M. Harris and C. E. Waring, J. Phys. Chem. **41**, 1077 (1937).
[5] C. E. Waring and G. Gibson (unpublished work).
[6] C. E. Waring and G. Robison, Rev. Sci. Inst. **14**, 143 (1943).

The temperature at the cell was read to ±0.1°C by using a Chromel-P-Alumel thermocouple. The thermocouple was periodically calibrated against the steam point. Potentials were measured on a recording potentiometer (Model No. 153X10V, range 0–10 mv, standard speed, Brown Instrument Company).

Figure 2 shows the electrical circuit used with the cell. The potential applied across the cell could be varied from 0 to 140 volts by changing the positions of the contacts on the resistors, R_4 and R_5. The potential drop across R_2 could be measured on the recording potentiometer, P. From this reading and the known resistance of R_3 the potential drop across the cell and R_1 was calculated. Since the resistance of the cell was always greater by a factor of about 10^4 than the resistance of R_1, the potential applied to the cell was essentially the potential drop calculated from the measurement with R_2. The current through the cell was obtained by measuring the potential drop across R_1 with the same recording potentiometer. By an arrangement of sealed mercury switches not shown in Fig. 2 one could record at will the potential drop across R_1 or across R_2 or the potential of the thermocouple.

The quartz plates, 2.54 cm² and of varying thicknesses, were purchased from The Premier Crystal Laboratories, New York. They were cut from optically clear Brazilian rock crystal. Chemically pure sodium and mercury were used to prepare the amalgams. The preparation, storage, and transfer of amalgams to the cell were carried out in an atmosphere of dry nitrogen. Amalgams were analyzed by acid titration of the sodium hydroxide formed when they were boiled with distilled water. After the cell had been filled and placed in the furnace, a rapid flow of dry nitrogen was used to flush out residual air. The flow rate through the furnace was then adjusted to 0.5 cc per second for the duration of the run. The loss of mercury by vaporization around the caps was not sufficiently great to expose the surface of the quartz plate or change the amalgam concentration appreciably.

In order to eliminate possible variables in making measurements, a definite procedure was adhered to for each run unless otherwise indicated. When the cell temperature was 230°C, a potential of 140 volts was applied across the cell and the furnace heating circuit put on the automatic thyratron control which eventually adjusted the temperature to 240°C. Under these conditions the current through the quartz plate rose to a constant value in about ten hours. No measurements were made until the cell current had been constant for at least four hours. Current readings were taken at applied potentials of 100, 80, 60, 40, and 20 volts at a given constant temperature. When a set of readings had been completed, the voltage was increased to 140 volts and the temperature control adjusted for the next lower temperature. Here, the equilibrium temperature and current at 140 volts were attained in one to three hours. Another set of readings were taken and the above process repeated for a total of four temperatures. An upper voltage of 140 was arbitrarily selected since in preliminary work crystals cracked at potentials of about 300 volts.

III. DATA AND DISCUSSION

In early experiments considerable difficulty was experienced in obtaining reproducible results until the quartz plates were treated as follows. The quartz plate was placed on the surface of a solid eight percent sodium amalgam and was heated to about 280°C. The plate was allowed to float on the hot liquid amalgam at 280°C for 30 minutes; vigorous bubbling occurred under the plate during this time. The plate was then lifted off the surface of the hot amalgam, cooled, washed with distilled water, and dried with a paper towel. The surface of the plate which was thus treated was slightly etched while the opposite face remained unchanged. In all future runs this etched face was placed in contact with the amalgam in the anode compartment while the mercury cathode was in contact with the untreated, opposite face. In seven runs prior to this treatment equilibrium currents for identical conditions varied 34 percent while after this treatment the maximum deviation of four runs was 1.5 percent. The possibility that a surface layer (perhaps a sodium silicate) was formed on the plate by the concentrated amalgam treatment was investigated. Electron diffraction patterns of the plate, however, showed only the presence of a "slightly disturbed" quartz lattice.

Since the current passing through the quartz plate was used to determine the amount of sodium migrating, it was necessary to establish unequivocally that all current passing through the cell was carried by sodium ions. Two runs were made at 240°C with two different quartz plates with an 0.0416 mole fraction sodium amalgam in the anode compartment using 140 volts across the cell. The almost constant current was plotted against time for several days on the recording potentiometer. The resulting graph was graphically integrated. The mercury in the cathode compartment was analyzed for sodium in the manner previously outlined. For a 0.0764-cm thick plate, graphical integration

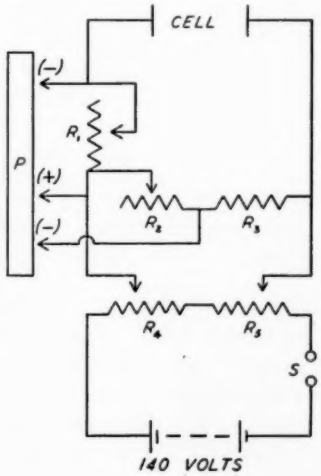

FIG. 2. Diagram of the electrical circuit. P, Brown Instrument Company recording potentiometer; R_1 and R_2, Leeds and Northrup variable resistors, No. 4776 accurate to ±0.1 percent, 0 to 999.9 ohms; R_3, wire-wound, standard 1-megohm resistor; R_4, 10-megohm variable resistor; R_5, 1-megohm variable resistor; and S, S.P.S.T. switch.

TABLE I. Kinetic data for migration of sodium ions through quartz plates (mole fraction of sodium 0.0416).

Run No. (1)	Plate thickness (cm) (2)	Potential gradient (3)	a (4)	ΔE^* kcal. mole^{-1} (5)	b (6)	Av. percent dev. of calc. i from exp. i (7)
1	0.0508	1969	4849.51	22.2	10.8646	0.3
		1575	4914.58	22.5	10.8803	0.1
		1181	4946.28	22.6	10.8008	0.1
		787	4997.54	22.9	10.7065	0.3
		394	5110.72	23.4	10.6050	0.3
2	0.0508	1969	4774.76	21.8	10.7213	0.8
		1575	4823.86	22.1	10.7033	0.8
		1181	4886.77	22.4	10.6851	0.9
		787	4955.14	22.7	10.6218	0.8
		394	5070.16	23.2	10.5230	0.7
3	0.0764	1309	4879.64	22.3	10.7126	1.2
		1047	4884.31	22.3	10.6103	1.0
		785	4939.51	22.6	10.5803	1.0
		523	4991.89	22.8	10.4906	1.1
		262	5052.15	23.1	10.2851	1.0
4	0.0764	1309	4937.75	22.6	10.8040	0.6
		1047	4950.01	22.6	10.7168	0.8
		785	4971.27	22.7	10.6173	0.8
		523	5023.92	23.0	10.5284	0.8
		262	5096.96	23.3	10.3377	1.4
5	0.0925	1081	4927.66	22.5	10.6601	0.5
		865	4985.41	22.8	10.6633	0.6
		649	5033.68	23.0	10.6185	0.6
		432	5133.99	23.5	10.6226	0.6
		216	5201.55	23.8	10.4290	0.6
6	0.0925	1081	5028.57	23.0	10.8444	0.2
		865	5065.37	23.2	10.8069	0.8
		649	5103.46	23.3	10.7412	0.2
		432	5164.61	23.6	10.6663	0.2
		216	5235.66	23.9	10.4844	0.1
7	0.1041	961	4926.77	22.5	10.6177	1.0
		769	4966.51	22.7	10.5857	1.2
		576	5053.93	23.1	10.6201	1.3
		384	5093.95	23.3	10.5091	1.4
		192	5198.97	23.8	10.4043	1.5
8	0.1041	961	5002.14	22.9	10.7592	0.4
		769	5035.57	23.0	10.7161	0.5
		576	5112.44	23.4	10.7325	0.6
		384	5182.16	23.7	10.6819	0.8
		192	5211.30	23.8	10.4276	1.1
9	0.1257	796	5173.47	23.7	10.9968	1.0
		636	5186.05	23.7	10.9157	0.9
		477	5297.92	24.2	11.0066	0.8
		318	5348.38	24.5	10.9234	0.8
		159	5434.19	24.9	10.7889	0.8
10	0.1257	796	5250.94	24.0	11.1094	0.2
		636	5285.41	24.2	11.0731	0.2
		477	5319.17	24.3	11.0082	0.3
		318	5325.05	24.4	10.8356	0.2
		159	5330.94	24.4	10.5417	0.5

showed that 2.43×10^{-4} faraday of electricity had been transferred. Analysis of the cathode contents indicated 2.36×10^{-4} mole of sodium had migrated. Thus, apparently all but 2.8 percent of the current was carried by migration of sodium ions. Similarly, a 0.0508-cm thick plate gave 3.71×10^{-4} faraday by graphical integration while 3.59×10^{-4} mole of sodium were found in the cathode compartment at the end of the run, a difference of 3.2 percent. This difference may not be real, since it is felt that the sodium analysis may be low due to mechanical difficulties in quantitatively transferring the catholyte from the cell. These results definitely established the fact that there was no important mechanism responsible for the passage of current other than the migration of sodium ions through the quartz plate.

A run at 240°C was made to verify the work of other investigators[1,7] who claimed that sodium ions under a potential gradient would not migrate through quartz plates cut with the major faces parallel to the principal axis. The plate used was 0.0787 cm thick and was etched before use as were those employed for the kinetic studies. A 0.0416 mole fraction sodium amalgam was used in the anode compartment with mercury as the cathode. With a potential of 140 volts the current fell in a few minutes from a high value of 0.03 down to 0.01 microamperes cm^{-2}, thereafter remaining constant. Under identical conditions, a quartz plate with major faces cut perpendicular to the principal axis of the crystal would be expected to give a current of approximately 25 microamperes cm^{-2}. This experiment definitely confirms that the migration of sodium ions through quartz plates is anisotropic.

Further support for the mechanism of current conduction was obtained from two runs using pure mercury in both cell compartments and quartz plates cut with major faces perpendicular to the principal axis of the crystal. At 240°C and a potential of 140 volts, a 0.0764-cm plate gave a current less than 0.02 microampere cm^{-2} and a 0.0508-cm plate, a current of about 0.035

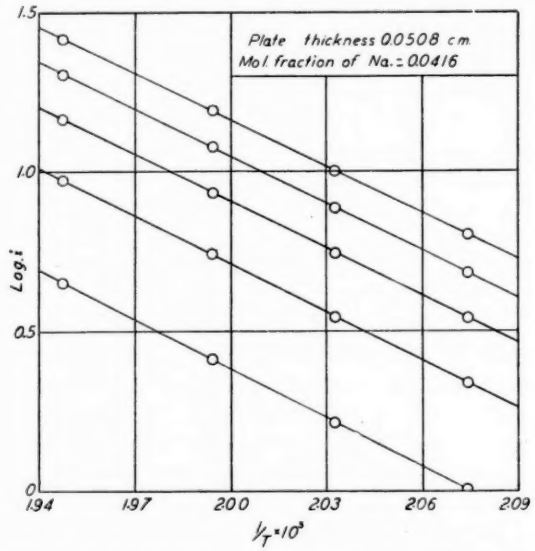

FIG. 3. Plot of log$i$ (i in μa cm^{-2}) *versus* the reciprocal of the absolute temperature, $1/T$ for Run 1. The plotted lines reading from top to bottom are for potential gradients of 1969, 1575, 1181, 787, and 394 volts cm^{-1}, respectively.

[7] Joffé, *Physics of Crystals* (McGraw-Hill Book Company, Inc., New York, 1928), Chapter IX.

microampere cm^{-2}. With an amalgam in the anode compartment one would expect current values of about 25 and 35 microamperes cm^{-2}, respectively, for these two quartz plates.

After these preliminary experiments had been completed, the kinetic runs were carried out as previously described. The data for a typical run are plotted in Fig. 3. In each run five current readings were made at each of five potential gradients for a particular temperature. This procedure was repeated for four temperatures. The temperature dependence of the data for a given potential gradient, amalgam concentration, and plate thickness is well represented by the Arrhenius equation,

$$\log_{10} i = -(a/T) + b, \qquad (1)$$

where i is the current in microamperes per square centimeter of exposed plate face, T is the absolute temperature, and a and b are constants. By the method of least squares the best values of a and b were found for a particular potential gradient, amalgam concentration, and quartz plate thickness.

Table I gives the data for a series of runs with plates of various thicknesses in which the amalgam concentration was 0.0416 mole fraction in all cases. In Table I, column 3 gives the potential gradient in volts cm^{-1}. Column 5 gives the activation energy for the sodium ion migration process and was calculated in the usual manner from the value of a. Column 7 gives the average percent deviation of the experimentally determined currents at four different temperatures from the corresponding currents calculated using Eq. 1. It can be seen that the data for a particular potential gradient generally fits Eq. 1 to better than one percent. The activation energies for identical potential gradients and duplicate runs generally agree to better than 0.4 kcal. per mole.

The increase in activation energy with decreasing potential gradient for each run should be noted. This general trend also exists if the activation energy is plotted *versus* the potential gradient for all the quartz plates. The magnitude of the trend is so close to that of the experimental error, however, that no quantitative significance can be ascribed to such a plot.[8]

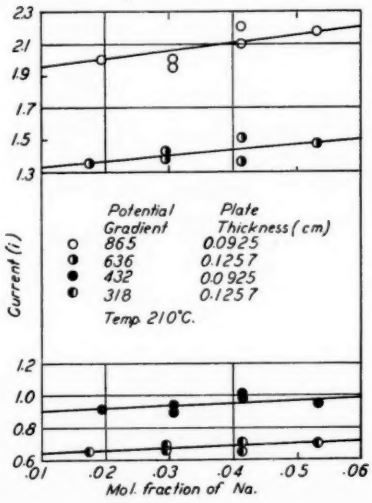

FIG. 4. Current (μa cm^{-2}) *versus* concentration of Na in the amalgam for a given plate thickness, temperature, and potential gradient (volts cm^{-1}).

TABLE II. Kinetic data for migration of sodium ions through quartz plates. Effect of amalgam concentration.

Run No. (1)	Plate thickness (cm) (2)	Amalgam conc. mole fract. (3)	Pot. grad. (4)	a (5)	ΔE^* kcal. mole^{-1} (6)	b (7)	Av. percent dev. of calc. i from exp. i (8)
11	0.0925	0.0202	1081	4986.58	22.8	10.7373	0.4
			865	5025.18	23.0	10.7026	0.5
			649	5084.21	23.3	10.6809	0.6
			432	5130.32	23.5	10.5784	0.7
			216	5203.22	23.8	10.4008	0.7
12	0.0925	0.0307	1081	4961.68	22.7	10.6748	0.2
			865	4998.52	22.9	10.6374	0.1
			649	5058.18	23.1	10.6190	0.4
			432	5148.17	23.5	10.6050	0.2
			216	5217.73	23.9	10.4239	0.4
13	0.0925	0.0307	1081	5035.42	23.0	10.8481	0.5
			865	5085.07	23.3	10.8378	0.6
			649	5124.00	23.4	10.7767	0.5
			432	5233.10	23.9	10.8043	0.6
			216	5312.17	24.3	10.6473	0.8
5	0.0925	0.0416	See Table I				
6	0.0925	0.0416					
14	0.0925	0.0534	1081	5135.62	23.5	11.0616	0.5
			865	5168.66	23.6	11.0167	0.6
			649	5222.96	23.9	10.9864	0.5
			432	5276.85	24.1	10.9017	0.4
			216	5354.64	24.5	10.7394	0.6
15	0.1257	0.0173	796	5108.39	23.4	10.8133	0.2
			636	5152.18	23.6	10.7966	0.1
			477	5173.06	23.7	10.7063	0.2
			318	5222.56	23.9	10.6212	0.4
			159	5220.13	23.9	10.3105	0.5
16	0.1257	0.0297	796	5183.45	23.7	10.9936	0.4
			636	5220.39	23.9	10.9626	0.2
			477	5251.53	24.0	10.8930	0.2
			318	5278.24	24.1	10.7629	0.1
			159	5352.50	24.5	10.6060	0.2
17	0.1257	0.0297	796	5130.68	23.5	10.8674	0.9
			636	5169.17	23.6	10.8402	0.9
			477	5205.81	23.8	10.7836	0.8
			318	5230.68	23.9	10.6490	0.6
			159	5242.27	24.0	10.3688	0.8
9	0.1257	0.0416	See Table I				
10	0.1257	0.0416					
18	0.1257	0.0538	796	5195.39	23.8	11.0288	0.5
			636	5210.08	23.8	10.9530	0.6
			477	5276.89	24.1	10.9562	0.6
			318	5284.95	24.2	10.7888	0.5
			159	5346.58	24.5	10.6070	0.5

[8] A number of investigators (J. Frenkel, *Kinetic Theory of Liquids* (Clarendon Press, Oxford, 1946); p. 43. Glasstone, Laidler, and Eyring, *The Theory of Rate Processes* (McGraw-Hill Book Company, Inc., New York, 1941), p. 552, have explained why the observed activation energy might gradually decrease with increasing potential gradient. They suggest that there is a series of

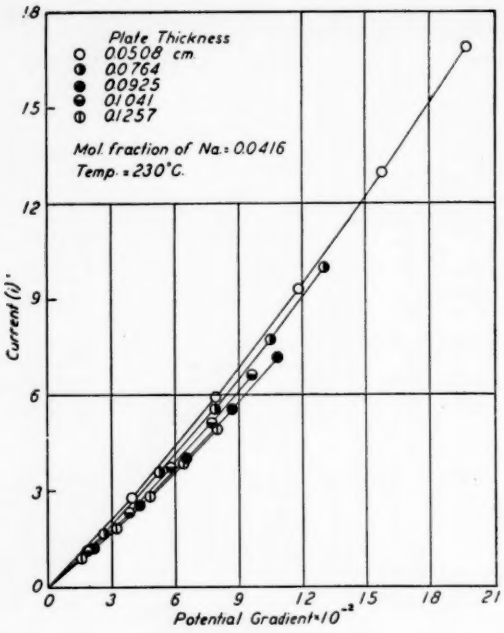

FIG. 5. Plot of current in μa cm^{-2} *versus* the potential gradient in volts cm^{-1}.

Table II presents data showing the effect of amalgam concentration. It is interesting to note that the activation energy increases slightly with amalgam concentration. The small effect of amalgam concentration can also be seen by reference to Fig. 4 in which the current is plotted against amalgam concentration for two potential gradients for each of two different quartz plates.

Figure 5 is a plot of current *versus* potential gradient for five quartz plates at a temperature of 230°C at an amalgam concentration of 0.0416 mole fraction of sodium. Each curve is the average of the data for two runs on a single crystal. The average percent deviation of each run from the mean is 0.3, 3.0, 1.8, 0.6, and 4.7 percent for the 0.0508-, 0.0764-, 0.0925-, 0.1041-, and 0.1257-cm crystals, respectively. There is a regular drop in this family of curves with one exception; the curve for the 0.0925 cm plate falls below that of the 0.1041-cm plate. This behavior may possibly be explained as a slight lattice irregularity in one of these two plates. Visually, both these plates appeared perfectly normal. The regular drop of the curves may be explained by assuming that as the thickness increases more tunnels through the quartz plate are blocked off.

In another set of experiments an attempt was made to measure the amount of sodium within the tunnels after an equilibrium current was attained at 240°C with a potential of 100 volts across the cell. Using the 0.0508-cm plate the equilibrium current was obtained with a 0.0416 mole fraction sodium amalgam in the anode compartment. The plate was then removed, washed with distilled water, dried, and replaced in the clean cell assembly. Both cell compartments were filled with mercury. At 240°C 140 volts was applied across the plate. The current fell rapidly to 0.035 microampere cm^{-2}, remaining constant at this value until the apparatus was shut off after four hours. This plot of current *versus* time was graphically integrated to obtain the amount of sodium carried into the cathode compartment. The area, when corrected for the constant residual current, indicated that 8.3×10^{-8} mole of sodium had migrated out of the crystal. When this experiment was repeated using a 0.0764-cm plate, a residual current of 0.02 microampere cm^{-2} was obtained. Graphical integration showed that 4.5×10^{-8} mole of sodium had migrated out of the plate. We are inclined to view these values as being qualitative in nature since we have no assurance that all of the sodium ions migrate out of the plate under these particular experimental conditions. The important point is that some sodium ions appear to remain in the tunnels. Perhaps the application of radioactive sodium as a tracer would help solve this particular problem which has been the subject of some discussion in the literature.[2]

equilibrium positions and that the passage of an ion from one position to another requires a certain activation energy. If a potential gradient is applied, the free energy in the initial state is increased while that in the final state is decreased by amounts proportional to the potential gradient. Thus, the free energy change from an equilibrium position to the top of the barrier will be decreased by an amount proportional to the potential gradient. Approximate calculations show, however, that this decrease probably would be smaller than the change in activation energy which we observe.

ACKNOWLEDGMENT

The authors wish to thank Mr. James J. Brophy of the Physics Department of the Illinois Institute of Technology for the electron diffraction data and its interpretation.

The Mercury Photosensitized Reactions of Methyl Alcohol*

M. K. PHIBBS AND B. DEB. DARWENT
Chemistry Division, National Research Council, Ottawa, Canada
(Received October 7, 1949)

The mercury photosensitized reactions of methyl alcohol have been investigated at pressures of 30 and 100 mm Hg and over a temperature range from 25° to 500°C. Below 400°C the products are almost entirely hydrogen and ethylene glycol and small amounts of carbon monoxide, formaldehyde and methane. It has been established that the primary step in the reaction mechanism is $Hg(^3P_1)+CH_3OH \rightarrow CH_2OH+H+Hg(^1S_0)$. There is considerable supporting evidence that the alternative split into $H+CH_3O$ does not occur.

Above 400°C the rates of production of CH_2O and CO become significant and increase with rising temperature which has been explained by the fact that the decomposition of the CH_2OH radical is taking place. An activation energy of 29 kcal. has been obtained for this decomposition reaction.

INTRODUCTION

RECENTLY, the mercury photosensitized reactions of several simple organic molecules containing an oxygen atom have been studied.[1-3] In the case of dimethyl ether it was found that the primary act involved the abstraction of an H atom. With CH_3OH there are obviously two possibilities for such a split. Either an O−H or a C−H bond might be broken, with the production of a CH_3O or a CH_2OH radical respectively. It was considered to be worth while to study the behavior of CH_3OH in an effort to find out which process is predominant and then to get some information about the resultant radical.

Other workers have reported qualitative results on the Hg sensitized reactions of CH_3OH. Berthelot and Gaudechon[4] found that an analysis of the non-condensable products gave 92 percent H_2 and 8 percent CO: As indicated previously,[3] it is probable that here too, they were studying the Hg sensitized reaction. Later, in a rough survey of Hg sensitized reactions, Taylor[5] reported that the non-condensable products from CH_3OH were 58 percent H_2 and 42 percent $CO+CH_4$. It is not possible to draw any conclusions about the details of the reaction mechanism from these data.

EXPERIMENTAL

The methyl alcohol used in this work was a Brickman and Company product, free of acetone. The usual technique of degassing and bulb to bulb distillation under vacuum was carried out on the methyl alcohol which was finally stored in a vessel above a Hg cut-off. It had the correct vapour pressure at 25°C and was used without further purification.

All of the quantitative results were obtained in a circulating system almost identical with that described in previous communications.[3] The reaction cell had a volume of 75 cc. A two liter bulb was inserted into the reaction system so that appreciable amounts of product could be obtained even though the percentage conversion of CH_3OH was kept below 1 percent. The temperature of the furnace around the reaction cell was controlled manually to ±1°C.

Standard technique was used in analyzing the non-condensable products. No ethane was detected in any of the runs. The residual methyl alcohol was frozen out into a small bulb at the end of each run, after the removal of the non-condensables, and analyzed for formaldehyde by a titration method.[6] Monochloracetic acid was used as the actinometric fluid in order to determine the light input to the cell.

Several preliminary runs were conducted in a single pass system to determine the nature of the products of reaction. An annular cell was used to ensure a high light input (3×10^{-6} einsteins/sec.) and the flow rate was adjusted to give about 20 percent conversion of reactant. An analysis of a sample of the non-condensable products revealed the presence of 72 percent H_2, 21 percent CO and 7 percent CH_4. A high boiling liquid formed in droplets on the walls of the cell during a run. Boiling water had to be placed around the cell after each run so that the liquid would distil into a small side tube surrounded by liquid air. The liquid product from ten runs amounted to about 1 cc and was carefully fractionated in a column of small capacity.[7] A refractive index determination was made on each fraction. The first 3 percent was CH_3OH which had been retained in the liquid product in spite of continuous evacuation of the reaction system during a run. The major part of the distillate (about 95 percent) had a refractive index agreeing closely with that of ethylene glycol. The infra-red spectrum[8] of a sample of the liquid was similar to that of ethylene glycol. After most

* Contribution No. 2098 from the National Research Council, Ottawa, Canada.
[1] Darwent, Steacie, and Van Winckel, J. Chem. Phys. **14**, 551 (1946).
[2] Phibbs, Darwent, and Steacie, J. Chem. Phys. **16**, 39 (1948).
[3] Marcus, Darwent, and Steacie, J. Chem. Phys. **16**, 987 (1948).
[4] D. Berthelot and H. Gaudechon, Comptes Rendus **151**, 478 (1910).
[5] J. R. Bates and H. S. Taylor, J. Am. Chem. Soc. **49**, 2438 (1927).
[6] I. M. Kolthoff and N. H. Furman, *Volumetric Analysis* (John Wiley and Sons, Inc., New York, 1929), Vol. II, p. 450.
[7] L. C. Craig, Ind. Eng. Chem. (Anal. Ed.) **9**, 441 (1937).
[8] We are indebted to Dr. R. N. Jones of the Laboratory for the infra-red spectrum.

TABLE I.*

Run No.	Temperature °C	Pressure (mm Hg)	Time hr.	H_2 cc gas at NTP/hr	CO	CH_4	Total CH_2O produced during run
2	25	100	1.38	0.212	0.009	0.001	0.033
3	25	100	1.33	0.228	0.010	0.001	0.029
4	25	100	4.00	0.211	0.012	0.001_6	0.051
5	25	30	3.05	0.184	0.034	0.006	0.047
6	25	30	1.00	0.196	0.029	0.006	0.014

* Volume of system 2470 cc; λ2537 absorbed einsteins $hr.^{-1}$ Hg pressure 1.5×10^{-3} mm.

of the glycol had been taken off, the fractionation was continued under a reduced pressure of 10 mm Hg. The last fraction collected had a refractive index of 1.4524 which indicated the presence of some other component, possibly a higher boiling alcohol such as glycerol (r.i. 1.4727). In any case, it did not amount to more than 2 percent of the liquid product. The fractionation indicated that no detectable amount of water was present. A quantitative test for organic peroxides[9] (dimethyl peroxide) was conducted on the residual CH_3OH from all the runs. Any peroxide would be expected to accumulate in the alcohol. The test indicated the absence of any peroxide.

Several runs were made in the circulatory system at two temperatures with $CH_3O\,D$. The $CH_3O\,D$ was prepared by adding D_2O (99.9 percent) to $NaOCH_3$ and fractionation of the resultant mixture. An infrared spectrum[10] of a sample showed that the material was 81 mol percent CH_3OD, the rest being largely CH_3OH. There was no information on how much, if any, CH_2DOH was present. The total hydrogen (H_2+HD) from all the runs at each temperature was converted into water. The percentage of HDO in the water was determined by vapor pressure measurements with a sensitive differential manometer.[11]

RESULTS

All of the quantitative results are collected in Tables I and II. Runs 2 and 6 show that the rates of production of H_2, CO, CH_4 are independent of time and that there is little change in the rates of production on increasing the initial pressure of methyl alcohol from 30 to 100 mm Hg. This latter fact indicates that the quenching of Hg ($^3P_1$) atoms by CH_3OH is essentially complete even at 30 mm.

It is evident that between 25°C and 400°C, H_2 is the only important measurable product in the circulating runs. In the discussion it is assumed that one molecule of $CH_2OH\cdot CH_2OH$ is produced along with each molecule of H_2 in this temperature range. This seems fairly certain in view of the results of the single pass runs and by analogy with the results of the work on dimethyl ether where it was possible to determine the amount of dimer quantitatively. It was impossible to measure the rate of production of ethylene glycol directly, in the circulating system, largely because it has such a small vapour pressure at room temperature and was dispersed over the whole reaction volume during a run.

At 400°C and above it can be seen that the production of CH_2O and CO as well as H_2 becomes more important with increasing temperature. No useful information could be obtained above 500°C because the thermal decomposition became too important.

There is a very small production of CO, CH_2O and CH_4 between 25°C and 400°C which is approximately independent of temperature. It is evident that a different reaction leads to the production of CO and CH_2O in this temperature range than the one which becomes important at 400°C and above. The values for CO and CH_2O used in plotting Fig. 1 were obtained by subtracting 0.008 cc CO and 0.014 CH_2O from observed values between 400°C and 500°C to correct for the unimportant temperature-independent production of CO and CH_2O. The amounts of all the products were also corrected for the small thermal decomposition at 500°C.

One run was conducted with a reduced reaction volume (400 cc) to determine the ratio of CH_3OH decomposed to hydrogen produced; this ratio was found to be 2.28. The quantum yield for H_2 production is seen to be about 0.43 at 25°C and rises to a value greater than unity, above 400°C.

DISCUSSION

The results obtained between 25°C and 400°C can be explained by the following sequence of steps.

$$Hg(^3P_1)+CH_3OH\rightarrow CH_2OH+H+Hg(^1S_0), \quad (1)$$

$$H+CH_3OH\rightarrow CH_2OH+H_2, \quad (2)$$

$$CH_2OH+CH_2OH\rightarrow CH_2OH\ CH_2OH. \quad (3)$$

On this basis hydrogen and ethylene glycol are the only important products in agreement with experi-

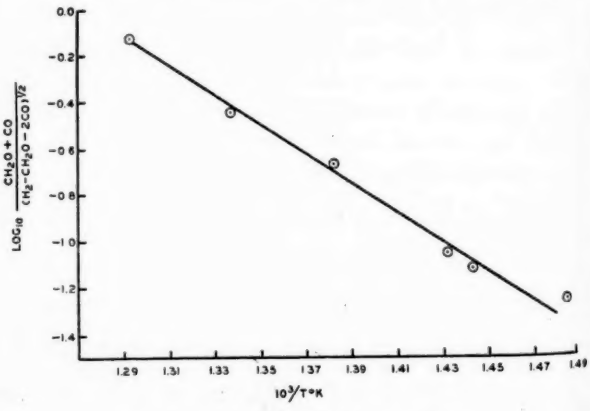

FIG. 1. Plot of $\log_{10}k_4/k_3^{\frac{1}{2}}$ against $1/T$.

[9] K. Nozaki, Ind. Eng. Chem. (Anal. Ed.) **18**, 583 (1946).

[10] We are indebted to Dr. D. Ramsay of this Laboratory for the infra-red spectrum.

[11] These measurements were kindly made by Dr. I. E. Puddington of this Laboratory and a description of the method is given in the Can. J. Research **B27**, 1 (1929).

ment. If these are the only steps involved one would expect

$$\frac{CH_3OH \text{ decomposed}}{H_2 \text{ produced}} = 2.$$

The experimental result of 2.28 for this ratio is valuable evidence that no other reactions which upset that ratio are important under these conditions.

Previous work on the Hg sensitized reactions of the saturated hydrocarbons and of the simple ethers have revealed that there is no tendency towards the splitting of the C−C or C−O bonds in the initial act and this is substantiated for the C−O bond in CH_3OH by the present work. The primary act in all these cases seems to be the abstraction of H atom.

In the case of CH_3OH there is an alternative way in which the H atom might be removed and one might expect the following reaction to take place along with reaction (1)

$$Hg(^3P_1)+CH_3OH \rightarrow CH_3O+H+Hg(^1S_0). \quad (1^1)$$

There is considerable evidence that reaction (1^1) is not significant. If it did occur, one would expect to find appreciable amounts of $CH_3-O-O-CH_3$ among the products. There was no indication of the presence of any peroxide. However, it has been shown[12] that $CH_3-O-O-CH_3$ is extremely unstable under certain conditions, even at 25°C and by analogy with the behaviour of diethyl peroxide, probably decomposes readily into CH_3OH+CH_2O. But if this were the case, one would expect the CH_3OH used/H_2 produced to be considerably less than 2 and also that considerable CH_2O would be produced. Both of the conclusions are contrary to our results. Reaction (1^1) is also excluded on the basis of the results with CH_3OD at 25°C. If reaction (1^1) were important followed by reaction (2) the experiments with CH_3OD would lead to the production of considerable HD. However the results indicated that there is only 6.6 percent HD in the hydrogen and even this small amount may be due to some CH_2DOH in the original reactant. For similar reasons the obvious alternative to reaction (2)

$$H+CH_3OH \rightarrow CH_3O+H_2 \quad (2^1)$$

must also be unimportant. The average O−H bond energy in H_2O is 110 kcal. and by analogy the O−H bond strength in CH_3OH is probably at least this large. The O−H bond is then 10 kcal. or more stronger than the C−H bond and this may be the explanation for the predominance of reactions (1) and (2) over (1^1) and (2^1).

Reaction (3) is interesting because it involves the recombination of radicals which should have a permanent dipole moment. Weiss[13] has indicated that in such cases disproportionation might be favored over recombination because of the tendency for orientation of the radicals on collision. Recombination of CH_2OH will involve the close approach of the positive CH_2 groups of two radicals. The importance of reaction (3) indicates that some other factor, such as a lower activation energy for the recombination process, must outweigh the orientation effect, unless a considerable rearrangement of atoms can occur after the orientation of the dipoles.

Although the above reactions explain the general nature of the products they do not account for the fact that ϕH_2, the quantum yield of hydrogen production, is only 0.43 at 25°C; the above mechanism demands a value of 1.0. It has been found that low quantum yields, in mercury photosensitized reactions of ammonia,[14] phosphine,[14] methane[15] and neopentane[16] are due to inefficiencies in the primary act, reaction (1), and Thomas and Gwinn[17] have suggested that the reaction

$$Hg(^3P_1)+H_2 \rightarrow 2H+Hg(^1S_0)$$

is not by any means 100 percent efficient. However, it is likely that the similar reactions with ethane[18] and dimethyl ether[3] are about 100 percent efficient and recent work[19] has shown that ϕ_{H_2} for the mercury photosensitized reaction of butane and the pentane increases with pressure, as was found for ethane, and actually values of 0.9 have been obtained at high pressures. In the present investigation, the indications are

TABLE II.*

Run No.	Temperature °C	H_2	CO	CH_3O cc. gas at N.T.P.	CH_4
16	25	0.525	0.019	0.025	0.012
11	100	0.618	0.008	0.024	0.005
13	200	0.657	0.008	0.013	0.008
14	300	0.661	0.008	0.016	0.011
15	400	0.675	0.015	0.051	0.022
22	420	0.710	0.0236	0.059	0.018
23	426	0.665	0.030	0.059	0.017
18	450	0.935	0.051	0.154	0.030
24	475	1.13	0.082	0.254	0.035
17	500	1.741	0.274	0.434	0.050
Thermal run					
20	500	0.064	0.006	0.027	0.013
Runs with CH_3OD 4 (2 hr. runs) at each temperature % HD in hydrogen					
27	25	6.6			
28	460	25.8			

* Conditions as in Table I but light input 2.72×10^{-5} einsteins/hr; all runs done at 100 mm CH_3OH and for 2 hours.

[12] A. Rieche, Berichte **61**, 951 (1928), see also E. J. Harris and A. C. Egerton, Proc. Roy. Soc. **A168**, 1 (1938).
[13] J. Weiss, Trans. Faraday Soc. **36**, 856 (1940).
[14] E. A. B. Birse and H. W. Melville, Proc. Roy. Soc. (London) **A175**, 187 (1940).
[15] Morikawa, Benedict, and Taylor, J. Chem. Phys. **5**, 212 (1937).
[16] B. deB. Darwent and E. W. R. Steacie, Can. J. Res. **B27**, 181 (1949).
[17] L. B. Thomas and W. D. Gwinn, J. Am. Chem. Soc. **70**, 2643 (1948).
[18] B. deB. Darwent and E. W. R. Steacie, J. Chem. Phys. **16**, 381 (1948).
[19] B. deB. Darwent, unpublished results.

that ϕ_{H_2} increases and the rates of production of CH_2O, CO and CH_4 decrease slightly with increasing pressure and temperature. These facts agree with the type of mechanism suggested to account for the low quantum yield and "atomic cracking" reactions of ethane[18] which, for methanol, will take the form:

$$H+CH_2OH\rightarrow CH_3OH^*, \quad (4)$$

$$CH_3OH^*+M\rightarrow CH_3OH+M \quad (5)$$

$$CH_3OH^*\rightarrow \text{decomposition products}, \quad (6)$$

$$2H\xrightarrow{M}H_2. \quad (7)$$

Reactions (4), (5) and (7) account for the low value of ϕ_{H_2} and for the decrease in the rates of production of CO, CH_2O and CH_4 with increasing pressure and temperature since both of these factors will increase the rate of reaction (2) relative to that of (4) and (7).

At 400°C and above the two following reactions

$$CH_2OH\rightarrow CH_2O+H \quad (8)$$

$$CH_2O\rightarrow CO+H_2 \quad (9)$$

must be added to explain the increasing importance of CO and CH_2O along with the greater production of hydrogen. Reaction (8) is the most probable decomposition of CH_2OH since it involves the formation of a C=O from a C−O bond with a considerable release of energy.[20] Any other reaction path would involve a much higher activation energy. Reaction (9) is the over-all thermal decomposition reaction[21] of formaldehyde.

The results show that there is a very small production of CO and CH_2O between 25°C and 400°C which is temperature independent while the production of these products between 400°C and 500°C is strongly temperature independent. It is clear that reactions (8) and (9) cannot be responsible for the production of these products between 25° and 400°C. Hence we have assumed that for the production of CH_2O and CO between 400 and 500°C the true values for CO and CH_2O are taken to be the total amounts produced less the amounts produced below 400°C.

On the basis of the reaction mechanism suggested above, it can be seen that

$$d/dt[CH_2O+CO]=k_4[CH_2OH]$$

$$d/dt[\text{dimer}]=d/dt[H_2-2CO-CH_2O]=k_3[CH_2OH]^2,$$

if we assume that the production of H_2 by (7) is negligible compared to (2),* and therefore at any given reaction time

$$A/B=\frac{[CH_2O+CO]}{[H_2-2CO-CH_2O]^{\frac{1}{2}}}=\frac{k_4}{(k_3)^{\frac{1}{2}}}.$$

If one then assumes that the activation energy of reaction (3) is zero, which should be approximately true, and plots $\log_{10} A/B$ *versus* $1/T$ as given in Fig. 1 one gets an activation energy for the decomposition of the CH_2OH radical which is equal to 29 kcal.

Further support for reactions (8) and (9) is given by the result of the experiment with CH_3OD at 460°C. The analysis of the hydrogen produced indicated that it contained 25.8 percent HD. This value should be corrected for the 6.6 percent HD found in the run with CH_3OD at 25°C (taken as a blank) to give a true value at 460°C of 19.2 percent HD. Assuming that the HD is produced solely via $CH_2OD\rightarrow CH_3O+D$ and $D+CH_3OD\rightarrow HD+CH_2OD$ and remembering that the original material was 81 percent CH_3OD, one can see that

$$\frac{CH_2O+CO}{H_2}=\text{percent HD}\times\frac{100}{81}=0.25.$$

Using the results of Table II at 460°C, interpolation gives values of (H_2=1.0 cc, CO=0.05, CH_2O=0.17 cc) which when substituted in the above expression make the left-hand side equal to 0.22 which agrees well with the right-hand side and therefore adds support to the reaction mechanism set forth.

[20] C. E. H. Bawn, Trans. Faraday Soc. **33**, 598 (1937).

[21] C. J. M. Fletcher, Proc. Roy. Soc. (London), **A146**, 357 (1934).

* This will probably be true at 400°C and higher.

THE JOURNAL OF CHEMICAL PHYSICS VOLUME 18, NUMBER 4 APRIL, 1950

On the Photographic Reciprocity Law Failure and Related Effects. II. The Low Intensity Sequence Effect

E. KATZ
Physics Department, University of Michigan, Ann Arbor, Michigan
(Received October 17, 1949)

A quantitative theory of all details of the low intensity sequence effect is given on the basis of the following assumptions. A monatomic Ag speck is unstable against thermal agitation, a diatomic speck is stable, but for development a speck of more than two atoms is required. The theory is based on that for low intensity failure as developed in paper I.

I. INTRODUCTION

IF a plate is given first an exposure (=intensity ×time) of pE with intensity I_1 and subsequently an exposure $qE=(1-p)E$ with intensity I_2 it is known that the resulting density D, after development etc., will differ from what would have been obtained if the sequence of these two exposures had been reversed. This sequence effect has been studied experimentally for intensities not exceeding the optimum intensity by J. H. Webb and C. H. Evans.[1] The effect was discovered by Weinland.[2] P. C. Burton and W. F. Berg who call this the "Weinland effect" have published a series of very interesting studies[3] in which the effect proves to be a useful tool for obtaining qualitative information concerning the latent image in its first stages of formation (sub-latent image).

The density D as a function of the four independent variables p, E, I_1, I_2 may be represented in a number of ways, for instance by plotting $e\equiv\log E$ as a function of p for constant values of the parameters D, I_1, I_2 (isodense curves) or by plotting D as a function of p for constant values of E, I_1, I_2 (iso-exposure curves). For the purpose of the present paper the isodense plots are the most important ones for reasons given below. Of course any other type of plotting can be converted to the isodense type provided there are sufficient data available.

For both iso-exposure and isodense plots a pair of curves with p, I_1, I_2 and q, I_2, I_1 forms a sequence loop as shown in Fig. 1. In such a loop any pair of points on a vertical line corresponds to sequence reversal. We shall call them conjugate points. Webb's results are mainly given in terms of iso-exposure loops but enough data are available for effectively transforming them into isodense plots. The results of Burton and Berg are given in neither way; these authors mostly keep either pE or qE constant, varying both E and D. Not enough data are available for replotting isodense curves from their results. Besides, their papers admittedly do not aim at quantitative relations, for which isodensity is essential, as will be shown below. Rather their results yield valuable support to the hypotheses concerning latent image formation as postulated previously by Webb and Evans and used extensively in the previous paper.[4]

For the loops obtainable from Webb's data we note three significant features as shown schematically in Fig. 1, *viz.*:

(a) The loops have a peculiar asymmetric shape.
(b) The curves have flat portions near their I_1 terminals.
(c) The upper curve in Fig. 1a and the lower one in Fig. 1b often have a typical sigmoid bend as they approach the right I_2 terminal point.

Weinland, and Webb and Evans more fully, recognized qualitatively the relation between the sequence effect and the reciprocity law failure (r.l.f.), in particular the low intensity failure (l.i.f.). The theory of the l.i.f. given in paper I therefore affords a basis for a complete theory of the low intensity sequence effect. The present paper aims at developing this theory and confronting it with Webb and Evans' experimental results.

II. ELEMENTARY RELATIONS

After choosing two fixed intensity values I_H and $I_L(I_H>I_L)$ we consider two types of conjugate exposure sequences:

(a) $I_1=I_H$; $I_2=I_L$
(b) $I_1=I_L$; $I_2=I_H$.

If a plate is given an exposure pE with I_1 and $(1-p)E$ with I_2 the resulting density D is one function of p and E in case a and another function of p and E in case b. It will be assumed that the result is independent of the time interval between the end of I_1 and the beginning of I_2 and also independent of the time between termination of I_2 and development. According to Burton and Berg these assumptions are reasonable at low intensities. If required the theory is strictly valid for short interexposure time and short times between exposure and development. Then, for each case, at any point of the $D(p, E)$ surface the following identity holds:

$$(\partial D/\partial p)_E=-(\partial D/\partial \log E)_p.(\partial \log E/\partial p)_D. \quad (1)$$

[1] J. H. Webb and C. H. Evans, J. Opt. Soc. Am. **28**, 431 (1938).
[2] C. E. Weinland, J. Opt. Soc. Am. **16**, 295 (1928).
[3] P. C. Burton and W. F. Berg, Phot. J. **86B**, 2 (1946) and **88B**, 84 (1948); P. C. Burton, Phot. J. **86B**, 62 (1946) and **88B**, 13 and 123 (1948).
[4] E. Katz, J. Chem. Phys. **17**, 1132 (1949), referred to hereafter as "paper I."

The quantity

$$\gamma \equiv (\partial D/\partial \log E)_p \qquad (2)$$

is the slope of characteristic curves such as shown in Fig. 2. This quantity is practically constant for a large range of intermediate D values. Moreover, for any value of D, γ is only very weakly dependent on p. Finally γ is even to a higher degree of approximation equal for conjugate points, because at the terminals of the loop its two branches necessarily meet. Form. (1) links Fig. 1a and 1b as illustrated in Fig. 2. Where Fig. 1a has a horizontal segment F, Fig. 1b must have the same. Insofar as γ is constant Fig. 1b is an upside down view of Fig. 1a, apart from a vertical scale factor γ. This simple rule effects the transformation from iso-exposure to isodense curves. The constancy of γ for a large D range means that the shape of the sequence loops in Figs. 1a and 1b is within the corresponding limits independent of the value of E and D.

III. THE RELATION BETWEEN DENSITOMETRIC AND SINGLE GRAIN DATA

In order to correlate experimental density measurements with single grain theory we postulate the order principle (o.p.): "The order in which the grains of a given plate become developable in the course of any exposure is independent of the conditions of exposure and development." This postulate is extensively discussed in paper I. A consequence of the o.p. is that isodense exposures produce exactly equal effects in the last grain(s) rendered developable. Deviations from the o.p. and their influence on the present theory will be discussed in Section VIIc.

The o.p. should at this point be compared with the ideas of Burton and Berg. The purpose of this comparison is to show why the present paper is essentially limited to isodense exposures and why, consequently, Burton and Berg's results are not amenable to the same degree of quantitative analysis unless many more details about the grains are known. This can best be seen with the aid of diagrams similar to those designed by Burton and Berg on page 21 of their first paper. We consider a multi-dimensional diagram. The ordinate is the amount of silver S of that speck which is going to be developable first in any particular grain as a result of a certain type of exposure. The abscissa is the total exposure. Along the other axes are plotted all (n) independent parameters of exposure and development. Each grain is then represented by an $(n+1)$-dimensional supersurface S_{n+1}. The developability is given by another $(n+1)$-dimensional supersurface D_{n+1} (presumably flat). The n-dimensional intersection supercurve of S and D determines the developability of the grain in question. Such a supercurve can in principle be drawn for each grain.

The o.p. may now briefly be stated in terms of this diagram as follows: "Supercurves do not intersect." It has been shown in paper I that the o.p. is the necessary and sufficient condition for establishing a $1-1$ relation between single grain data and densitometric measurements and this is exactly what is expressed by the non-intersection of the supercurves. Another

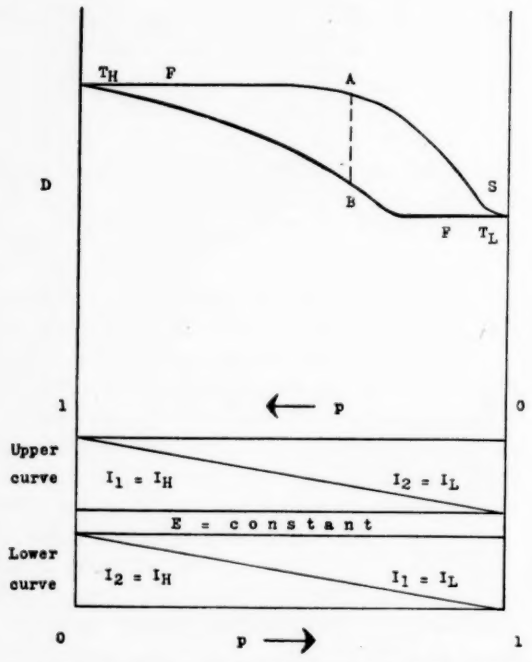

FIG. 1a. Iso-exposure plot. Typical "sequence loops" (schematic for various proportions of exposures at a high intensity I_H and at a low intensity I_L. A, B; A', B'=conjugate points, F=flat portions; S=sigmoid bend.

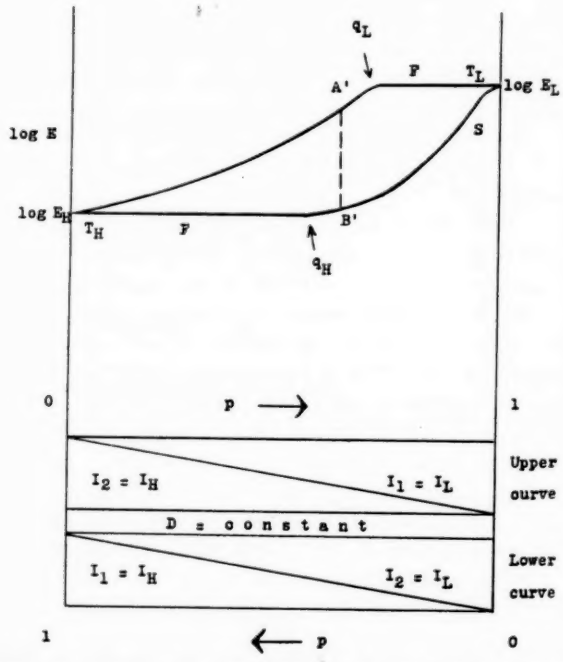

FIG. 1b. Isodense plot. The exposure fraction pE given first at I_1 (either I_H or I_L) is followed by qE at I_2 (either I_L or I_H) $(p+q=1)$. q_L, q_H=corners, T_L, T_H=low and high intensity terminals.

way of expressing the o.p. is that each supercurve (each grain) may be labeled with the density at which it becomes developable.

By comparing isodense exposures one deals with one and the same grain. One has only to derive the shape of one supercurve. In order to compare non-isodense exposures one has to know, in addition, something about the distances between the supercurves and about the possibilities of intersections of the supersurfaces S_{n+1} at lower levels than D_{n+1}. These are governed by grain properties which may differ widely among the various grains of an emulsion even if the comparison is restricted to grains of the same size and at the same depth, as is evidenced for instance by Webb's analysis of H & D curves.[5] Apart perhaps from very special circumstances, the required details are not known so that in general a quantitative analysis along the ideas of Burton and Berg will not be feasible. Only for isodense exposures where such detailed information is not required may basic single grain theory be expected to succeed.

IV. THE MECHANISM OF THE SEQUENCE EFFECT AND ITS CONSEQUENCES

The idea of Webb and Evans as corroborated by the work of Burton and Berg is to divide the process of latent image formation into the following two parts: (a) the building of a stable Ag speck (sub-latent image); (b) the building of a developable speck from a stable one.

Until part *a* is completed thermal motion will tend to destroy the result. Therefore, the efficiency of this part is sensitive to the temperature and to the light intensity. During part *b* the efficiency of the process is assumed to be independent of these factors insofar as we restrict ourselves to low intensities. Therefore, changes in intensity during the last part of an exposure will affect the result less than changes during the first part. Qualitatively this picture explains the sequence loops and at the same time the l.i.f. The terminals of the loops are different because of different efficiencies of part *a* for different intensities, and this is simply the l.i.f.

The parts *F* in Fig. 1 are flat because of the constant efficiency of part *b*. Because the flat part of the lower curve in Fig. 1b generally extends to $p>0.5$ Webb and Evans concluded that the size of the stable speck is about half that of the developable speck. No other quantitative conclusions on the subject were drawn in their paper. The interpretation of the length of the flat part was criticized by Burton and will become clear in the present paper.

In paper I extensive use was made of this picture for the theory of the l.i.f. Likewise we shall assume here that a monatomic Ag speck is unstable against thermal agitation whereas a diatomic one is stable. An additional number of Ag atoms has to be added in order to reach developability. The efficiency of the process of

[5] J. H. Webb, J. Opt. Soc. Am. **29**, 314 (1939).

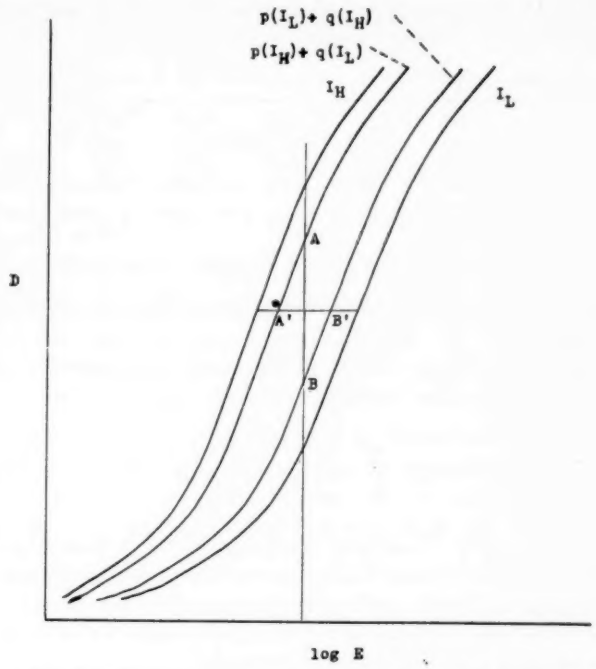

FIG. 2. Schematic representation of terminal characteristic curves and of one pair of conjugate sequence characteristic curves. Vertical section corresponds to iso-exposure diagram Fig. 1a. Horizontal section corresponds to isodense diagram Fig. 1b.

latent image formation is governed by the time spacings of successive quanta (interquantic times) during the formation of the stable speck.

We wish to find the probabilities that a certain type of exposure will produce in a grain a stable speck or a developable speck. We define the survival function $F(t)$ as the probability that a grain, absorbing at $t=0$ a quantum which produces a conduction electron, will at time t still have this electron "alive." This electron may wander around, being captured and released at intervals, until it finally "dies" either by being trapped stably at a silver speck or by being recaptured in its hole. Let $E.P(T, t)dt$ be the probability of finding in an exposure E of duration T an interquantic time between t and $t+dt$. Let c be the chance of building a stable speck if two electrons are alive. Then the probability of not building a stable speck by two quanta, separated by one interquantic time t is $(1-cF(t))$. The chance N of not building a stable speck by any of the interquantic times occurring in the exposure E is:

$$N=\prod_{t=0}^{t=\infty}(1-cF(t))^{E.P(T,t)dt}$$

$$=\exp\left\{\int_0^\infty E.P(T,t)\ln(1-cF(t))dt\right\}. \quad (3)$$

Finally the probability of forming one or more stable specks during E is $1-N$. In these expressions the upper limit of integration may be taken as T or ∞ since $P=0$ for $t>T$. We have neglected the probability of a first electron reacting with a third or later one. This

TABLE I. Parameter values from analysis of Webb and Evans' data.

Emulsion	γ	ϵ	ω	x	p_H	Ag atoms per speck
I	4.64	2.37	3.78	0.19	0.49	4
III	1.17	4.08	15.1	0.39	0.22	9
IV	1.10	4.15	9.35	0.32	0.38	5
V	0.76	4.60	14.7	0.39	0.26	8
II	—	3.94	13.0	0.37	0.25	8

is justified in the low intensity domain we are dealing with here. For the same reason and because $c<1$ we may legitimately break off the series development of $\ln(1-cF(t))$ after the first term in (3) and we find:

$$\ln N=-cE\int_0^\infty P(T,t).F(t)dt\equiv -cEW. \tag{4}$$

The quantity W defined by this relation is dependent in general on I and T. For exposures with many interquantic times P, and hence W, becomes independent of T. For two successive exposures E_1 with T_1 and E_2 with T_2 a similar reasoning leads to:

$$\ln N=\ln N_1+\ln N_2=-c(E_1.W_1+E_2.W_2) \tag{5}$$

for the probability N that neither exposure will produce a stable Ag speck. We have neglected the probability that the last electron of the first exposure may react with the first one of the second exposure in accordance with the assumption stated in Section II. For many short breaks such as occur in the intermittence effect this probability has to be taken into account (see paper III) but for only one break its influence is calculable but very small.

The probability of forming a developable grain can now be found with good approximation from the previous result by reserving a last part E_0 of the total exposure E for the purpose of bringing up to or beyond the developable size all specks that were stabilized during $E-E_0$ but no specks that were not. In accordance with Webb, Evans, Burton and Berg, we shall take E_0 to be independent of the intensity at which this part of the process is effected. Owing to the statistical fluctuations of the number of quanta received during E_0 this procedure is an approximation. The effect of the fluctuations will be estimated in Section VII.

We conclude that the probability for rendering a grain developable is governed by the quantity Q defined as follows:

(a) For an exposure pE at I_1 followed by $qE\geqslant E_0$ at $I_2(p+q=1)$

$$Q=c\{W_1pE+W_2(qE-E_0)\}. \tag{6a}$$

(b) For an exposure pE at I_1 followed by $qE\leqslant E_0$ at $I_2(p+q=1)$

$$Q=c.W_1(E-E_0). \tag{6b}$$

(c) For only one exposure E at I

$$Q=c.W(E-E_0). \tag{6c}$$

Case c can be considered as a special case of b for $q=0$. Assuming the order principle, isodense exposures must correspond to the same probability for developability for the type of grains that become developable last at the density considered. Consequently isodense exposures should satisfy the relation:

$$Q=\text{constant}. \tag{7}$$

This then is the general expression for the sequence effect and at the same time for the l.i.f. Its explicit form depends on the P and F.

V. THE STATISTICS OF LIGHT ABSORPTION P AND THE SURVIVAL FUNCTION F

Let a grain absorb $I=1/i$ quanta per second during a time T with $E=I.T$. It is easily shown that the probability $E.P(T,t)dt$ of finding an interquantic time between t and $t+dt$ in E is exactly:

$$\left.\begin{matrix}E.P(T,t)dt=E(1-t/T)\exp(-t/i)dt/i & (0\leqslant t\leqslant T)\\ P=0 & (t\geqslant T)\end{matrix}\right\}. \tag{8}$$

For $E\gg 1$, P approaches Eq. (5) in paper I, becoming independent of T. For $E\ll 1$ the only interquantic times that can occur are $\ll i$. The number of interquantic times during E is exactly:

$$E\int_0^\infty P dt=E-1+e^{-E}, \tag{9}$$

which approaches $E-1$ for large E and $E^2/2$ for small E.

The survival function $F(t)$ was discussed in paper I. Its relevant features are: independence of the light intensity in the l.i.f. region, and $F(t)\sim t^{-x}$ for low in-

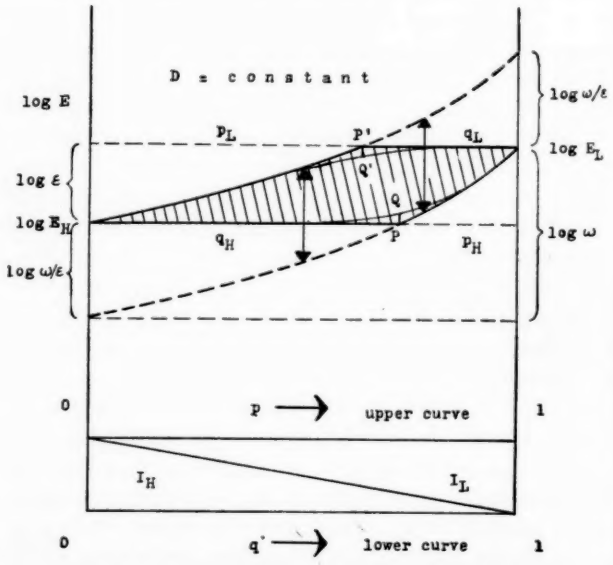

FIG. 3. Schematic illustration of theoretical relations 10...16 for isodense loops.

tensities. Here x is the slope of the straight part of isodense l.i.f. diagrams. The indepencence of light intensity amounts to interaction only between successive quanta.

VI. THEORY OF THE ISODENSE LOOPS

a. First Approximation

In first approximation W as defined by (4) is assumed to be independent of the exposure time T. According to Eqs. (6) and (7) the terminals of the loops should then satisfy:

$$W_H(E_H-E_0)=W_L(E_L-E_0) \tag{10}$$

and the loops are given by:

$$W_1(E-E_0)=W_H(E_H-E_0) \tag{11a}$$

if $qE\leqslant E_0$ and by:

$$W_1pE+W_2(qE-E_0)=W_H(E_H-E_0) \tag{11b}$$

if $qE\geqslant E_0$.

The meaning of the symbols is defined in Section II. Equation (11a) represents the flat parts F. The upper and lower branch correspond, respectively, to $I_1<I_2$ and $I_1>I_2$. At the points $q_H=E_0/E_H$ and $q_L=E_0/E_L$ the curves have a discontinuous slope, caused by the discontinuous change from unstable to stable specks and the neglection of statistical fluctuations in the number of quanta absorbed during E_0. The different lengths of the flat parts of the two branches, which contribute to the asymmetry of the loop are now seen to be connected with the difference of E_H and E_L.

We abbreviate

$$W_H/W_L=\omega \tag{12a}$$

$$E_L/E_H=\epsilon, \tag{12b}$$

where ω and ϵ are >1.

According to paper I, for low intensities, W is proportional to I^x where x is the l.i.f. exponent. Since the bending of the l.i.f. curve towards the optimum was primarily due to the factor $E-E_0$ we shall assume the validity of this relation up to the optimal intensity. A glance at Fig. 5 on p. 129 of Burton's last-mentioned paper supports the correctness of this assumption. Then:

$$\omega=(I_H/I_L)^x. \tag{13}$$

If is seen that for given intensities the knowledge of the l.i.f. yields directly ϵ and ω. It will be shown that these two parameters determine the shape of the loops completely. By straightforward manipulation of Eqs. (10), (11), and (12) the equations of the curved parts of the isodense loop become:

upper branch:

$$\log E=\log E_H-\log(1-p(1-1/\omega)) \tag{14a}$$

lower branch:

$$\log E=\log E_H-\log(1-q(1-1/\omega))+\log\epsilon/\omega. \tag{14b}$$

Since p for the upper branch and q for the lower branch both run from left to right in Fig. 1b the two curves have exactly the same shape and differ only by a vertical sift of

$$\Delta\log E=\log\omega/\epsilon. \tag{15}$$

The shape of the curves is only dependent on one parameter ω. These results are illustrated schematically in Fig. 3.

The following relations are helpful in the analysis of experimental curves and are easily verified:

$$q_H/q_L=\epsilon, \tag{16a}$$

$$q_Hp_L/q_Lp_H=\omega, \tag{16b}$$

from which the p's and q's may be derived separately.

The area of the loop can also be computed. It approaches zero if the two intensities are very low, because $\omega\rightarrow\epsilon$, and also if the two intensities are near the

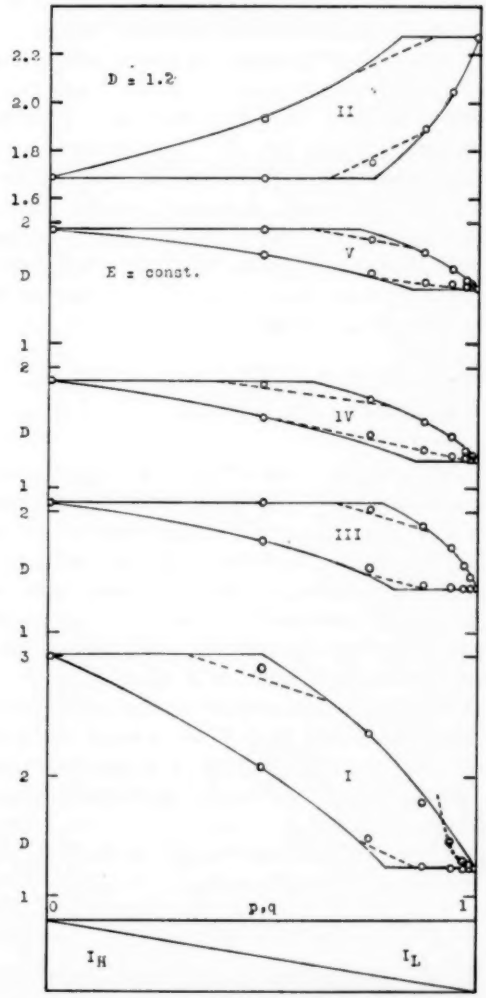

FIG. 4. Comparison of theory with Webb and Evans' experimental results (reference 1). Points are experimental. Full lines are drawn according to the theory in first approximation. Dotted lines represent estimated second approximation. Top loop for emulsion II: isodense plot. Other loops are iso-exposure plots. Used values of the constants are listed in Table I.

optimal region, because $\epsilon \to 0$. We find

$$\text{area} = 0.434(\omega-\epsilon)(\epsilon-1)/(\omega-1)\epsilon, \quad (17)$$

which is maximum for

$$\epsilon = \omega^{0.5} = (I_H/I_L)^{x/2}, \quad (18)$$

in which case the corners are conjugate points. This condition was intuitively satisfied remarkably closely by Webb and Evans (see Table I).

b. Comparison of First Approximation with Experiment

The lower part of Fig. 4 shows Webb and Evans' measured points for their emulsions I, III, IV, V. Here only iso-exposure data were available, so that the theory has three adjustable parameters: γ, ω, and ϵ. The full curves give the lines according to (14) transformed to iso-exposure plots according to Section II. The values of γ, ω, and ϵ, given in Table I, have been derived from the following sets of three data:

(a) The vertical distance between the terminals $\gamma \log\epsilon$.

(b) The vertical distance between the curves $\gamma \log\omega/\epsilon$ (see (15) and Fig. 3).

(c) The slope at the low intensity terminal $0.434\,\gamma(\omega-1)$, disregarding the sigmoid bend if present.

A more stringent test is possible for emulsion II, for which Webb and Evans, in their Figs. 4 and 5, give enough information for plotting a number of isodense points. Here the theory has only two adjustable parameters:

(a) The vertical distance between the terminals $\log\epsilon$.

(b) The slope at the low intensity terminal $0.434\,(\omega-1)$.

The results of Fig. 4 show that a satisfactory description is achieved with reasonable values of the parameters γ, ω, ϵ. The values of the l.i.f. slope x that follow with (13) from $\omega(I_H/I_L$ being 1000) are tabulated and also turn out reasonable. In particular emulsion I which according to reference 1 has very low speed and thus probably fine grains, has a lower x-value in agreement with the rule found in paper I.

In two respects systematic deviations appear between the points and lines. The corners are actually rounded and the sigmoid bend S (Fig. 1) is ignored. These features will be cleared satisfactorily in the second approximation.

In order to interpret the length of the flat part q_H the following relation is useful:

$$1/p_H = E_H/(E_H-E_0). \quad (19)$$

If one assumes that for optimal intensity the stabilization of the Ag speck occurs with the same efficiency as the further growth of the stable speck, then according to (19) the value of $1/p_H$ for $I_H = I_{\text{opt}}$ should be an integral multiple of 0.5, assuming a diatomic speck to be the smallest stable one. The permissible values of p_H are then: 0.67; 0.50; 0.40; 0.33; 0.285; 0.25; 0.22; ..., corresponding to a developable speck of 3, 4, 5, 6... Ag atoms. Only the first four or so values are sufficiently separated for checking the assumption concerning the efficiency experimentally. The value of $p_H = 0.50$ apparently was taken by Webb and Evans as an average value but the present analysis proves, as shown in Table I that also other values occur. So far the observed values are close enough to the permitted ones not to contradict the assumption made. The number of atoms per just developable Ag speck corresponding to these p_H values are also listed.

TABLE II. Rounding of corners resulting from various causes. Values of PQ and $P'Q'$ for emulsions II in units of $\log E$, others in units of D.

Emuls.	Fluct. E_0 PQ	Fluct. E_0 $P'Q'$	Light grad. $PQ=P'Q'$	Grain size $PQ=P'Q'$	Resultant PQ	Resultant $P'Q'$
I	0.24	0.12	0.02	0.03	0.24	0.12
II	0.09	0.03	0.05	0.06	0.10	0.07
III	0.13	0.04	0.05	0.06	0.13	0.07
IV	0.12	0.06	0.04	0.05	0.12	0.07
V	0.08	0.02	0.05	0.06	0.09	0.06

VII. SECOND APPROXIMATION

The theory needs refinement in three ways: (a) The dependence of W on E should be taken into account, especially for small values of E. (b) The statistical fluctuations in the number of quanta received during the last part of the exposure E must be taken into account. (c) Deviations from the order principle, resulting from a light gradient in the plate and inhomogeneous grain size, have to be analyzed. The correction under (a) will explain the sigmoid bend, whereas the other two causes round off the corners of the curves.

a. The Dependence of W on E

The flat parts are obviously not affected by any dependence of W on E. The effect for the upper curve left terminal (Fig. 3) turns out to be negligible. The discussion may thus be restricted to the lower curve right terminal.

For small values of p the first term in (11b), in view of (8) and (4) becomes $(pE)^2/2$. The second term is not altered. The resulting equation for the isodense curve near the terminal is

$$\log E/E_L = 0.434(p - \epsilon\omega E_H p^2/2W_H \ldots), \quad (20)$$

whereas (14b) originally would yield

$$\log E/E_L = 0.434(-p(\omega-1) + p^2(\omega-1)^2/2 \ldots). \quad (21)$$

Equation (20) represents the sigmoid bend. The horizontal distance between the two curves (20) and (21) has a maximum of

$$\Delta p_{\max} = 0.5\omega^2/(\omega-1)((\omega-1)^2 + \epsilon\omega E_H/W_H)$$

around the point

$$p = \omega/((\omega-1)^2 + \epsilon\omega E_H/W_H).$$

Using the values for ϵ and ω from Table I it is seen that emulsion I can be fitted near the terminal by (20) with $E_H/W_H=10$ (dotted curve in Fig. 4). With the observed $q_H=0.5$ one finds with (10) $E_HW_H=4$ or $W_H=0.65$ and $E_H=6.5$. These values are reasonable. In general $W_{H.\text{opt}}$ must be less than, but of the order of unity. Using the same value of E_H/W_H also for the other emulsions one finds $\Delta p_{\max}=0.01$. This is almost unobservably small, showing the reason why the other curves have, if anything, only a trace of this bend.

b. The Statistical Fluctuations of E_0

In Eq. (11) E_0 represents the exposure, required for bringing a just stable speck to the just developable size. This requires a constant number of quanta for the grains that become developable last. Hence the magnitude of E_0 that will furnish these quanta fluctuates statistically about some average value E_a. The influence of these fluctuations is to round off the curves at the sharp corners resulting from the first approximation (see Fig. 3). The curves for grains with various values of E_0 coincide along the horizontal parts since ϵ is independent of E_0, but their corners occur at different values of q which is proportional to E_0 according to (11). We shall measure the degree of rounding of the corner by the vertical distance PQ between the corner of the simple curve corresponding to E_a and the resultant curve. The distribution of E_0 is given by

$$P(E_0)dE_0=E_0{}^{E_a-1}e^{-E_0}/(E_a-1)\,!dE_0. \qquad (22)$$

From (22) PQ can be estimated. It is found that Q at q_H must lie on a curve with an E_0 value about 10–20 percent lower than the E_a value defining P. The percentage depends very insensitively on E_a, being lower if E_a and q_H are larger.

In view of (16a) $P'Q'$ for the q_L corner must be of the order ϵ times smaller than PQ at the q_H corner. The actually observed rounding of the q_L corner is much greater than this amount and is due to other causes discussed under *c*. The roundings estimated in this way are shown in Table II.

c. Deviations from the Order Principle

Deviations from the o.p. may result from the light intensity gradient in the plate and from the grain size inhomogeneity. Their effects can be treated, as outlined in paper I, by considering the emulsion as a sum of fractions, indicated by a parameter α such that in each fraction the o.p. holds. The total density is then the sum of all fractional densities

$$D=\int D(\alpha, e, p)d\alpha, \qquad (23)$$

where $e=\log(\text{incident exposure on the plate})$. Applying the requirement of isodensity $\delta D=0$, setting

$$(\delta D(\alpha, e, p)/\delta e)_p=\gamma_\alpha,$$

and noticing

$$\int \gamma_\alpha d\alpha=\gamma.$$

We find with (1)

$$\partial e/\partial p=1/\gamma\cdot\int \gamma_\alpha(\partial e/\partial p)_D d\alpha=(\partial e/\partial p)_{M.\alpha}. \qquad (24)$$

I.e. the slope of the sequence loop at any point p is the average slope at that point for the various α-groups. We have to analyze now what causes spreading values of the slope $\partial e/\partial p$.

For the intensity gradient deviations from the o.p. the l.i.f. exponent x, hence ω is not dependent on α, but ϵ is. E_H is practically independent of α but $\log E_L$, and hence $\log\epsilon$, varies as $x\log I$. For the grain size deviations from the o.p. it has been shown in paper I that x, hence ω, may depend very slightly on α but ϵ is much more affected, mainly through variations in the rate of quanta reception that go with variations in grain size. Practically then for both types of deviations ω is constant and ϵ varies. Since ω determines the shape of the curved parts of the loop and E_H is unaffected the entire left half of the loop is practically without spread. The right half has a vertical spread, given by the mean absolute deviation Δ in $\log\epsilon$. The resulting roundings of the upper and lower corners, PQ and $P'Q'$, are now both equal to $\Delta/2$. Values of Δ can be estimated in the following way.

For the intensity drop through the plate a factor of 10 is a commonly occurring order of magnitude. The mean absolute spread in $\log I$ is then 0.25 hence $PQ=P'Q'=0.125x$. For the mean absolute grain size spread, according to paper I, a common order of magnitude is $0.8((\Delta\log\alpha)^2{}_M)^{0.5}=0.32$. This is effectively an intensity spread and hence $PQ=P'Q'=0.16x$. A little geometrical consideration will show that the combination of several spreading causes results in a lengthening of the rounded section, leaving the height PQ practically equal to the greatest partial PQ value of the separate causes. The effects of the various spreads are collected in Table II. They should be interpreted only as a rough estimate because of the unknown exact values that go into them. The dotted lines in Fig. 4 are drawn according to the resultant values of the table. The agreement with the experimental points is remarkably good. It is seen that the rounding of q_H is mainly determined by the fluctuations of E_0, whereas that of q_L comes mainly from the grain size spread except for emulsion I.

It is noteworthy that the theory of the loops at this point permits ruling out the hypothesis mentioned in paper I, that the l.i.f. slope x should be the result of the combination of two groups of grains, one group with slope 0 and the other with slope 1. According to Eq. (21) the slope of the curved part near the low intensity terminal, disregarding the S shape, is 0.434 $(\omega-1)$

where $\omega=1000^x$. The slope would be 0 for the first group and 434 for the second one. The average for $\bar{x}_{Av}=0.33$, according to (24) would be about 150. This is incompatible with the observed slopes of about 5. The basic idea of this argument is that the r.l.f. averages x and the terminal slope of the loops averages $(1000)^x$; these two averages are quite different. This argument, therefore, proves again the basic idea of paper I, that the value of x observed is essentially a single grain feature.

VIII. CONCLUSION

The theoretical considerations in this paper yield these conclusions: (1) The available data for isodense and iso-exposure sequence loops are described quantitatively by the theory in terms of l.i.f. The latter in turn was covered in paper I in terms of the fundamental processes in the grain. (2) The number of Ag atoms in a just developable speck seems to vary somewhat according to circumstances between 4 and 10. (More data may reveal even larger values.)

THE JOURNAL OF CHEMICAL PHYSICS VOLUME 18, NUMBER 4 APRIL, 1950

The Raman Spectrum of Hexachlorodisilane

MIKIO KATAYAMA, TAKEHIKO SIMANOUTI, YONEZO MORINO, AND SAN-ICHIRO MIZUSHIMA
Chemical Laboratory, Tokyo University, Bunkyo-ku, Tokyo, Japan
(Received October 13, 1949)

The Raman spectrum of hexachlorodisilane was observed in the liquid state and the normal vibrations of this molecule were calculated by use of the Urey-Bradley field. The seven observed Raman frequencies could be assigned to the fundamental vibrations and the molecule was found to belong to the D_{3h}' symmetry. This means that the molecule exerts internal free rotation around the Si-Si bond as axis. This is in conformity with the experimental result of the electron diffraction investigation.

DURING the last few years many investigations of the molecules of ethane type have been made in connection with the mutual position of the two methyl groups and the potential barrier restricting internal rotation about the carbon-carbon single bond as axis. It would be interesting from this point of view to study the internal rotation of hexachlorodisilane $Cl_3Si—SiCl_3$ about the Si—Si single bond, whose length is much greater than that of the C—C bond, so that the interaction potential of the two rotating groups would decrease considerably. L. O. Brockway and J. Y. Beach[1] concluded by electron diffraction investigation that this molecule has a staggered form, but recently more accurate analysis of the electron diffraction pattern showed that this molecule exerts almost free internal rotation about the Si—Si axis.[2]

F. Stitt and D. M. Yost[3] observed the frequencies, relative intensities and depolarization factors of the Raman lines of this molecule, but they could not decide whether the molecular configuration corresponds to D_{3d} or D_{3h}'. It is the object of this paper to determine the configuration of this molecule by the measurement of the Raman effect together with the calculation of normal vibrations.

EXPERIMENTAL

The apparatus for the measurement of the Raman effect was previously described.[4] The hexachlorodisilane (b.p. 36.0°C at 10 mm Hg) kindly prepared by Professor K. Yamasaki by the reaction between metallic silicon and chlorine gas[2] was distilled into the Raman tube in vacuum. To avoid the decomposition of the sample by ultraviolet rays dilute solution of sodium nitrite was used as a filter. The observed Raman frequencies ($\Delta\nu$) and visually estimated intensities (I) are shown in Table I, which agree well with the results obtained by Stitt and Yost. The minor differences are that we observed one broad line at 379 cm^{-1} instead of the two lines at 377 cm^{-1} and 387 cm^{-1} and that we assigned the e-565 cm^{-1} line reported by them as f-622 cm^{-1}.

CALCULATION OF NORMAL VIBRATION AND ASSIGNMENT OF FREQUENCIES

This molecule consisting of eight atoms has twelve normal frequencies, of which six correspond to doubly degenerate vibrations. One of these corresponds to the internal rotation of $SiCl_3$ groups about the Si—Si bond as axis and is inactive both in the Raman effect and the infra-red. The selection rule for the remaining eleven vibrations is shown in the left part of Table II, from which we see that six fundamental frequencies will be observed in the Raman effect if the molecule belongs to D_{3d} symmetry (staggered form), while nine frequencies will be expected both for D_{3h} (eclipsed form) and D_{3h}' symmetry (free rotation). Stitt and Yost considered that one cannot discriminate D_{3h}' from D_{3d} by the Raman data, because the frequencies of E_g vibrations coincide with those of E_u vibrations so that only six fundamentals become Raman active in both cases. Their reasoning is not, however, sound, since it

[1] L. O. Brockway and J. Y. Beach, J. Am. Chem. Soc. **60**, 1836 (1938).
[2] Yamasaki, Kotera, Tatematsu, and Iwasaki, J. Chem. Soc. Japan **69**, 104 (1947).
[3] F. Stitt and D. M. Yost, J. Chem. Phys. **5**, 90 (1937).
[4] S. Mizushima and Y. Morino, Proc. Ind. Acad. Sci. **8**, 351 (1938).

TABLE I. The Raman spectrum of hexachlorodisilane.

Present data			Stitt and Yost's data		
$\Delta\nu$ cm^{-1}	I	excitation	$\Delta\nu$ cm^{-1}	I	ρ
124	8	$e\pm, k\pm, i$	124	8	
132	8	$e\pm, k\pm, i$	132	5	0.72±0.02
179	5	e	179	0.4	
211	8	$e\pm, k\pm, i$	212	4	0.86±0.02
354	10	$e\pm, k\pm, i, f, g$	354	10	0.05
379	3b	e	377 387	1 1	
420	4	e	421	<<<1	
454	3	e	460	<<<1	
484	3	e	487	<<<1	
			565	<<1	
588	6b	$e\pm, k\pm, i, f$	590	3	0.88±0.03
622	6	$e\pm, k\pm, i, f$	625	2	<0.5
651	1	e			
710	2	e	706	<<<1	

TABLE II. The normal vibrations of hexachlorodisilane.

Irreducible representation D_{3d}	D_{3h}'	D_{3h}		Selection rule for the Raman effect D_{3d}	D_{3h}'	D_{3h}	Calculated frequencies (cm^{-1})	Observed frequencies (cm^{-1})	
			ν(Si-Si)[a]	p[c]	p	p	626	622(6)	ρ<0.5
A_{1g}	A_1	A_1'	ν(Si-Cl)	p	p	p	375	354(10)	p
			ν(Si-Cl)	p	p	p	127	124(8)	p
			ν(Si-Cl)	d[d]	d	d	625	622(6)	
E_g	$\bar{E}$	E'	δ(Si-Cl)[b]	d	d	d	145	132(8)	
			δ(Si-Cl)	d	d	d	202	211(8)	d
A_{2u}	$\bar{A}_2$	A_2''	ν(Si-Cl)	i[e]	i	i	478		
			δ(Si-Cl)	i	i	i	249		
			ν(Si-Cl)	i	d	d	588	588(6b)	d
E_u	E	E''	δ(Si-Cl)	i	d	d	80	—	
			δ(Si-Cl)	i	d	d	188	179(5)	

[a] ν: valency vibration.
[b] δ: deformation vibration.
[c] p: Raman-active and polarized.
[d] d: Raman-active and depolarized.
[e] i: Raman-inactive.

TABLE III. Force constants (10^5 dynes/cm) and molecular parameters of hexachlorodisilane used in the calculation of normal vibration.

$K_{SiSi}=2.20$, $H_{ClSiCl}=0.04$, $F'_{ClCl}=-0.06$, $F'_{SiCl}=-0.05$, $\kappa=0.15$,
$K_{SiCl}=2.60$, $H_{ClSiSi}=0.05$, $F_{ClCl}=0.30$, $F_{SiCl}=0.1$,
$R_0(\text{Si—Si})=2.34A$, α } = tetrahedral angles
$r_0(\text{Si—Cl})=2.02A$, β }

will be evident from the following calculation that all the frequencies of E_u vibrations do not coincide with those of E_g vibrations. Furthermore, as shown in Table II, E_u vibrations are Raman-active for D_{3h}', while they are not for D_{3d}. Therefore, the determination of molecular configuration can at once be made by observing if the E_u-type vibrations appear in the Raman effect or not.

For the assignment of the Raman line we have calculated the normal vibrations of this molecule, using the Urey-Bradley field, which has been shown to be successful in obtaining the normal frequencies for various molecules.[5] The potential energy in the present case is thus expressed as follows:

$$\begin{aligned}V=&\{K'_{SiSi}R_0\Delta R+\tfrac{1}{2}K_{SiSi}(\Delta R)^2\}\\&+\sum_{i=1}^{6}\{K'_{SiCl}r_0\Delta r_i+\tfrac{1}{2}K_{SiCl}(\Delta r_i)^2\}\\&+\sum_{j=1}^{6}\{H'_{ClSiCl}r_0^2\Delta\alpha_j+\tfrac{1}{2}H_{ClSiCl}r_0^2(\Delta\alpha_j)^2\}\\&+\sum_{k=1}^{6}\{H'_{ClSiSi}r_0R_0\Delta\beta_k+\tfrac{1}{2}H_{ClSiSi}r_0R_0(\Delta\beta_k)^2\}\\&+\sum_{l=1}^{6}\{F'_{ClCl}q_0\Delta q_l+\tfrac{1}{2}F_{ClCl}(\Delta q_l)^2\}\\&+\sum_{m=1}^{6}\{F'_{ClSi}p_0\Delta p_m+\tfrac{1}{2}F_{ClSi}(\Delta p_m)^2\},\end{aligned}\qquad(1)$$

where R and r_i are the bond distances of Si—Si and Si—Cl, α_j and β_k the interbond angles ∠Cl—Si—Cl and ∠Cl—Si—Si, q_l the distances between Cl-atoms bonded to the same Si-atom, p_m those between Si and Cl not bonded directly, and R_0, r_0, q_0 and p_0 the equilibrium values of R, r, q, and p. They are shown in Fig. 1. The first and the second terms of Eq. (1) are the potentials for the change of bond distances, and the third and the fourth terms are those for the change of interbond angles. The last two terms refer to the repulsions between non-bonded atoms. The interaction between Cl-atoms attached to different Si-atoms is neglected, because if the repulsive force constant between two chlorine atoms bonded to the different Si-atoms is calculated from Eq. (3) to be described below, it is found to be less than 0.01×10^5 dynes/cm. The secular equation is calculated by the method presented by Wilson:[6]

$$|\mathbf{GF}-\lambda\mathbf{E}|=0,\qquad(2)$$

of which the G- and F-matrices are given in Eqs. (4) and (6) in the preceding paper.[7] So far as we neglect the interaction between atoms bonded to different Si-atoms, we can at once show that the frequencies of the normal vibrations of ethane-like molecules are independent of the angle of internal rotation, since the **G**- and **F**-matrices are the same for all internal positions.

For the calculation of the vibrational frequencies from this secular equation using the potential function stated above, nine force constants, K_{SiSi}, K_{SiCl}, H_{ClSiCl}, H_{ClSiSi}, F'_{ClCl}, F_{ClCl}, F'_{ClSi}, F_{ClSi} and an intramolecular tension κ are necessary.* Four of these constants, K_{SiCl}, H_{ClSiCl}, F'_{ClCl}, and F_{ClCl}, can be obtained directly from

[5] T. Simanouti, J. Chem. Phys. **17**, 245, 734 (1949).

[6] E. Bright Wilson, Jr., J. Chem. Phys. **7**, 1047 (1939); **9**, 76 (1941).

[7] T. Simanouti, J. Chem. Phys. **17**, 848 (1949).

* For the significance of κ refer to T. Simanouti, J. Chem. Phys. **17**, 245 (1949). The other constants K' and H' are represented in terms of F' and κ.

TABLE IV. Assignment of the combination tones and overtones of hexachlorodisilane.

Observed frequency (cm^{-1})	Assignment	Symmetry and selection rule for the Raman effect D_{3h}'		D_{3d}	
377	$124\times3=372$	A_1	active	A_{1g}	active
387	$132\times3=396$	$\bar{A}_1+\bar{A}_2+\bar{E}$	active	$A_{1g}+A_{2g}+E_g$	active
	$211+179=390$	$\bar{A}_1+\bar{A}_2+\bar{E}$	active	$A_{1u}+A_{2u}+E_u$	inactive
420	$211\times2=422$	A_1+E	active	$A_{1g}+E_g$	active
	$179+124\times2=427$	E	active	E_u	inactive
454	$211+124\times2=459$	$\bar{E}$	active	E_g	active
484	$354+124=478$	$\bar{A}_1$	active	A_{1g}	active
	$354+132=486$	$\bar{E}$	active	E_g	active
	$211+132\times2=475$	$\bar{A}_1+\bar{A}_2+2\bar{E}$	active	$A_{1g}+A_{2g}+2E_g$	active
651	$354+179+124=657$	E	active	E_u	inactive
	$211+179+132\times2=654$	$2\bar{A}_1+2\bar{A}_2+4\bar{E}$	active	$2A_{1u}+2A_{2u}+4E_u$	inactive
	$179\times3+124=661$	A_1+A_2+E	active	$A_{1u}+A_{2u}+E_u$	inactive
	$132\times4+124=652$	$\bar{A}_1+2\bar{E}$	active	$A_{1g}+2E_g$	active
	$132\times5=660$	$\bar{A}_1+\bar{A}_2+2\bar{E}$	active	$A_{1g}+A_{2g}+2E_g$	active
710	$354\times2=708$	A_1	active	A_{1g}	active
	$354+179\times2=712$	A_1+E	active	$A_{1g}+E_g$	active
	$354+211+132=697$	A_1+A_2+E	active	$A_{1g}+A_{2g}+E_g$	active

the normal frequencies of $SiCl_4$.[7] As to the other five we have taken the values shown in Table III so as to give the best fit with the observed frequencies.

In Table II are shown the calculated frequencies which are in good agreement with those observed, if these are assigned as in the last column of that table. The most remarkable difference between our assignment and that of Stitt and Yost lies in that for the vibration of ν(Si—Si). Assuming both SiH_3 and $SiCl_3$ as one particle, Stitt and Yost calculated this frequency as 200 cm^{-1} by use of the force constants 1.7×10^5 dynes/cm obtained from the analysis of the spectra of disilane Si_2H_6, and they assigned the observed frequency of 179 cm^{-1} to the ν(Si—Si) vibration. Our calculation has given 626 cm^{-1} as the frequency of ν(Si—Si) of Si_2Cl_6, so that the observed frequency of 622 cm^{-1} should be assigned to this vibration, while the line at 179 cm^{-1} is assigned to the deformation vibration of E_u type† computed as 188 cm^{-1}. The valency vibration of E_g type, computed by the calculation as 625 cm^{-1}, seems to overlap with the frequency 626 cm^{-1} of A_{1g} type. This assignment is justified by the fact reported by Stitt and Yost that the degree of depolarization of this line is larger than the other two frequencies of A_{1g} type.

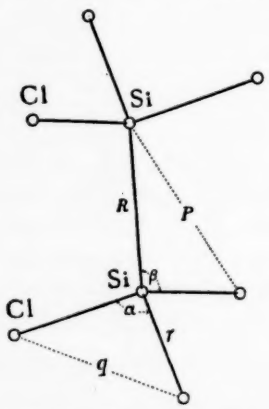

FIG. 1. Coordinates used for hexachlorodisilane.

The weak lines observed in the Raman spectra may correspond to combination tones or overtones. Their possible assignments and the selection rules are given in Table IV, which shows that almost all the Raman lines are well explained by the model of D_{3h}' as well as by that of D_{3d} except the frequency of 651 cm^{-1}. As to this frequency there are many possibilities of assignment, but all the higher harmonics of the Raman-active vibrations of the model of D_{3d} do not probably appear in the Raman effect. This fact favors the model of D_{3h}' (freely rotating model).

Stitt and Yost assumed the existence of the frequency of 252 cm^{-1} to explain combination tones. Since this frequency is not observed in the Raman spectra, it must belong to the class of $\bar{A}_2$ for the model of D_{3h}' and to that of A_{2u} or E_u for the model of D_{3d}. Accordingly, some of their assignments of the combination tones are not acceptable from the selection rules. We did not use such an unobserved frequency in our assignment, and could explain all of the observed frequencies without any contradiction to the selection rules.

DISCUSSION

The most important point of our assignment refers to the fact that the frequencies 588 cm^{-1} and 179 cm^{-1} of E_u type for D_{3d} are observed in the Raman effect. This shows that the molecule is not of the staggered form, since E_u frequencies are not Raman-active for D_{3d} symmetry as shown in Table II. Of course they might be explained by the eclipsed form (D_{3h}), but this

† Naming the symmetry of the vibrations in accord with the D_{3d} configuration is not to be interpreted as eliminating the D_{3h}' or D_{3h} possibility.

possibility is excluded by the result of the electron diffraction experiment described below. Accordingly, we have to conclude that this molecule should belong to the D_{3h}' symmetry.

As to the electron diffraction investigation Brockway and Beach[1] observed four halos in the region of $s=2\sim8$, and by comparing the calculated intensity curves with the observed result they concluded that this molecule has the staggered form. The eclipsed form was excluded by their result, and also by the recent investigation by Yamasaki, Kotera, Tatematsu, and Iwasaki.[2]

The experiment of Brockway and Beach is not sufficient for the final determination of the molecular form, because in the region of scattering angle corresponding to $s=2\sim8$, there is no difference between the intensity curve for the staggered form and that for the freely rotating model. In the next outer region, however, there is a conspicuous difference between the staggered and freely rotating models,[2] i.e., the staggered form must have a halo of $s=11$, while the freely rotating model has none. Yamasaki, Kotera, Tatematsu, and Iwasaki ascertained that there is no halo of $s=11$, which is a conclusive evidence for the freely rotating model. The result obtained by the Raman effect stated above also confirms this conclusion.

For hexachloroethane Cl_3CCCl_3 it was concluded from the investigation of the Raman spectrum[8,9] and electron diffraction [10] that the equilibrium configuration is the staggered form (D_{3d}), and that the forces stabilizing this form result mainly from the steric repulsion between chlorine atoms. As we have shown above, hexachlorodisilane exerts free internal rotation, which can be explained from the greater distance between the chlorine atoms of different rotating groups. In fact, if we calculate the interatomic potential between chlorine atoms by use of the potential function

$$V=-\frac{1.515\times10^{-10}}{r^6}+\frac{1.620\times10^{-7}}{r^{12}}$$

erg/molecule (r in A unit), (3)

which[11] was obtained from the second virial coefficient of chlorine gas, we can show that the hindering potential is negligibly small for hexachlorodisilane, while its barrier amounts to 12 kcal./mole for hexachloroethane.

One might consider that owing to the free rotation around the Si—Si axis the Raman lines would become broad. If, however, we neglect the interaction between atoms bonded to different Si-atoms, the frequencies of the normal vibrations are independent upon the angle of internal rotation, and the said interaction is expected to be very small, as stated before. Therefore, even in the case of free rotation the Raman lines do not necessarily become broad.

As the Raman spectra reported above were observed in the liquid state, the intermolecular forces might deform the molecule as in the case of liquid benzene[12] and the selection rule for the D_{3d} symmetry might be broken. This deformation would, however, take place most probably through the internal rotation of $SiCl_3$-groups about the Si—Si axis. We need not, therefore, change our explanation of the Raman spectra of hexachlorodisilane, even if we take into account such intermolecular forces in the liquid state.

ACKNOWLEDGMENT

We wish to express our sincere thanks to Professor K. Yamasaki of the Nagoya University who supplied us with the sample of hexachlorodisilane used in this experiment. Our thanks are also due to Ministry of Education in aid of this research.

[8] Mizushima, Morino, Kawano, and Otiai, J. Chem. Soc. Japan **65**, 127 (1944); Sci. Pap. Inst. Phys. Chem. Research (Tokyo) **42**, 1 (1944).

[9] D. T. Hamilton and F. F. Cleveland, J. Chem. Phys. **12**, 249 (1944).

[10] Morino, Yamaguchi, and Mizushima, Sci. Pap. Inst. Phys. Chem. Research (Tokyo) **42**, 5 (1944); Y. Morino and M. Kimura, J. Chem. Soc. Japan **68**, 77 (1947); Y. Morino and M. Iwasaki, J. Chem. Phys. **17**, 216 (1949).

[11] Y. Morino and I. Miyagawa, J. Chem. Soc. Japan **68**, 62 (1947).

[12] C. K. Ingold, Proc. Roy. Soc. **A169**, 149 (1939).

Hexacovalent Bond Orbitals III

GEORGE H. DUFFEY
Chemistry Department, South Dakota State College, Brookings, South Dakota
(Received October 19, 1949)

A set of six equivalent orthogonal bond orbitals of trigonal antiprism symmetry are considered. The orbitals are of type $s^n p^3 d^{3-n}$. The strongest orbitals are obtained when n equals 0.8427. These orbitals are only slightly stronger than the octahedral orbitals. The trigonal antiprism orbitals are stronger than the corresponding trigonal prism orbitals. The SF_6, $Fe(CN)_6^{\equiv}$, and $Fe(CN)_6^{=}$ structures are discussed. The relation used for estimating energies is used to estimate bond energies of CH bonds in the structures $-\overset{\diagdown}{\underset{\diagup}{C}}-H$, $=\overset{\diagdown}{\underset{\diagup}{C}}-H$, and $\equiv C-H$.

THERE is a family of non-cylindrical bond orbitals related to the cylindrical octahedral orbitals as the orbitals discussed in papers I and II[1] of this series are related to the cylindrical trigonal prism orbitals. This family is of type $s^n p^3 d^{3-n}$ and the orbitals possess trigonal antiprism symmetry. One may wonder whether some of these trigonal antiprism orbitals are stronger than the cylindrical octahedral orbitals since non-cylindrical trigonal prism orbitals slightly stronger than the cylindrical trigonal prism orbitals were found.

Set up the following functions:

$$\psi_1=\{[1/(6)^{\frac{1}{2}}]\cos\alpha\}s+[1/(6)^{\frac{1}{2}}]p_z+(1/\sqrt{3})p_x+\{[1/(6)^{\frac{1}{2}}]\sin\alpha\}d_z+[(1/\sqrt{3})\cos\beta]d_{xy}+[(1/\sqrt{3})\sin\beta]d_{x+z}, \quad (1)$$

$$\psi_2=\{[1/(6)^{\frac{1}{2}}]\cos\alpha\}s+[1/(6)^{\frac{1}{2}}]p_z-(1/2\sqrt{3})p_x+(1/2)p_y+\{[1/(6)^{\frac{1}{2}}]\sin\alpha\}d_z-[(1/2\sqrt{3})\cos\beta]d_{xy}-[(1/2)\cos\beta]d_{x+y}-[(1/2\sqrt{3})\sin\beta]d_{x+z}+[(1/2)\sin\beta]d_{y+z}, \quad (2)$$

$$\psi_3=\{[1/(6)^{\frac{1}{2}}]\cos\alpha\}s+[1/(6)^{\frac{1}{2}}]p_z-(1/2\sqrt{3})p_x-(1/2)p_y+\{[1/(6)^{\frac{1}{2}}]\sin\alpha\}d_z-[(1/2\sqrt{3})\cos\beta]d_{xy}+[(1/2)\cos\beta]d_{x+y}-[(1/2\sqrt{3})\sin\beta]d_{x+z}-[(1/2)\sin\beta]d_{y+z}, \quad (3)$$

$$\psi_4=\{[1/(6)^{\frac{1}{2}}]\cos\alpha\}s-[1/(6)^{\frac{1}{2}}]p_z-(1/\sqrt{3})p_x+\{[1/(6)^{\frac{1}{2}}]\sin\alpha\}d_z+[(1/\sqrt{3})\cos\beta]d_{xy}+[(1/\sqrt{3})\sin\beta]d_{x+z}, \quad (4)$$

$$\psi_5=\{[1/(6)^{\frac{1}{2}}]\cos\alpha\}s-[1/(6)^{\frac{1}{2}}]p_z+(1/2\sqrt{3})p_x-(1/2)p_y+\{[1/(6)^{\frac{1}{2}}]\sin\alpha\}d_z-[(1/2\sqrt{3})\cos\beta]d_{xy}-[(1/2)\cos\beta]d_{x+y}-[(1/2\sqrt{3})\sin\beta]d_{x+z}+[(1/2)\sin\beta]d_{y+z}, \quad (5)$$

$$\psi_6=\{[1/(6)^{\frac{1}{2}}]\cos\alpha\}s-[1/(6)^{\frac{1}{2}}]p_z+(1/2\sqrt{3})p_x+(1/2)p_y+\{[1/(6)^{\frac{1}{2}}]\sin\alpha\}d_z-[(1/2\sqrt{3})\cos\beta]d_{xy}+[(1/2)\cos\beta]d_{x+y}-[(1/2\sqrt{3})\sin\beta]d_{x+z}-[(1/2)\sin\beta]d_{y+z}. \quad (6)$$

See Eqs. (1)–(9) of paper I[1] for the notation used in these functions. These functions represent six equivalent orthogonal bond orbitals cf type $s^n p^3 d^{3-n}$ where

$$n=\cos^2\alpha. \quad (7)$$

Setting

$$\cos\alpha=1 \quad (8)$$

and

$$\cos\beta=1/\sqrt{3} \quad (9)$$

yields the cylindrical octahedral orbitals discussed by Pauling[2] and Hultgren.[3] The Z axis coincides with a threefold axis. Changing α and β from the values given by Eqs. (8) and (9) yields orbitals of trigonal antiprism symmetry D_{3d}.

Three functions orthogonal to $\psi_1, \cdots \psi_6$ can be set up as follows:

$$\psi_7=(\sin\alpha)s-(\cos\alpha)d_z, \quad (10)$$

$$\psi_8=(\sin\beta)d_{xy}-(\cos\beta)d_{x+z}, \quad (11)$$

$$\psi_9=(\sin\beta)d_{x+y}+(\cos\beta)d_{y+z}. \quad (12)$$

The results from the calculations on the trigonal antiprism orbitals are given in Tables I and II. β was chosen to obtain the strongest orbitals for each α. The range $0\leqslant\alpha\leqslant\pi/2$ is covered in Table I. The range $0\geqslant\alpha\geqslant-\pi/2$ is covered in Table II. In these tables S is the maximum value of ψ_1 and is called the strength of an orbital; θ_1 is the angle between the axis and the maximum in ψ_1 and is called the angle between the axis and bond one.

For the trigonal prism bonds discussed in papers I and II[1] $(\partial S/\partial\alpha)_\beta$ is always positive when α equals zero. Also calculations at representative points indicate that when α is considerably different from zero, the orbitals with $0\leqslant\alpha\leqslant\pi/2$ are considerably stronger than the orbitals with $0\geqslant\alpha\geqslant-\pi/2$. Hence only the results with α in the former region were reported. We may note that it is difficult to explain the observed angles in MoS_2 unless the principal contribution to the molybdenum structure is from the orbitals reported.

From Table I it is evident that strong trigonal antiprism orbitals can be formed when n is greater than about 0.2. The strongest orbitals result when n equals 0.8427. The maximum strength is only slightly greater than the strength of octahedral orbitals so one would expect octahedral orbitals to be employed when the

[1] G. H. Duffey, J. Chem. Phys. **17**, 1328 (1949); *ibid.* **18**, 128 (1950).

[2] L. Pauling, J. Am. Chem. Soc. **53**, 1367 (1931).

[3] R. Hultgren, Phys. Rev. **40**, 891 (1932).

TABLE I. Results of calculations on trigonal antiprism orbitals[a] with β chosen to obtain the strongest orbitals and with α positive.

n	$\cos\beta$	S, Strength of an orbital	θ_1, Angle between axis and bond 1
1.0000	0.5774	2.9239	54° 44′
0.9000	0.4942	2.9252	48° 40′
0.8427	0.4748	2.9254	47° 10′
0.7000	0.4403	2.9239	44° 27′
0.5000	0.4070	2.915	41° 43′
0.3000	0.3824	2.893	39° 37′
0.1000	0.3627	2.840	37° 54′
0.0000	0.3542	2.732	37° 8′

[a] The orbitals are of type $s^n p^3 d^{3-n}$. Also $n=\cos^2\alpha$.

interaction energy[4] of the electrons in the sp^3d^2 structure is more than a small amount greater than that in the structure with n equal to 0.8427. (In the discussion in this paper it is assumed that the structures are more stable than possible trigonal prism structures. See paper II.[1])

In structures of the SF_6 type there are no unshared electrons in the valence shell and the d orbitals are considerably less stable than the s orbital. One would expect that octahedral orbitals would be used in these structures.

As examples of structures containing unshared electrons in the valence shells consider complexes of the ferrous and the ferric ions such as $Fe(CN)_6^{\equiv}$ and $Fe(CN)_6^{=}$. Spectroscopic evidence[5] indicates that the $4s$ orbital is here more stable than the $3d$ orbitals. In changing n from 1 to n_1 an unshared electron pair (in either the ferrous or the ferric ion) passes from a d level to a hybrid level (see Eqs. (10), (11), and (12)) containing some s. Simultaneously the shared pairs pass to hybrid levels containing less s. In effect $1-n_1$ unshared electron pairs are demoted and $1-n_1$ shared electron pairs are promoted. Since the interaction energy of a shared pair is less than that of an unshared pair, one would expect energy to be evolved in the process for some values of n_1 if the repulsion between the attached groups is small. It is probable that the repulsion is large enough to stabilize the octahedral structure.

Of the elements Fe, Co, Ni, Ru, Rh, Pd, Ir, Pt the s level is lowest[5] with respect to the d level in Fe. Thus one would expect the strain preventing the assumption of the trigonal antiprism structure to be the lowest in an iron complex, or in a complex of one of the somewhat larger ions such as an osmium complex where the repulsive forces are less, with a given attached group.

The use of terms in paper II[1] is similar to that of Kuhn.[4] It seems less confusing if bond energy is redefined so that with the proper choice of the zero of energy the energy of the molecule is the sum of the bond energies.

[4] See H. Kuhn, J. Chem. Phys. **16**, 727 (1948).

[5] In Fe the state $3d^64s^2\ {}^5D_4$ is 19.7 kcal./mole more stable than the state $3d^74s\ {}^5F_5$. See F. R. Bichowsky and F. D. Rossini, *The Thermochemistry of the Chemical Substances* (Reinhold Publishing Corporation, New York, 1936).

TABLE II. Strongest trigonal antiprism orbitals with α negative.

n	$\cos\beta$	S, Strength of an orbital	θ_1, Angle between axis and bond 1
1.0000	0.5774	2.9239	54° 44′
0.9417	0.6456	2.9243	59° 24′
0.9000	0.6670	2.9241	60° 49′
0.7000	0.7319	2.918	65° 2′
0.5000	0.7738	2.903	67° 44′
0.3000	0.8051	2.874	69° 47′
0.1000	0.8297	2.814	71° 24′
0.0000	0.8402	2.700	72° 7′

Thus for a general $A-B$ bond one is led to the empirical equation

$$E=kS_AS_B+R-W. \tag{13}$$

Here E is the bond energy, S_A and S_B are the strengths of the orbitals of atoms A and B used to form the bond, k is a constant evaluated from the energy of a bond, R is the resonance energy to be associated with the bond, W is the energy required to excite the shared pair above the valence states of A and B which are obtained when the molecule is dissociated.[6]

Equation (13) should give the energy required to break the $A-B$ bond when all bonds are broken simultaneously. (Zero point energies are neglected in view of the approximate nature of the theory.) Equation (13) was used to estimate the bond energy of the CH bond in structures containing no unshared electrons when the C orbital of the CH bond is of type $s^{1-n}p^n$. The following equation[7] was obtained:

$$E=58.5S_c+6-(n-\tfrac{1}{2})(1.04)(96.4). \tag{14}$$

It was assumed that the CH bond energy is 98 kcal./mole when the C orbital is $s^{\frac{1}{2}}p^{\frac{3}{2}}$. When the C orbital is $s^{\frac{1}{3}}p^{\frac{3}{2}}$ or $s^{\frac{1}{4}}p^{\frac{3}{4}}$, one would expect the bond energies to be 106 or 119 kcal./mole respectively. These values agree qualitatively with the variation of the stretching force constants[8] and the dissociation energies.[9] Among the corrections to be applied to the latter for ethane and ethylene in making the comparison are corrections for the change in delocalization energies on dissociation and possible changes in bond energies of the bonds not broken.

The conclusions drawn in the discussions of the examples are limited by the very approximate nature of Eq. (13). This is indicated in this paper by the use of the word "expect" in the discussion.

[6] Equation (13) reduces to the equation developed by Pauling and Sherman (J. Am. Chem. Soc. **59**, 1450 (1937)) when W and R are zero.

[7] Data were obtained from K. S. Pitzer, J. Am. Chem. Soc. **70**, 2140 (1948) and L. Pauling, *The Nature of the Chemical Bond* (Cornell University Press, Ithaca, New York, 1940).

[8] G. Herzberg, *Infrared and Raman Spectra of Polyatomic Molecules* (D. Van Nostrand Company, Inc., New York, 1945).

[9] J. S. Roberts and H. A. Skinner, Trans. Faraday Soc. **45**, 339 (1949).

THE JOURNAL OF CHEMICAL PHYSICS VOLUME 18, NUMBER 4 APRIL, 1950

The Intrinsic Viscosity, Translational and Rotatory Diffusion Constants of Rod-Like Macromolecules in Solution

JACOB RISEMAN
Institute of Polymer Research, Polytechnic Institute of Brooklyn, Brooklyn, New York

AND

JOHN G. KIRKWOOD
Gates and Crellin Laboratories, California Institute of Technology, Pasadena, California

(Received October 21, 1949)

A theory of the intrinsic viscosities, translational and rotatory diffusion constants of rod-like macromolecules in solution is developed on the basis of a rigid-chain model made up of monomeric elements separated by rigid bonds. The general methods of previous papers are used to take proper account of the hydrodynamic interactions of the monomeric units of the molecule. The theory developed leads to results showing qualitatively, marked similarity to that obtained for cylindrical and ellipsoidal particles. The intrinsic viscosities, translatory and rotatory diffusion constants are shown, as in the case of flexible macromolecules, to be related through a pair of parameters. A method for obtaining the molecular weight of rod-like macromolecules is proposed, based on the combination of intrinsic viscosity and rotatory diffusion constant measurements.

INTRODUCTION

IN attempting to evaluate the molecular size and weight of macromolecular substances by determination of their hydrodynamical properties, it has been customary to associate with these substances corresponding models assumed to behave in a manner similar to that of the actual material. For this purpose rigid molecules have been assumed to behave as spheres, rods or ellipsoids, flexible molecules as spherical, ellipsoidal and pearl-necklace types of models. Kuhn[1] and Huggins[2] have also investigated the viscosity behavior of a model analogous to the pearl-necklace type, that of a set of elements separated by rigid bonds with zero angle between successive bonds as representative of a rigid rod-like macromolecule. As in the case of flexible molecules, however, the hydrodynamic interaction between the monomer units composing the rigid chain have been neglected. Consequently such theories must fail for the same reasons as set forth previously.[3,4]

In this paper we shall employ as a hydrodynamic representation of a linear rigid rod-like macromolecule a set of $2n+1$ groups, in which the hydrodynamic interactions of the monomeric elements composing the chain are located, separated by $2n$ bonds such that the angle between successive bond vectors is equal to zero. It is interesting to note that this model is identical to that used in current light-scattering theory,[5] and one might therefore expect that the molecular size obtained by that method should be similar to those obtained by the hydrodynamical methods to be given here. Utilizing the method of our previous papers[4,6] we shall evaluate the intrinsic viscosity, translatory frictional coefficient and rotatory frictional coefficients for the above-mentioned model. Some of the results of our earlier papers will be repeated here. For greater detail the reader is referred to those papers.

INTRINSIC VISCOSITY

A rigid macromolecule introduced into a solvent having a prior condition of stationary two-dimensional viscous flow will have a set of forces acting on it. As a result the particle will tend to follow the local translatory and rotatory components of the fluid flow. The particle will thus take up two types of forced motions. A translatory motion of its center of mass equal to that of the local fluid and an angular velocity equal to that of the rotational component of velocity of the fluid. In addition to these motions there will be a third motion connected with the random rotatory Brownian movement tending to disorient any orienting effect of the original flow. The magnitude of this random motion will be dependent on the rotatory diffusion constant of the molecule, and therefore on its size and shape.

For a fluid, whose original flow pattern is given by

$$\mathbf{V}^0=\dot{\epsilon}(\mathbf{R}\cdot\mathbf{e}_y)\mathbf{e}_x, \tag{1}$$

the velocity at an element l imposed by the fluid alone can be represented by

$$\begin{aligned}\mathbf{V}_l&=\boldsymbol{\Omega}_0\times\mathbf{R}_l\\ \boldsymbol{\Omega}_0&=-\mathbf{e}_x\sin\phi\dot{\theta}+\mathbf{e}_y\cos\phi\dot{\theta}+\mathbf{e}_z\dot{\phi}\end{aligned} \tag{2}$$

where $\mathbf{e}_x$, $\mathbf{e}_y$, $\mathbf{e}_z$ are a set of unit vectors in the direction of the coordinate axis, θ and ϕ the usual angles in a spherical coordinate system and $\mathbf{R}_l$ is the vector from the center of mass of the rigid chain to element l. Expanding Eqs. (1) and (2) into components parallel and perpendicular to the chain direction, and comparing, we obtain for the fluid imposed angular velocities of the

[1] W. Kuhn, Helv. Chim. Acta **28**, 97 (1944).
[2] M. L. Huggins, J. Phys. Chem. **43**, 439 (1939).
[3] P. Debye, Reports to the Office of Rubber Reserve, Reconstruction Finance Corporation, October 10, 1946.
[4] J. G. Kirkwood and J. Riseman, J. Chem. Phys. **16**, 565 (1948).
[5] P. Debye, J. Phys. Coll. Chem. **51**, 18 (1947).
[6] J. Riseman and J. G. Kirkwood, J. Chem. Phys. **17**, 442 (1949).

chain

$$\dot{\theta}=\dot{\epsilon}\sin\theta\cos\theta\sin\phi\cos\phi$$
$$\dot{\phi}=\dot{\epsilon}\sin^2\phi \tag{3}$$

which in the absence of Brownian movement will tend to align the rigid chains parallel to the direction of fluid flow. Brownian movement will distort this alignment to an extent determined by both the magnitude of the flow gradient and the rotatory diffusion constant. The combined effects of fluid flow and Brownian movement will therefore result in an orientation described by the distribution function $\rho(\theta, \phi)$ satisfying the equation of Brownian movement.

$$\nabla\cdot\mathbf{j}+\partial\rho/\partial t=0$$
$$\mathbf{j}=-\mathbf{D}\cdot\nabla\rho+\mathbf{u}\rho$$
$$u_\theta=\dot{\theta}$$
$$u_\phi=\sin\theta\dot{\phi}. \tag{4}$$

To apply our methods it is necessary to know the value of $\mathbf{u}_l$, the velocity with which element l of the chain is moving. In general this would demand solving the partial differential Eqs. (4). In the case of overwhelming Brownian movement, in which case we have a uniform distribution $\rho(\theta, \phi)=$ constant, the average contributions to $\mathbf{u}_l$ from the fluid flow effect and the Brownian movement will each vanish, and the particle can be considered as fixed at some definite orientation. In this article, we will restrict ourselves to this condition.

The methods of our previous article[4] are immediately applicable here, the only difference involved is that we are now considering a rigid particle and averages over internal configurations are no longer necessary. In our present averaging procedure, we only need make use of our assumed uniform distribution. We can immediately write for the intrinsic viscosity

$$[\eta]=N\zeta G/100M\eta_0$$

$$G=-\frac{1}{\zeta\dot{\epsilon}}\sum_{l=-n}^{+n}\langle(\mathbf{R}_l\cdot\mathbf{e}_y)(\mathbf{F}_l\cdot\mathbf{e}_x)\rangle_{Av}$$

$$\mathbf{F}_l=-\zeta\mathbf{V}_l{}^0-\zeta\sum_{\substack{s=-n\\ \neq l}}^{+n}\mathbf{T}_{ls}\cdot\mathbf{F}_s \qquad -n\leqslant l\leqslant+n \tag{5}$$

$$\mathbf{T}_{ls}=\frac{1}{8\pi\eta_0}R_{ls}\left\{\mathbf{I}+\frac{\mathbf{R}_{ls}\mathbf{R}_{ls}}{R_{ls}{}^2}\right\}$$

$$\mathbf{R}_{ls}=\mathbf{b}|l-s|$$

$$\mathbf{V}_l{}^0=\dot{\epsilon}(\mathbf{R}_l\cdot\mathbf{e}_y)\mathbf{e}_x,$$

where our symbols have the same significance as in our previous paper. To obtain an explicit expression for the intrinsic viscosity it is convenient to define quantities $\phi_{l,l'}$ and F by

$$\langle(\mathbf{F}_l\cdot\mathbf{e}_x)(\mathbf{R}_{l'}\cdot\mathbf{e}_y)\rangle_{Av}=-(2/9)n^2b^2\zeta\dot{\epsilon}\phi_{l,l'}$$

$$F=\frac{1}{n}\sum_{l=-n}^{+n}\phi_{l,l}$$

$$[\eta]=\frac{N\zeta b^2Z^2F}{3600\eta_0M_0}$$

$$\phi_{l,l'}=f_{l,l'}+\frac{9}{2n^2b^2\dot{\epsilon}}\sum_{\substack{s=-n\\ \neq l}}^{+n}\langle(\mathbf{e}_y\cdot\mathbf{R}_{l'})(\mathbf{e}_x\cdot\mathbf{T}_{ls}\cdot\mathbf{F}_s)\rangle_{Av} \tag{6}$$

$$-n\leqslant l\leqslant+n$$
$$-n\leqslant l'\leqslant+n$$

$$f_{l,l'}=3/(2n^2)ll'$$

$$Z=M/M_0=2n.$$

Introducing the approximation

$$\langle(\mathbf{e}_y\cdot\mathbf{R}_{l'})(\mathbf{e}_x\cdot\mathbf{T}_{ls}\cdot\mathbf{F}_s)\rangle_{Av}=\langle(\mathbf{e}_y\cdot\mathbf{R}_{l'})(\mathbf{e}_x\cdot\langle\mathbf{T}_{ls}\rangle_{Av}\cdot\mathbf{F}_s)\rangle_{Av}$$

$$\langle\mathbf{T}_{ls}\rangle_{Av}=\frac{1}{6\pi\eta_0b}\mathbf{I}/|l-s|. \tag{7}$$

For large n, and utilizing Eq. (5) the set of Eqs. (6) defining $\phi_{l,l'}$ is asymptotically approximated by the integral equation

$$\phi(x, y)=f(x, y)-\lambda\int_{-1}^{1}K(x, t)\phi(t, y)dt$$

$$K(x,t)=\begin{cases}\dfrac{1}{x-t} & -1\leqslant t\leqslant x-\delta\\ 0 & x-\delta<t<x+\delta\\ \dfrac{1}{t-x} & x+\delta\leqslant t\leqslant+1\end{cases} \tag{8}$$

$$f(x, y)=\tfrac{3}{2}xy,$$

$$\lambda=\frac{\zeta}{6\pi\eta_0b},$$

$$\delta=1/n,$$

$$x=l/n.$$

It should be noted that explicit recognition has been taken in the integral Eq. (8) of the fact that the sum in Eq. (9) does not extend over the index s equal to l. Failure to take this into account would result in a kernel singular as $1/t$, for which the existence of a solution is questionable. The solution of (8) in Fourier series form

is given by*

$$\phi(x,y)=\sum_{k=\substack{-\infty\\ \neq 0}}^{\infty}\frac{f_k(y)e^{i\pi kx}}{1-2\lambda Ci\{|k|\pi\delta\}}$$

$$f_k(y)=\frac{3}{2}\frac{(-1)^k}{k\pi}iy \tag{9}$$

$$Ci(x)=\int_{\infty}^{x}\frac{\cos t}{t}\,dt.$$

For large n the sum defining F is replaced by the integral

$$F=\int_{-1}^{1}\phi(x,x)dx \tag{10}$$

to give for the intrinsic viscosity

$$[\eta]=\frac{N\zeta l^2}{3600\eta_0 M_0}F(\lambda\delta)$$

$$l=\text{length of rigid chain}=Zb \tag{11}$$

$$F(\lambda\delta)=\frac{6}{\pi^2}\sum_{k=1}^{\infty}\frac{1}{k^2(1-2\lambda Ci(k\pi\delta))}.$$

It is interesting to examine the behavior of the intrinsic viscosity of our model in the mathematical limits of large and small molecular weights. For this purpose we make use of the properties of the cosine integral function**

$$Ci(x)=\log\gamma x \text{ for small } x$$

$$Ci(x)=\frac{\sin x}{x} \text{ for large } x \tag{11a}$$

$$\gamma=\text{Euler's constant}=1.781,$$

whereby

$$\lim_{\substack{Z\to 0\\ \text{or}\\ \lambda\to 0}}F(\lambda\delta)=1 \tag{12}$$

and, for large Z,

$$F(\lambda\delta)=\frac{6}{\pi^2}\sum_{k=1}^{\infty}\frac{1}{2\lambda k^2\{\log Z-(\log 2\gamma k\pi-\tfrac{1}{2}\lambda)\}}.$$

Thus for small molecular weight the intrinsic viscosity is proportional to the square of the particle length and except for a factor of $\frac{1}{3}$ is identical with the result of a dumbbell, if ζ is used for $6\pi\eta_0 a$ of Simha's notation.[7] For large molecular weights we compare our result with that for ellipsoidal particles of large axis ratio.[8]

$$\eta_{sp}=4\pi a^3 n/45(\log 2a/b-1.80) \tag{13}$$

where a and b are the semimajor and minor axis with length $l=2a$. Our results, therefore, bear some analogies to those for elongated ellipsoids in containing a logarithmic term with argument Z proportional to the length $2a$. For a rod-shaped particle with b constant (Burger's notation) we rewrite the logarithmic term of Eq. (13) to emphasize the similarity with our Eq. (12).

$$\eta_{sp}=\frac{4\pi a^3 n}{45\{\log l-(\log b+1.8)\}}$$

$$F(\lambda\delta)=\frac{6}{\pi^2}\sum_{k=1}^{\infty}\frac{1}{2\lambda k^2\{\log l-(\log 2\gamma k\pi b-\tfrac{1}{2}\lambda)\}}. \tag{13a}$$

In a formal manner we may perhaps regard the rigid rod-like particle as the limit approached by our model, in a manner similar to the relationship between weighted and continuous string.

THE TRANSLATIONAL DIFFUSION CONSTANT

The friction constant Ξ of a rigid chain-like molecule is obtained by considering the mean force $\langle\mathbf{F}\rangle_{Av}$ exerted by the fluid on its center of mass when it is immersed in a solvent relative to which its center of mass is moving with relative velocity $\mathbf{u}$. The averages are taken over all random orientations of the rigid chain.

$$\langle\mathbf{F}\rangle_{Av}=-\sum_{l=-n}^{+n}\langle\mathbf{F}_l\rangle_{Av};\quad \langle\mathbf{F}\rangle_{Av}=\Xi\mathbf{u}$$

$$\langle\mathbf{F}_l\rangle_{Av}=-\zeta\mathbf{u}-\zeta\sum_{s=\substack{-n\\ \neq l}}^{+n}\langle\mathbf{T}_{ls}\cdot\mathbf{F}_s\rangle_{Av}\qquad -n\leqslant l\leqslant +n. \tag{14}$$

Neglecting the fluctuations, $\langle(\mathbf{T}_{ls}-\langle\mathbf{T}_{ls}\rangle_{Av})\cdot\mathbf{F}_s\rangle_{Av}$ and defining functions ψ_l by

$$\langle\mathbf{F}_l\rangle_{Av}=-\zeta\psi_l\mathbf{u} \tag{15}$$

we obtain

$$\psi_l=1-\lambda\sum_{s=\substack{-n\\ \neq l}}^{+n}\frac{\psi_s}{|l-s|} \tag{16}$$

from which ψ_l is to be evaluated. For large n Eq. (16) is replaced by the asymptotic integral equation

$$\psi(x)=1-\lambda\int_{-1}^{1}K(x,t)\phi(t)dt$$

$$K(x,t)=\begin{cases}\dfrac{1}{x-t} & -1\leqslant t\leqslant x-\delta\\ 0 & x-\delta<t<x+\delta\\ \dfrac{1}{t-x} & x+\delta\leqslant t\leqslant +1\end{cases} \tag{17}$$

$$x=l/n$$

where again explicit recognition has been made that the

* See Appendix I.

** See E. Jahnke and F. Emde, *Funktiontafeln* (Dover Publications, New York, 1943).

[7] Robert Simha, Research Nat. Bur. Stand. 42, 409 (1949).

[8] See J. M. Burgers, Chapter III, Second Report on Viscosity and Plasticity of the Amsterdam Academy of Sciences, Nordemann, 1938.

sum in Eq. (16) does not extend over l. Equation (17) differs from Eq. (8) encountered in the viscosity theory, only through its inhomogeneous part. The solution of Eq. (17) is therefore

$$\psi(x)=\sum_{k=-\infty}^{\infty}\psi_k e^{i\pi kx} \tag{18}$$

and the friction constant, in view of Eqs. (14) and (15) is given by

$$\Xi=\frac{Z}{2}\zeta\int_{-1}^{1}\psi(x)dx \tag{19}$$

or

$$\Xi=Z\zeta\psi_0. \tag{20}$$

ψ_0, the constant term in the Fourier expansion, is shown in Appendix I to be

$$\psi_0=\frac{1}{1-2\lambda\log\delta+2\lambda(\log 2-1)} \tag{21}$$

giving for the friction constant,

$$\Xi=\frac{Z\zeta}{2\lambda\{\log Z-[1-(1/2\lambda)]\}}$$
$$\lambda=\frac{\zeta}{6\pi\eta_0 b}. \tag{22}$$

With this value for the friction constant the translational diffusion and sedimentation constants, become

$$D=\frac{kT}{Z\zeta}2\lambda\{\log Z-[1-(1/2\lambda)]\}$$
$$s=\frac{M_0(1-V\rho)}{\zeta}2\lambda\{\log Z-[1-(1/2\lambda)]\}. \tag{23}$$

It should be noted that the friction constant is, as in the case of flexible molecules, proportional to Z for small molecular weight but proportional to $Z/\log Z$ for large molecular weights. For the latter, it is of interest, that the sedimentation constant is proportional to $\log Z$ and therefore to the logarithm of the molecular weight. To illustrate the close analogy with the results for long straight cylinders, which was already mentioned in the intrinsic viscosity theory, we present here the equations for the frictional resistance of the latter for the cases where its motion is parallel and perpendicular to the long axis.[8]

$$\Xi_p=\frac{4\pi\eta_0 a}{\log(2a/b)-0.72},$$
$$\Xi_s=\frac{8\pi\eta_0 a}{\log(2a/b)+0.5}, \tag{24}$$

$2a$=length of cylinder where the notation is that of Burgers.

THE ROTATORY DIFFUSION TENSOR

The rotatory resistance tensor of a rod-like chain can be defined in terms of the total torque about the center of mass

$$\mathbf{T}=\varrho\cdot\boldsymbol{\Omega}_0$$
$$\mathbf{T}=\sum_{l=-n}^{+n}\mathbf{T}_l \tag{25}$$
$$\mathbf{T}_l=-\mathbf{R}_l\times\mathbf{F}_l$$
$$D=kT\varrho^{-1},$$

where $-\mathbf{F}_l$, the force acting on element l is calculated from the Oseen equation.

$$\mathbf{F}_l=-\zeta(\mathbf{V}_l{}^0-\mathbf{u}_l)-\zeta\sum_{\substack{s=-n\\ \neq l}}^{+n}\mathbf{T}_{ls}\cdot\mathbf{F}_s \quad -n\leqslant l\leqslant+n. \tag{26}$$

If the velocity $\mathbf{u}_l$ of the chain elements relative to the solvents is derivable from the angular motion of the rigid chain, Eq. (26) becomes

$$\mathbf{F}_l=-\zeta\mathbf{u}_l-\zeta\sum_{\substack{s=-n\\ \neq l}}^{+n}\mathbf{T}_{ls}\cdot\mathbf{F}_s$$
$$\mathbf{u}_l=\boldsymbol{\Omega}_0\times\mathbf{R}_l \tag{27}$$
$$\boldsymbol{\Omega}_0=-\mathbf{e}_x\sin\phi\dot{\theta}+\mathbf{e}_y\cos\phi\dot{\theta}+\mathbf{e}_z\dot{\phi}.$$

Defining quantities

$$\langle\mathbf{R}_{l'}\times\mathbf{F}_l\rangle_{Av}=-(4/9)\zeta b^2n^2\phi_{l,l'}\boldsymbol{\Omega}_0$$
$$\langle\mathbf{T}\rangle_{Av}=(4/9)\zeta b^2n^3\boldsymbol{\Omega}_0F$$
$$F=\int_{-1}^{1}\phi(x,x)dx \tag{28}$$
$$x=l/n;\quad y=l'/n.$$

Again assuming that the fluctuation

$$\langle\mathbf{R}_{l'}\times(\mathbf{T}_{ls}-\langle\mathbf{T}_{ls}\rangle_{Av})\cdot\mathbf{F}_s\rangle_{Av}$$

can be neglected we obtain from Eq. (27) using Eq. (28)

$$\phi_{l,l'}=f_{l,l'}-\lambda\sum_{\substack{s=-n\\ \neq l}}^{+n}\frac{\phi_{l,s}}{|l-s|}$$
$$f_{l,l'}=\frac{3\,ll'}{2\,n^2} \tag{29}$$
$$\lambda=\zeta/6\pi\eta_0 b$$

which yields exactly the same asymptotic integral equation as Eq. (8) in the intrinsic viscosity section. Consequently, the value of F in Eq. (28) will also be the same as that given in Eq. (10) so that

$$\langle\mathbf{T}\rangle_{Av}=(4/9)\zeta b^2n^3\boldsymbol{\Omega}_0F(\lambda\delta)$$
$$F(\lambda\delta)=\frac{6}{\pi^2}\sum_{k=1}^{\infty}\frac{1}{k^2(1-2\lambda Ci(k\pi\delta))}. \tag{30}$$

The mean rotatory resistance tensor, in dyadic form, is thus given by

$$\langle \varrho \rangle_{Av} = (4/9)\zeta b^2 n^3 F(\lambda, \delta)\mathbf{I}$$
$$\langle \rho_{\theta\theta} \rangle_{Av} = \langle \rho_{\phi\phi} \rangle_{Av} = \langle \rho \rangle_{Av} \tag{31}$$
$$\langle D_{\theta\theta} \rangle_{Av} = \langle D_{\phi\phi} \rangle_{Av} = -\frac{9}{4}\frac{kT}{b^2\zeta n^3 F(\lambda, \delta)}.$$

It is very interesting to note that the intrinsic viscosity and rotatory resistance constants of both flexible and rigid chain-like molecules have exactly the same form, differing only in the coefficients $F(\lambda)$. This result was only to be expected since using identical molecular parameters a dimensional analysis would show the necessity of such similarities of form.

For the limiting properties of $F(\lambda, \delta)$ we refer back to Eq. (12). For purpose of comparison we quote here the corresponding expression for the rotatory resistance constant of a cylinder about a transverse axis[8]

$$\rho = \frac{8\pi\eta_0 a^3}{3(\log(2a/b) - 0.80)}. \tag{32}$$

Equation (11) combined with Eq. (31) gives the same relationship, except for a factor of two, between the frictional resistance constant and intrinsic viscosity as was obtained with flexible molecules.[6]

$$\langle \rho_{\phi\phi} \rangle_{Av} = 200(M/N)\eta_0[\eta],$$
$$\langle D_{\phi\phi} \rangle_{Av} = \frac{NkT}{200M\eta_0[\eta]}. \tag{33}$$

This relationship, except for the numerical factor, is the same for spherical and flexible molecules, in which case the factors are 240 and 400 respectively. For cylindrical molecules, it would appear, from the results that we have quoted, Eqs. (13) and (32), that except for very large axial ratios, the quotient $\langle \rho_{\phi\phi} \rangle_{Av}/[\eta]$ not only depends on the molecular weight but also on the axial ratio. For very large axial ratios the numerical factor is of order 3000. It should be noted that Eq. (33) offers an independent method for making molecular weight determinations, from, for example, birefringence and intrinsic viscosity measurements, somewhat analogous to the well-known pair, sedimentation and diffusion constant.

APPENDIX I

Solution of the Integral Equations

The integral equations considered in this article are of the form

$$\phi(x) = f(x) - \lambda \int_{-1}^{1} K(x, t)\phi(t)dt$$
$$K(x, t) = \begin{cases} \dfrac{1}{x-t} & -1 \leqslant t \leqslant x-\delta \\ 0 & x-\delta < t < x+\delta \\ \dfrac{1}{t-x} & x+\delta \leqslant t \leqslant +1 \end{cases} \tag{A1}$$

in which we suppose that

$$\phi_0 = \tfrac{1}{2}\int_{-1}^{1} \phi(x)dx \tag{A2}$$

vanishes. If this condition does not apply we consider the subsidiary integral equation

$$\phi^*(x) = f^*(x) - \lambda \int_{-1}^{1} K(x, t)\phi^*(t)dt$$
$$\begin{aligned} \phi^*(x) &= \phi(x) - \phi_0 \\ f^*(x) &= f(x) - \phi_0\mu(x) \\ \mu(x) &= 1 + \lambda \log[(1-x^2)/\delta^2] \end{aligned} \tag{A3}$$

in which the condition corresponding to Eq. (A2) does apply. We represent the kernel $K(x, t)$ by

$$K(x, t) = \begin{cases} \displaystyle\int_0^\infty e^{-(x-t)z}dz, & -1 \leqslant t \leqslant x-\delta \\ 0 & x-\delta < t < x+\delta \\ \displaystyle\int_0^\infty e^{-(t-x)z}dz, & x+\delta \leqslant t \leqslant +1. \end{cases} \tag{A4}$$

We substitute this value of the kernel into Eq. (A3), and interchange the order of integration, which is permissible under the condition of Eq. (A2), and obtain the set of equations

$$\phi^*(x) = f^*(x) - \lambda \int_0^\infty g(x, z)dz$$
$$\frac{\partial^2 g}{\partial x^2} = z^2 g + e^{-\delta z}F(x, z) \tag{A5}$$
$$F(x, z) = \frac{\partial}{\partial x}[\phi^*(x-\delta) - \phi^*(x+\delta)] - z[\phi^*(x-\delta) + \phi^*(x+\delta)],$$

where the second of Eqs. (A5) arises from the integral equation defining $g(x)$

$$g(x) = \int_{-1}^{x-\delta} e^{-(x-t)z}\phi^*(t)dt + \int_{x+\delta}^{1} e^{-(t-x)z}\phi^*(t)dt \tag{A6}$$

and is obtained by differentiating twice with respect to x. From here on the procedure is identical with that of our previous paper,[4] so that using Fourier expansions for $\phi^*(x)$ $g(x, z)$ and $f^*(x)$ on the interval $-1 \leqslant x \leqslant 1$ we obtain

$$\phi_k^* = \frac{f_k^*}{1 - 2\lambda Ci(|k|\pi\delta)}$$
$$Ci(x) = \int_\infty^x \frac{\cos t}{t}dt \tag{A7}$$

and since f_0^* vanishes

$$\phi_0 = f_0/\mu_0$$
$$\mu_0 = \tfrac{1}{2}\int_{-1}^{1} \mu(x)dx \tag{A8}$$
$$\mu_0 = 1 - 2\lambda(1 - \log 2/\delta)$$

and the Fourier representation of $\phi(x)$ is given by

$$\phi(x) = \frac{f_0}{1 - 2\lambda\log\delta + 2\lambda(\log 2 - 1)} + \sum_{\substack{k=-\infty \\ \neq 0}}^{\infty} \frac{(f_k - (\mu_k/\mu_0)f_0)e^{i\pi kx}}{1 - 2\lambda Ci(|k|\pi\delta)},$$
$$f_k = \tfrac{1}{2}\int_{-1}^{1} f(x)e^{-i\pi kx}dx, \tag{A9}$$
$$\mu_k = \tfrac{1}{2}\int_{-1}^{1} \{1 - 2\lambda\log\delta + \lambda\log(1-x^2)\}e^{-i\pi kx}dx.$$

The above is the desired solution of the integral Eq. (A1) employed in the foregoing work.

A Viscosity Equation for Gas Mixtures

C. R. WILKE
Department of Chemistry and Chemical Engineering, University of California, Berkeley, California
(Received October 24, 1949)

By application of the kinetic theory, with several simplifying assumptions, the previous equation of Buddenberg and the author has been modified to give a general equation for viscosity as a function of molecular weights and viscosities of the pure components of the mixture. Agreement of the equation with experimental data is demonstrated for a number of highly irregular binary gas systems and mixtures of three to seven components.

RECENTLY, Curtiss and Hirschfelder[1,2] have developed relations for calculation of gas mixture viscosities, based on quantitative evaluation of intermolecular forces and the use of collision integrals, which reproduce the experimental data for non-polar gases with high precision. In the present paper are presented alternate, although less rigorous, equations which may prove useful from the standpoint of simplicity and convenience in numerical use, and which are believed sufficiently accurate for many purposes.

Buddenberg and Wilke[3] have shown that the Sutherland type equation[4] may be expressed in the general form for binary mixtures given by Eq. (1).

$$\mu_m=\frac{\mu_1}{1+(1.385\mu_1x_2/D_{12}\rho_1x_1)}+\frac{\mu_2}{1+(1.385\mu_2x_1/D_{12}\rho_2x_2)}\cdots, \quad (1)$$

where the dimensionless constant 1.385 is an average value determined empirically by examination of a large body of data.

Equation (1) was further extended to include multicomponent systems in the general form:

$$\mu_m=\sum_{i=1}^{n}\frac{\mu_i}{1+\left[\dfrac{1.385\mu_i}{x_i\rho_i}\sum\limits_{\substack{j=1\\ j\neq i}}^{n}\dfrac{x_j}{D_{ij}}\right]} \quad (2)$$

A major source of uncertainty in the use of these equations lies in the need for the diffusion coefficients for the various gas pairs involved, so that it is often necessary to estimate the diffusion coefficients from empirical correlations.

Equation (1) may be written in a more general form:

$$\mu_m=\frac{\mu_1}{1+(\beta\mu_1x_2/D_{12}\rho_1x_1)}+\frac{\mu_2}{1+(\beta\mu_2x_1/D_{21}\rho_2x_2)}\cdots, \quad (3)$$

where β is a constant for the gas pair under consideration. Considering Eq. (3) for the special case of a mixture of component 1 in itself, say for 50 percent of 1 in 1, and solving for β gives the result:

$$\beta=\beta_1=(D_{11}\rho_1)/\mu_1. \quad (4)$$

Similarly, considering component 2 alone:

$$\beta=\beta_2=(D_{22}\rho_2)/\mu_2. \quad (5)$$

According to the kinetic theory[5] the group $D\rho/\mu$ for self-diffusion ranges in numerical value from 1.2 for hard spheres to 1.543 for inverse-fifth-power repulsion, which supports the average value of 1.385 obtained for the constant in Eq. (1). It is probable, therefore, that β is not equal to a single constant, but rather that it may have various values in the vicinity of 1.385, depending upon the gases under consideration.

The diffusion coefficient in a binary mixture is given by the expression:[5]

$$D_{12}=(1+\lambda_{12})\frac{3}{8}\left(\frac{\pi}{2}\right)^{\frac{1}{2}}\frac{1}{nS_{12}}\left(\frac{m_1+m_2}{m_1m_2}kT\right)^{\frac{1}{2}}\cdots \quad (6)$$

where for hard spherical molecules S_{12} is given by the relation

$$S_{12}=(\pi/4)(\sigma_1+\sigma_2)^2\cdots. \quad (7)$$

Writing (6) and (7) for self-diffusion yields expressions for σ_1 and σ_2 as functions of the coefficients of self-diffusion. Substituting these values of σ_1 and σ_2 in (6) for the binary case, and assuming $(1+\lambda_{11})\approx(1+\lambda_{22})\approx(1+\lambda_{12})$, gives an expression for the binary diffusion coefficient in terms of the coefficients of self-diffusion:

$$D_{12}=\frac{(4/\sqrt{2})(m_1+m_2/m_1m_2)^{\frac{1}{2}}}{[(1/D_{11}^2m_1)^{\frac{1}{4}}+(1/D_{22}^2m^2)^{\frac{1}{4}}]^2}\cdots. \quad (8)$$

Equations (4) and (5) may be combined with (8) to give a further expression for the diffusion coefficient:

$$D_{12}=\frac{[4/\sqrt{2}(1/M_1+1/M_2)^{\frac{1}{2}}]}{[(\rho_1^2/\beta_1^2\mu_1^2M_1)^{\frac{1}{4}}+(\rho_2^2/\beta_2^2\mu_2^2M_2)^{\frac{1}{4}}]^2}\cdots. \quad (9)$$

Assuming $\beta=\beta_1=\beta_2$, Eqs. (3) and (9) may be com-

[1] C. F. Curtiss and J. O. Hirschfelder, "The kinetic theory of multicomponent systems of gases," University of Wisconsin, CF-727 (July, 1947).
[2] Hirschfelder, Bird, and Spotz, Chem. Rev. 44, 205 (1949).
[3] J. W. Buddenberg and C. R. Wilke, Ind. Eng. Chem. 41, 1349 (1949).
[4] W. Sutherland, Phil. Mag. 40, 421 (1895).
[5] E. H. Kennard, *Kinetic Theory of Gases* (McGraw-Hill Book Company, Inc., New York, 1938), p. 195.

TABLE I. Properties of gases used in Fig. 1 and Table II.*

Gas pair	t°C	$\mu_1 \times 10^6$	$\mu_2 \times 10^6$	ϕ_{12}	ϕ_{21}	Reference for viscosity data
He-A	20	197.3	221.1	2.417	0.2716	a,b
N_2-O_2	27	178.1	205.7	0.994	1.014	c
C_2H_6-C_3H_8	250	152.6	136.3	1.276	0.779	d
H_2-CCl_2F_2	25	88.4	124.0	3.943	0.0920	e
H_2-C_3H_8	26.9	89.1	81.7	3.674	0.1539	f
H_2-A	20	87.5	221.1	1.870	0.2384	a
Ne-A	200	422.0	320.8	1.606	0.6166	a
Ne-He	200	422.0	267.2	0.4862	1.552	a
He-A	200	267.2	320.8	2.318	0.2789	a
N_2-CO_2	25	176.8	147.8	1.368	0.7281	e
H_2-CO_2	25	88.4	147.8	2.470	0.1977	e
H_2-N_2	25	88.4	176.8	1.905	0.2750	e
Ne-CO_2	25	313.3	147.8	2.250	0.5011	e
Ne-CCl_2F_2	25	313.3	124.0	3.987	0.2628	e
Ne-N_2	25	313.3	176.8	1.612	0.6552	e
CO_2-CCl_2F_2	25	147.8	124.0	1.751	0.5351	e
N_2-CCl_2F_2	25	176.8	124.0	2.358	0.3830	e

* All data at atmospheric pressure.
[a] M. Trautz and H. E. Benkele, Ann. d. Physik **5**, 561 (1930).
[b] M. Trautz and K. F. Kipphan, Ann. d. Physik **2**, 743 (1929).
[c] M. Trautz and A. Melster, Ann. d. Physik **7**, 409 (1930).
[d] M. Trautz and K. G. Sorg, Ann. d. Physik **10**, 81 (1931).
[e] J. W. Buddenberg, M.S. thesis, University of California (1948). Data determined relative to N_2.
[f] M. Trautz and F. Kurz, Ann. d. Physik **9**, 992 (1931).

bined* to eliminate the diffusion coefficient from the viscosity equation:

$$\mu_m = \frac{\mu_1}{1+\dfrac{x_2/x_1\{1+[(\mu_1/\mu_2)(\rho_2/\rho_1)]^{\frac{1}{2}}(M_1/M_2)^{\frac{1}{4}}\}^2}{(4/\sqrt{2})[1+(M_1/M_2)]^{\frac{1}{2}}}} + \frac{\mu_2}{1+\dfrac{x_1/x_2\{1+[(\mu_2/\mu_1)(\rho_1/\rho_2)]^{\frac{1}{2}}(M_2/M_1)^{\frac{1}{4}}\}^2}{(4/\sqrt{2})[1+(M_2/M_1)]^{\frac{1}{2}}}} \cdots \quad (10)$$

For ideal gas behavior, Eq. (10) may be reduced to the relatively simple expression:

$$\mu_m = \frac{\mu_1}{1+\dfrac{(x_2/x_1)[1+(\mu_1/\mu_2)^{\frac{1}{2}}(M_2/M_1)^{\frac{1}{4}}]^2}{(4/\sqrt{2})[1+(M_1/M_2)]^{\frac{1}{2}}}} + \frac{\mu_2}{1+\dfrac{(x_1/x_2)[1+(\mu_2/\mu_1)^{\frac{1}{2}}(M_1/M_2)^{\frac{1}{4}}]^2}{(4/\sqrt{2})[1+(M_2/M_1)]^{\frac{1}{2}}}} \cdots \quad (11)$$

Equation (11) constitutes the final recommended relation for binary mixtures. This relation is relatively convenient to use, requiring only the molecular weights and viscosities of the pure components for the prediction of the entire viscosity concentration curve. It should be noted that the equation contains no empirical numerical constants, the constant $4/\sqrt{2}$ coming from the kinetic theory.

* Values of β_1 and β_2 need not necessarily be viewed as equal to a single value of β in combining (3) and (9), but rather that $\beta=\beta_1$, in calculating D_{12}, and $\beta=\beta_2$ in calculating D_{21}. Thus it is possible that errors due to deviations between β_1 and β_2 may fortuitously cancel in each of the partial viscosity terms in (3).

TABLE II. Calculated and experimental data for multicomponent mixtures.

	Volume percent of components							Viscosity $\times 10^6$, g/cm-sec.	
t,°C	Ne	A	He	H_2	CO_2	N_2	CCl_2F_2	μ_{calc}	μ_{exp}
200	31.93	32.13	35.94					360.0	357.4[a]
25	33.33			33.33	33.33			190.2	185.7[b]
25				33.33		33.33	33.33	145.7	146.9[b]
25					33.33	33.33	33.33	144.6	145.8[b]
25	25.00			25.00	25.00		25.00	159.3	168.1[b]
25				25.00	25.00	25.00	25.00	146.7	147.1[b]

[a] See Table I, reference b.
[b] See Table I, reference e.

COMPARISON OF CALCULATED WITH EXPERIMENTAL DATA

To offer a severe test of Eq. (11) a number of binary systems exhibiting highly irregular and dissimilar viscosity-concentration curves were selected from the literature. These data are plotted and compared with the calculated curves in Fig. 1. Properties of the pure components and literature sources for these systems are given in Table I. It is believed that the close correspondence between these calculated and observed data indicates the ability of Eq. (11) to reproduce gas viscosity behavior with sufficient precision for most purposes. The average deviation between calculation and experiment for the data shown in Fig. 1, excluding terminal points, is 0.97 percent. Prediction of the hydrogen-argon curve is the least satisfactory, and by excluding these data the average deviation between calculated and experimental points is reduced to 0.49 percent.

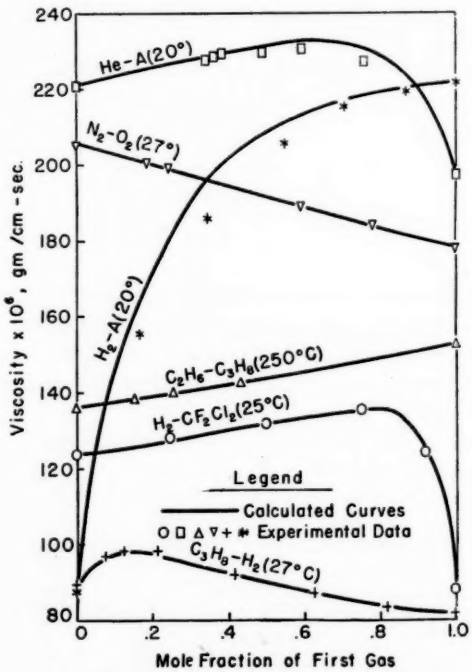

FIG. 1. Comparison of calculated and experimental viscosities for some binary mixtures.

TABLE III. Calculated and experimental data for some industrial gases.*

Components	CO_2	O_2	CO	H_2	CH_4	N_2	Higher hydrocarbons[a]	Viscosity $\times 10^6$ g/cm-sec.	
Component viscosity[b]	147.2	201.9	174.9	87.55	108.7	178.1	90.9	μ_{calc}	μ_{exp}
Volume percent of components	6.2	10.7				83.1		178.1	179.3
Volume percent of components	10.4		28.5	1.6		59.5		172.9	173.8
Volume percent of components	10.6		29.8	3.9	0.3	55.4		172.4	174.3
Volume percent of components	2.5	0.8	14.9	53.0	18.1	9.1	1.6	142.7	135.5
Volume percent of components	2.2	1.0	4.0	52.3	29.9	9.4	1.2	130.7	130.7
Volume percent of components	4.8	0.3	26.4	17.2	2.6	48.2	0.5	171.4	171.4
Volume percent of components	3.5	0.3	27.3	14.4	3.7	50.0	0.8	171.1	171.2

* Data of F. Herning and L. Zipperer, Gas-u Wasserfach **79**, 49–54, 69–73 (1936), all at 293°K, atmospheric pressure.
[a] Assumed to be ethane.
[b] Based on data summarized by Hirschfelder, Bird, and Spotz (see reference 2).

GENERAL EQUATION FOR MULTICOMPONENT SYSTEMS

Equation (2) may be written in a general form analogous to (3) and combined with equations such as (9) in the same manner as for the binary case to give a general viscosity equation for a mixture of any number of components. Thus:

$$\mu_m = \frac{\mu_1}{1+(x_2/x_1)\phi_{12}+(x_3/x_1)\phi_{13}+\cdots} + \frac{\mu_2}{1+(x_1/x_2)\phi_{21}+(x_3/x_2)\phi_{23}+\cdots}+\cdots. \quad (12)$$

Equation (12) may be written in the general form:

$$\mu_m = \sum_{i=1}^{n} \frac{\mu_i}{1+\frac{1}{x_i}\sum_{\substack{j=1\\ j\neq i}}^{j=n} x_j\phi_{ij}} \quad (13)$$

where ϕ_{ij} is given by the equation:

$$\phi_{ij} = \frac{[1+(\mu_i/\mu_j)^{\frac{1}{2}}(M_j/M_i)^{\frac{1}{4}}]^2}{(4/\sqrt{2})[1+(M_i/M_j)]^{\frac{1}{2}}}\cdots. \quad (14)$$

Table II compares experimental data with those calculated by Eqs. (13) and (14), for several mixtures of three and four components. Pure component viscosities and calculated values of ϕ_{ij} for these systems are given in Table I. Table III shows the results obtained for some industrial gases of three to seven components. The average deviation between calculated and experimental data for these thirteen mixtures is 1.9 percent It is believed that these results demonstrate satisfactory application of the general equation to multicomponent systems.

NOMENCLATURE

D—diffusion coefficient, cm²/sec.; D_{11}, D_{22}, etc. for self-diffusion, D_{12} for a binary mixture.
k—Boltzmann's constant.
m—mass of a single molecule.
M—molecular weight.
n—number of molecules per unit volume in the portion of gas under consideration.
S—collision cross section for diffusion; S_{11}, S_{22}, etc. for pure components, S_{12} for dissimilar molecules.
t—temperature, °C.
T—temperature, °K.
x—mole fraction of a component in the mixture.
β—dimensionless constant.
λ—correction factor for deviation from inverse-fifth-power behavior.
μ—viscosity, g/cm-sec.; μ_1, μ_2, etc. refer to the pure components at the temperature and pressure of the mixture, μ_m is the viscosity of the mixture.
ϕ—dimensionless constant defined by Eq. (14).
ρ—density, g/cu.cm; ρ_1, ρ_2, etc. refer to the pure components at the temperature and total pressure of the mixture.
σ—molecular diameter.

Subscripts

1, 2, i, j, n—refer to the pure components of the mixture.
m—refer to the mixture.

The Catalysis of the Ortho-Para Conversion in Liquid Hydrogen

C. A. SWENSON*
The Clarendon Laboratory, Oxford University, England
(Received November 7, 1949)

The catalysis of the ortho-para conversion in liquid hydrogen is of importance for the quantity production of pure parahydrogen. Parahydrogen is of interest in itself: however, from a purely practical standpoint, if liquid hydrogen were to be kept for any considerable length of time, it would be much more economical to store liquid parahydrogen than normal (25 percent para) liquid hydrogen. Rough determinations of the conversion constant, both in the adsorbed layer of the catalyst and in the actual liquid, are given for activated charcoal and for silica gel onto which oxygen gas had been adsorbed. The heat of mixing of ortho- and parahydrogen was also measured, and found to be smaller than the accuracy of measurement.

THE difference in the internal energies of ortho- and parahydrogen leads to a heat of conversion between these two modifications. As was pointed out in a previous paper,[1] the effect of this heat conversion, combined with the spontaneous conversion process in pure liquid hydrogen, leads to a very appreciable heat influx into liquid hydrogen, and a corresponding loss of the liquid by evaporation. If liquid hydrogen were to be stored for any length of time, while normal heat influxes could be reduced by means of radiation shields, etc., this source of heat could only be decreased by reducing the orthohydrogen content of the liquid. The most practical solution would be to store pure parahydrogen directly, and it was with this end in view that the following experiments on the catalysis of the ortho-para conversion in liquid hydrogen were performed.

There have been several instances in the literature[2–5] where the ortho-para conversion in liquid hydrogen has either been used or observed, but no quantitative data as to conversion constants, etc., have been given. In fact, for the two cases where large quantities of liquid hydrogen were produced, using adsorption-type catalysts, the rates of conversion seem to differ by a factor of ten or so.[2,3] Probably the most interesting case is that of catalysis by small quantities of solid oxygen floating in the liquid, as reported by Brickwedde, Scott, Urey, and Wahl.[4] A modification of this effect was recently reported by van Itterbeck,[5] who observed that supersonics catalyze the reaction, but only if small quantities of solid oxygen are present.

For most purposes, the use of solid oxygen would not be satisfactory, both from a safety point of view and from the standpoint of experimental technique. The ideal situation would be to have a catalyst placed in the liquefaction chamber of the hydrogen liquefier, so that, while the heat of conversion would result in a drop in the efficiency of the liquefier, this would be somewhat compensated for the extra amounts of cold gas passing through the final heat exchanger.

For gaseous hydrogen adsorbed onto a catalyst, the ortho-para conversion rate has been shown to be of the general form[6]

$$d\alpha/dt = -\alpha/\tau, \tag{1}$$

where α is the orthohydrogen fraction present, and τ is the reciprocal conversion constant. This can easily be solved to give

$$\alpha = (\alpha_0 - \alpha_f)\exp(-t/\tau), \tag{2}$$

where α_0 and α_f represent the initial and final orthohydrogen fractions, respectively.

Values for τ in the adsorption layer have been determined at various temperatures for various substances, probably the most important of which is charcoal. A rather complete account of the variation of the conversion on charcoal with temperature, pressure, and degree of activation of the charcoal is given by Farkas[7] and will not be reproduced here.

For catalysis of the ortho-para conversion in liquid hydrogen, the reaction rate would be expected to be given by

$$d\alpha/dt = -(\alpha/\tau_1) - (\alpha^2/\tau_2), \tag{3}$$

where τ_1 is the reciprocal conversion constant due to the catalyst, and τ_2 is that due to the homogeneous conversion (caused by the interaction between two ortho molecules discussed previously).[1] For any useful catalyst, $\tau_1 \ll \tau_2$, since $\tau_2 = 79$ hr.

APPARATUS

The apparatus used is shown in Fig. 1. The cryostat consisted of two compartments, A and B, which could be connected by means of the needle valve, C, and which were enclosed in a vacuum jacket, D. Replacement of the catalyst in A was facilitated by Wood's metal joints at A_1 and D_1. The connections from A and B through

* Now at Harvard University.

[1] Larsen, Simon, and Swenson, Rev. Sci. Inst. **19**, 266 (1948).

[2] L. W. Alvarez and K. S. Pitzer, Phys. Rev. **58**, 1003 (1940); Sutton, Hall, Anderson, Bridge, DeWire, Lavatelli, Long, Snyder, and Williams, Phys. Rev. **72**, 1147 (1947).

[3] Brickwedde, Dunning, Hoge, and Manley, Phys. Rev. **54**, 266 (1938).

[4] Brickwedde, Scott, Urey, and Wahl, J. Chem. Phys. **2**, 454 (1934).

[5] A. van Itterbeek, reported in a paper read before the International Conference on Very Low Temperature Physics at M.I.T. (September, 1949).

[6] A. Farkas, *Ortho-Hydrogen, Para-Hydrogen, and Heavy Hydrogen* (Cambridge University Press, London, England, 1935), p. 79.

[7] See reference 6, p. 92.

the vacuum jacket were 4-mm o. d., 0.1-mm w.t. German silver tubes, 10 cm long. The vacuum jacket was in turn placed in a Dewar of liquid hydrogen, *E*.

Liquid hydrogen from the outer Dewar could be admitted into either *A* or *B* by means of the needle valves, F_1 and F_2, which were controlled from the cap of the cryostat. Hydrogen could also be condensed into either compartment from an external cylinder, *G*. The needle valve, *C*, connecting *A* and *B* could also be opened or closed from the outside, and all three valves, *C*, F_1, and F_2, were made vacuum-tight by using a graphite and asbestos packing at their upper ends in the conventional manner.

The external arrangement was such that either *A* or *B* could be evacuated with a mercury pump for vacuum testing. The rate of evaporation of liquid hydrogen from either could be measured by means of a capillary flowmeter, while total amounts of gas were measured using an ordinary gasmeter.

Any temperature difference between *A* and *B* was made as small as possible by a heavy slotted copper cylinder which was fitted over *B* and extended well down into *A*. The temperature difference between the two compartments was determined by putting liquid hydrogen from the outer Dewar into both *A* and *B*, and with the liquid hydrogen in *B* evaporating into the atmosphere while the liquid in *A* was isolated, measuring the vapor pressure difference between the two by means of the differential oil manometer, H. This difference was found to be less than 1 cm of oil—or 0.003°K. This differential manometer was later used in the same manner to measure the vapor pressure difference (and, hence, the concentration difference) between liquid hydrogen samples in *A* and *B*.

Finally, to prevent recondensation of the hydrogen gas evaporating from the inner compartments, the liquid hydrogen in the outer Dewar was kept at a slightly higher temperature than that of the hydrogen in *A* and *B* by sealing the Dewar to the cap with a rubber sleeve and using the water bubbler, *J*.

EXPERIMENTAL PROCEDURE

The procedure used to measure the conversion rate was roughly as follows. The catalyst was heated (200°C) under high vacuum for several hours, and then was placed in *A*, being kept continuously in a helium atmosphere. The Wood's metal joints, A_1 and D_1, were then soldered, and with the vacuum jacket and *A* and *B* evacuated, liquid oxygen was placed in the outer Dewar and the set-up was cooled to liquid oxygen temperature by means of a few millimeters of helium "exchange" gas in the vacuum jacket. Liquid hydrogen was then placed in the Dewar, and the cooling to liquid hydrogen temperature continued in the same manner. The catalyst was kept continuously in contact with gaseous hydrogen at atmospheric pressure, so that the charcoal was "saturated" with hydrogen gas at 20°K in an hour or so. The exchange gas also removed the heat of adsorption (approximately 500 cal./mole).

The exchange gas was pumped after an hour, and liquid hydrogen from the Dewar was put into *B* through F_2. The rate of evaporation of the hydrogen in *B* was then measured on the capillary flowmeter with *A* isolated. This was continued until a relatively steady value for the evaporation was reached (due to the homogeneous conversion in *B*). This indicated that the adsorbed layer on the catalyst in *A* was completely converted. The conversion constant could be determined from the conventional logarithmic plot of the net flow due to the conversion against time. This was necessarily inaccurate, but gave the conversion constants to 20 percent or so. A better scheme would have been to place pure parahydrogen in *B*, since then the background flow would have been zero.

Finally, liquid hydrogen from the outer Dewar was placed in *A*, and the rate of conversion measured again by means of the net evaporation from *B*.

RESULTS

In all, three catalysts were tried—activated charcoal, activated silica gel, and oxygen adsorbed on the activated silica gel. An experiment was performed with the silica gel immediately after activation, and then with the silica gel saturated with gaseous oxygen (at 90°K) to show the effect of oxygen as a catalyst.

The results are given in Table I, where τ_a is the characteristic time in the adsorbed layer, and τ_e is the characteristic time for the liquid in contact with the catalyst. To verify that the conversion had actually

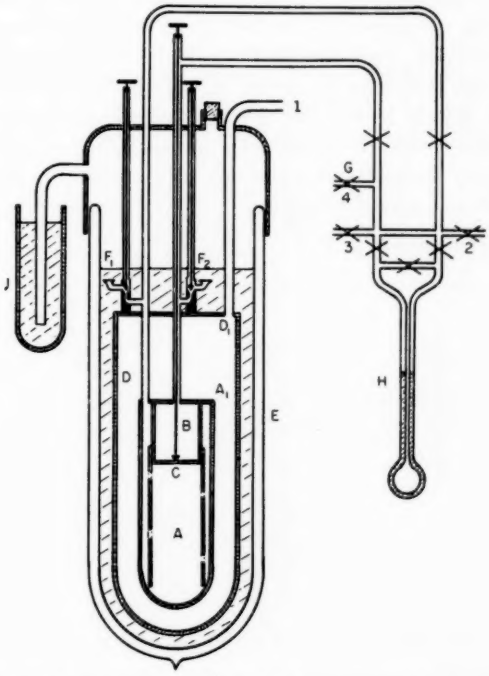

FIG. 1. The cryostat: (1, 2) to high vacuum; (3) to capillary flowmeter; (4) to cylinder of normal hydrogen gas.

TABLE I. Catalysts and amounts of hydrogen used in each experiment. τ_a and τ_e are the reciprocal conversion constants in hours in the adsorbed layer and the liquid, respectively.

Catalyst	τ_a (hr.)	Hydrogen in adsorption layer	τ_e (hr.)	Liquid H_2 around catalyst (cc)
16 g coconut charcoal (40 cc)	0.25	12.5 l. (N.T.P.)	0.7	1
	—	12.5 l. (N.T.P.)	0.6	45
45 cc silica gel	1.5	11.5 l. (N.T.P.)	—	—
Same, +8 l. O_2 gas	0.4	11.5 l. (N.T.P.)	0.6	25

taken place, the vapor pressure difference between the liquid hydrogen in *A* and liquid hydrogen condensed into *B* (75 percent ortho) was checked using the oil manometer. This vapor pressure difference (42 cm of Apiezon A oil between pure parahydrogen and normal hydrogen)[8] was easily measured and showed the expected concentration difference. This method was also used to verify that the Clarendon hydrogen liquefier produces liquid hydrogen of roughly 50 percent ortho concentration.

The characteristic times given for the conversion in the adsorbed layer of activated charcoal agree roughly with those given by Farkas, in spite of the fact that the activation was not as thorough as is recommended. Since the conversion rate in the adsorbed layer of activated silica gel was so small, conversion of liquid hydrogen was not attempted. However, the increased effect due to oxygen adsorbed on the silica gel is shown quite nicely. A much greater effect would be expected if oxygen were to be adsorbed onto the charcoal, but this is a rather dangerous procedure, as the mixture of hydrogen, oxygen, and charcoal would be highly explosive. However, a charcoal cleaner at liquid air temperatures, which serves to remove the last traces of oxygen and nitrogen from the hydrogen gas before liquefaction, probably serves as an excellent catalyst because of this oxygen gas adsorbed on it.

[8] See reference 6, p. 39.

It will be noted that the conversion rate is always less for the liquid than it is for the adsorbed layer. This probably points to an exchange of molecules between the adsorbed layer and the liquid. The volume of liquid hydrogen used was always about the same as the volume of the catalyst, so nothing is known of the effect of a small amount of charcoal in a large volume of liquid hydrogen. Presumably, the reaction rate would decrease as the volume of the liquid hydrogen was increased.

THE HEAT OF MIXING OF ORTHO- AND PARAHYDROGEN

This same apparatus can easily be used to determine whether or not a heat of mixing exists between ortho- and parahydrogen. The following experiment was performed. Two hundred cc of 50 percent orthohydrogen were placed in *A* (no catalyst), and 70 cc of 75 percent orthohydrogen were placed in *B*. The concentration difference was checked by means of the vapor pressure difference using the oil manometer, and the flow from *A* with *B* isolated, as measured with the capillary flowmeter, gave the normal evaporation. The needle valve, *C*, was then opened, and the two lots of hydrogen were mixed. The resulting effect (as determined by the change in evaporation) was less than one-half calorie, and could be explained by the rise in the boiling point of the mixture in *A* (parahydrogen having a larger vapor pressure than orthohydrogen).[8] An experiment performed with hydrogen of the same concentration in both *A* and *B* showed no measurable effect.

Thus, it would seem that the discrepancies between our previous results[1] and theory cannot be explained by a heat of mixing between ortho- and parahydrogen. These previous measurements should probably be repeated before any decision is made as to the agreement between theory and experiment.

I wish to express my appreciation to Professor F. E. Simon for his constant interest and advice on this problem. I also wish to thank Mr. J. Milligan for his technical assistance. This work was made possible through a grant from the Carnegie Fund for Overseas Students.

The Magnetic Susceptibility of Bromine-Graphite

M. GOLDSMITH
Argonne National Laboratory, Chicago, Illinois
(Received October 3, 1949)

The magnetic susceptibilities of graphite and bromine-graphite have been measured. Possible structures of bromine-graphite are discussed.

INTRODUCTION

IF graphite is exposed to an atmosphere containing bromine vapor, bromine is intercalated[1] between the layer planes of the graphite lattice; the substance thus formed is known as "bromine-graphite." Rüdorff[1] has found that the bromine-graphite which is formed, at room temperature, in the presence of an atmosphere continuously saturated with bromine vapor has the empirical formula: C_8Br. If this "saturated" bromine-graphite is allowed to stand in air, more than 90 percent of its bromine is lost to the atmosphere.

Considerations based on x-ray analyses[1] of saturated bromine-graphite exclude the possibility that the greater part of the intercalated bromine is present in ionic form and this, together with the rapid decomposition of the substance in air, has lead Rüdorff to the conclusion that either atomic or molecular bromine occupies interlamellar positions in the graphite lattice.

Since the feeble diamagnetism[2] of molecular bromine is essentially temperature independent, and since atomic bromine should possess a strong paramagnetic susceptibility[3] which is temperature dependent, it was thought that measurements of the magnetic susceptibility of bromine-graphite might lead to a more detailed knowledge of its electronic structure.

EXPERIMENTAL PROCEDURE

Apparatus

Magnetic susceptibilities were determined by the Gouy method. A partitioned Gouy tube similar to that described by Freed[4] was used. The lower half of the tube was permanently evacuated; the upper half was packed with the sample up to a mark near the top. The tube was suspended in a Pyrex jacket filled with dry nitrogen, and nitrogen was circulated through the upper portion of this jacket to prevent the diffusion of air into the atmosphere around the Gouy tube. The jacket and its contents were surrounded by a Dewar flask which was shaped to fit between the pole pieces of an electromagnet (Consolidated Engineering Corporation's Model 23–104A). Calibrated copper-constantan thermocouples, inserted in the space between the Gouy tube and the jacket wall, were employed to measure the temperature of the sample.

The current which passed through the magnet coils also flowed through a 0.005 ohm resistor; the potential drop due to this resistor was measured with a Rubicon potentiometer (Model 2732). It was found that a given magnet current could be reproduced with a precision of ±0.2 percent.

Magnetic susceptibilities were calculated with the aid of the following formula:

$$X=\left[\frac{(\Delta W_p-\Delta W_N)\kappa_{H_2O}}{\Delta W_{H_2O}-\Delta W_N}-\kappa_A(1-\rho/\rho')\right]1/\rho,$$

where X is the gram susceptibility, ΔW_p is the apparent change in weight of the Gouy tube (upper half filled with powder) occasioned by the magnetic field, κ is the cm^3 susceptibility, ρ is the density of the powdered sample, and ρ' is the density of the solid component of the powder.

The subscripts p, N, H_2O, and A refer to the powdered sample, nitrogen, water, and air, respectively.

The Gouy tube was calibrated with water distilled through a Barnstead still and reboiled, immediately before measurement, to expel oxygen. The cm^3 susceptibility[5] of this water was assumed to be -0.720×10^{-6} at 20°C. The calibration was checked with benzene purified according to the procedure described previously.[6] The value obtained for the benzene, using the above value for water, was -0.706×10^{-6} at 26°C, which is in satisfactory agreement with the value -0.7020×10^{-6} at 20°C found by French and Trew.[7]

The correction for air in the powdered samples was made in the manner described by Hutchison and Elliott.[8]

Magnetic measurements were made at field strengths corresponding to potentiometer readings of 20.00 mv and 40.00 mv. These field strengths, as estimated from the data used to calibrate the Gouy tube, were 6.4 and 9.3 kilogauss respectively.[9]

[1] W. Rüdorff, Zeits. f. anorg. u. allg. Chem. **245**, 383 (1941).
[2] International Critical Tables, Vol. 6, p. 354.
[3] J. H. Van Vleck, *Electric and Magnetic Susceptibilities* (Oxford University Press, London, 1932), pp. 232–235.
[4] S. Freed, J. Am. Chem. Soc. **52**, 2705 (1930).
[5] P. W. Selwood, *Magnetochemistry* (Interscience Publishers, Inc., New York, 1943), pp. 45–46.
[6] M. Goldsmith and G. W. Wheland, J. Am. Chem. Soc. **70**, 2632 (1948).
[7] C. M. French and V. C. G. Trew, Trans. Faraday Soc. **41**, 439 (1945).
[8] C. A. Hutchison, Jr. and N. Elliott, J. Chem. Phys. **16**, 924 (1948).
[9] E. C. Stoner, *Magnetism and Atomic Structure* (Methuen and Co. Ltd., London, 1926), p. 40.

TABLE I. Magnetic susceptibilities of graphite and bromine-graphite.

Temp. (°K)	Composition (g Br/g C)	Density (g cm^{-3})	Approximate field strength (kilogauss)	$-\Delta W_p$ (mg)	$-X\times10^6$
305	0	0.854	9.3	37.9	5.23
305	0	0.854	6.4	18.2	5.29
75.6	0	0.854	9.3	53.2	7.38
302	0	0.855	9.3	37.3	5.15
302	0	0.855	6.4	18.0	5.22
298	0	0.871	9.3	39.1	5.29
298	0	0.871	6.4	18.7	5.32
75.0	0	0.871	9.3	54.5	7.43
298	0.051	0.671	9.3	23.6	4.17
298	0.051	0.671	6.4	11.3	4.20
75.6	0.051	0.671	9.3	30.2	5.41
75.6	0.051	0.671	6.4	14.4	5.42
296	0.051	0.694	9.3	24.1	4.13
76.0	0.051	0.694	9.3	31.0	5.37
298	0.67	0.881	9.3	1.99	0.31
298	0.67	0.881	6.4	0.932	0.31
75.6	0.67	0.881	9.3	1.38	0.29
299	0.71	0.856	9.3	1.95	0.31
75.6	0.71	0.856	9.3	1.25	0.29

The values of ΔW_N, 0.098 mg at 6.4 kilogauss and 0.184 mg at 9.3 kilogauss, were temperature independent from 75°K to room temperature. The "tube constant," $(\Delta W_{H_2O}-\Delta W_N)/\kappa_{H_2O}$, was 4.068×10^6 at 6.4 kilogauss and 8.558×10^6 at 9.3 kilogauss.

Chemical Preparations and Analyses

Bromine-graphite samples were prepared from "SP-1" spectroscopic graphite powder obtained from the National Carbon Company. Spectrographic analysis of this powder revealed less than 1 part per million of the following elements: Ag, B, Be, Bi, Cr, Cu, Fe, Li, Mg, Mn, Ni, Sb, Sn, Ti, and V; less than 2 p/m of: Ba, Co, Na, and Si; less than 20 p/m of: Al, As, Hg, K, Pb, Sr, Zn, and Zr.

The powdered graphite was allowed to stand in a desiccator over Merck Reagent grade bromine for 24 hours; after this time the sample was transferred as rapidly as possible to a Gouy tube. The open Gouy tube was then placed for an additional 24 hours in an atmosphere saturated with bromine vapor.

When its susceptibility had been determined, the weighed sample was transferred to an open weighing bottle which was allowed to stand first in air and then over KOH until it had come to constant weight. The bromine which still remained was determined by combustion of the sample and subsequent precipitation of AgBr. It was found that the bromine-graphite samples contained approximately 0.7 g Br/g C before exposure to air and approximately 0.05 g Br/g C after standing over KOH.

RESULTS AND DISCUSSION

Experimental data and results are tabulated in Table I.

In correcting for the susceptibility of air in the various powders, the x-ray densities of graphite, bromine-graphite containing 0.05 g Br/g C, and bromine-graphite containing 0.7 g Br/g C have been assumed to be 2.25, 2.3, and 2.6 g/cm^3, respectively.

The assumption that the vapor pressure of bromine above bromine-graphite is no greater than the vapor tension of liquid bromine at the same temperature enables one to neglect the contribution of bromine vapor to the magnetic suceptibility of bromine-graphite.

The values in Table I do not indicate the presence of a ferromagnetic impurity; such an impurity would cause the measured susceptibilities to be less diamagnetic at the lower field strength. That the finely powdered graphite crystals have a random, or at least a constant, orientation in the tightly packed Gouy tube is indicated by the precision of the measurements which is within the ±2 percent usually obtainable when isotropic powders are measured by the Gouy method.

If it is assumed that all the intercalated bromine is present as free bromine molecules, the susceptibility of bromine-graphite may be calculated from Wiedmann's Law:

$$mX=\sum_i m_iX_i,$$

where m is the weight of the mixture, X the gram susceptibility of the mixture, m_i the weight of the ith component of the mixture, and X_i the susceptibility of that component. Applying the appropriate data from Table I and taking the gram susceptibility of molecular bromine[2] to be -0.4×10^{-6}, we obtain -3.3×10^{-6} at 298°K and -4.5×10^{-6} at 75.6°K as values of the susceptibility of a bromine-graphite sample containing 0.7 g Br/g C. These values are in serious disagreement with the observed values: -0.31×10^{-6} at 298°K and -0.29×10^{-6} at 75.6°K.

On the other hand, the assumption that the sample discussed in the preceding paragraph contains only atomic bromine leads, if one assumes complete quenching of the orbital contribution to the susceptibility, to the values: $+3.3\times10^{-6}$ at 298°K and $+21.2\times10^{-6}$ at 75.6°K. The differences between observed and calculated values are found to be even greater if one assumes no quenching of the orbital angular momenta.

It is believed that a qualitative explanation of the observed susceptibilities may be given in terms of the band theory of solids. Using the "tight-binding" approximation, Peierls[10] has shown that an important contribution to the susceptibility of an intrinsic semiconductor, such as graphite, is dependent upon the integration, over the surface of the Fermi distribution of

[10] R. Peierls, Zeits. f. Physik **80**, 786 (1933).

occupied energy states, of the quantity

$$\frac{1}{|\mathrm{grad}_k E|}\left\{\frac{\partial^2 E}{\partial k_x^2}\frac{\partial^2 E}{\partial k_y^2}-\left(\frac{\partial^2 E}{\partial k_x \partial k_y}\right)^2\right\},$$

where, within the confines of a given Brillouin zone, the values of energy (E) which may be assumed by a conduction electron are approximated as the range of a continuous function of the wave vector k, whose components are k_x, k_y, and k_z. (The magnetic field is parallel to the z direction.) It has been re-emphasized by Wallace[11] that the "Peierls diamagnetism" of the graphite is strongly dependent upon those electrons which are near the top of the first zone and those near the bottom of the second zone; in addition, Wallace calculated that the number of electrons in the second zone is only a small fraction of 1 percent of the total number of conduction electrons. One would therefore expect that the removal of these electrons from the second zone would appreciably affect the diamagnetism of graphite; thus the formation of a relatively small number of carbon-bromine covalent or ionic bonds could account for the observed susceptibilities of the bromine-graphite mixtures. This point of view is supported by the fact that the gram susceptibility at room temperature of a bromine-graphite sample containing only 0.05 g Br/g C is 20 percent lower than the susceptibility of pure graphite.

Our data together with those of Rüdorff[1] indicate the possible presence of both molecular bromine and a small number of carbon-bromine bonds in bromine-graphite.

[11] P. R. Wallace, Phys. Rev. **71**, 622 (1947).

THE JOURNAL OF CHEMICAL PHYSICS VOLUME 18, NUMBER 4 APRIL, 1950

Argon Repulsive Potential from Collision Cross-Section Measurements

I. Amdur, D. E. Davenport, and M. C. Kells
Department of Chemistry, Massachusetts Institute of Technology, Cambridge, Massachusetts
(Received November 10, 1949)

The total collision cross section has been measured for argon atoms, with energies between 300 and 1100 electron volts, scattered in room temperature argon. In the region between 700 and 1000 volts, the cross section shows a maximum indicative of inelastic scattering, probably due to ionization by the high energy atoms.

The repulsive potential between two argon atoms has been evaluated from elastic collision cross sections (deduced from observed values of the total collision cross section) using a method which takes account of the greater probability of small angle scattering by averaging the cross section over the length of the scattering path. The results may be expressed by

$$V(r)=4.61\times10^{-11}/r^{4.33}\ \text{ergs}$$

or

$$V(r)=3.66\times10^{-8}\exp(-6.88r^{\frac{1}{2}})\ \text{ergs}$$

for values of r between 1.37 and 1.84A.

HIGH velocity argon atoms, with energies in the range 300–1100 electron volts, have been scattered in room temperature argon to obtain experimental values of the total collision cross section, as part of a program for the determination of repulsive potentials at close distances of interaction.

EXPERIMENTAL

The apparatus and experimental procedure were essentially those previously described[1] in connection with the measurement of total collision cross sections of high velocity hydrogen atoms scattered in room temperature molecular hydrogen. In the present experiments, the single-junction radiation thermocouple originally used as the detector was replaced by a forty-junction thermopile kindly supplied for the purpose by Professor L. Harris.[2] The receiver surface of the new detector was square, 0.254 cm on a side, and was covered symmetrically with a circular mask, 0.132 cm in diameter. The geometric average angular aperture of the detector was 2.88°, and was computed by averaging linearly, with respect to distance along the beam axis, all half-angles subtended by the detector at its fixed position, 7.738 cm from the origin of the beam. The essential features of the scattering path which determine the geometric average angular aperture are shown in Fig. 1. In calculating the average aperture, it is necessary to take cognizance of the angular limitations imposed by the tip of the second collimating channel, the lower edge of the detector mask, and the edge of the thermopile. This is done by dividing the scattering path into three sections, each characterized by a range of angle, θ_1, θ_2, or

[1] I. Amdur and H. Pearlman, J. Chem. Phys. **8**, 7 (1940).

[2] L. Harris, J. Opt. Soc. Am. **36**, 597 (1946).

TABLE I. Summary of collision cross-section results.

Voltage	$\bar{S}$ A²	S A²	$\bar{L}$ cm	Percent error (±)
300	10.10	10.52	0.0280	2.7
400	9.91	9.38	0.0286	2.2
500	8.39	8.50	0.0377	2.4
600	7.78	7.78	0.0364	1.7
700	7.39	7.19	0.0383	1.8
800	7.58	6.72	0.0373	1.8
900	7.18	6.37	0.0394	1.8
1000	6.31	6.10	0.0448	1.3
1100	5.85	5.86	0.0484	2.7

θ_3, through which a beam particle may be scattered and still strike the detector.

Total collision cross sections were computed, as heretofore, from ratios of beam intensities after traversing the scattering path containing argon at two different pressures. A total of 139 determinations were made, from 8 to 24 at each voltage, and the usual tests were applied for the absence of multiple scattering, namely, constancy, at a given voltage, of cross sections computed from runs in which widely different scattering pressures were used. The final results of the present experiments are summarized in Table I which includes values of $\bar{S}$, the arithmetic average of all total collision cross sections measured at a given voltage, S, *elastic* collision cross sections as read from the smooth curve which eliminates the maximum near 800 volts as shown in Fig. 2, and $\bar{L}$, the average mean free path at 1 mm of Hg and 0°C computed from the relation

$$\bar{L}=1/(n\bar{S})$$

where n is the number of scattering molecules at 1 mm of Hg and 0°C. The percentage errors are the probable errors of the tabulated $\bar{S}$ and $\bar{L}$ values. The purity of the argon used in the experiments was better than 99.6 percent.

DISCUSSION

A. Inelastic Scattering

The relative maximum at 800 volts in Fig. 2 is assumed to be due to ionization of the argon scattering gas by the argon beam for the following reasons:

1. In the absence of diffraction effects (a condition which is met in the present experiments since the de Broglie wave-length of the scattering system is extremely small compared to the collision radius), the collision cross section should everywhere decrease with increasing voltage if the repulsive potential between two argon atoms depends only upon the separation distance.

2. Rostagni[3] and Berry[4] have measured ionization cross sections for argon atoms in argon in the energy ranges 0–1000 and 1000–5000 volts, respectively. The absolute values of their cross sections are somewhat uncertain due to experimental difficulties, but both investigators agree on a value of the order of 1A². Although Rostagni's results do not show the effect, Berry states that the correct ionization curve would exhibit a maximum between 700 and 1000 volts. The smooth curve in Fig. 2 which is taken to represent elastic collision cross sections indicates that the increment in cross section due to ionization at 800 volts is about 0.9A² in agreement with the order of magnitude value of the ionization cross section as determined by Rostagni and by Berry.

Although it is possible that a slight maximum exists near 400 volts, it has not been shown in Fig. 2 since the deviations of the 300- and 400-volt points from the smooth curve are not sufficiently greater than the probable errors shown in Table I.

B. Calculation of Repulsive Potential

Since the angular aperture of the present detecting system is sufficiently large to eliminate diffraction effects, the total elastic cross sections of Table I may be used to calculate the repulsive potential for the A–A system using classical scattering theory. As shown recently in connection with the recalculation of the repulsive potentials for the He–He and H–H_2 systems,[5] it is necessary to take account of the variation of scattering intensity with angle by averaging the theoretical expression for the total elastic cross section over the entire scattering path, 7.738 cm, in the present case. A procedure for carrying out this averaging process when the potential function, $V(r)$, can be represented by K/r^n, where r is the separation distance, was originally

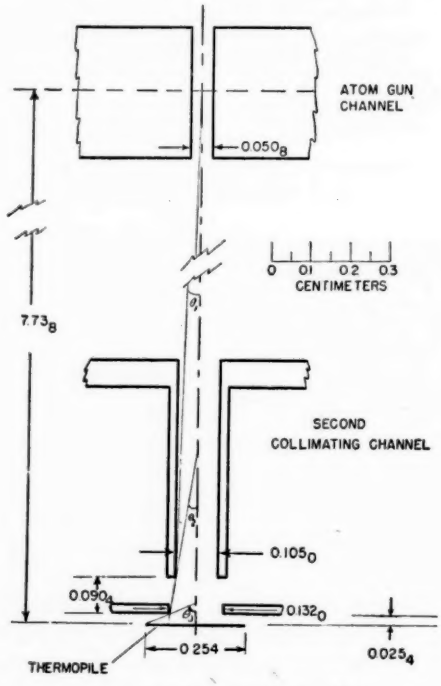

FIG. 1. Details of scattering path.

[3] A. Rostagni, Nature 134, 626 (1934); Nuovo Cimento 12, 134 (1935); 13, 389 (1936).
[4] H. W. Berry, Phys. Rev. 62, 378 (1942).
[5] I. Amdur, J. Chem. Phys. 17, 844 (1949).

suggested by Simons, Fontana, Muschlitz, and Jackson[6] and by Simons, Muschlitz, and Unger[7] and improved by Kells[8] for the case of small angle scattering which is treated by Kennard.[9] Kells' treatment is applicable in the present case and leads to the following relations

$$S=(\pi/l)\int_0^l b^2dx$$
$$=(\pi/l)\int_0^l r_0^2dx-[2K\pi/(\mu v^2 l)]\int_0^l r_0^{2-n}dx$$
$$=(\pi/l)[KC/(\mu v^2)]^{2/n}(\phi-2\psi/C), \quad (2)$$

where

$$\phi=\int_0^{7.271}[(7.622-x)/0.0515]^{2/n}dx$$
$$+\int_{7.271}^{7.698}[(7.713-x)/0.0660]^{2/n}dx$$
$$+\int_{7.698}^{7.738}[(7.738-x)/0.1796]^{2/n}dx \quad (3)$$

and

$$\psi=\int_0^{7.271}[(7.622-x)/0.0525]^{(2-n)/n}dx$$
$$+\int_{7.271}^{7.698}[(7.713-x)/0.0660]^{(2-n)/n}dx$$
$$+\int_{7.698}^{7.738}[(7.738-x)/0.1796]^{(2-n)/n}dx. \quad (4)$$

Symbols in Eq. (2) which have not been defined previously are: l, length of scattering path, 7.738 cm; x, any point on the scattering path; b, impact parameter defined by $b^2=[1-2V(r_0)/(\mu v^2)]r_0^2$; r_0, distance of closest approach of centers of beam particle and scatterer; μ, reduced mass of scattering system; v, relative initial velocity of scattering system; and C, a constant, $\pi^{\frac{1}{2}}\Gamma(n/2+\frac{1}{2})/\Gamma(n/2)$. The separate integrals which appear in Eqs. (3) and (4) arise from the necessity, previously referred to, of dividing the scattering path into three sections as follows: 7.271 cm in which the scattering is limited by the tip of the second collimating channel, 0.427 cm (from $x=7.271$ to $x=7.698$) in which the scattering is limited by the lower edge of the detector mask, and the remaining 0.040 cm of path in which the thermopile surface itself is the limiting factor. For simplicity, it has been assumed that this surface may be approximated by the area of a circle, 0.1796 cm in radius, which can be circumscribed about the actual square receiver. Since this approximation enters into only 0.040 cm of the scattering path, the error introduced is negligible, less than 0.1 percent.

The potential function is obtained by taking logarithms of both sides of Eq. (2), whereupon a straight line relation should result between $\log S$ and $\log(\mu v^2)$ in which the slope, $-2/n$, gives the index of r, and the intercept, $(\pi/l)(KC)^{2/n}(\phi-2\psi/C)$, gives the constant, K, in the expression $V(r)=K/r^n$. The extent to which the straight line relation is valid is a direct measure of the ability of the expression K/r^n to represent the variation of potential energy with separation distance. The method of least squares was used to obtain the equation

$$\log S=-0.462\log(\mu v^2)$$
$$-19.2780\ (\mu v^2 \text{ in ergs; } S \text{ in cm}^2) \quad (6)$$

whose calculated S values show a maximum deviation of 1.2 percent and an average absolute deviation of 0.6 percent from the values of Table I. Accordingly, the assumed potential form is valid and the required function is

$$V(r)=1.08\times10^{-45}/r^{4.33}\text{ ergs } (r \text{ in cm}) \quad (7)$$

or

$$V(r)=4.61\times10^{-11}/r^{4.33}\text{ ergs } (r \text{ in A}), \quad (8)$$

for values of r in the range 1.37–1.84A. Equation (8) is equivalent, within 0.9 percent, to

$$V(r)=3.66\times10^{-8}\exp(-6.88r^{\frac{1}{2}})\text{ ergs } (r \text{ in A}), \quad (9)$$

which is shown in graphical form in Fig. 3.

The potential calculated from Eqs. (8) or (9) is 0.33 that obtained by assuming that the average relative angular deflection of a beam particle which just misses the detector is 5.76°, twice the geometric average angular aperture of the detecting system. This illustrates the importance of calculating potentials by taking account of the distribution of scattered intensity with angle along the scattering path, since the *effective* relative angular aperture for scattering is, in the present case, only one-third of the geometric average relative angular aperture.

After the present experiments had been completed, results on the scattering of 500–3500 electron volt argon

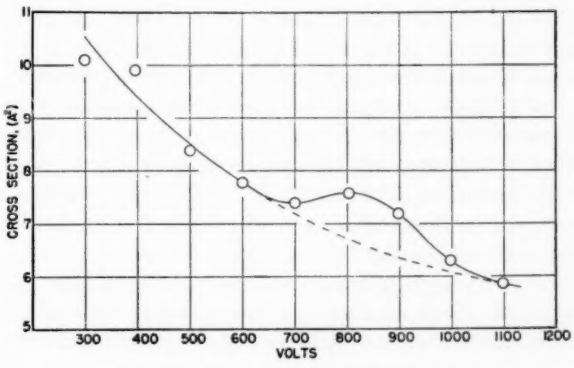

FIG. 2. Total collision cross sections.

[6] Simons, Fontana, Muschlitz, and Jackson, J. Chem. Phys. **11**, 307 (1943).
[7] Simons, Muschlitz, and Unger, J. Chem. Phys. **11**, 332 (1943).
[8] M. C. Kells, J. Chem. Phys. **16**, 1174 (1948).
[9] E. H. Kennard, *Kinetic Theory of Gases* (McGraw-Hill Book Company, Inc., New York, 1938), pp. 115 ff.

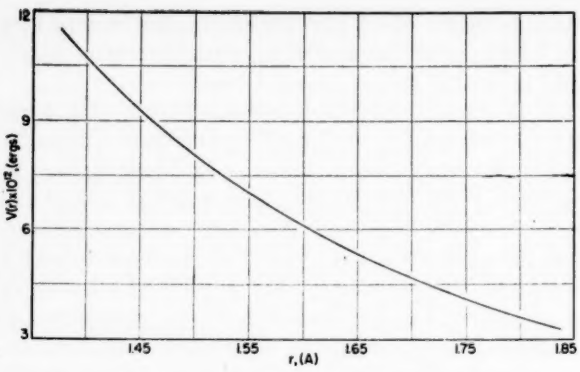

FIG. 3. Repulsive potential between two argon atoms.

atoms in argon were published by Berry.[10] His method involved the measurement of the intensity of scattered beam particles, in terms of the number of secondary electrons ejected from a tantalum detector, as a function of angle over as wide a range as possible. Collision cross sections were calculated from the relation $S=\int_\theta^\pi f(\theta_r)d\theta_r$ where $f(\theta_r)$ is the polar scattering coefficient for the relative angle of scattering, θ_r, and may be defined by the condition that $f(\theta_r)d\theta_r$ shall represent the fraction of the beam molecules incident on unit area which are scattered by one scattering molecule in all directions making an angle between θ_r and $\theta_r+d\theta_r$ with the direction of the incident beam. Berry deduced a repulsive potential in graphical form for separation distances between 0.6 and 1.2A. Although the potential derived from the present experiments is valid only between 1.37 and 1.84A, comparison of numerical values of the respective potentials at 1.2A and 1.37A indicates that, if the energy range had been extended in the two investigations so as to obtain repulsive potentials covering the same range of separation distance, Berry's potential would be considerably larger than that shown in Fig. 3, but that order of magnitude agreement would exist. It is not possible to account for the disparity without more detailed information than that given in Berry's paper, but the following factors might be responsible for the disagreement: (1) the use of approximate methods to obtain $f(\theta_r)$ for θ_r greater than 90° due to low accuracy in measurement of intensity and angular position at the larger angles; and (2) the effect of the presence of scattering gas upon the efficiency of secondary electron emission from the tantalum detector. The authors feel that, in view of the much greater difficulty in obtaining accurate cross sections by measuring scattered intensities as a function of angle at all angles, as compared with the measurement of axis intensities at two scattering pressures, the probable order of magnitude agreement between the two potentials should not be considered unsatisfactory.

A word of caution seems in order with respect to the danger of extrapolating potential energy functions, derived for separation distances near the minimum, to the very small distances involved in the scattering of atoms with energies of the order of hundreds or thousands of electron volts. For example, Berry finds that the repulsive portion of a potential function deduced from experimental values of the second virial coefficient by Buckingham,[11]

$$V(r)=1.69\times10^{-8}\exp(-r/0.273)\text{ ergs }(r\text{ in A}),\quad(10)$$

when extrapolated to $r=0.6$ to 1.2A, agrees well with his potential. Yet, the repulsive portion of the potential function deduced from the lattice constant and heat of sublimation of solid argon by Herzfeld and Goeppert-Mayer,[12]

$$V(r)=1.34\times10^{-9}\exp(-r/0.345)\text{ ergs }(r\text{ in A}),\quad(11)$$

when similarly extrapolated, gives $V(r)$ values which are eightfold smaller at 0.6A and fivefold smaller at 1.2A than those of Buckingham. Finally, the repulsive portion of a potential function also deduced from the lattice constant and heat of sublimation of solid argon by Kane,[13]

$$V(r)=8.30\times10^{-7}\exp(-r/0.2091)\text{ ergs }(r\text{ in A}),\quad(12)$$

gives $V(r)$ values which are twenty-six fold greater at 0.6A and thirteen-fold greater at 1.2A than those of Buckingham. At 3.6A, which is the approximate distance of closest approach of two argon atoms at room temperature, the energies of repulsion as calculated from Eqs. (10)–(12) agree quite well, the values being 3.2×10^{-14}, 3.8×10^{-14}, and 2.8×10^{-14} ergs, respectively. Since at this distance, the repulsive potential is a minor fraction of the net potential, which is attractive, the agreement among the net potentials is even better due to compensation of the slightly different attractive terms for the discrepancies in the repulsive terms. Because of this compensation, and the fact that the experimental information upon which the potential functions are based are not likely to involve interaction distances much smaller than that at which $V(r)$ is zero, or much larger than that at which $V(r)$ is a minimum (about 3.4A and 3.8A, respectively for argon), the repulsive portion of the potential taken by itself is not of much significance, particularly when extrapolated far beyond the original range of validity. Even in the case of helium, where satisfactory theoretical calculations of the repulsive potential alone have been made for r as small as 1A, and where the calculated potential and that derived from scattering experiments agree well at 1A, extrapolation to 0.52A results in a discrepancy of over 100 percent.[5]

ACKNOWLEDGMENT

The authors wish to express their thanks to Mr. L. O. Mitchell for technical assistance.

[10] H. W. Berry, Phys. Rev. **75**, 913 (1949).

[11] R. A. Buckingham, Proc. Roy. Soc. **168**, 264 (1938).

[12] K. F. Herzfeld and M. Goeppert-Mayer, Phys. Rev. **46**, 995 (1934).

[13] G. Kane, J. Chem. Phys. **7**, 603 (1939).

Time Lag in the Nucleation of Supercooled Water Clouds by Silver Iodide Smokes*

HOWARD REISS
Department of Chemistry, Boston University, Boston, Massachusetts
(Received November 14, 1949)

A mechanism is proposed by means of which the time lag in phase transitions initiated by foreign bodies may be calculated. Calculations are performed for silver iodide nucleating supercooled water clouds, and the results are compared with experimental data.

I. INTRODUCTION

RECENTLY, B. Vonnegut[1,2] discovered that silver iodide smokes were able to transform supercooled water clouds into large numbers of ice crystals. He assumed that the structural similarity between ice and silver iodide enabled the latter to "trick" the surrounding water vapor into condensation on its surface, the transition being vapor to ice, directly. The net process, then, consisted of the evaporation of water droplets in favor of the ice crystals.

Vonnegut observed a very curious fact about the course of the transition, namely, that not every silver iodide particle could immediately be an ice nucleus, but that a particle reached this state, only, after the passage of a random period of time. It is the purpose of this paper to inquire into the nature of this behavior.

II. THE SUB-CRITICAL HYPOTHESIS

Vonnegut suggested that the time lag was associated with the arrangement of the condensate molecules into an orderly lattice; a chance occurrence. This viewpoint must, of course, be partly correct, but it can be reformulated as part of a more general scheme which is applicable to liquid droplets as well as crystals. This scheme shall be called the *sub-critical hypothesis*.

It is well known that the condensation of a supersaturated vapor can occur only when there are present, in the body of the vapor, small embryos[3] of the condensed phase which have attained certain critical dimensions (self-nucleation). Sometimes, condensation can be facilitated by the presence of a foreign bodies whose surfaces are "wetted" by the vapor, i.e., upon whose surfaces the condensation of the vapor can occur with a decrease of free energy (foreign nucleation). If the over-all dimensions of a foreign particle "wetted," in this manner, are greater than the critical dimensions, mentioned above, then the particle can continue to collect vapor by means of a process involving a decrease in free energy, and a stable fragment of the condensed phase will be formed. *Every* particle of this size will be a nucleus.

On the other hand, suppose that the "wetted" particle is below the critical size. After the initial decrease in free energy, associated with the wetting process, the particle can only continue to collect vapor by means of a process involving an increase of free energy, at least, until it attains critical dimensions. Under this restriction the attainment of critical dimensions (becoming a nucleus) is a chance occurrence with which a time lag must be associated. The sub-critical wetted particle behaves, approximately, as a sub-critical embryo.

This scheme has significance, not only for crystal formation, but also for processes which do not include orientational steps, e.g., the formation of droplets. In the former case the orientational factor, mentioned by Vonnegut, must, surely, be operative, and acts, undoubtedly to reduce the chance of attaining the critical size.

Accordingly, the sub-critical hypothesis supposes that only foreign bodies having sub-critical dimensions will exhibit the time lag effect.

On the basis of this hypothesis it is interesting to consider why this effect has not been reported, previously (except for the case of self-nucleation). An examination of the critical sizes corresponding to various degrees of supersaturation indicates that, generally, they are quite small. Only the lowest, significant degree of supersaturation will permit the critical radius to be as large as 10^{-6} cm. In systems where the degree of supersaturation is so low, there is not enough condensate available to form particles of appreciable size. This means that foreign bodies which are to exhibit the time lag effect must be so small that they cannot conveniently be subjected to experiment, or else, the supersaturation must be so low that no appreciable disperse system of condensate can form.

The nucleation of supercooled water clouds constitutes a special case. Although, here, it is true that the degree of supersaturation is quite low, being determined by the vapor pressure of supercooled water relative to that of ice, the droplets in the cloud are able to supply water vapor continually by evaporating so that the ice crystals grow to appreciable size, in spite of the low degree of supersaturation. The vapor pressure in the cloud remains essentially constant during the major course of the transition. Furthermore, because of the low supersaturation, the critical size is large enough

* This work has been made possible through the sponsorship of the Geophysical Research Directorate of the Air Force Cambridge Research Laboratories under Contract No. AF 19 (122)-168.

[1] B. Vonnegut, Chem. Rev. 44, 277 (1949).
[2] B. Vonnegut, J. App. Phys. 18, 593 (1947).
[3] Frenkel, *Kinetic Theory of Liquids* (Oxford University Press, London, 1946), p. 374.

so that the silver iodide particles can exhibit the time lag effect.

III. CALCULATION OF THE TIME LAG

The time lag will be calculated upon the assumption that the condensation does not involve an orientational step. Since the transition does lead to the formation of ice, an error in viewpoint is introduced at the outset. However, the data, currently available is so inexact that no more than a semiquantitative comparison of theory and experiment is possible, even under the most favorable circumstances. Under these conditions the simplification introduced by the omission of the orientational factor is desirable.

The present author hopes to conduct experiments which will provide more quantitative data. When these data are available it may be necessary to solve the more exact problem.

According to a theory proposed by Becker and Doring[4] and fortified by Zeldovich[5] *self-nucleation* can be regarded as a process in which sub-critical embryos grow, stepwise, by the acquisition of single molecules. In this manner, during the transition, a distribution of embryos among all possible sizes is set up in which the concentration of embryos containing g molecules can be represented at the time, t, by the function, $f(g, t)$. This function satisfies the following partial differential equation.[6]

$$\frac{\partial f}{\partial t}=\frac{\partial}{\partial g}\left(D\frac{\partial f}{\partial g}\right)+\frac{1}{kT}\frac{\partial}{\partial g}\left(Df\frac{\partial \Delta\varphi}{\partial g}\right), \tag{1}$$

where

$$D=\frac{(4\pi)^{\frac{1}{3}}(3v)^{\frac{2}{3}}p}{(2\pi mkT)^{\frac{1}{2}}}g^{\frac{2}{3}}=Rg^{\frac{2}{3}} \tag{2}$$

$$\Delta\varphi=-\left(kT\ln\frac{p}{p_0}\right)g+4\pi\sigma\left(\frac{3v}{4\pi}\right)^{\frac{2}{3}}g^{\frac{2}{3}}$$

$$=-kTAg+kTBg^{\frac{2}{3}}. \tag{3}$$

In these expressions p is the constant vapor pressure, p_0 is the saturation vapor pressure, k is the Boltzman constant, v is the molecular volume in the condensed phase, m is the molecular mass, σ is the tension of the vapor-condensate interface, and T is the absolute temperature. Comparison of (1) with the equation of continuity[7] reveals that the flux of embryos, $I(g, t)$, passing through the size, g, at the time, t, is

$$I(g, t)=-D(g)N(g)\frac{\partial}{\partial g}\left(\frac{f(g, t)}{N(g)}\right), \tag{4}$$

where

$$N(g)=ce^{-\Delta\varphi/kT}, \tag{5}$$

c, being the concentration of single molecules at the pressure, p, and temperature, T. $N(g)$ is the equilibrium distribution of embryos at this temperature and pressure. If

$$g^*=(2B/3A)^3 \tag{6}$$

represents the critical size, then, the nucleation rate is given by $I(g^*, t)$.

Now, the preceding equations are only valid when the pressure, p, remains constant, and the vapor molecules conserve a Maxwellian distribution. Therefore, any results derived from them can be valid only at the inception of the nucleation process, and as much information as will have any meaning can be obtained if it is assumed that a stationary state exists in which I is independent of g and t, f depends only upon g, and $f(\infty)=0$.

Under this assumption it is an easy matter to compute the depencence of I upon p/p_0, the *supersaturation ratio*. It turns out that as this ratio is increased a critical value is reached at which I increases suddenly (but not discontinuously) from almost zero to almost infinity. The entire phase transition seems to take place at this critical value of the supersaturation ratio. The critical ratios computed, in this manner, compare well with those obtained experimentally.

It can also be demonstrated that whenever the degree of supersaturation is less than the critical value $f(g)$, like I itself, is practically zero for all $g>30$.

The preceding ideas will be utilized in calculating the time lag in foreign nucleation. However, Eq. (1) will appear as part of a new boundary value problem, and unlike the procedure used by Becker, Doring, and Zeldovich for the discussion of *self-nucleation*, we shall attempt to obtain the time-dependent solution of this problem. In all cases the degree of supersaturation will be below the critical value, and the conditions just mentioned will exist. It may be imagined that foreign particles, equal in size to embryos for which $g=\gamma>30$, are introduced at the zero of time, and are wetted in such a manner that they behave like embryos of size, γ, with the one exception that, unlike real embryos, they cannot reduce their size to values of g less than γ. In the interval, $\gamma\leqslant g\leqslant\infty$, the initial distribution of embryos may be represented as

$$\begin{aligned} &f(\gamma, 0)=P \\ &f(g, 0)=0, \quad \gamma<g\leqslant\infty, \end{aligned} \tag{7}$$

where P is the concentration of foreign particles of size, γ. In writing (7) it has been assumed, in accordance with what has been said above, that the concentration of real embryos in this interval may be regarded as zero. In consequence of this, and also because the foreign particles are unable to reduce their size below the value, γ,

$$I(\gamma, t)=0$$

[4] Becker and Doring, Ann. d. Physik **24**, 719 (1935).
[5] Zeldovich, J. Exp. Theor. Phys. (Russia) **12**, 525 (1942).
[6] See reference 3, p. 394.
[7] Slater and Frank, *Introduction to Theoretical Physics* (McGraw-Hill Book Company, Inc., New York, 1932), p. 187.

or by reference to (4)

$$\partial/\partial g(f/N)_{g=\gamma}=0. \tag{8}$$

Of course,

$$f(\infty, t)=0. \tag{9}$$

The rate at which foreign particles become nuclei in this system is determined by $I(g^*, t)$, and this function can be derived by the application of (4) to the solution of the boundary value problem defined by (1), (7), (8), and (9), i.e.,

$$\frac{\partial f}{\partial t}=\frac{\partial}{\partial g}\left(D\frac{\partial f}{\partial g}\right)+\frac{1}{kT}\frac{\partial}{\partial g}\left(Df\frac{\partial \Delta\varphi}{\partial g}\right)$$

$$f(\gamma, 0)=P$$

$$f(g, 0)=0, \quad \gamma<g\leqslant\infty$$

$$\frac{\partial}{\partial g}\left(\frac{f}{N}\right)_{g=\gamma}=0, \quad t>0$$

$$f(\infty, t)=0, \quad t>0.$$

In contrast to the situation in the case of self-nucleation, the time dependent solution of (1) *has* physical significance when it is applied to nucleation in supercooled water clouds. In this case the pressure, p, which is the vapor pressure of supercooled water is, as has been mentioned, conserved during the major part of the transition. p_0 is the vapor pressure of ice.

This boundary value problem is quite similar to certain diffusional problems treated by the author in a recent paper.[8] These belonged to a certain limiting class to which a simplifying approximation could be applied. The above problem also belongs to this class. The reason lies in the fact that the flux of embryos through any size, g, is much larger than the rate of change of concentration, $\partial f/\partial t$, at g. Consequently (1) may be replaced by the approximate equation

$$0=\frac{\partial}{\partial g}\left(D\frac{\partial f}{\partial g}\right)+\frac{1}{kT}\frac{\partial}{\partial g}\left(Df\frac{\partial \Delta\varphi}{\partial g}\right)$$

which yields, upon quadrature,

$$I(t)=-D(g)N(g)\frac{\partial}{\partial g}\left(\frac{f(g, t)}{N(g)}\right). \tag{11}$$

In view of (11) which states that the flux defined by (10) is independent of g, condition (8) which demands that the flux be zero, at γ, cannot be applied without rendering the solution of (10) trivial. Fortunately, it can be replaced by an alternative condition which has approximately the same physical significance. In order to see this it is necessary to realize that the net effect of (8) is to require that all embryos which pass out of the system at $g=\infty$, originate within the interval, $\gamma\leqslant g\leqslant\infty$. This follows from the requirement that no embryos penetrate the boundary at γ. Now, at γ, the concentration, f, decreases so rapidly in the direction of increasing g (at all times) that $f(\gamma, t)$ almost equals the total concentration of embryos, summed over the entire interval, $\gamma\leqslant g\leqslant\infty$. According to (8), the rate of decrease of this sum must be the negative of the flux of embryos penetrating the boundary, at infinity, i.e.

$$-(\partial f/\partial t)_{g=\gamma}=I(\infty, t)=I(t). \tag{12}$$

Equation (12) can be utilized in place of (8), and is, in no way, inconsistent with (10).

It is also not possible to apply the discontinuous initial condition (7) to (10), for no solution of the latter can satisfy it. If (7) is weakened so that it assumes the form

$$\begin{aligned} f(\gamma, 0)&=P \\ f(\infty, 0)&=0 \end{aligned} \tag{13}$$

it will then be applicable to (10). Furthermore, the function, $f(g, 0)$ so determined, will nearly satisfy (7), anyhow, because of its sharp decrease, in the direction of increasing g, mentioned above. In this manner, a new, approximate boundary value problem can be formed from (10), (13), (12), and (9).

$$0=\frac{\partial}{\partial g}\left(D\frac{\partial f}{\partial g}\right)+\frac{1}{kT}\frac{\partial}{\partial g}\left(Df\frac{\partial \Delta\varphi}{\partial g}\right)$$

$$f(\gamma, 0)=P$$

$$f(\infty, 0)=0$$

$$-\left(\frac{\partial f}{\partial t}\right)_{g=\gamma}=I(t)$$

$$f(\infty, t)=0.$$

This procedure is more thoroughly justified in another place.[8] The approximate boundary value problem will now be solved.

The solution of (10) is obtained upon integrating (11). The result is

$$f(g, t)=-I(t)N(g)\int_\gamma^g\frac{dg}{D(g)N(g)}+\frac{N(g)}{N(\gamma)}f(\gamma, t). \tag{14}$$

Integration of (12), subject to the first part of (13) yields

$$f(\gamma, t)=P-\int_0^t I(t)dt \tag{15}$$

and this expression, substituted into (14) gives

$$f(g, t)=-I(t)N(g)\int_\gamma^g\frac{dg}{D(g)N(g)}+\frac{N(g)}{N(\gamma)}\left[P-\int_0^t I(t)dt\right]. \tag{16}$$

[8] H. Reiss and V. K. La Mer, J. Chem. Phys. **18**, 1 (1950).

TABLE I.

Temperature, deg. K	A	B	R
248	0.251	15.1	1.62×10^{3}
253	0.199	14.8	2.50×10^{3}
258	0.144	14.4	3.73×10^{3}
263	0.100	14.2	6.45×10^{3}
268	0.0488	14.0	8.07×10^{3}

Condition (9) is applied to (16)

$$f(\infty,t)=0=N(\infty)\left\{-I(t)\int_{\gamma}^{\infty}\frac{dg}{D(g)N(g)}\right.$$
$$\left.\frac{1}{N(\gamma)}[P-\int_{0}^{t}I(t)dt]\right\}. \quad (17)$$

Define

$$J(\gamma)=\int_{\gamma}^{\infty}\frac{dg}{D(g)N(g)}. \quad (18)$$

Equation (17) will be satisfied if

$$I(t)J(\gamma)=\frac{1}{N(\gamma)}[P-\int_{0}^{t}I(t)dt] \quad (19)$$

or, by differentiation with respect to time

$$\frac{dI}{I}=-\frac{dt}{J(\gamma)N(\gamma)}. \quad (20)$$

The solution of (20) is

$$I=I(0)e^{-t/[J(\gamma)N(\gamma)]} \quad (21)$$

and $I(0)$ can be determined by setting $t=0$ in (19):

$$I(0)=\frac{P}{J(\gamma)N(\gamma)}. \quad (22)$$

The rate at which the foreign particles become nuclei is then

$$I(t)=\frac{P}{J(\gamma)N(\gamma)}e^{-t/[J(\gamma)N(\gamma)]}. \quad (23)$$

The probability, α_0, at the zero of time, that a given foreign particle will become a nucleus during the time interval, $t\rightarrow t+dt$, is

$$\alpha_0=\frac{I(t)dt}{P}=\frac{dt}{J(\gamma)N(\gamma)}e^{-t/[J(\gamma)N(\gamma)]} \quad (24)$$

while the probability, α_t, at the time, t, that the foreign particle will become a nucleus during the time interval, $t\rightarrow t+dt$, is

$$\frac{I(t)dt}{P-\int_{0}^{t}I(t)dt}=\frac{dt}{J(\gamma)N(\gamma)}=\frac{I(0)}{P}dt. \quad (25)$$

TABLE II.

Radius (cm) / Temperature (deg. K)	0.8×10^{-6}	10^{-6}	1.3×10^{-6}	1.9×10^{-6}	3.8×10^{-6}
268	10^{65000}	10^{61000}	10^{52000}	10^{38000}	10^{-430}
263	10^{16000}	10^{9100}	10^{2800}	2.1×10^{-4}	
258	10^{7800}	10^{1800}	3.8×10^{-4}		
253	10^{520}	5.6×10^{-4}			
248	10^{-38}				

The half-life, $t_{\frac{1}{2}}$, of a typical foreign particle, prior to becoming a nucleus, is determined by the condition

$$P/2=\int_{0}^{t_{\frac{1}{2}}}I(t)dt \quad (26)$$

or

$$t_{\frac{1}{2}}=(\ln2)J(\gamma)N(\gamma)=\frac{P\ln2}{I(0)} \quad (27)$$

while the average life, $\bar{t}$, prior to becoming a nucleus is

$$\bar{t}=\frac{\int_{0}^{\infty}tI(t)dt}{P}=J(\gamma)N(\gamma)=\frac{P}{I(0)}. \quad (28)$$

IV. THE CALCULATION OF $J(\gamma)$

In computing the various aspects of the time lag phenomenon it is apparent that the product $J(\gamma)N(\gamma)$ is important. The factor, $N(\gamma)$, can be obtained in a straight-forward manner by reference to (5), while $J(\gamma)$ can be obtained by means of a transformation of variable. Introduce the new variable

$$x=g^{\frac{1}{3}} \quad (29)$$

so that $J(\gamma)$ can be written in the form

$$J(\gamma)=\frac{3}{RC}\int_{\gamma^{\frac{1}{3}}}^{\infty}\exp[-(Ax^3-Bx^2)]dx \quad (30)$$

where R, A, and B have been defined in (2) and (3). The integrand has an extremely sharp maximum at the point

$$x^*=2B/3A \quad (31)$$

so that almost the entire value of the integral is derived from a narrow interval including this point. Because of this, Ax^3-Bx^2 can be replaced by its quadratic approximation in the neighborhood of x^*

$$Ax^3-Bx^2\simeq-\frac{4B^3}{27A^2}+B\left(x-\frac{2B}{3A}\right)^2. \quad (32)$$

Now introduce the translation

$$z=x-(2B/3A) \quad (33)$$

so that (32) is reduced to

$$Ax^3-Bx^2\simeq-(4B^3/27A^2)+Bz^2 \quad (34)$$

and

$$J(\gamma)=\frac{3}{RC}\left(\frac{\pi}{B}\right)^{\frac{1}{2}}\exp[(4B^3/27A^2)]$$

$$\times\left[\frac{1}{(2\pi)^{\frac{1}{2}}}\int_{[\gamma^{\frac{1}{2}}-2B/3A](2B)^{\frac{1}{2}}}^{\infty}\exp[-u^2/2]du\right]. \quad (35)$$

The factor in brackets is simply the error integral. If

$$\gamma^{\frac{1}{2}}<\frac{2B}{3A}-\frac{3}{(2B)^{\frac{1}{2}}} \quad (36)$$

it may be equated to unity. If not, its value may be obtained by reference to standard tables.[9]

V. RESULTS

Expression (27) may now be used to compute the half-lives of silver iodide particles in supercooled water clouds. In performing these computations the surface tension of ice, σ, may be estimated to be

$$\sigma=100 \text{ dynes/cm}, \quad (37)$$

while the molecular volume, v, of an ice molecule is

$$v=3.44\times10^{-23} \text{ cm}^3. \quad (38)$$

Both these values may be considered to be independent of temperature.

Vonnegut[1] investigated the nucleation process in the temperature range, 248–263°K, and, according to the results of electron microscopic examinations, the radii of his silver iodide particles varied from 0.3×10^{-6} to 10^{-5} cm. The values of p and p_0, the vapor pressures of supercooled water and of ice, respectively, for the above temperature range, are available in the critical tables.[10] They lead to the following assignment of values for A, B, and R.

Using (27), together with the values compiled in Table I the half-lives of silver iodide particles in the size range investigated by Vonnegut were computed over the temperature range he investigated. In Table II, the half-life, in seconds, corresponding to a given radius and temperature, can be found at the intersection of the column and row headed, respectively, by the given radius and temperature.

Vonnegut states that at 268°K the half-life was many years while at 253°K it was a few seconds, and at 248°K, a few milliseconds. It will be seen that Table II compares well with his observations, especially for particles of radius 0.8×10^{-6} cm of which, undoubtedly, many were present in his smokes.

There is an extremely sharp dependence on both radius and temperature. The five degree decrease in temperature from 253° to 248° transforms the half-life of particles of radius 0.8×10^{-6} cm from what is almost an infinity to a virtual zero. This means that a fraction of a degree change in temperature, somewhere, in this interval, transforms the silver iodide particle from essentially a non-nucleus to a nucleus. Similar observations can be made, concerning the radius. Notice that at 253° increasing the radius from 0.8×10^{-6} cm to 10^{-6} cm also reduces the half-life from an infinity to zero.

Perhaps, the most important thing to be learned from this calculation is the fact that this sharp dependence upon temperature and radius renders the performance of a crucial experiment difficult. Only the most precisely controlled experiment will be sufficient.

In closing, it should be remarked that Vonnegut's smokes were quite polydisperse so that all of the sizes represented in Table II were present. It might be expected that the larger particles would nucleate immediately, while the time lag would be associated with the smaller ones.

[9] Lange's *Handbook of Chemistry* (Handbook Publishers Inc., Sandusky, Ohio, 1941), fourth edition, p. 257.
[10] I.T.C. Vol. III, p. 211.

Erratum: Vector Model for Spin-Orbit Interaction in Polyatomic Molecules

S. I. Weissman
[J. Chem. Phys. 18, 234 (1950)]

THE fifth sentence of the third paragraph of the above named article should read: "The classifications of triplet wave functions are obtained from the product representations of the spin functions and orbital functions."

The Absorption Spectra of Manganese Fluoride, Zinc Fluoride, and Manganese-Activated Zinc Fluoride*

W. W. PARKINSON, JR.† AND FERD E. WILLIAMS‡
Department of Chemistry, University of North Carolina, Chapel Hill, North Carolina
(Received December 12, 1949)

Thin films of MnF_2, ZnF_2, and ZnF_2:Mn have been prepared by evaporation, and their optical absorption spectra have been measured from 1500 to 2600A. The absorption coefficient of MnF_2 has a maximum of 8.64×10^4 cm^{-1} at 1613A, corresponding to an oscillator strength of 0.042; while there appears to be a maximum of lower value at 1470A for ZnF_2. An unresolved weaker band at 2050A is also evident for MnF_2. For the phosphor, ZnF_2:Mn, the absorption coefficient is intermediate between those of ZnF_2 and MnF_2, but the peak characteristic of the Mn^{++} activator is shifted to 1666A and the oscillator strength of the transition is increased to 1.2.

The relative excitation spectrum of ZnF_2:Mn was determined, and maximum response occurred between 1600 and 1670A, indicating that radiation in the strong absorption band characteristic of the activator is most effective in exciting luminescence. Less efficient excitation occurs to 2200A.

It is concluded that a transition to an excited atomic state of the activator, rather than an electron transfer process, is responsible for the first absorption peaks in MnF_2 and ZnF_2:Mn.

I. INTRODUCTION

OPTICAL absorption spectra of luminescent solids are prerequisite for the determination of the precise transitions involved in luminescence. Phosphors in general, however, have not been prepared in thin homogeneous deposits suitable for absolute absorption measurements at the wave-lengths of strong absorption. Such deposits can be formed of manganese-activated zinc fluoride which is unique in being capable of evaporation and condensation in a vacuum to form thin transparent layers without loss of high luminescent efficiency.[1] This material, in common with other manganese activated phosphors, requires relatively high concentrations of activator and is insensitive to minute traces of foreign ions, making it especially suitable for experimental work.

Previous work on the manganese activated phosphors[2,3] has shown that the manganese ion is situated substitutionally in the host lattice so that calculations of the forces acting on the activator ion can be made. The phosphor ZnF_2:Mn has a compact, ionic, rutile lattice reducing the possibility of extraneous effects from interstitial ions and making experimental work susceptible to theoretical interpretation. For these reasons ZnF_2:Mn was selected for optical absorption measurements.

From diffuse reflectance measurements on powdered ZnF_2:Mn, Fonda and Studer[4] inferred that significant absorption occurs at 2200A. To obtain absolute absorption data at wave-lengths of strong absorption, measurements in the vacuum ultraviolet on evaporated deposits are necessary.

II. APPARATUS

The apparatus for measurement of absorption consisted of a high voltage hydrogen discharge tube as a source of ultraviolet, a vacuum grating monochromator, and a 1P21 photo-multiplier tube as a detector. To enable the photo-multiplier to respond to ultraviolet, a thin layer of willemite phosphor was deposited on the back of the sample chamber, in the optical path and immediately in front of the photo-multiplier. This equipment has been described in an earlier paper[5] and is shown schematically in Fig. 1.

For the preparation of the thin film samples, a vacuum evaporation system was used. A mercury diffusion pump, a liquid air trap, and a small eccentric rotor type pump comprised the pumping system. The evaporating chamber was made up of a conical bell jar resting on a silicone rubber gasket on a flat brass plate. A cold finger protruded down from the top of the bell jar for final clean-up of condensible gases. Enclosed in the bell jar was an electrical heating element formed by a V-shaped trough of 0.004-cm platinum foil held in stainless steel, conducting supports. For out-gassing the system an asbestos oven was constructed to fit the bell jar.

III. PREPARATION OF SAMPLES

For evaporation to deposit thin films of the materials, fused or pressed lumps were required. For MnF_2, pressed pellets were prepared in a hydraulic press from C. P. MnF_2 powder. In the case of ZnF_2 and the phosphor, pure ZnF_2 was first prepared by adding spectroscopically pure ZnO to excess C. P. 40 percent HF in a platinum dish, evaporating to dryness and finally heating at

* Part of a thesis submitted by W. W. Parkinson, Jr. to the University of North Carolina in partial fulfillment of the requirements for the degree of Doctor of Philosophy. This work was supported by the ONR through Contract N7onr-284, Task Order 1.
† Present address: Carbide and Carbon Chemicals Corporation, Oak Ridge, Tennessee.
‡ Present address: General Electric Research Laboratory, Schenectady, New York.
[1] F. E. Williams, J. Opt. Soc. Am. **37**, 302 (1947).
[2] F. A. Kroeger, Physica **6**, 369 (1939) and Zeits. f. Krist. **100**, 543 (1939).
[3] Jenkins, McKeag, and Rooksby, Nature **143**, 978 (1939).
[4] G. R. Fonda and F. J. Studer, J. Opt. Soc. Am. **38**, 1007 (1948).
[5] W. W. Parkinson, Jr. and F. E. Williams, J. Opt. Soc. Am. **39**, 705 (1949).

350°C for half an hour. Fused lumps of the ZnF_2 were prepared by mixing the ZnF_2 with about half its weight of C. P. NH_4F to give a slightly acid atmosphere and fusing in a covered platinum crucible for five minutes. After cooling the melt was broken up to provide lumps for evaporation. The phosphor was prepared by grinding the proper weight of C. P. MnF_2 powder with the pure, dried ZnF_2 in an agate mortar. NH_4F was added as before and the mixture was treated in the same manner as the ZnF_2.¶

The thin films for optical measurements were evaporated onto lithium fluoride plates which, during the evaporation, were shielded over half their area by quartz plates to provide blanks. The procedure for evaporation was similar to that described by Williams.[1] Before evaporation, the vacuum system was baked to outgas, cooled, and liquid air was added to the cold finger. The lump of sample was partially evaporated by adjusting the heating current to bring the platinum trough containing the sample to a bright red heat. The thickness of the films was controlled by the time of heating.

IV. ANALYSIS OF SAMPLES

The manganese concentration in the phosphor samples was determined by oxidation of the manganous ion to permanganate by KIO_4 in strongly acid solution.[6] The concentration of permanganate was then determined by optical transmission measurements with a spectrophotometer.

The bulk phosphor used for evaporation contained 4.47 ± 0.04 mole percent Mn while the evaporated films, taken from the quartz shields, showed 1.0 ± 0.2 mole percent. The concentration in the films appeared to vary within the limits indicated, from one specimen to another, depending on the conditions of evaporation.

V. EXPERIMENTAL MEASUREMENTS AND THEIR PRECISION

Measurements of the photo-current in the detector tube, after corrections for dark current and scattered light, gave for each wave-length the absorption coefficient k, defined by the relation:

$$I=I_0e^{-kd}, \tag{1}$$

where d is thickness in centimeters and I_0 and I are the intensities of incident and transmitted light respectively. The incident light was that measured through the blank, the bare half of the lithium fluoride plates; and the transmitted light was observed by shifting the plate to place the film-coated half before the exit slit of the monochromator. The thickness of the films, d, was determined by weighing the lithium fluoride plates before and after deposition of the film, and then measuring the area of the film. Due to the difficulty of illuminating the films in the measuring microscope the area could be measured to only plus or minus 3 percent.

Corrections for dark current and light scattered within the monochromator were simple because the photo-current of the 1P21 is directly proportional to the intensity of incident light.[7] The dark current of the 1P21 was recorded for each wave-length and was subtracted from the current reading for transmission of the blank and of the sample to give the photo-current. From the photo-currents observed for the blank and the sample, the correction for scattered light was subtracted to give net values proportional, respectively, to the intensity of monochromatic light incident upon and transmitted by the sample. These net values were substituted for I_0 and I in (1) to give the absorption coefficient for each wave-length.

Scattered light within the monochromator came largely from the direct reflection from the face of the

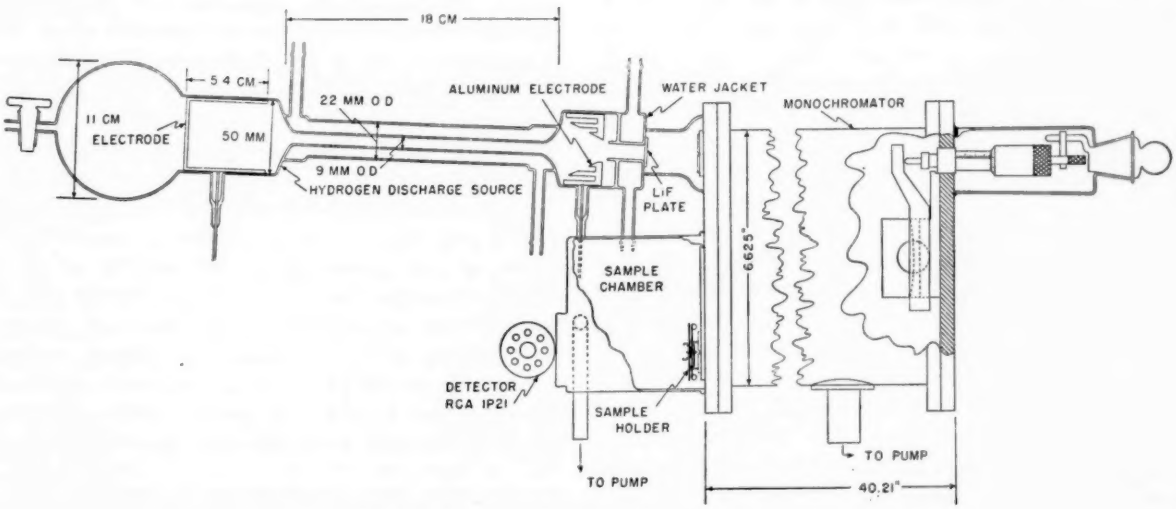

FIG. 1. Apparatus for absorption measurements.

¶ The samples of phosphor and ZnF_2 were supplied by Dr. Peter D. Johnson.

[6] N. H. Furman, *Scott's Standard Methods of Chemical Analysis* (D. Van Nostrand Company, Inc., New York, 1939), p. 573.

[7] R. W. Engstrom, J. Opt. Soc. Am. **37**, 420 (1947).

grating mirror; consequently the intensity varied with each wave-length setting on the grating. This variation was found to be almost linear with the micrometer scale indicating wave-length. Therefore, a curve of photo-currents due to scattered light *versus* wave-length was established before each absorption run by observing photo-currents at several settings for very short wave-lengths where only polychromatic, scattered light occurred. The curve was then extrapolated to the wave-length region of absorption measurement to give the correction for scattered light.

The micrometer screw for wave-length on the monochromator was calibrated by calculating from the dimensions a curve of wave-length *versus* grating movement. This curve was checked with the lines of the mercury spectrum and, in addition, an absorption curve was run on NaCl. The first absorption peak for NaCl agreed with that reported by Hilsch and Pohl[8] and Schneider and O'Bryan[9] within less than 10A.

The resolution of the monochromator was sacrificed to obtain sufficient intensity for measurement. The band width was 7A at the setting for 1200A and broadened to about 10A below 1000 and above 2000A. At this band width the resolution was adequate to separate the 3126 and 3132A mercury lines without difficulty.

During the absorption measurements it was necessary to interchange the coated and uncoated halves of the LiF plate bearing the sample, very quickly, because of slight variations in the intensity of the source. This was accomplished by placing the sample plate in a holder mounted on a pivoted, vertical, counterbalanced arm. The arm could be shifted to the proper position by momentarily energizing one or the other of a pair of a.c. electromagnets mounted outside the sample chamber. Intermittent use of a.c. precluded magnetic disturbance of the photo-multiplier.

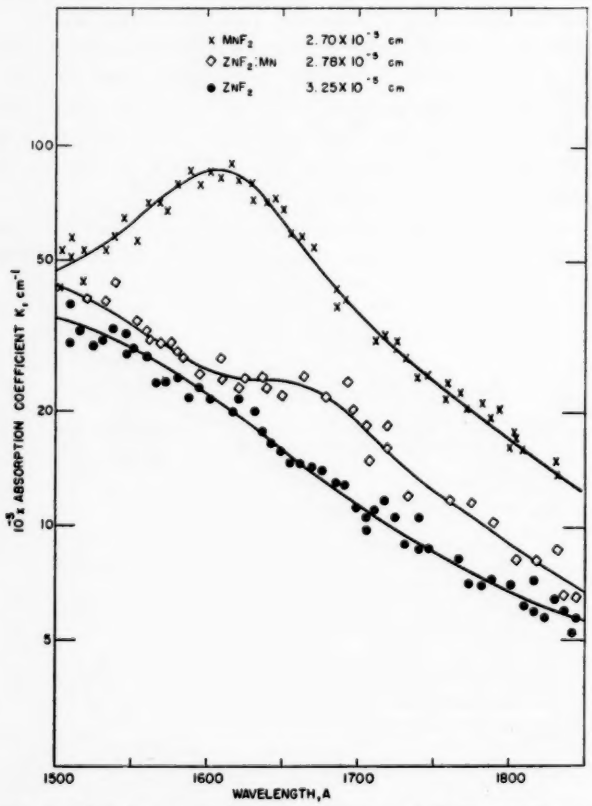

FIG. 2. The short wave-length absorption of ZnF_2, MnF_2, and ZnF_2:Mn containing 1.0 mole percent Mn.

The reproducibility of the intensity measurements was seriously affected by the slight variations in the intensity of the source and in the dark current of the detector. To reduce uncertainty in the position of the absorption curves, measurements were taken at many points. Typical points, only about half those recorded, are shown in Figs. 2 and 3.

An additional precaution to improve reproducibility was duplication of meter readings. For each point, intensity readings for blank and sample were repeated as quickly as possible and if corresponding readings differed by more than $\frac{1}{4}$-scale division, they were not recorded. Furthermore, these intensity readings were discarded if, between adjacent wave-length settings, the dark current of the detector had changed by more than $\frac{1}{4}$ division (5×10^{-11} amp.), which, due to fluctuations, was the limit to which the meter could be read. These two $\frac{1}{4}$-division tolerances could be cumulative in subtracting dark current from gross reading to obtain the photo-current, and the net photo-current was as low as 4 divisions in two spectral regions. Therefore the reproducibility for photo-current readings was no better than 1 part in 8 in these regions, 1524–1550 and 1710-1730A. The transmitted light, having low intensity in the region of strong absorption, showed even poorer reproducibility, although very thin samples were used for this region. The logarithmic dependence of the absorption coefficient equation reduces the possible error in the coefficient to 1 part in 5 in this portion of the curve, but requires the use of thick samples in the region of low absorption.

Measurements on samples of thicknesses other than those shown indicated that, in every case, the observed absorption coefficient was lower for the thicker samples. This discrepancy can be attributed to loss of light by reflection and scattering at the surfaces of the film sample. Samples could not be prepared thick enough to provide a precise correction for this effect. In the case of each material at least four samples covering a variation in thickness of a factor of at least two, were measured in the absorptive region. The greatest difference between curves for samples of this thickness range was 22 percent.

VI. THE ABSORPTION DATA AND THEIR SIGNIFICANCE

The absorption data for ZnF_2, MnF_2, and the ZnF_2:Mn phosphor containing 1.0 mole percent MnF_2 are shown in Figs. 2 and 3, with the thickness of each

[8] R. W. Pohl, Proc. Phys. Soc. 49, Extra Part 1, 3 (1937).
[9] E. G. Schneider and H. M. O'Bryan, Phys. Rev. 51, 293 (1937).

sample indicated. The MnF_2 exhibits a maximum absorption peak of 8.64×10^4 cm^{-1} at 1613A. From the following equation:[10]

$$f\simeq\frac{mc\Delta\nu k}{\pi Ne^2}, \tag{2}$$

where $\Delta\nu$ is the band width and k the absorption coefficient, the oscillator strength f is determined as 0.042. An unresolved weaker absorption band at 2050A is also evident for MnF_2.

ZnF_2 exhibits no absorption structure between 2500 and 1500A but only a continuously increasing absorption coefficient with decreasing wave-length. A few isolated measurements below 1500A indicate that the first peak is at 1470A and the corresponding coefficient is less than that of the peak for MnF_2.

The absorption of the phosphor is intermediate between that of the pure substances. However the absorption coefficient of ZnF_2:Mn is much higher than is predicted from a simple additive relationship. For example, the oscillator strength of the MnF_2 peak has increased to 1.2, as calculated from (2). Furthermore, the energy of transition is decreased as shown by the shift in peak position from 1613A or 7.66 ev for MnF_2 to 1666A or 7.42 ev for ZnF_2:Mn. There is some evidence in the experimental data for the presence of the 2050A MnF_2 band in the phosphor.

To determine the nature of the transitions involved, the energy of the transfer of an electron from the fluoride ion to the manganese ion was calculated. Neglecting polarization, the electron transfer energy U for nearest neighbors,[11] the anion monovalent and the cation divalent, is:

$$U=\frac{(2A-1)e^2}{2r}+E-I', \tag{3}$$

where A is the Madelung constant, E the electron affinity of the anion, and I' the second ionization potential of the cation. For MnF_2, U is calculated to be 18 ev. Because polarization could reduce U only by a few electron volts, it is apparent that an electron transfer process is not responsible for the 7.66- and 6.0-ev bands in ZnF_2 or the 7.42-ev band in ZnF_2:Mn.

Atomic excitations within the Mn^{++} are more probably the transitions taking place both in MnF_2 and ZnF_2:Mn. Seitz[12] has attributed the long wave-length absorption bands in thallium-activated alkali halide phosphors to such processes. The long temperature independent afterglow and the multiplicity change accompanying excitation[13] for the ZnF_2:Mn demonstrate that a forbidden atomic transition is responsible for the emission process. The strong absorption peaks at 7.66 and 7.42 ev for MnF_2 and ZnF_2:Mn, respectively,

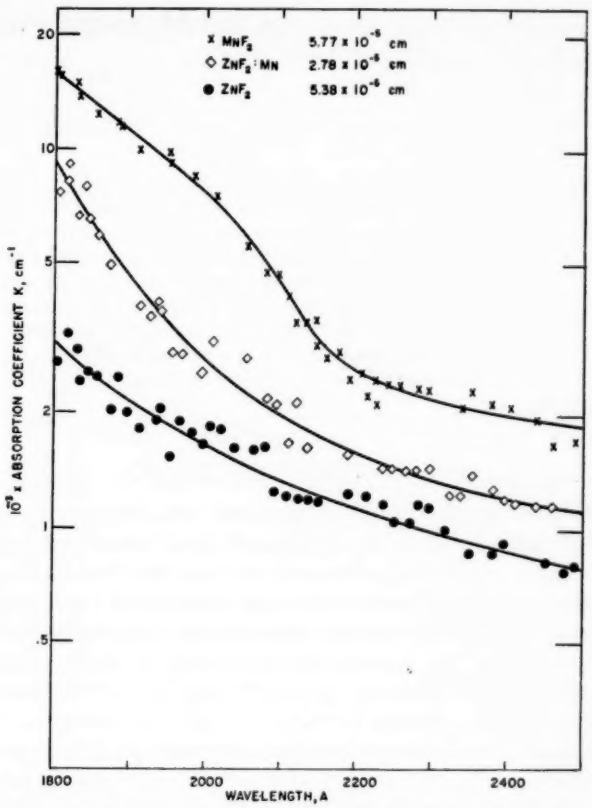

FIG. 3. The long wave-length absorption of ZnF_2, MnF_2, and ZnF_2:Mn containing 1.0 mole percent Mn.

probably result from an allowed atomic transition such as $3d^5\rightarrow3d^44p$, whereas the weak absorption band at 6.0 ev probably is a forbidden transition such as $3d^5\rightarrow3d^44s$ possibly with a multiplicity change. Quantitative calculation on these interpretations are in progress.

To correlate the absorption data with excitation, the relative response of ZnF_2:Mn to radiation of various wave-lengths was measured. This was accomplished by substituting the ZnF_2:Mn for the willemite deposited on the back of the sample chamber to sensitize the photo-multiplier to ultraviolet. The excitation curve showed a maximum from 1610 to 1670A, the region where the strong absorption peak occurs. Measurable excitation occurred to 2200A.

The absolute absorption and excitation characteristics of manganese activated zinc fluoride are similar to the results of relative measurements reported for manganese activated zinc sulfide[14] and zinc orthosilicate.[15] With each material, the manganese increases the absorption of the long wave-length edge of the peak of the host substance, and the response of each phosphor exhibits a peak in this long wave-length edge. The determination of the absolute absorption spectrum of ZnF_2:Mn, however, permits evaluation of peak absorption energy, band width and oscillator strength. These data are prerequisite to the determination of the precise transitions involved.

[10] N. F. Mott and R. W. Gurney, *Electronic Processes in Ionic Crystals* (Oxford Press, London, 1948), p. 103.
[11] A. von Hippel, Zeits. f. Physik **101**, 680 (1936).
[12] F. Seitz, J. Chem. Phys. **6**, 150 (1938).
[13] P. D. Johnson and F. E. Williams, J. Chem. Phys. **17**, 435 (1949).
[14] F. A. Kroeger, Physica **6**, 369, 764 (1939).
[15] J. T. Randall, Proc. Roy. Soc. **170A**, 272 (1939).

On the Magnetic Properties of Liquid He_3*,†

L. GOLDSTEIN AND M. GOLDSTEIN
Los Alamos Scientific Laboratory, Los Alamos, New Mexico
(Received November 7, 1949)

The object of this paper is to investigate the possibility that liquid He_3 might have a tendency toward nuclear ferromagnetism in the approximation where this fluid is considered to be an antisymmetrical collection of atoms having an angular momentum of $\hbar/2$ and a finite nuclear magnetic moment. In the rather crude approximation where the motion of the individual atoms is described with the help of plane de Broglie waves, the exchange energy, originating in the interatomic mutual potential energy of He_3 atoms, favors the parallel alignment of all spins at the temperature of absolute zero. The total energy of the fluid is, however, smaller in the antiferromagnetic configuration because its kinetic energy is smaller than in the ferromagnetic configuration. To the approximation of these studies then, liquid He_3 does not show nuclear ferromagnetism. Its nuclear paramagnetism is then discussed.

1. INTRODUCTION

ONE of the interesting problems raised by a collection of particles having an angular momentum of $\hbar/2$ and a finite magnetic moment concerns its magnetic behavior. Antisymmetrical statistics resulting from first principles lead for such a collection of completely free particles to the well-known balancing of their spins and magnetic moments. At the temperature of absolute zero in such a system the total angular momentum and magnetic moment vanish. This, however, is not necessarily true if the particles of the collection exert forces upon each other. Indeed, as first shown by Bloch,[1] for a so-called free electron gas, in which the potential energy of any electron is constant or vanishes on the average, the Coulomb repulsion between the electrons leads to a quantum mechanical exchange energy for electrons of parallel spin. This exchange energy is negative and favors ferromagnetism. However, this energy is to be regarded as a correction to the first approximation energy (e.g., the kinetic energy) of the electrons, which is positive. Actually the preceding method of obtaining the total energy of the free electron gas may be said to be equivalent to an approximation method which proceeds according to the increasing powers of the coupling parameter, $e^2/\hbar v_f$, where v_f is the electron velocity at the top of the Fermi distribution associated with the antiferromagnetic configuration.[2] Ferromagnetism cannot occur in this model unless the coupling parameter is larger than unity. This latter condition is however equivalent to that of the breakdown in the validity of the approximation method. Within the region of validity of this method then, the free electron gas cannot exhibit ferromagnetism.

A collection of He_3 atoms at liquid He_3 densities may be regarded as approximating what one might call an antisymmetric assembly of loosely bound particles. It appears that a study of the magnetic properties of liquid He_3 using the admittedly crude model of describing, in a first approximation, the motion of individual atoms by plane de Broglie waves and computing the total energy of such a system by including the mutual potential energy of He atoms, is of interest. It is realized that there will be objections to this limiting gas model. It may, however, be expected that as long as the quantum mechanical exchange energy corrections are of reasonable magnitude in comparison with the average classical potential energy or the average kinetic energy, such an approximation method would be justified.

2. THE TOTAL ENERGY OF LIQUID He_3

In the present studies it was assumed that liquid He_3 stays liquid down to the absolute zero temperature, a situation often conjectured in connection with liquid He_4. Since the latter fluid does not solidify down to the lowest temperature at which it has been observed, unless subjected to external pressure, it is to be expected that this conjecture is better justified in the case of liquid He_3 which is considerably more volatile and less dense[3] than liquid He_4. The present investigation refers essentially to the temperature of absolute zero, where the density of the liquid was taken to be somewhat larger than the highest density observed at Los Alamos, namely $\rho(0°\text{K})$ was assumed to be 0.08 g/cc. This density determines the maximum kinetic energy or linear momentum at the top of the Fermi distributions in both the ferromagnetic (f) and antiferromagnetic (a) configurations. One has, ρ_0 denoting the liquid density at the temperature of absolute zero, for the maximum momentum p_f and kinetic energy E_f,

$$p_f=h(3\rho_0/4\pi M)^{\frac{1}{3}},$$
$$E_f=p_f^2/2M=(h^2/2M)(3\rho_0/4\pi M)^{\frac{2}{3}}, \quad (1)$$

M being the mass of a He_3 atom (5×10^{-24} g), and

$$p_a=p_f/2^{\frac{1}{3}}, \quad E_a=E_f/2^{\frac{2}{3}}. \quad (2)$$

* This paper has been reported on at the Cambridge meeting of the American Physical Society, June 16–18, 1949.

† This document is based on work performed at Los Alamos Scientific Laboratory of the University of California under Government Contract W-7405-Eng-36.

[1] F. Bloch, Zeits. f. Physik **57**, 545 (1929).

[2] L. Goldstein, J. de phys. et rad. **7**, 141 (1936).

[3] See Sydoriak, Grilly, and Hammel, Phys. Rev. **75**, 303 (1949) and Grilly, Hammel, and Sydoriak, *ibid.* **75**, 1103 (1949).

The ratios of $2^{\frac{1}{3}}$ and $2^{\frac{2}{3}}$ between the moments p_f/p_a and kinetic energies E_f/E_a in the (f) and (a) configurations result from the inflated momentum or energy spheres in the former as compared with the latter. Indeed in the (a) configuration two atoms of opposite spin are accommodated per free particle state, while in the (f) configuration there being only one atom per state, the volume of the momentum sphere has increased by a factor two with respect to that in the (a) configuration.

The average kinetic energy per atom is then

$$\bar{E}_{f,a}=\tfrac{3}{5}E_{f,a}, \tag{3}$$

as in a completely degenerate collection of antisymmetric particles, since in our approximation the kinetic energy of an atom in liquid He_3 is that of a free particle within an ideal Fermi-Dirac fluid.

The total wave function of the system in the ferromagnetic configuration, normalized to unity in the volume V, is, in the present approximation, the determinant:

$$\psi_f(\mathbf{r}_1,\mathbf{r}_2,\cdots\mathbf{r}_N)=(N!V^N)^{-\frac{1}{2}}\sum_{P=1}^{N!}(-)^P P \times\exp[i(\mathbf{k}_1\mathbf{r}_1+\cdots+\mathbf{k}_N\mathbf{r}_N)], \tag{4}$$

where the summation extends over all the $N!$ permutations of the permutation operator P acting on the radius vectors $\mathbf{r}_j$ of the He_3 atoms of wave vector $\mathbf{k}_j(=\mathbf{p}_j/\hbar)$ in the system formed by N atoms. In the antiferromagnetic configuration the wave function is a product of two determinants associated with the $(N/2)$ atoms in the two spin states respectively. Let the $\mathbf{r}$'s denote the radius vectors of the atoms in one spin state and the $\mathbf{R}$'s those of the second group of $(N/2)$ atoms in the other spin state, the approximate wave function is

$$\psi_a(\mathbf{r}_1,\cdots\mathbf{r}_{N/2};\mathbf{R}_1\cdots\mathbf{R}_{N/2})=[(N/2)!V^{N/2}]^{-1}\times\sum_{p=1}^{(N/2)!}\sum_{P=1}^{(N/2)!}(-)^{p+P}pP\exp\{i[(\mathbf{k}_1\mathbf{r}_1+\cdots+\mathbf{k}_{N/2}\mathbf{r}_{N/2})+(\mathbf{K}_1\mathbf{R}_1+\cdots+\mathbf{K}_{N/2}\mathbf{R}_{N/2})]\}. \tag{5}$$

Here, the permutation operators p and P operate on the $\mathbf{r}$'s and $\mathbf{R}$'s respectively, the $\mathbf{K}$'s being the wave vectors associated with the atoms $\mathbf{R}$ in one of the spin states. It is, of course, fully realized that the extreme ideal gas wave functions may be worse approximations here than in the case of the electron gas in the theory of metals. While in the latter case a relatively good justification can be given in some types of metals for describing the less tightly bound electrons as forming an antisymmetric assembly of practically free particles, no such justification is attempted in the present problem of liquid He_3. We should like to invoke here the experimental results of the Argonne workers[4] on the flow properties of liquid He_3. According to these results the viscosity coefficient of this liquid is of the same order of magnitude as that of liquid He_4I, i.e., some 10^{-5} c.g.s. unit.[5] This in turn is of the same order of magnitude as, or somewhat larger than, the viscosity coefficient of He_4 vapor at liquid He temperatures. This argument should merely be considered as an indirect indication of the gas-like behavior of liquid He_3 where the atoms have a small but finite binding energy.[6]

One finds with the wave functions (5) or (6), the following potential energy of two He_3 atoms:

$$E_p=\frac{1}{V^2}\int\Phi(r)dv_1dv_2-\frac{1}{V^2}\delta(\mathbf{s}_1-\mathbf{s}_2)\int\Phi(r)\times\exp[i(\mathbf{k}_1-\mathbf{k}_2)\mathbf{r}]dv_1dv_2=E_{p,c}+E_x(|\mathbf{k}_1-\mathbf{k}_2|). \tag{6}$$

Here, $E_{p,c}$ is simply the classical potential energy of two stationary He_3 atoms averaged over their positions in the volume V of the fluid, with $\Phi(r)$ denoting the mutual potential energy of two stationary atoms at a distance r. This was taken to be given by either one of the following two expressions due respectively to Slater and Kirkwood[7] and Margenau:[8]

$$\Phi_{S-K}(r)=Ae^{-\alpha r}-Br^{-6}, \tag{7}$$

$$\Phi_M(r)=Ae^{-\alpha r}-B_1r^{-6}-B_2r^{-8}. \tag{8}$$

In these formulas, the distance $r=|\mathbf{r}_1-\mathbf{r}_2|$ of the two atoms is expressed in angstrom units, the constants having the following numerical values:

A	B	B_1	B_2
77	0.149	0.139	0.37×10^{-11} erg,

while α is equal to 4.60A^{-1}.

E_x is the quantum mechanical exchange energy of two He_3 atoms whose distance in wave vector space is $|\mathbf{k}_1-\mathbf{k}_2|$ while the δ-function simply indicates that in the (a) configuration only atoms of parallel spin direction give rise to exchange energy $(\mathbf{s}_1=\mathbf{s}_2)$. The coordinate integrations in (7) extend over the volume V. With the origin of the coordinate system placed at one of the atoms, one obtains

$$E_{p,c}=\frac{4\pi}{V}\int\Phi(r)r^2dr,$$

$$E_x(k)=-\frac{4\pi}{V}\int\Phi(r)\frac{\sin kr}{kr}r^2dr;\ k=|\mathbf{k}_1-\mathbf{k}_2|. \tag{10}$$

$$(k\neq0)$$

The integrals (9) and (10) diverge on account of the peculiar behavior of the interatomic potential energies (8), so that the integrations have to be cut off at some

[4] Osborne, Weinstock, and Abraham, Phys. Rev. **75**, 988 (1949).

[5] See the monograph of W. H. Keesom, *Helium* (Elsevier Publishing Company, Inc., Amsterdam, 1942).

[6] It is to be noted that the equality in order of magnitude of the liquid and vapor viscosity coefficients also holds for hydrogen but the difference in viscosities becomes increasingly large with heavy elements.

[7] J. C. Slater and J. G. Kirkwood, Phys. Rev. **37**, 682 (1931).

[8] H. Margenau, Phys. Rev. **56**, 1000 (1939).

finite small distance a. Physically, only those lower limits are acceptable which lead to a large enough negative average potential energy, since the atoms are evidently bound in the liquid. One obtains thus, at once,

$$E_{p,c}(a)_{S-K}=\frac{4\pi}{V}\left[\frac{A}{\alpha^3}e^{-a\alpha}(2+2a\alpha+a^2\alpha^2)-\frac{B}{3a^3}\right], \quad (11)$$

$$E_{p,c}(a)_{M}=\frac{4\pi}{V}\left[\frac{A}{\alpha^3}e^{-a\alpha}(2+2a\alpha+a^2\alpha^2)-\frac{B_1}{3a^3}-\frac{B_2}{5a^5}\right]. \quad (12)$$

It is found that the preceding averages become negative at values of a, such that $a\geq 2.14$A in the $S-K$ case and $a\geq 2.02$A in the M case.

The exchange energy of a pair of He_3 atoms becomes, after an elementary calculation, with the $S-K$ potential energy,

$$E_x(k)_R=-\frac{4\pi}{V}\frac{1}{k^3}\frac{Ae^{-a\alpha}}{1+\beta^2}\left[\left(a\alpha+\frac{\beta^2-1}{\beta^2+1}\right)\sin ka+\left(ka+\frac{2\beta}{1+\beta^2}\right)\cos ka\right], \quad (13)$$

due to the repulsive part (R) of the potential energy or the term $Ae^{-a\alpha}$. The attractive part, (A), leads to:

$$E_x(k)_A=\frac{\pi Bk^3}{V}\left[\left(\frac{1}{(ka)^2}-\frac{1}{6}\right)\frac{\sin ka}{(ka)^2}+\left(\frac{1}{(ka)^2}-\frac{1}{2}\right)\frac{\cos 2ka}{3ka}+\pi/12-\tfrac{1}{6}Si(ka)\right], \quad (14)$$

where

$$\beta=\alpha/k; \quad Si(x)=\int_0^x\frac{\sin x}{x}dx.$$

With the Margenau potential energy, the repulsive exchange energy is of course, the same as with the Slater-Kirkwood potential energy, while the attractive exchange term has a form similar to (14). The oscillating character of these exchange energies is of course already evident in the original formula (10).

The total energy of the liquid, in the ferromagnetic configuration becomes:

$$E_{T,f}=\tfrac{3}{5}NE_f+\tfrac{1}{2}N(N-1)E_{p,c}(a)+\tfrac{1}{2}\textstyle\sum_{\mathbf{k}_1}\sum_{\mathbf{k}_2}E_x(|\mathbf{k}_1-\mathbf{k}_2|). \quad (15)$$

The first term on the right-hand side is the free particle kinetic energy in a system of N atoms, with E_f being given by Eq. (1); the second term is the total classical potential energy of the system, there being $N(N-1)/2$ pairs of energy $E_{p,c}(a)$ per pair of atoms. Finally the last term represents the total exchange energy. In the latter, one has to sum over all possible $\mathbf{k}$-values of both atoms up to $\mathbf{k}_f$.

Similarly, in the antiferromagnetic configuration one obtains

$$E_{T,a}=\tfrac{3}{5}NE_a+\tfrac{1}{2}N(N-1)E_{p,c}(a)+2(\tfrac{1}{2}\textstyle\sum_{\mathbf{k}_1}\sum_{\mathbf{k}_2}E_x(|\mathbf{k}_1-\mathbf{k}_2|)). \quad (16)$$

In this expression, the maximum kinetic energy E_a is given by Eq. (2); the classical potential energy term is the same as in the (f) configuration, since this quantity does not depend on the spin configuration. In the last exchange energy term, the summations over the $\mathbf{k}$'s extend only up to $\mathbf{k}_a(=2^{-\frac{1}{3}}\mathbf{k}_f)$, the radius of the contracted wave vector sphere associated with ($N/2$) parallel spins, in either direction. The total exchange energy is of course the sum of the exchange energies in either spin direction, and this is indicated by the factor 2 in front of the single spin direction exchange term. We now turn to the evaluation of these exchange energies.

3. THE FREE PARTICLE EXCHANGE ENERGY IN LIQUID He_3

The summations appearing in the total exchange energy expressions in Eqs. (15) and (16) may be replaced by integrations over the distribution of free particle levels, with a level density,

$$\frac{dn(k,\theta)}{2\pi\sin\theta d\theta}=\frac{V}{(2\pi)^3}k^2dk,$$

associated with the solid angle $2\pi\sin\theta d\theta$ and wave vector band $(k,k+dk)$, so that:

$$\tfrac{1}{2}\textstyle\sum_{\mathbf{k}_1}\sum_{\mathbf{k}_2}E_x(|\mathbf{k}_1-\mathbf{k}_2|)=N\frac{V}{2\pi^2}\int_0^K E_x(k)k^2dk,$$

where the origin of the coordinate system in k-space was chosen to coincide with one of the particles, say atom 1, so that an integration over the k-space of this atom leads just to N, while the polar axis coinciding with the direction of $(\mathbf{k}_1-\mathbf{k}_2)$, the integrand in the second integral becomes independent of the polar angle θ, leading to a factor 4π of the total solid angle. It is now seen that by substituting $E_x(k)$, as given by Eqs. (13) and (14), one obtains a series of definite integrals all expressible in terms of impractical infinite series at worst. Instead of following this procedure it appeared more useful to express the total exchange energy in another form. With the definition (10) one finds

$$\tfrac{1}{2}\textstyle\sum_{\mathbf{k}_1}\sum_{\mathbf{k}_2}E_x(|\mathbf{k}_1-\mathbf{k}_2|)=-\sum_{\mathbf{k}_2}\frac{1}{(2\pi)^2}\int\Phi(r)r^2dr\int\frac{\sin|\mathbf{k}_1-\mathbf{k}_2|r}{|\mathbf{k}_1-\mathbf{k}_2|r}d\mathbf{k}_1,$$

with $d\mathbf{k}_1$ denoting the volume element in $\mathbf{k}_1$-space. Choosing a polar coordinate system whose axis coincides with $\mathbf{k}_2$, applying the Gegenbauer addition the-

orem[9] to $\sin|\mathbf{k}_1-\mathbf{k}_2|r/(|\mathbf{k}_1-\mathbf{k}_2|r)$, integrating over $\mathbf{k}_1$, replacing the summation over $\mathbf{k}_2$ by an integral with the level density $(V(2\pi)^3)d\mathbf{k}_2$, and integrating again one obtains finally

$$E_{x,\,\substack{f\\a}}=-\tfrac{3}{2}N\int_a^\infty \Phi(r)J_{\frac{3}{2}}^2(k_{\substack{f,\\a}}r)\frac{dr}{r}, \qquad (17)$$

where $J_{\frac{3}{2}}(z)$ is the Bessel function of order $\frac{3}{2}$, k_f and k_a denote the maximum wave vectors in the two configurations, respectively, e.g.,

$$k_f=p_f/\hbar, \quad k_a=2^{-\frac{1}{3}}k_f.$$

Replacing, in Eq. (17), $\Phi(r)$ by the Coulomb energy e^2/r acting between two electrons, one obtains at once the total exchange energies in the two configurations of the free electron gas model.[10]

In the present case of the He-He interaction the total exchange energy has no simple analytical expression. It is, however, easy to see that the exchange energy, for a chosen cut-off length a, is in general larger, the smaller the radius of the momentum or wave vector sphere of the system, a result similar to the simpler case of electrostatic coupling, where this is always true. The complication which exists in the case of helium results from a superposition of effects due to the attractive and repulsive components of the potential energy $\Phi(r)$.

Since a simple analytical expression of the exchange energy is lacking here, a discussion of the limitations in the validity of these calculations is not as straightforward as in the electron gas problem. A further complication arises here from the somewhat arbitrary choice of the cut-off length a. It appears, however, that the limitations on the validity of the exchange energy in the He_3 case should be somewhat different from those of the electron problem. In the latter because the average classical potential energy vanishes or becomes constant, the exchange energy can only be compared with the kinetic energy or first approximation energy of the electrons. In our case, where the plane de Broglie wave approximation of the one atom wave function is postulated at the start also, the exchange energy may be compared to both the average potential and kinetic energies. Since the atoms are bound in the liquid, necessarily the potential energy is larger than the kinetic energy per atom. The comparison of the approximate exchange energy to the potential energy rather than to the smaller kinetic energy would then lead in the present calculations to a wider validity range in the wave vectors or particle densities than in the electron case.

The exchange energies have been computed here by evaluating numerically the integrals in (17).* In all the cases studied here with the smaller Slater-Kirkwood potential energy, the exchange energy turned out to be a small fraction of both the kinetic and potential energies for the same physically significant cut-off lengths, e.g., $a\geq 2.2$A. As expected, the exchange energy is negative for the small cut-off values, since there, the repulsive portion of the potential energy is more important than the attractive part. For cut-off lengths a which are physically significant the exchange energy starts by being negative, it then increases with increasing a, at constant k_f, becomes positive and reaches a maximum corresponding to that value of a, beyond which the potential energy $\Phi(r)$ is negative, e.g., for a equal to the root of $\Phi(r)$. The positive exchange energy is associated with the predominance of the attractive part of the potential energy.

At the temperature of absolute zero, with the assumed liquid He_3 density, the exchange energies have been investigated with both types of potential energies and the results are given in Figs. 1 and 2.** It is seen that with both types of potential energies, the exchange energy alone favors the ferromagnetic configuration since one has always $E_{x,f}<E_{x,a}$. However, in the whole physically significant region of the cut-off lengths, as a function of which the exchange and average potential

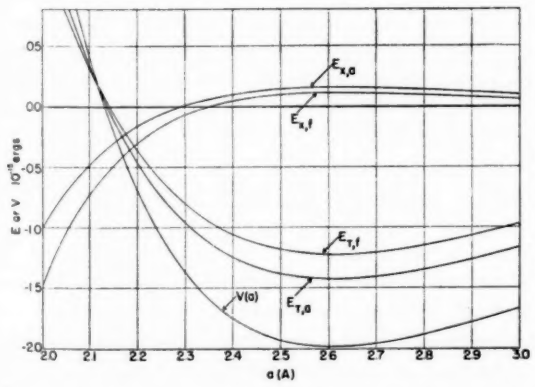

FIG. 1. Average potential, exchange, and total energies per atom in liquid He_3. (Slater-Kirkwood interaction.)

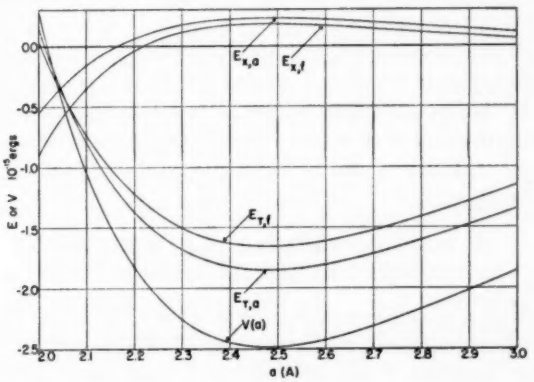

FIG. 2. Average potential, exchange and total energies per atom in liquid He_3. (Margenau interaction.)

[9] G. N. Watson, *Theory of Bessel Functions* (Cambridge University Press, London, 1922), p. 363 or 366.

[10] See reference 1 or F. Seitz, *Modern Theory of Solids* (McGraw-Hill Book Company, Inc., New York, 1940), p. 341.

* We should like to thank here Mr. D. W. Sweeney for his cooperation in this work.

** One finds that the kinetic energy is $\bar{E}_a=4.05\times10^{-16}$ erg/atom.

TABLE I. Paramagnetic, (χ_T/ρ), and total, (χ_{tot}/ρ), mass susceptibilities of liquid He_3.

T °K	(χ_T/ρ) 10^{-7} c.g.s.	$-(\chi_{tot}/\rho)$ 10^{-7} c.g.s.
0*	0.508	5.80
0.245*	0.507	5.80
0.490*	0.504	5.81
1.2	0.478	5.83
1.5	0.464	5.85
2.0	0.431	5.88
2.5	0.404	5.91
2.8	0.391	5.92
3.1	0.384	5.93
3.34	0.400	5.91

* These values correspond to the same liquid He_3 extrapolated density of 0.08 g/cc.

energies have been investigated, the total energy $E_{T,a}$ of the antiferromagnetic configuration is smaller than that of the ferromagnetic configuration $E_{T,f}$. Hence, in the present, rather crude, model of liquid He_3 with a density value assumed at the temperature of absolute zero, the liquid would not exhibit nuclear ferromagnetism.

It is not entirely without interest to notice that with the larger Margenau potential energy there is, in a small but physically acceptable cut-off length region, some evidence for the somewhat increased stability of the ferromagnetic configuration. Clearly, it is not justifiable to attach any particular importance to this result beyond noticing its existence. The main reason for this lies in the fact that for these smaller cut-off lengths the exchange energies are about equal to the potential and kinetic energies. The validity of the exchange energy at these cut-off lengths cannot, however, be justified. This situation is similar to the one encountered in the electron case, insofar as the electron gas model leads also to ferromagnetism in the extrapolation of the approximation method to exchange energy regions where the method ceases to be valid.

We should like to add here that the model could be improved along lines suggested by Wigner's work[11] in the electron case. This improvement would correspond to the introduction of correlation between He_3 atoms of opposite spin in the antiferromagnetic configuration. It is likely that one would thus be led to a further strengthening of the conclusions reached above on the larger stability of the vanishing total spin configuration of the system.

4. ON THE NUCLEAR PARAMAGNETIC SUSCEPTIBILITY OF LIQUID He_3

Since our crude model of liquid He_3 leads to a stable non-ferromagnetic configuration, the finite nuclear magnetic moment of the He_3 atoms should manifest itself through a small paramagnetism of the liquid. The main interest of this paramagnetism of this liquid lies in that its experimental study might be of importance in showing, together with other thermodynamic properties, the possible intervention of antisymmetric statistics in the behavior of this fluid.

In the limit of the ideal antisymmetric fluid model, the paramagnetic susceptibility is given by[12]

$$\chi_T=\frac{n\mu^2}{kt}\frac{[-F'(\alpha)]}{F(\alpha)}, \tag{18}$$

where n is the atomic concentration, the spin per atom being $\hbar/2$, μ is the nuclear magnetic moment of He_3 ($\mu=-1.07\times10^{-23}$ c.g.s.),[13] $F(\alpha)$ is the statistical function determined by the temperature and concentration of the fluid according to

$$F(\alpha)=\frac{nh^3\Gamma(\frac{3}{2})}{(2s+1)(2\pi mkT)^{\frac{3}{2}}}$$
$$=\tfrac{2}{3}(T_0/T)^{\frac{3}{2}};\quad F'(\alpha)=dF/d\alpha,$$

with m denoting the mass of a He_3 atom (5.008×10^{-24} g), and T_0 the degeneration temperature at the concentration n,

$$T_0=(h^2/2mk)(3n/4\pi(2s+1))^{\frac{2}{3}}.$$

At the limit of very low temperatures, e.g., $T\ll T_0$,

$$\lim_{T\ll T_0}\chi_T=\frac{3}{2}\frac{n\mu^2}{kT_0},$$

χ_T reduces to the temperature independent Pauli paramagnetic susceptibility. The resultant magnetic susceptibility of liquid He_3 is the sum of its diamagnetic and paramagnetic susceptibilities. The latter is given by the Langevin formula

$$\chi_D=-n(r_0/6)\sum_{i=1}^{Z}\bar{r}_i^2. \tag{19}$$

Here, r_0 denotes the classical electron radius (e^2/mc^2), and $\bar{r}_i^2$ is the mean square of the distance of the i'th atomic electron to the nucleus, the sum being extended over all the Z electrons of the atom. The resultant or total susceptibility, per unit mass, is then

$$\chi_{tot}=(\chi_T-\chi_D)/\rho$$
$$=\frac{\chi_{A,D}(He_4)}{3}+\frac{\mu^2}{m_{He_3}(kT)}\frac{[-F'(\alpha)]}{F(\alpha)}, \tag{20}$$

since the atom-gram diamagnetic susceptibility of He_3 should be practically the same as that of He_4.

Using the approximate Los Alamos liquid He_3 densities together with the experimental value of $\chi_{A,D}(He_4)$ ($=-1.90\times10^{-6}$ c.g.s.),[14] we have collected in Table I,

[11] E. P. Wigner, Phys. Rev. **46**, 1002 (1934) and Trans. Faraday Soc. **34**, 678 (1938).

[12] L. Brillouin, *Les Statistiques Quantiques* (Les Presses Universitaires, Paris, 1930).

[13] H. A. Anderson and A. Novick, Phys. Rev. **73**, 919 (1948).

[14] A. P. Wills and L. G. Hector, Phys. Rev. **23**, 209 (1924); **2A**, 418 (1924); G. G. Havens, Phys. Rev. **43**, 992 (1933).

a series of liquid He_3 susceptibilities per unit mass.[15] Since the diamagnetic mass susceptibility of He_3 is $(-6.31\times10^{-7}$ c.g.s.), it is seen that its paramagnetic mass susceptibility is but a small fraction, 6–8 percent of the former.The paramagnetic mass susceptibility is practically temperature independent in this ideal antisymmetric fluid model, in contrast with the Curie paramagnetism.

It is, of course, realized that the experimental investigation of the very feeble magnetic properties of liquid He_3 would encounter serious difficulties. One of these is the problem of the establishment of statistical equilibrium in an external magnetic field necessary for the nuclear paramagnetic susceptibility to manifest itself in a physically acceptable way. It appears that an extension of the experimental methods of Bloch, Bloembergen, Purcell, and Pound[16] to the investigation of liquid He_3 could yield important information on the statistical behavior of a rather elementary monatomic system in the liquid phase. It is, indeed, clear that the understanding of the laws governing the elementary processes of energy exchange between the nuclear spin system, and the "rest" of this liquid could be of great help in furthering the knowledge of similar phenomena in more complicated systems. We should like then to conclude by saying that the experimental investigation of the magnetic properties of liquid He_3 could yield, together with its other thermal properties, information regarding the possible intervention of antisymmetrical statistics in the general behavior of this fluid. Simultaneously, the nuclear paramagnetism of this liquid offers interesting possibilities in the study of approach to statistical equilibrium, in an external magnetic field and, at very low temperatures, of a unique monatomic system.

[15] The ratios $(-F'(\alpha)/F(\alpha))$ have been obtained with the help of the tables of J. McDougall and E. C. Stoner, Phil. Trans. Roy. Soc. London **A237**, 67 (1938).

[16] F. Bloch, Phys. Rev. **70**, 460 (1946); Bloembergen, Purcell, and Pound, Phys. Rev. **73**, 679 (1948).

THE JOURNAL OF CHEMICAL PHYSICS VOLUME 18, NUMBER 4 APRIL, 1950

Vibration Spectra and Normal Coordinate Treatment of Perfluorocyclobutane*†

HOWARD H. CLAASSEN
Department of Physics, University of Oklahoma, Norman, Oklahoma
(Received November 28, 1949)

The Raman spectra of gaseous and liquid cyclic C_4F_8 at room temperature have been obtained and polarization measurements made for the liquid state. The infra-red absorption spectrum of the gas between 2 and 23.1μ obtained by Dr. D. C. Smith of the Naval Research Laborotory is also reported here. A normal coordinate treatment, based on the assumption that the molecular symmetry is D_{4h}, has been made and applied to assign the 23 fundamental vibration frequencies and to evaluate a set of force constants. The observed spectra have been interpreted in detail.

INTRODUCTION

ALTHOUGH considerable interest has recently been shown in the spectroscopic properties of fluorocarbons, few papers[1,2] have discussed potential functions for fluorinated compounds other than methane derivatives. Values reported for C–F bond stretching force constants have ranged from 9.15 to 3.80×10^5 dynes/cm. Perfluorocyclobutane is an example of a relatively complicated molecule which, because of its high symmetry, is amenable to a vibrational analysis. If a fairly simple potential function is assumed, force constants can be calculated for this molecule. The Raman spectrum of liquid perfluorocyclobutane has been studied by Edgell,[3] who also reported four infra-red absorption maxima and made an assignment of fundamentals.

As a part of a larger project on the spectroscopic properties of fluorocarbons and fluorinated hydrocarbons the vibration spectra of perfluorocyclobutane have been investigated. This paper reports the spectra, their interpretation and a normal coordinate analysis.

EXPERIMENTAL

The sample of perfluorocyclobutane was prepared and purified in the Jackson Laboratory of E. I. du Pont de Nemours and Company. No information was available about its purity. Since it has been possible to interpret satisfactorily all but a very few of the faintest infra-red and Raman bands, the purity is probably high.

The infra-red absorption from 2 to 23.1μ was studied by Dr. D. C. Smith of the Naval Research Laboratory by means of a prism spectrometer of high resolution.[4]

* This work has been supported by the Office of Naval Research under contract N7-onr-398, Task Order I.

† From a dissertation submitted to the Faculty of the Graduate College of the University of Oklahoma in partial fulfillment of the requirements for the degree of Doctor of Philosophy.

[1] E. L. Pace, J. Chem. Phys. **16**, 74 (1948).

[2] W. F. Edgell and W. E. Byrd, J. Chem. Phys. **17**, 740 (1949).

[3] W. F. Edgell, J. Am. Chem. Soc. **69**, 660 (1947).

[4] Nielsen, Crawford, and Smith, J. Opt. Soc. Am. **37**, 296 (1947).

The cell length was 10 cm. The entire spectrum was recorded at 775 mm pressure and regions of high absorption at several lower pressures.

The Raman spectra of gaseous and liquid perfluorocyclobutane were photographed by means of a Lane-Wells Raman Spectrograph. This instrument and the irradiation apparatus used have been described[5] briefly, as has the apparatus for obtaining depolarization factors.[6] The liquid sample was irradiated at room temperature in a sealed Raman tube of 9 mm outside diameter and 15 cm effective length. Although all of the Raman bands interpreted below as fundamentals could be observed for the liquid with an exposure of one hour, exposures of 4, 12, and 50 hours duration were made to obtain as many weaker bands as possible. The gaseous sample was irradiated in a Raman tube 32 mm in outside diameter and of 30 cm effective length at its vapor pressure at room temperature, about three atmospheres. Frequencies were measured on enlarged prints by interpolation between iron arc lines photographed adjacent to the Raman spectra.

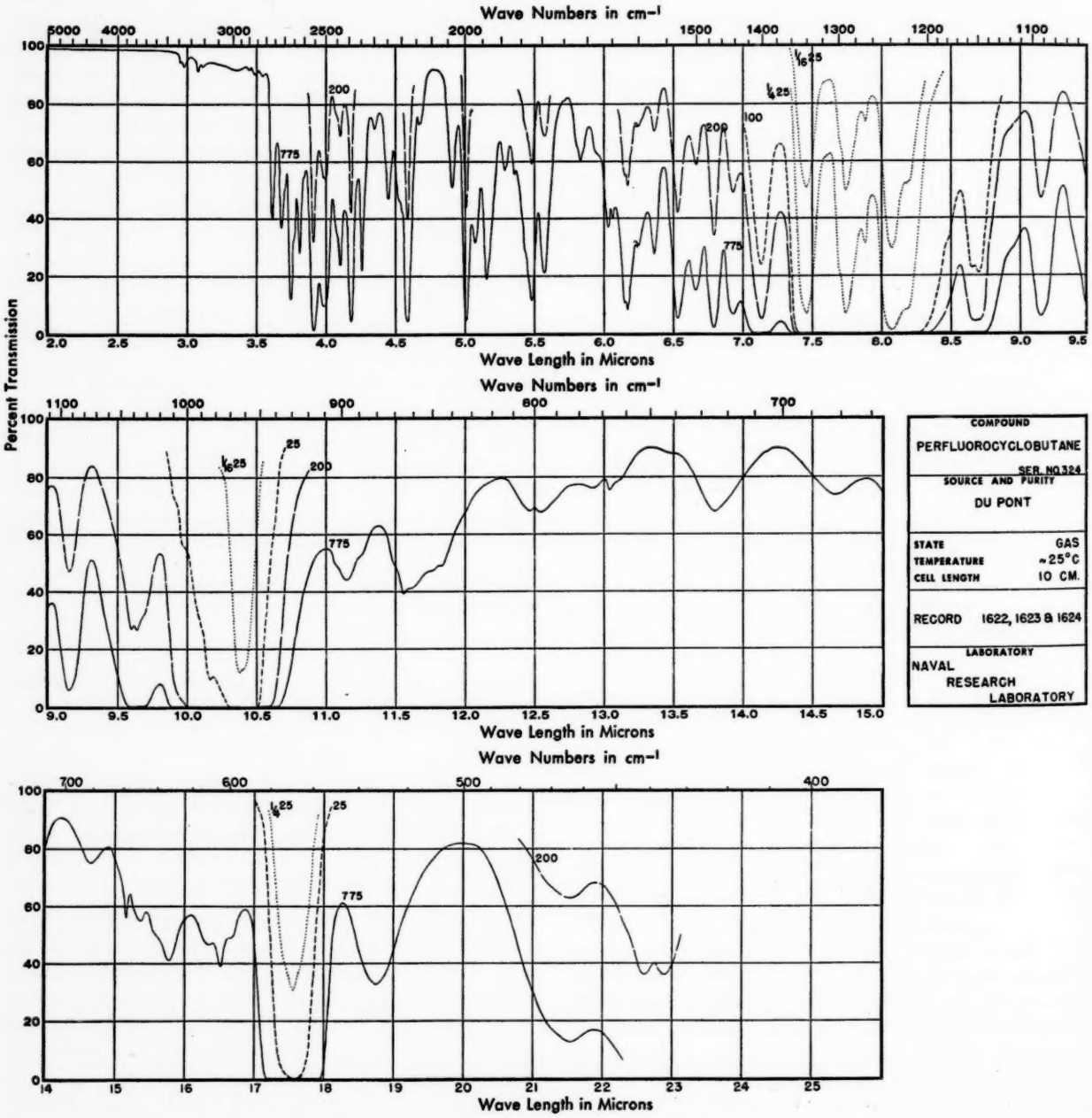

FIG. 1. Infra-red spectrum of perfluorocyclobutane.

[5] Smith, Nielsen, and Claassen, J. Chem. Phys. **18**, 326 (1950).
[6] Nielsen, Claassen, and Smith, J. Chem. Phys. **18**, 485 (1950).

TABLE I. Infra-red spectrum of perfluorocyclobutane (gas).

Wave number	Description	Interpretation
437	*m*	$1008-569=439(E_u)$
442	*m*	$273+173=446(E_u)$
464	*s*	$285+192=477(E_u)$; $2\times86+285=457(E_u)$
533	*m*	$439+(86)=525(E_u)$; $1239-699=540\ (A_{2u})$
569	*vs*	E_u Fundamental
598	*w*	$439+(173)=612(E_u)$
605	*m*	$963-359=604(E_u)$
611	*w*	$(388)+273=611(E_u)$; $439+(173)=612(E_u)$
634	*w*	$2\times173+(285)=631(E_u)$
640	*w*	$359+(285)=644(E_u)$
650	*w*	$1220-569=651(E_u)$
659	*w sh*	$2\times192+(285)=669(E_u)$
682	*vw*	$439+(250)=689(E_u)$
725	*w*	$439+(285)=724(A_{2u}+A_{1u}+B_{1u}+B_{2u})$; $1008-(285)=723(E_u)$
743	*vw*	$660+(86)=746(A_{2u})$
763	*vw*	$569+192=761(E_u)$
767	*vw*	
774	*vw*	$439+(338)=777(E_u)$
797	*vw*	$359+273+(173)=805(A_{2u})$
802	*vw*	$(613)+192=805(A_{2u})$
845	*w*	$569+273=842(A_{2u}+A_{1u}+B_{1u}+B_{2u})$
850	*w*	
858	*w*	$3\times(285)=855(E_u)$
865	*m*	$1431-569=862(E_u)$
870	*w*	$439+258+(173)=870(E_u)$
890	*vw*	$(613)+273=886(E_u)$
897	*w*	$359+(285)+258=902(E_u)$
905	*vw*	$(745)+(173)=918(A_{2u})$; $439+(285)+192=916(A_{2u}+A_{1u}+B_{1u}+B_{2u})$
963	*vs*	E_u Fundamental
983	*s*	$699+285=984(E_u)$
1003	*w*	$1285-(285)=1000(A_{2u}+A_{1u}+B_{1u}+B_{2u})$
1010	*w*	$439+569=1008(A_{2u}+A_{1u}+B_{1u}+B_{2u})$
1030	*w*	$(745)+(285)=1030(E_u)$
1037	*s*	$699+(338)=1037(A_{2u})$
1042	*s*	$(613)+439=1052(E_u)$
1093	*m*	$1008+(86)=1094(A_{2u})$
1149	*s*	$1340-192=1148(E_u)$
1156	*s*	$963+192=1155(E_u)$
1180	*w*	$(745)+273+173=1191(E_u)$; $699+(285)+192=1176(E_u)$
1223	*m*	$963+258=1221(E_u)$; $660+569=1229(E_u)$
1239	*vvs*	A_{2u} Fundamental
1269	*s*	$699+569=1268(E_u)$; $660+(613)=1273(A_{2u})$
1292	*vvs*	$1008+(285)=1293(E_u)$
1304	*w*	$(745)+569=1314(E_u)$
1340	*vvs*	E_u Fundamental

TABLE I.—*Continued.*

Wave number	Description	Interpretation
1403	*s*	$963+439=1402(A_{2u}+A_{1u}+B_{1u}+B_{2u})$
1443	*m*	$1285+173=1458(E_u)$
1473	*s*	$1220+(250)=1470(A_{2u})$
1502	*s*	$1220+(285)=1505(E_u)$
1531	*s*	$1340+192=1532(E_u)$
1572	*m*	$1008+569=1577(E_u)$; $1285+(285)=1570(A_{2u}+A_{1u}+B_{1u}+B_{2u})$
1600	*w*	$1239+359=1598(A_{2u})$; $1340+258=1598(E_u)$
1621	*s*	$963+660=1623(E_u)$; $1008+(613)=1621(A_{2u})$
1626	*s*	$1285+(388)=1623(E_u)$
1649	*w*	$1008+359+(285)=1652(E_u)$
1658	*m*	$963+699=1662(E_u)$; $(1385)+273=1658(E_u)$
1680	*vw*	$1239+439=1678(E_u)$
1715	*w*	$1431+(285)=1716(E_u)$
1795	*m*	$1220+569=1789(E_u)$
1825	*s*	$(1385)+439=1824(E_u)$
1866	*vw*	$1220+358+(285)=1863(E_u)$
1893	*w*	$1285+(613)=1898(E_u)$
1940	*s*	$1239+699=1938(A_{2u})$
1971	*m*	$1008+963=1971(E_u)$
1996	*s sh*	$1431+569=2000(E_u)$; $1340+660=2000(E_u)$
2037	*w*	$1340+699=2039(E_u)$
2135	*vw*	
2141	*vw*	
2180	*s*	$1220+963=2183(E_u)$
2247	*vw*	$1285+963=2248(A_{2u}+A_{1u}+B_{1u}+B_{2u})$
2300	*vw*	$2\times1008+(285)=2301(E_u)$
2347	*m sh*	$1340+1008=2348(E_u)$
2392	*s sh*	$1431+963=2394(E_u)$; $(1385)+1008=2393(A_{2u})$
2437	*m*	$1431+569+439=2439$; $1285+963+192=2440(A_{2u}+A_{1u}+B_{1u}+B_{2u})$.
2508	*s*	$1220+1008+(285)=2513(E_u)$
2557	*s*	$1340+1220=2560(E_u)$
2625	*m sh*	$1340+1285=2625(A_{2u}+A_{1u}+B_{1u}+B_{2u})$
2670	*s*	$1431+1239=2670(A_{2u})$; $(1385)+1285=2670(E_u)$
2718	*m*	$1431+1008+(285)=2724(E_u)$ $2\times1220+(285)=2725(E_u)$
2766	*m*	$1431+1340=2771(E_u)$
2825	*vvw*	$1340+1220+273=2833(A_{2u}+A_{1u}+B_{1u}+B_{2u})$
2869	*vvw*	$1220+963+699=2882(E_u)$
2903	*vvw*	$1285+963+660=2908(A_{2u}+A_{1u}+B_{1u}+B_{2u})$
2976	*vvw*	$2\times1008+963=2979(E_u)$
3213	*vvw*	$1431+1220+569=3220(E_u)$
3250	*vvw*	$2\times1008+1239=3255(A_{2u})$; $1008+1285+963=3256(A_{2u}+A_{1u}+B_{1u}+B_{2u})$.
3356	*vvw*	$2\times1008+1340=3356(E_u)$
3390	*vvw*	$1431+1008+963=3402(E_u)$

RESULTS

The infra-red absorption spectrum of gaseous perfluorocyclobutane from 2 to 23.1μ is shown in Fig. 1. The wave numbers for the observed absorption maxima are given in the first column of Table I. In the second column the relative intensities are indicated by the abbreviations: *vs* very strong, *s* strong, *m* medium, *w* weak, etc.

The Raman shifts observed for gaseous and liquid perfluorocyclobutane are given in the first two columns of Table II. In the third column are given rough estimates of the relative intensities of the bands and, for some bands, information about exceptionally sharp or diffuse appearance. The depolarization ratios measured for the liquid sample are listed in the fourth column. All of the Raman frequencies listed were observed as Stokesian shifts from Hg 4358A, a few from Hg 4047 and 4078A, and several as anti-Stokesian shifts from Hg 4358A. All but the weakest bands were observed on more than one exposure. The listed frequencies are weighted averages.

The Raman spectrum as observed in the present work agrees well with that reported by Edgell, except that more than twice as many bands were found. Two of the shifts reported by Edgell have been observed as pairs of bands. Thus, in place of his value 267 cm^{-1}, 258 and 273 cm^{-1} have been observed; in place of his 651 cm^{-1}, 642.9 and 659.5 cm^{-1} have been observed.

INTERPRETATION OF SPECTRA

Cyclobutane is believed[7] to have the symmetry D_{4h}. That perfluorocyclobutane has the same symmetry was

[7] T. P. Wilson, J. Chem. Phys. **11**, 369 (1943).

TABLE II. Raman spectrum of perfluorocyclobutane (gas and liquid).

Wave Number Gas cm^{-1}	Wave Number Liquid cm^{-1}	Description	Polarization	Interpretation
	192	*m d*	*dp**	B_{2g} Fundamental
	258	*s d*	0.87	B_{1g} Fundamental
	273	*s d*	0.87	E_g Fundamental
	347.0	*s*	*p**	$2\times173=346(A_{1g})$
358.2	360.6	*vs sh*	0.22	A_{1g} Fundamental
	384	*m*	0	$2\times192=384(A_{1g})$
439	438	*vs d*	0.82	E_g Fundamental
	570	*vw*		$2\times(285)=570(A_{1g}+B_{1g}+B_{2g})$
	603	*w*		$358+258=616(B_{1g})$; $2\times173+258=604(B_{1g})$
	659.5	*m sh*	*dp**	B_{2g} Fundamental
	675	*w*		$2\times(338)=676(A_{1g})$
699.3	698.7	*vvs*	0.04	A_{1g} Fundamental
719.3	721.9	*m sh*	0.3	$2\times358.2=716.4(A_{1g})$
	767	*vvw*		
	810	*vvw*		$569+(250)=819(E_g)$
	854	*vvw*		$569+(285)=854(E_g)$; $192+660=852(A_{1g})$
	972	*w*		$699+273=972(E_g)$
1008	1006.5	*s d*	0.82	B_{2g} Fundamental
	1051	*vw*		$963+(86)=1049(E_g)$
	1117	*vvw*		
1220	1215.0	*s*	1**	B_{1g} Fundamental
1285	1281	*m d*	0.9**	E_g Fundamental
	1337***	*vw d*		
1431.3	1429.2	*s sh*	0.69**	A_{1g} Fundamental
	1747	*vvw*		$1285+(745)=1753(E_g)$
	2020	*vvw*		$2\times1008=2016(A_{1g})$

* Cannot be measured accurately because of overlapping.
** Cannot be measured accurately because of uncertainty in background correction.
*** May possibly be the very intense 1340 E_u due to violation of selection rules in the liquid.

TABLE III. Active fundamental vibration frequencies for perfluorocyclobutane.

Symmetry species	Approximate character*	Infra-red (gas) Wave number	Infra-red (gas) Description	Raman (gas) Wave number	Raman (gas) Description
A_{1g}	CF Stretching			1431.3 cm^{-1}	*s sh*
A_{1g}	Ring Stretching			699.3	*vvs sh*
A_{1g}	CF_2 Deformation			358.2	*vs sh*
A_{2u}	CF Stretching	1239 cm^{-1}	*vs*		
A_{2u}	CF_2 Rocking	(338)			
B_{1g}	CF Stretching			1220	*s*
B_{1g}	CF_2 Wagging			258**	*s d*
B_{2g}	CF Stretching			1008	*s d*
B_{2g}	CF_2 Deformation			659.5**	*m sh*
B_{2g}	In-plane Ring Bending			192**	*m d*
E_g	CF Stretching			1285	*m*
E_g	CF_2 Rocking			439	*vs d*
E_g	CF_2 Twisting			273**	*s d*
E_u	CF Stretching	1340	*vs*		
E_u	Ring Stretching	963	*vs*		
E_u	CF_2 Deformation	569	*vs*		
E_u	CF_2 Wagging	(285)			

* Only very rough meaning can be attached to the terms in this column.
** Observed in the liquid only.

TABLE IV. Inactive fundamental vibration frequencies for perfluorocyclobutane.

Symmetry species	Approximate character	Wave number
A_{1u}	CF_2 Twisting	(173)
A_{2g}	CF_2 Wagging	(745)
B_{1u}	CF Stretching*	(1385)
B_{1u}	CF_2 Rocking*	(613)
B_{1u}	Out-of-plane ring bending*	(86)
B_{2u}	CF_2 Twisting	(250)

* Only very rough meaning can be attached to this term.

concluded by Edgell on the basis of his spectral data. The spectra obtained in the present research are much more complete, and several approximate coincidences between infra-red and Raman frequencies are observed, namely at 438, 569, 605, 659, 767, 1010, 1220, and 1337 cm^{-1}. Four of these bands are weak or extremely weak in the Raman spectrum and are observed only in the liquid state, in which the selection rules may possibly break down. This leaves four coincidences to be explained as accidental if the symmetry is D_{4h}. This does not seem unreasonable in view of the large number of frequencies observed. Both the number of intense infra-red bands and the number of intense polarized Raman bands observed are in agreement with the predictions based on the D_{4h} symmetry. Further, it may be noted that no infra-red absorption maxima have been observed near the frequencies of 1431 and 699 cm^{-1}, at which intense polarized Raman bands occur. If the carbon ring were non-planar and the symmetry C_{2v}, the totally symmetrical vibrations would also be infra-red-active. Hence, it seems fairly certain that the symmetry is D_{4h}.

If this is the case, the fundamentals divide themselves in the following manner: $3A_{1g}+1A_{1u}+1A_{2g}+2A_{2u}+2B_{1g}+3B_{1u}+3B_{2g}+1B_{2u}+3E_g+4E_u$. The species A_{1g}, B_{1g}, B_{2g}, and E_g are Raman-active, A_{1g} giving polarized and the other species depolarized bands. A_{2u} and E_u are infra-red-active, whereas A_{1u}, A_{2g}, B_{1u}, and B_{2u} are forbidden in both spectra. The observed infra-red bands cannot be classified as "parallel" or "perpendicular" on the basis of their contours. This is not surprising since the moments of inertia, when computed from plausible assumptions of molecular dimensions, are large and do not differ greatly.

Five Raman bands have been observed to be definitely polarized. Of these the two weakest are readily explained as overtones, so that the three A_{1g} fundamentals are known with certainty. The assignments for the other Raman-active species given in Table III depend largely on the calculations discussed below.

Six intense infra-red absorption bands are observed at 1340, 1292, 1239, 963, 569, and 440 cm^{-1}. Since these lie higher on the average than the intense Raman bands, it is likely that one or two of these six are combination bands and that one or two fundamentals lie below the observed frequency range. The band at 1340 cm^{-1} can be definitely assigned to E_u on the basis of the activity of binary sums. Thus, E_u frequencies can combine with each of the four Raman-active species to give infra-red-active combination bands, whereas A_{2u} frequencies, combining with B_{2g} and with B_{1g} frequencies, give inactive combination bands. Now, all of the frequencies obtained by adding 1340 to the B_{2g} and B_{1g} frequencies of 1008, 660, 192, 1220, and 258 cm^{-1}, are observed as 2347 *m*, 1996 *s*, 1531 *s*, 2557 *s*, and 1600 *w*. For 1292 two sums with B_{2g} and B_{1g} frequencies

namely, 1292+1008=2300 and 1292+1220=2512, are observed as 2300 *vw* and 2508 *s*. For 1239 two such sums, 1008+1239=2247 and 1239+1258=1497, are observed as 2247 *vw* and 1502 *s*, but these can be satisfactorily interpreted otherwise as 1285+693=2248 and 1220+(285)=1505 (E_u). Thus, the indication is that 1239 belongs to A_{2u} and 1340 and 1292 belong to E_u. Now, 1292 can be interpreted as an E_u combination band, 1008 (B_{2g})+(285) (E_u)=1293 (E_u), the intensity of which is presumably enhanced by its proximity to 1340. The value of 285 cm^{-1} for the lowest E_u fundamental, first suggested by its overtone, 570 *vw*, in the Raman spectrum is amply verified by its usefulness in combinations. Eight of the 11 possible combinations of 285 with Raman-active fundamentals are observed in the infra-red. The other three would occur at 543, 558, and 945 cm^{-1}, and are probably masked by the intense infra-red bands at 963 and 569 cm^{-1}. The frequency 285 cm^{-1} cannot belong to any of the other *u* species, because none of the other species can combine with all Raman-active species to give infra-red-active combinations. The other infra-red fundamentals have been assigned largely on the basis of calculations. They are listed in Table III.

The assigned inactive fundamentals are listed in Table IV. These have been evaluated by searching near the computed values for frequencies that would explain by combinations the strongest of the observed infra-red bands not explainable by binary sums of the active fundamentals. All of the inactive frequencies are in at least rough agreement with computed frequencies, but some of the values listed are based on only two or three observed combination bands, and hence are not known with great certainty.

The interpretation of the infra-red and Raman spectra is given in the last columns of Tables I and II. Fundamentals not directly observed are written in parentheses. Of the 88 observed infra-red bands, four are interpreted as fundamentals, 51 as binary sums, six as binary differences, 23 as ternary sums, and four weak or very weak bands are left unexplained. Only such ternary sums have been considered for which the sum of two of the fundamentals was observed in the infra-red or in the Raman spectrum. Of the 26 observed Raman bands, 11 are interpreted as fundamentals, 12 as binary sums or first overtones, and three are left unexplained. One of the unexplained bands practically coincides with the very intense infra-red band at 1340 cm^{-1}, is very weak, and is observed only for the liquid. Hence it is probably a result of violation of the selection rules. The other two are extremely weak and they, as well as the five unexplained infra-red bands, may be caused by impurities.

The agreement between calculated and observed frequencies for binary combination bands is generally very good. Only a few differ by more than 5 cm^{-1}. The intensity relations between corresponding sum and difference bands is plausible in all cases with possibly

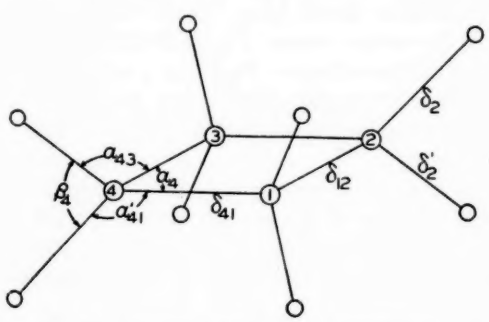

FIG. 2. Numbering of internal coordinates.

TABLE V. Internal symmetry coordinates for perfluorocyclobutane and dependency relations.

Definition of Coordinates

$$^*S_1(A_{1g})=2^{-1}(\alpha_1+\alpha_2+\alpha_3+\alpha_4)$$
$$S_2(A_{1g})=2^{-1}(\beta_1+\beta_2+\beta_3+\beta_4)$$
$$^*S_3(A_{1g})=2^{-2}(\alpha_{12}+\alpha_{21}+\alpha_{23}+\alpha_{32}+\alpha_{34}+\alpha_{43}+\alpha_{41}+\alpha_{14}+\alpha_{12}'+\alpha_{21}'+\alpha_{23}'+\alpha_{32}'+\alpha_{34}'+\alpha_{43}'+\alpha_{41}'+\alpha_{14}')$$
$$S_4(A_{1g})=(2\sqrt{2})^{-1}(+\delta_1'+\delta_2'+\delta_3'+\delta_4'+\delta_1+\delta_2+\delta_3+\delta_4)$$
$$S_5(A_{1g})=2^{-1}(\delta_{12}+\delta_{23}+\delta_{34}+\delta_{41})$$
$$S_1(A_{1u})=2^{-2}(\alpha_{12}-\alpha_{21}+\alpha_{23}-\alpha_{32}+\alpha_{34}-\alpha_{43}+\alpha_{41}-\alpha_{14}-\alpha_{12}'+\alpha_{21}'-\alpha_{23}'+\alpha_{32}'-\alpha_{34}'+\alpha_{43}'-\alpha_{41}'+\alpha_{14}')$$
$$S_1(A_{2g})=2^{-2}(\alpha_{12}-\alpha_{21}+\alpha_{23}-\alpha_{32}+\alpha_{34}-\alpha_{43}+\alpha_{41}-\alpha_{14}+\alpha_{12}'-\alpha_{21}'+\alpha_{23}'-\alpha_{32}'+\alpha_{34}'-\alpha_{43}'+\alpha_{41}'-\alpha_{14}')$$
$$S_1(A_{2u})=2^{-2}(\alpha_{12}+\alpha_{21}+\alpha_{23}+\alpha_{32}+\alpha_{34}+\alpha_{43}+\alpha_{41}+\alpha_{14}-\alpha_{12}'-\alpha_{21}'-\alpha_{23}'-\alpha_{32}'-\alpha_{34}'-\alpha_{43}'-\alpha_{41}'-\alpha_{14}')$$
$$S_2(A_{2u})=(2\sqrt{2})^{-1}(\delta_1+\delta_2+\delta_3+\delta_4-\delta_1'-\delta_2'-\delta_3'-\delta_4')$$
$$S_1(B_{1g})=2^{-2}(\alpha_{12}+\alpha_{21}-\alpha_{23}-\alpha_{32}+\alpha_{34}+\alpha_{43}-\alpha_{41}-\alpha_{14}+\alpha_{12}'+\alpha_{21}'-\alpha_{23}'-\alpha_{32}'+\alpha_{34}'+\alpha_{43}'-\alpha_{41}'-\alpha_{14}')$$
$$S_2(B_{1g})=2^{-1}(\delta_{12}-\delta_{23}+\delta_{34}-\delta_{41})$$
$$S_1(B_{1u})=2^{-2}(\alpha_{12}-\alpha_{21}-\alpha_{23}+\alpha_{32}+\alpha_{34}-\alpha_{43}-\alpha_{41}+\alpha_{14}-\alpha_{12}'+\alpha_{21}'+\alpha_{23}'-\alpha_{32}'-\alpha_{34}'+\alpha_{43}'+\alpha_{41}'-\alpha_{14}')$$
$$S_2(B_{1u})=(2\sqrt{2})^{-1}(-\delta_1+\delta_2-\delta_3+\delta_4+\delta_1'-\delta_2'+\delta_3'-\delta_4')$$
$$S_3(B_{1u})=\gamma$$
$$S_1(B_{2g})=2^{-1}(\alpha_1-\alpha_2+\alpha_3-\alpha_4)$$
$$S_2(B_{2g})=2^{-1}(\beta_1-\beta_2+\beta_3-\beta_4)$$
$$^*S_3(B_{2g})=2^{-2}(\alpha_{12}-\alpha_{21}-\alpha_{23}+\alpha_{32}+\alpha_{34}-\alpha_{43}-\alpha_{41}+\alpha_{14}+\alpha_{12}'-\alpha_{21}'-\alpha_{23}'+\alpha_{32}'+\alpha_{34}'-\alpha_{43}'-\alpha_{41}'+\alpha_{14}')$$
$$S_4(B_{2g})=(2\sqrt{2})^{-1}(\delta_1-\delta_2+\delta_3-\delta_4+\delta_1'-\delta_2'+\delta_3'-\delta_4')$$
$$S_1(B_{2u})=2^{-2}(\alpha_{12}+\alpha_{21}-\alpha_{23}-\alpha_{32}+\alpha_{34}+\alpha_{43}-\alpha_{41}-\alpha_{14}-\alpha_{12}'-\alpha_{21}'+\alpha_{23}'+\alpha_{32}'-\alpha_{34}'-\alpha_{43}'+\alpha_{41}'+\alpha_{14}')$$
$$S_{1a}(E_g)=(2\sqrt{2})^{-1}(\alpha_{12}+\alpha_{21}-\alpha_{34}-\alpha_{43}-\alpha_{12}'-\alpha_{21}'+\alpha_{34}'+\alpha_{43}')$$
$$S_{1b}(E_g)=(2\sqrt{2})^{-1}(\alpha_{23}+\alpha_{32}-\alpha_{41}-\alpha_{14}-\alpha_{23}'-\alpha_{32}'+\alpha_{41}'+\alpha_{14}')$$
$$S_{2a}(E_g)=(2\sqrt{2})^{-1}(\alpha_{23}-\alpha_{32}-\alpha_{41}+\alpha_{14}-\alpha_{23}'+\alpha_{32}'+\alpha_{41}'-\alpha_{14}')$$
$$S_{2b}(E_g)=(2\sqrt{2})^{-1}(-\alpha_{12}+\alpha_{21}+\alpha_{34}-\alpha_{43}+\alpha_{12}'-\alpha_{21}'-\alpha_{34}'+\alpha_{43}')$$
$$S_{3a}(E_g)=(2\sqrt{2})^{-1}(\delta_1+\delta_2-\delta_3-\delta_4-\delta_1'-\delta_2'+\delta_3'+\delta_4')$$
$$S_{3b}(E_g)=(2\sqrt{2})^{-1}(-\delta_1+\delta_2+\delta_3-\delta_4+\delta_1'-\delta_2'-\delta_3'+\delta_4')$$
$$S_{1a}(E_u)=2^{-1}(\alpha_1-\alpha_2-\alpha_3+\alpha_4)$$
$$S_{1b}(E_u)=2^{-1}(\alpha_1+\alpha_2-\alpha_3-\alpha_4)$$
$$S_{2a}(E_u)=2^{-1}(\beta_1-\beta_2-\beta_3+\beta_4)$$
$$S_{2b}(E_u)=2^{-1}(\beta_1+\beta_2-\beta_3-\beta_4)$$
$$S_{3a}(E_u)=(2\sqrt{2})^{-1}(\alpha_{12}-\alpha_{21}-\alpha_{34}+\alpha_{43}+\alpha_{12}'-\alpha_{21}'-\alpha_{34}'+\alpha_{43}')$$
$$S_{3b}(E_u)=(2\sqrt{2})^{-1}(\alpha_{23}-\alpha_{32}-\alpha_{41}+\alpha_{14}+\alpha_{23}'-\alpha_{32}'-\alpha_{41}'+\alpha_{14}')$$
$$^*S_{4a}(E_u)=(2\sqrt{2})^{-1}(-\alpha_{23}-\alpha_{32}+\alpha_{41}+\alpha_{14}-\alpha_{23}'-\alpha_{32}'+\alpha_{41}'+\alpha_{14}')$$
$$^*S_{4b}(E_u)=(2\sqrt{2})^{-1}(\alpha_{12}+\alpha_{21}-\alpha_{34}-\alpha_{43}+\alpha_{12}'+\alpha_{21}'-\alpha_{34}'-\alpha_{43}')$$
$$S_{5a}(E_u)=(2\sqrt{2})^{-1}(+\delta_1-\delta_2-\delta_3+\delta_4+\delta_1'-\delta_2'-\delta_3'+\delta_4')$$
$$S_{5b}(E_u)=(2\sqrt{2})^{-1}(+\delta_1+\delta_2-\delta_3-\delta_4+\delta_1'+\delta_2'-\delta_3'-\delta_4')$$
$$^*S_{6a}(E_u)=2^{-\frac{1}{2}}(\delta_{23}-\delta_{41})$$
$$^*S_{6b}(E_u)=2^{-\frac{1}{2}}(-\delta_{12}+\delta_{34})$$

Dependency Relations

$$S_1(A_{1g})=0$$
$$S_1(A_{1g})+\sqrt{2}S_2(A_{1g})+\sqrt{5}S_3(A_{1g})=0$$
$$S_1(B_{2g})+\sqrt{2}S_2(B_{2g})+\sqrt{5}S_3(B_{2g})=0$$
$$DS_{1a}(E_u)-\sqrt{2}S_{6a}(E_u)=0$$
$$DS_{1b}(E_u)-\sqrt{2}S_{6b}(E_u)=0$$
$$2S_{1a}(E_u)+2\sqrt{2}S_{2a}(E_u)+(10)^{\frac{1}{2}}[S_{3a}(E_u)+S_{4a}(E_u)]=0$$
$$2S_{1b}(E_u)+2\sqrt{2}S_{2b}(E_u)+(10)^{\frac{1}{2}}[S_{3b}(E_u)+S_{4b}(E_u)]=0$$

TABLE VI. *G* Matrices for perfluorocyclobutane.

A_{1g}

$G_{11}=2\mu\epsilon^2+2\eta\epsilon^2(1-\cos\beta)=10.89\times10^{38}$, $G_{12}=-2^{\frac{1}{2}}\eta\epsilon\sin\beta=-4.84\times10^{30}$,
$G_{13}=4\eta\epsilon(\cot\beta-\csc\beta)\cos\alpha=8.66\times10^{30}$, $G_{22}=\mu+4\eta\cos^2\alpha=6.31\times10^{22}$,
$G_{23}=2^{\frac{3}{2}}\eta\cos\alpha=-5.62\times10^{22}$, $G_{33}=2\eta=10.05\times10^{22}$

A_{1u}

$G_{11}=\mu\epsilon^2\csc^2\alpha=2.03\times10^{38}$

A_{2g}

$G_{11}=\mu\epsilon^2\csc^2\alpha+2\eta(\epsilon\csc\alpha-2\tau\cot\alpha)^2=20.7\times10^{38}$

A_{2u}

$G_{11}=\mu\epsilon^2(1-\cot^2\alpha)-4\eta\epsilon^2\cot^2\alpha\cos2\alpha=2.78\times10^{38}$,
$G_{12}=-2^{\frac{3}{2}}\eta\epsilon\cot\alpha\cos2\alpha=-3.09\times10^{30}$, $G_{22}=\mu-2\eta\cos2\alpha=10.08\times10^{22}$

B_{1g}

$G_{11}=\mu\epsilon^2\csc^2\alpha+2\eta\epsilon^2\csc^2\alpha=8.47\times10^{38}$, $G_{12}=-2\eta\epsilon\csc\alpha=-8.04\times10^{30}$, $G_{22}=2\eta=10.05\times10^{22}$

B_{1u}

$G_{11}=\mu\epsilon^2(1-\cot^2\alpha)-4\eta\cos2\alpha(2\tau\csc\alpha-\epsilon\cot\alpha)^2=43.1\times10^{38}$,
$G_{12}=2^{\frac{3}{2}}\eta\cos2\alpha(\epsilon\cot\alpha-2\tau\csc\alpha)=17.0\times10^{30}$, $G_{13}=4\eta\sin\beta/2(2\tau\csc\alpha-\epsilon\cot\alpha)=28.8\times10^{30}$,
$G_{22}=\mu-2\eta\cos2\alpha=10.08\times10^{22}$, $G_{23}=2^{\frac{3}{2}}\eta\sin\beta/2=11.78\times10^{22}$, $G_{33}=4\eta=20.1\times10^{22}$

B_{2g}

$G_{11}=8\eta\tau^2=17.16\times10^{38}$, $G_{12}=8\eta\tau\epsilon(\csc\beta-\cot\beta)\cos\alpha=-11.32\times10^{38}$,
$G_{13}=-2^{5/2}\eta\tau\cos\alpha=7.34\times10^{30}$, $G_{22}=2\mu\epsilon^2+2\eta\epsilon^2(1-\cos\beta)=10.89\times10^{38}$,
$G_{23}=-2^{\frac{1}{2}}\eta\epsilon\sin\beta=-4.84\times10^{30}$, $G_{33}=\mu+4\eta\cos^2\alpha=6.31\times10^{22}$

B_{2u}

$G_{11}=\mu\epsilon^2\csc^2\alpha=2.03\times10^{38}$

E_g

$G_{11}=\mu\epsilon^2-2\eta\epsilon^2\cot^2\alpha\cos2\alpha=2.41\times10^{38}$, $G_{12}=-\mu\epsilon^2\cot^2\alpha-2\eta\cot\alpha(\epsilon^2\cot\alpha-2\tau\epsilon\csc\alpha)\cos2\alpha=3.49\times10^{38}$,
$G_{13}=-2\eta\epsilon\cot\alpha\cos2\alpha=-2.18\times10^{30}$, $G_{22}=\mu\epsilon^2-2\eta\cos2\alpha(2\tau\csc\alpha-\epsilon\cot\alpha)^2=22.6\times10^{38}$,
$G_{23}=2\eta\cos2\alpha(2\tau\csc\alpha-\epsilon\cot\alpha)=-12.01\times10^{30}$, $G_{33}=\mu-2\eta\cos2\alpha=10.08\times10^{22}$

E_u

$G_{11}=4\eta\tau^2=8.58\times10^{38}$, $G_{12}=\eta\epsilon\tau\sec\alpha\sin\beta=-5.66\times10^{38}$, $G_{13}=2^{\frac{3}{2}}\eta\tau(2\tau\cot\alpha-\epsilon\cot\alpha\cos\alpha)=-6.39\times10^{38}$,
$G_{14}=-2^{\frac{3}{2}}\eta\tau\cos\alpha=3.67\times10^{30}$, $G_{22}=2\mu\epsilon^2+2\eta\epsilon^2(1-\cos\beta)=10.89\times10^{38}$,
$G_{23}=2^{-\frac{1}{2}}\mu\epsilon^2\sin\beta\csc2\alpha+2^{\frac{1}{2}}\eta\epsilon\sin\beta(\tau\csc\alpha-\epsilon\cot\alpha)+2^{\frac{1}{2}}\eta\epsilon^2\sin\beta\csc2\alpha=-1.47\times10^{38}$,
$G_{24}=-2^{\frac{1}{2}}\eta\epsilon\sin\beta=-4.84\times10^{30}$, $G_{33}=\mu\epsilon^2+2\eta(4\tau^2\cot^2\alpha+\epsilon^2\cot^2\alpha\cos2\alpha+\epsilon^2-4\tau\epsilon\cot^2\alpha\cos\alpha)=11.04\times10^{38}$,
$G_{34}=-2\eta(2\tau\cot\alpha\cos\alpha+\epsilon\cot\alpha-2\epsilon\cot\alpha\cos^2\alpha)=-0.05\times10^{30}$, $G_{44}=\mu+4\eta\cos^2\alpha=6.31\times10^{22}$

one exception. Thus, the band at 437 cm^{-1}, interpreted as 1008–569, and the corresponding sum band are both listed as being of medium intensity. The intensity estimate for the 437 cm^{-1} band, however, is very unreliable, since the intensity maximum falls only 5 cm^{-1} from that of the sum band at 442 cm^{-1}, and since this region is at the extreme transmission limit of potassium bromide optics.

The present assignment of observed fundamentals does not agree with that given by Edgell[3] except for two frequencies belonging to A_{1g}, one belonging to A_{2u}, and one to E_u. The discrepancy is not surprising, since Edgell's experimental data included only eleven Raman bands and four infra-red bands so that it was not possible for him to check assignments by the activity of combination bands.

NORMAL COORDINATE TREATMENT

Wilson's[8] F–G matrix method was used to set up the secular equations for the various species. The internal coordinates used for the C_4F_8 molecule are: the changes from the equilibrium values in the four C–C–C angles, designated by α_i; in the four F–C–F angles, designated by β_i; in the sixteen C–C–F angles, designated by α_{ij} (or α_{ij}'); in the eight C–F distances, designated by δ_i (or δ_i'); in the four C–C distances, designated by δ_{ij}; and an out-of-plane distortion of the carbon ring, designated by γ. The subscripts, i, $j=1, 2, 3, 4$ refer to different carbon atoms, and the primes refer to fluorine atoms lying "below" the "horizontal" plane of the carbon atoms. Figure 2 illustrates the numbering of the coordinates. There are a total of 37 coordinates; since the molecule has only 30 vibrational degrees of freedom, seven dependency relations exist among them.

The set of 37 symmetry coordinates used to effect the factorization of the secular equation were derived by Mr. L. H. Berryman using a method recently devised.[9] The coordinates and the seven dependency rela-

[8] E. B. Wilson, Jr., J. Chem. Phys. **7**, 1047 (1939); **9**, 76 (1941).

[9] J. Rud Nielsen and L. H. Berryman, J. Chem. Phys. **17**, 659 (1949).

tions existing among them are listed in Table V. The seven coordinates considered as redundant are indicated by asterisks. These were ignored in computing the G matrices but were algebraically eliminated in obtaining the F matrices.

The G matrices for the different symmetry species are given in Table VI. Only elements on and above the main diagonals are listed, since the matrices are symmetrical. In the algebraic expressions α and β are the equilibrium values of the F−C−C and F−C−F angles, respectively; τ and ϵ are the reciprocals of the equilibrium values of the C−C and C−F distances, respectively; and μ and η are the reciprocals of the masses of fluorine and carbon atoms, respectively. The numerical values of order of magnitude 10^{38} have the dimension $g^{-1}\ cm^{-2}$, those of order 10^{30} have the dimension $g^{-1}\ cm^{-1}$, and those of order 10^{22} the dimension g^{-1}. These values are based on assumed molecular dimensions since no electron diffraction data are available for perfluorocyclobutane. The C−F distance was taken as 1.36A, since approximately this value has been observed for several difluoromethanes. The C−C distance was taken as 1.53A, the distance commonly observed in saturated hydrocarbons. The F−C−F angle was assumed to be 112 degrees.

The potential function that has been considered for perfluorocyclobutane is given by the following quadratic expression in the internal coordinates:

$$
\begin{aligned}
2V = {} & x\sum_{i=1}^{4}(\delta_i^2+\delta'_i{}^2)+y\sum_{i=1}^{4}\delta_{i,i+1}{}^2+r\sum_{i=1}^{4}\alpha_i^2+u\sum_{i=1}^{4}\beta_i^2 \\
& +s\sum_{i=1}^{4}(\alpha_{i,i+1}{}^2+\alpha_{i,i-1}{}^2+\alpha'_{i,i+1}{}^2+\alpha'_{i,i-1}{}^2)+v\gamma^2 \\
& +2b\sum_{i=1}^{4}(\delta_{i,i+1}(\alpha_i+\alpha_{i+1}) \\
& +2f\sum_{i=1}^{4}\delta_{i,i+1}(\alpha_{i,i+1}+\alpha_{i+1,i}+\alpha'_{i,i+1}+\alpha'_{i+1,i}) \\
& +2g\sum_{i=1}^{4}[\delta_i(\alpha_{i,i+1}+\alpha_{i,i-1})+\delta'_i(\alpha'_{i,i+1}+\alpha'_{i,i-1})] \\
& +2c\sum_{i=1}^{4}\beta_i(\delta_i+\delta'_i) \\
& +2h\sum_{i=1}^{4}(\alpha_{i,i+1}\alpha_{i+1,i}+\alpha'_{i,i+1}\alpha'_{i+1,i}) \\
& +2k\sum_{i=1}^{4}(\delta_i+\delta'_i)(\delta_{i,i+1}+\delta_{i-1,i}) \\
& +2a\sum_{i=1}^{4}\delta_i\delta'_i,
\end{aligned}
$$

where sums such as $i+1$ are reduced modulo four.

TABLE VII. F matrices for perfluorocyclobutane.

A_{1g}

$u+2(s+h)/5$	$2^{\frac{1}{2}}c-2g/5^{\frac{1}{2}}$	$-2^{\frac{1}{2}}f/5$
	$x+a$	$2^{\frac{1}{2}}k$
		y

B_{1u}

$s-h$	$-2^{\frac{1}{2}}g$
	$x-a$

0	
0	
v	

B_{2g}

$r+(s-h)/5$	$2^{\frac{1}{2}}(s-h)/5$	$2^{\frac{1}{2}}g/5^{\frac{1}{2}}$
	$u+2(s-h)/5$	$2^{\frac{1}{2}}c-2g/5^{\frac{1}{2}}$
		$x+a$

E_g

$s+h$	0
	$s-h$

g	
g	
$x-a$	

B_{1g}

$s+h$	$2f$
	y

A_{2u}

$s+h$	$2^{\frac{1}{2}}g$
	$x-a$

A_{1u} A_{2g} B_{2u}

$s-h$	$s-h$	$s+h$

E_u

$r+2(s+h)/5+D^2y/2$	$4(s+h)/50^{\frac{1}{2}}$	$2(s+h)/10^{\frac{1}{2}}+2^{\frac{1}{2}}Df$	$-2g/10^{\frac{1}{2}}-2^{\frac{1}{2}}Dk$
$-2Db+4Df/5^{\frac{1}{2}}$	$+2^{\frac{1}{2}}Df/5^{\frac{1}{2}}$		$2^{\frac{1}{2}}c-2g/5^{\frac{1}{2}}$
	$u+4(s+h)/5$	$2(s+h)/5^{\frac{1}{2}}$	0
		$2s$	$x+a$

This potential function contains the so-called valence force constants for each internal coordinate, i.e., for the bond lengths and the interbond angles. Interaction constants are included for products of changes of two C−F bonds to the same carbon atom and for products of changes of C−C and C−F bonds to the same carbon atom. Interaction constants are also included for products of the change in each interbond angle with that in each of the bonds forming its sides. Because of the extreme electronegativity of fluorine, repulsions between fluorine atoms may be expected to influence the potential function. Hence, it seems reasonable to consider additional interaction terms for any pairs of coordinates whose relative values will markedly influence the distances between neighboring fluorine atoms. For this reason there has been included an interaction constant for the products of changes in F−C−C angles lying on the same side of the carbon plane and having a C−C bond in common. The symbols that have been used for force constants are: x and y for bond stretching; r, s, u, and v for bond bending, and a, b, c, f, g, h, and k for interaction terms.

The F matrices obtained from this potential function for the different symmetry species are given in Table VII. Only terms on and above the diagonal are listed. For the C−C distance the symbol D is used. For the species A_{1g}, B_{2g}, and E_u, the redundant symmetry coordinates were eliminated by writing out the quadratic forms corresponding to the matrices and making use of the redundancy identities listed in Table V.

The secular equations for the different species were then used to evaluate force constants. The total number of fundamental frequencies is considerably greater than the number of force constants in the assumed potential function. However, for each single species the number of force constants is greater than the number of frequencies. Thus, in no case, can force constants be evaluated from the frequencies of a single species. Further difficulties are caused by the lack of knowledge of the inactive fundamentals and of the species to which a number of the observed frequencies belong. Evaluation of force constants and calculation of several observed

TABLE VIII. Calculated and observed frequencies for perfluorocyclobutane.

Species	Calculated frequencies cm^{-1}	Observed frequencies cm^{-1}
A_{1g}	1431*	1431
	699*	699
	359*	359
A_{1u}	221	(173)
A_{2g}	705	(745)
A_{2u}	1239*	1239
	278	(338)
B_{1g}	1220*	1220
	258*	258
B_{1u}	1453	(1385)
	568	(613)
	86*	(86)
B_{2g}	1066	1008
	554	660
	192*	192
B_{2u}	292	(250)
E_g	1285*	1285
	439*	439
	273*	273
E_u	1399	1340
	935	963
	544	569
	277	(285)

* These frequencies were used to evaluate force constants.

fundamentals as independent checks was possible, however, when use was made of the following assumptions: that the eight Raman-active fundamentals belonging to B_{1g}, B_{2g}, and E_g could be identified with eight of the strongest observed depolarized bands, and that the interaction force constants were so small that calculations in which some of them were set equal to zero could be used as a guide in assignment to species.

Thus, setting interaction constants equal to zero, rough values were obtained for the constants x and y by means of the A_{1g} secular equation and the observed frequencies. These could then be used in further rough computations that indicated: that either 1220 or 1285 cm^{-1} and one of the low frequencies, 273, 258 or 192 cm^{-1} must be assigned to B_{1g}, that the lower A_{2u} fundamental must lie well below 435 cm^{-1}, and that 1285, 439, and one of the low frequencies, 273, 258, or 192 cm^{-1} should be assigned to E_g.

When interaction constants are considered, no single species can be used to evaluate force constants. However, the two species, E_g and A_{2u}, when considered simultaneously, can be used to evaluate force constants. Only the four independent constants, s, $x-a$, g, and h enter these equations, while five equations may be written for the five frequencies belonging to these species. Now, the infra-red band at 1239 cm^{-1} can be assigned to A_{2u} on the basis of infra-red combinations. Using the four equations obtained from this frequency and the frequencies 1285, 439, and 273 cm^{-1}, as suggested above for E_g, four force constants were evaluated: $x-a=5.63\times10^{5}$ dyne/cm, $s=1.17\times10^{-11}$ dyne cm, $h=0.32\times10^{-11}$ dyne cm, and $g=0.39\times10^{-3}$ dyne. This assignment for E_g was supported by later calculations, whereas other assignments which were tried led to absurd results. The second frequency belonging to A_{2u} was calculated at 278 cm^{-1}. By means of the B_{1g} secular equation two further force constants were evaluated: $y=4.07\times10^{5}$ dyne/cm and $f=-0.05\times10^{-3}$ dynes. The Raman bands at 1220 and 258 cm^{-1} were used for the B_{1g} fundamentals. The other plausible choice, 1220 and 192 cm^{-1}, yielded unreasonable force constants.

Next the A_{1g} secular equation and frequencies were used. Although only three frequencies belong to this species, four force constants were considered by treating one of them as a parameter. If the interaction constant, k, is assigned the value 0.2×10^{5} dyne/cm, a solution for the other three is $x+a=6.49\times10^{5}$ dyne/cm, $u=1.44\times10^{-11}$ dyne cm, and $c=0.55\times10^{-3}$ dyne. If k is set equal to zero there is obtained $x+a=5.52\times10^{5}$, $u=1.92\times10^{-11}$, and $c=0.95\times10^{-3}$. If k is set equal to -0.2×10^{5} no real solution exists for the others.

One Raman-active species, B_{2g}, remains to be treated. Five of the force constants evaluated above enter the secular equation for this species, as does the still unknown angle constant r. If the assignments for the other species are correct, there remain only 192, 347, 660 and 1008 cm^{-1} of the intense Raman bands, three of which must belong to B_{2g}. If 192 cm^{-1} is used to evaluate r, the other two can be calculated. This was done for each of the two sets of values above for k, $x+a$, u, and c. The first of the two sets was found to give the best results: 192, 554, and 1066 cm^{-1}. Although this fits the observed values 192, 660, and 1008 cm^{-1} only roughly, the assignment is clearly indicated. It does not seem that the agreement here could be improved materially by choosing another value for k. The other intense Raman band at 347 cm^{-1} is very probably the overtone of an inactive fundamental, the intensity being enhanced by the band's proximity to the very intense A_{1g} fundamental at 359 cm^{-1}.

For E_u, the infra-red-active species having a fourth degree secular equation, all force constants are known except b, an interaction constant for C—C stretching and C—C—C angle change. If this constant is given the value, $b=-0.17\times10^{-3}$ dyne, approximately the average of the values indicated by the two frequencies 1340 and 285 cm^{-1} which were assigned to E_u on the basis of infra-red combinations, there is obtained 1399, 935, 544, and 275 cm^{-1}. This definitely indicates the assignment 1340, 963, 569, and 285 cm^{-1}, and furnishes a strong indication that the earlier work is essentially correct.

The inactive frequencies remain to be calculated. Using the force constants given above we obtain for the A_{1u}, A_{2g}, and B_{2u} fundamentals the values, 221, 705, and 292 cm^{-1}, respectively. In the secular equation for the other inactive species, B_{1u}, to which three frequencies belong, there occurs the constant v for out-of-plane distortion of the carbon ring, about whose magnitude nothing is known. Inspection of the secular equation showed that a frequency between about 140 and

200 cm^{-1} would lead to absurdly high values of v. In the range below 140 cm^{-1} some evidence could be found in combination bands for a B_{1u} fundamental at 86 cm^{-1}. Using this, the value of 0.58×10^5 dynes/cm was found for v. The three calculated frequencies belonging to B_{1u} were then calculated at 1453, 568, and 86 cm^{-1}.

The complete list of calculated and observed fundamentals is given in Table VIII. The frequencies that were used to evaluate force constants are marked by asterisks. Experimental values for the inactive frequencies are listed in parentheses. These were evaluated by searching near the computed values for frequencies that could be used in binary combinations to explain infra-red or Raman bands not interpreted by binary sums of the active fundamentals. Several of the inactive frequencies listed in the observed column must be regarded as doubtful, since only a few combinations could be found in which they occurred.

DISCUSSION

The agreement between calculated and observed frequencies is perhaps as good in most instances as could be expected in view of the uncertainty in the molecular dimensions. The calculations are precise enough to establish with some confidence the assignment of the observed fundamentals. It would be highly desirable to obtain the infra-red spectrum out to 35 microns to look for the two infra-red-active bands predicted at 285 and 338 cm^{-1}. It seems likely that the inaccuracy in B_{2g} may be caused in part by the failure to include interaction terms for pairs of C—C stretching coordinates. Inclusion of such terms, however, would require the evaluation of six force constants from 6 simultaneous equations.

The force constants evaluated are listed in Table IX. These must not be considered as highly accurate in view of the uncertainty in molecular dimensions and of the lack of perfect fit between computed and observed frequencies in a few instances. It is interesting to note that the constants for interaction of pairs of C—F stretching coordinates involving the same carbon atom, and for interaction of F—C—F deformations with the bonds forming the sides are both rather high. This might be expected if repulsions exist between the fluorines in a CF_2 group. The value of 6.06×10^5 dynes/cm for the C—F bond constant is in good agreement with 5.96×10^5 reported by Crawford and Brinkley[10] for CH_3F, but rather far from the values of 9.15×10^5 reported by Pace[1] for C_2F_6 and of 3.80×10^5 reported by Edgell and Byrd[2] for $CF_2=CH_2$. The present assignment leads to a value of 39.2 calories per degree per mole for the heat capacity at constant pressure at 42°C, assuming an ideal gas. Edgell[1] reported that the measured value at this temperature was 37.4. Since many compounds with boiling points comparable to that of perfluorocyclobutane have lower heat capacities, it seems possible that the measured value may be in error on the low side because of impurities. It is also possible that some of the assigned values of the inactive fundamentals are in error.

TABLE IX. Force constants for perfluorocyclobutane.

Description	Symbols	Value dyne/cm
Valence Force Constants		
C—F bond	x	6.06×10^5
C—C bond	y	4.07
C—C—C angle	r/D^2	0.07
F—C—C angle	s/dD	0.56
F—C—F angle	u/d^2	0.78
C distance out of plane	v	0.58
Interaction Constants		
C—C—C angle with C—C dist.	b/D	−0.11
F—C—F angle with C—F dist.	c/d	0.40
F—C—C angle with C—C dist.	f/D	−0.03
F—C—C angle with C—F dist.	g/d	0.29
F—C—C angle with F—C—C angle	h/d^2	0.17
C—C dist. with C—F dist.	k	0.20
C—F dist. with C—F dist.	a	0.43

ACKNOWLEDGMENTS

The writer wishes to acknowledge his indebtedness to Professor J. Rud Nielsen for suggesting the problem and for much helpful criticism; to Dr. D. C. Smith of the Naval Research Laboratory for providing the infra-red absorption data; and to E. I. du Pont de Nemours and Company for the sample.

[10] B. S. Crawford Jr. and S. R. Brinkley, J. Chem. Phys. 9, 69 (1940).

Infra-Red Absorption Spectra at Low Temperatures

A. WALSH AND J. B. WILLIS
Division of Industrial Chemistry, Commonwealth Scientific and Industrial Research Organization, Melbourne, Australia
(Received October 10, 1949)

An infra-red absorption cell for use at low temperatures is described. Use of the cell requires no modification of the optical system of the spectrometer. Spectra of several organic substances which are solid or liquid at room temperature have been recorded and the changes in spectrum on cooling to −170°C observed. The results show that there is no systematic narrowing of infra-red absorption bands on cooling from room temperature to −170°C. The narrowing reported by previous workers is not of general occurrence but is restricted to certain compounds which undergo a change of state in this temperature range.

INTRODUCTION

VERY few data have hitherto been published on infra-red absorption spectra at low temperatures, although it has been pointed out that such data may be of practical value in the analysis of hydrocarbon mixtures[1,2] and of considerable importance in the study of crystal dynamics.[3]

Avery and Ellis[1] measured the spectra of several hydrocarbons as gases at room temperature and as condensed films at −195°C, using a reflection-type absorption cell, and found that the widths of the absorption bands decreased by roughly 50 percent on passage from room temperature to −195°C. In order to investigate whether this narrowing on cooling is of general occurrence, as suggested by Avery and Morrison,[2] we have recorded the spectra over the range 3μ–15μ of several other substances at room temperature and at −170°C.

The reflection-type cell used by Avery and other workers[1,2,4,5] for obtaining low temperature spectra suffers from the disadvantage of requiring a modification of the optical system of most spectrometers. The transmission-type cell described below requires no such modification of the spectrometer (in our case a Perkin-Elmer Model 12B) and is more suitable for use with solids and non-volatile liquids. It can also be used for gases which condense to solids at the temperature of the cooling agent employed, though it is not so suitable as the reflection-type for the study of samples in the vapor state. It seems to resemble in principle the cell described briefly by Axford and Rank in a very recent paper.[6]

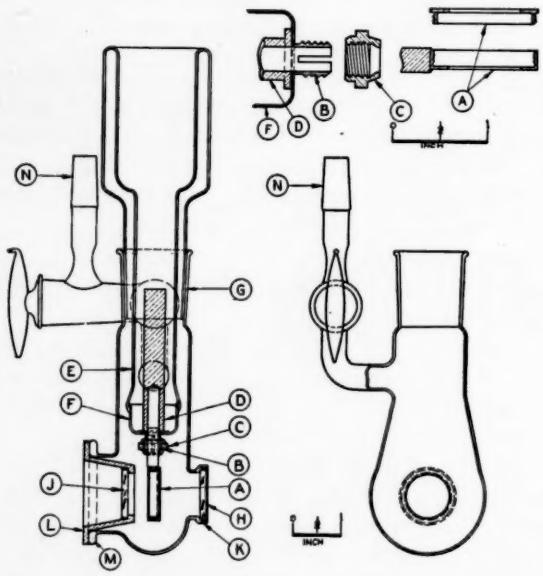

FIG. 1. Low temperature absorption cell.

EXPERIMENTAL

The cell is shown in Fig. 1. The specimen to be studied is carried on a 1-in. diameter rocksalt plate, which is inserted into the brass holder *A* and held firmly by screwing the two halves of *A* tightly together. The inside surfaces of the holder are plane, and thin lead washers are interposed between them and the rocksalt plate in order to ensure good heat transfer from the rocksalt to the metal. The shaft of the holder is inserted into the hollow sprung tube *B* and gripped by tightening the lockscrew *C*. *B* forms the end of a ½-in. diameter copper rod *D* which is sealed through the end of the Pyrex tube *E* by soldering through the "Kovar" metal ring *F*; the latter is sealed to "Kodial" C40 glass and so through a graded seal to the Pyrex tube. This assembly forms the inner part of the complete cell, and is inserted into the outer part by means of the B34 "Quickfit" joint *G*. The outer windows *H* and *J* are 1-in. diameter rocksalt plates, *H* resting on a narrow annular constriction *K*, and *J* on an annular ring at the end of the tapered duralumin holder *L*. The polished flange at the outer end of *L* fits closely over the ground glass flange *M*. The rocksalt windows and flanges are sealed into place with "Apiezon" wax (W40). A B14 joint, *N*, allows for easy attachment to a gas-handling system for evacuation or filling with gas. The inside surfaces of the cell are silvered.

The cell is clamped in the convergent light beam of the spectrometer with the window *H* against the mono-

[1] W. H. Avery and C. F. Ellis, J. Chem. Phys. **10**, 10 (1942).
[2] W. H. Avery and J. R. Morrison, J. App. Phys. **18**, 960 (1947).
[3] D. F. Hornig, J. Chem. Phys. **16**, 1063 (1948).
[4] Conn, Lee, and Sutherland, Proc. Roy. Soc. **176A**, 484 (1940).
[5] R. E. Richards and H. W. Thompson, Proc. Roy. Soc. **195A**, 1 (1948).
[6] D. W. E. Axford and D. H. Rank, J. Chem. Phys. **17**, 430 (1949).

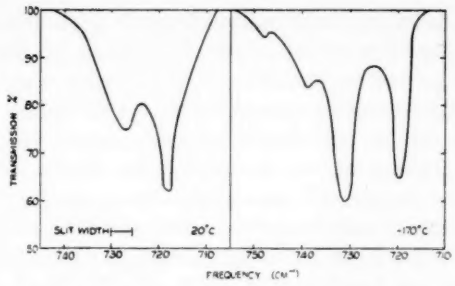

FIG. 2. The absorption at 720–730 cm^{-1} in the spectrum of 4-eicosanone at 20° and −170°C.

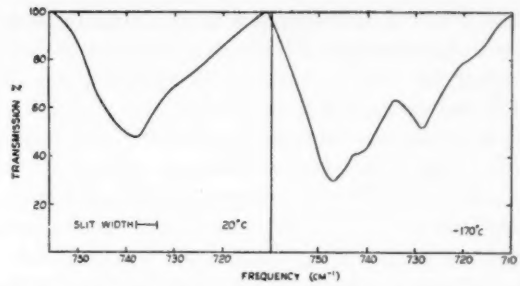

FIG. 3. The 737-cm^{-1} absorption band in the spectrum of 1,4,5,8-tetrahydroxyanthraquinone at 20° and −170°C.

chromator housing. With the dimensions given here there is a slight obstruction of the incident beam by the cell, but the transmission with the windows in position is greater than 80 percent of the light flux obtained with no cell in position.

After evacuating the cell to a Dewar vacuum the cooling agent is poured into the center tube. The temperature attained by the rocksalt plate holding the specimen was tested by means of a thermocouple inserted in a fine hole drilled obliquely into the plate. When liquid oxygen (b.p.−183°C) was used as a cooling agent the rocksalt reached a steady temperature of −167°C in about 10–15 minutes, while with liquid nitrogen (b.p. −195°C) the temperature attained was −178°C. Tests showed that the passage of the infra-red beam through the rocksalt produced a negligible heating effect.

In the case of a solid, the specimen is deposited on a 1-in. diameter rocksalt plate, when possible by vacuum sublimation, though other methods such as deposition from a suspension or solution can be employed. Vacuum-sublimed layers have generally been found in this laboratory to have a fine uniform grain-size with little tendency to scatter infra-red light. When a non-volatile liquid is to be studied, a drop is placed between two thin rocksalt plates with or without a metal shim and the plates inserted in the holder *A* in the usual way. If a condensable gas is to be studied at low temperatures, a rocksalt plate is inserted in the holder and the gas admitted after evacuating the cell and introducing the cooling agent, so that the gas condenses immediately as a solid on the cooled surface of the rocksalt.

The following substances were studied:

(1) Vacuum-sublimed layers of *n*-eicosane, 4-eicosanone, 1,4,5,8-tetrahydroxyanthraquinone and glycine, at room temperature and −170°C.

(2) Ammonium chloride and ammonium nitrate as vacuum sublimed layers at room temperature, −10°, −40°, −70° and −170°C.

(3) Dibutyl phthalate and "Nujol" as liquids at room temperature, as glasses at −70°C and as solids at −170°C.

(4) Methanol as a vapor at room temperature and as a solid at −170°C.

RESULTS

(1) All four organic compounds studied as vacuum-sublimed layers show a number of effects in common on cooling to −170°C. The intensities of the absorption bands, measured as percentage absorption, increase, more particularly in the low frequency region (<1200 cm^{-1}). The high frequency region is almost unaffected. Minor bands which appear only as shoulders on stronger bands at room temperatures are slightly better resolved at the lower temperature. Some of the bands, again almost always in the low frequency region, are narrowed a little, though never to the extent found by Avery and Ellis. Bands sometimes shift in position by several wave numbers but the directions of the shifts seem quite random.

The specimen of *n*-eicosane scattered light badly at frequencies greater than about 1500 cm^{-1}, thus limiting severely the accuracy of measurement for the high frequency region of its spectrum.

Two striking examples of increase of absorption intensity on cooling are given in Figs. 2 and 3 which show the 720-cm^{-1} and 731-cm^{-1} bands of 4-eicosanone and the 737-cm^{-1} band of 1,4,5,8-tetrahydroxyanthraquinone.

(2) Our results for ammonium chloride are in agreement with the data given by Wagner and Hornig[7] for the temperature-dependence of the shape and position of the 1750-cm^{-1} band. The 1410-cm^{-1} band also exhibits a considerable change on going to −170°C. The shoulder on the high frequency side of this band becomes progressively less intense as the temperature is lowered, and the width of the main band decreases (Fig. 4).

In agreement with the work of Keller and Halford,[8]

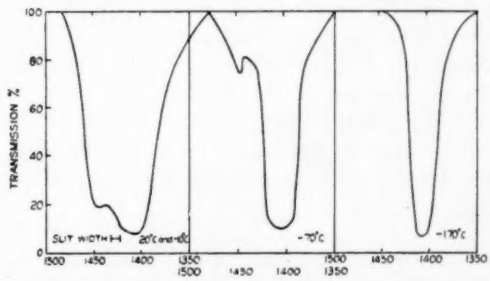

FIG. 4. The 1410-cm^{-1} absorption band in the spectrum of ammonium chloride at 20°, −70° and −170°C.

[7] E. L. Wagner and D. F. Hornig, J. Chem. Phys. **17**, 105 (1949).
[8] W. E. Keller and R. S. Halford, J. Chem. Phys. **17**, 26 (1949).

our spectrum of ammonium nitrate shows little variation with temperature. The band at 1790 cm^{-1} sharpens on cooling to −40°C, shows little further alteration at −70°C, but is considerably sharper at −170°C.

(3) In spite of the change of state on cooling to −170°C, the spectrum of dibutyl phthalate shows practically no difference except that the bands of frequency below 900 cm^{-1} show, in general, an increase of intensity with lowering of temperature, while in the high frequency region the intensities are practically identical for room temperature and −170°C.

In "Nujol" (a mixture of higher paraffins) no frequency shifts are found on lowering the temperature, but there is an over-all increase in the intensities, particularly with the band at 722 cm^{-1}, which increases from 10 percent absorption at room temperature to 30 percent at −170°C.

(4) Although the resolution of our spectrometer is not sufficient to show the rotational lines in the 1034-cm^{-1} band of methanol vapor, the envelope of the *P Q*, and *R* branches is well defined. In the solid, the *P* and *R* branches disappear and there is a single symmetrical band at 1028 cm^{-1}. The positions of the bands at 2850 cm^{-1} and 2980 cm^{-1} do not change significantly on transition from the gaseous state to the solid, but the band at 3680 cm^{-1} is shifted to 3220 cm^{-1} in the solid.

DISCUSSION

As mentioned earlier, Avery and Ellis[1] state that for ethane, propylene, and 2,2-dimethylbutane, which they studied as gases at room temperature and as liquids or solids at −195°C, there is a general decrease of about 50 percent in the band widths. Later, Avery and Morrison[2] reported a similar narrowing for a number of trimethylpentanes in going from the liquid at 0°C to the solid at −195°C. They explained their results on the basis of Bjerrum's[9] formula, $\Delta\nu=(1/\pi c)(KT/I)^{\frac{1}{2}}$, for the wave number separation of the maxima of the *P* and *R* branches of the vibration band of a diatomic molecule. While it has been shown[10] that this formula also holds for a symmetrical top molecule, it is clear that it can only apply where the molecular rotation is quantized, even though the individual rotational lines may not be resolvable. Apart from hydrogen and perhaps methane,[11] no cases are known in which rotational quantization is detectable in the solid state, and therefore the application of the Bjerrum formula must be restricted to gases. There is no reason to expect that the temperature dependence of the widths of the absorption bands of solids should be governed by the same law.

We have recently pointed out[12] that the band-narrowing observed by Avery and Ellis in 2,2-dimethylbutane on passing from the vapor at room temperature to the supercooled liquid at −195°C takes place almost entirely at the gas-liquid transition, and that little further change occurs on cooling the liquid. The fact that the degree of narrowing observed for several bands agreed well with that predicted by the formula is thus to be regarded as fortuitous. Accurate measurement of the band widths using the published spectra is unfortunately difficult, especially as Avery and Ellis do not state whether the widths have been corrected for the spectral slit-width which, in the low frequency part of the spectrum, may be appreciable compared with the band width.

In the spectra of the trimethylpentanes, band-narrowing on cooling certainly occurs, but here again there is a liquid-solid transition between 0° and −195°C which may well cause a large and abrupt spectral change. It is perhaps significant that very considerable band-narrowing was found in ethane on passing from the liquid to the solid.*

With the organic compounds studied in the present work there is no systematic narrowing of the absorption bands with temperature, although minor changes in spectrum do occur in some cases. In the case of methanol, which undergoes a transition from the gaseous state to the solid on cooling, considerable changes are found.

Richards and Thompson[5] have examined the spectra of a number of organic compounds in the solid and liquid state and found that the absorption bands are usually sharper and more numerous in the spectrum of the solid. They suggest that "the broad nature of some of the bands with liquids may arise from the influence of intermolecular collisions, two or more close bands thus being broadened and caused to overlap."

On the other band Halford and Schaeffer[13] predict that, quite generally, substances should show more bands in the liquid than in the solid state, since no selection rules are expected to operate in the liquid state. They also predict that absorption bands which do not appear in the vapor state, but which appear in both liquid and solid should have the greater intensity in the solid state, since intermolecular forces, which serve to bring about such bands, are more powerful in the solid state. The data presented by these authors for the spectrum of benzene fulfil these predictions well,

[9] See G. Herzberg, *Molecular Spectra and Molecular Structure. I. Diatomic Molecules* (Prentice Hall Inc., New York, 1939), p. 131.

[10] S. L. Gerhard and D. M. Dennison, Phys. Rev. **43**, 197 (1933).

[11] G. Herzberg, *Infrared and Raman Spectra of Polyatomic Molecules* (D. Van Nostrand Company, Inc., New York, 1945), p. 532.

[12] A. Walsh and J. B. Willis, J. Chem. Phys. **17**, 838 (1949).

* There is some doubt as to whether Avery and Ellis studied ethane as a liquid. The melting point of ethane is −172°C but while the absorption curves given are labelled "−180°C," they are referred to in the text as having been obtained at −170°C. The authors also state that the temperatures are in doubt by ±10°. However, it seems unlikely that the specimen was solid at this temperature, because of the large changes in the spectrum on cooling to −195°C.

[13] R. S. Halford and O. A. Schaeffer, J. Chem. Phys. **14**, 141 (1946).

but in the case of cyclohexane[14] the spectrum of the liquid is practically identical with that of the solid, both with regard to the positions and the intensities of the bands. The explanation offered is that there is a more orderly arrangement of molecules in liquid cyclohexane than in benzene, so that the intermolecular forces change less on transition to the solid.

It is clear that at the present time no satisfactory explanation of the effect of state of aggregation on spectra can be given. This is not surprising since, as yet, there is no theory which can explain the intensities and shapes of absorption bands in the condensed phases. Until such a theory is forthcoming the temperature dependence of band widths cannot be predicted.

In special cases where rotational isomerism is present in the liquid, a simplification of the spectrum may be expected on solidification, since only the isomer of lower energy is present in the solid state.[6]

Dibutyl phthalate and "Nujol," which are liquids at room temperature, do not show more bands in the liquid state than in the solid. Indeed, the spectra in the two states are virtually identical except that the intensities of the absorption bands, certainly in the low frequency region, are considerably greater in the solid state. However, the solids were examined at a much lower temperature than the liquids, and since the substances which were solid at room temperature also showed increased absorption intensities at −170°C, this increase cannot be ascribed with certainty to an abrupt change at the freezing point. It is of interest to note that Carpenter and Halford[12] also found an increase of band intensity on cooling solid cyclohexane from −3°C to −75°C, together with some narrowing of the bands. Unfortunately, however, the resolution of their spectrometer was higher at the time of taking the readings at −75°C, so it is not possible to say whether the narrowing observed by them was due solely to the decrease of temperature.

The increase of intensity of absorption bands found in the solid specimens on lowering the temperature is rather puzzling. It does not seem to be due to the cracking of the crystalline layer on cooling, since in this event the absorption intensity would presumably decrease, owing to the extra transmission through the holes, and both high and low frequencies would be affected to an approximately equal degree. In all the compounds studied in the present work increase of intensity was confined chiefly to bands in the low frequency region. Measurement of the areas under typical examples of these absorption bands showed that in most cases the integrated intensity also increased a little on proceeding to low temperatures.

The fact that it is the low frequency bands which are most affected on cooling may suggest that it is the skeletal and deformation vibrations of the molecule which are more influenced by intermolecular forces than the stretching vibrations. Attention has already been drawn to the considerable changes undergone by the band in the 720–730-cm^{-1} region in the spectra of "Nujol" and 4-eicosanone which is due to the CH_2 rocking mode.[15,16] However, the results of other workers show that in many compounds the high frequency bands are markedly affected by changes of state. It can be seen, therefore, that it is not possible to give even the most approximate generalization regarding the effect of the state of aggregation on band intensities and positions.

Hornig[3] has discussed the theoretical principles governing the vibration spectra of crystals, and shown that if the vibrations are harmonic, the infra-red spectrum should consist of a series of sharp lines. When there is anharmonicity, combination of the molecular vibrations with lattice vibrations will be possible, and the sharp lines will be converted into the more or less broad bands actually observed. He points out that at sufficiently low temperatures, when only the lower lattice states are occupied, the anharmonicity will be at a minimum, so that each line should be exceedingly sharp, and any anharmonicity present will give combination bands only on the high frequency side of the fundamental. At higher temperatures, on account of the increased population of the higher lattice states, difference bands will be possible, and these will appear on the low frequency side of the fundamental so that at sufficiently high temperatures the bands should become symmetrical. In view of our results it seems that temperatures considerably lower than those obtained with liquid nitrogen are necessary to test Hornig's prediction.†

The considerable changes which take place in the spectrum of a gas on cooling to a condensed state are illustrated by the behavior of the 1034-cm^{-1} band of methanol which arises from the parallel vibration ν_5 between the methyl and hydroxyl groups.[17] Apparently the intermolecular forces in the solid state do not greatly perturb either the frequency of this vibration or the frequencies of the C—H vibrations, ν_1 and ν_2 at 2850 cm^{-1} and 2980 cm^{-1} respectively. The OH vibration, ν_7, which occurs at 3680 cm^{-1} in the vapor,

[14] G. B. Carpenter and R. S. Halford, J. Chem. Phys. **15**, 99 (1947).

[15] N. Sheppard and G. B. B. M. Sutherland, Nature **159**, 739 (1947).

[16] N. Sheppard, J. Chem. Phys. **16**, 690 (1948).

† Since this paper was written, an account of work on the infra-red absorption spectra of some polymers at liquid-helium temperatures has appeared (King, Hainer, and McMahon, J. App. Phys. **20**, 559 (1949)). These authors found little change of spectrum on cooling even to 4°K, except that in the case of polythene the doublet at 720 cm^{-1} undergoes alteration, the 715-cm^{-1} component remaining unchanged on cooling and that at 730 cm^{-1} becoming sharper. This behavior is in close agreement with that of the corresponding band in 4-eicosanone, which is shown in Fig. 2 of the present paper.

[17] A. Borden and E. F. Barker, J. Chem. Phys. **6**, 553 (1938).

appears at 3220 cm^{-1}. As might be expected on account of the increased intermolecular forces in the solid state this frequency is lower than that of 3400 cm^{-1} found[18] for the liquid.

Methanol would repay further study with a reflection-type absorption cell, in which the thickness of the solid layer could be carefully controlled, and it would be interesting to investigate the problem of free rotation in the solid above the λ-point at −113°C.

In conclusion we wish to thank Dr. A. L. G. Rees for his interest and advice, Dr. N. Sheppard for valuable discussion, and Mr. W. G. Jones for his patience and skill in constructing the absorption cell.

This work forms part of the research program of the Division of Industrial Chemistry, Commonwealth Scientific and Industrial Research Organization, Australia.

[18] Buswell, Deitz, and Rodebush, J. Chem. Phys. **5**, 501 (1937).

THE JOURNAL OF CHEMICAL PHYSICS VOLUME 18, NUMBER 4 APRIL, 1950

Surfaces of Solids XIX. Molecular Interaction between Metals and Hydrocarbons

WILLIAM D. HARKINS AND E. H. LOESER
Department of Chemistry, University of Chicago, Chicago, Illinois

(Received November 22, 1949)

The energy of interaction between a hydrocarbon and a metal increases rapidly in the order copper, silver, lead, and iron (Fig. 8), and with the value of P/P_0. Tables Ia and Ib give the values of the energy at $p/p_0=1$; i.e., at saturation of the vapor. The values of the work of adhesion W_A at 25°C for the clean metals are copper 69, silver 77, lead 89, iron 93. For the oxide coated metals the values are only slightly higher (Table Ib). These increase with decrease of temperature. For *n*-hexane they are essentially the same at 0°C as for *n*-heptane at 25°C. Isotherms for *n*-heptane are given for both 25°C and 15°C. Figure 7 illustrates a common phenomenon: a first-order change at 0.02-mm Hg on clean silver.

The method in general use for calculation of the work of adhesion from the adhesion tension is absurd, since for the usual case in which the liquid wets the solid the work of adhesion is given as twice the free surface energy of the liquid. Thus this states that the nature of the solid has nothing to do with the work of adhesion. Unfortunately, all of the books on surface chemistry give this entirely fallacious method of calculation. On this account it is recommended that the use of adhesion tension should be abandoned, since it is one of the most prolific sources of error in Surface Science.

I. WORK OF ADHESION, SPREADING PRESSURE AND SPREADING COEFFICIENT

THIS is the first of a series of papers in which the surfaces of metals or their oxides are considered. The work was begun at the request of the National Advisory Committee on Aeronautics and was a continuation of a project carried out in another institution. In this earlier work the work of adhesion between a metal and a liquid had been calculated from what is known as the adhesion tension (A) between a solid and a liquid, where

$$A=\gamma_L\cos\theta, \qquad \text{(a)}$$

in which θ is the angle of contact between the solid and the liquid and γ_L is the surface tension of the liquid. As this quantity is employed it has led in all cases to incorrect results, as considered later.

The correct equations were developed by the writer, and these were published with some experimental values by Livingston.[1] These values were not accurate since Livingston determined the extent of the adsorption by the use of a quartz spring which does not give accurate results unless the areas are much larger than those involved in his work with anatase and graphite. For these low areas the volumetric method used in the present investigation is much superior.

The number of determinations of the work of adhesion between non-porous solids and liquids thus far made is very small, since no other laboratory than this has engaged in the work, which, if done accurately, is very time-consuming.

The equations applied in this work are the same as those of the earlier paper,[1] except that a symbol π, which gives the film pressure $\gamma_S-\gamma_{Sf}$ is introduced. Here γ_S is the free surface energy of the clean surface and γ_{Sf}, of the surface covered by a film. When the vapor is saturated π is represented by π_e and the film is duplex.

Harkins' spreading coefficient S for a duplex film over a clean surface S is:

$$\pi_e=S_{L/S}=\gamma_S-\gamma_{SL}-\gamma_L. \qquad (1)$$

The increase of free energy on emersion of a clean powder is:

$$f_{E(SL)}=\gamma_S-\gamma_{SL}=\pi_e+\gamma_L. \qquad (2)$$

When the solid and liquid are pulled apart to give 1 sq. cm of the surface of each, the work of adhesion is

$$W_{A(SL)}=\gamma_S-\gamma_{SL}+\gamma_L=f_{E(SL)}+\gamma_L=\pi_e+2\gamma_L. \qquad (3)$$

[1] W. D. Harkins and H. K. Livingston, J. Chem. Phys. **10**, 348 (1942).

The values of these quantities for systems which consist of a metal and an organic substance give valuable knowledge of the magnitude of their molecular interaction, and should be of interest in connection with lubrication.

Equations (2) and (3) are valid in the usual case in which θ, the angle of contact, is zero. For other angles the equations are:

$$f_{E(SL)}=\pi_e+\gamma_L\cos\theta \qquad (2')$$

$$W_A=\pi_e+\gamma_L(1+\cos\theta). \qquad (3')$$

Experimental

The volumetric apparatus used for the determination of the adsorption isotherms was similar to that used earlier in this laboratory[2] except that it was made more complicated by the use of Stock valves instead of stopcocks. As in their work the vapor pressure was obtained to 0.002 to 0.003 mm by use of a differential manometer and traveling microscope sensitive to 0.001 mm, compared with an invar bar calibrated in Paris and Washington by the respective bureaus of standards.

The isotherms (Figs. 1 to 4 at 25°C and 5 and 6 at 15°C, 0.02-mm Hg) differ from those usually obtained in representing a large number of experimental points. The vapor pressure of *n*-heptane at 24.9° is 45.77 mm, and the attainment of equilibrium, especially at the lowest and the highest pressures, is very slow, so a single isotherm requires from two to three weeks for its completion.

The number of molecules of *n*-heptane adsorbed on unit area of iron is at all pressures below $p/p_0=0.9$ greater than on silver. At 0.5 p/p_0 the amount is greater on iron than on silver or lead and on these greater than on copper.

The energy of interaction increases in the order Cu, Ag, Pb, Fe.

At 15°C a first-order change appears at 0.02 mm in the adsorption of *n*-heptane on clean silver.

II. FREE ENERGY OF INTERACTION BETWEEN CLEAN OR OXIDE COATED METALS AND *n*-HEPTANE

Table Ia presents values of the free energy of interaction for surfaces which were reduced by passing hydrogen over them, initially in a high vacuum, at as high a temperature as was judged possible without a modification of the surface otherwise.

Figure 8 gives the values of π, the film pressure, at all values of P/P_0, and Fig. 9 as a function of the mean molecular area σ.

The values for *n*-hexane at 0°C are almost the same as those given above for *n*-heptane at 25°C.

Table Ib gives values for the unreduced (*u*) surfaces.

On reduction of the surface by hydrogen water was given off, and this was collected. The conclusion was reached that the film on the unreduced solids was a very thin film of the oxide.

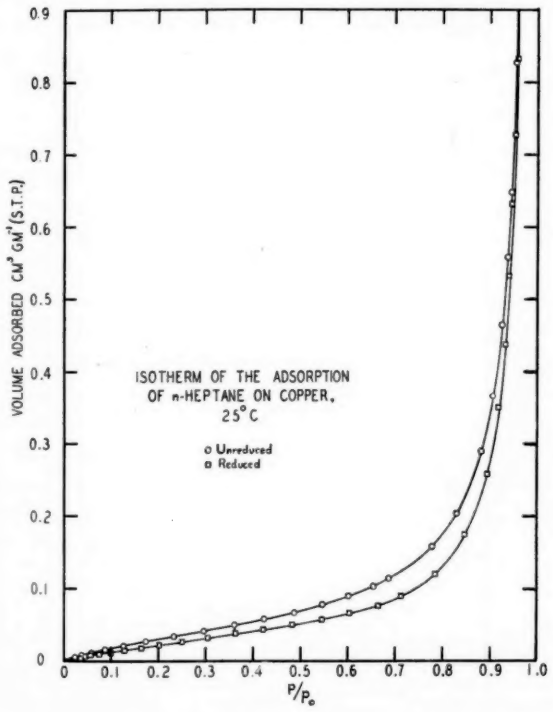

FIG. 1.

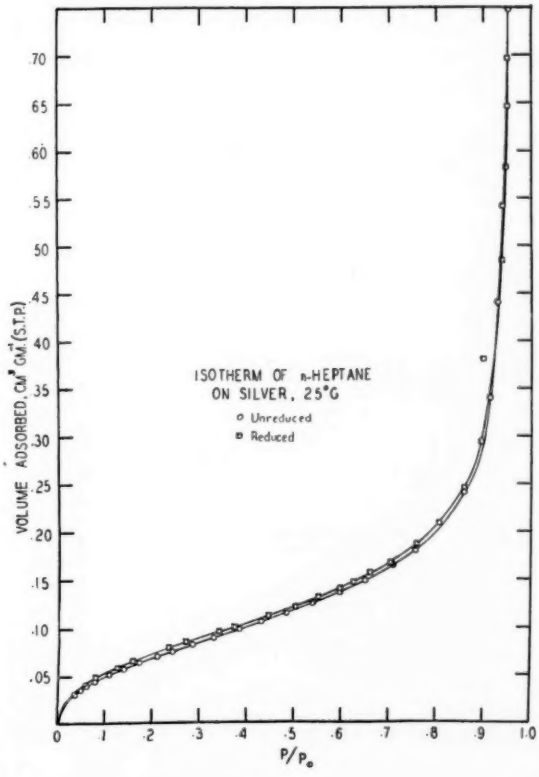

FIG. 2.

[2] G. Jura and William D. Harkins, J. Am. Chem. Soc. **66**, 1358 (1944).

The values for the unreduced surfaces, covered with oxide, are only very slightly higher, one to three ergs per sq. cm, than those for the clean metal, so the presence of the oxide has very little effect in the energy of attraction for a hydrocarbon.

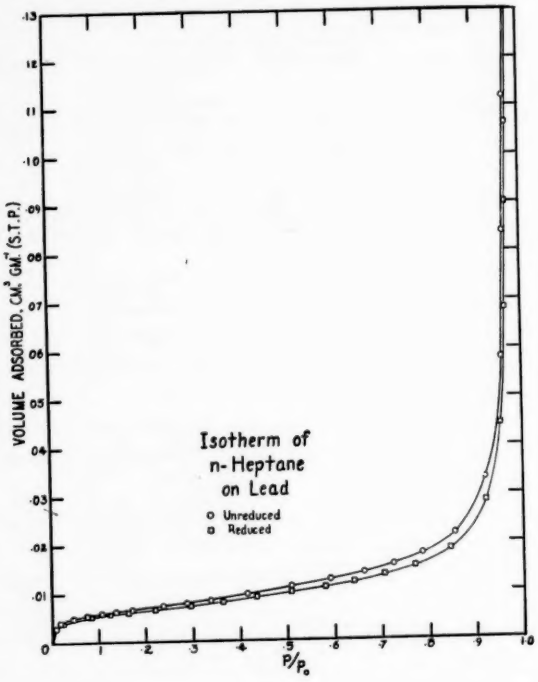

FIG. 3.

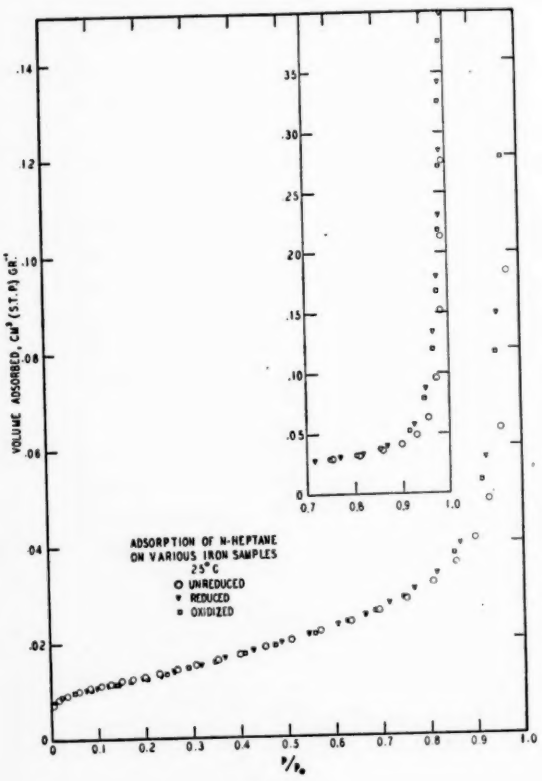

FIG. 4.

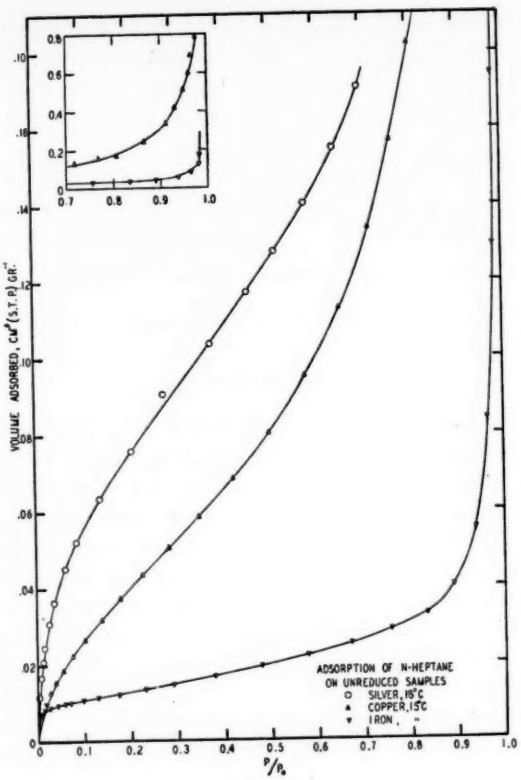

FIG. 5.

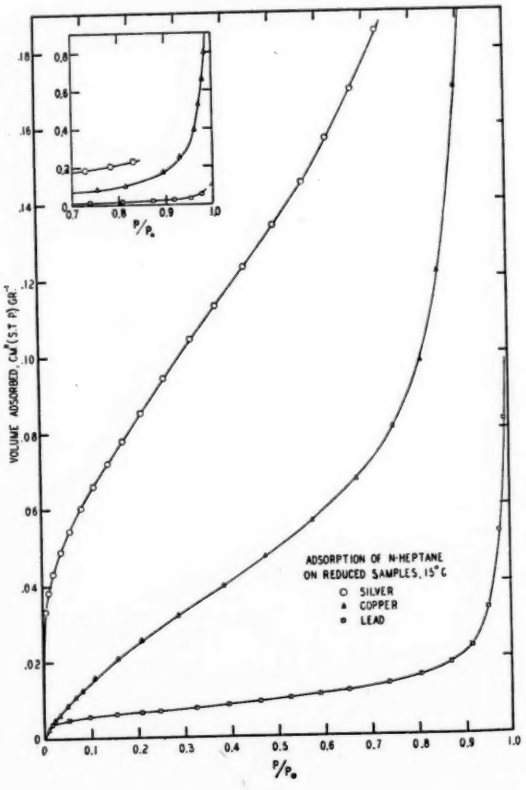

FIG. 6.

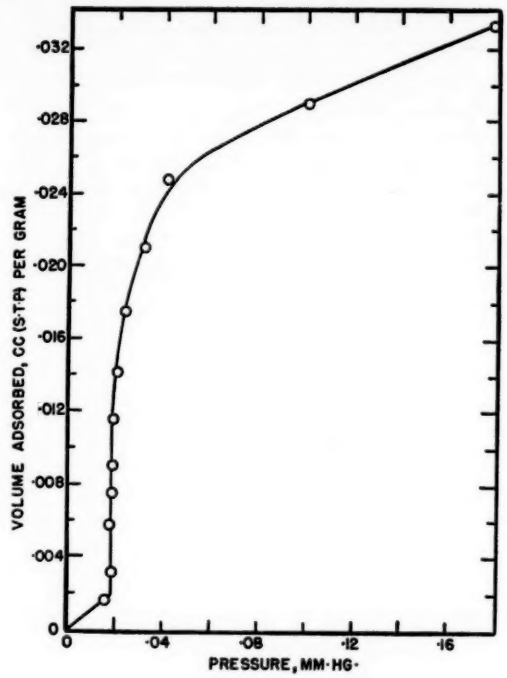

FIG. 7.

This is far from true if alcohols and other compounds containing hydrogen bound to oxygen are involved. In such a case the oxide film produces a large increase in the work of adhesion or any other quantity which is a measure of the attraction between the solid and the liquid. This may be considered as due to a hydrogen bond between the polar group of the liquid and the oxide of the surface.

These values for the physical interaction between metals and an organic liquid may be compared with those obtained earlier in ths laboratory for the work of adhesion at 25° for the following anatase (TiO_2)—liquid systems: water 334, *n*-butane 73, and *n*-heptane 86. Thus the values for *n*-heptane are almost the same for lead and for anatase. For graphite-*n*-heptane the value obtained was 69 erg cm^{-1}, or about the same as with copper.

On water as a subphase the values in ergs per sq. cm at 20°C of the work of adhesion vary from 44 for *n*-octane to 94 for *n*-heptylic acid, and on mercury from 116 for *n*-hexane and 123 for *n*-octane to 157 for *n*-octyl alcohol, 178 for water and 213 for acetylene tetrabromide. Thus the values for liquid mercury are higher than for any of the four solid metals.

III. ADHESION TENSION

During the late war, as well as both earlier and later, a very considerable amount of effort was wasted by governmental and by private agencies in an attempt to determine the energy of interaction between solids, particularly metals, and liquids. This waste was due to the use of incorrect equations based on the *adhesion tension A*, defined by the relation:

$$A = \gamma_L \cos\theta, \qquad (a)$$

as given in Section I. This does not represent an energy of adhesion, since it is merely the component of the surface tension of the liquid along the surface of the solid.

From this the equation which represents the work of adhesion ($W_{A(SL)}$) between the solid and the liquid was derived as:

$$W_{A(SL)} = \gamma_L(1+\cos\theta_{SL}). \qquad (b)$$

TABLE Ia. Free energy of interaction between clean metals and *n*-heptane at 25°C.

	Ergs per cm		
	Spreading coefficient π	Free energy of emersion $f_{E(SL)}$	Work of adhesion W_A
Copper	29	49	69
Silver	37	57	77
Lead	49	69	89
Iron	53	73	93

TABLE Ib. Values for the solids of Table Ia, but before reduction.

Solid	Area sq. meters per gram	Spreading coefficient	Free energy of emersion	Work of adhesion
Cu	0.773	33	53	73
Ag	1.05	38	58	82
Pb	0.099_2	51	71	91
Fe	0.174	54	74	94

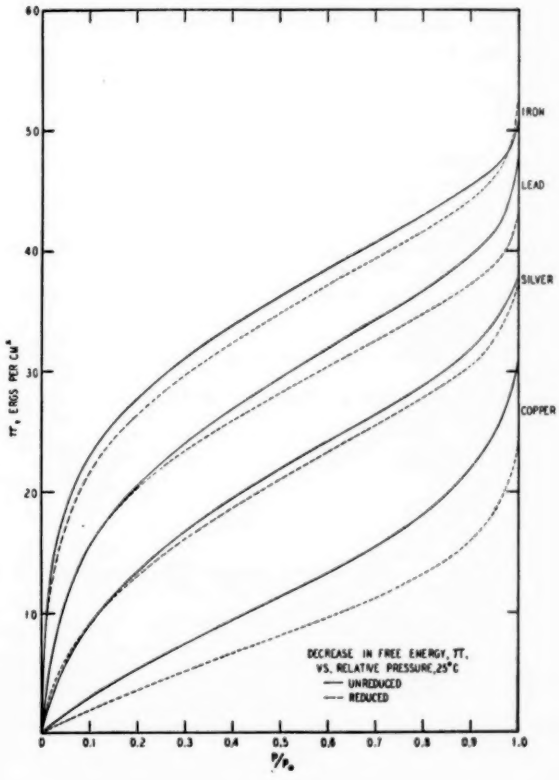

FIG. 8.

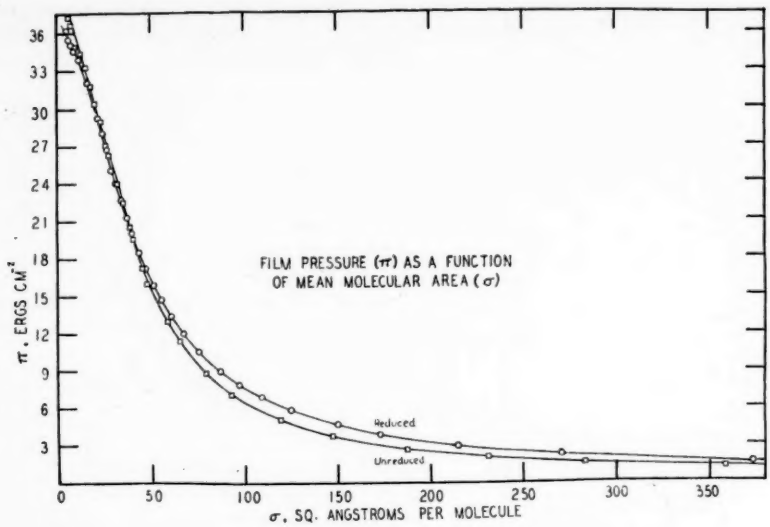

FIG. 9.

This, if the angle of contact is zero, reduces to

$$W_A = 2\gamma_L. \qquad \text{(c)}$$

These equations appear to their users as entirely justified, since they find them to be given by Rideal,[3] Adam,[4] Bikerman[5] and even in the latest book[6] from the Department of Colloid Science, Cambridge University. They are applied more often[7,8] than the correct equations.

However, consider what Eq. (c) expresses: For all cases in which the angle of contact is zero (the usual case with inorganic solids) the work required to pull the liquid completely from the surface of the solid is twice the free surface energy (surface tension) of the liquid and has nothing to do with the surface of the solid.

Obviously this is absurd. The correct equation for the simple case (c) is

$$W_{A(SL)} = \pi_e + 2\gamma_L. \qquad (1)$$

Here π_e is the film pressure at equilibrium with the saturated vapor of the liquid. For *n*-propyl alcohol and anatase, or any other solid at 25°C which this liquid wets, the false Eq. (c) of references 1 to 5 gives the value of the work of adhesion as 46 erg cm^{-1} at 25°C, whereas the true equation gave on the basis of experimental work in this laboratory 154 erg cm^{-1} for anatase. Thus the correct value is 335 percent of the false value obtained if the most prominent books on surface chemistry are followed.

Also the work of adhesion is *not* independent of the nature of the solid. For example, our experiments give 112 erg cm^{-1} for silver instead of the 154 erg cm^{-1} for anatase at 25°C.

The use of Adhesion Tension should be abandoned, since it is one of the most prolific sources of error in Surface Science. With oxides the results it gives are particularly erroneous. For water and anatase π_e has the value 190 erg cm^{-2}, and $W_A = 334$, but on the basis of the equations based on adhesion tension is only 144. Thus the value calculated according to the textbooks is much less than half the correct value.

[3] E. K. Rideal, *Surface Chemistry* (Cambridge University Press, London, 1930), p. 6.
[4] N. K. Adam, *The Physics and Chemistry of Surfaces* (Clarendon Press, Oxford, 1938), p. 179.
[5] J. J. Bikerman, *Surface Chemistry for Industrial Research* (Academic Press, Inc., New York, 1948).
[6] A. E. Alexander and P. Johnson, *Colloid Science* (Clarendon Press, Oxford, 1949).
[7] F. E. Bartell and H. J. Osterhof, Colloid Symposium Monograph 5, 113 (1928), Ind. Eng. Chem. **19**, 1277 (1927, and later papers).
[8] N. F. Miller, J. Phys. Chem. **50**, 300 (1946).

Erratum: Some Observations of the Epitaxy of Sodium Chloride on Silver

GERALD W. JOHNSON
[J. Chem. Phys. **18**, 153 (1950)]

IN the Letter to the Editor of the above title, the captions to Figs. (1) and (3) were reversed. The caption to Fig. 3 should be that appearing under Fig. 1 and *vice versa*.

Letters to the Editor

THIS section will accept reports of new work, provided these are terse and contain few figures, and especially few half-tone cuts. The Editorial Board will not hold itself responsible for opinions expressed by the correspondents. Contributions to this section should not exceed 600 words in length and must reach the office of the Managing Editor not later than the first of the month preceding that of the issue in which the letter is to appear. No proof will be sent to the authors. The usual publication charge ($8.00 per page) will not be made and no reprints will be furnished free.

Application of the Activated State Method to Thermal Diffusion of Solutions (Preliminary Report)

KOZO HIROTA AND ISAO MIYASHITA
Research Institute of Applied Electricity, Hokkaido University, Sapporo, Japan
February 14, 1950

AS is well known, the ordinary diffusion coefficient is derived theoretically, by the activated state method, as follows:

$$D=\lambda^2\frac{kT}{h}\exp(-\Delta H^{\ddagger}/RT+\Delta S^{\ddagger}/R), \quad (1)$$

where λ is the distance of neighboring cages; T, the absolute temperature; $\Delta H^{\ddagger}$ and $\Delta S^{\ddagger}$, the enthalpy and entropy of activation of a particle crossing the cage barrier, respectively; k, h and R, Boltzmann's, Planck's and the gas constant, respectively. In the course of deriving Eq. (1), the rate of flow $\vec{v}$ of the particle to cross the barrier in one direction is defined by the equation

$$\vec{v}=c\lambda(kT/h)\cdot\exp(-\Delta H^{\ddagger}/RT+\Delta S^{\ddagger}/R), \quad (2)$$

where $\mathbf{c}$ is the concentration of the diffusing particles at the initial cage and $\mathbf{v}$ in the opposite direction is defined by the similar equation.

In the previous research,[1] it seemed promising to apply the method to the solute system where thermal gradient exists, provided that the temperatures of the cage barrier (i.e., activated state) and initial cage or final cage are substituted in Eq. (2) or similar equation, according as the direction of crossing is to or against the temperature gradient. Thus it was found that the calculated thermal diffusion coefficient, defined by the ratio $\vec{v}-\overleftarrow{v}$ to $(\mathbf{dT/dX})\cdot\mathbf{c}$, fell in the range of usual experimental values, but it was impossible to make a satisfactory check due to the absence of the data necessary in calculations at that time.

Now, it can be shown by a similar assumption, slightly modifying the derivation, that the thermal diffusion coefficient D' is expressed by

$$D'=\frac{\lambda^2}{2}\frac{k}{h}\frac{\Delta H^{\ddagger}}{RT}\exp\left(-\frac{\Delta H^{\ddagger}}{RT}+\frac{\Delta S^{\ddagger}}{R}\right), \quad (3)$$

which is convenient in comparing the theory with experiment.

For the systems to be utilized in comparison, dilute aqueous solutions of alcohol and cane sugar are adopted, because in these non-electrolyte systems the thermal diffusion potential,[2] which complicates the argument, does not occur, and also because fairly reliable data of $\Delta H^{\ddagger}$, $\Delta S^{\ddagger}$, and λ can be estimated at present, besides the experimental D', as will be shown.

According to Eyring's theory with respect to dielectric relaxation, relaxation time τ_0 is given by

$$1/\tau_0=(kT/h)\exp(-\Delta H^{\ddagger}/RT+\Delta S^{\ddagger}/R). \quad (4)$$

Thus $\Delta H^{\ddagger}$ and $\Delta S^{\ddagger}$ can be evaluated from the temperature dependency of τ_0. As the cage distance λ, the diameter of water $(0.75\text{A})^3$ which is estimated from its self-diffusion coefficient is used.

Together with $\Delta H^{\ddagger}$ and $\Delta S^{\ddagger}$ thus determined, the calculated thermal diffusion coefficients are shown in Table I. For the sake of reference, $\Delta H^{\ddagger}$ calculated from viscosity data is also described in the table. The agreement of the calculated D' with the observed is fairly good, considering the assumptions made in the theory, while the agreement of cane sugar-water system is not so good, probably due to the large size of cane sugar compared with that of the solvent.

TABLE I.

	Calc. values* from Eq. (4) $\Delta H^{\ddagger}$ (kcal.)	$\Delta S^{\ddagger}$ (e.u.)	Experimental values of D' calc.	obs.	Calc. values** from viscosity $\Delta H^{\ddagger}$ (kcal.)
Ethyl alcohol (20 wt. %)—Water	6.0	10	8	1.5[a](40°C)	5.3
Cane sugar (10 wt. %)—Water	4.6	9	40	0.4[b](30°C)	4.3

* Ken'ichi Higashi and Kenji Nukazawa, private communication. Measurement was done at 0°–30°C by use of electric wave of 10.45 cm.
** Landolt-Bornstein *Tables*, H.W. p. 140 for alcohol (Noack) and p. 139 for cane sugar (Hosking).
[a] van Velden, van der Voort, and Gorter, Physica **12**, 151 (1946).
[b] J. van Draner and F. Bergsma, Physica **13**, 558 (1947).

From Eqs. (1) and (3), the relation between thermal diffusion coefficient and ordinary diffusion coefficient will easily be given by

$$D'=\tfrac{1}{2}(d\log D/dT-D/T). \quad (5)$$

The theoretical formula for D' was already derived by Wirtz[4] by the use of the kinetic method, but his equation

$$D'=d\log D/dT \quad (6)$$

is different from Eq. (5).

The check of Eqs. (5) and (6) is carried out with respect to hydrochloric acid of one normal solution. The result is given in Table II.

TABLE II.

	Observed value† at 50°C	Calculated value from Eq. (5)	Calculated value from Eq. (6)
$D'(\times 10^{+7})$	1.7	3.1	8.1

† K. Hirota, Bull. Chem. Soc. Japan **16**, 232 (1941). Clusius-Dickel's column (annular space distance 1.5 mm) was used. The "forgotten effect" (de Groot, Hoogenstraaten, and C. J. Gorter, Physica **9**, 923 (1942)) was not taken into account.

The agreement of Eq. (5) with experiment is very good, thus the validity of Eq. (3) being also supported.

Detailed derivation of Eq. (3) and other discussions will be published in another journal.

[1] K. Hirota and Osamu Kimura, Bull. Chem. Soc. Japan **18**, 111 (1943).
[2] Guthrie, Wilson, and Schomaker, J. Chem. Phys. **17**, 310 (1949); Hirota, J. Chem. Soc. Japan (in Japanese) **64**, 112 (1943).
[3] Glasstone, Laidler, and Eyring, *Theory of Rate Process* (1941).
[4] K. Wirtz, Naturwiss. **27**, 369 (1939); Ann. d. Physik **36**, 295 (1939).

The O—O Bond Dissociation Energy in Tertiary-Butyl-Peroxide

M. SZWARC AND J. S. ROBERTS
Department of Chemistry, University of Manchester, Manchester, England
February 17, 1950

THE very extensive studies of the thermal decomposition of tertiary butyl-peroxide, carried out recently by Vaughan and his colleagues,[1–4] demonstrated beyond any doubt that this decomposition was initiated by the breaking of the O—O bond

according to Eq. (1):

$$(CH_3)_3.C.O-O.C.(CH_3)_3 \rightarrow 2(CH_3)_3.C.O^{\cdot}. \quad (1)$$

Vaughan *et al.* showed also that the character of the subsequent reactions of the $(CH_3)_3.C.O^{\cdot}$ radicals was dependent on the nature of the environment—in the gas phase they decomposed according to Eq. (2):

$$(CH_3)_3.C.O^{\cdot} \rightarrow CH_3.CO.CH_3+CH_3^{\cdot}. \quad (2)$$

It followed also from their observations that the stationary concentration of CH_3 radicals was high, and therefore the association:

$$2CH_3^{\cdot} \rightarrow C_2H_6 \quad (3)$$

was the main reaction responsible for the removal of CH_3 radicals.

From the kinetics of the gas phase decomposition Vaughan and his colleagues concluded that: (1) The over-all reaction is a homogeneous first-order gas reaction; (2) The rate of the over-all reaction is equal to the rate of initial decomposition (1), and therefore the over-all activation energy (39 kcal./mole) is identical with the activation energy of dissociation (1).

Since the above result led to an extremely high frequency factor (3.2×10^{16} sec.$^{-1}$) for the dissociation (1), we decided to reinvestigate the decomposition of tertiary butyl-peroxide. Our work was carried out in a static system, over a temperature range of 40°C (from 120°C to 160°C), tertiary butyl-peroxide being admitted to the reaction vessel together with a great excess of toluene vapor. The rate of reaction was measured by the rate of formation of $CH_4+C_2H_6$, the former being produced by reaction (4):

$$C_6H_5.CH_3+CH_3^{\cdot} \rightarrow C_6H_5.CH_2^{\cdot}+CH_4, \quad (4)$$

the latter resulting from reaction (3). The following observations were made:

(1) The reaction was a homogeneous gas reaction, shown by packing the reaction vessel with short tubing which increased the surface by a factor of 6.

(2) The rate of decomposition obeyed a first-order law, shown by changing the partial pressure of peroxide by a factor of 4. (from 10 mm Hg to 40 mm Hg), and by changing the time of reaction from 15 min. to 240 min.

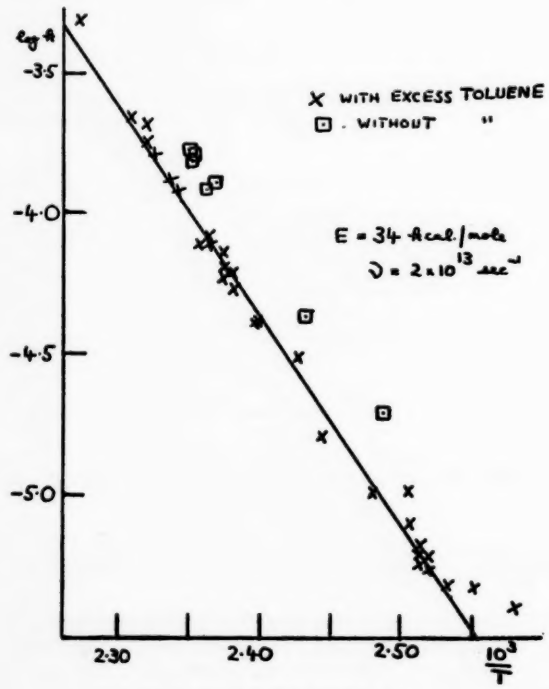

FIG. 1. Plot of log$k$ against $1/T$

(3) The rate of decomposition was independent of the toluene pressure, although the toluene/peroxide ratio was changed from 5 to 25. The increase of the toluene/peroxide ratio caused an increase in the CH_4/C_2H_6 ratio in the products of reaction. This result was to be expected, since the importance of reaction (4) compared with reaction (3) increases with increasing pressure of toluene.

(4) The plot of log$k$ against $1/T$, shown in Fig. 1, yielded $E=34$ kcal./mole and $\nu=2.10^{13}$ sec.$^{-1}$.

(5) The rate of decomposition in the absence of toluene was found to be higher by about 50 percent than the rate observed in the presence of toluene. This observation seems to point to reaction (5):

$$CH_3^{\cdot}+(CH_3)_3.CO.O.C.(CH_3)_3 \rightarrow C_2H_6+CH_3.CO.CH_3+(CH_3)_3CO^{\cdot} \quad (5)$$

which takes place in the absence of toluene, and leads to a very short chain process. This conclusion was supported by further results obtained by a flow technique.

(6) The rates of decomposition in the absence of toluene, measured in our experiments by the rate of formation of $CH_4+C_2H_6$, approximated closely to the rates reported by Vaughan *et al.* although they measured the progress of the decomposition by the increase of pressure.

In view of the above facts we conclude that the O—O bond dissociation energy in tertiary butyl-peroxide is 34 kcal./mole. It seems to us that the higher value recommended by Vaughan *et al.* has to be attributed to:

(a) a very narrow range of temperature, which increases the experimental errors in the estimation of activation energy;

(b) an arbitrary way of measuring the rate (the final pressure, which should be 3 times the initial pressure, was found experimentally to be 2.88 times the initial pressure); and

(c) some minor side reaction, which caused the final pressure to be less than three times the initial pressure and which might cause a great change in the numerical value of the experimental activation energy in view of (a).

A fuller account of this work is in course of preparation.

[1] Raley, Rust, and Vaughan, J. Am. Chem. Soc. **70**, 88 (1948).
[2] Rust, Seabold, and Vaughan, J. Am. Chem. Soc. **70**, 95 (1948).
[3] Raley, Rust, and Vaughan, J. Am. Chem. Soc. **70**, 1336 (1948).
[4] Rust, Seabold, and Vaughan, J. Am. Chem. Soc. **70**, 3259 (1948).

Certain Fourier Transforms and the Structure of Proteins*

DOROTHY WRINCH
Department of Physics, Smith College, Northampton, Massachusetts
February 15, 1950

A RESULT with a bearing on the structure of proteins has emerged from a study of the Fourier transforms of certain point sets. The P_n set is a $216n^2$-point distribution on laminae of a diamond network associated with a truncated tetrahedron $(1\frac{1}{2}, 1\frac{1}{2}, 12n-1\frac{1}{2})_{12}$ of height $h_n=8na$, where a is the metric of the network and $k=a/\sqrt{3}$ the scale of the cubic coordinates. It is derived from the C_n structures[1] which are among those proposed as models for the skeletons of protein molecules;[2] in these structures, in which a value intermediate between the lengths of C—C and C—N single bonds may be represented by $a\sim1.5$A, all atoms of the $72n^2$ (N—C—C) amino acid backbones are replaced by points of equal weight.

The general outline of the transforms of P_n is implicit in previous studies,[3] and we can readily obtain precise information regarding their morphology along various central lines. Thus, with $e_r\equiv e^{2\pi irt^*}$ and t^* in the scale of $3/a$, the section in [111] directions is given by

$$72n^2T(t^*)=9n^2c_{12n}(e_1+e_2)+ins_{12n}(e_1-e_2)+nfs_{12n}/s_4,$$

where $f\equiv4e_{-3}+5e_{-2}+5e_1+4e_2$, an expression in which the fact that there is a single underlying diamond network for all values

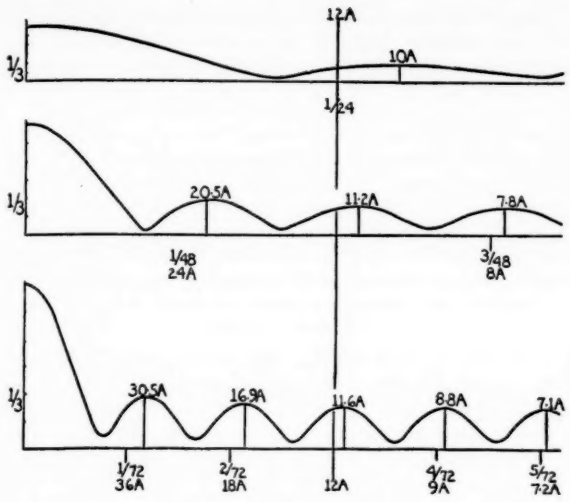

FIG. 1. $T(t^*)$ for $n=1, 2, 3$.

of n interestingly emerges, as, for example in the secondary peak[4] at $t^*=\frac{1}{4}$ for which $|T|=\frac{1}{3}$. A study of this expression elicits the fact that $|T|$ has maxima which are "associated" with natural subdivisions of the unit cell, defined by $t^*=1/24n$, at distance $1/8na=1/h_n$ from the origin. Figure 1 depicts $T(t^*)$ (up to the point $t^*=0.072$), for $n=1$, 2 and 3. The "spacings" with which maxima are "associated" are then $8a\sim$12A, 16a, and 24a, and submultiples. As shown in the figure, actual values of $|T|$ and of these inverse distances are found by calculation to be 0.32, 10A; 0.315, 20.5A; 0.27, 11.2A; 0.25, 7.8A; 0.315, 30.5A; 0.27, 16.9A; 0.25, 11.6A; 0.25, 8.8A; 0.24, 7.1A.

To pass from these results to the case of the C_n structures, we segregate points representing carbons from points representing nitrogens and introduce the damping atomic scattering factors and it is readily verified that the C_n structures have intensity maxima very close to those here given for P_n. Attention may be focused on the fact that all the C_n structures thus have intensity maxima at sets of cube vertices with spacings 10–12A, since outstanding reflections have been found in this neighborhood for a wide range of proteins.[5] Noteworthy cases in the literature include edestin[6] with 11.4A spacings: also tobacco mosaic virus protein[7] with spacings at 11A, the reflexions occurring close to *a set of cube vertices*.

It may be emphasized that in devising any proposed structure for a protein crystal, with a view to testing it against x-ray diffraction data, a formulation of the electron density function is required over the complete unit cell. Such a function will include entries for the molecular skeletons, of which there may be several in the unit of pattern, entries for their interiors (if they have interiors) and for their R-substituents, and entries for the ubiquitous water molecules. Transforming such a distribution into reciprocal (or vector) space is an immensely complicated matter. However, it is often useful in the early stages of a structure analysis if outstanding reflections can be shown to be correlatible with groups of atoms in specified positions, particularly if these groups may constitute what has been called *the major theme*[8] of a range of crystals. In this connection we may recall the outstanding reflexions, at 1.453–1.495A, for olivine and the minerals of the chondrodite series,[9] which are, in fact, a manifestation of the oxygens in hexagonal close packing which constitute the common major theme. If, as has been suggested, protein crystals also have a major theme—which is then necessarily the molecular skeletons —such themes being responsible for pseudosymmetry and twinning and intergrowths of particular types,[10] then it seems possible that making a contact between the transforms of proposed skeletons and outstanding reflections may provide an approach to the structure analyses of protein crystals. Such a contact, it may be claimed, has now been achieved for the C_n skeletons and the 10–11A reflections.

* This work is supported by the ONR under contract N8onr-579.

[1] D. Wrinch, Nature **139**, 972 (1937) *et seq.*
[2] D. Wrinch, Phil. Mag. **31**, 177 (1941); Science **107**, 445 (1948).
[3] D. Wrinch, "Fourier transforms and structure factors, 1946" (Monograph No. 2 of the American Society for X-Ray and Electron Diffraction).
[4] D. Wrinch, Acta Crystallographica (in press).
[5] I. Fankuchen, N. Y. Acad. Sci. **41**, 157 (1941).
[6] Astbury, Dickinson, and Bailey, Biochem. J. **24**, 2351 (1935).
[7] J. D. Bernal and I. Fankuchen, J. Gen. Physiol. **25**, 111 (1941).
[8] D. Wrinch, Am. Mineral. **32**, 695 (1947); Biol. Bull. **95**, 66 (1948).
[9] W. L. Bragg, *Atomic Structure of Minerals* (Cornell University Press, Ithaca, 1937), p. 153.
[10] D. Wrinch, Biol. Bull. **89**, 48 (1945); Am. Mineral. **33**, 781 (1948).

On the Contraction of Organic Chain Molecules

P. GOMBÁS AND T. A. HOFFMANN
Physical Institute of the Hungarian University for Technical Sciences, Budapest, Hungary

February 20, 1950

IN this paper we should like to show that some interesting mechanical properties of organic chain molecules, especially those of the polypeptide chain, may be derived on the basis of simple quantum mechanical conceptions. These properties may offer a possibility for explaining the contraction and relaxation of muscle as well as other biophysical problems.

It is often assumed[1] that in the polypeptide chain the nitrogen atoms are ionized. Let us follow this assumption and consider first the following chain:

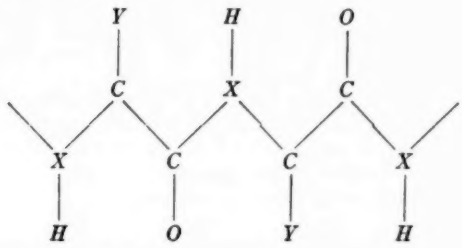

In this chain Y shall represent at first an atom with one valency, that is, the CY bond corresponds to the CH bond. At the X point there are N atoms or N^+ ions, respectively.

We begin with assuming that all the X represent N^+ ions. Both the C atoms and the N^+ ions have the electronic configuration $1s^2\ 2s\ 2p^3$ and are in the trigonal valence state, that is, the 3 valencies are lying in a plane forming angles of 120° with one another. By the p_z orbitals, which are perpendicular to that plane, a resonating π-bond is formed and that causes all the atoms of the chain to lie in a plane.

Let us now consider what would happen if we had at some X points of the chain neutral N atoms instead of the N^+ ions, that is if in the chain considered before some of the N^+ ions were neutralized. The neutral N atom has the electronic configuration $1s^2\ 2s^2\ 3p^3$ with the 3 valence orbitals $p_x\ p_y\ p_z$ which are mutually orthogonal. If we now assume that the chain lies in a plane again, then it can be seen immediately that the chain will contract, since the CNC valence angle decreases with 30° compared to the CN^+C valence-angle (see Fig. 1).

If all the N^+ ions are substituted by N atoms, that is if all N^+ ions are neutralized, this contraction can be calculated with the help of the simplifying assumption that the nuclear distances in every bond and the valence-angles at the C atoms remain the same. With this assumption we obtain in this case a contraction reducing the length of the chain to 0.92 times of its original length.

In the case that only every second N^+ ion is replaced by an N atom, the chain—if we do not take into account the steric effects —would curl up to a ring with a diameter 7.7 times the length of the CCN^+ group. So, for example, a chain of the length of 24 CCN^+

groups would contract to a ring with a diameter of 0.32th of the original chain length.

Similarly we obtain that if in the original chain every 4th, 6th, 8th, 2nth, etc. N^+ ion were neutralized, the chain that contained originally 48, 72, 96, 24n CCN^+ groups, respectively, would close to a ring with a diameter of 0.32th of its former length. Let us, for example, consider a chain containing 12,000 CCN^+ groups. If we neutralized only 12 of the N^+ ions altogether, so that every 1000th N^+ ion would be neutralized, the chain would contract to a ring with a diameter of 0.32th of the original chain length again. This effect is caused in our example by the neutralization of only 1°/00 of the N^+ ions originally present, provided that the ions to be neutralized are distributed equidistant. In the case of equidistant distribution of the 12 neutral N atoms the contraction of the chain is maximal, any other distribution would cause a smaller contraction.

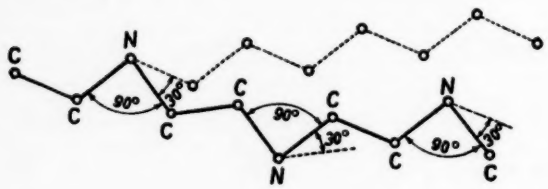

FIG. 1.

The situation is changed if we take into consideration the steric effects too. Taking the spin orientation of the H and O atoms into account, a rough estimation will show us, that the neighboring (CCN^+ CCN^+...CCN) planes are forming an angle different from zero. It follows that by neutralizing the N^+ ions the chain is twisted to a cylinder as a helical curve; that means that a contraction results also in this case.

Let us now assume that one-half of the C atoms is still in the trigonal while the other half is in the tetragonal state, in accordance with that we replace all CY bonds with the CHR groups. In this case the atoms of the chain are not lying in a plane any more. The atoms of the following configurations,

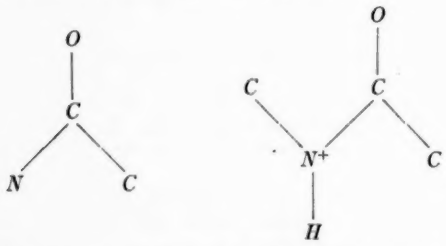

lie again in planes, which are however inclined to one another. If all the N atoms in this chain were again ionized, the arrangement of the atoms would not be very different from that one in a plane. If the chain contained also neutral N atoms the chain links would become twisted in space. The neutralization of the N^+ ions causes a contraction also in this case.

The single chains are joined together by hydrogen-bonds through the NH and CO groups in the following way: $NH.OC$. This structure shows immediately the impossibility to build up a set of chains in a plane-like surface, and shows that a chain complex must have a spatial structure.

Finally we should like to make a remark on the electron mobility in the chain. In this respect there is an essential difference between the chain containing only N^+ ions and the chain that contains neutral N atoms too. While the first one, owing to its unsaturated resonating π-bonds possesses, like the benzene ring, an electron mobility, that is not the case in the second one where the electrons are localized, because of the 3 saturated valencies of the N atoms. The electron mobility is restricted also in the chain with the CHR groups even in the stretched case.

These calculations are only of informative character. A closer and rather difficult investigation of the energy relations would of course lead to more quantitative results.

[1] K. G. Denbigh, Nature **154**, 642 (1944).

The Infra-Red Spectrum and Structure of Ozone

H. S. GUTOWSKY AND ELIZABETH M. PETERSEN
Noyes Chemical Laboratory, University of Illinois, Urbana, Illinois
February 23, 1950

IN the interpretation of the infra-red spectrum of ozone, the appearance of the band envelopes at 1043 cm^{-1} and 2108 cm^{-1} has been questioned[1] and discussed[2,3] in some detail. Recently we had occasion to examine the infra-red spectrum of ozone while investigating the operation of an "ozonizer,"[4] and our observations on the 1043 cm^{-1} and 2108 cm^{-1} bands may be of some general interest. In these observations the contours of the two bands, under the same experimental conditions, are very similar. In particular, the 1043 cm^{-1} band definitely has a Q branch and a detailed comparison with the available data on the 2108 cm^{-1} band indicates the band envelopes are identical in every essential characteristic.

The infra-red spectrum of the gas was observed at room temperature with a Perkin-Elmer Model 12B spectrophotometer equipped with rock salt optics. A number of runs were made with equivalent results. Figure 1 gives the spectra observed for: (A) ozone at a pressure of about 20 cm in a 10-cm gas cell; (B) ozone at an estimated pressure of 10 cm in the spectrometer case containing the primary optics for which the light path is about 40 cm. Under these conditions only the bands at 1043 cm^{-1} and 2108 cm^{-1} were observed in the covered range from 625 cm^{-1} to 4000 cm^{-1}; in addition, faint traces of absorption were apparent in (B) in the region of the 705 cm^{-1} band.

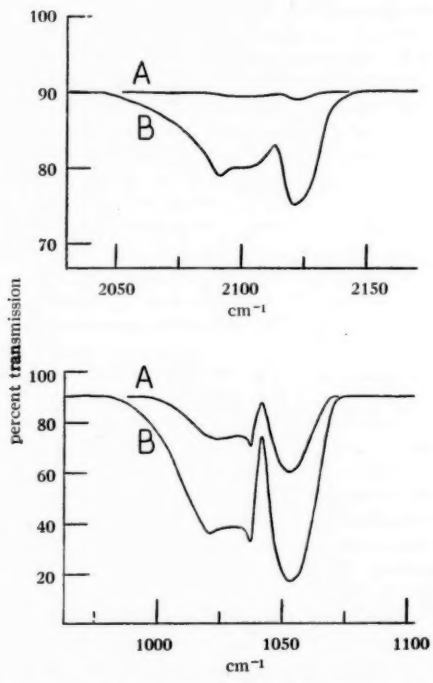

FIG. 1. The 1043 cm^{-1} and 2108 cm^{-1} infra-red absorption bands of ozone.

Both of the band envelopes in Fig. 1 have sharp R branches with considerably broader P branches. The separation of the P

and R maxima is 31 cm^{-1} for the 1043-cm^{-1} band and 28 cm^{-1} for the 2108-cm^{-1} band. As ozone is a near-symmetrical top in either the acute or obtuse-angled model,[1] these separations may be used to estimate the near-equal moments of inertia by means of the expression[5] $\Delta\nu(P-R)=2.358(TB)^{\frac{1}{2}}$ which applies to parallel type bands. The results of 49×10^{-40} g/cm^2 and 60×10^{-40} g/cm^2, respectively, are in good agreement with the values ranging from 50 to 60×10^{-40} g/cm^2 calculated from the fine structure[1,3] of the 705-cm^{-1} band and thus the assignment of both the 1043 cm^{-1} and 2108-cm^{-1} bands as parallel type is confirmed. The one disagreement in the band structures in Fig. 1 is the absence of a well-defined Q branch in the 2108-cm^{-1} band. This is probably due to the poorer resolution of the sodium chloride prism in that region as well as to the relative weakness of the band. However, a comparison of the band envelope in Fig. 1 for the 1043-cm^{-1} band with that given by Adel and Dennison[3] for the 2108-cm^{-1} band in their Fig. 3 can leave little doubt about these bands being of the same type.

This conclusion, while essential for ozone to have an acute-angled structure,[3] is not necessarily inconsistent with the data and frequency assignments of Wilson and Badger[2] which favor the obtuse-angled model. Although their interpretation is probably the most attractive one, perhaps one should point out that on the basis of available spectral data it is not unique. Table I lists the observed spectrum and band types along with possible frequency assignments on the basis of both structures.

TABLE I. The infra-red spectrum of ozone and frequency assignments for acute-angled and obtuse-angled models.

Observed* ν cm^{-1}	Acute-angled model†	Obtuse-angled model
705 D	ν_2	ν_3
1043 Q	ν_3	ν_2
1110 D	ν_1	$\nu_1-\nu_2$; 1062 Q $3\nu_3-\nu_2$; 1072 D
1740 D?	$\nu_2+\nu^0$; 1748 Q	$\nu_2+\nu_3$; 1748 D
2105 Q	$\nu_1+\nu_3$; 2153 Q	ν_1
2800 Q?	$\nu_2+2\nu_3$; 2791 D $\nu_1+\nu_2+\nu_3$; 2858 Q	$\nu_1+\nu_3$; 2810 D $2\nu_2+\nu_3$; 2791 D
3050 Q	$3\nu_3$; 3129 Q	$\nu_1+\nu_2$; 3148 Q $3\nu_2$; 3129 Q

* D—doublet structure; Q—parallel type band with Q branch.
† See reference 2.

[1] D. M. Simpson, J. Chem. Phys. **15**, 846 (1947).
[2] M. K. Wilson and R. M. Badger, J. Chem. Phys. **16**, 741 (1948).
[3] A. Adel and D. M. Dennison, J. Chem. Phys. **14**, 379 (1946).
[4] We are indebted to Professor Murray Sanders, University of Miami, and Dr. E. J. Ryan, Miami, Florida, for the preparation of the ozone.
[5] G. Herzberg, *Infrared and Raman Spectra of Polyatomic Molecules* (D. Van Nostrand Company, Inc., New York, 1945), p. 391.

The Background Scattering of CO_2 and CCl_4, Correction

I. L. KARLE AND J. KARLE
U. S. Naval Research Laboratory, Washington, D. C.
February 2, 1950

IN a recent paper[1] we stated that the background scattering of electrons for CO_2 and CCl_4 appeared to be in disagreement with theory. The theoretical formula for the background scattering is given by

$$\Sigma_i S_i/s^4+\Sigma_i (Z_i-f_i)^2/s^4, \qquad (1)$$

where the summation is over-all atoms in the molecule, S_i is the incoherent atomic scattering factor for x-rays, $(Z_i-f_i)/s^2$ is the coherent atomic scattering factor for electrons and s is a function of the angle of scattering. In comparing our experimental results with theory, Eq. (1) was multiplied erroneously by s^2. The opening in our sector was proportional to s^2. For comparison Eq. (1) should have been multiplied by s since an opening of s^2 in the sector multiplies the scattered intensity by a factor of $s^2/r\cong ks$ where k is a proportionality constant. The agreement between experiment and the recomputed theoretical curves is seen in Fig. 1.

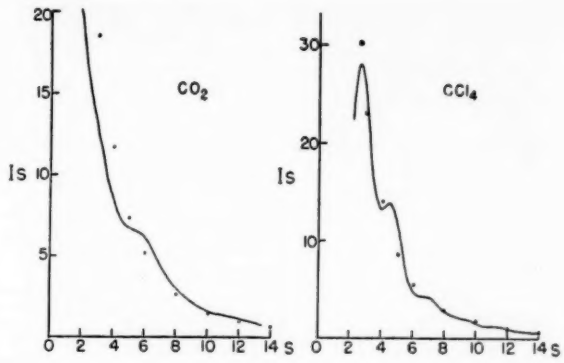

FIG. 1. The solid lines are the experimental scattering curves obtained with a sector whose opening is proportional to s^2. The dots represent the background scattering calculated from tabulated values.

This correction in no way affects our results for the molecular structure and average vibrational amplitudes, since our method does not involve the use of a theoretical background curve. We obtain one experimentally by drawing a line through the oscillations of the experimental intensity curves. It is assumed that this drawn line represents the correct background scattering. The agreement with theory shown in Fig. 1 is additional evidence for the validity of this assumption.

[1] I. L. Karle and J. Karle, J. Chem. Phys. **17**, 1058 (1949).

Microwave Determination of the Structure of Chloroform*

R. R. UNTERBERGER, RALPH TRAMBARULO, AND WILLIAM V. SMITH
Department of Physics, Duke University, Durham, North Carolina
February 10, 1950

THE $J=6$ to $J=7$ rotational transitions of chloroform ($CHCl_3^{35}$) and deuterochloroform ($CDCl_3^{35}$) have been recorded using the Stark modulation technique.[1] In order to obtain the stronger absorptions associated with the high frequencies and low temperatures,[2] a standard K-band two meter Stark cell, provided with cooling and frequency doubling equipment, was used in preference to the longer coiled cell previously utilized in the observations[3] of the $J=2$ and $J=3$ and the $J=3$ to $J=4$ rotational transitions of $CHCl_3^{35}$. Since the chlorine quadrupole moment interacts with the molecular field, the energy levels are split, resulting in weak individual lines. By using pressures near 0.01 millimeter of mercury, the individual lines form an integrated pattern with a single peak and a width of approximately one megacycle at the half power points (see Fig. 1).

Frequency standard[4] measurements of the peaks of the recorded absorptions yield:

$J=6\rightarrow7$	$CHCl_3^{35}$	46,227.2±0.15 MC
$J=6\rightarrow7$	$CDCl_3^{35}$	45,502.4±0.15 MC.

Since the C−H bond in chloroform has some ionic character, the C−H (or C−D) distance was assumed to be 1.090A±0.005A, slightly less than the C−H distance in CH_3Cl [5] and CH_4.[6] These assumptions, together with the observed frequencies and the corresponding moments of inertia, determine the other molecular

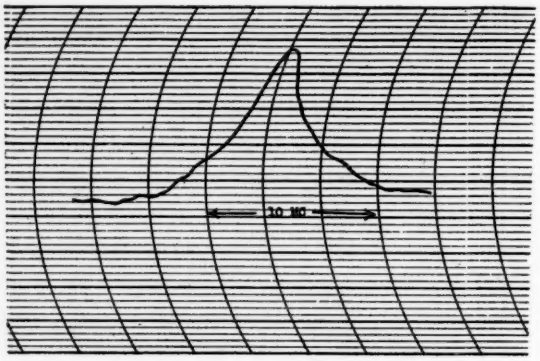

FIG. 1. $J=6-7$; absorption of $CHCl_3^{35}$.

parameters as:

$$d_{C-Cl}=1.761\mp0.004\text{A} \qquad d_{Cl-Cl}=2.908\mp0.004\text{A}$$
$$\angle H-C-Cl=108°\,0'\mp40' \qquad \angle Cl-C-Cl=112°-0'\mp40'.$$

The C−Cl bond is shorter than the value[5] of 1.783A found for methyl chloride and is, within experimental error, equal to the value of 1.760±0.005A found by electron diffraction[7] for CCl_4. The data also agrees with the somewhat less precise electron diffraction data on chloroform[8] and with Pauling's value of 1.76 for the sum of the single bond radii of carbon and chlorine.[9]

Further investigations with C^{13} enriched chloroform are planned to determine completely the structure as preliminary investigations show that the structure is insensitive to variations in the chlorine mass.

* The research reported in this document has been made possible through support and sponsorship extended by the Geophysical Research Directorate of the Air Force Cambridge Research Laboratories under Contract No. W(19-122)ac-35. It is published for technical information only and does not represent recommendations or conclusions of the sponsoring agency.

[1] R. H. Hughes and E. B. Wilson, Jr., Phys. Rev. **71**, 562 (1947).
[2] W. Gordy, Rev. Mod. Phys. **20**, 668 (1948), pp. 695–696.
[3] William V. Smith and R. R. Unterberger, J. Chem. Phys. **17**, 1348 (1949).
[4] R. R. Unterberger and William V. Smith, Rev. Sci. Inst. **19**, 580 (1948).
[5] J. W. Simmons, Phys. Rev. **76**, 686 (1949). Gordy, Simmons, and Smith, Phys. Rev. **74**, 243 (1948). Dailey, Mays, and Townes, Phys. Rev. **76**, 136 (1949).
[6] G. Herzberg, *Infrared and Raman Spectra* (D. Van Nostrand Company, Inc., New York, 1945), p. 439.
[7] L. E. Sutton and L. O. Brockway, J. Am. Chem. Soc. **57**, 473 (1935).
[8] S. H. Bauer, J. Chem. Phys. **4**, 406 (1936). L. R. Maxwell, J. Opt. Soc. Am. **30**, 374 (1940). L. Pauling and L. O. Brockway, J. Am. Chem. Soc. **57**, 2684 (1935). L. O. Brockway, J. Phys. Chem. **41**, 747 (1937).
[9] L. Pauling, *The Nature of the Chemical Bond* (Cornell University Press, Ithaca, New York, 1948), p. 164.

The Planarity of the Urea Molecule*

ROBERT D. WALDRON AND RICHARD M. BADGER
Gates and Crellin Laboratories of Chemistry, California Institute of Technology, Pasadena, California
February 10, 1950

ARGUMENTS based on infra-red observations were recently presented by W. E. Keller for the planarity of the urea molecule in the crystalline state.[1] Though plausible, we have not found these completely convincing since the statement that in a nonplanar model one of the A_1 hydrogen bending fundamentals should be essentially inactive is based on certain assumptions, and not on a selection rule required by symmetry. The really conclusive evidence is to be found in the 3μ region where the resolving power of the spectrometer employed by Keller seems to have been inadequate. In the planar model four N–H valence frequencies may be active, two of which have the character A_1. In the nonplanar C_{2v} model only three of these fundamentals can be active, and only one of these has the character A_1.

Excellent absorption spectra with very high resolution were recently obtained in this laboratory, using polarized radiation and single micro crystals of urea. These observations were made possible by a reflecting microscope or "microilluminator," with polarizing attachment, designed especially to match the optical systems of both the Beckman IR-2 spectrometer and our large vacuum grating instrument.[2] The latter instrument, with lead sulfide detector cooled by solid CO_2, was used in the work mentioned.

As may be seen in Fig. 1, two pairs of intense bands were observed in the 2.9μ region, accompanied by much weaker bands on the long wave side, which are presumably combination frequencies or overtones. These pairs are incompletely resolved in ordinary light but with polarized radiation each was very definitely

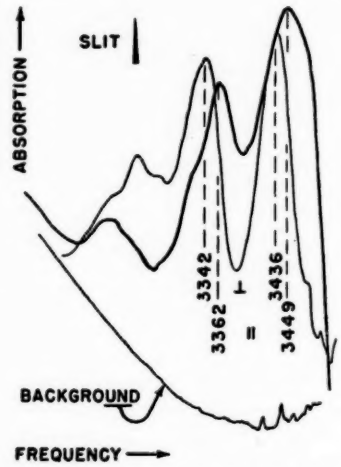

FIG. 1. Recorder tracings of the spectrum of a single urea crystal in polarized infra-red at 2.9μ, obtained with reflecting microscope and vacuum grating spectrometer. Frequencies of the four intense maxima are given. Symbols ⊥ and ∥ indicate direction of electric vector with respect to the tetragonal axis.

shown to consist of two components, one polarized perpendicular, and one parallel to the tetragonal axis. Because of their high intensity we regard it as very probable that the four strong bands are NH stretching fundamentals, and consider that the complete planarity of the urea molecule in the crystal is now reasonably well established by spectroscopic evidence.

* Contribution No. 1391 from the Gates and Crellin Laboratories of Chemistry. The investigation here described was supported in part by the Bureau of Ordnance under Contract N6-ori-102, VI with the ONR.

[1] W. E. Keller, J. Chem. Phys. **16**, 1003 (1948).
[2] Badger, Zumwalt, and Giguère, Rev. Sci. Inst. **19**, 861 (1948).

Eclipsed Configuration of the Hydrazine Molecule in the Solid State[1]

ROBERT L. COLLIN[2] AND WILLIAM N. LIPSCOMB
School of Chemistry, University of Minnesota, Minneapolis, Minnesota
February 20, 1950

THE configuration of the hydrogen atoms in the hydrazine molecule has been discussed for some time. Although the spectroscopic data have been interpreted on the basis of the staggered configuration of C_2 symmetry, they are apparently not in serious conflict with the *cis*-configuration, which is the eclipsed form of C_{2v} symmetry[3] (Fig. 1). The observed dipole moment[4,5] of 1.90 debyes suggests an angle φ, between the projected bisectors of the HNH bonds, of about 84°. Because of the nature of this argument, this value might well be ±20° or more. These dipole moment results are supported by the theoretical considerations of Penny and Sutherland[6] who find φ to be about 90°, or slightly greater. From the nature of hydrogen bonding in hydrazinium difluoride[7] and in hydrazinium dichloride[8] it is inferred that the

$N_2H_6^{++}$ ion has the staggered configuration in these crystals. Thus on the basis of the above evidence, and from the configurations of other related molecules, a configuration for N_2H_4 not far different from the staggered form of C_2 symmetry would be expected.

Our crystal structure investigation has yielded the results shown in Fig. 2. The short N...N distances suggest hydrogen

General	Staggered, C_2	Staggered, C_{2h}	Eclipsed, C_{2v}	Eclipsed, C_2
$\mu=2.55\cos(\varphi/2)$	$\mu=2.2$ $\varphi=60°$	(trans) $\mu=0$ $\varphi=180°$	(*cis*) $\mu=2.55$ $\varphi=0°$	$\mu=1.3$ $\varphi=120°$

FIG. 1. The hydrazine molecule.

bonds in zig-zag chains along the *b* axis, and it is assumed that these bonds require all of the electron pairs and half of the hydrogen atoms. The remaining hydrogen atoms are then inferred to be in the positions indicated in Fig. 2. The short N...N distance in the a.c. plane may also involve some hydrogen bonding, but probably not a specific electron pair, since it is assumed that all are employed for the other hydrogen bonds.

As a result of some preliminary calculations which indicated that inclusion of hydrogen atoms improved slightly the agreement between observed and calculated intensities of x-ray diffraction, the electron density map of Fig. 3 was calculated by the usual method. The coefficients were obtained by taking the difference between the observed structure factors[9] and those calculated from

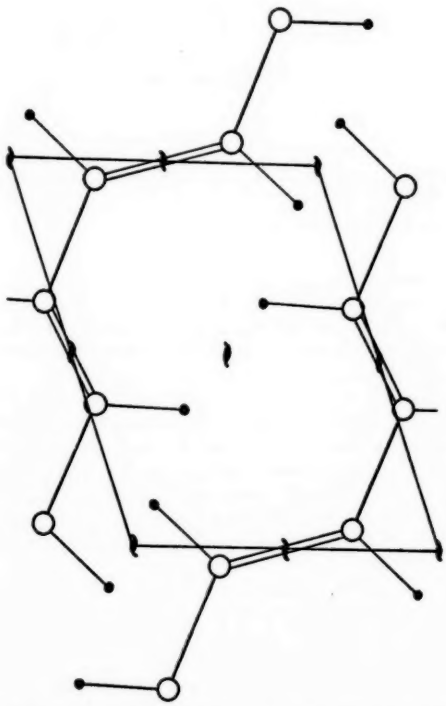

FIG. 2. Projection of the crystal structure of hydrazine along the *b*(5.78A) axis. Hydrogen bond distances, indicated, by double lines, are 3.19A approximately along the *c*(4.53A) axis and 3.30A approximately along the *a*(3.56A) axis. In addition, a short N...N distance of 3.25A occurs in the *ac* plane. The N−N bond distance is 1.46A. The space group is $C_{2h}^2-P_{2_1/m}$.

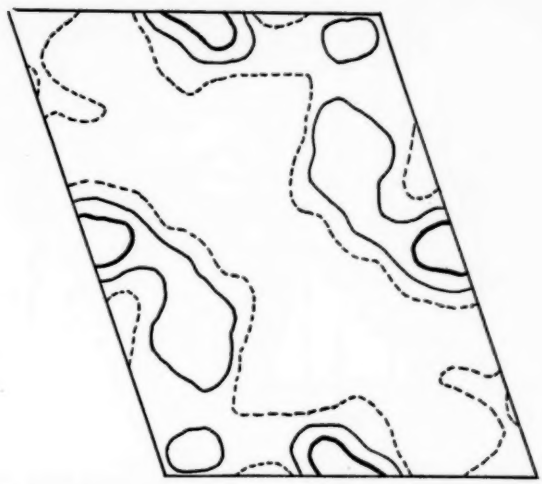

FIG. 3. Electron density map of hydrogen contributions in hydrazine. Contour levels are at 1/2 (dotted) 3/4 (solid, light), and 1 (solid, heavy) electron/A^3.

the positions of the nitrogen atoms alone, and hence the resulting map should yield the hydrogen contributions, provided errors in estimates of the intensities are sufficiently small or random. The correspondence of the high regions in Fig. 3 with the hydrogen atom positions shown in Fig. 2 is rather good. These results are in agreement with those inferred from the short N...N distances, and indicate that in the solid state the hydrazine molecule has one or the other of the eclipsed configurations. It is not necessarily inferred that the configuration in the gas phase is eclipsed inasmuch as the thermochemical data suggest to us that hydrogen bonding stabilizes the crystal by about 7 kcal./mole over that estimated for dispersion forces alone. Hence a small barrier could easily be overcome in the formation of the solid from the gas molecules.

The possibility of a residual entropy of about 0.44 cal./mole degree was suggested by the calorimetric study.[3] However, the positions of hydrogen bonds indicated in our diffraction study do not permit measureable residual entropy to be retained at absolute zero.

[1] This research was supported by Contract N8onr-66203 between the ONR and the University of Minnesota, and by a predoctoral fellowship to Robert L. Collin sponsored by the Shell Oil Company.
[2] Present address: Department of Research in Chemical Physics, Mellon Institute, Pittsburgh, Pennsylvania.
[3] Scott, Oliver, Cross, and Hubbard, J. Am. Chem. Soc. **71**, 2293 (1949).
[4] Ulrich, Peisker, and Audrieth, Ber. der Deutsch. Chem. Ges. **B68**, 1677 (1935).
[5] Combination of the N−H bond moment of 0.9 debye, estimated from the electronegativity difference, with the observed moment of 1.46 debyes in NH_3 gives an effective moment of 0.55 debye for the electron pair. These values then lead to the expression, listed in Fig. 1, for the dipole moment of N_2H_4 on the assumption of tetrahedral configuration about the nitrogen atoms.
[6] W. G. Penny and G. B. B. M. Sutherland, Trans. Faraday Soc. **30**, 898 (1934); J. Chem. Phys. **2**, 492 (1934).
[7] W. L. Kronberg and D. Harker, J. Chem. Phys. **10**, 309 (1942).
[8] R. W. G. Wyckoff, Am. J. Sci. **5**, 15 (1923); J. Donohue and W. N. Lipscomb, J. Chem. Phys. **15**, 115 (1947).
[9] These data and the methods of the structure determination will be published in the Acta Crystallographica. The scattering curve for nitrogen was that listed in the *Internationale Tabellen zur Bestimmung von Kristallstrukturen* (Gebruder Borntraeger, Berlin, 1935), with a temperature factor $\exp(-2.9\sin^2\theta/\lambda^2)$.

Osmosis in an Alternating Electric Field

Z. LÁSZLÓ
Budapest, Hungary
January 12, 1950

WE have filled a vessel divided in two parts by a diaphragm (for instance a glass plate with a hole or a glass filter) in the first part with a polar and in the other part with a non-polar

FIG. 1. Vessel for the osmosis.

liquid. Placing into each part of the vessel an electrode and applying some thousand volts of alternating voltage to these condenser plates we have found that the process of osmosis has changed in respect to that without field.[1]

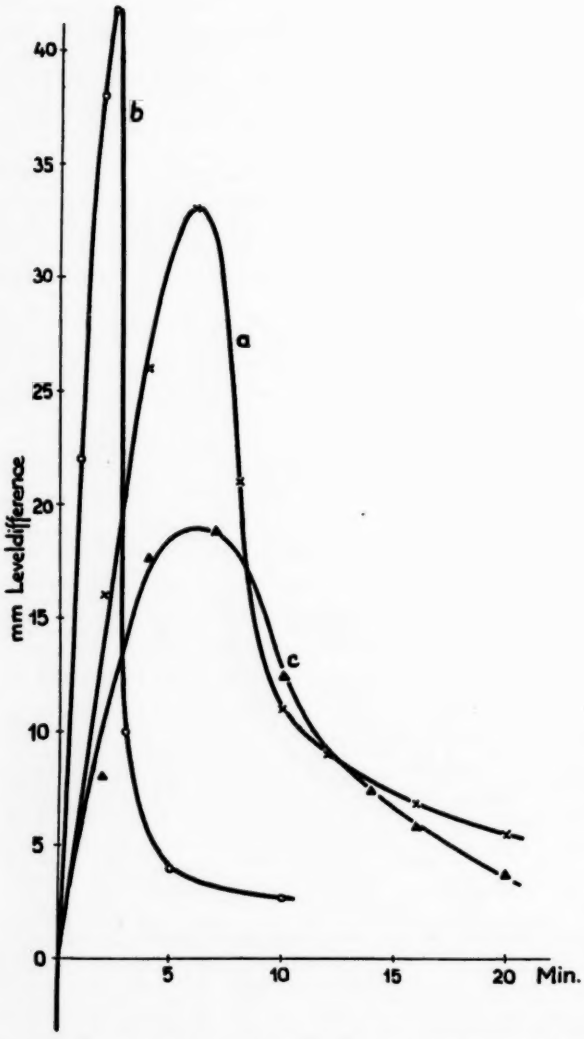

FIG. 2. Osmosis in the case of a glass plate with a hole diaphragm in a 4000 v a.c. field with systems (a) isobutylalcohol-methylalcohol, (b) nitrobenzene-methylalcohol, (c) diethyloxalate-ethylalcohol.

In this note we report observations made with the vessel filled in both sides with a polar liquid. In the first case our vessel was a U-shaped glass receptacle which was divided into two parts by means of a glass plate soldered in. This glass plate had a hole of *ca.* 0.4 mm diameter at the middle (Fig. 1). In the two parts of the vessel two platinum electrodes were immerged. The alternating voltage was supplied by a transformer from the 50 c/s mains. The vessel was cooled by means of circulating water.

We filled both parts of the vessel with different polar liquids to a height such that the hydrostatic pressure in them should be equal. In the absence of an electrical field we found that the two liquids mixed slowly in both compartments with levels approaching each other. Applying some thousand volts of a.c. to the condensers the osmotic process changed. This change could be seen by the rising of the first liquid and the sinking of the second. After a maximum difference of levels—these differences disappeared slowly—owing to the mixing of the liquids.

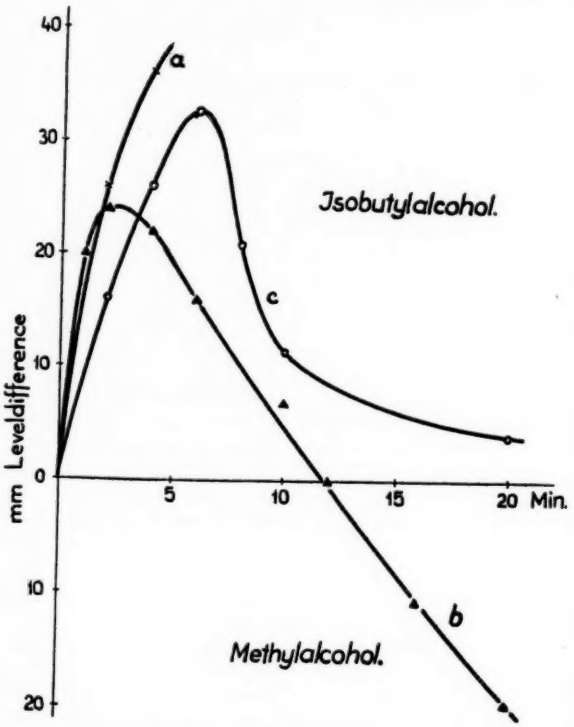

FIG. 3. Osmosis in the case of a glass plate with a hole diaphragm in a 4000 v d.c. field with the system isobutylalcohol-methylalcohol. The electrode is negative in the (a) methylalcohol, (b) in the isobutylalcohol. (c) Osmosis in the 4000 v a.c. field.

The liquid-pairs which we have examined were the following: ethylalcohol-methylalcohol, isobutylalcohol-methylalcohol, isobutylalcohol-ethylalcohol, isobutylalcohol-acetone, acetone-methylalcohol, acetone-ethylalcohol, diethyloxalate-isobutylalcohol, diethyloxalate-methylalcohol, diethyloxalate-ethylalcohol, diethyloxalate-acetone, nitrobenzene-methylalcohol, nitrobenzene-ethylalcohol, nitrobenzene-isobutylalcohol, nitrobenzene-acetone, nitrobenzene-diethyloxalate.

The experiments have been carried out at 4000 v a.c. Of the above-mentioned liquid-pairs always the first rose. Figure 2 shows the osmotic process of some liquid-pairs in an a.c. field in function of the time. On the figures the time is plotted on the horizontal and the level difference on the vertical axis.

We have carried out our experiments with some liquid-pairs also at 4000 v direct voltage with one electrode being positive, the other negative, and again with reversed polarity. The results of our measurements with d.c. are shown on Figs. 3 and 4 together with the observations with a.c.

The theoretical background of our experimental results is not yet cleared completely. Except nitrobenzene liquid-pairs the liquid with the less dielectrical constant rose. The rising of the liquid with the less dielectrical constant is tentatively explained by ponderomotoric forces as the order of magnitude of the level

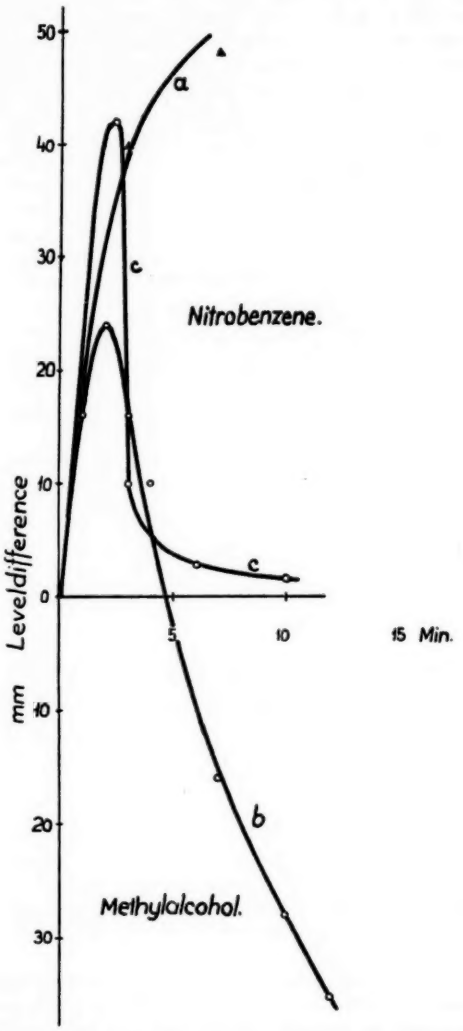

FIG. 4. The same as Fig. 3, but with the system of methylalcohol-nitrobenzene. The negative electrode is in (a) methylalcohol, (b) in nitrobenzene. (c) Osmosis in the 4000 v a.c. field.

differences equals roughly with the approximate calculation. In any case the rising of nitrobenzene is not explicable by ponderomotoric forces.

During the d.c. measurements it was found that independent of polarity the same liquid rose at first which has risen with a.c. When the concentration difference of the liquids is great the effect of the a.c. is the same as of the d.c. This experience proves that the phenomenon is independent of the polarity, i.e., it increases with the square of the field intensity, a fact also verified by prior measurements. If the concentration difference is diminishing the effect dependent on the square of the field intensity also lessens, and the phenomenon of electro-osmosis is prevailing. It was found, that during electro-osmosis the liquid at the positive pole has risen, which can be explained perhaps by the adhesion of the liquid of greater dielectric constant to the diaphragm.

The other vessel used in our measurements was also a U-shaped pipe, but the diaphragm was a soldered Jena glass filter "G 3."

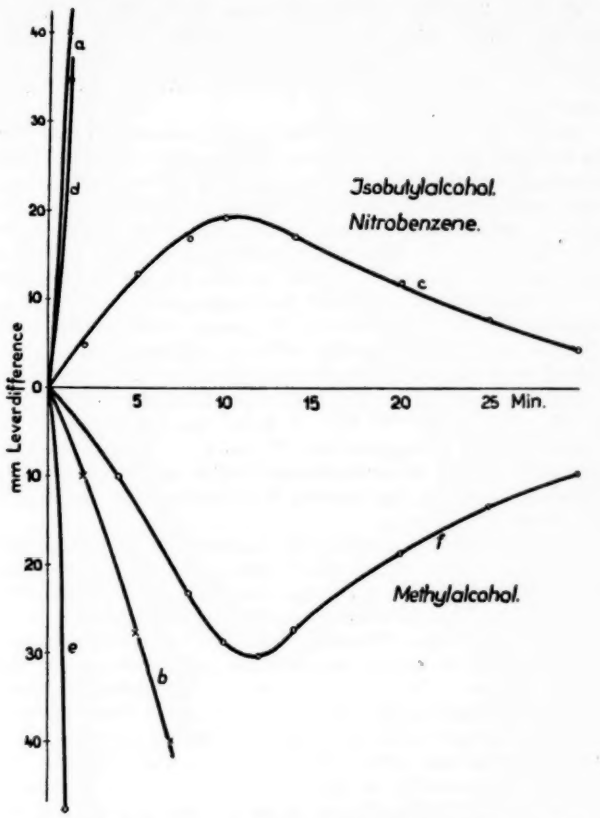

FIG. 5. Osmosis in the case of a glass filter diaphragm in 2000 v d.c. field with systems isobutylalcohol-methylalcohol, methylalcohol-nitrobenzene. The electrode is negative in the (a) isobutylalcohol, (b) in the methylalcohol. (c) Osmosis in the 3000 v a.c. field. (d) The electrode is negative in the nitrobenzene. (e) in the methylalcohol. (f) Osmosis in the 3000 v a.c. field.

The examined liquid pairs were the same as above. During the investigation we found differences in comparison with the results of similar measurements performed with the former vessel. The rising in the methylalcohol-acetone and in the ethylalcohol-acetone system were reversed in respect of the former vessel. Further we found a deviation with the nitrobenzene liquid-pairs where in every case the nitrobenzene was sinking.

In case of measurements carried out with d.c. the level differences independent of the polarity were not observed. By applying the voltage the electro-osmosis immediately appears, consequently the liquid at the negative pole rises (Fig. 5). The absence of the quadratic effect can be explained easily, because the diameter of the pores in a glass filter diaphragm is substantially less than the diameter of the hole in the glass plate and so the electro-osmotic pressure is greater than in the case of a great hole, surpassing instantly the quadratic effect.

[1] Z. László, Hungarica Acta Physica **1**, 44 (1949); J. Chem. Phys. **17**, 507 (1949); Kolloid Zeits. 114 (1949) (to be published).

Evidence for a Non-Planar Carbon Ring in Octafluorocyclobutane*

H. P. LEMAIRE AND R. L. LIVINGSTON
Department of Chemistry, Purdue University, West Lafayette, Indiana
December 8, 1949

PRELIMINARY results of an electron diffraction investigation of the structure of octafluorocyclobutane have led to the conclusion that the four-membered carbon ring is non-planar.

Electron diffraction photographs were prepared from a highly purified sample which was obtained from the Central Research Laboratories of the Minnesota Mining and Manufacturing Company. The photographs showed diffraction patterns extending to about $q=75$.

Models having a planar carbon ring (D_{4h} symmetry) gave rise to intensity curves which are in disagreement with the visual appearance of the diffraction patterns. Non-planar models were then constructed from planar models in the following way: One pair of diametrically opposite carbon atoms was raised above the plane while the other pair was lowered to the same extent keeping the CF_2 groups oriented so that a plane through the carbon atom of this group and the two adjacent carbon atoms bisected the FCF angle of the CF_2 group. These models have $D_{2d}(V_d)$ symmetry. Agreement with the diffraction data is obtained with models having this configuration and parameters within the following limits: C−F=1.31 to 1.34A, C−C=1.57 to 1.62A, ∠FCF=107° to 112°, α (angle between planes which bisect opposite CF_2 groups)=157° to 163°. Further work is necessary in order to choose the best models and to estimate uncertainties but the final results should fall within the ranges indicated.

It is interesting to compare this compound with cyclobutane and hexafluoropropene. In the former, spectroscopic evidence[1] favors a planar carbon ring indicating that the non-planar ring in C_4F_8 may be attributed to repulsions between fluorine atoms attached to different carbon atoms. These repulsions may also be responsible for an increase in the C−C distance above the value of about 1.54A which is observed in many hydrocarbons. In the case of hexafluoropropene, evidence has been obtained[2] for the fact that the closest approach of fluorine atoms attached to different carbon atoms is about 2.70A, which is twice the van der Waals radius of fluorine. This same value appears in the acceptable models of C_4F_8 as the shortest distance between fluorine atoms attached to different carbon atoms. It thus appears likely that twice the van der Waals radius of fluorine does represent the closest distance of approach of fluorine atoms which are not attached to the same carbon atom. This is not the case with the other halogens.

Independent evidence for the non-planar carbon ring in C_4F_8 has been obtained from spectroscopic studies by Edgell and Weiblen.[3]

The authors wish to thank the Research Corporation for financial support of this work. They are grateful to Professor Edgell of the Chemistry Department who suggested the problem, and to Professor H. J. Yearian of the Physics Department for the use of his diffraction equipment and for many stimulating discussions.

* From the Ph.D. thesis of H. P. Lemaire, Research Corporation Fellow in Chemistry, Purdue University.

[1] T. P. Wilson, J. Chem. Phys. 11, 361 (1943).
[2] F. A. M. Buck and R. L. Livingston, J. Chem. Phys. 18, 570 (1950).
[3] W. F. Edgell and D. G. Weiblen, J. Chem. Phys. 18, 571 (1950).

The Molecular Structure of Hexafluoropropene*

F. A. M. Buck
Shell Oil Company, Martinez, California
AND
R. L. Livingston
Department of Chemistry, Purdue University, West Lafayette, Indiana
December 8, 1949

THE preparation of electron diffraction photographs of C_3F_6 and their interpretation on the basis of a model of hexafluoropropene have been described in a previous article.[1] It is the purpose of this letter to indicate the nature of the acceptable models and those models which were rejected.

The models of hexafluoropropene were drawn graphically using the methods and techniques of descriptive geometry. This

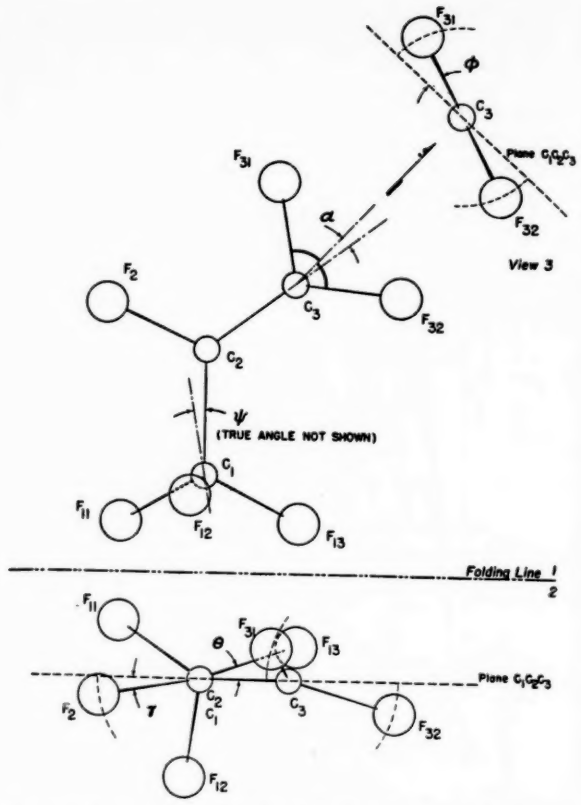

FIG. 1. Orthogonal projections of a molecular model of hexafluoropropene. The angle α is the angle between the line bisecting the $F_3C_3F_3$ angle and the extension of the C_2C_3 bond, ϕ is an angle describing a rotation of the $F_3C_3F_3$ group about the double bond, γ describes the rotation of F_2 about the direction C_1-C_2 as an axis and ψ is the angle between the trigonal axis of the CF_3 group and the direction C_1C_2. The angle θ is the angle between two planes, one plane being determined by the three carbon atoms and the other by C_1, C_2 and F_{13}.

afforded a convenient method of finding models consistent with the prominent peaks on the radial distribution curve.[1] During the investigation theoretical intensity curves were calculated for sixty-five models; many more models were rejected at the drawing board stage because they did not agree with the radial distribution curve.

The models considered may be conveniently classified as (1) "planar" models (having all atoms in one plane except the fluorine atoms in the CF_3 group) and (2) "strained" models (having some or all of the fluorine atoms of the $-CF=CF_2$ group not in the plane determined by the three carbon atoms). The values chosen for interatomic distances were those supported by spectroscopic and (unpublished) electron diffraction results on fluorocarbons and were always compatible with at least some of the major peaks on the radial distribution curve.

While in previous investigations it has been either assumed or demonstrated that atoms attached to double-bonded carbon atoms lie in the same plane, it was not possible in the case of hexafluoropropene to find a "planar" model with would give rise to an intensity curve agreeing with the visual appearance of the diffraction photographs. The "planar" models also fail to account for the radial distribution peak at 2.72A unless the C−C or C−F distances are made unusually long, in which case disagreement with other peaks arises. The peak at 2.72A is interpreted as corresponding to distances between fluorine atoms attached to different carbon atoms.

In order to construct models compatible with the radial distribution peaks at 1.32, 2.16, 2.32, 2.72 and 3.52A, it was necessary to consider "strained" models. The strain parameters chosen are indicated in Fig. 1. Models in which these parameters are

given values of from 2° to 5° and with $\theta=25°$ give rise to acceptable intensity curves. A typical model has bonded C−F distances ranging from 1.31 to 1.35A, the bonded C−C distances about 0.02A less than the frequently observed values of 1.34 and 1.54A, the FCF angles nearly tetrahedral, $\angle C_1C_2C_3=126°$ and $\angle C_1C_2F_2=114°$.

Because of the large number of parameters it is not possible to eliminate all "planar" models but in view of the failure to find an acceptable "planar" model after many trials, the authors believe that the structure of this compound is best represented by a "strained" model in which none of the fluorine atoms is in the plane determined by the three carbon atoms. The strains are attributed to repulsions between fluorine atoms which are attached to different carbon atoms; these repulsions apparently twist the double bond to such an extent that the closest approach of fluorine atoms is almost exactly twice the van der Waals radius of fluorine, i.e., 2×1.35A. Additional and somewhat more conclusive evidence for the importance of such strains has been found in the halogenated benzenes[2] and in C_4F_8.[3]

* From the Ph.D. thesis of F. A. M. Buck, du Pont Fellow in Chemistry, Purdue University, 1947–48.

[1] F. A. M. Buck and R. L. Livingston, J. Am. Chem. Soc. **70**, 2817 (1948).
[2] O. Bastiansen and O. Hassel, Acta Chemica Scandinavica **1**, 489 (1947).
[3] H. P. Lemaire and R. L. Livingston, J. Chem. Phys. **18**, 569 (1950).

On the Molecular Configuration of Cyclic C_4F_8

WALTER F. EDGELL[1]
Department of Chemistry, State University of Iowa, Iowa City, Iowa
AND
DONOVAN G. WEIBLEN
Central Analytical Laboratories, Minnesota Mining and Manufacturing Company, St. Paul, Minnesota
December 8, 1949

SEVERAL years ago one of us[2] studied the Raman spectrum of perfluorocyclobutane and concluded that it and the data then available on the infra-red spectrum "are in harmony with the planar ring model of symmetry D_{4h}." The spectra have been investigated again with better equipment and new data obtained.

The sample used in this work was prepared by the pyrolysis of teflon.[3] Experimental details will be presented later. The Raman spectrum was determined in the liquid state at about −25°C using a Lane-Wells spectrograph of camera aperture $F/3$. The results are found in Table I. Lines were also found shifted 301, 382, 598, 643, 906, and 954 cm^{-1} from the Hg 4358A exciting line. These are believed to be the fundamentals 361, 440, 699, and 1008 cm^{-1} excited by Hg 4348 or Hg 4339A.

TABLE I. The Raman spectrum of cyclic C_4F_8 (to 1450 cm^{-1}).

ω (cm^{-1})	Density*	ω (cm^{-1})	Density*
190	*m*	783	*vw*
256	*s*	857	*vw*
272	*s*	971	*w*
346	*m*+	1008	*s*
361	*vs*	1052	*w*
440	*vs*	1216	*s*
573	*vw*	1278	*m*+
605	*w*+	1340	*w*
659	*m*	1398	*vw*
699	*vs*		
722	*m*	1431	*m*+

* *s*=strong, *m*=medium, *w*=weak, *v*=very.

The infra-red spectrum was obtained with a Perkin-Elmer spectrometer, Model 12B, using NaCl and KBr optics. The results, through the region of the fundamentals, are found in Table II. Relative intensities are based on the scale: *vvs*, 50 percent absorption at 2.5 mm pressure; *vs*, 50 percent at 12.5 mm; *s*, 50 percent at 50 mm; *m*, 50 percent at 500 mm; *w*, 50–25 percent at 500 mm; *vw*, <25 percent at 500 mm, all in a 10-cm cell.

In general, the data obtained in another recent study of this molecule[4] are in good agreement with those presented here. They have been interpreted in terms of the planar ring model.

TABLE II. The infra-red spectrum of cyclic C_4F_8 (400 to 1450 cm^{-1}).

ω (cm^{-1})	Intensity*	ω (cm^{-1})	Intensity*
425	*vw*	864†	*w*
444	*m*	890	*w*
467	*w*	899	*w*
502	*vvw*	962	*vvs*
531	*vw*	981	*m*
571	*vs*	1002	*m*
606	*vw*	1093	*m*
632	*vw*	1120	*w*
659	*w*	1153	*s*
684	*w*	1224†	*vs*
729†	*w*	1239†	*vvs*
731†	*w*	1268	*m*
799	*vw*	1290	*vvs*
845†	*w*	1229	*vvs*
851†	*w*	1394	*s*
858†	*w*	1448	*w*

* *s*=strong, *m*=medium, *w*=weak, *v*=very.
† Peaks in a "single band" or region of absorption.

If cyclic C_4F_8 has a planar ring structure of symmetry D_{4h}, eleven fundamentals would be Raman active. Almost twice this number of lines are found in the spectrum range of the fundamentals, fifteen of which are of sufficient intensity to appear on all films of reasonable exposure. A molecule with this point group has a center of symmetry and transitions permitted in the Raman spectrum are forbidden in the infra-red spectrum and vice-versa. More than half of the Raman lines in the region of common observation correspond to infra-red bands with almost exact numerical coincidence or within the limits to be expected of spectra taken in different phases.

With the D_{4h} model, these features of the spectra must be attributed to the breakdown of selection rules either in the liquid state or at higher pressures, near coincidences in the frequencies of similar fundamental modes of vibration and the appearance of overtones or combinations in the Raman spectra. Because of the number of the "discrepancies" and the fact that allowed fundamentals of highly fluorinated molecules often appear weakly in Raman and infra-red spectra, it is believed that a question should be raised as to the correctness of the D_{4h} model. Independent evidence is required to prove this point.

An electron diffraction study of this molecule has been carried out by Lemaire and Livingston.[5] They were unable to interpret their results in terms of the planar ring model of symmetry D_{4h}. Agreement between calculated and observed patterns were obtained for a model of symmetry V_d, the most likely non-planar ring structure.

One of us (W. F. E.) wishes to express his gratitude to the Research Corporation for a grant which made the purchase of the Lane-Wells spectrograph possible. Thanks are also due Mr. H. D. Mallory for preparing several Raman spectrograms and the Central Research Laboratories, Minnesota Mining and Manufacturing Company, for the samples.

[1] Now at the Department of Chemistry, Purdue University, Lafayette, Indiana.

[2] Walter F. Edgell, J. Am. Chem. Soc. **69**, 660 (1947).
[3] E. Lewis and M. Naylor, J. Am. Chem. Soc. **69**, 1968 (1949).
[4] H. Claasen and J. R. Nielsen, Symposium on Molecular Structure, Ohio State University (June, 1949).
[5] H. Lemaire and R. L. Livingston, J. Chem. Phys. **18**, 569 (1950).

The Mechanism of the Decomposition of N_2O on ZnO as Catalyst

M. BOUDART
Frick Chemical Laboratory, Princeton University, Princeton, New Jersey
February 3, 1950

UNDER this heading, Wagner[1] reports an attempt to correlate catalytic activity with conductive properties. Observing that the conductivity of ZnO+1 percent Ga_2O_3 is 50 times greater than that of ZnO but that the rate of N_2O decomposition on these catalysts differs by a factor less than two, he concludes that the

". . . attempt to develop a mixed catalyst with an outstanding activity has been a failure." This failure however is not due to an absence of correlation between activated adsorption and conductive characteristics of the adsorbent but to a deceptive choice of the operative parameter. Volkenshtein[2] has shown that the main features of activated adsorption (activation energy, isotherms, differential adsorption heats decreasing with coverage) can be obtained with an energetically homogeneous but temperature sensitive surface. Active centers may be originally present but new ones are produced either on filling up at constant temperature or by a temperature increase, at the expense of an energy E which appears as an activation energy in the rate equation for adsorption. In certain cases, we may identify E with the energy ϵ necessary to send a bound electron into the conduction band. Details will be described elsewhere. Let it be said only that such an activation throws much light on some facts which were obscure from the standpoint of the usual theories. Since 1932, Taylor[3] has repeatedly emphasized that the observed adsorption rates were not compatible with the assumption that every molecule hitting the surface with the necessary activation energy is adsorbed. Pace and Taylor,[4] reporting that the adsorption rates for H_2 and D_2 on Cr_2O_3 and ZnO-Cr_2O_3 are identical, suggested that *"the activation energy of the adsorption process is required by the solid adsorbent."* This activation of the solid has also been considered by Hedvall[5] whose concepts have been examined by Möglich.[6]

Assuming that the concentration of quasi-free electrons is rate determining, Wagner concludes that 1 percent Ga_2O_3 has no influence on the reaction velocity and he defines active centers of a special nature. No such restrictive hypothesis is needed if absolute values of K (specific conductivity) are of little interest but if ϵ has to be measured and appreciated as the determining parameter. There is a relationship between K and ϵ (Meyer's "straight line") but from the data which led Meyer to his systematisation and from their analysis by Gisolf,[7] it can be seen that large differences in conductivities do not entail a large difference $\Delta\epsilon$ between the corresponding values of ϵ; $\Delta\epsilon$ actually depends on changes in concentrations of both defects and electron traps and can be quite small. If it were 1350 cal. mole^{-1}, the reaction rates would differ at 725°C by a factor of two only.

We thus think that Wagner underestimated the scope of his own work. Further attempts to correlate adsorption and catalysis with semiconductivity ought to include measurements of both K and ϵ.[8] We wish to express our indebtedness to Professor H. S. Taylor who suggested a large number of the ideas contained in this note.

[1] C. Wagner, J. Chem. Phys. **18**, 69 (1950).
[2] F. F. Volkenshtein, Zeits. f. Khim. **23**, 917 (1949).
[3] H. S. Taylor, Trans. Faraday Soc. **28**, 137 (1932).
[4] J. Pace and H. S. Taylor, J. Chem. Phys. **2**, 578 (1934).
[5] J. A. Hedvall, Zeits. f. angew. Chemie **54**, 505 (1941).
[6] F. Möglich and R. Rompe, Physik. Zeits. **44**, 77 (1943).
[7] J. H. Gisolf, Ann. d. Physik **1**, 3 (1947).
[8] Bevan, Shelton, and Anderson, J. Chem. Soc. 1729 (1948).

Quasi-Unimolecular and Quasi-Bimolecular Steps in Complex Reactions. The Dissociation of Nitrogen Pentoxide

RICHARD A. OGG, JR.*
Mallinckrodt Chemical Laboratory, Harvard University, Cambridge, Massachusetts
February 15, 1950

THE mechanism previously proposed[1] for the decomposition of N_2O_5 entails a hitherto unemphasized prediction of an apparent "falling off" of the first-order rate constant at *extreme low pressure*. In the reformulation below, the symbol M denotes the molecular species responsible for collisional activation and deactivation.

$N_2O_5 \rightarrow NO_3+NO_2$	$k_1=f_1[(M)]$
$NO_3+NO_2\rightarrow N_2O_5$	$k_2=f_2[(M)]$
$NO_3+NO_2\rightarrow NO_2+O_2+NO$	k_3
$NO_3+NO \rightarrow 2NO_2$	k_4

(The rate constant for step 4, not comprised in the original formulation, does not appear in the rate expression for the decomposition. It is required to explain the kinetics of the reaction between N_2O_5 and added NO.) The various detailed theories[2] of quasi-unimolecular reactions allow derivation (on the basis of assumed molecular models) of specific mathematical forms for the function f_1. Inasmuch as k_1/k_2 is an equilibrium constant, f_1 and f_2 are identical in form, in the sense that $f_1[(M)_A]/f_1[(M)_B] = f_2[(M)_A]/f_2[(M)_B]$. The various theories converge in the region of extreme low pressure—i.e., as $(M)\rightarrow 0$, $k_1\rightarrow k_{act}(M)$, where k_{act} is the collisional activation constant.

The following rate expression results for the decomposition.

$$\frac{-d(N_2O_5)}{dt}=k_{ex}(N_2O_5)=\frac{2k_1k_3}{k_2+2k_3}(N_2O_5).$$

As previously shown, when $(M)\rightarrow\infty$, $k_2\gg 2k_3$ and hence

$$k_{ex,\infty}=\frac{2k_1k_3}{k_2}.$$

At all values of (M)

$$\frac{1}{k_{ex}}=\frac{k_2}{2k_1k_3}+\frac{1}{k_1}=\frac{1}{k_{ex,\infty}}+\frac{1}{k_1}.$$

As $(M)\rightarrow 0$, $k_1\rightarrow k_{act}(M)$,

$$\frac{1}{k_{ex,0}}\rightarrow\frac{1}{k_{ex,\infty}}+\frac{1}{k_{act}(M)}.$$

The above conclusion as to eventual falling off of k_{ex} is strikingly confirmed by the studies of Linhorst and Hodges[3] performed at pressures of the order of 10^{-3} mm Hg. Their empirical equation is of exactly the above linear form. From their data at various temperatures, for M simply N_2O_5 itself, the collisional activation rate constant

$$k_{act}=10^{18.9}e^{-\frac{18{,}300}{RT}}\ \text{mole}^{-1}\ \text{cm}^3\ \text{sec.}^{-1}.$$

The activation energy of step 1 at high pressures cannot be less in absolute value than the energy change associated with this process. From the previous estimate[1] a value of about 21.6 kcal./mole seems very probable for this activation energy. It is seen above that the limiting value at extreme low pressures is some 18.3 kcal./mole. In the Kassel[2] classical model based theory, this difference is merely $(s-3/2)RT$, where s is the effective number of classical oscillators. Noting that these figures apply to some 300°K, the corresponding value for s is about 7. This is entirely reasonable in view of the maximum possible value of 15 for N_2O_5. Using $s=7$, the above frequency factor leads to a collisional *deactivation* rate constant of some 10^{15} mole^{-1} cm^3 sec.$^{-1}$. The collision diameter corresponding to this figure is in sensible agreement with the viscosity studies on N_2O_5.[4]

The above estimated activation energy and a "normal" frequency factor lead to an expected limiting high pressure value of k_1 at 300°K of the order of magnitude of 10^{-1} sec.$^{-1}$. From the above estimate of s the classical theory of Kassel[2] predicts that N_2O_5 pressures of the order of hundreds of millimeters of Hg would be necessary to reach *one-half* of the limiting high pressure value of k_1. Thus step 1, when studied separately, is expected to show very marked falling off of rate constant at moderate pressures, and should be markedly accelerated by addition of chemically indifferent gases.

The work of Smith and Daniels[5] on the kinetics of the reaction

$$N_2O_5+NO\rightarrow 3NO_2$$

offers one approach to study of the rate of step 1. Neglecting step 3 the resulting rate expression is

$$\frac{-d(NO)}{dt}=\frac{k_1(N_2O_5)}{1+[k_2(NO_2)/k_4(NO)]}.$$

The reaction was observed to be zero order with respect to NO, but no marked inhibitory effect of NO_2 was found. At the relatively very low pressures used, the value of k_2 has apparently

fallen off so much that $k_2 \ll k_4$. The first-order constants show a systematic trend with increase of pressure, suggesting the above predicted quasi-unimolecular behavior. It is to be expected that addition of chemically indifferent gases, such as CO_2 and SF_6, would greatly accelerate the reaction.

* Currently on leave from Stanford University, California.
[1] R. A. Ogg, Jr., J. Chem. Phys. **15**, 613 (1947).
[2] L. S. Kassel, *Kinetics of Homogeneous Gas Reactions* (Chemical Catalogue Company, New York, 1932).
[3] E. F. Linhorst and J. H. Hodges, J. Am. Chem. Soc. **56**, 836 (1934).
[4] H. Eyring and G. A. Van Valkenburgh, J. Am. Chem. Soc. **52**, 2619 (1930).
[5] J. H. Smith and F. Daniels, J. Am. Chem. Soc. **69**, 1735 (1947).

Experimental Evidence for the Quasi-Unimolecular Dissociation of Nitrogen Pentoxide

RICHARD A. OGG, JR.,* WILLIAM S. RICHARDSON, AND M. KENT WILSON
Mallinckrodt Chemical Laboratory, Harvard University, Cambridge, Massachusetts
February 15, 1950

REACTION rate studies involving nitrogen pentoxide have been carried out, concentrations of respective components being determined by intensity measurements on suitable infra-red absorption bands. Use was made of the double beam recording spectrophotometer Model B manufactured by Baird Associates. Absorption cells were of Pyrex glass tubing 4.5 cm long and 4.0 cm in diameter, fitted with interchangeable windows or rocksalt, silver chloride or fluorite. Of the "strong" bands of N_2O_5 between 2 and 16μ, only that at approximately 1350 cm^{-1} is clearly resolved from strong bands of N_2O_4. For the isotopic nitrogen exchange studies, use was made of the very strong ν_3 fundamental of NO_2 at 1621 cm^{-1}. The appearance of the band envelope proved particularly sensitive to pressure broadening caused by admixture of foreign gases, the *P* and *R* branches showing an apparent intensity increase much greater than that of the *Q* branch. When NO_2 was prepared (by heating with PbO) from KNO_3 containing 57 atomic percent of N^{15}, the resulting additional spectrum displayed the expected isotope displacement to longer wavelength, amounting to about 40 cm^{-1}. In the presence of considerable foreign gas the *P* branch of $N^{15}O_2$ is clearly resolved, and its intensity is a satisfactory concentration index. Concomitantly in such an isotopic mixture, the intensity of the *R* branch of $N^{14}O_2$ may be used to measure the concentration of this species.

N^{15} enriched N_2O_5 was prepared by ozonization of enriched NO_2. After separation from oxygen and ozone, it was vaporized into the evacuated absorption cell. After tracing the relevant region of the spectrum, the spectrophotometer was stopped at the maximum of the *P* branch of $N^{15}O_2$. Opening a stopcock to an attached bulb caused admission of a mixture of CO_2 and isotopically normal NO_2. The transmission scale was read at measured time intervals, the change corresponding to production of $N^{15}O_2$. When exchange equilibrium was reached, the entire spectrum was traced, the intensities of the N_2O_5, NO_2, and CO_2 bands yielding the composition of the reaction mixture. (Concentration-intensity relations had been determined empirically.) In typical experiments the respective partial pressure ranges for these three components were some 5–25, 10–50, and 50–500 mm Hg. Experiments were also performed in which isotopically normal N_2O_5 was admitted to the cell containing enriched NO_2. These latter showed qualitatively the rapid exchange, but for rather apparent reasons are not well suited to accurate measure of the rate.

The above studies show the equilibrium

$$N_2{}^{14}O_5 + N^{15}O_2 \rightleftarrows N_2{}^{15}O_5 + N^{14}O_2$$

to be established very rapidly, the rate being apparently first order with respect to N_2O_5 and zero order with respect to NO_2 (although greater precision is required to establish these orders exactly). This indicates that at least the major rate determining step is the dissociation

$$N_2O_5 \rightarrow NO_3 + NO_2.$$

At 27°C the rate constant of this step is of the order of magnitude of 0.5 $sec.^{-1}$ when the partial pressure of CO_2 is 500 mm Hg. Decrease of CO_2 concentration markedly decreases the rate, the above velocity constant decreasing by a factor of about five when the CO_2 partial pressure is reduced tenfold. It appears that still higher pressures would be required to attain the limiting value of the rate constant. It is to be noted that this behavior qualitatively substantiates the prediction of quasi-unimolecular behavior with "falling off" at relatively high pressures.[1] Probably the principal value at this stage of the studies is the first experimental demonstration of the expected isotopic exchange reaction *in the gas phase*. The previous studies[2] with N^{13} were confined to solutions in CCl_4, and gave an even rougher indication of the magnitudes of the rates.

Rate studies of the reaction

$$N_2O_5 + NO \rightarrow 3NO_2$$

were carried out at 27°C by following the disappearance of N_2O_5. The cell initially contained pure N_2O_5 vapor at some 40 mm Hg pressure, and the spectrophotometer was set at the maximum of the 1350 cm^{-1} band. After admission of an NO–CO_2 mixture, the procedure was as above. (The characteristic NO fundamental does not overlap other bands of interest.) Initial concentrations of NO varied from some 60 to 200 mm Hg, and that of CO_2 from 50 to 500 mm Hg. The NO_2 formed by the reaction proved to have a marked inhibiting effect, which was quantitatively greater, the higher the concentration of CO_2. As nearly as could be judged from the experiments, this inhibition is in agreement with the form of the rate expression given by the proposed mechanism.[1] Initial rates were determined by extrapolation, and proved to be zero order with respect to NO, and first order with respect to N_2O_5. At a partial pressure of CO_2 of 500 mm Hg, the first-order rate constant is within experimental uncertainty identical with that found from the isotope exchange. Decrease of CO_2 concentration produced a marked decrease of the initial rate constant—again in a fashion indistinguishable from that of the isotope exchange reaction. To be sure, the relatively low precision of both sets of measurements does not warrant more than the statement that it seems highly probable that the same rate determining step must be common to both reactions. Further evidence for the correctness of the proposed mechanism is found in the experimental observation of the increase of the inhibitory effect of NO_2 with increasing CO_2 concentration—an effect to be expected from the necessarily quasi-bimolecular character of the association reaction $NO_3 + NO_2 \rightarrow N_2O_5$.

Current continuation of both sets of studies is aimed at improvement of precision, and the extension to other temperatures, as well as the use of various chemically indifferent gases. These studies hold promise of completion of the first body of experimental evidence adequate for comparison with the refined theories of quasi-unimolecular reactions.

* Currently on leave from Stanford University, California.
[1] R. A. Ogg, Jr., J. Chem. Phys. **18**, 572 (1950).
[2] R. A. Ogg, Jr., J. Chem. Phys. **15**, 613 (1947).

The Behavior of Glass Electrodes in Acid Solutions

MALCOLM DOLE
Department of Chemistry, Northwestern University, Evanston, Illinois
February 24, 1950

UNDER the above title, Sinclair and Martell[1] have recently published a description of a study of glass electrodes which they have made in concentrated hydrochloric and sulfuric acid solutions. In their paper they state, "In view of the experimental results presented in this paper in comparison with the results predicted by Dole's theory of the negative errors, it is to be concluded that the assumption of water transport through the glass membrane does not satisfactorily account for the negative errors of the glass electrode. It would seem, therefore, that the only remaining possibility of accounting for these deviations would be to attribute them to anions."

There is another possible explanation which the authors have apparently not considered and that is, that the potentials they measured, at least some if not all of those which deviate from my theory, are not true, reversible thermodynamic potentials. In a paper published in 1941, which Sinclair and Martell do not mention, we showed[2] that, whereas neither the fluoride ion nor hydrogen ion by itself causes deviations of the glass electrode, as soon as the molecular hydrogen fluoride concentration became as high as 0.0013 molar, strong deviations of the glass electrode occurred even in the normal *p*H range of validity. It is thus evident that chemical attack of the surface of the glass electrode can cause marked errors. E.m.f. values drifting with time as observed by Sinclair and Martell are signs of non-reversibility of the electrode and of chemical attack.

If Sinclair and Martell's data in the range of glass electrode stability are considered, agreement with my theory within the range of glass electrode reproducibility in acid solution is obtained. Thus, using their Table II data which include e.m.f. values of four individual electrodes, we find −11.2, −5.4, −9.9, and −6.5 mv error in 5 N HCl, average −8.2 mv while the error calculated by my theory is −9.8 mv. In 1 N HCl, measured errors were −2.4, +0.3, −0.5, −1.3 mv, average −1.0 mv while the error calculated by my theory is −1.3 mv. Hence in these HCl solutions the data of Sinclair and Martell confirm my theory within the accuracy attainable with glass electrodes. In 5 N H_2SO_4 solutions e.m.f. values of three glass electrodes gave −4.1, −1.2 and −3.6 mv error, average −3.0 mv, calculated by theory −4.0 mv. In 1 N H_2SO_4 solution measured errors were −0.4, −0.4, −0.2, −0.1, +0.6 mv, calculated by theory −0.6 mv. This agreement is not quite as close as in the case of the HCl data, but the data are in the direction predicted by theory and have the correct order of magnitude.

For years I have attempted to discover a negative ion function of the glass electrode, that is to say an e.m.f. response of the glass electrode which bears a quantitative relation to variations in the negative ion activity, but without success.[2,3]

Such a function might be demonstrated thermodynamically or kinetically. Ion transference experiments have shown that both hydrogen and other positive ions and water molecules are transported into glass on the passage of electric current.[4] Thus both kinetic and thermodynamic evidence indicate the passage of positive ions and water molecules across the solution-glass boundary on the passage of electric current, but no evidence of a negative ion function of the glass electrode either of a thermodynamic or kinetic nature exists. Until such evidence is forthcoming any conclusion that the acid errors are due to negative ions is without foundation.

[1] E. E. Sinclair and A. E. Martell, J. Chem. Phys. **18**, 224 (1950).
[2] Dole, Roberts, and Holley, Jr., J. Am. Chem. Soc. **63**, 725 (1941).
[3] M. Dole, J. Am. Chem. Soc. **54**, 3095 (1932).
[4] For the water transport see the valuable paper by G. Haugaard, J. Phys. Chem. **45**, 148 (1940); for positive ion transport see F. Quittner, Ann. d. Physik [4] **85**, 745 (1928).

The Effect on Reaction Rates Caused by the Substitution of C^{14} for C^{12}

WILLIAM H. STEVENS AND RICHARD W. ATTREE*
Chemistry Branch, Atomic Energy Project, National Research Council of Canada, Chalk River, Ontario, Canada
February 13, 1950

SEVERAL observations of an isotope effect on reaction rates, both with C^{13} and C^{14}, have recently been reported.[1] In view of the importance of this effect in quantitative tracer experiments, and because a study of the effect may make a contribution to an understanding of the mechanism of the reactions concerned, an extensive investigation as to the extent and magnitude of the effect has been started in this laboratory. This letter reports preliminary results of experiments with the Cannizzaro reaction, the benzoin condensation, and the benzilic acid rearrangement.

With benzaldehyde, the Cannizzaro reaction produces benzyl alcohol and benzoic acid. If benzaldehyde-carbonyl-C^{14} is used, the activity in the alcohol and acid produced, per mole, will be equal unless the rate constant for the reaction involving labeled molecules differs from that for the unlabeled molecules. The alcohol and acid are easily separated, and any difference in their molar specific activities can be directly related to a reaction rate difference.

In the benzoin condensation, with benzaldehyde-carbonyl-C^{14}, two differently labeled products are possible, *viz.*:

$$2C_6H_5C^{14}HO \rightarrow C_6H_5.C^{14}HOH.CO.C_6H_5 \quad \text{I}$$
$$2C_6H_5C^{14}HO \rightarrow C_6H_5.CHOH.C^{14}O.C_6H_5. \quad \text{II}$$

These will be produced in equal quantities unless the rate constants for their formation are unequal. Analysis for these two species may be performed by cleaving the benzoin produced in the reaction with periodic acid. Reaction I will yield benzaldehyde-carbonyl-C^{14}, while II will yield benzoic acid-carboxyl-C^{14}. The benzaldehyde and benzoic acid may be readily separated, and since the cleavage is quantitative,[2] the ratio of the molar specific activities of the benzaldehyde and benzoic acid will be equal to the ratio of the concentrations of I and II, provided the specific activities are low. Any divergence from unity for this ratio can be related to a reaction rate difference.

These reactions have been carried out, and it has been found that any difference in the rate constants for the C^{14}-labeled and unlabeled molecules which may exist is less than the probable counting sample preparation and counting error (±1.5 percent) in both the Cannizzaro reaction and benzoin condensation. No very appreciable isotope effect exists therefore in these two reactions. This may be of some interest as it is the first reported case where an isotope effect has been sought and found to be inappreciable.†

In the benzilic acid rearrangement, with mono-carbonyl labeled benzil, two differently labeled products are possible, *viz.*: benzilic acid-1-C^{14} (III) and benzilic acid-2-C^{14} (IV).

$$C_6H_5C^{14}OCOC_6H_5 \rightarrow (C_6H_5)_2COHC^{14}O_2H \text{ (III)} \rightarrow (C_6H_5)_2CO + C^{14}O_2$$
$$C_6H_5C^{14}OCOC_6H_5 \rightarrow (C_6H_5)_2C^{14}OHCO_2H \text{ (IV)} \rightarrow (C_6H_5)_2C^{14}O + CO_2$$

On treatment with lead tetra-acetate, benzilic acid is decarboxylated to benzophenone. The ratio of the quantities of benzilic acids III and IV formed may readily be obtained from the molar specific activities of the initial benzilic acid produced in the reaction and the resulting benzophenone obtained by decarboxylation, provided low specific activity material has been used.

This reaction has been carried out, and it has been found that the ratio of the amount of benzilic acid-2-C^{14} to benzilic acid-1-C^{14} produced in the rearrangement is equal to 1.11±0.01.

Experimental details and discussion of results will be reported elsewhere.

* Now at Frick Chemical Laboratory, Princeton University, Princeton, New Jersey.
[1] J. Bigeleisen and L. Friedman, J. Chem. Phys. **17**, 998 (1949). Lindsay, McElcheran, and Thode, J. Chem. Phys. **17**, 589 (1949). W. H. Stevens and R. W. Attree, Can. J. Research **27B**, 807 (1949). (See this paper for references to previous earlier work by others.) J. W. Weigl and M. Calvin, J. Chem. Phys. **17**, 210 (1949).
[2] P. W. Clutterbuck and F. Reuter, J. Chem. Soc. 1467 (1935).
† Pyrolysis of barium adipate, containing C^{13} of natural abundance, to produce barium carbonate and cyclopentanone has been found to produce an isotope fractionation of only about 0.1 percent of the C^{13}/C^{12} ratio. Bothner-By, Bigeleisen, and Friedman, reported at Brookhaven Chemistry Conference No. 4, January 19, 1950 (unpublished work).